



U.S. DEPARTMENT OF  
**ENERGY**

Office of  
Science

# **Benchmarking CATALYSIS SCIENCE**

**Meeting of the Catalysis Science Program  
Chemical Sciences, Geosciences and  
Biosciences Division  
Office of Basic Energy Sciences  
U.S. Department of Energy**

**Westin Annapolis  
Annapolis, Maryland  
July 19–22, 2015**

This document was produced under contract number DE-AC05-06OR23100 between the U.S. Department of Energy and Oak Ridge Associated Universities.

## FOREWORD

The 2015 Catalysis Science Program Meeting is sponsored by the Division of Chemical Sciences, Geosciences and Biosciences, Office of Basic Energy Sciences (BES), U.S. Department of Energy. It is being held on July 19-22, 2015, at the Westin Annapolis Hotel, Annapolis, Maryland. The purposes of this meeting are to discuss the recent advances in the chemical, physical, and biological bases of catalysis science, to foster exchange of ideas and cooperation among participants, and to discuss the new challenges and opportunities recently emerging in energy technologies.

Catalysis activities within BES emphasize fundamental research aimed at understanding mechanisms and ultimately controlling the chemical conversion of natural and synthesis substances. The long-term goal of this research is to discover fundamental principles and produce insightful approaches to predict structure-reactivity properties. Such knowledge, integrated with advances in chemical and materials synthesis, *in situ* and *operando* analytical instrumentation, and chemical kinetics and quantum chemistry methods, will allow the control of chemical reactions along desired pathways. This new knowledge will impact the efficiency of conversion of matter into fuels, chemicals, materials, or other forms of energy, while minimizing the impact to the environment.

This year's meeting participants will discuss how to benchmark the approaches used for acquiring and sharing new catalytic knowledge. The goal will be to identify best practices and also new approaches for the study of transformations relevant to DOE's missions, such as C-H and C-H-O activation in general, selective reduction and oxidation, fossil- and biomass-related conversions, polymer synthesis, energy generation and storage, and others. Methods classical in organic and organometallic chemistry can be combined with solid state and surface chemistry to study reaction mechanisms and structures of catalytic sites, and so arrive at reliable, easily shareable information among the catalysis community in order to accelerate progress towards new discoveries.

Special thanks go to the program investigators and their students, postdocs, and collaborators for their dedication to the continuous success and visibility of the BES Catalysis Science Program, and to the session moderators for their invaluable help. We also thank Diane Marceau from DOE BES<sup>3</sup> and Connie Lansdon from Oak Ridge Institute for Science and Education for the logistical and web support.

Jingguang Chen<sup>1</sup>, Susannah Scott<sup>2</sup> and Raul Miranda<sup>3</sup>

<sup>1</sup>Columbia University and Brookhaven National Laboratory

<sup>2</sup>University of California-Santa Barbara

<sup>3</sup>Office of Basic Energy Sciences - U.S. Department of Energy

This page is intentionally blank.

## Schedule for 2015 Catalysis Science PI Meeting

### Benchmarking Catalysis Science

July 19–22, 2015  
Annapolis, MD

**Program chairs:**  
Jingguang Chen and Susannah Scott

<b>Sunday, July 19</b>	
3:00 pm	<b>Registration opens</b>
<i>Opening session</i>	Session Chairs: <b>J. Chen, S. Scott</b>
6:30-6:40 pm	Welcoming Remarks ( <b>R. Miranda</b> )
6:40-7:00 pm	Benchmarking theme and outcomes ( <b>J. Chen, S. Scott</b> )
<b>Plenary session</b>	Session chair: <b>S. Scott</b>
7:00-8:00 pm	<b>Plenary lecture (M. Bullock)</b> <i>Design of Molecular Electrocatalysts for Production and Oxidation of Hydrogen</i>
8:00-10:00 pm	<b>Poster Session I</b>

<b>Monday, July 20</b>	
7:00-8:30 am	<b>Breakfast</b>
8:30-9:00 am	DOE BES Update ( <b>T. Pietrass</b> )
<b>Plenary session</b>	Session chair: <b>J. Chen</b>
9:00-10:00 am	<b>Plenary lecture (J. Nørskov)</b> <i>The Need for Benchmarking Catalysis, with particular emphasis on Computational Methods and Models</i>
10:00-10:30 am	<b>Coffee Break</b>
<i>I. Advances in Theoretical and Computational Modeling</i>	Session Chair: <b>T. Rahman</b>
10:30-11:10 am	Keynote speaker ( <b>D. Vlachos</b> )
11:10-11:35 am	Invited speaker ( <b>D. Sholl</b> )
11:35-12:00 pm	Invited speaker ( <b>A. Selloni</b> )
12:00-1:30 pm	<b>Lunch</b>
<i>II. Advances in Heterogeneous Catalysis</i>	Session Chair: <b>U. Ozkan</b>
1:30-2:10 pm	Keynote speaker ( <b>J. Lercher</b> )

2:10-2:35 pm	Invited speaker ( <b>R. Crooks</b> )
2:35-3:00 pm	Invited speaker ( <b>P. Dauenhauer</b> )
3:00-3:15 pm	<b>Transition to Breakouts, Coffee Break</b>
<b><i>Breakout Session I</i></b>	<b><i>Benchmarking:</i></b>
3:15-4:45 pm	Topic 1: <i>Computational approaches</i> Discussion leaders: <b>J. Kitchin, T. Bligaard</b> Topic 2: <i>Molecular and hybrid catalysts</i> Discussion leaders: <b>C. Jones, W. Jones</b> Topic 3: <i>Non-molecular catalysts</i> Discussion leaders: <b>C. Campbell, B. Gates</b> Topic 4: <i>Photo- and electrocatalysts</i> Discussion leaders: <b>M. Bullock, R. Gorte</b>
5:00-6:30 pm	<b>Dinner</b>
<b><i>III. Advances in Small Molecule Activation, I: H<sub>2</sub>O, CO<sub>2</sub>, N<sub>2</sub>, etc.</i></b>	Session Chair: <b>C. Friend</b>
6:30-7:10 pm	Keynote speaker ( <b>T. Rauchfuss</b> )
7:10-7:35 pm	Invited speaker ( <b>T. Jaramillo</b> )
7:35-8:00 pm	Invited speaker ( <b>B. Bartlett</b> )
8:00-10:00 pm	<b>Poster Session II</b>

<b>Tuesday, July 21</b>	
7:00-8:30 am	<b>Breakfast</b>
<b>Plenary session</b>	Session chair: <b>S. Scott</b>
8:30-9:30 am	<b>Plenary lecture (R. Schlögl)</b> <i>Benchmarking and Standardization of Electro- and Chemo-Catalysts. Basic Considerations and Experimental Procedures</i>
9:30-10:00 am	<b>Coffee Break</b>
<b>Reports from Breakout Sessions</b>	<i>Benchmarking</i> Session Chair: <b>J. Chen</b>
10:00-10:15 am	Topic 1: <i>Computational approaches</i>
10:15-10:30 am	Topic 2: <i>Molecular and hybrid catalysts</i>
10:30-10:45 am	Topic 3: <i>Non-molecular catalysts</i>
10:45-11:00 am	Topic 4: <i>Photo- and electrocatalysts</i>
11:00-11:30 am	Discussion
11:30-1:30 pm	<b>Lunch</b>
<b>IV. Advances in Small Molecule Activation, 2: CO, CH<sub>4</sub>, H<sub>2</sub>, etc.</b>	Session Chair: <b>F. Zaera</b>
1:30-2:10 pm	Keynote speaker ( <b>J. Rodriguez</b> )
2:10-2:35 pm	Invited speaker ( <b>P. Balbuena</b> )
2:35-3:00 pm	Invited speaker ( <b>W. Mustain</b> )
3:00-3:15 pm	<b>Transition to Breakouts, Coffee Break</b>
<b>Breakout Session II</b>	<i>Benchmarking (cont.):</i>
3:15-4:45 pm	Topic 1: <i>Computational approaches</i> Discussion leaders: <b>J. Kitchin, T. Bligaard</b> Topic 2: <i>Molecular and hybrid catalysts</i> Discussion leaders: <b>C. Jones, W. Jones</b> Topic 3: <i>Non-molecular catalysts</i> Discussion leaders: <b>C. Campbell, B. Gates</b> Topic 4: <i>Photo- and electrocatalysts</i> Discussion leaders: <b>M. Bullock, R. Gorte</b>
5:00-6:30 pm	<b>Dinner</b>
<b>V. Advances in Molecular and Hybrid Catalysis</b>	Session Chair: <b>R. Finke</b>
6:30-7:10 pm	Keynote speaker ( <b>T. B. Gunnoe</b> )
7:10-7:35 pm	Invited speaker ( <b>A. Katz</b> )
7:35-8:00 pm	Invited speaker ( <b>A. Sen</b> )
8:00-10:00 pm	<b>Poster Session III</b>

<b>Wednesday, July 22</b>	
7:00-8:30 am	<b>Breakfast</b>
<i>VI. Advances in Multifunctional Molecule Disassembly</i>	Session Chair: <b>L. Grabow</b>
8:30-9:10 am	Keynote speaker ( <b>R. Davis</b> )
9:10-9:35 am	Invited speaker ( <b>M. Abu-Omar</b> )
9:35-10:00 am	Invited speaker ( <b>A. Bhan</b> )
10:00-10:15 am	<b>Coffee Break</b>
<i>Reports from Breakout Sessions</i>	Session Chair: <b>S. Scott</b>
10:15-10:30 am	Topic 1: <i>Computational approaches</i>
10:30-10:45 am	Topic 2: <i>Molecular and hybrid catalysts</i>
10:45-11:00 am	Topic 3: <i>Non-molecular catalysts</i>
11:00-11:15 am	Topic 4: <i>Photo- and electrocatalysts</i>
11:15-12:00 pm	Discussion and Conclusions
12:00-12:30 pm	<b>Departure</b>

## Table of Contents

<b>Foreword</b> .....	i
<b>Agenda</b> .....	iii
 <b>Sunday Evening: Plenary Session</b>	
R. Morris Bullock – <i>Design of Molecular Electrocatalysts for the Production and Oxidation of Hydrogen</i> .....	3
 <b>Monday Morning: Plenary Session</b>	
Jens K. Nørskov – <i>The Need for Benchmarking Catalysis, with Particular Emphasis on Computational Methods and Models</i> .....	7
 <b>Monday Morning: Advances in Theoretical and Computational Modeling</b>	
Dion G. Vlachos – <i>Comparing Simulation and Experiments: Successes and Gaps</i> .....	11
David Sholl – <i>Challenges and Opportunities in High-Throughput Computational Modeling of Nanoporous Materials</i> .....	12
Annabella Selloni – <i>Trapping and Dynamics of Excess Electrons and Holes at TiO<sub>2</sub> Anatase Surfaces and Interfaces</i> .....	13
 <b>Monday Afternoon: Advances in Heterogeneous Catalysis</b>	
Johannes Lercher – <i>Impact of the Steric and Chemical Environment of Active Sites on Catalytic Activity</i> .....	21
Richard M. Crooks – <i>Testing the Predictive Power of Theory for Determining the Structure and Activity of Nanoparticle Electrocatalysts: Design of Pt-shell Nanoparticles with Alloy Cores for the Oxygen Reduction Reaction</i> .....	22
Paul J. Dauenhauer – <i>Alkali-Catalyzed Cellulose Conversion to Furans: Techniques for Benchmarking High Temperature Condensed-Phase Kinetics</i> .....	28
 <b>Monday Evening: Advances in Small Molecule Activation, 1: H<sub>2</sub>O, CO<sub>2</sub>, N<sub>2</sub>, etc.</b>	
Thomas B. Rauchfuss – <i>Organometallic Catalysis Inspired by the Hydrogenase Enzymes</i> .....	31

Thomas F. Jaramillo – *Benchmarking Catalysts for the Hydrogen Evolution Reaction (HER) and the Oxygen Evolution Reaction (OER): The Importance of Turnover Frequency (TOF)* .....35

Bart M. Bartlett – *Using Semiconductor Photoelectrodes to Engender Catalytic Transformations in Small Molecules on Solid Surfaces* .....39

### **Tuesday Morning, Plenary Session**

R. Schlögl – *Benchmarking and Standardization of Electro- and Chemo-Catalysis. Basic Considerations and Experimental Procedures* ..... 45

### **Tuesday Afternoon, Advances in Small Molecule Activation, 2: CO, CH<sub>4</sub>, H<sub>2</sub>, etc.**

José A. Rodriguez – *Benchmark Studies for the Water-Gas Shift and CO<sub>2</sub> Hydrogenation* ..... 49

Perla B. Balbuena – *Nanocatalyst Structure and Composition during Reaction* .....57

William Mustain – *Near Room Temperature Electrochemical Upgrading of Methane to Oxygenate Fuels* .....63

### **Tuesday Evening: Advances in Molecular and Hybrid Catalysis**

T. Brent Gunnoe – *Transition Metal Catalyzed Hydroarylation of Olefins* .....67

Alexander Katz – *Organic-Ligand Control of Binding in Supported Molecular Cluster Catalysts* .....71

Ayusman Sen – *Self-Powered Catalytic Nanomotors and Pumps* .....75

### **Wednesday Morning, Advances in Multifunctional Molecule Disassembly**

Robert J. Davis – *Isotopic Transient Analysis of the Ethanol Coupling Reaction over Hydroxyapatite and Magnesia* .....81

Mahdi M. Abu-Omar – *Mechanistic Aspects of New C-H Activation Chemistries to Afford Bimetallic Complexes: Implication for Alkane Upgrading with Biorenewables* .....85

Aditya Bhan – *Catalytic Deoxygenation on Metal Carbides* .....89

## Poster Presentations

1. Radoslav Adzic (BNL) – *Structure and Function in Electrocatalysis of Reactions for Direct Energy Conversion* .....93
2. Aaron M. Appel (PNNL) – *Increasing Catalytic Performance for the Reduction of CO<sub>2</sub> by Controlling Free Energies for Proton and Hydride Transfers* ..... 101
3. Ludwig Bartels (Univ. of California–Riverside) – *Multiscale Imaging and DFT Analysis of Reactant Interactions on Single-Layer MoS<sub>2</sub> and Related Molybdenum-Sulfur Materials*..... 102
4. Alexis T. Bell (LBNL) – *Catalysts for the Selective Oxidation of Fuels and Chemicals* ..... 108
5. Thomas Bligaard (SLAC) – *Adsorbate Interactions in Catalytic Trend Studies* ..... 114
6. Jesse Q. Bond (Syracuse Univ.) – *Catalytic Processing of Levulinic Acid: Expanding Applications while Building Fundamental Insights*..... 116
7. Charles T. Campbell (Univ. of Washington) – *Supported Metal Nanoparticles: Correlating Structure with Catalytic Function through Energetics* ..... 117
8. Matteo Cargnello (Stanford Univ.) – *Benchmarking Active Phases, Supports and Reaction Conditions using Monodisperse Nanocrystals* ..... 122
9. Fuat E. Celik (Rutgers Univ.) – *Research in the Celik Catalysis Group* ..... 123
10. Eugene Y. Chen (Colorado State Univ.) – *DHMF: A C<sub>12</sub> Building Block for Renewable Chemicals, Liquid Fuels, and Polymeric Materials*..... 126
11. David F. Cox (Virginia Tech) – *Interaction of Na, Water and CO<sub>2</sub> with MnO(100): Modeling a Complex Mixed Oxide System for Thermochemical Water Splitting*..... 130
12. Abhaya K. Datye and Yong Wang (Univ. of New Mexico and Washington State Univ.) – *Sub Nanometer Sized Clusters for Heterogeneous Catalysis* ..... 133
13. David A. Dixon (Univ. of Alabama) – *Computational Studies of Catalytic Reactions of Alcohols on Oxide Nanoclusters*..... 139
14. Jonah D. Erlebacher (Johns Hopkins Univ.) – *Control of Reactivity in Nanoporous Metal/Ionic Liquid Composite Catalysts*..... 140
15. Joshua S. Figueroa (Univ. of California–San Diego) – *Mechanism of CO<sub>2</sub> Reductive Disproportionation by Base Metal Isocyanometalates* ..... 144

16. Richard G. Finke (Colorado State Univ.) – <i>Agglomerative Sintering of an Atomically Dispersed Ir<sub>1</sub>/Zeolite Y Catalyst: Compelling Evidence against Ostwald Ripening but for Bimolecular and Autocatalytic Agglomeration Catalyst Sintering Steps</i> .....	148
17. Alison R. Fout (Univ. of Illinois–Urbana-Champaign) – <i>The Reduction of Inorganic Anions: Ligand Redox Tautomerism Supports Base Metal Reactivity</i> .....	152
18. Bruce C. Gates (Univ. of California–Davis) – <i>Well-Defined Molecular Single-Site Catalysts on Crystalline Supports</i> .....	153
19. Andrew J. Gellman (Carnegie Mellon Univ.) – <i>Surface Structure Sensitive Enantioselectivity in Surface Explosion Reactions</i> .....	157
20. Michael Gordon (Univ. of California–Santa Barbara) – <i>Unconventional Oxidants and Reaction Schemes for Propane Dehydrogenation</i> .....	158
21. Raymond J. Gorte (Univ. of Pennsylvania) – <i>Oxide-Metal Interactions Studied on Core-Shell Catalysts</i> .....	162
22. Lars C. Grabow (Univ. of Houston) – <i>Hydrodeoxygenation of Furan on Oxygen Vacancy Sites of MoO<sub>3</sub>(010): A DFT investigation</i> .....	167
23. Michael A. Henderson (PNNL) – <i>Photodesorption of Molecular Hydrogen from the Surface of RuO<sub>2</sub>(110)</i> .....	170
24. Graeme Henkelman (Univ. of Texas–Austin) – <i>A Theoretical and Experimental Approach for Correlating Nanoparticle Structure and Electrocatalytic Activity</i> .....	171
25. Adam S. Hock (Illinois Institute of Technology, ANL) – <i>Mechanistic Insights from Rationally Designed Single Site Catalysts for Alkane Activation</i> .....	176
26. Rongchao Jin (Carnegie Mellon University) – <i>Atomically Precise Metal Nanoclusters for Catalytic Application</i> .....	184
27. William D. Jones (Univ. of Rochester) – <i>Selectivity of Intermolecular C-H Activation at [Tp’Rh(PMe<sub>3</sub>)]: How Does the Ancillary Ligand Affect the Metal-Carbon Bond Strength?</i> .....	187
28. Christopher W. Jones (Georgia Tech) – <i>Immobilized Molecular Catalysts in Cooperative Catalysis and Cascade Reactions</i> .....	189
29. John R. Kitchin (Carnegie Mellon Univ.) – <i>Electrolyte Dependent Oxygen Evolution Catalysis on Ni-based Electrocatalysts</i> .....	195
30. Ping Liu (BNL) – <i>Promoting the Activity and Selectivity of Catalysts towards CO<sub>2</sub> Activation: Mechanistic Understanding and Rational Catalyst Optimization</i> .....	198
31. Daniel A. Lutterman (ORNL) – <i>Neutron Spectroscopy in Catalysis</i> .....	210

32. Jean-Sabin McEwen (Washington State Univ.) – <i>Elucidating the Mechanism for the Catalytic Hydrodeoxygenation of Phenols</i> .....	211
33. C. Buddie Mullins (Univ. of Texas–Austin) – <i>Pd-Au Surface Chemistry - Effects of Water on Ethanol Oxidation over Au/TiO<sub>2</sub></i> .....	215
34. SonBinh T. Nguyen (Northwestern Univ.) – <i>Institute for Catalysis in Energy Processes</i> .....	219
35. Colin P. Nuckolls (Columbia Univ.) – <i>Catalytic Growth of Molecular Scale Wiring</i> .....	226
36. Ralph G. Nuzzo (Univ. of Illinois–Urbana-Champaign) – <i>In situ/Operando Investigations of Structural Dynamics of Supported Metal Catalysts</i> .....	228
37. Zhenmeng Peng (Univ. of Akron) – <i>Solid-State Chemistry Production and Property of Platinum Group Metal Nanoparticle Catalysts with Tailored Particle Morphology</i> .....	236
38. Marek Pruski (Ames Laboratory) – <i>Characterization of Catalytic Materials by DNP-Enhanced Solid-State NMR</i> .....	237
39. Talat S. Rahman (Univ. of Central Florida) – <i>Reactivity of Oxide and Sulfide Supported Metal Nanoparticles: Role of the Interface</i> .....	240
40. Ashwin Ramasubramaniam (Univ. of Massachusetts–Amherst) – <i>Influence of Support Effects on CO Oxidation by Graphene–Pt<sub>13</sub> Nanocomposites</i> .....	241
41. Andrew M. Rappe (Univ. of Pennsylvania) – <i>Synergistic Oxygen Evolving Activity of a TiO<sub>2</sub>-Rich Reconstructed SrTiO<sub>3</sub>(001) Surface</i> .....	244
42. Fabio H. Ribeiro (Purdue Univ.) – <i>Fundamental Studies of Oxidation Reactions on Model Catalysts: Catalytic Sites for Propylene Epoxidation by O<sub>2</sub> and H<sub>2</sub> over Au/Titanium Silicalite-1</i> .....	247
43. Fabio H. Ribeiro (Purdue Univ.) – <i>Heterogeneous and Homogeneous Catalyst Design by Discovery Informatics</i> .....	251
44. Aaron D. Sadow and Igor I. Slowing (Ames Laboratory) – <i>Hybrid Organic-Inorganic-Organometallic Catalysts for Reactions of Oxygenates: Characterization, Catalytic Activity and Reaction Mechanisms</i> .....	255
45. Aditya (Ashi) Savara (ORNL) – <i>Simulation of Temperature Programmed Reactions: TPR Mechanism Following Adsorption of Methanol on CeO<sub>2</sub>(111)</i> .....	266
46. William F. Schneider (Univ. of Notre Dame) – <i>New Approaches to Non-Ideal Surface Adsorption and Reaction</i> .....	268
47. Wendy J. Shaw (PNNL) – <i>Enhancing the Performance of Hydrogenase Mimics with an Enzyme-Inspired Outer Coordination Sphere</i> .....	273

48. Darío J. Stacchiola (BNL) – <i>The Catalytic Power of Interfaces in Catalysts Determined by In-Situ Studies</i> .....	278
49. Steven L. Suib (Univ. of Connecticut) – <i>Porous Transition Metal Oxides: Synthesis, Characterization, and Catalytic Activity</i> .....	279
50. Christine M. Thomas (Brandeis Univ.) – <i>C=O Bond Cleavage Reactions Facilitated by Early/Late Heterobimetallic Complexes</i> .....	285
51. Ian A. Tonks (Univ. of Minnesota) – <i>Catalytic Formal [2+2+1] Synthesis of Pyrroles from Alkynes and Diazenes via Ti<sup>II</sup>/Ti<sup>IV</sup> Redox Catalysis</i> .....	289
52. David A. Vicić (Lehigh Univ.) – <i>Accessing Nickel(II), (III), and (IV) Complexes Bearing a Readily Attached [C<sub>4</sub>F<sub>8</sub>] Ligand</i> .....	290
53. Jason F. Weaver (Univ. of Florida) – <i>Characterization of Propane <math>\sigma</math>-Complexes on PdO(101) using Vibrational Spectroscopy</i> .....	297
54. Michael G. White (BNL/Stony Brook Univ.) – <i>Influence of Cluster-Support Interactions on Reactivity of Size-Selected Metal Oxide Clusters</i> .....	303
55. Bingjun Xu (Univ. of Delaware) – <i>Surface Mediated Thermocatalytic and Electrocatalytic Processes—Reaction Mechanism and Catalyst Design</i> .....	309
56. Judith C. Yang (Univ. of Pittsburgh) – <i>Development and Applications of Quantitative and In Situ Environmental Electron Microscopy to Structural Characterization of Supported Nanoparticles</i> .....	310
57. Francisco Zaera (Univ. of California–Riverside) – <i>Yolk-Shell Catalysts for Regular and Photo Catalysis</i> .....	311
58. Steven H. Overbury (ORNL) – <i>Fundamentals of Catalysis and Chemical Transformations</i> .....	318
 <b>Additional Abstracts</b>	
59. Jingguang Chen (Columbia Univ.) – <i>Metal Carbide and Bimetallic Alloys as Low-Cost and Active Electrocatalysts</i> .....	331
60. Cynthia M. Friend (Harvard Univ.) – <i>Molecular-Scale Understanding of Selective Oxidative Transformations Promoted by Au</i> .....	336
61. Susannah L. Scott (Univ. of California–Santa Barbara) – <i>Dramatic Improvement in a Re-Based Olefin Metathesis Catalyst via Ligand-Exchange-Mediated Activation on Chlorinated Alumina</i> .....	338
 <b>Participant List</b> .....	345
6YbW@a Uf_]b[ `6fYU_ci h'GYgg]cbg'!! `7cbW g]cbg"..... (*	

**Sunday Evening**

**Plenary Session**

This page is intentionally blank.

## Design of Molecular Electrocatalysts for the Production and Oxidation of Hydrogen

Center for Molecular Electrocatalysis (efrc.pnnl.gov)  
Pacific Northwest National Laboratory, Richland, Washington USA 99352

Solar and wind are carbon-neutral, sustainable energy sources, but their intermittent nature requires reliable energy storage. Catalysts that efficiently interconvert between electrical energy and chemical bonds (fuels) are needed for sustainable, secure energy in the future. Electrocatalysts based on inexpensive, earth-abundant metals (“Cheap Metals for Noble Tasks”) are needed since low-temperature fuel cells generally use platinum, an expensive, precious metal.

We are developing nickel(II) complexes that catalyze the electrocatalytic production of H<sub>2</sub> by reduction of protons. Pendant amines in the ligands function as proton relays, facilitating *intramolecular* and *intermolecular* proton mobility. Most of our studies have been carried out in acetonitrile solution, but recent studies in a protic ionic liquid / aqueous medium show very fast reactions, with turnover frequencies as high as 10<sup>7</sup> s<sup>-1</sup>, with an overpotential of about 400 mV. Organometallic Fe(II) complexes derived from CpFe(diphosphine)H, with pendant amines in the diphosphine ligands, mimic the reactivity of [FeFe]-hydrogenase enzymes, leading to new iron catalysts for oxidation of H<sub>2</sub>. Evaluation of the turnover frequencies is carried out by measuring the current in cyclic voltammograms, providing a benchmark for comparison to synthetic and natural (hydrogenase) catalysts.

This research was supported as part of the Center for Molecular Electrocatalysis, an Energy Frontier Research Center funded by the U.S. Department of Energy, Office of Science, Office of Basic Energy Sciences.

This page is intentionally blank.

**Monday Morning**

**Plenary Session**

This page is intentionally blank.

## **The need for benchmarking catalysis, with particular emphasis on computational methods and models.**

Jens K. Nørskov

SUNCAT Center for Interface Science and Catalysis  
Stanford University and SLAC

Catalysis in the science of controlling reaction rates: absolute rates as well as relative rates for different reaction pathways. A good catalyst provides a high rate and/or a high selectivity for a special product. Since catalyst performance is the essence of catalysis, it is essential that any new development is held up against previous state-of-the-art. That is benchmarking of catalysts. There is additional benchmarking that is important. It is important that experimental and theoretical methods are benchmarked against other measurements or calculations to make sure that they perform as we think they do. This is particularly true of theoretical methods, which must always be benchmarked against well-defined experiments to assess their reliability.

In the talk I will discuss the general need for benchmarking of catalysts in the field of catalysis. I will then turn to the question of benchmarking theoretical methods. Electronic structure theory of catalytic processes is dominated by density functional theory (DFT) calculations, and I will discuss benchmarking of different methods against experiment. I will also discuss how benchmarking can be used to develop a systematic theory of error estimation in DFT calculations. Finally, I will discuss benchmarking of theories of catalysis, that is, how well current models are able to make predictions of catalytic trends, and, ultimately, of new catalysts.

This page is intentionally blank.

# **Monday Morning**

## **I. Advances in Theoretical and Computational Modeling**

This page is intentionally blank.

**Dion G. Vlachos**

**Comparing simulation and experiments: Successes and gaps**

Dion Vlachos

Department of Chemical and Biomolecular Engineering, Center for Catalytic Science and Technology, and Catalysis Center for Energy Innovation, University of Delaware, Newark, DE 19716-3110

**Presentation Abstract**

The advances in multiscale computations and experiments enable us to compare model predictions to experimental data, obtain insights into the mechanisms, predict in silico new materials, and interrogate model predictions experimentally. In this talk, grand challenges in closing the gap between experiments and simulations will be presented. We will demonstrate how descriptor-based modeling can enable search of novel materials and assess this framework with experiments. Outstanding questions include how reliable and robust are model predictions and our quest for searching new materials and how critical are the aforementioned gaps. We will present a new computational formalism that addresses this problem. We will demonstrate this methodology with examples of ammonia decomposition and ethanol steam reforming on single metals and bimetallic catalysts.

**Grant Information**

- Biomass work is supported by the Catalysis Center for Energy Innovation (CCEI), an Energy Frontier Research Center funded by the U.S. Department of Energy, Office of Science, Office of Basic Energy Sciences under award number DE-SC0001004.
- The mathematical work is being funded by the U.S. Department of Energy, Office of Basic Energy Sciences, under Contract No. DE-AC02-98CH10886 and DE-SC0010723.
- Computational work was carried out at the TeraGrid provided by Texas Advanced Computing Center (TACC) of the University of Texas at Austin, at the Center for Functional Nanomaterials at Brookhaven National Laboratory, and at National Energy Research Scientific Computing Center (NERSC).

**Challenges and Opportunities in High-Throughput Computational Modeling of Nanoporous Materials**

School of Chemical & Biomolecular Engineering, Georgia Institute of Technology

Nanoporous materials are relevant to heterogeneous catalysis both as supports for catalytic sites and more broadly as examples of chemically and structurally diverse materials where computational modeling can help drive materials innovation. In this talk, I will give several examples of successes and challenges of using high-throughput computational methods to describe molecular adsorption and diffusion in crystalline nanoporous materials such as zeolites and metal-organic frameworks and draw analogies between progress in this area and related problems in heterogeneous catalysis.

## Trapping and dynamics of excess electrons and holes at TiO<sub>2</sub> anatase surfaces and interfaces

Sencer Selcuk, Ye-Fei Li, Annabella Selloni  
Department of Chemistry, Princeton University, Princeton, N.J. 08544

### Presentation Abstract

The common picture of excess and photoexcited carriers in TiO<sub>2</sub> is based on the polaron model, where electrons are localized at Ti sites to form Ti<sup>3+</sup> species while holes are trapped by oxygen anions to form O<sup>-</sup> species. The location and energies of the trapped species at or near the surface play a key role in the (photo-)reactivity and have been probed by a variety of experimental techniques, but there is no consensus on whether the carriers are located at subsurface or surface sites and in the latter case which type of site is preferred. There are also indications that the trapping process is affected by the surrounding environment, i.e. the trapping sites on a dry surface may be different from those on a surface in an aqueous environment, but understanding of these effects is still limited also because solid/liquid interfaces are more difficult to probe experimentally than surfaces in vacuum. Our goal is to address these issues and obtain a complete picture of excess carriers at TiO<sub>2</sub> surfaces, interfaces and nanoparticles using a theoretical/computational approach based on First Principles Molecular Dynamics (FPMD) simulations combined with accurate hybrid functional and DFT+U calculations of the electronic structure. Here we shall present results of our ongoing studies, focusing on the localization and dynamics of excess electrons and holes on bare TiO<sub>2</sub> anatase surfaces and anatase-water interfaces. We shall discuss the effects of different surface terminations, showing, e.g., that electrons localize easily on (101) surfaces but tend to avoid (001) facets by forming delocalized two-dimensional states below the surface. We shall also examine the influence of surfaces steps, surface hydroxyls and subsurface impurities as well as the interaction between localized carriers and water at the interface.

### DE-FG02-12ER16286: Understanding Surfaces and Interfaces of Photocatalytic Oxide Materials with First Principles Theory and Simulations

**Postdocs:** Ye-Fei Li<sup>(a)</sup>

**Students:** Sencer Selcuk, Xiao Shi

**Affiliations:** <sup>(a)</sup> Present address: Department of Chemistry, Fudan University, Shanghai, China

### RECENT PROGRESS

*Ab initio simulations of the structure of thin water layers on defective anatase TiO<sub>2</sub>(101) surfaces.* We have studied the effects of reducing and oxidizing defects on the structure of thin water layers on TiO<sub>2</sub> anatase (101) by ab initio molecular dynamics. On the stoichiometric defect-free surface, water-surface interactions dominate over intermolecular water-water interactions. This leads to substantial vertical and in-plane ordering of the first two layers in direct contact with the surface. This

ordering is strongly perturbed in the presence of both oxidizing (surface bridging oxygen dimers,  $(O_2)_O$ 's) and reducing (subsurface oxygen vacancies and Ti interstitials) defects. On the oxidized surface, H-bonds formed with an  $(O_2)_O$  dimer rather than regular  $O_{2c}$  surface sites lead to a locally altered H-bonding pattern around the dimer. This perturbation of the regular H-bond structure results in desorption of water molecules from  $Ti_{5c}$  sites and their migration to subsequent water layers. On the reduced surface we also observe desorption of a water molecule and its migration to higher lying layers. In contrast to the oxidized surface, the process on the reduced surface is however triggered by water dissociation and a stronger H-bond formation between water and the resulting OH groups. This leads to a more marked and long-range disturbance of the water structure above the reduced surface. These results also suggest a difference in the dynamical properties of the interfacial water on the oxidized and reduced surfaces, with higher water diffusivity on the latter.

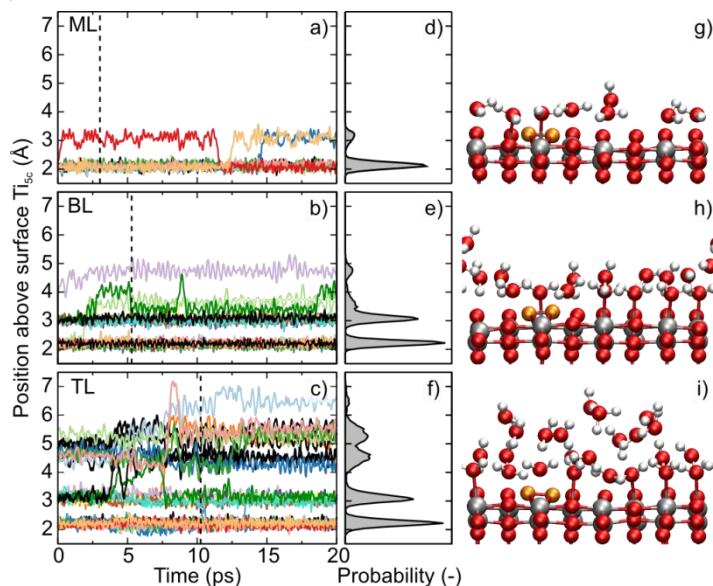


**Figure 1:** Time evolution of the water-surface vertical distances and corresponding probability distributions for a water monolayer (a, d), bilayer (b, e), and trilayer (c, f) on the oxidized anatase (101) surface, characterized by the presence of a bridging oxygen dimer,  $(O_2)_O$ , defect. Snapshots for the monolayer (g), bilayer (h), and trilayer (i), viewed along the  $[-101]$  direction, with the dimer highlighted in orange; the instant of the snapshot is indicated by the dashed vertical line in a)-c) respectively.

**Localized excitation of  $Ti^{3+}$  ions in the photoabsorption and photocatalytic activity of reduced rutile  $TiO_2$**  In reduced  $TiO_2$ , electronic transitions originating from the  $Ti^{3+}$ - induced states in the band gap are known to contribute to the photoabsorption, being in fact responsible for the material's blue color, but the excited states accessed by these transitions have not been characterized in detail. In this work we investigate the excited state electronic structure of the prototypical rutile  $TiO_2(110)$  surface using two-photon photoemission spectroscopy (2PPE) and density functional theory (DFT) calculations. Using 2PPE, an excited resonant state derived from  $Ti^{3+}$  species is identified at  $2.5 \pm 0.2$  eV above the Fermi level ( $E_F$ ) on both the reduced and hydroxylated surfaces. DFT calculations reveal that this excited state is closely related to the gap state at  $\sim 1.0$  eV below  $E_F$ , as they both result from the Jahn-Teller induced splitting of the  $3d-t_{2g}$  orbitals of  $Ti^{3+}$  ions in reduced  $TiO_2$ . Localized excitation of  $Ti^{3+}$  ions via  $3d \rightarrow 3d$  transitions from the gap state to this empty resonant state increases significantly the  $TiO_2$  photoabsorption and extends the absorbance to the visible region. This can explain the observed enhancement of the visible light induced photocatalytic activity of  $TiO_2$  through  $Ti^{3+}$  self-doping.

**Structural and Electronic Properties of Photoexcited  $\text{TiO}_2$  Nanoparticles.** In this study we have tried to quantify the effects of different DFT functionals on the structure and energetics of excitons and individual electron and hole polarons in a  $(\text{TiO}_2)_{38}$  cluster representative of a small anatase  $\text{TiO}_2$  nanoparticle (NP). An inherent difficulty of this study is that small  $\text{TiO}_2$  NPs are highly distorted, leading to the occurrence of many possible localization sites for the photoexcited carriers, so that several different solutions must be examined. We have used pure GGA (BLYP) and hybrid functionals with different HF-exc percentages (B3LYP-15, B3LYP, and the long-range corrected CAM-B3LYP functional) and also compared the performances of TD-DFT and SCF-DFT approaches for the description of the photoexcited polaron states. Computed properties are found to depend significantly on the fraction of HF-exc, as well as on the introduction of long-range corrections. For instance, the two employed B3LYP and B3LYP-15 hybrid functionals yield self-trapping energies that differ by  $\sim 0.26$  eV for trapped electrons. The solvent (here introduced using a continuum model) also plays a relevant role, self-trapping energies being higher in vacuo than in DMF and water solvent by  $\sim 0.1$  eV for the exciton and excess electron states, and by  $\sim 0.3$  eV for an excess hole. Finally, the results of this study also show that the nanoscale size of the  $\text{TiO}_2$  NPs gives rise to important differences in the structure and energetics of trapped charge carriers with respect to anatase bulk and extended surfaces.

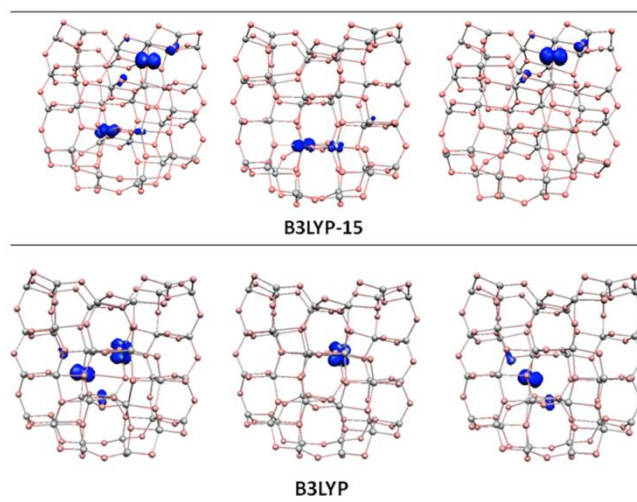


**Figure 2.** Electron spin densities for the triplet exciton state (left), single extra electron (middle) and single extra hole (right) in a  $(\text{TiO}_2)_{38}$  cluster in DMF solvent. Results at the B3LYP-15 and B3LYP levels are shown in the top and bottom row respectively.

### **Results on the surface structure of Co, Fe, and Ni oxides**

#### ***(i) DFT+U Study of the Surface Structure and Stability of $\text{Co}_3\text{O}_4(110)$ : Dependence on U***

The DFT+U method is widely used to theoretically describe transition metal oxides, where the correlated nature of d electrons is not well captured by standard DFT. Although first principles methods are available to determine the U parameter, it is generally accepted that no single value of U can accurately predict different physical quantities. As a result, studies using very different U values are often found for the same material. This is the case for  $\text{Co}_3\text{O}_4$ , an important oxidation catalyst. We have thus decided to examine the effects of U on the stability diagram of the (110) surface of  $\text{Co}_3\text{O}_4$ , by considering three representative U values often used in previous studies, notably U = 0, 3.0, and 5.9 eV. For all U values, the hydrated B surface, exposing only octahedral Co ions, is predicted to be the thermodynamically stable

termination under ambient conditions and at low temperatures. In other situations, the predicted stability generally depends on U, smaller (larger) U values favoring the B (A) termination. By combining our results with those of previous studies, we conclude that U = 3.0 eV provides a better overall description of the electronic structure and surface reactivity, whereas U = 5.9 eV is better suited for the description of the magnetic properties.

(ii) Structure of the NiFe<sub>2</sub>O<sub>4</sub>(001) surface in contact with gaseous O<sub>2</sub> and water vapour

Using DFT+U calculations, we have studied the structural and electronic properties of the (001) surface of NiFe<sub>2</sub>O<sub>4</sub>, a promising catalyst for the oxygen evolution reaction. Our results show that, unlike in the bulk, oxygen vacancies form quite easily on the nickel ferrite surface, especially at oxygen sites that are coordinated mainly to Ni ions. Our results also indicate that dissociative adsorption of water at vacancy sites is much more favorable than adsorption at regular surface sites thus suggesting that a humid environment may help the creation of oxygen vacancies. From our computed surface phase diagram we infer that the NiFe<sub>2</sub>O<sub>4</sub>(001) is hydroxylated at ambient conditions, while water desorption should lead to a defective surface containing a significant fraction of oxygen vacancies at higher temperature. Due to its tendency to easily form surface oxygen vacancies, NiFe<sub>2</sub>O<sub>4</sub> is predicted to be a promising catalyst for oxidation reactions occurring through the Mars-Van Krevelen mechanism.

(iii) Structure of  $\beta$ -NiOOH from DFT and Genetic Algorithm Calculations.  $\beta$ -NiOOH is a widely used electrode material for rechargeable alkaline batteries as well as a promising catalyst for water oxidation. Two observed but not well understood structural features of  $\beta$ -NiOOH are the doubling of the *c*-axis periodicity and the presence of a mosaic texture produced by an irreversible microstructural transformation during the first oxidation of  $\beta$ -Ni(OH)<sub>2</sub>. We have used a genetic algorithm approach for predicting crystal structures in combination with DFT calculations to identify a number of stable low-energy structures which could explain the experimental observations for  $\beta$ -NiOOH. In two of these candidate structures, the NiO<sub>6</sub> units form a layered framework, whereas in the others they form tunnel structures isostructural with polymorphs of MnO<sub>2</sub>. The picture of the  $\beta$ -NiOOH structure that is suggested by our results can be summarized as follows. Starting from  $\beta$ -Ni(OH)<sub>2</sub>, which has a well-defined layered ABAB structure, removal of half of the protons from the voids between NiO<sub>6</sub> octahedral layers in the first oxidation transforms the initial ABAB stacking to ABBCCA, with a doubling of the *c* axis periodicity. During this process, low energy tunnel structures can easily form to relieve the strain in the ABBCCA structure, thus giving rise to the mosaic texture observed in TEM experiments. During discharge, only the layered structure of  $\beta$ -NiOOH transforms back to  $\beta$ -Ni(OH)<sub>2</sub>, whereas the tunnel structures are not healed. This explains why the mosaic texture is maintained throughout subsequent charge/discharge cycles as well.

### **Publications Acknowledging this Grant in 2012-2015**

1. U. Aschauer, A. Tilocca, A. Selloni, Ab initio simulations of the structure of thin water layers on defective anatase TiO<sub>2</sub>(101) surfaces, *Int. J. Quantum Chemistry* **2015**, *115*, DOI: 10.1002/qua.24918
2. Martin Setvin, Maria Buchholz, Weiyi Hou, Cui Zhang, Bernhard Stöger, Mingchun Xu, Yuemin Wang, Michael Schmid, Christof Wöll, Annabella Selloni, Ulrike Diebold, CO adsorption on the TiO<sub>2</sub> anatase (101) surface (under review).
3. Zhiqiang Wang, Bo Wen, Qunqing Hao, Li-Min Liu, Chuanyao Zhou, Xinchun Mao, Xiufeng Lang, Wen-Jin Yin, Dongxu Dai, Annabella Selloni, Xueming Yang, Localized excitation of Ti<sup>3+</sup> ions in the photoabsorption and photocatalytic activity of reduced rutile TiO<sub>2</sub> (under review).

4. U. Aschauer, A. Selloni, Adsorption of Biomedical Coating Molecules, Amino Acids and Short Peptides on Magnetite (110) (under review).
5. F. Nunzi, S. Agrawal, A. Selloni, F. De Angelis, Structural and Electronic Properties of Photoexcited TiO<sub>2</sub> Nanoparticles from First Principles, *J. Chem. Theory Comput.* **2015**, *11*, 635-645.
6. S. Selçuk, A. Selloni, DFT+U Study of the Surface Structure and Stability of Co<sub>3</sub>O<sub>4</sub>(110): Dependence on U, *J. Phys. Chem. C*, **2015**, *119*, 9973-9979.
7. Xiao Shi, Ye-Fei Li, S. L. Bernasek, A. Selloni, Structure of the NiFe<sub>2</sub>O<sub>4</sub>(001) surface in contact with gaseous O<sub>2</sub> and water vapor, *Surf. Sci.* **2015**, in press.
8. Ye-Fei Li and Annabella Selloni, Mosaic Texture and Double c-axis Periodicity of β-NiOOH: Insights from First Principles and Genetic Algorithm Calculations, *J. Phys. Chem. Lett.* **2014**, *5*, 3981-3985.
9. Martin Setvin, Benjamin Daniel, Ulrich Aschauer, Weiyi Hou, Ye-Fei Li, Michael Schmid, Annabella Selloni, Ulrike Diebold, "Identification of Adsorbed Molecules Via STM Tip Manipulation: CO, H<sub>2</sub>O, and O<sub>2</sub> on TiO<sub>2</sub> Anatase (101)", *Phys. Chem. Chem. Phys.* **2014**, *16*, 21524.
10. S. Selçuk, A. Selloni, "Influence of External Electric Fields on Oxygen Vacancies at the Anatase (101) Surface", *J. Chem. Phys.* **2014**, *141*, 084705.
11. F. De Angelis, C. Di Valentin, S. Fantacci, A. Vittadini, A. Selloni, Theoretical Studies on Anatase and Less Common TiO<sub>2</sub> Phases: Bulk, Surfaces and Nanomaterials, *Chem. Rev.* **2014**, 9708-9753.
12. Jun Hee Lee and A. Selloni, TiO<sub>2</sub>/Ferroelectric Heterostructures as Dynamic Polarization-Promoted Catalysts for Photochemical and Electrochemical Oxidation of Water, *Phys. Rev. Letters* **2014**, *112*, 196102.
13. Ye-Fei Li, Ulrich Aschauer, Jia Chen, and Annabella Selloni, Adsorption and Reactions O<sub>2</sub> with Anatase TiO<sub>2</sub>, *Acc. Chem. Res.* **2014**, *47*, 3361-3368.
14. Y. F. Li and A. Selloni, Mechanism and Activity of Water Oxidation on Selected Surfaces of Pure and Fe-doped NiO<sub>x</sub>, *ACS Catal.* **2014**, *4*, 1148-1153.
15. J. Chen, Y.-F. Li, P. Sit, A. Selloni, Chemical Dynamics of the First Proton-Coupled Electron Transfer of Water Oxidation on TiO<sub>2</sub> Anatase, *J. Am. Chem. Soc.*, **2013**, *135*, 18774 (Communication).
16. M. Setvín, U. Aschauer, P. Scheiber, Y.-F. Li, W. Hou, M. Schmid, A. Selloni, and U. Diebold, Reaction of O<sub>2</sub> with Subsurface Oxygen Vacancies on TiO<sub>2</sub> Anatase (101), *Science* **2013**, *341*, 988.
17. J. Chen, A. Selloni, First Principles Study of Cobalt (Hydr)Oxides under Electrochemical Conditions, *J. Phys. Chem. C* **2013**, *117*, 20002-20006.
18. T. Xia, Neng Li, Y. Zhang, M. B. Kruger, J. Murowchick, A. Selloni, and Xiaobo Chen, Directional Heat Dissipation across the Interface in Anatase–Rutile Nanocomposites, *ACS Appl. Mater. Interfaces*, **2013**, *5* (20), 9883–9890
19. Y.-F. Li, A. Selloni, Theoretical Study of Interfacial Electron Transfer from Reduced Anatase TiO<sub>2</sub>(101) to Adsorbed O<sub>2</sub>, *J. Am. Chem. Soc.*, **2013**, *135*, 9195.
20. R. Ciancio, A. Vittadini, A. Selloni, R. Arpaia, C. Aruta, F. M. Granozio, U. Scotti di Uccio, G. Rossi, E. Carlino, Evolution of nanostructures of anatase TiO<sub>2</sub> thin films grown on (001) LaAlO<sub>3</sub>, *J. Nanopart. Res.*, **2013**, *15*, 1735.
21. S. Selçuk, A. Selloni, Surface Structure and Reactivity of Anatase TiO<sub>2</sub> Crystals with Dominant {001} Facets, *J. Phys. Chem.*, **2013**, *117*, 6358-6362.
22. F. Nunzi, E. Mosconi, L. Storchi, E. Ronca, A. Selloni, M. Graetzel, F. De Angelis, Inherent electronic trap states in TiO<sub>2</sub> nanocrystals effect of saturation and sintering, *Energy & Environmental Science*, **2013**, *6*, 1221-1229.
23. P. Scheiber, M. Fidler, O. Dulub, M. Schmid, U. Diebold, W. Hou, U. Aschauer, A. Selloni, (Sub)surface mobility of oxygen vacancies at the TiO<sub>2</sub> anatase (101) surface, *Phys. Rev. Lett.* **2012**, *109*, 136193.

24. R. Ciancio, E. Carlino, G. Rossi, C. Aruta, U. Scotti di Uccio, A. Vittadini, A. Selloni, Magnéli-like phases in epitaxial anatase TiO<sub>2</sub> thin films, *Phys. Rev. B* **2012**, *86*, 104110.
25. J. Chen, A. Selloni, Water adsorption and oxidation at the Co<sub>3</sub>O<sub>4</sub>(110) surface, *J. Phys. Chem. Lett.* **2012**, *3*, 2808-2814.
26. U. Aschauer, A. Selloni, Hydrogen interaction with the anatase TiO<sub>2</sub>(101) surface, *Phys. Chem. Chem. Phys.* **2012**, *14*, 16595-16602.
27. J. Chen, A. Selloni, Electronic states and magnetic structure at the Co<sub>3</sub>O<sub>4</sub>(110) surface: A first-principles study, *Phys. Rev. B* **2012**, *85*, 085306.
28. A. Tilocca, A. Selloni, DFT-GGA and DFT+U simulations of thin water layers on reduced TiO<sub>2</sub> anatase, , *J. Phys. Chem. C* **2012**, *116*, 9114-9121.
29. E. Mosconi, A. Selloni, F. De Angelis, Solvent Effects on the Adsorption Geometry and Electronic Structure of Dye-sensitized TiO<sub>2</sub>: a First Principles Investigation, *J. Phys. Chem. C* **2012**, *116*, 5932-5940.

**Monday Afternoon**

**II. Advances in  
Heterogeneous  
Catalysis**

This page is intentionally blank.

**Impact of the steric and chemical environment of active sites on catalytic activity**

Institute for Integrated Catalysis, Pacific Northwest National Laboratory, Richland, WA

The unsurpassed reactivity of enzymes is usually explained by the specific interaction of reacting molecules at the catalytic center, which is surrounded by a very specific environment. A large role is ascribed to the specificity in which the molecule interacts with the active site directed by the surrounding. The lecture will describe approaches to match such specificity with inorganic oxides and nanoparticles of metals by tailoring the environment around the active site. Molecular sieves, which are usually used to exclude reaction pathways, will be shown to be able to enhance selectively reaction rates by subtly adjusting the space around the Brønsted acid site or metal cation via the addition of cations, oxidic clusters, or organic fragments. The impact of such changes on mono- and bimolecular reactions such as eliminations from alcohols, cracking, and alkylation of hydrocarbons are discussed for gas and liquid phase reactions. Experimental methods to define the state of the reacting molecules combined with detailed kinetic analyses and theory will be used to explain the principal contributions of the interactions and the confinement to determine reaction rates. It will be discussed, how reaction rates and pathways can be tailored using the space available for a transition state and the chemical constituents around the active site.

**Testing the Predictive Power of Theory for Determining the Structure and Activity of Nanoparticle Electrocatalysts: Design of Pt-shell Nanoparticles with Alloy Cores for the Oxygen Reduction Reaction**

Richard M. Crooks, Graeme Henkelman, Liang Zhang, Ravikumar Iyyamperumal,  
and David F. Yancey  
The University of Texas at Austin, Department of Chemistry

**Presentation Abstract**

We report that the oxygen binding energy of alloy-core@Pt nanoparticles can be linearly tuned by varying the alloy core composition. Using this tuning mechanism, we are able to predict optimal compositions of alloy-core@Pt nanoparticles for the oxygen reduction reaction (ORR). Subsequent electrochemical measurement of ORR activities of AuPd@Pt dendrimer-encapsulated nanoparticles (DENs) are in a good agreement with the theoretical prediction that the peak of activity is achieved for a 28% Au / 72% Pd alloy core supporting a single-atom-thick Pt shell. Importantly, these findings represent an unusual case of first-principles theory leading to nearly perfect agreement with experimental results.

**DE-FG02-13ER16428: Testing the Predictive Power of Theory for Determining the Structure and Activity of Nanoparticle Electrocatalysts**

**PI:** Richard M. Crooks

**Co-PI:** Graeme Henkelman

**Postdocs:** Liang Zhang and Ravikumar Iyyamperumal

**Graduate Student:** David F. Yancey

**RECENT PROGRESS**

***Introduction***

The overall goal of this research project is development of high-throughput computational-based screening methods for discovery of catalyst candidates and subsequent experimental validation using appropriate catalytic nanoparticles. This concept is illustrated in Figure 1.

Effective comparison of theory and experiment requires that the theoretical and experimental models map onto one-another perfectly. Accordingly, we use novel synthetic methods, advanced characterization techniques, and density functional theory (DFT) calculations to approach this ideal. For example, well-defined core@shell DENs can be synthesized by electrochemical underpotential deposition (UPD), and the observed deposition potentials can be compared to those calculated by DFT. Theory is also used to learn more about structure than can be determined by analytical characterization alone. For example, density functional theory molecular dynamics (DFT-MD) has been used to show that the core@shell configuration of Au@Pt DENs undergoes a surface reconstruction that dramatically affects its electrocatalytic properties. A separate Pd@Pt DENs study has revealed reorganization, in this case a core-shell

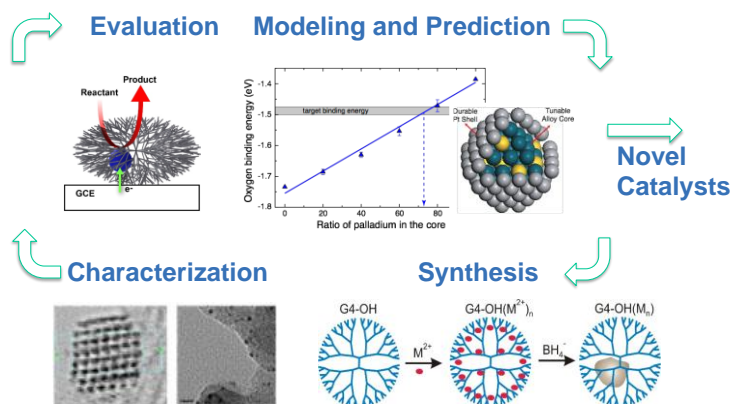
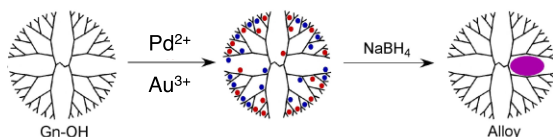


**Figure 1.** Illustration of the iterative process we use to couple theory and experiment for discovery of improved catalysts.

1. Co-complexation of the core metals followed by  $\text{BH}_4^-$ .



2. Electrode immobilization, Cu UPD, Pt galvanic exchange

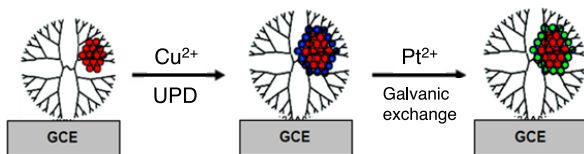


**Figure 2.** Illustration showing the synthetic method used to prepare the experimental model (dendrimer-encapsulated nanoparticles) used in this study. In Step 1, two different metal ions are co-complexed within a sixth-generation PAMAM dendrimer and then chemically reduced to yield a bimetallic core. In Step 2, the bimetallic core is immobilized on an electrode surface, a sacrificial monolayer of Cu is electrodeposited onto the core surface by underpotential deposition, and then the Cu monolayer is replaced with Pt by galvanic exchange.

alloy-core@Pt-shell nanoparticles using DFT calculations with oxygen binding as the reactivity descriptor. The combination of Au and Pd in the nanoparticle core was found to be particularly interesting, because variations of the core composition between pure Au and pure Pd are calculated to shift the oxygen binding on the Pt shell to values both weaker and stronger than bulk Pt. Our predicted trends in ORR activity, as well as the optimal core composition, provide a testable model for experiments.

We selected PdAu@Pt DENs as our model system for comparison with the calculations. Pd<sub>n</sub>Au<sub>140-n</sub>@Pt DENs were synthesized electrochemically by Cu UPD onto Pd<sub>n</sub>Au<sub>140-n</sub> alloy cores, followed by galvanic exchange of the Cu layer for Pt (Figure 2). Note that the subscripts used here reflect the nominal elemental compositions of the DENs based on the percentages of

inversion to a Pt@Pd structure. Understanding these types of structural changes is critical to building correlations between structure and catalytic function.

The specific aim of this presentation is to use novel nanostructures and appropriate theory to better understand the oxygen reduction reaction (ORR). Specifically, catalytic materials containing an atomically thin Pt surface layer are a promising alternative to pure Pt nanoparticle catalysts for the oxygen reduction reaction (ORR). Pt-shelled catalysts can be quite stable, have significantly less Pt loading than commercial alternatives, and can lead to higher activities.<sup>1-3</sup> Recent progress has also been made using near-surface alloys to tune the activity of the catalytic surface. One such promising geometry is a monolayer shell covering a random alloy core of variable composition (Figure 2). These alloy-core@shell nanoparticles have both the robustness of core@shell structures and the tunability of random alloy particles.<sup>4</sup> Indeed, Adzic and coworkers recently reported that adding Au to a Pd nanoparticle core covered by a Pt monolayer shell enhances stability under ORR conditions.<sup>5,6</sup>

### Experimental Design

In this presentation, we predicted the ORR activity trends of ~2 nm

Pd and Au used to prepare them. We have previously shown that these values are good (but not perfect) estimates of the experimentally determined stoichiometry of the nanoparticles.

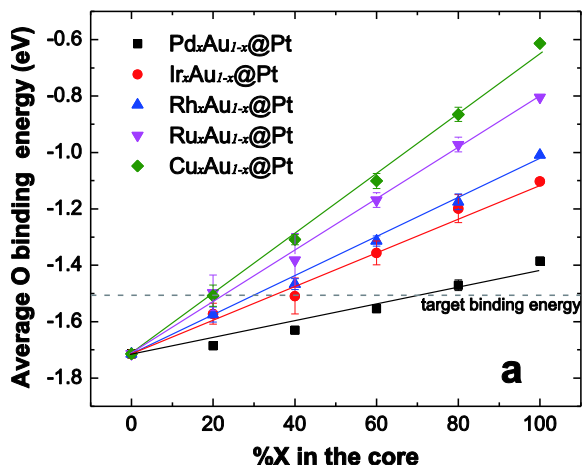


**Figure 3.** Oxygen binding energy trends for  $X_x\text{Au}_{1-x}\text{@Pt}$  nanoparticles ( $X = \text{Pd}, \text{Ir}, \text{Rh}, \text{Ru},$  and  $\text{Cu}$ ). The grey dashed line represents the target oxygen binding energy.

### Theoretical Findings

Figure 3 shows the average calculated O binding energies of  $X_x\text{Au}_{1-x}\text{@Pt}$  nanoparticles as a function of core composition. The near-linear O binding trends are consistent with our earlier reports for alloy-core@Pd-shell nanoparticles.<sup>4</sup> Optimal alloy-core compositions are predicted at the intersections of linear O binding trends and the target O binding energy (solid and dashed lines in Figure 3, respectively).

### Experimental Findings

Figure 4a shows a series of rotating disk voltammograms (RDVs) for glassy carbon electrodes modified with  $\text{Au}_n\text{Pd}_{140-n}\text{@Pt}$  and  $\text{Pt}_{140}$  DENs, and Figure 4b shows an expanded portion of these RDVs in the vicinity of the onset of current. The RDVs were obtained in  $\text{O}_2$ -saturated, aqueous 0.10 M  $\text{HClO}_4$  using a rotation rate of 1600 RPM at a scan rate of 5 mV/s. The onset potential for the ORR, which is defined as the potential of the inflection point on the quasi-steady-state polarization curve, at the  $\text{Pd}_{70}\text{Au}_{70}$  DEN-modified electrode is -0.30 V. However, upon addition of the Pt shell, this value shifts positive to 0.10 V. For comparison, the ORR onset potential for the  $\text{Pt}_{140}$  DENs is at 0.15 V, which is more positive than that of the  $\text{Pd}_{70}\text{Au}_{70}\text{@Pt}$  electrocatalyst. However, the ORR onset potentials for  $\text{Pd}_{90}\text{Au}_{50}\text{@Pt}$  and  $\text{Pd}_{120}\text{Au}_{20}\text{@Pt}$  DENs are shifted even more positive, to 0.17 V. The onset potential for the  $\text{Pd}_{105}\text{Au}_{35}\text{@Pt}$  DENs shifts much more positive, to 0.23 V, than any of the other DENs and hence it has the lowest overpotential and highest activity. Figure 4c summarizes the

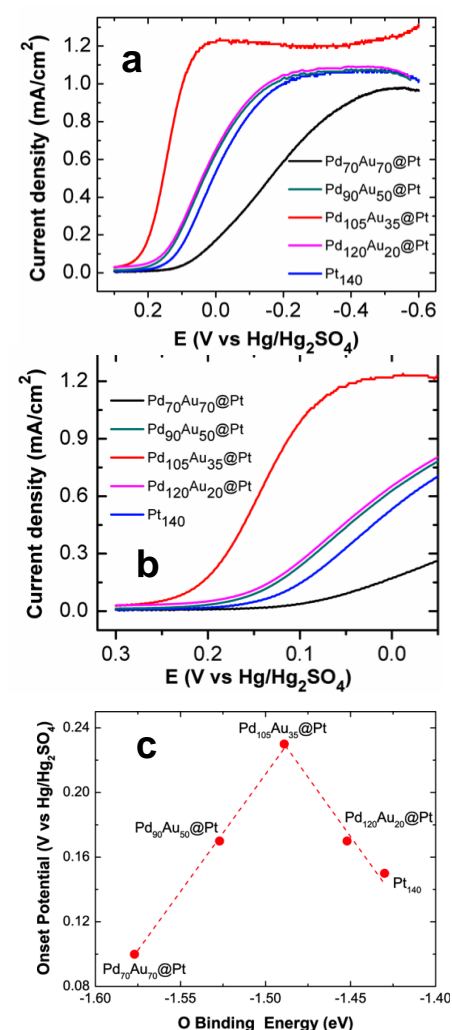


**Figure 4.** (a) Rotating disk voltammograms for glassy carbon electrodes modified with  $\text{Pd}_n\text{Au}_{140-n}\text{@Pt}$  ( $n = 70, 90, 105, 120$ ) and  $\text{Pt}_{140}$  DENs. The electrode rotation rate was 1600 PRMs, the scan rate was 5 mV/s, the electrolyte solution was  $\text{O}_2$ -saturated, aqueous 0.10 M  $\text{HClO}_4$ , and the electrode was scanned from -0.6 to 0.3 V (vs  $\text{Hg}/\text{Hg}_2\text{SO}_4$ ). (b) An enlargement of part (a) in the region of the onset potential for the ORR. Note that the current axes in (a) and (b) are normalized to the electrochemical surface area of Pt determined by measuring hydrogen UPD. (c) Onset potential for the ORR at  $\text{Pd}_x\text{Au}_{1-x}\text{@Pt}$  DENs measured by RDVs and plotted as a function of the corresponding oxygen binding energy calculated by DFT. The dashed line corresponds to the linear fit of the two branches of the activity volcano.

RDV data by showing the onset potential for the ORR as a function of corresponding O binding energy calculated from DFT. The measured activities exhibit a volcano-shaped trend when plotted against the theoretically determined O-binding energy. The peak of the volcano, corresponding to Pd<sub>105</sub>Au<sub>35</sub>@Pt or 75% Pd in the core, is in excellent agreement with our theoretical prediction of 72% Pd. Additionally, a Pt shell reduces the Pt loading as compared to a pure Pt particle.

### **Summary and Conclusions**

In summary, we have shown that the oxygen binding energy of alloy-core@Pt-shell nanoparticles can be linearly tuned by varying the composition of the alloy core. An important point pertains to the way this experiment was carried out. First, we obtained the experimental data shown in Figure 3c for just two DEN compositions: Pd<sub>70</sub>Au<sub>70</sub>@Pt and Pd<sub>105</sub>Au<sub>35</sub>@Pt. On the basis of these results, we anticipated a simple linear relationship between alloy core composition and ORR activity. Second, DFT calculations were carried out, and they predicted a volcano-shaped relationship between the onset potential for the ORR, catalyzed by PdAu@Pt 140-atom nanoparticles, and the oxygen binding energy. The peak activity was predicted to occur at a core composition corresponding to 105 Pd atoms and 35 Au atoms (Figure 4c). Third, we synthesized and tested additional Pd<sub>n</sub>Au<sub>140-n</sub>@Pt DEN compositions, and were gratified to find that the activity of these electrocatalysts fell almost exactly on the predicted trend lines. Hence, this is an unusual case of first-principles theory leading to nearly perfect agreement with experimental results. We believe that this tuning mechanism is a general property of the alloy-core@shell system, and hence provides a systematic means for designing nanoparticles to have desirable catalytic activity.

### **References**

1. Adzic, R. R.; Zhang, J.; Sasaki, K.; Vukmirovic, M. B.; Shao, M.; Wang, J. X.; Nilekar, A. U.; Mavrikakis, M.; Valerio, J. A.; Uribe, F. *Top. Catal.* **2007**, *46*, 249–262.
2. Adzic, R. R. *Electrocatalysis* **2012**, *3*, 163–169.
3. Wang, C.; Chi, M.; Li, D.; Strmcnik, D.; Vliet, D. Van Der; Wang, G.; Komanicky, V.; Chang, K.; Paulikas, A. P.; Tripkovic, D.; *et al.* *J. Am. Chem. Soc.* **2011**, *133*, 14396–14403.
4. Zhang, L.; Henkelman, G. *J. Phys. Chem. C* **2012**, *116*, 20860–20865.
5. Sasaki, K.; Naohara, H.; Choi, Y.; Cai, Y.; Chen, W.-F.; Liu, P.; Adzic, R. R. *Nat. Commun.* **2012**, *3*, 1115.
6. Koenigsmann, C.; Sutter, E.; Adzic, R. R.; Wong, S. S. *J. Phys. Chem. C* **2012**, *116*, 15297–15306.

### **Publications Acknowledging this Grant in 2012-2015**

1. Myers, V. S.; Frenkel, A. I.; Crooks, R. M. In-situ Structural Characterization of Platinum Dendrimer-Encapsulated Oxygen Reduction Electrocatalysts. *Langmuir* **2012**, *28*, 1596-1603.\*
2. Dumitrescu, I.; Yancey, D. F.; Crooks, R. M. Dual-Electrode Microfluidic Cell for Characterizing Electrocatalysts. *Lab Chip* **2012**, *12*, 986-993.\*
3. Yancey, D. F.; Zhang, L.; Crooks, R. M.; Henkelman, G. Au@Pt Dendrimer Encapsulated Nanoparticles as Model Electrocatalysts for Comparison of Experiment and Theory. *Chem. Sci.* **2012**, *3*, 1033-1040.\*
4. Carino, E. V.; Kim, H. Y.; Henkelman, G.; Crooks, R. M. Site-Selective Cu Deposition on Pt Dendrimer-Encapsulated Nanoparticles: Correlation of Theory and Experiment. *J. Am.*

5. *Chem. Soc.* **2012**, *134*, 4153-4162.\*
6. Dumitrescu, I.; Crooks, R. M. Effect of Mass Transfer on the Oxygen Reduction Reaction Catalyzed by Platinum Dendrimer Encapsulated Nanoparticles. *Proc. Natl. Acad. Sci., USA* **2012**, *109*, 11493-11497.\*
7. Anderson, R. M.; Zhang, L.; Loussaert, J. A.; Frenkel, A. I.; Henkelman, G.; Crooks, R. M. An Experimental and Theoretical Investigation of the Inversion of Pd@Pt Core@Shell Dendrimer-Encapsulated Nanoparticles. *ACS Nano* **2013**, *7*, 9345-9353.
8. Zhang, L.; Iyyamperumal, R.; Crooks, R. M.; Henkelman, G. Design of Pt-shell Nanoparticles with Alloy Cores for the Oxygen Reduction Reaction. *ACS Nano* **2013**, *7*, 9168-9172.
9. Yancey, D. F.; Chill, S. T.; Zhang, L.; Frenkel, A. I.; Henkelman, G.; Crooks, R. M. Systematic Ligand-Induced Disorder in Au<sub>147</sub> Dendrimer-Encapsulated Nanoparticles. *Chem. Sci.* **2013**, *4*, 2912-2921.
10. Iyyamperumal, R.; Zhang, L.; Henkelman, G.; Crooks, R. M. Efficient Electrocatalytic Oxidation of Formic Acid using Au@Pt Dendrimer-Encapsulated Nanoparticles. *J. Am. Chem. Soc.* **2013**, *135*, 5521-5524.
11. Kim, H.-Y.; Henkelman, G. CO Adsorption-driven Surface Segregation of Pd on Au/Pd Bimetallic Surfaces: Role of Defects and Effect on CO Oxidation. *ACS Catal.* **2013**, *3*, 2541-2546.
12. Zhang, L.; Kim, H.-Y.; Henkelman, G. CO Oxidation at the Au-Cu Interface of Bimetallic Nanoclusters Supported on CeO<sub>2</sub>(111). *J. Phys. Chem. Lett.* **2013**, *4*, 2943-2947.
13. Anderson, R. M.; Yancey, D. F.; Loussaert, J. A.; Crooks, R. M. Multistep Galvanic Exchange Synthesis Yielding Fully Reduced Pt Dendrimer-Encapsulated Nanoparticles. *Langmuir* **2014**, *30*, 15009-15015.
14. Loussaert, J. A.; Fosdick, S. E.; Crooks, R. M. Electrochemical Properties of Metal-Oxide-Coated Electrodes Prepared by Atomic Layer Deposition. *Langmuir* **2014**, *30*, 13707-13715.
15. Duan, Z.; Henkelman, G. CO Oxidation on the Pd(111) Surface. *ACS Catal.* **2014**, *4*, 3435-3443.
16. Anderson, M.; Crooks, R. M. High-Efficiency Generation-Collection Microelectrochemical Platform for Interrogating Electroactive Thin Films. *Anal. Chem.* **2014**, *86*, 9962-9969.
17. Zhang, L.; Henkelman, G. Computational Design of Alloy-Core@Shell Metal Nanoparticle Catalyst. *ACS Catal.* **2015**, *5*, 655-660.
18. Duan, Z.; Henkelman, G. CO Oxidation at the Au/TiO<sub>2</sub> Boundary: The Role of the Au/Ti<sub>5c</sub> Site. *ACS Catal.* **2015**, *5*, 1589-1595.
19. Zhang, L.; Anderson, R. M.; Crooks, R. M.; Henkelman, G. Correlating Structure and Function of Metal Nanoparticles for Catalysis. *Surf. Sci.*, April, **2015** (published on the Elsevier website, DOI:10.1016/j.susc.2015.03.018).
20. Chill, S. T.; Anderson, R. M.; Yancey, D. F.; Frenkel, A. I.; Crooks, R. M.; Henkelman, G. Probing the Limits of Conventional EXAFS Analysis using Thiolated Au Nanoparticles. *ACS Nano* **2015**, *9*, 4036-4042.
21. Anderson, R. M.; Yancey, D. F.; Zhang, L.; Chill, S. T.; Henkelman, G.; Crooks, R. M. A Theoretical and Experimental Approach for Correlating Nanoparticle Structure and Electrocatalytic Activity. *Acc. Chem. Res.*, May, **2015** (published on the ACS website,

22. DOI: 10.1021/acs.accounts.5b00125).

23. Luo, L.; Zhang, L.; Henkelman, G.; Crooks, R. M. Unusual Electrocatalytic Activity Trend of Pd<sub>x</sub>Au<sub>(140-x)</sub>@Pt (x: 0-140) Core@shell Nanoparticles for CO Oxidation. *J. Phys. Chem. Lett.*, May, **2015** (submitted).

\*Indicates that these publications cite an earlier DOE BES Catalysis Program grant number:  
DE-FG02-09ER16090

**Alkali-Catalyzed Cellulose Conversion to Furans:  
Techniques for Benchmarking High Temperature Condensed-Phase Kinetics**

Paul J. Dauenhauer, Associate Professor  
University of Minnesota, Department of Chemical Engineering & Materials Science

High temperature thermolysis of cellulose, a dehydration polymer of  $\beta$ -glucan monomers, occurs via a myriad of condensed-phase, millisecond reactions to volatile organic compounds in gasification, combustion and/or pyrolysis of lignocellulosic biomass. Naturally-occurring alkali species including Calcium and Magnesium are generally known to catalyze pyran ring opening, formation of permanent gases, and C-C bond formation to condensed products while inhibiting transglycosylation to levoglucosan and other anhydrosugars. However, the precise catalytic role of  $\text{Ca}^{++}$  and  $\text{Mg}^{++}$  and its oxides including their mechanisms and associated kinetics remains unknown. In this work, we invented a new experimental technique called “pulsed-film kinetics” that allows for characterization at millisecond reaction times of inorganic/organic reactions at temperatures above 400 °C within isothermal substrates. Millisecond temporal resolution of the hundreds of chemicals formed from cellulose at high temperature allows for the first measurement of the intrinsic kinetics of both uncatalyzed (melt-phase) reactions of cellulose and alkali-catalyzed reactions. Proposed mechanisms for furan formation evaluated via CPMD are compared with measured activation energies of formation of furfural, hydroxymethylfurfural (HMF), and methylfuran. Furan formation was shown to occur via a direct pyran-to-furan mechanism, while an alternative pathway via hydrolysis to intermediate glucose was energetically unviable. Further work with supported Pd/ $\text{Al}_2\text{O}_3$  allowed for selective decarbonylation of thermolysis-derived furans. Obtained fundamental catalytic mechanisms are broadly applicable to thermochemical biomass technologies; pulsed-film kinetics allows for measurement of reaction-limited catalytic rates which are apparatus agnostic. Additionally, new techniques and methods developed herein provide capability for expanding fundamental catalytic research into other high temperature reacting systems with complex chemical mechanisms within porous catalytic particles and on surfaces where fast quench and intricate analytical methods are required.

**Award No. DE-SC0006640: Natural Catalysts for Molten Cellulose Pyrolysis to Targeted Bio-Oils**

**PI:** Paul J. Dauenhauer

**Students:** Alex D. Paulsen, Christoph Krumm, Cheng Zhu

**Publications Acknowledging this Grant in 2012-2015**

- M.S. Metter, A.D. Paulsen, D.G. Vlachos, P.J. Dauenhauer, "The Chain Length Effect in Pyrolysis: Bridging the Gap between Glucose and Cellulose," *Green Chemistry* **2012**, 14, 1284-1288.
- M.S. Mettler, A.D. Paulsen, D.G. Vlachos, P.J. Dauenhauer, "Pyrolytic Conversion of Cellulose to Fuels: Levoglucosan Deoxygenation via Elimination and Cyclization within Molten Biomass," *Energy & Environmental Science* **2012**, 5, 7864-7868.
- A.D. Paulsen, M.S. Mettler, P.J. Dauenhauer, "The Role of Sample Dimension and Temperature in Cellulose Pyrolysis," *Energy & Fuels* **2013**, 27(4), 2126-2134.
- M.S. Mettler, A.D. Paulsen, D.G. Vlachos, P.J. Dauenhauer, "Tuning Cellulose Pyrolysis Chemistry: Selective Decarbonylation via Catalyst-Impregnated Pyrolysis," *Catalysis Science & Technology*, **2014**, 4, 3822-3825.
- C. Krumm, P.J. Dauenhauer, "Finding Chemistry in Cellulose Pyrolysis," Submitted. **2015**.
- C. Krumm, A.D. Paulsen, S. Maduskar, P.J. Dauenhauer, "On the Method of Pulsed-Film Kinetics," Submitted, **2015**.
- C. Krumm, P.J. Dauenhauer, "Pulsed-Film Kinetics Reveals the Mechanism of Furan Formation from Cellulose," Submitted, **2015**.
- C. Zhu, A.D. Paulsen, S. Maduskar, A.R. Teixeira, P.J. Dauenhauer, "Calcium Catalysis in Cellulose Pyrolysis," Submitted, **2015**.

# **Monday Evening**

## **III. Advances in Small Molecule Activation, 1: H<sub>2</sub>O, CO<sub>2</sub>, N<sub>2</sub>, etc.**

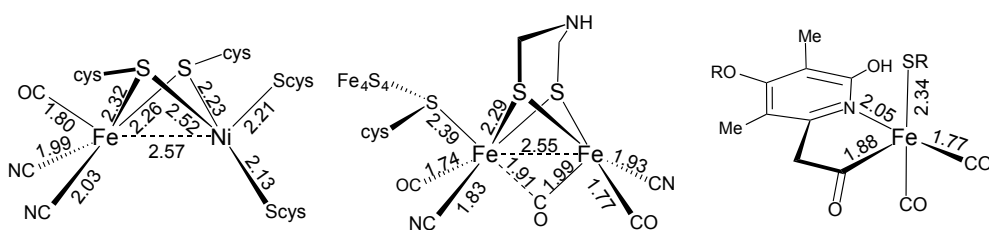
This page is intentionally blank.

# Organometallic Catalysis Inspired by the Hydrogenase Enzymes

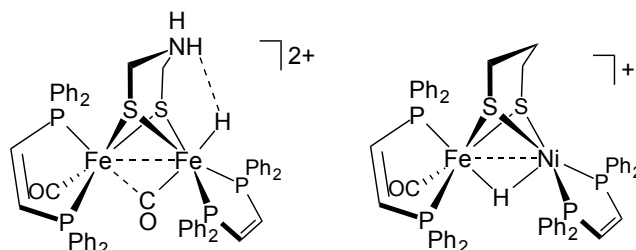
Thomas B. Rauchfuss  
 School of Chemical Sciences  
 University of Illinois at Urbana-Champaign

## Presentation Abstract

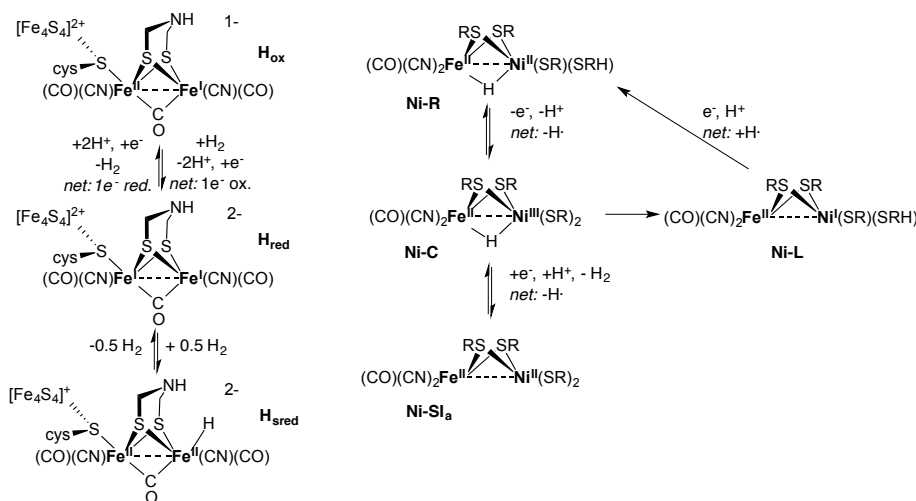
The active sites of the three hydrogenase ( $H_2ase$ ) enzymes provide templates and benchmarks for the design of homogeneous catalysts for transformations involving hydrogen. These catalytic centers are of special interest because (i) they utilize unusual pathways involving mixed valence intermediates, (ii) only first row metals are required, and (iii) the cofactors inspire fruitful catalytic platforms (e.g., PNNL's program on amine-phosphines). This presentation will give a critical update on the analogues of the enzyme active sites of the  $[Fe]$ -,  $[FeFe]$ -, and  $[NiFe]$ - $H_2ases$ .



Two bimetallic hydride systems will be emphasized:  $[HFe_2[(SCH_2)_2NH_2](CO)_2(diphos)_2]^{2+}$  and  $[HFeNi(SR)_2(CO)_2(diphos)_2]^+$ , catalysts for producing  $H_2$ .



Benchmarking is provided by the structures of the active sites, operating conditions (summary: super fast, very low overpotentials). Benchmarking is also provided by comparisons of spectroscopic signatures of the catalytic states ( $[FeFe]$  states:  $H_{sred}$ ,  $H_{red}$ ,  $H_{ox}$ ;  $[NiFe]$ -states: Ni-L, Ni-SI, Ni-R, Ni-C).



Complementing these *biomimetic* sites, are studies on related *bioinspired* systems with distinctly nonbiological centers, e.g.  $[\text{HCp}_2\text{Co}_2(\text{SR})_2]^+$ ,  $[\text{Cp}_2\text{Ni}_3(\text{SR})_4]$ ,  $[\text{HFe}_2(\text{SR})_2(\text{CNMe})_6]^+$ . These systems display wide ranging reactivity toward small molecules that provide new insights as well as new mechanistic challenges.

## defg02-90er14146

### "Organometallic and Catalytic Chemistry of Functionalized Complexes"

**Postdocs:** Ryan Gilbert Wilson, Xiaoyuan Zhou, Wenguang Wang, Joyee Mitra

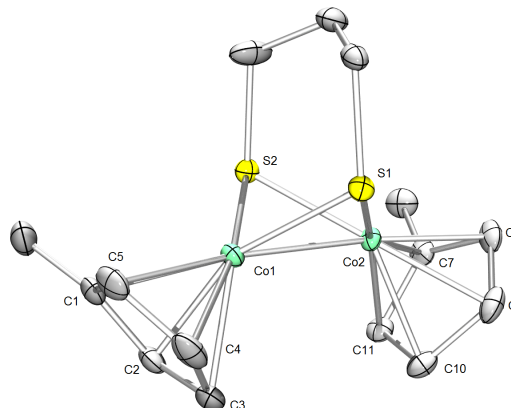
**Students:** Michaela Carlson, Geoffrey Chambers, Wan-Yi "Amy" Chu, James Lansing, Aaron Royer

#### RECENT PROGRESS

##### *Dicobalt Analogues of Hydrogenase Active Sites*

*Coworkers:* Geoffrey Chambers, Maria Carroll, James Lansing

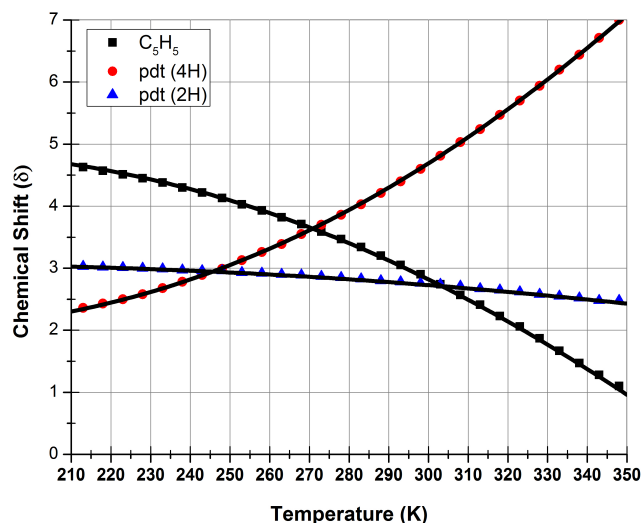
The goal of this effort is to replicate and expand upon the reactivity of the hydrogenase active sites using CpCo (14e center) in place of  $\text{FeL}_3$  (14e) centers. The species  $\text{Cp}_2\text{Co}_2(\text{SR})_2$  indeed give active catalysts for hydrogen evolution, proceeding via  $\mu$ -hydrides. Unlike simple  $\text{Fe}_2$  systems, the  $\text{Co}_2$  species also appears to catalyze oxidation of  $\text{H}_2$ . The mixed valence species  $[\text{Cp}_2\text{Co}_2(\text{SR})_2]^+$  differs from  $[\text{Fe}_2(\text{SR})_2\text{L}_{6-x}(\text{CO})_x]^+$  in that it has a delocalized ground state, whereas the Fe-CO-species desymmetrizes to a trapped state involving  $\mu$ -CO. This delocalized mixed valence species exhibits unusual reactions that will be discussed in the lecture.



##### *Cp<sub>2</sub>Ni<sub>2</sub> Analogues of Hydrogenase Active Sites: Advantages to Deplanarizing M<sub>2</sub>X<sub>2</sub> Cores*

*Coworkers:* Geoffrey Chambers

The goal of this effort is to elucidate the effect of "deplanarizing"  $\text{M}_2\text{S}_2$  cores and the consequences of such distortions in terms of reactivity/catalysis. The 36 e dimers  $\text{Cp}_2\text{Ni}_2(\text{SR})_2$  complexes have been known for decades as inert compounds with uninteresting properties. We have prepared the corresponding pyramidalized dimers using short chain dithiolate ligands. Upon distortion, the  $\text{Ni}_2\text{S}_2$  core becomes redox active and triplet states become populated.

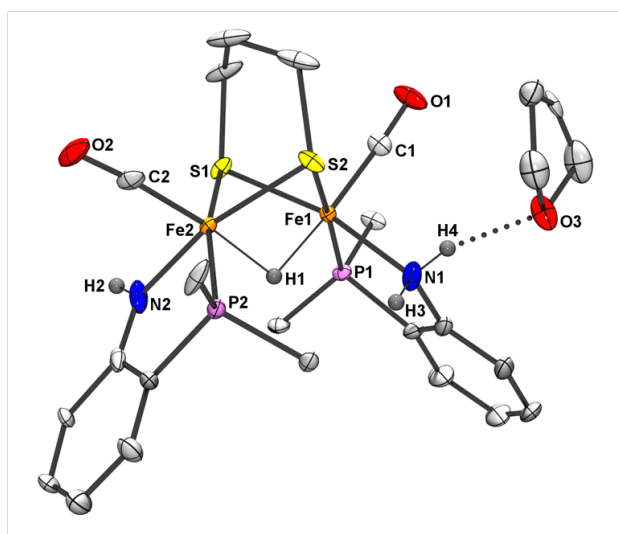


<sup>1</sup>H-NMR shifts vs T for  $\text{Cp}_2\text{Ni}_2(\text{pdt})$ .

### Oxidative Addition of N-H Bonds at $\text{Fe}_2(\text{SR})_2$ Centers

Coworkers: Michaela Carlson, Ryan Gilbert-Wilson, Joyee Mitra

The goal of this effort is to introduce pi-donor sites and protic N-H functionality adjacent to hydride ligands in hydrogenase models. These goals are being met by reactions of the diiron(I) carbonyl dithiolates with *o*- $\text{Ph}_2\text{PC}_6\text{H}_4\text{NH}_2$  (PNH<sub>2</sub>). The first chelate attaches normally, but the second induces oxidative addition of the N-H bond. Even though the amino-amido-hydride is unsymmetrical, the NMR data indicate rapid site exchange even at -85 °C. The acid-base and redox properties of these hydrides are being examined.

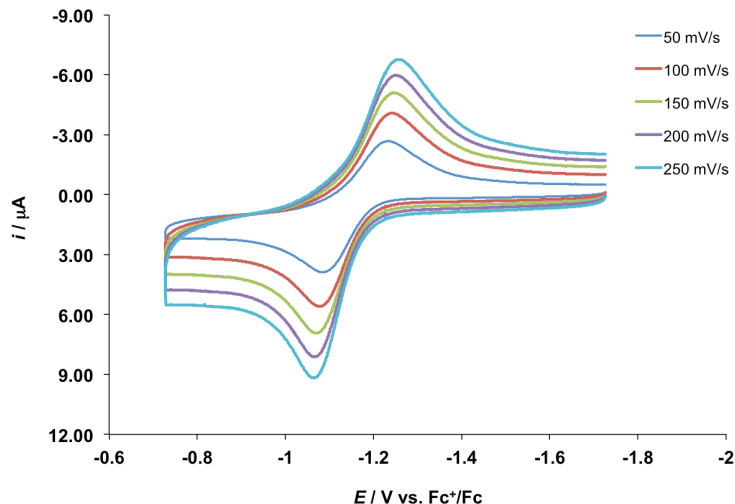


Structure of the amido-hydride  $\text{HFe}_2(\text{S}_2\text{C}_3\text{H}_6)(\text{CO})_2(\kappa^2\text{-PNH})(\kappa^2\text{-PNH}_2)$ .

### Unusual Reducing Properties of $\text{Fe}_2(\text{SR})_2(\text{CNMe})_6$

Bryan C. Barton, Xiaoyuan Zhou

The goal of this effort is to produce highly reducing diiron centers as platforms for reactions with small molecule substrates of relevance to the DoE mission. The thermal reaction of  $\text{Fe}_2(\text{SR})_2(\text{CO})_6$  with MeNC produces  $\text{Fe}_2(\text{SR})_2(\text{CNMe})_6$ , which has been characterized crystallographically. Protonation ( $\text{p}K_{\text{a}}^{\text{MeCN}} > 18$ ) occurs initially at CNMe prior to formation of a cationic Fe-H-Fe species. Both  $\text{H}_2$  and  $\text{CO}_2$  react readily (1 atm, RT), but the nature of these products is unknown.



Cyclic voltammogram of  $\text{Fe}_2(\text{SR})_2(\text{CNMe})_6$  in MeCN solution (0.1 M  $n\text{Bu}_4\text{NPF}_6$ ) at scan rates of 50-250 mV/s. The waveform reflects the effect of a combined chemical-electrochemical process.

## Publications Acknowledging this Grant in 2012-2015

### 2015

- Ogata, H.; Krämer, T.; Wang, H.; Schilter, H.; Pelmentschikov, H.; van Gastel, M.; Neese, F.; Rauchfuss, T. B.; Gee, L. B.; Scott, A. B.; Yoda, Y.; Tanaka, Y.; Lubitz, W.; Cramer, S. P. "Hydride bridge in [NiFe]-hydrogenase observed by nuclear resonance vibrational spectroscopy" *Nature Comm.* **2015**, in press.
- Gilbert-Wilson, R.; Chu, W.-Y.; Rauchfuss, T. B., "Phosphine-Iminopyridines as Platforms for Catalytic Hydrofunctionalization of Alkenes", *Inorg. Chem.* **2015**, *54*, 0000.
- Chu, W.-Y.; Zhou, X.; Rauchfuss, T. B., "Cooperative Metal–Ligand Reactivity and Catalysis in Low-Spin Ferrous Alkoxides", *Organometallics* **2015**, *34*, 1619-1626
- Mitra, J.; Zhou, X.; Rauchfuss, T., "Pd/C-catalyzed reactions of HMF: decarbonylation, hydrogenation, and hydrogenolysis", *Green Chem.* **2015**, *17*, 307-313

### 2014

- Chambers, G. M.; Mitra, J.; Rauchfuss, T. B.; Stein, M., "Ni/L Model for the Ni-L State of the [NiFe]Hydrogenases: Synthesis, Spectroscopy, and Reactivity", *Inorg. Chem.* **2014**, *53*, 4243–4249
- Zhou, X.; Mitra, J.; Rauchfuss, T. B., "Lignol Cleavage by Pd/C Under Mild Conditions and Without Hydrogen: A Role for Benzylic C-H Activation?", *ChemSusChem* **2014**, *7*, 1623-1626
- Wang, W.; Rauchfuss, T. B.; Zhu, L.; Zampella, G., "New Reactions of Terminal Hydrides on a Diiron Dithiolate", *J. Am. Chem. Soc.* **2014**, *136*, 5773-5782

### 2013

- Chambers, G. M.; Angamuthu, R.; Gray, D. L.; Rauchfuss, T. B., "Organo Ruthenium-Nickel Dithiolates with Redox-Responsive Nickel Sites", *Organometallics* **2013**, *32*, 6324-6329;
- Zhou, X.; Rauchfuss, T. B., "Production of Hybrid Diesel Fuel Precursors from Carbohydrates and Petrochemicals Using Formic Acid as a Reactive Solvent", *ChemSusChem* **2013**, *6*, 383-388
- Appel, A. M.; Bercaw, J. E.; Bocarsly, A. B.; Dobbek, H.; DuBois, D. L.; Dupuis, M.; Ferry, J. G.; Fujita, E.; Hille, R.; Kenis, P. J. A.; Kerfeld, C. A.; Morris, R. H.; Peden, C. H. F.; Portis, A. R.; Ragsdale, S. W.; Rauchfuss, T. B.; Reek, J. N. H.; Seefeldt, L. C.; Thauer, R. K.; Waldrop, G. L., "Frontiers, Opportunities, and Challenges in Biochemical and Chemical Catalysis of CO<sub>2</sub> Fixation", *Chem. Rev.* **2013**, *113*, 6621-6658

### 2012

- Lei, H.; Royer, A. M.; Rauchfuss, T. B.; Gray, D., "C<sub>2</sub>-Symmetric Iron(II) Diphosphine-Dialkoxide Dicarbonyl and Related Complexes", *Organometallics* **2012**, *31*, 6408-6414.
- Ringenberg, M. R.; Rauchfuss, T. B., "Protonation-Enhanced Lewis Acidity of Iridium Complexes Containing Noninnocent Amidophenolates", *Eur. J. Inorg. Chem.* **2012**, 490–495

**Benchmarking catalysts for the hydrogen evolution reaction (HER) and the oxygen evolution reaction (OER): The importance of turnover frequency (TOF)**

Thomas F. Jaramillo (PI)  
Department of Chemical Engineering  
443 Via Ortega, Shriram Center Room  
Stanford University  
Stanford, CA 94305-5025  
Phone: (650) 498-6879; Fax: (650) 725-7294  
E-mail: jaramillo@stanford.edu

**Presentation Abstract**

Fundamental studies of catalyst materials provide design principles that govern performance, knowledge that is enabling the development of catalysts that are active, selective, and stable for important electrochemical reactions involving energy conversion. Two particular reactions of interest include the hydrogen evolution reaction (HER) and the oxygen evolution reaction (OER), which have significant importance in the areas of water electrolysis and solar fuels. Objective comparisons of electrocatalyst activity and stability using standard methods under identical conditions are necessary to evaluate the viability of existing electrocatalysts for integration into solar-fuels devices as well as to help inform the development of new catalytic systems.

This talk will begin by describing different means to compare electrocatalyst materials, followed by description of a standard protocol that has been developed to serve as a primary screening tool for evaluating the activity, short-term (2-h) stability, and electrochemically-active surface area (ECSA) of 17 hydrogen evolution reaction (HER) electrocatalysts and 26 oxygen evolution reaction (OER) electrocatalysts under conditions relevant to an integrated solar-water splitting device in aqueous acidic or alkaline solution. Trends will be discussed among these high-performance materials, with a specific emphasis on drawing comparisons among geometric area activity versus turnover frequency (TOF). Opportunities and challenges will be described for catalyst development, followed by recent efforts to produce highly active and stable catalysts for these reactions. The paper will conclude with a discussion of efforts to integrate the latest catalysts onto semiconductor photoelectrodes to produce active and stable systems.

**DOE Grant #: DE-SC0008685: Directed surface structures and interfaces for enhanced electrocatalyst activity, selectivity, and stability for energy conversion reactions**

**PI:** Thomas F. Jaramillo (PI)  
**Postdoc(s):** Jakob Kibsgaard  
**Student(s):** Ariel Jackson

**RECENT PROGRESS**

***Hydrogen evolution on molybdenum phosphide and molybdenum phosphosulfide materials***

Introducing sulfur into the surface of molybdenum phosphide (MoP) produces a molybdenum phosphosulfide (MoP|S) catalyst with superb activity and stability for the hydrogen evolution reaction (HER) in acidic environments. The MoP|S catalyst reported herein exhibits among the

highest HER activity of any non-noble metal electrocatalyst investigated in strong acid, while remaining perfectly stable in accelerated durability testing. Whereas mixed metal alloy catalysts are well-known, MoP|S represents a more uncommon mixed anion catalyst where synergistic effects between sulfur and phosphorous produce a more active, high surface area electrode than those based on either the pure sulfide or the pure phosphide. The extraordinarily high activity and stability of this catalyst opens up avenues to replace Pt in technologies relevant to renewable energy such as proton exchange membrane (PEM) electrolyzers and solar photoelectrochemical (PEC) water-splitting cells.

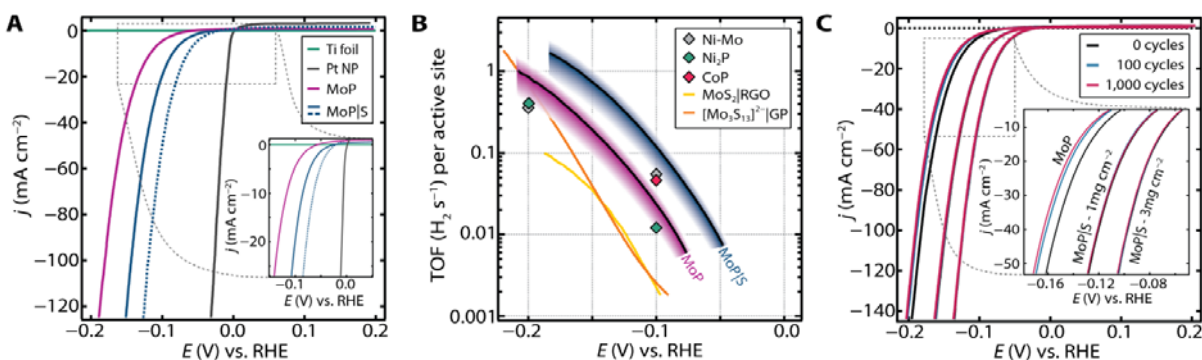


**Figure 1.** HER activity of MoP and MoP|S. (A) Linear sweep voltammograms of MoP and MoP|S. The solid and dotted lines represent samples with a loading of  $\sim 1$  and  $\sim 3$   $\text{mg cm}^{-2}$ , respectively. The HER activity of Pt nanoparticles (NP) is displayed for comparison. (B) Plot that displays the TOF of MoP and MoP|S together TOFs for Ni-Mo (1), Ni<sub>2</sub>P (2), CoP (3), MoS<sub>2</sub> (4) and [Mo<sub>3</sub>S<sub>13</sub>]<sup>2-</sup> (5) catalysts. For MoP and MoP|S the black line represent TOF calculated using 40  $\mu\text{F cm}^{-2}$  as specific capacitance standard and the borders of the colored gradients represent using 20 and 60  $\mu\text{F cm}^{-2}$  for a lower and upper limit. MoP|S exhibit among the highest TOF of any non-precious metal HER catalyst synthesized by a scalable route. (C) Accelerated stability test. Initial and post potential linear sweep voltammograms of MoP with  $\sim 1$   $\text{mg cm}^{-2}$  loading and MoP|S with  $\sim 1$  and  $\sim 3$   $\text{mg cm}^{-2}$  loadings. Whereas MoP experiences a slight decrease in current density upon increased potential cycling, MoP|S remains perfectly stable.

### ***Understanding the hydrogen evolution reaction (HER) on molybdenum sulfide catalysts***

We discuss recent developments in nanostructured molybdenum sulfide catalysts for the electrochemical hydrogen evolution reaction. To develop a framework for performing consistent and meaningful comparisons between catalysts, we review standard experimental methodologies for measuring catalyst performance and define two metrics used in this perspective for comparing catalyst activity: the turn over frequency, an intrinsic activity metric, and the total electrode activity, a device-oriented activity metric. We discuss general strategies for synthesizing catalysts with improved activity, namely increasing the number of electrically accessible active sites or increasing the turn over frequency of each site. Then we consider a number of state-of-the-art molybdenum sulfide catalysts, including crystalline MoS<sub>2</sub>, amorphous MoS<sub>x</sub>, and molecular cluster materials, to highlight these strategies in practice. Comparing these catalysts reveals that most of the molybdenum sulfide catalysts have similar active site turn over frequencies, so the total electrode activity is primarily determined by the number of accessible active sites per geometric electrode area. Emerging strategies to overcome current catalyst limitations and potential applications for molybdenum sulfide catalysts including

photoelectrochemical water splitting devices and electrolyzers are also considered in this analysis.

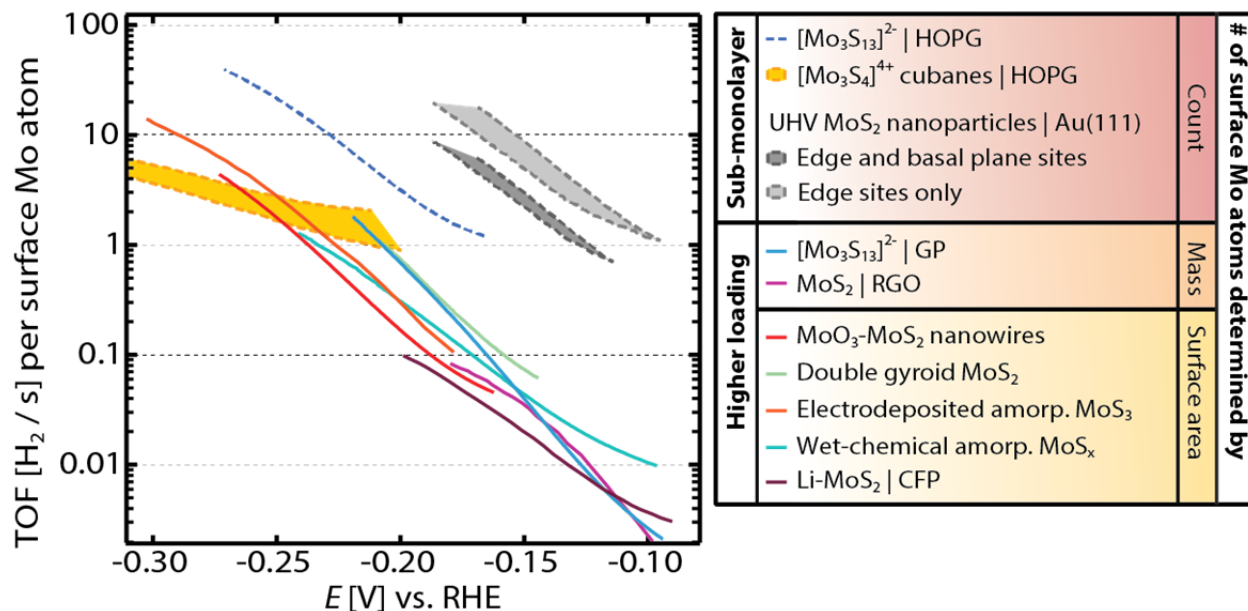


**Figure 2.** Turn over frequencies of different molybdenum sulfide catalysts normalized to the number of surface Mo atoms.

### Cited References

1. J. R. McKone, B. F. Sadtler, C. A. Werlang, N. S. Lewis, H. B. Gray, Ni–Mo Nanopowders for Efficient Electrochemical Hydrogen Evolution. *ACS Catal.* **3**, 166 (2012).
2. E. J. Popczun *et al.*, Nanostructured Nickel Phosphide as an Electrocatalyst for the Hydrogen Evolution Reaction. *J. Am. Chem. Soc.* **135**, 9267 (2013).
3. E. J. Popczun, C. G. Read, C. W. Roske, N. S. Lewis, R. E. Schaak, Highly Active Electrocatalysis of the Hydrogen Evolution Reaction by Cobalt Phosphide Nanoparticles. *Angew. Chem.* **53**, 5427 (2014).
4. Y. Li *et al.*, MoS<sub>2</sub> Nanoparticles Grown on Graphene: An Advanced Catalyst for the Hydrogen Evolution Reaction. *J. Am. Chem. Soc.* **133**, 7296 (2011).
5. J. Kibsgaard, T. F. Jaramillo, F. Besenbacher, Building an appropriate active-site motif into a hydrogen-evolution catalyst with thiomolybdate [Mo<sub>3</sub>S<sub>13</sub>]<sup>2-</sup> clusters. *Nature Chem.* **6**, 248 (2014).

### Publications Acknowledging this Grant in 2012-2015

1. J.D. Benck, T.R. Hellstern, J. Kibsgaard, P. Chakhranont, T.F. Jaramillo, "Catalyzing the Hydrogen Evolution Reaction (HER) with Molybdenum Sulfide Nanomaterials," *ACS Catalysis* **2014**, *136*, 3957-3971.

2. J. Kibsgaard and T.F. Jaramillo, "Molybdenum Phosphosulfide: An Active, Acid-Stable Earth-Abundant Catalyst for the Hydrogen Evolution Reaction," *Angewandte Chemie* **2014**, *53*, 14433-14437.
3. Kibsgaard, J.; Jaramillo, T.F.; Besenbacher, F. Building an appropriate active-site motif into a hydrogen evolution catalyst with thiomolybdate  $[\text{Mo}_3\text{S}_{13}]^{2-}$  clusters. *Nature Chemistry* **2014**, *6*, 248-253.
4. Jackson, A.; Viswanathan, V.; Forman, A.J.; Larsen, A.H.; Nørskov, J.K.; Jaramillo, T.F. Climbing the Activity Volcano: Core-Shell Ru@Pt Electrocatalysts for Oxygen Reduction. *ChemElectroChem* **2014**, *1*, 67-71.

**Using Semiconductor Photoelectrodes to Engender Catalytic Transformations in Small Molecules on Solid Surfaces**

Bart M. Bartlett, James J. Brancho, Tanya M. Breault, Samuel L. Esarey, Benjamin M. Klepser, and Kayla J. Pyper  
University of Michigan, Department of Chemistry

**Presentation Abstract**

Semiconductor materials allow for solar-driven fuel forming reactions such as water splitting from renewable sustainable sources and allow for green chemistry routes toward activating functional moieties of organic molecules. Although traditional metal oxide materials such as TiO<sub>2</sub> have the drawback of a large energy band gap (> 3 eV) that render them active only in the UV part of the solar spectrum, stable co-alloyed compositions such as Ti<sub>1-(5x/4)</sub>Nb<sub>x</sub>O<sub>2-y</sub>N<sub>y</sub> prepared in our lab are responsive to visible light for oxygen evolution. Moreover, photoelectrodes composed of CuWO<sub>4</sub>, an *n*-type semiconductor with a band-gap energy of 2.4 eV photooxidize water with simulated solar radiation with a nearly quantitative Faradaic efficiency for O<sub>2</sub> evolution in borate-buffered saline solution. CuWO<sub>4</sub> is selective for water oxidation in the presence of the Cl<sup>-</sup> or HSO<sub>4</sub><sup>-</sup>, common anions in aqueous electrolytes. These characteristics are a significant improvement to the more commonly studied binary phase, WO<sub>3</sub>. Moreover, we can anchor derivatives of known molecular water oxidation catalysts such as Fe(tebppmcn)Cl<sub>2</sub> (tebppmcn is the κ<sup>4</sup>-nitrogen donor, tetraethyl *N,N'*-bis(2-methylpyridyl-4-phosphonate)-*N,N'*-dimethyl-cyclohexyl-diamine) that binds to the surface of WO<sub>3</sub> using pendant phosphonate groups to improve its efficiency for selective photoelectrochemical water oxidation. Characterizing surface-bound species in aqueous solution continues to pose a significant challenge in bridging homogeneous and heterogeneous catalysis. Therefore, current efforts focus on extending the reaction scope beyond water oxidation to include chemoselective oxidative amine coupling on CuWO<sub>4</sub> under non-aqueous conditions.

**DE-SC0006587: Chemoselective Oxidations Using Visible-light Responsive Semiconducting Oxides**

Student(s): James J. Brancho, Tanya M. Breault, Samuel L. Esarey, Benjamin M. Klepser, and Kayla J. Pyper

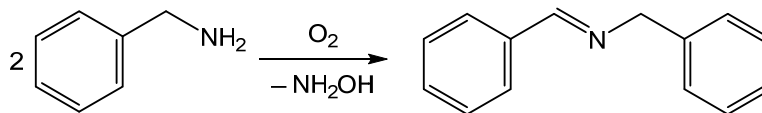
**RECENT PROGRESS**

This project builds on our DOE-sponsored program from previous funding period by expanding the scope of molecular catalysts, reactions of interest, and semiconductor compositions to effect energy-relevant photochemical and photoelectrochemical oxidation reactions. The single theme bidding the three aims of this proposal is that a semiconducting photoelectrode will replace harsh chemical oxidants, thereby improving the atom-

efficiency of oxidation reactions. Semiconducting oxides chemically stable, but are often indiscriminant oxidants due highly oxidizing holes that give rise to  $\bullet\text{OH}$  in water, 2.7 V (vs. RHE). Therefore, new reactivity focuses on working in organic solvents and/or tethering molecular catalysts to oxidize compound containing multiple functional groups chemoselectively. In this funding cycle, we are honing reactions in which  $\text{O}_2$  can potentially serve as an oxidant, but we are probing differences in selectivity, reaction rate, and elementary steps when  $\text{O}_2$  serves as the oxidant opposed to oxidation by photogenerated holes. The primary challenge is designing chemically robust tethers that will also rapidly shuttle holes from the valence band of the semiconductor to attached catalyst molecules or substrates for high turnover number with high turnover frequency.

***Expanding the scope of reactions for semiconducting oxide photo(electro)catalysts to include selective oxidation of amines***

Our group has developed  $\text{CuWO}_4$  photoelectrodes for the oxygen evolution reaction (OER) through NSF-sponsored work.<sup>1</sup> However, the electronic structure of this material renders it an excellent candidate for carrying out oxidation reactions of organic substrates (DOE-funded work). This approach of using semiconductor photoelectrochemistry allows us to replace sacrificial chemical oxidants with either valence-band holes or active oxygen species derived from valence-band holes. For our preliminary work, we focus on the oxidative coupling of benzylamine to form the imine according to the reaction:



We started with amine oxidations because they have relevance in synthetic organic chemistry and they have biological implications.<sup>2</sup> Also, there is synthetic precedence of this reaction occurring photocatalytically on  $\text{TiO}_2$  using  $\text{O}_2$  as the external oxidant.<sup>3</sup> The importance of  $\text{O}_2$  in the catalytic cycle was realized as the reaction proceeds through a benzaldehyde intermediate for both alcohol and amine oxidation.<sup>4,5</sup> However, one

1. a) Yourey, J. E.; Bartlett, B. M. Electrochemical Deposition of and Photoelectrochemistry of  $\text{CuWO}_4$ , a Promising Photoanode for Water Oxidation. *J. Mater. Chem.* **2011**, *21*, 7651-7660; b) Yourey, J. E.; Kurtz, J. B.; Bartlett, B. M. Water Photooxidation on a  $\text{CuWO}_4$ - $\text{WO}_3$  Composite Electrode in the Presence of  $[\text{Fe}(\text{CN})_6]^{3-}$ : toward Z-scheme Water Splitting at Zero Bias. *J. Phys. Chem. C* **2012**, *116*, 3200-3250; c) Yourey, J. E.; Pyper, K. J.; Kurtz, J. B.; Bartlett, B. M. Chemical Stability of  $\text{CuWO}_4$  for Photoelectrochemical Water Oxidation. *J. Phys. Chem. C* **2013**, *117*, 8708-8718; d) Pyper, K. J.; Yourey, J. E.; Bartlett, B. M. Reactivity of  $\text{CuWO}_4$  in Photoelectrochemical Water Oxidation is Dictated by a Mid-gap Electronic State. *J. Phys. Chem. C* **2013**, *117*, 24726-24732.

2. Murahashi, S-I. Synthetic Aspects of Metal-Catalyzed Oxidations of Amines and Related Reactions *Angew. Chem. Int. Ed. Engl.* **1995**, *34*, 2443-2465.

3. Lang, X.; Ma, W.; Chen, C.; Ji, H.; Zhao, J. Selective Aerobic Oxidation Mediated by  $\text{TiO}_2$  Photocatalysis *Accounts Chem. Res.* **2013**, *47*, 355-363.

4. Lang, X.; Ma, W.; Zhao, Y.; Chen, C.; Ji, H.; Zhao, J. Visible-Light-Induced Selective Photocatalytic Aerobic Oxidation of Amines into Imines on  $\text{TiO}_2$  *Chem. Eur. J.* **2012**, *18*, 2624-2631.

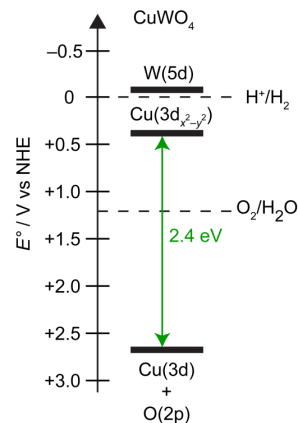
5. Zhang, M.; Wang, Q.; Chen, C.; Zang, L.; Ma, W.; Zhao, J. Oxygen Atom Transfer in the Photocatalytic Oxidation of Alcohols by  $\text{TiO}_2$ : Oxygen Isotope Studies *Angew. Chem. Int. Ed.* **2009**, *48*, 6081-6084.

drawback of using TiO<sub>2</sub> is that its band gap is large (3.0 – 3.2 eV), resulting only in a UV response.

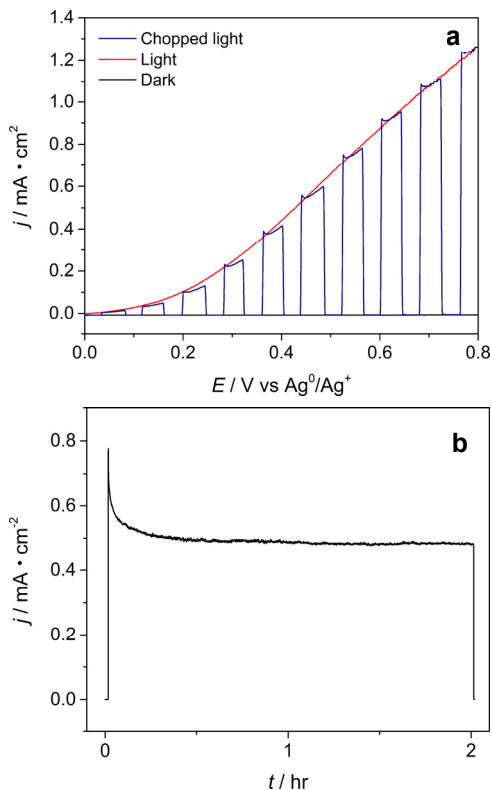
CuWO<sub>4</sub> is attractive because its valence band edge is higher less oxidizing (2.7 eV), and its band gap is smaller (2.3 eV) due to the Cu(3d) orbital contribution, illustrated in Figure 1. Moreover, mid-gap electronic states that dictate water oxidation may provide a lower overpotential pathway for amine oxidation. The reaction was carried out on a film electrode of CuWO<sub>4</sub> synthesized by sol-gel processing. Benzylamine was added to an acetonitrile solution with tetrabutylammonium hexafluorophosphate (TBAPF<sub>6</sub>) as supporting electrolyte. Linear sweep voltammetry was performed on the electrode in the dark, under continuous irradiation using a 150 W Xe lamp fitted with a blue cut-on filter from 300-600 nm and focuser producing 450 mW/cm<sup>2</sup>, and under chopped light.

Figure 2a shows there is oxidation that is taking place at the surface of the electrode with minimal transient photocurrent, meaning that undesired carrier recombination at the surface is minimal. Controlled potential coulometry was carried out under illumination on an electrode poised at 0.7 V vs Ag<sup>0</sup>/Ag<sup>+</sup> in which 3.5 C of charge was passed in order to produce enough product for gas chromatography (GC) detection. The bulk electrolysis in Figure 2b shows an initial spike in current that decreases over the span of ~15 minutes, after which it remains constant for the remainder of the experiment. This initial decrease could be due to oxidation of a small amount of water since the acetonitrile used is not dried, and requires further investigation. Nevertheless, gas chromatography on shows that the coupled imine is the only product formed, corroborated by a measured Faradaic efficiency of ~90%.

Although electrochemistry allows for direct measurement of Faradaic efficiency, we have also shown that we can carry out this oxidation reaction on CuWO<sub>4</sub> powder to decrease the conversion time. Powdered catalysts have the advantage of having more surface catalytic sites. CuWO<sub>4</sub> powder was synthesized by a co-precipitation reaction and further treated hydrothermally.<sup>6</sup> In



**Figure 1.** Electronic structure of CuWO<sub>4</sub> as determined by UV-Vis spectroscopy, EIS Mott-Schottky analysis, and XPS analysis.



**Figure 2** a) Dark current (black), photocurrent (red), and chopped-light photocurrent (navy) in LSV traces of benzylamine oxidation on CuWO<sub>4</sub>; b) Bulk electrolysis on a CuWO<sub>4</sub> electrode poised at 0.7 V vs Ag<sup>0</sup>/Ag<sup>+</sup> in 0.5 M benzylamine solution with 0.1 M TBAPF<sub>6</sub> in acetonitrile.

6. Chen, H.; Leng, W.; Xu, Y. Enhanced Visible-Light Photoactivity of CuWO<sub>4</sub> through a Surface-Deposited CuO *J. Phys. Chem. C* **2014**, *118*, 9982-9989.

this experiment, the reaction conditions were mimicked to that of the TiO<sub>2</sub> powder reactions described in Zhang *et al.*<sup>5</sup> The reaction conditions are 10 mg of CuWO<sub>4</sub> powder, bromobenzene as the internal standard for GC analysis, and 0.1 mmol of benzylamine in 2 mL of acetonitrile. The illumination conditions were held the same as with the electrode at 450 mW/cm<sup>2</sup> measured lamp power with a blue cut-on filter (300 – 600 nm) and focuser in a single quartz cell. Notable is that after 8 h of continuous illumination, all of the starting material is converted cleanly to the imine.

***Preparing stable titanium oxide, nitride, and carbide photocatalysts or electrocatalysts based on the synthesis work on our TiO<sub>2</sub>:(Nb,N) work***

Building on previous work in synthesizing visible-light absorbing anatase-phase derivatives with composition Ti<sub>1-(5x/4)</sub>Nb<sub>x</sub>O<sub>2-y</sub>N<sub>y</sub> (termed TiO<sub>2</sub>:(Nb,N) in our lab), we have generated rock salt phase TiN<sub>x</sub>C<sub>1-x</sub> (XRD pattern shown in Figure 3). The N(1s) XPS peak at 397 eV binding energy is indicative of TiN, but the Ti(2p) lines suggest that titanium is present in its formal +3 and +4 oxidation states at the surface. The material is generated under air-free conditions starting from the precipitate that forms from a THF solution of Ti(NMe<sub>2</sub>)<sub>4</sub> and NH<sub>3</sub> that is annealed in a quartz tube at 600 °C under argon. Next steps are to introduce oxygen to generate oxynitrides that absorb in the visible. As the inset shows, these TiN<sub>x</sub>C<sub>1-x</sub> compositions are black, but in the interim, we are exploring them as thin films for electrocatalytic oxygen reduction.

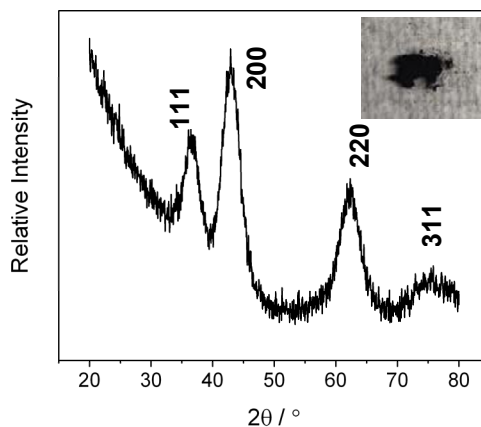


**Figure 3.** XRD pattern and photograph of TiN<sub>x</sub>C<sub>1-x</sub>.

**Publications Acknowledging this Grant in 2012-2015**

1. Breault, T. M.; Bartlett, B. M. Lowering the Band Gap of Anatase-structured TiO<sub>2</sub> by Co-Alloying with Nb and N: Electronic Structure and Photocatalytic Degradation of Methylene Blue Dye. *J. Phys. Chem. C* **2012**, *116*, 5986-5994.
2. Breault, T. M.; Bartlett, B. M. Composition-Dependence of TiO<sub>2</sub>:(Nb,N)-x Compounds on the Rate of Photocatalytic Methylene Blue Dye Degradation. *J. Phys. Chem. C* **2013**, *117*, 8611-8618.
3. Breault, T. M.; Brancho, J. J.; Guo, P.; Bartlett, B. M. Visible Light Water Oxidation Using a Co-Catalyst Loaded Anatase-Structured Ti<sub>1-(5x/4)</sub>Nb<sub>x</sub>O<sub>2-y-δ</sub>N<sub>y</sub> Compound. *Inorg. Chem.* **2013**, *52*, 9363-9368.
4. Klepser, B. M.; Bartlett, B. M. Anchoring a Molecular Iron Catalyst to Solar-Responsive WO<sub>3</sub> Improves the Rate and Selectivity of Photoelectrochemical Water Oxidation. *J. Am. Chem. Soc.* **2014**, *136*, 1694-1697.
5. Pyper, K. J.; Bartlett, B. M. Oxidative Coupling of Benzylamine on CuWO<sub>4</sub> Powder and Photoelectrodes. **2015**, *Submitted*.

**Tuesday Morning**

**Plenary Session**

This page is intentionally blank.

**Robert Schlögl**

**Benchmarking and Standardization of Electro- and Chemo-Catalysts  
Basic Considerations and Experimental Procedures**

**Robert Schlögl**

Fritz Haber Institute of the Max Planck Society  
Department of Inorganic Chemistry  
Berlin, Germany

This page is intentionally blank.

**Tuesday Afternoon**

**IV. Advances in  
Small Molecule  
Activation, 2:  
CO, CH<sub>4</sub>, H<sub>2</sub>, etc.**

This page is intentionally blank.

**José A. Rodriguez**

## **Benchmark Studies for the Water-gas Shift and CO<sub>2</sub> Hydrogenation**

**José A Rodriguez, Ping Liu, Dario Stacchiola, Sanjaya Senanayake, Mike G. White and Jonathan C. Hanson.**

**Chemistry Department , Brookhaven National Laboratory**

### **Presentation Abstract**

This program pursues an improved understanding of chemical catalysis for advanced fuels synthesis and energy conversion processes by elucidating catalytically important properties of well-defined surfaces, powders and nanostructures. The presentation will focus on benchmark studies for the water-gas shift and CO<sub>2</sub> hydrogenation on well-defined model catalyst. Starting with single crystals of metal {Cu(111) and Au(111)} and oxide surfaces {TiO<sub>2</sub>(110) and CeO<sub>2</sub>(111)}, we have performed detailed tests of catalytic activity and performed mechanistic studies that illustrate the importance of the metal-oxide interface. Extremely high catalytic activity was found after depositing nanoparticles of CeO<sub>x</sub> on Cu(111) and Au(111) or after dispersing them together with Cu or Au nanoparticles on TiO<sub>2</sub>(110). IR and AP-XPS indicate that this enhancement in catalytic activity is the result of opening new reaction paths that lead to the formation of a HOCO intermediate at the metal-oxide interface. Data of IR spectroscopy and DFT calculations indicate that formate species are not necessarily involved in the main reaction paths for the water-gas shift and CO<sub>2</sub> hydrogenation on the model catalysts. The benchmark studies have been extended to include work with well-characterized powder catalysts. The work with the powder catalysts have shown the validity of the concepts and ideas for catalyst design derived from the benchmark studies.

## **BNL FWP CO-009: Catalysis for Advanced Fuels**

### **Subtask 1: Catalysis, Structure and Reactivity**

**Postdoctoral fellows:** Wenqian Xu (partly), Huanru Wang

**Students:** Si Luo, Zongyen Liu, Siyu Yao

## RECENT PROGRESS

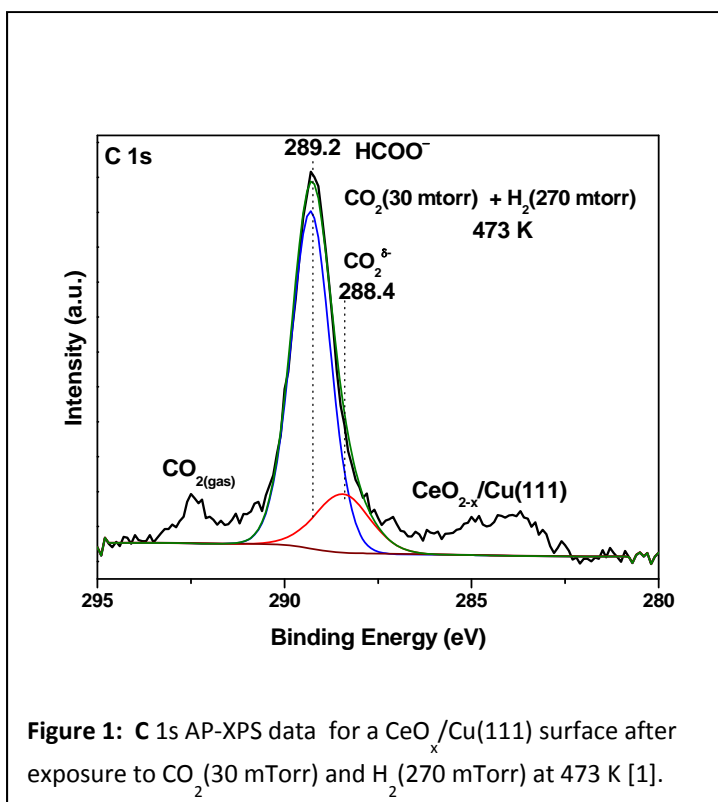
The main research themes in this FWP are inspired by challenges in the production and use of chemical fuels [1-35]. Specific themes are (i) the cleaning of oil-derived fuels through hydrodesulfurization [3,26], (ii) the reforming of alcohols [12,21,28], (iii) the synthesis of higher (C<sub>1</sub>-C<sub>4</sub>) alcohols by the hydrogenation of CO<sub>2</sub> or CO [1,4,15,30], and (iv) CO oxidation [5,13,23,29,31]. The last two topics are associated with C1 chemistry. These research efforts are also linked by an interest in the properties of oxides [1,5,11,14,27,28], carbides [2-4,9,15-17] and sulfides [3], materials which may be able to replace scarce noble metals in energy-related catalysis involving hydrogen transfer, e.g. hydrogenation and hydrodesulfurization processes. In many of our studies, the catalytic processes are carried out on multifunctional catalysts which contain metal-oxide, metal-carbide or metal-sulfide interfaces [1,4,9,28]. The research team has a strong interest in the development of tools for the *in-situ* characterization of model and powder catalysts under reaction conditions [8,12,18-20,23,29]. Since 2012, more than 30 papers have been published showing the work done under this FWP [1-35].

### *Role of Metal-Oxide Interface on the Hydrogenation of CO<sub>2</sub> to Methanol*

Methanol is a key commodity used to produce acetic acid, formaldehyde, and a number of key chemical intermediate. Of particular interest is the synthesis of methanol from CO<sub>2</sub> not only as a way to mitigate this greenhouse gas but also because of the potential use of CO<sub>2</sub> as an alternative and economical feedstock. The combination of metal and oxide centers in the copper-ceria interface provides favorable reaction pathways for the CO<sub>2</sub>→CH<sub>3</sub>OH conversion not seen over conventional catalysts for methanol synthesis [1].

Using a combination of ambient-pressure X-ray photoelectron (Figure 1) and infrared spectroscopies, we investigated the interaction of CO<sub>2</sub> and CO<sub>2</sub>/H<sub>2</sub> mixtures with Cu(111), CeO<sub>2</sub>(111) and CeO<sub>x</sub>/Cu(111) surfaces at temperatures between 300

and 500 K [1]. Pure CO<sub>2</sub> did not adsorb on Cu(111) at these temperatures. On the



other hand, the adsorption of CO<sub>2</sub> on a CeO<sub>2</sub>(111) surface produced strongly bound carbonate (CO<sub>3</sub><sup>2-</sup>) species [1]. A carboxylate (CO<sub>2</sub><sup>δ-</sup>) species was detected in appreciable amounts only when ceria-copper interfaces were present in the catalyst. The low stability of the CO<sub>2</sub><sup>δ-</sup> species made it an excellent intermediate in the CO<sub>2</sub>→CH<sub>3</sub>OH conversion [1]. Indeed, the results of DFT calculations indicate that on a ceria-copper

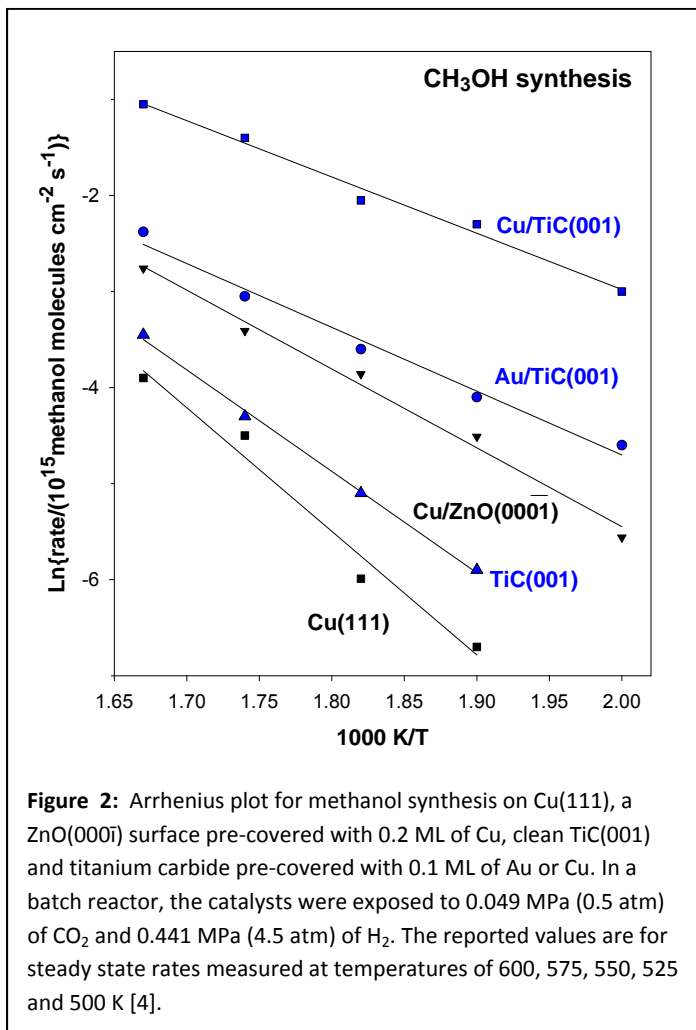
interface CO<sub>2</sub> is activated in a bent conformation and hydrogenated to yield a carboxyl OCOH species. A low energy barrier is associated with the OCOH → OC + OH transformation. Subsequent steps achieve the hydrogenation of CO to methanol through expected intermediates: HCO (formyl), H<sub>2</sub>CO (formaldehyde), and H<sub>3</sub>CO (methoxy). In general, our theoretical results indicated that the thermochemistry of the reaction steps associated with the formation of methanol on a ceria-copper interface is predominantly downhill with an overall exothermic process [1].

Our study illustrates the substantial benefits that can be obtained by properly tuning the properties of a metal-oxide interface in catalysts for methanol synthesis [1]. In a metal-oxide interface, one can have truly bifunctional sites which would be very difficult to generate on the surface of a pure metal or alloy systems.

*Activation of Noble Metals on Metal-Carbide Surfaces: Novel Catalysts for the CO<sub>2</sub> Hydrogenation and the Water-gas shift Reaction*

Transition-metal carbides exhibit broad and amazing physical and chemical properties. These properties may be viewed as resulting from a combination of those of covalent solids, ionic crystals and transition metals. High-resolution photoemission, scanning tunneling microscopy (STM) and first-principles periodic density-functional (DF) calculations have been used to study the interaction of metals of Groups 9, 10 and 11 with MC(001) (M= Ti, Zr, V, Mo) surfaces [2,3,4]. DF calculations give adsorption energies that range from 2 eV (Cu, Ag, Au) to 6 eV (Co, Rh, Ir) [3]. STM images show that Au, Cu, Ni and Pt grow on the carbide substrates forming two-dimensional islands at very low coverage, and three-dimensional islands at medium and large coverage [3]. In many systems, the results of DF calculations point to the preferential formation of admetal-C bonds with significant electronic perturbations in the admetal [2-4]. A comparison of the behavior of Au deposited on MC(001) (M= Ti, Mo, V, Zr) indicates that the electronic perturbations on the admetal vary depending on the nature of the carbide substrate [3]. TiC(001) and ZrC(001) transfer some electron density to the admetals facilitating bonding of the adatom with electron-acceptor molecules (CO, O<sub>2</sub>, C<sub>2</sub>H<sub>4</sub>, SO<sub>2</sub>, thiophene, etc) [3,4]. In general, the Au/TiC system is more chemically active than systems generated by depositing Au nanoparticles on oxide surfaces [2,3,4]. Thus, metal carbides are excellent supports for enhancing the chemical reactivity of noble metals.

Our studies indicate that the charge polarization undergone by small Cu and Au particles in contact with a TiC(001) surface makes them very active for CO<sub>2</sub> activation and the catalytic synthesis of methanol [4,30]. The binding energy of CO<sub>2</sub> on these systems is in the range of 0.6 to 1.1 eV, much larger than those observed on surfaces or nanoparticles of Cu and Au. Thus, in spite of the poor CO<sub>2</sub> hydrogenation performance of Cu(111) and Au(111), the Cu/TiC(001) and Au/TiC(001) systems display a catalytic activity for methanol synthesis substantially higher than that of conventional Cu/ZnO catalysts, see Figure 2 [4,30]. The turnover frequencies for methanol production on Cu/TiC(001) are 170-500 times much larger than on Cu(111) [4]. Thus, our study illustrates the advantages of using a metal carbide as a support for noble metals for CO<sub>2</sub> hydrogenation.



We have also found that the Au/TiC system is a very good catalyst for the low-temperature water-gas shift (CO + H<sub>2</sub>O → H<sub>2</sub> + CO<sub>2</sub>, WGS) reaction exhibiting turnover frequencies orders of magnitude larger than those observed for conventional metal/oxide catalysts [2]. The results of DFT calculations indicate that the WGS reaction follows an associative mechanism with a carboxyl OCOH species as a key intermediate [2]. The same intermediate is formed during the hydrogenation of CO<sub>2</sub> [30].

*Development of Techniques for In-situ Characterization of Powder Catalysts: Time-resolved PDF, XAFS/XRD, XAFS/IR and XAFS/Raman*

The development of techniques for characterizing the structural properties of catalysts under the high-pressure conditions of industrial processes is widely recognized as a top priority in the area of heterogeneous catalysis. In the last years, the Catalysis Group at BNL has been very active in developing instrumentation for the characterization of catalysts with pair-distribution function (PDF) analysis and the integration of XAFS and XRD or XAFS and IR or Raman [18-20,23,25]. The integration of IR or Raman with XAFS (Figure 3) allows a simultaneous

determination of the reaction intermediates on the surface and the chemical state and structure of the catalyst [23]. Raman spectroscopy adds sensitivity to crystallographic phase and long range order that both XANES and EXAFS are lacking. *In-situ* PDF has been used to study the structure of amorphous metal and metal oxide nanoparticles under reaction [31]. Using a XAFS/IR combination, we have investigated reaction mechanisms and correlations between structure/reactivity for CO oxidation [29].

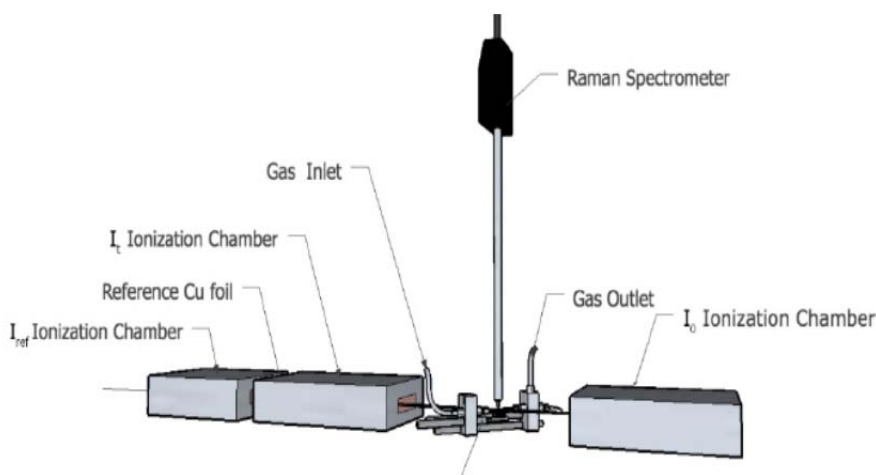


Figure 3. Instrumental set-up for combining XAFS and Raman [23].

### Publications acknowledging this grant in 2012-2015

1. Graciani, J., et al. *Science*, **2014**, *345*, 546-550.
2. Rodriguez, J., et al. *Angew. Chem. Int. Ed.* **2014**, *53*, 11270-11274.
3. Rodriguez, J.; Illas, F. *Physical Chemistry Chemical Physics*, **2012**, *14*, 427-438.
4. Vidal, A., et al., *Journal of Physical Chemistry Letters*, **2012**, *3*, 2275-2280.
5. Stacchiola, D.J., et al., *Chemical Reviews*, **2013**, *113*, 4373-4390.
6. Yao, S.Y., et al. *Physical Chemistry Chemical Physics*, 2014, *16*, 17183-17195.
7. Liu, P., *Journal of Physical Chemistry C*, **2012**, *116*, 25337-25343.
8. Mudiyansele, K., et al., *Angewandte Chemie Int. Ed.* **2013**, *52*, 5101-5105.

9. Mudiyansele, K., et al., *Topics in Catal.* **2015**, *58*, 271-280.
10. Dos Santos Politi, J.A., et al, *Phys. Chem. Chem. Phys.*, **2013**, *15*, 12617-12625.
11. Carrasco, J., et al., *Journal of Physical Chemistry C*, **2013**, *117*, 8241–8250.
12. Xu, W., et al., *ACS Catalysis*, **2013**, *3*, 975-984.
13. Yan, T., et al., *Journal of Catalysis*, **2012**, *294*, 216-222.
14. Wang, H., et al., *Journal of the American Chemical Society*, **2013**, *135*, 4149-4158.
15. Xu, W.; Ramirez, P.J.; Stacchiola, D.; Rodriguez, J.A.. *Catal. Lett.* **2014**, *144*, 1418-1424.
16. Posada-Perez, S.; Vines, F.; Ramirez, P.J.; Vidal, A.; Rodriguez, J.A. Illas, *F. Phys. Chem. Chem. Physics.* **2014**, *16*, 14912-14921
17. Asara, G., et al., *Journal of Physical Chemistry C*, **2014**, *118*, 19224-19231.
18. Frenkel, A.I.; Rodriguez, J.A.; Chen, J.G. *ACS Catalysis*, **2012**, *2*, 2269-2280.
19. Rodriguez, J. A.; Senanayake, S. D.; Stacchiola, D.; Liu, P.; Hrbek, J., *Acc. Chem. Res.*, **2014**, *47*, 773–782.
20. Rodriguez, J.A.; Hanson, J.C.; Chupas, P. *Goals and Challenges for the In-situ Characterization of Heterogeneous Catalysts*, in *In-situ Characterization of Heterogeneous Catalysts*, J.A. Rodriguez, J.C. Hanson, and P. Chupas, Editors. 2013, Wiley: New York.
21. Zhao, F., et al., *J. Phys. Chem. C*, **2014**, *118*, 2528–2538.
22. Kundu, S., et al., *Journal of Physical Chemistry C*, **2012**, *116*, 4767-4773.
23. Platolla, A., et al., *Topics in Catalysis*, **2013**, *56*, 896-904.
25. Rodriguez, J.A., et al., *Physical Chemistry Chemical Physics*, **2013**, *15*, 12004-12025.
26. Senenayake, S.D.; Stacchiola, D.; Rodriguez, J.A. *Accounts of Chemical Research*, **2013**, *46*, 1702-1711.
27. Johnston-Peck, A., et al., *Journal of Physical Chemistry C*, **2013**, *117*, 14463-14471.
28. Senanayake, S.D.; Rodriguez, J.A.; Stacchiola, D., *Topics in Catalysis*, **2013**, *56*, 1488-1498.
29. Yao, S.Y. et al., *ACS Catalysis*, **2014**, *4*, 1650-1661.
30. Rodriguez, J.A. et al., *Journal of Catalysis*, **2013**, *307*, 162-169.
31. Hanson, J.C. et al, *Catalysis Today*, **2014**, *229*, 64-71.
32. Guzman-Blas, R. et al, *Electrocatalysis*, **2014**, *5*, 50-61.

33. Wang, H. et al, *Angew. Chem. Int. Ed.* **2013**, *52*, 9210-9214.
34. Baber, A.E. et al, *Angew. Chem. Int. Ed.* **2014**, *53*, 5336-5340.
35. Zhao, F. et al., *Catal. Lett.* **2015**, *145*, 808-815.

**Nanocatalyst structure and  
composition during reaction**

Perla B. Balbuena<sup>1</sup>, Jose L. Gomez-  
Ballesteros<sup>1</sup> and Juan C. Burgos;<sup>1</sup> Pin Ann  
Lin<sup>2,3</sup> and Renu Sharma<sup>2</sup>

<sup>1</sup>Department of Chemical Engineering, Texas A& M University,  
College Station, TX 77843

<sup>2</sup>Center for Nanoscale Science and Technology, National Institute  
of Standards and Technology, Gaithersburg, MD 20899-6203

<sup>3</sup>University of Maryland – IREAP, College Park, MD 20742

**Presentation  
Abstract**

Transition metal nanoparticles deposited over MgO substrates are used as catalysts for the synthesis of single-walled carbon nanotubes via decomposition of  $C_2H_2$  over the catalytic surface. The dynamic evolution of nanocatalyst particle shape and carbon composition is examined through the initial stages of nucleation and growth of carbon structures via classical reactive and ab initio molecular dynamics simulations along with environmental tunneling electron microscope video imaging techniques. The analysis reveals a clear migration of carbon from the nanocatalyst/MgO interface, leading to a C-gradient showing C enrichment of the nanocatalyst layers in the immediate vicinity of the contact layer. However, as the metal nanocatalyst particle becomes saturated with carbon, a dynamic equilibrium is established with carbon precipitating on the surface and nucleating a carbon cap that is the precursor of nanotube growth. A carbon composition profile that decreases in the direction of the nanoparticle region in contact with the nucleating cap is revealed by the computational and experimental results. The development of the described carbon composition profile is synergic with a well-defined shape evolution of the nanocatalyst driven by the various opposite forces acting upon it both from the substrate and from the nascent carbon nanostructure. This new understanding suggests that tuning the nanoparticle/substrate interaction would provide unique ways of controlling the nanotube synthesis.

## DE-FG02-06ER15836: Modeling catalyzed growth of single-wall carbon nanotubes

**PI:** Perla B. Balbuena

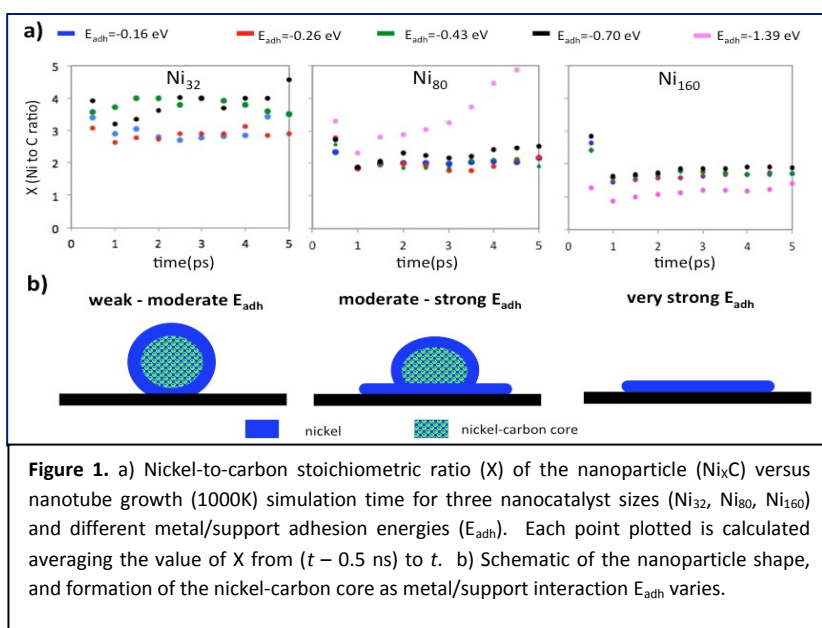
**Postdoc(s):** Juan Carlos Burgos

**Student(s):** Jose L. Gomez-Ballesteros

### RECENT PROGRESS

#### Insights into growth mechanism

Figure 1a shows the average stoichiometry of the nanoparticle ( $\text{Ni}_x\text{C}$ ) during growth (in 0.5 ns



intervals), suggesting that a Ni-C core is stabilized during induction/nucleation.

Various nanoparticle compositions resemble common carbide stoichiometries, such as  $\text{Ni}_3\text{C}$  (e.g.  $P6_322$  structure) and  $\text{Ni}_2\text{C}$  (e.g.  $Pbcn$  or  $Pnmm$  structures). A correlation between nanoparticle composition and  $E_{adh}$  can be explained by the sensitivity of nanoparticle shape to  $E_{adh}$  (Figure 1b). From the analyses of various Ni catalyst sizes and nickel/support interaction

strengths a seemingly layered structure of the nanoparticle emerges. The interlayer separation is more irregular than that for interlayer distance between (111) planes in nickel. However, the observed separation is also consistent with Ni-Ni interlayer distance ( $\sim 2.1$  Å) along the [001] direction in  $\text{Ni}_3\text{C}$  bainite ( $P6_322$ ) model structures. Furthermore, the Ni (001) plane in this structure is identical to that of (111) planes in pure fcc Ni. Hemiacarbide  $\text{Ni}_2\text{C}$  model structures ( $Pnmm$  and  $Pbcn$ ) also show a  $2.0$  Å Ni-Ni interlayer distance along the [100] direction. It is concluded that the formation of the Ni-C core has only a small effect in the Ni-Ni interlayer separation, which is consistent with Ni atoms approximately retaining their fcc arrangement, but also compatible with carbide structures of different stoichiometries. The latter statement may explain why no significant differences in Ni-Ni interlayer separation were found between  $\text{Ni}_{32}$ ,  $\text{Ni}_{80}$ , and  $\text{Ni}_{160}$  despite their different  $\text{Ni}_x\text{C}$  stoichiometry.

**Dynamics of defects on nanotube walls during CVD growth** Topological defects that nucleate in the nanotube wall relate to the catalyst shape and therefore to the metal-support interaction energy ( $E_{MS}$ ). The 5-7 type of defect was found in every nanotube grown from our reactive molecular dynamics (RMD) simulations independently of the  $E_{MS}$  value. As  $E_{MS}$  increases and the catalyst becomes flatter, 5-7 defects are more frequently found as a result of rapid detachment of carbon

rings and interrupted carbon diffusion (Figure 2). Although Stone-Wales (SW) defects can be found at low  $E_{MS}$  (associated with low amount of defects), their presence in the nanotube sidewall arises from 5-7's recombining into 5-7-7-5 arrangements. At even higher  $E_{MS}$ , 5 and 7-membered rings are no longer the exclusive source of topological defects on the structure. Flat catalysts lead to the formation of larger rings associated with vacancies and di-vacancies. Vacancy defects are more often found in nanotubes grown on bi/mono-layer catalysts. At these conditions, carbon caps lift-off so rapidly that they are not able to minimize dangling bond through structural rearrangements on the catalyst surface. Therefore, low coordinated carbon atoms were frequently observed in the tube sidewall during growth on catalysts with these particular shapes. Figure 3 illustrates a defect formation mechanism valid for vacancies and di-vacancies. The mechanism follows six steps after starting with the formation of nanotube edge delimited by carbon atoms potentially forming a defect. Rapid addition of catalyzed carbon to the edge as a result of high pressures, leads to the fast growth of carbon chains in close interaction with the support. Carbon chains formed in the second step bend as a consequence of substrate repulsion to neighbor carbon atoms. Highly unstable pentagons are formed due to rapid formation of rings, which leads to ring recombination into larger rings assisted by carbon diffusion on the catalyst surface. Part of the large

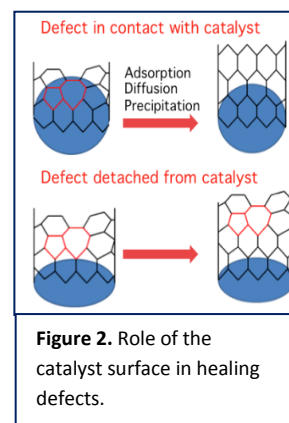


**Figure 2.** Role of the catalyst surface in healing defects.

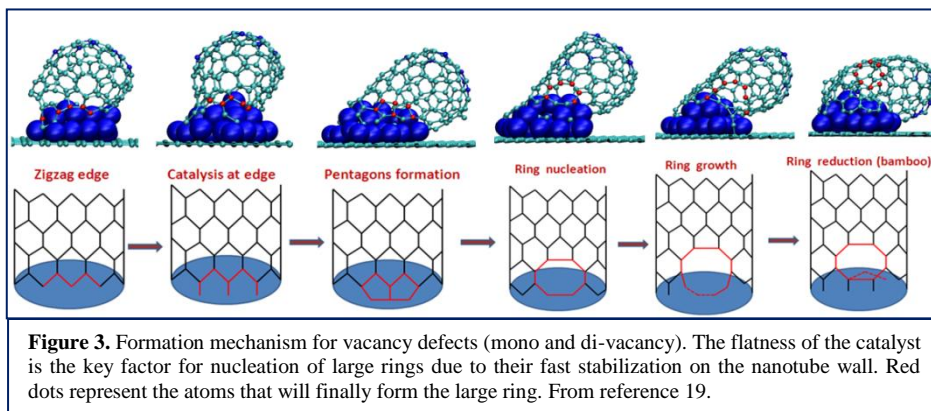


**Figure 3.** Formation mechanism for vacancy defects (mono and di-vacancy). The flatness of the catalyst is the key factor for nucleation of large rings due to their fast stabilization on the nanotube wall. Red dots represent the atoms that will finally form the large ring. From reference 19.

less stable carbon squares and triangles that end incorporated into a bigger carbon ring. However, very large rings are also unstable and low coordinated carbon atoms from the large ring try to interact with metal atoms at the top of the catalyst. This favors the ring size reduction by imposing a bamboo growth through formation of carbon chains at the inner part of the nanotube cap. Once the large ring lifts off from the catalyst surface eliminating any kind of interaction with it, the defect becomes stable and the catalytic healing is impossible. However, very large rings are also unstable and low coordinated carbon atoms from the large ring try to interact with metal atoms at the top of the catalyst. This favors the ring size reduction by imposing a bamboo growth through formation of carbon chains at the inner part of the nanotube cap. Once the large ring lifts off from the catalyst surface eliminating any kind of interaction with it, the defect becomes stable and the catalytic healing is impossible. This mechanism differs in some details for different growths at the same conditions. Intermediate states may vary

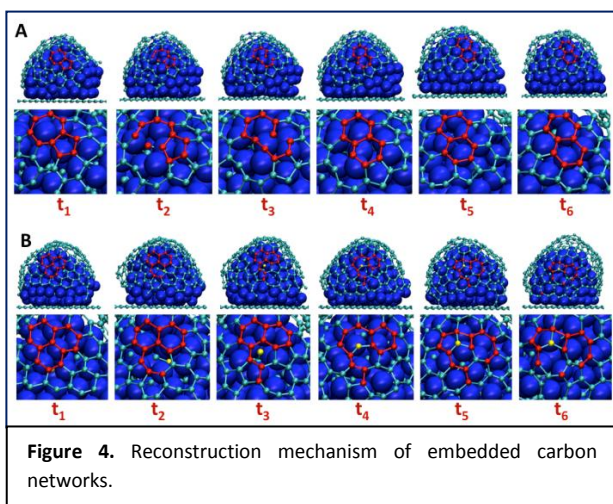


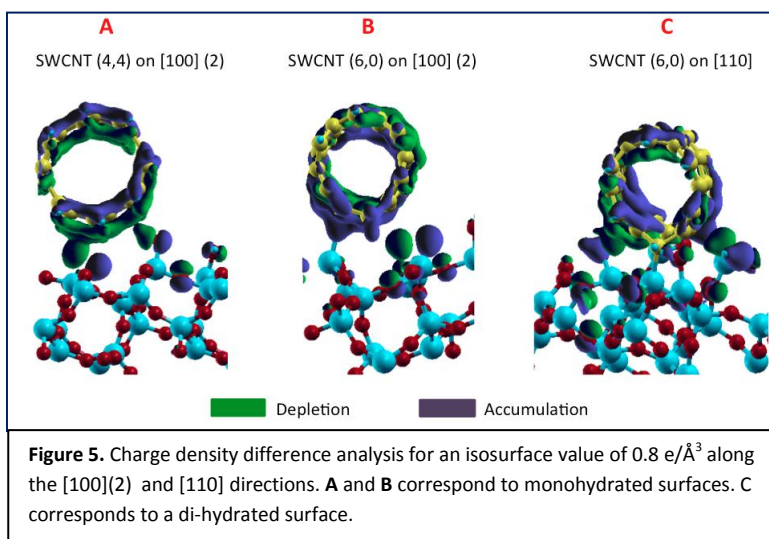
**Figure 4.** Reconstruction mechanism of embedded carbon networks.

(Figure 3), such as the number of pentagons formed at the edge, the size of the first ring, and/or the extent of ring growth and reduction. Nonetheless, the overall defect formation mechanism remains the same, and vacancy/di-vacancy defects are generally related to bamboo growth. This is in agreement with our previous results in which inner walls were grown only on flat catalysts at high metal-support interactions.

Enhanced surface areas of large catalyst particles not only assist defect healing but also favor defect formation. Hexagons embedded into a near perfect graphitic network are exposed to network reconstruction, as they remain deposited on the catalyst surface (Figure 4A). The stability of the hexagonal network might be then jeopardized by the high kinetic energy at the catalyst-cap interface and the mass transfer from the bulk of the catalyst toward the interface. As seen in Figure 5B, an embedded network comprising three adjacent hexagons ( $t_1$ ) is disrupted by surface diffusion and reorganization into a transitional 6-6-7 configuration ( $t_2$ ). The instability of this arrangement allows the reconfiguration of the network back to six adjacent hexagons ( $t_3$ ). A single carbon (yellow atom in Figure 4B) is precipitated into the nanotube-catalyst interface at  $t_3$  and favors breaking of a C-C bond in order to accommodate in the middle of two heptagons at  $t_4$ . After this event takes place, the original perfect hexagonal network is never recovered despite the probability for defect healing inherent to the cap-catalyst interaction. The carbon precipitation at the interface has a significant effect on the defect concentration.

### Factors that influence horizontal growth on quartz surfaces

Adsorption of nanotubes of various chiralities on a *mono-hydrated* surface (one water molecule per unit cell) revealed that the (4,4) armchair tube is not energetically favored for alignment along any direction. The metallic character of this tube and the significant differences in adsorption energy with respect to zigzag tubes, made evident the existence of an effect of the substrate on the preferential deposition of semiconducting tubes. In contrast, zigzag tubes were clearly favored to adsorb on the mono-hydrated surface of quartz, although SWCNTs (6,0) and (7,0) did not align preferentially along the same direction. For the SWCNT (7,0), the direction parallel to the [010](2) y-axis was found to be that of strongest adsorption energy as found previously on the clean (*non-hydrated*) ST-cut surface of quartz. Along this direction, nanotubes with a diameter within the range of the three nanotubes studied ( $\sim 5$  Å) were exposed to close interactions with low-coordinated Si and O atoms. In the hydrated surfaces, low saturated sites along that direction become saturated with products of water dissociation, i.e. having OH terminations side by side of the [010](2) direction. It is also remarkable that the nanotube (6,0) undergoes a very weak attraction along the same y direction. The nanotube (6,0) has a smaller diameter than the (7,0), which places it in disadvantage respect to the (7,0). This is because the [010](2) direction is characterized by



having a channel delimited by low-coordinated Si atoms at the topmost layer and the subsurface. A nanotube with a larger diameter is able to reach the effect of low-coordinated Si atoms at *both* sides of the channel. On the other hand, semiconducting (7,0) and metallic (4,4) have very similar diameters but different adsorption strengths on this direction, which confirms that the *electronic behavior of each nanotube defines its adsorption preferences*. A general scenario of depletion and accumulation of charges before and after

nanotube adsorption provides insightful information about the repulsive/attractive nature of each

interaction and the migration of charges upon adsorption. The results confirm the repulsion experienced by the (4,4) tube as charges are depleted at the interface and accumulated inside the nanotube, (Figure 5A). In the top half of the (4,4) nanotube, charges are also displaced in the positive direction of the z-axis. This overall charge shift in the SWCNT (4,4) denotes a strong repulsion undergone by the nanotube after contact with the surface that results in a displacement of carbon nuclei away from the surface. In contrast, SWCNT (6,0) shows the strongest adsorption energy along the same direction of the monohydrated surface, and allows a significant charge accumulation at the interface (Figure 5B). Electron cloud depletion at the interface was occasionally observed for hydrated surfaces, unlike the behavior on clean surfaces. Localized migration of charges away from the interface combined with accumulation at Si-C connections, are a result of structural deformation of strongly adsorbed nanotubes. As a consequence of these deformations, nuclei might move away from the surface at specific locations, such as stiff OH functional groups, and approach lower energy spots such as unsaturated Si sites. Therefore, simultaneous electron depletion *and* accumulation is observed at different points of the interface (Figure 5C). We conclude that low-coordinated Si atoms guide preferential alignment of carbon nanotubes on the ST-surface of quartz. It was previously reported that unsaturated O atoms at the surface were critical on defining preferential alignment through partial oxidation of nanotubes. Here we demonstrated that if the low-coordinated O is bonded to low-coordinated Si, as in the case of the ST-cut, the unsaturated Si is most likely to cause the attraction and charge concentration at the interface. These results can be extended to other silica surfaces no matter the spatial arrangement of atoms within the lattice. Only the coordination states of the Si and O atoms will define the adsorption strength of carbon nanotubes on the surface, and therefore, the surface concentration and distribution of this kind of atoms will establish the directions of *preferential alignment*.

### Nucleation of SWCNTs over $\text{Co}_2\text{C}$ supported on MgO

Anchoring of graphene on  $\text{Co}_2\text{C}$  (020) surfaces detected in 2D images by our experimental collaborators (R. Sharma et al., NIST) employing an environmental scanning transmission electron (ESTEM) equipped with an image corrector and a digital video recording system, and its detachment from  $\text{Co}_2\text{C}_{(210)}$  surfaces was explained by our DFT calculations, where we study the 3D graphene/nanoparticle interaction. The stable (020) and (210) surfaces are identified as Co and Co-C terminated respectively. It is found that the graphene sheet is almost flat and in close contact with

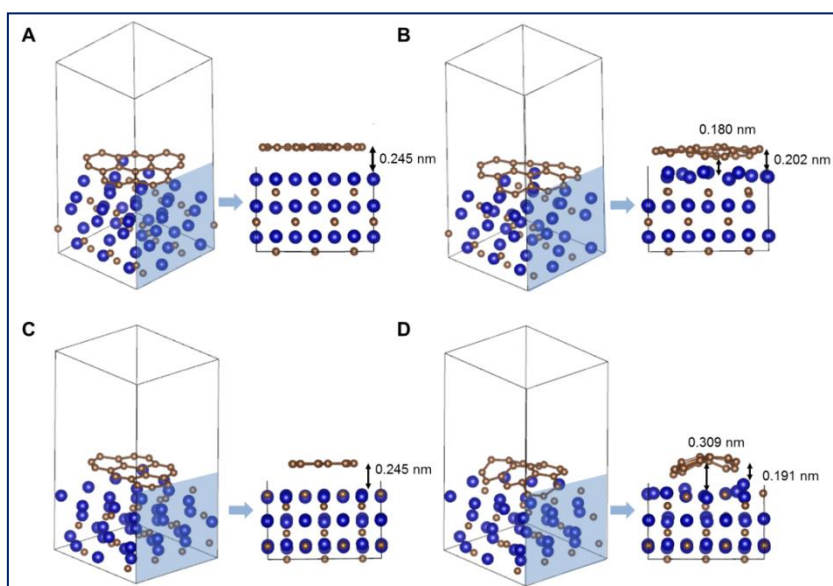


**Figure 6.** DFT simulation of graphene relaxation on  $\text{Co}_2\text{C}_{(020)}$  and  $\text{Co}_2\text{C}_{(210)}$  surfaces. (A, C) Graphene sheets initially placed at 0.245 nm from a Co terminated  $\text{Co}_2\text{C}_{(020)}$  surface and at the same distance from a Co-C terminated  $\text{Co}_2\text{C}_{(210)}$  surface. After relaxation of graphene on  $\text{Co}_2\text{C}$  surfaces, distance changes to 0.180 nm - 0.202 nm from  $\text{Co}_2\text{C}_{(020)}$  (B) and to 0.191 nm to 0.309 nm from  $\text{Co}_2\text{C}_{(210)}$  (D). For each panel, a 3D view (left) and a side view are proposed for visual clarity.

Co terminated (020) surface. The calculated distance between graphene and the NP are shown in Fig. 6B. On the other hand, it forms a dome on Co-C terminated (210) surface (Figure 6D). These values are in close agreement with experimental measurements. The calculated work of adhesion for graphene on Co terminated (020) surface is higher than for Co-C terminated (210) surface with corresponding values of adhesion to be  $-26.5 \text{ eV nm}^{-2}$  and  $-14.4 \text{ eV nm}^{-2}$ , respectively.

Therefore, the NP surface termination plays a

critical role in determining the work of adhesion between graphene and the NP: a Co terminated surface favors graphene anchoring and a Co-C terminated surface promotes graphene detachment and cap lift-off. In both simulation and experiment, the central part of the graphene sheet is observed to be lifted from the (210) surface, but the edge of the graphene sheet is maintained in close contact with (210) forming a convex-like structure. Despite a low work of adhesion, the growing structure remains attached. This can be explained by the presence of dangling bonds at the graphene edges which tend to bind with the NP to be stabilized.

### **Publications Acknowledging this Grant in 2012-2015**

#### *(1) Sole funding by DOE-BES and this particular grant*

1. D. A. Gómez-Gualdrón, G. D. McKenzie, J. F. J. Alvarado, and Perla B. Balbuena, "Dynamic Evolution of Supported Metal Nanocatalyst/Carbon Structure during Single-Walled Carbon Nanotube Growth," *ACS Nano*, 6, 720-735, (2012).
2. D. A. Gómez-Gualdrón and P. B. Balbuena, "Characterization of Carbon Atomistic Pathways during Single-Walled Carbon Nanotube Growth on Supported Metal Nanoparticles", *Carbon*, 57, 298-309, (2013)
3. D. A. Gómez-Gualdrón, J. M. Beetge, J. C. Burgos, and P. B. Balbuena, "Effects of precursor type on the CVD growth of single-walled carbon nanotubes," *J. Phys. Chem. C*, 117, 10397-10409, (2013);
4. D. A. Gómez-Gualdrón, J. M. Beetge, and P. B. Balbuena, "Characterization of metal nanocatalyst state and morphology during simulated single-walled carbon nanotube growth," *J. Phys. Chem. C*, 117, 12061-12070, (2013);
5. J. C. Burgos and P. B. Balbuena, "Preferential Adsorption of Zigzag Single-Walled Carbon Nanotubes on the ST-cut of Quartz," *J. Phys. Chem. C*, 117, 4639-4646, (2013).
6. J. C. Burgos, E. Jones, and P. B. Balbuena, "Dynamics of Topological Defects in Single-Walled Carbon Nanotubes during Catalytic Growth," *J. Phys. Chem. C*, 118, 4808-4817, (2014).
7. J. C. Burgos and P. B. Balbuena, "Engineering Preferential Adsorption of Single-Walled Carbon Nanotubes on Functionalized ST-cut Surfaces of Quartz," *ACS Appl. Mater. Inter.*, 6 (15) 12665-12673, (2014).
8. M. Picher, P. A. Linn, J. L. Gómez-Ballesteros, P. B. Balbuena, and R. Sharma, "Nucleation of Graphene and its Conversion to Single-Walled Carbon Nanotubes," *Nano Lett.*, 14, 6104-6108, (2014)
9. Jose L. Gomez-Ballesteros and Perla B. Balbuena, "Structure and dynamics of metallic and carburized catalytic Ni nanoparticles: effects on growth of single-walled carbon nanotubes," *Phys. Chem. Chem. Phys.*, in press, DOI: 10.1039/c5cp00835b.

#### *(2) Joint funding by DOE (including other DOE grants) and other Federal or Non-Federal Sources*

J. L. Gómez-Ballesteros, A. Callejas-Tovar, L. A. F. Coelho, and P. B. Balbuena, "Molecular dynamics studies of graphene exfoliation using supercritical CO<sub>2</sub>," in J. M. Seminario (Editor) "Design and applications of nanomaterials for devices and sensors," V. 16, p. 171-183, (2014).

## Near Room Temperature Electrochemical Upgrading of Methane to Oxygenate Fuels

William Mustain, Associate Professor and Associate Department Head

Department of Chemical & Biomolecular Engineering

University of Connecticut

DOE Award Number: DE-SC0010531

Methane is one of the most important industrial gases. Not only is it directly used for heat generation, it is the primary feedstock for several of the most widely produced commodity chemicals including hydrogen, ammonia, methanol and formaldehyde. Methane activation and conversion is typically accomplished through syngas production by steam reforming which requires high pressure (typically above 10 bar) and high temperature (above 650 °C). The syngas product is an over oxidized product, necessitating reduction back to methanol or other desired oxygenates. This process involves excessive intermediate reaction steps and has a large energy requirement

Since they allow for control of the catalyst surface free energy, electrochemical methods have the potential to reduce the thermal and overall energy barrier to convert methane to oxygenates.<sup>1, 4, 5</sup> Processing conditions for electrosynthesis can also be tailored to selectively and dynamically change the reaction selectivity, meaning that the several unit operations that are currently required for the conversion of methane to methanol or formaldehyde might be reduced to a single step. Methanol is a particularly high value target; it is used to synthesize numerous products, and has been touted as an important energy carrier of the future. Its high energy density and liquid state in atmospheric conditions make it ideal for stable transportation and storage that is compatible with existing petroleum infrastructure.<sup>6, 7</sup>

In this study, we will present two systems that are able to directly convert methane to methanol at low temperatures in alkaline media. Cell geometries, overall trends and variations in catalytic performance and the product profile will be presented while controlling the reacting environment. Trends from this promising technology will help to guide future cell design with the prospect of improving the applications for methane, natural gas resources and CO<sub>2</sub>.

### References:

1. N. Spinner and W. E. Mustain, *J. Electrochem. Soc.*, **160**, 11 (2013).
2. R. G. Bergman, *Nature (London, U. K.)*, **446**, 7134 (2007).
3. T. V. Choudhary and V. R. Choudhary, *Angew. Chem., Int. Ed.*, **47**, 10 (2008).
4. N. Spinner and W. E. Mustain, *J. Electrochem. Soc.*, **159**, 12 (2012).
5. N. Spinner and W. E. Mustain, *Electrochim. Acta.*, **56**, 16 (2011).
6. G. A. Olah, A. Goeppert and S. K. Surya-Prakash, *Beyond oil and gas: the methanol economy*, Wiley-VCH (2009).
7. G. A. Olah, *Angew Chem Int Ed Engl.*, **44**, 18 (2005).

This page is intentionally blank.

**Tuesday Evening**

**V. Advances in  
Molecular and Hybrid  
Catalysis**

This page is intentionally blank.

## Transition Metal Catalyzed Hydroarylation of Olefins

T. Brent Gunnoe<sup>a</sup>, Bradley A. McKeown<sup>a</sup>, Samantha A. Burgess<sup>a</sup>, Evan E. Joslin<sup>a</sup>, Benjamin A. Vaughan<sup>a</sup>, Michael S. Webster-Gardiner<sup>a</sup>, Thomas R. Cundari<sup>b</sup>

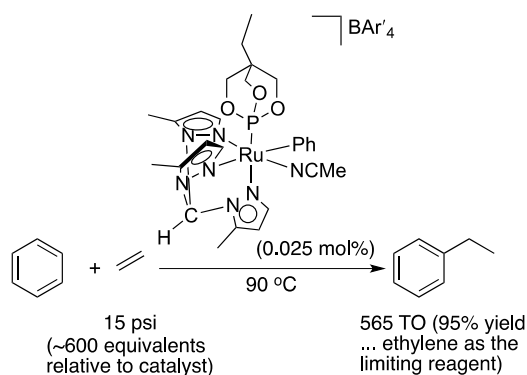
<sup>a</sup> Department of Chemistry, University of Virginia, Charlottesville, VA 22904

<sup>b</sup> Center for Advanced Scientific Computing and Modeling (CASCAM), Department of Chemistry, University of North Texas, Denton, TX 76203

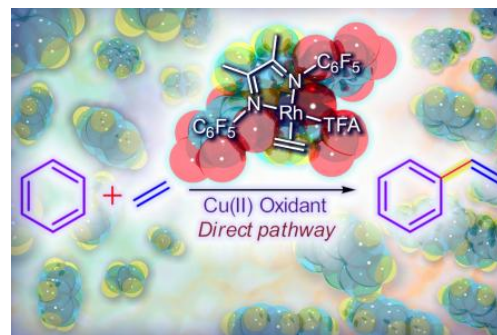
## Presentation Abstract

The selective catalytic functionalization of C–H bonds of hydrocarbons remains one of the foremost challenges facing synthetic chemists. The ability to selectively manipulate C–H bonds of arenes, alkanes and more complex organic molecules would open the door to a wide range of useful synthetic transformations. For example, the addition of aromatic C–H bonds across olefin C=C bonds, olefin hydroarylation, provides an atom economical reaction with broad potential including applications in both commodity

scale processes as well as fine chemical synthesis. We have been studying olefin hydroarylation (to produce alkyl aromatics) and oxidative olefin hydroarylation (to produce vinyl aromatics) catalyzed by well-defined Fe, Ru, Rh and Pt catalysts. For  $\text{TpRu(L)(NCMe)Ph}$  (Tp = hydridotris(pyrazolyl)borate; L = CO,  $\text{PMe}_3$ ,  $\text{P(OCH}_2)_3\text{CEt}$ ,  $\text{P}(N\text{-pyrrolyl})_3$ , etc.) catalyst precursors, which provide a range of Ru(III/II) redox potentials (vs. NHE) that span from  $\sim 0.3$  to 1.0 V, we have quantified the impact of the donor ability of the ligand "L" on the rate of stoichiometric benzene C–H activation and elucidated the primary catalyst deactivation pathway. As the donor ability of the ligand L is increased, ethylene C–H activation competes with ethylene insertion and results in the formation of very stable  $\eta^3$ -ally complexes. Our studies predicted that replacing anionic Tp ligands with charge-neutral tris(pyrazolyl)alkane ligands, to give overall cationic Ru(II) complexes, would provide increased catalyst longevity. In fact, using  $[(\text{HC}(\text{pz}'_3)\text{Ru}(\text{P}(\text{OCH}_2)_3\text{CEt})(\text{NCMe})\text{Ph})][\text{BAR}'_4]$  [ $\text{HC}(\text{pz}'_3)$  = tris(3,5-dimethylpyrazolyl)methane] as catalyst precursor gives > 500 turnover numbers (TONs) of ethylbenzene formation ( $\sim 95\%$  yield) while the corresponding  $\text{TpRu}(\text{P}(\text{OCH}_2)_3\text{CEt})(\text{NCMe})\text{Ph}$  complex gives 20 TONs under the same conditions.



For Pt(II) catalysts of the type  $[(^x\text{bpy})\text{Pt}(\text{Ph})(\text{THF})]^+$  ( $^x\text{bpy}$  = 4,4'-disubstituted-2,2'-dipyridyl ligands), kinetic studies suggest that catalyst deactivation occurs through a bimolecular pathway that suggests the possible formation of Pt(s). We hypothesized that Rh(I) catalysts would be less likely to decompose by reduction to elemental metal [i.e., Pt(s) or Rh(s)] and designed electron-deficient fluorinated ligands that would stabilize lower oxidation states under oxidizing conditions. Recently, we reported that  $(^{\text{Fl}}\text{DAB})\text{Rh}(\text{TFA})(\eta^2\text{-C}_2\text{H}_4)$  [ $^{\text{Fl}}\text{DAB}$  = *N,N'*-bis(pentafluorophenyl)-2,3-dimethyl-1,4-diaza-1,3-butadiene; TFA = trifluoroacetate] converts benzene, ethylene and Cu(II) acetate to styrene, Cu(I) acetate, and acetic acid with high selectivity and yields  $\geq 95\%$ . Turnover numbers > 800 have been demonstrated with catalyst stability up to 96 hours.



**Grant Number:** DE-SC0000776

**Grant Title:** Development of Transition Metal Catalysts for the Functionalization of Carbon-Hydrogen Bonds: Fundamental Studies of Catalytic Hydroarylation of Olefins

**PI:** T. Brent Gunnoe

**Postdocs:** N/A

**Students:** Bradley McKeown (G), Evan Joslin (G), Steve Kalman (G), Benjamin Vaughan (G), Max Friedfeld (U), Anna Brosnahan (U), Daniel Tate (U)

**Collaborators:** Thomas R. Cundari (University of North Texas), Daniel H. Ess (Brigham Young University), Brian Trewyn (Colorado School of Mines)

## Recent Progress

### Goal and Major Advancements

The goal of this project is to increase understanding of fundamental aspects surrounding homogeneous catalysts for the addition of carbon-hydrogen bonds across carbon-carbon multiple bonds. These studies will facilitate the rational design of future catalysts for the hydroarylation or hydroalkylation of carbon-carbon multiple bonds. Through development of mechanistic details, in the past funding period we have developed three of the most efficient *molecular* catalysts for the conversion of benzene and ethylene to ethylbenzene or styrene: 1. The cationic Ru(II) complex  $[(\text{HC}(\text{pz}')_3)\text{Ru}(\text{P}(\text{OCH}_2)_3\text{CEt})(\text{NCMe})\text{Ph}][\text{BAR}'_4]$  [ $\text{HC}(\text{pz}')_3$  = tris(3,5-dimethylpyrazolyl)methane]. 2. The Pt(II) complex  $[(\text{dpm})\text{Pt}(\text{THF})\text{Ph}]^+$  (dpm = 2,2'-dipyridylmethane). 3.  $(^{\text{F}}\text{DAB})\text{Rh}(\text{TFA})(\eta^2\text{-C}_2\text{H}_4)$  [ $^{\text{F}}\text{DAB}$  = *N,N'*-bis(pentafluorophenyl)-2,3-dimethyl-1,4-diaza-1,3-butadiene; TFA = trifluoroacetate].

## Recent Progress

**Objective 1.** Study catalytic olefin hydroarylation using  $\text{Ru}^{\text{II}}$  catalysts supported by poly(pyrazolyl) ligands with similar or reduced electron density relative to  $\text{TpRu}(\text{CO})(\text{NCMe})\text{Ph}$ .

Previous studies have indicated the potential for increased catalyst longevity upon moving from charge neutral  $\text{TpRu}(\text{L})(\text{NCMe})\text{Ph}$  catalyst precursors to cationic variants coordinated by poly(pyrazolyl)alkane ligands (rather than the anionic Tp ligand). We demonstrated

that heating the Ru(II) cation  $[(\text{C}(\text{pz})_4)\text{Ru}(\text{P}(\text{OCH}_2)_3\text{CEt})(\text{NCMe})\text{Me}]^+$  (pz = pyrazolyl) results in intramolecular C–H activation of a pyrazolyl 5-position C–H bond. Thus, we synthesized the 3,5-dimethyl variant  $[(\text{HC}(\text{pz}')_3)\text{Ru}(\text{P}(\text{OCH}_2)_3\text{CEt})(\text{NCMe})\text{Ph}][\text{BAR}'_4]$  [ $\text{HC}(\text{pz}')_3$  = tris(3,5-dimethylpyrazolyl)methane] to protect against C–H activation of the pyrazolyl 5-position C–H bond. Comparison of the TONs for ethylene hydrophenylation by  $\text{TpRu}(\text{P}(\text{OCH}_2)_3\text{CEt})(\text{NCMe})\text{Ph}$  and  $[(\text{HC}(\text{pz}')_3)\text{Ru}(\text{P}(\text{OCH}_2)_3\text{CEt})(\text{NCMe})\text{Ph}][\text{BAR}'_4]$  confirmed our hypothesis. The best TON for  $\text{TpRu}(\text{P}(\text{OCH}_2)_3\text{CEt})(\text{NCMe})\text{Ph}$  is 20 (24 h, 90 °C, 0.025 mol% catalyst, 15 psi  $\text{C}_2\text{H}_4$ ). In contrast,  $[(\text{HC}(\text{pz}')_3)\text{Ru}(\text{P}(\text{OCH}_2)_3\text{CEt})(\text{NCMe})\text{Ph}][\text{BAR}'_4]$  gives 565 TONs under these same conditions, which is a 28-fold improvement upon replacing Tp with a charge neutral tris(pyrazolyl)alkane ligand. Also, the increased stability of  $[(\text{HC}(\text{pz}')_3)\text{Ru}(\text{P}(\text{OCH}_2)_3\text{CEt})(\text{NCMe})\text{Ph}][\text{BAR}'_4]$  allows catalysis at higher temperatures, which can be used to overcome the slightly lower activity compared to  $\text{TpRu}(\text{L})(\text{NCMe})\text{Ph}$  catalysts. At 150 °C,  $[(\text{HC}(\text{pz}')_3)\text{Ru}(\text{P}(\text{OCH}_2)_3\text{CEt})(\text{NCMe})\text{Ph}][\text{BAR}'_4]$  is an effective catalyst, and the

**Table.** Comparison of TOF for ethylbenzene production for catalytic hydrophenylation of ethylene using Ru(II) complexes.

Catalyst	Temp (°C)	TOF (s <sup>-1</sup> )	rel TOF
$[(\text{HC}(\text{pz}^5)_3)\text{Ru}(\text{P}(\text{OCH}_2)_3\text{CEt})(\text{NCMe})\text{Ph}][\text{BAR}'_4]^{\text{a}}$	90	$3.6 \times 10^{-4}$	1
$\text{TpRu}(\text{P}(\text{OCH}_2)_3\text{CEt})(\text{NCMe})\text{Ph}^{\text{a}}$	90	$4.8 \times 10^{-4}$	1.3
$[(\text{HC}(\text{pz}^5)_3)\text{Ru}(\text{P}(\text{OCH}_2)_3\text{CEt})(\text{NCMe})\text{Ph}][\text{BAR}'_4]^{\text{b}}$	105	$3.2 \times 10^{-3}$	9
$[(\text{HC}(\text{pz}^5)_3)\text{Ru}(\text{P}(\text{OCH}_2)_3\text{CEt})(\text{NCMe})\text{Ph}][\text{BAR}'_4]^{\text{b}}$	150 <sup>c</sup>	$2.0 \times 10^{-2}$	56
$[(\text{HC}(\text{pz}^5)_3)\text{Ru}(\text{P}(\text{OCH}_2)_3\text{CEt})(\text{NCMe})\text{Ph}][\text{BAR}'_4]^{\text{b}}$	175 <sup>c</sup>	$2.1 \times 10^{-2}$	58

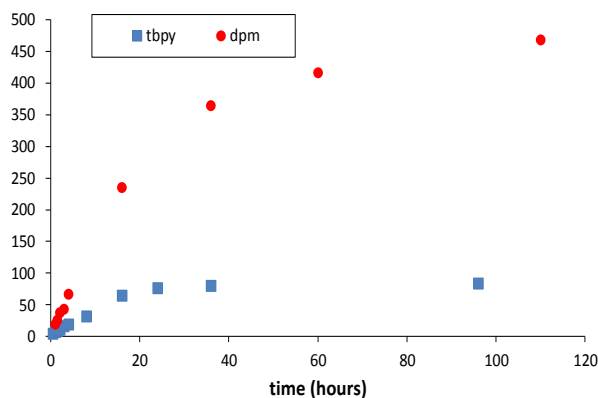
<sup>a</sup>TOF calculated after 4 h at 90 °C with 15 psi  $\text{C}_2\text{H}_4$  and 0.025 mol% of catalyst. <sup>b</sup>TOF calculated after 4 h with 15 psi  $\text{C}_2\text{H}_4$  and 0.01 mol% of catalyst. <sup>c</sup>Catalyst deactivation is significant, and TOF is a lower limit.

rate is ~42 times faster than using  $\text{TpRu}(\text{P}(\text{OCH}_2)_3\text{CET})(\text{NCMe})\text{Ph}$  at its optimized conditions at 90 °C (see Table).

**Objective 2.** Continue to study the influence of ancillary ligands on  $\text{Pt}^{\text{II}}$  catalyzed olefin hydroarylation using chelating *N,N*- and related chelating ligands.

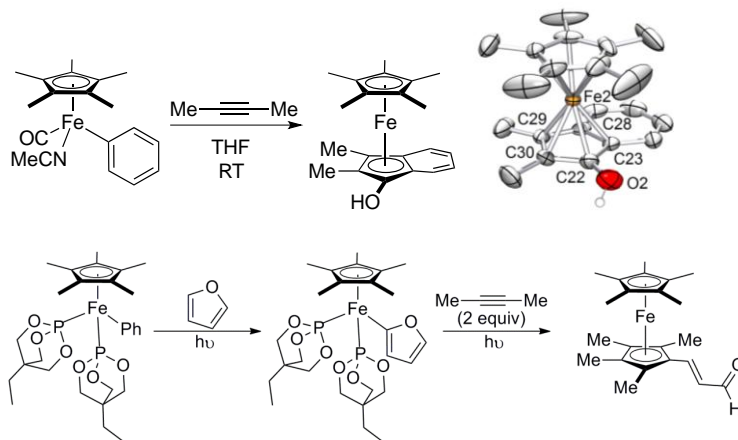
A detailed mechanistic study of ethylene hydrophenylation using  $[(^{\text{b}}\text{bpy})\text{Pt}(\text{Ph})(\text{L})]^+$  ( $^{\text{b}}\text{bpy}$  = 4,4'-di-tert-butyl-2,2'-bipyridyl;  $\text{L}$  = THF,  $\text{NC}_5\text{F}_5$ , or  $\text{NCMe}$ ) complexes has been completed. Recently, we demonstrated that selectivity for vinyl arene versus alkyl arene production can be controlled by the donor ability of 4/4'-substituents for  $[(^{\text{x}}\text{bpy})\text{Pt}(\text{Ph})(\text{L})]^+$  ( $^{\text{x}}\text{bpy}$  = 4,4'-X-2,2'-bipyridyl) catalysts for which the 4/4' "X" substituents are varied among  $^t\text{Bu}$ , H, OMe,  $\text{NO}_2$ , Br and  $\text{CO}_2\text{Et}$ . Also, substituting the 2,2'-bipyridyl ligand with 2,2'-dipyridylmethane (dpm) results in a substantial increase in catalyst efficiency. Using the dpm catalyst precursor  $[(\text{dpm})\text{Pt}(\text{THF})\text{Ph}]^+$  provides a TON of ~470, which, to our knowledge, is comparable to the best molecular catalysts for ethylene hydrophenylation by a non-acidic pathway. Interesting analyses of the elementary steps of the catalytic cycle (e.g., ethylene insertion and benzene C–H activation) demonstrate that the larger chelate ring of the dpm ligand provides an entropic advantage compared to  $^{\text{b}}\text{bpy}$ , which results in increased catalytic activity at elevated temperatures.

**Figure.** Comparison of TO versus time for ethylene hydrophenylation (100 °C) catalyzed by  $[(\text{N}\sim\text{N})\text{Pt}(\text{Ph})(\text{THF})]^+$  ( $\text{N}\sim\text{N}$ ) =  $^{\text{b}}\text{bpy}$  (■); dpm (●). 0.01 mol % Pt in  $\text{C}_6\text{H}_6$  with 0.1 MPa  $\text{C}_2\text{H}_4$ .



**Objective 3.** Extend chemistry of  $(^{\text{x}}\text{bpy})\text{Pt}^{\text{II}}$  to  $\text{Rh}^{\text{I}}$  catalysts.

Preliminary calculations suggest that  $\text{Rh}^{\text{I}}$  catalysts should have lower overall activation barriers (compared with analogous  $\text{Pt}^{\text{II}}$  catalysts) for olefin hydroarylation, and we believed that  $\text{Rh}^{\text{I}}$  catalysts would be advantageous due to enhanced thermal stability for oxidative olefin hydroarylation. The  $\text{Rh}$  catalyst  $(^{\text{F}}\text{DAB})\text{Rh}(\text{TFA})(\eta^2\text{-C}_2\text{H}_4)$  [ $^{\text{F}}\text{DAB}$  = *N,N'*-bis(pentafluorophenyl)-2,3-dimethyl-1,4-diaza-1,3-butadiene; TFA = trifluoroacetate] converts benzene, ethylene and  $\text{Cu}(\text{II})$  acetate to styrene,  $\text{Cu}(\text{I})$  acetate, and acetic acid with 100% selectivity and yields  $\geq 95\%$ . Turnover numbers > 800 have been demonstrated with catalyst stability up to 96 hours.



**Objective 4.** Begin to pursue catalysts for olefin hydroarylation based on first-row transition metals. A logical entry point is to extend our efforts on  $\text{Ru}^{\text{II}}$  catalysts to  $\text{Fe}^{\text{II}}$  catalysts.

Using  $\text{Cp}^*\text{Fe}(\text{CO})(\text{NCMe})\text{Ph}$  ( $\text{Cp}^*$  = pentamethylcyclopentadienyl) we have demonstrated that  $\text{Fe}(\text{II})$  is capable of

regioselective aromatic C–H activation at temperatures  $\leq 50$  °C. Kinetic studies, regioselectivities, isotopic labeling and computational studies are consistent with an Fe-mediated C–H activation without the formation of free radicals. In addition, new Fe-mediated C–C coupling reactions have been discovered. Extension of these reactions toward catalytic processes is being pursued.

### Publications (2012 – 2015)

14. "A Rhodium Catalyst for Single-Step Styrene Production" Vaughan, B. A., Webster-Gardiner, M. S., Cundari, T. R.\*, Gunnoe, T. B.\* *Science* **2015**, *348*, 421-424. This manuscript was highlighted in *Chemical and Engineering News* **2015**, *93* (17), 26.
13. "Phosphine and *N*-Heterocyclic Carbene Ligands on Pt(II) Shift Selectivity from Ethylene Hydrophenylation toward Benzene Vinylation" Brosnahan, A. M., Talbot, A., McKeown, B. A., Kalman, S. E., Gunnoe, T. B.\*, Ess, D. H.\*, Sabat, M. Manuscript accepted *J. Organomet. Chem.* **2015** (invited contribution for special issue in memoriam of Alexander E. Shilov)
12. "Formation of Hydroxyindenyl and Vinylidene Ligands by Reaction of Internal Alkynes with Cp\*Fe(CO)(NCMe)Ph" Kalman, S. E., Gunnoe, T. B.\*, Sabat, M. *Organometallics* **2014**, *33*, 5457-5463.
11. "Hydrophenylation of Ethylene using a Cationic Ru(II) Catalyst: Comparison to a Neutral Ru(II) Catalyst" Burgess, S. A., Joslin, E. E., Gunnoe, T. B.\*, Cundari, T. R.\*, Sabat, M., Myers, W. H. *Chem. Sci.* **2014**, *5*, 4355-4366.
10. "C–H Activation of Pyrazolyl Ligands by Ru(II)" Joslin, E. E., Quillian, B., Gunnoe, T. B.\*, Cundari, T. R.\*, Sabat, M., Myers, W. H. *Inorg. Chem.* **2014**, *53*, 6270-6279.
9. "Pt(II) Catalyzed Hydrophenylation of  $\square$ -Olefins: Variation of Linear:Branched Products as a Function of Ligand Donor Ability" McKeown, B. A., Prince, B. M., Ramiro, Z., Gunnoe, T. B.\*, Cundari, T. R.\* *ACS Catalysis* **2014**, *4*, 1607-1615.
8. "Control of Olefin Hydroarylation Catalysis via a Sterically and Electronically Flexible Pt<sup>II</sup> Catalyst Scaffold" McKeown, B. A., Gonzalez, H. E., Michaelos, T., Gunnoe, T. B.\*, Cundari, T. R.\*, Crabtree, R. H., Sabat, M. *Organometallics* **2013**, *32*, 3903-3913.
7. "Pt<sup>II</sup> Catalyzed Ethylene Hydrophenylation: Influence of Dipyridyl Chelate Ring Size on Catalyst Activity and Longevity" McKeown, B. A., Gonzalez, H. E., Gunnoe, T. B.\*, Cundari, T. R.\*, Sabat, M. *ACS Catalysis* **2013**, *3*, 1165–1171.
6. "Pt<sup>II</sup> Catalyzed Ethylene Hydrophenylation: Switching Selectivity between Alkyl and Vinyl Benzene Production" McKeown, B. A., Gonzalez, H. E., Friedfeld, M. R., Brosnahan, A. M., Gunnoe, T. B.\*, Cundari, T. R.\*, Sabat, M. *Organometallics* **2013**, *32*, 2857-2865.
5. "Facile and Regioselective C–H Bond Activation of Aromatic Substrates by an Fe(II) Complex Involving a Spin-Forbidden Pathway" Kalman, S. E., Petit, A., Gunnoe, T. B.\*, Ess, D. H.\*, Cundari, T. R.\*, Sabat, M. *Organometallics* **2013**, *32*, 1797-1806.
4. "2,2,2-Tris(pyrazolyl)ethoxide (Ep<sup>ox</sup>) Ruthenium (II) Complexes, (Ep<sup>ox</sup>)RuCl(L)(L'): Synthesis, Structure and Reactivity" Quillian, B., Joslin, E. E., Gunnoe, T. B.\*, Sabat, M. *Inorg. Chem.* **2013**, *52*, 1113-1121.
3. "Catalytic Hydroarylation of Ethylene using TpRu(L)(NCMe)Ph (L = 2,6,7-Trioxa-1-phosphabicyclo[2,2,1]heptane): Comparison to TpRu(L')(NCMe)Ph Systems (L' = CO, PMe<sub>3</sub> or P(OCH<sub>2</sub>)<sub>3</sub>CEt)" Joslin, E. E., McMullin, C. L., Gunnoe, T. B.\*, Cundari, T. R.\*, Sabat, M., Myers, W. H. *Organometallics* **2012**, *31*, 6851-6860.
2. "Coordination Chemistry of 4-Methyl-2,6,7-Trioxa-1-phosphabicyclo[2,2,1]heptane: Preparation and Characterization of Ru(II) Complexes" Joslin, E. E., McMullin, C. L., Gunnoe, T. B.\*, Cundari, T. R.\*, Sabat, M. *Inorg. Chem.* **2012**, *51*, 4791-4801.
1. "DFT Study of Group 8 Catalysts for the Hydrophenylation of Ethylene: Influence of Ancillary Ligands and Metal Identity" Morello, G. R., Cundari, T. R.\*, Gunnoe, T. B.\* *J. Organomet. Chem.* **2012**, *697*, 15-22.

**Organic-Ligand Control of  
Binding in Supported  
Molecular Cluster Catalysts**

Prof. Alexander Katz  
Department of Chemical and Biomolecular Engineering  
University of California, Berkeley

**Presentation Abstract**

The unique ability of sterically bulky calixarene ligands to offer accessibility to open “coordinatively unsaturated” sites of metal clusters while also stabilizing such clusters allows new control of molecular binding and, as such, potentially offers methods for imparting selective catalysis on metal surfaces. We specifically demonstrate that the apical position of supported molecular tetrairidium clusters consisting of three bound calixarene phosphine ligands on the basal plane binds ethylene and catalyzes its hydrogenation. In contrast, basal-plane P-substituted sites on the same cluster are unable to do this binding and catalysis due to electronic rather than steric factors. We also demonstrate that silica-supported closed clusters consisting of  $\text{Ir}_4(\text{CO})_9\text{L}_3$  (L = phosphine) bind dioxygen, which results in a catalysis rate increase of 100 fold for ethylene hydrogenation, whereas the activity of its isostructural L = phosphite analogue under similar conditions remained the same upon exposure to oxygen. The two examples above highlight organic ligand mediated binding of molecules to the metal core.

**Grant DEFG02-05ER15696: Control  
of Supported Molecular Catalysis  
Using Metallocalixarene Active Sites**

**PI:** Alexander Katz

**Postdoc(s):** Andrew Solovyov, Daniel Ertler, Alexander Okrut

**Student(s):** Michael Nigra, Lena Winner, Andrew Palermo, Nicholas Grosso-Giordano

**Collaborator(s):** Bruce Gates, David Dixon, Ilke Arslan

**RECENT PROGRESS**

***Calixarene-Bound Gold Cluster Catalysts***

The Katz-group goal within the area of calixarene-bound clusters is synthesis of accessible but protected metal cluster surfaces, which are tunable via choice of organic ligand. Our molecular design approach uses the high radius of curvature inherent to a rigid cone calix[4]arene ligand relative to the low radius of curvature of the metal core, as shown in Figure 1, in order to accomplish this.

Our first demonstration of the construct in Figure 1 used synthesis of gold clusters via  $\text{NaBH}_4$  reduction of Au(I) complexes shown in Figure 2 (left panel). This approach resulted in the synthesis of gold clusters within average sizes ranging from  $\text{Au}_{11}$  up to 2 nm diameter, depending on the ligand, when using HAADF-STEM. The smallest of these

clusters was characterized by ESI mass spectrometry, and exhibited an absorption band near 415 nm, which is characteristic of Au<sub>11</sub> clusters. Accessibility of the surface in the calixarene-bound gold clusters was quantified using steady-state fluorescence of a probe molecule consisting of 2-naphthalaene thiol (2NT). Data in Figure 2 demonstrates the accessibility not to be a function of calixarene-ligand substituents (i.e. N-heterocyclic carbene leads to same accessibility as similarly sized phosphine gold cluster), consistent with the mechanical model of accessibility shown in Figure 1. Catalysis related to H<sub>2</sub>O<sub>2</sub> synthesis with these metal clusters will be described.

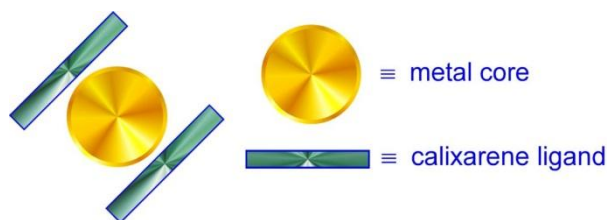


**Figure 1.** A mechanical model of cluster accessibility using rigid cone calix[4]arene ligands and small metal cores.

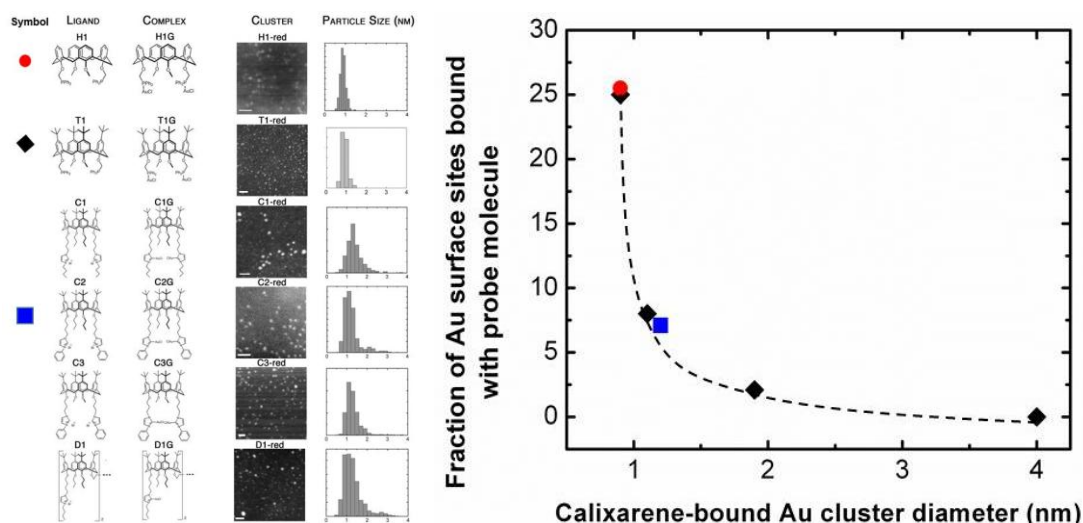
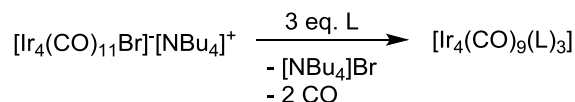


**Figure 2.** Left panel: Various calixarene phosphine and N-heterocyclic carbene ligands and their Au(I) complexes, as well as HAADF-STEM data of clusters synthesized from these complexes. Right panel: Amount of measured 2NT accessibility of gold clusters.

### *Calixarene-Bound Iridium Cluster Catalysts*

We apply the construct of cluster accessibility shown in Figure 1 to tetrairidium carbonyl clusters, which were synthesized with three P ligands on the basal plane according to the reaction scheme below.



Within this class of calixarene-substituted clusters, we recently demonstrated the apical position of silica-supported Ir<sub>4</sub>(CO)<sub>9</sub>L<sub>3</sub> (L = calixarene phosphine ligand) clusters to be the

unique location on the cluster that is active for ethylene hydrogenation, whereas open sites that occur on the substituted Ir atoms of the basal plane are inactive due to their inability to bind ethylene. We also demonstrated the importance of the calixarene in stabilizing clusters with open apical sites according to the mechanism of Figure 1, since ligands with less steric bulk led to aggregation of the metal cluster core.

We have further refined the selective formation of catalytically productive (apical) vacancies via oxidation of CO using trimethyl amine oxide, so as to only open vacancies at the apical position upon terminal CO oxidation and to minimize oxidation of bridging CO, which leads to basal-plane vacancies. Using this, we probe the effects of organic ligands on basal-plane sites on catalysis at the apical position, in a system that is geared to investigate and demonstrate action-at-a-distance ligand effects on a simple metal surface. Results shown in Figure 3 compare the effect of phosphite versus phosphine substituents on the ligand, whereas the calixarene and coordination geometry (2 equatorial and 1 axial ligand substitution on the basal plane) are preserved in both to maintain site isolation and a basis for comparison.

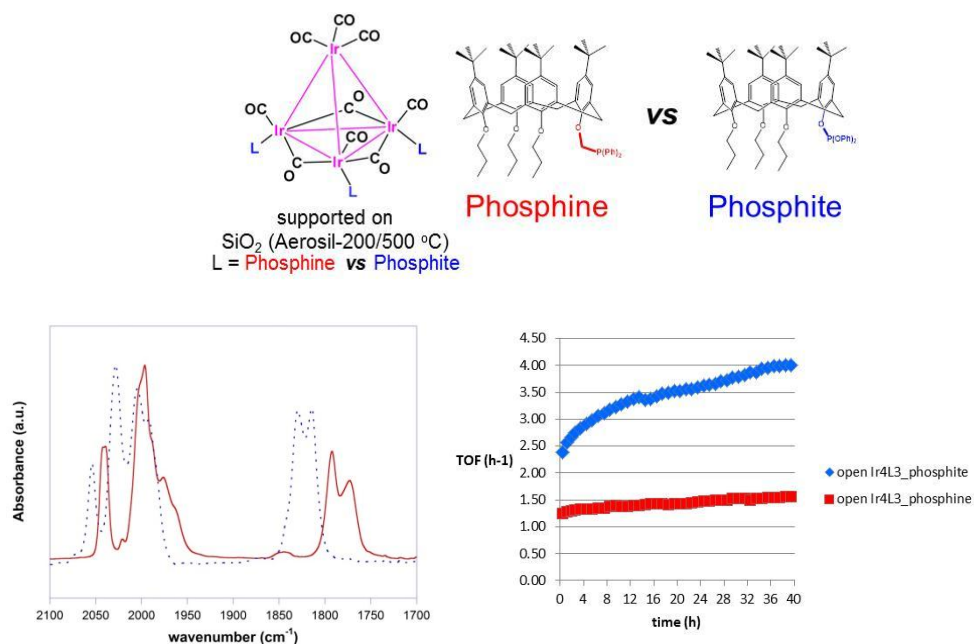


**Figure 3.** Top panel: comparison of supported molecular tetrairidium-calixarene catalysts on silica consisting of phosphine and phosphite substituents on the calixarene lower rim. Bottom left panel: the supported phosphite-containing cluster has blue shifted CO ligands and has a more electron deficient metal core relative to the supported phosphine-containing cluster. Bottom right panel: this leads to an enhanced per-site ethylene hydrogenation catalytic activity for the silica-supported phosphite relative to phosphine cluster.

We also describe the effect of dioxygen treatment of a silica-supported Ir<sub>4</sub>(CO)<sub>9</sub>L<sub>3</sub> cluster where L = phosphine shown in Figure 3. This treatment leads to a 100-fold increase in the activity. Data from a combination of in-situ FTIR spectroscopy, XANES, and EXAFS is consistent with lack of phosphine ligand oxidation and CO oxidation and dioxygen binding to the resulting open “coordinatively unsaturated” sites, which activates the cluster for

catalysis according to molecular modeling calculations. Yet the same treatment on the L = phosHITE cluster shown in Figure 3 demonstrates a lack of catalytic activity increase and suggests a lack of dioxygen interaction with the cluster. This suggests that the nature of organic ligands on the basal plane controls the interaction of dioxygen with the tetrairidium core.

### **Publications Acknowledging DOE-BES Grants in 2012-2015**

1. Katz, A.; Nandi, P.; Okrut, A.; Solovyov, A. AlIII–Calix[4]arene Catalysts for Asymmetric Meerwein–Ponndorf–Verley Reduction. *ACS Catal.* **2014**, *4*, 2492-2495.
2. Katz, A.; Nigra, M. M. Identification of Binding and Reactive Sites in Metal Cluster Catalysts: Homogeneous–Heterogeneous Bridges. In *Bridging Heterogeneous and Homogeneous Catalysis: Concepts, Strategies, and Applications*; Li, Can, Liu, Yan, Eds.; Wiley-VCH: Weinheim, Germany, 2014, Chapter 9.
3. Okrut, A.; Runnebaum, R. C.; Ouyang, X.; Lu, J.; Aydin, C.; Hwang, S.-J.; Zhang, S.; Olatunji-Ojo, O. A.; Durkin, K. A.; Dixon, D. A.; Gates, B. C.; Katz, A. Selective Molecular Recognition by Nanoscale Environments in a Supported Iridium Cluster Catalyst. *Nat. Nanotechnol.* **2014**, *9*, 459-465.
4. Katz, A.; Nigra, M. M. Cooperative Catalysis on Solid Surfaces versus Soluble Molecules. In *Cooperative Catalysis: Designing Efficient Catalysts for Synthesis*; Peters, R., Ed.; Wiley-VCH: Weinheim, Germany, 2015, Chapter 12.
5. Arslan, I.; Dixon, A.; Gates, B. C.; Katz, A. Beyond Relationships between Homogeneous and Heterogeneous Catalysis. *Catal. Lett.* **2014**, *144*, 1785-1789.
6. Winner, L.; Daniloff, G.; Nichiporuk, R. V.; Solovyov, A.; Katz, A. Patterned Grafted Lewis-Acid Sites on Surfaces: Olefin Epoxidation Catalysis Using Tetrameric Ti(IV)-Calix[4]arene Complexes. *Top. Catal.* **2015**, *58*, 441-450.
7. Chung, P.-W.; Charmot, A.; Click, T.; Yuchun, L.; Bae, Y.J.; Chu, J.-W.; Katz, A.; The Importance of Internal Porosity for Glucan Adsorption in Mesoporous Carbon Materials. *Langmuir.* **2015**, DOI: <http://dx.doi.org/10.1021/acs.langmuir.5b01115>.

## Self-Powered Catalytic Nanomotors and Pumps

Ayusman Sen  
Department of Chemistry  
The Pennsylvania State University  
University Park, PA 16802, USA  
Email: [asen@psu.edu](mailto:asen@psu.edu)

### Presentation Abstract

Self-powered nano and microscale moving systems are currently the subject of intense interest. We have discovered that catalyst particles (both colloidal and molecular scale) generate sufficient mechanical force through substrate turnover to cause their own movement. Furthermore, the movement becomes directional through the imposition of a gradient in substrate concentration. The same catalyst particles, when anchored on a surface, pump ambient fluid directionally in the presence of the substrate. Possible applications involve sorting of catalysts based on activity, enhanced substrate channeling in tandem catalysis, enhanced mixing, and precisely controlled microfluidics.

### DE-FG02-84ER13295: Transition Metal Mediated Transformations of Small Molecules

**PI:** Ayusman Sen

**Postdoc(s):** Chandrani Chatterjee

**Student(s):** Hua Zhang, Frances Pong, Scott Biltek

### RECENT PROGRESS

The major themes of our research in the current grant period are (a) the design of metal-catalyzed systems for the synthesis of novel classes of polymers, (b) the identification of new metal-mediated systems for the conversion of biomass to fuels and chemicals, and (c) catalysis-induced transport of particles and fluid. In addition, we are studying new materials to sense and capture carbon dioxide.

*Steric and Electronic Effects in Ethene/Norbornene Copolymerization by Neutral Salicylaldiminato-Ligated Palladium(II) Catalysts.* Late transition metal catalysts have been researched extensively for both homo- and co-polymerization of polar monomers. We have examined the effects of naphthoxyimine ligands, with different C8 functional groups, on the polymerization activity of the corresponding palladium(II) complex. Our group has previously studied Pd(II) catalysts extensively because of their ability to tolerate polar functional groups in monomers.<sup>3</sup>

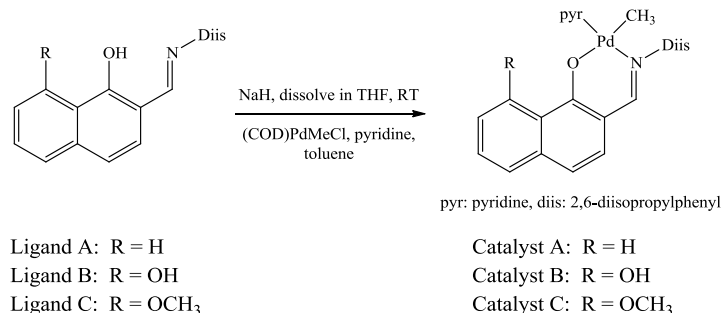


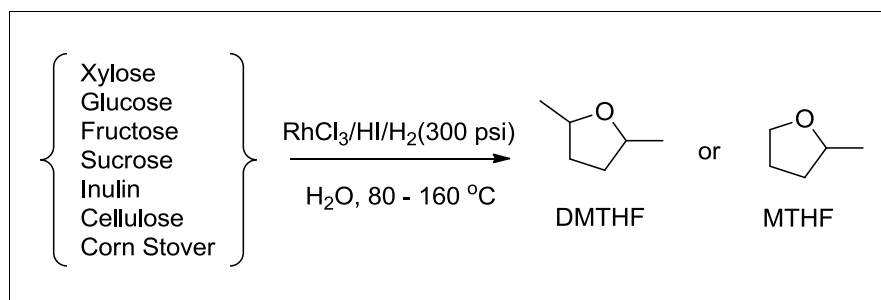
**Figure 1.** Naphthoxyimine ligands 1-3 used to synthesize Catalyst A-C.

Three palladium(II) catalysts, ligated with naphthoxyimine ligands, were synthesized, structurally characterized, and used to copolymerize ethene with norbornene derivatives (see Fig. 1).<sup>5</sup> Results show that modification of the functional group on the 8-carbon of the naphthol ligand can significantly influence polymer composition and structure. The three functional groups on the 8-carbon studied were: -H (Catalyst **A**), -OH (Catalyst **B**), and -OCH<sub>3</sub> (Catalyst **C**). Catalyst **B** significantly outperforms both **A** and **C** in production of ethene-norbornene copolymer. **B** yields over twice the amount of NB/E copolymer that **A** produces, and nearly five times as much as **C** under the same conditions. Both **A** and **B** are capable producing appreciable amounts of ethene/5-norbornene-*tert*-butyl-2-carboxylate copolymers which contain over 30% of functionalized norbornene. **C**, in contrast to both **A** and **B**, is incapable of copolymerizing functionalized norbornene with ethene.

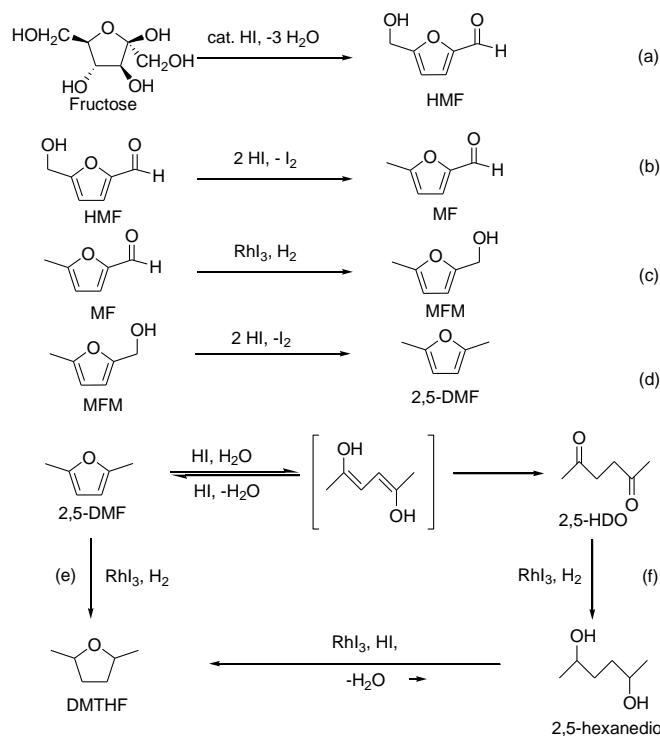
**One Step Catalytic Transformation of Cellulosic Biomass to 2,5-Dimethyltetrahydrofuran (DMTHF) for Liquid Fuel.** The production of liquid fuel directly from biomass is of great current interest, given the diminishing reserves of fossil fuels such as coal, oil, and natural gas – the current commercial sources of fuels.<sup>6</sup> We are attempting to develop a commercially viable, high yield process for the conversion of carbohydrates to the target liquid fuel 2,5-dimethyltetrahydrofuran (DMTHF). Carbohydrates, such as mono and polysaccharides and cellulose, typically constitute 50-80% of plant biomass.

Our experimental results obtained to date clearly demonstrate that it is possible to convert, *in one step*, a wide range of biomass derived carbohydrates and raw cellulosic biomass, the most abundant plant biomass, into liquid fuel (Scheme 1).<sup>8</sup> DMTHF, our initial fuel target, removes most oxygen atoms but keeps all the carbon and hydrogen content from the biomass, which preserves the highest energy content among all the liquid fuel candidates (such as ethanol). Compared to ethanol, the most common biomass-derived fuel, DMTHF possesses higher energy density (31.8 MJ/L), lower solubility in water (immiscible), and higher boiling point (90-92°C), and can be incorporated directly into the existing transportation infrastructure.

**Scheme 1:** One step transformation of carbohydrates and cellulosic biomass to tetrahydrofuran derivatives.<sup>1,2</sup>



We have examined in some detail the respective roles of HI and  $\text{RhX}_3/\text{H}_2$  in the conversion of carbohydrates to DMTHF.<sup>1,2</sup> HI serves to hydrolyze complex carbohydrates to fructose and glucose and then acts as a dehydration agent in converting these to 5-hydroxymethylfurfural (HMF). HI also acts as a reducing reagent to convert HMF to 5-methylfurfural (MF) by reducing conjugated carbinols and generates iodine as a byproduct. It also enables the hydration of 2,5-dimethylfuran (DMF) to 2,5-hexanedione (HDO), an important intermediate on route to DMTHF. The  $\text{RhX}_3$  catalyzes the conversion of iodine back to HI with hydrogen. The Rh catalyst is also necessary for the hydrogenation of the unsaturated C=C and C=O bonds of the intermediates which lead to the final product DMTHF. The overall series of reactions is shown in Scheme 2. The exact identity of the Rh catalyst under the reaction conditions could not be determined, but  $\text{RhI}_3$  was established as the catalyst precursor.



**Scheme 2.** Proposed reaction mechanism for the conversion of fructose to DMTHF.

**Novel Materials for the Reversible Capture and Sensing of Carbon Dioxide.** We have discovered a new class of absorbents for carbon dioxide, amino alcohols.<sup>7</sup> They reversibly absorb carbon dioxide at ambient temperature. Carbon dioxide is released back by simply purging the material with air or nitrogen. By coupling the process with a standard pH indicator,

the system acts as a sensitive and reversible carbon dioxide sensor with a visual color output (Fig. 2). The detection of carbon dioxide in confined spaces is of great interest for food, beverage, health, as well as for mining, biotechnology, and chemical industries and our sensors can detect carbon dioxide down to 500 ppm levels. Solid state sensors can be readily fabricated by supporting the amino alcohol and the pH indicator on alumina. This colorimetric response is completely reversible and is not interfered by moisture, oxygen or trace CO<sub>2</sub>, present in ambient air.

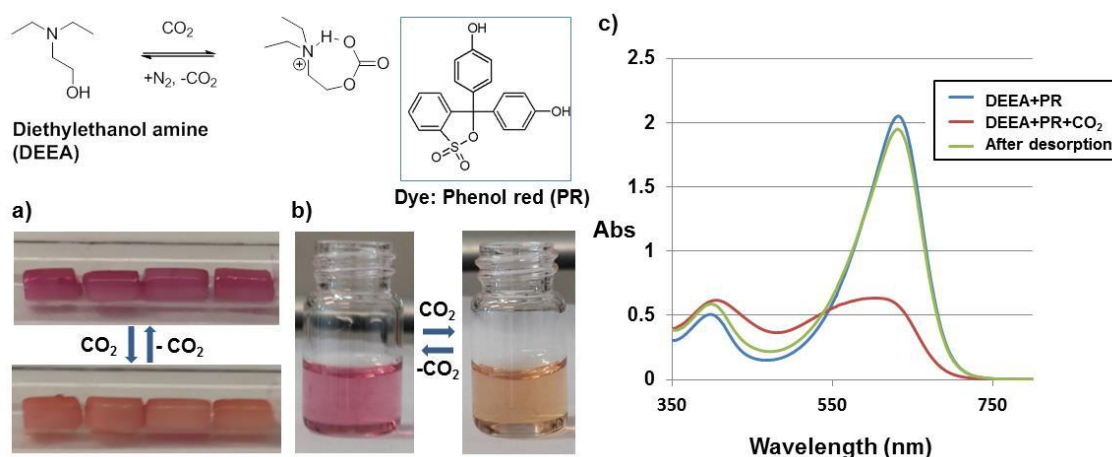


**Figure 2.** The observed colorimetric responses to pure CO<sub>2</sub> at ambient temperature, using pH sensitive phenol red dye in diethylethanolamine (DEEA). a) Visual color change observed with alumina-supported DEEA-phenol red system, b) visual color change observed in DEEA-phenol red solution, c) changes observed in the UV-visible spectra of DEEA-phenol red solution after absorption of pure CO<sub>2</sub> and the subsequent CO<sub>2</sub> desorption by purging N<sub>2</sub> at ambient temperature.

### Refereed Publications Acknowledging this Grant in 2012-2015

1. Yang, W.; Grochowski, M.; Sen, A. Selective Reduction of Biomass by Hydroiodic Acid and Its In Situ Regeneration from Iodine by Metal/Hydrogen. *ChemSusChem*, **2012**, *5*, 1218-1222..
2. Grochowski, M.; Yang, W.; Sen, A. Mechanistic Study of One Step Catalytic Conversion of Fructose to 2,5-Dimethyltetrahydrofuran. *Chem. Europ. J.*, **2012**, *18*, 12363-12371.
3. Nakamura, A.; Anselment, T. M. J.; Claverie, J.; Goodall, B.; Jordan, R. F.; Mecking, S.; Rieger, B.; Sen, A.; van Leewuen, P. W. N. M.; Nozaki, K. Ortho-Phosphonebenzenesulfonate: A Superb Ligand for Palladium-Catalyzed Coordination-Insertion Copolymerization of Polar Vinyl Monomers. *Acc. Chem. Res.*, **2013**, *46*, 1438-1449.
4. Biltek, S. R.; Sen, A.; Pedicini, A. F.; Reber, A. C.; Khanna, S. N. Isolation and Structural Characterization of a Silver-Platinum Nanocluster, Ag<sub>4</sub>Pt<sub>2</sub>(DMSA)<sub>4</sub>. *J. Phys. Chem. A*, **2014**, *118*, 8314-8319.
5. Pong, F. Y.; Mandal, S.; Sen, A. Steric and Electronic Effects in Ethene/Norbornene Copolymerization by Neutral Salicylaldiminato-Ligated Palladium(II) Catalysts. *Organometallics*, **2014**, *33*, 7044-7051.
6. Chatterjee, C.; Pong, F.; Sen, A. Chemical Conversion Pathways for Carbohydrates. *Green Chemistry*, **2015**, *17*, 40-71.
7. Chatterjee, C.; Sen, A. Sensitive Colorimetric Sensors for Visual Detection of Carbon Dioxide. *J. Mater. Chem. A*, **2015**, *3*, 5642-5647.
8. Sen, A.; Yang, W. One-step Catalytic Conversion of Biomass-derived Carbohydrates to Liquid Fuels. *U. S. Patent*, 8,674,150 B2 (2014).

**Wednesday Morning**

**VI. Advances in  
Multifunctional  
Molecule Disassembly**

This page is intentionally blank.

**Robert J. Davis**

**Isotopic Transient Analysis of the  
Ethanol Coupling Reaction over  
Hydroxyapatite and Magnesia**

Robert J. Davis, Sabra Hanspal, Ian Hill,  
Joseph Kozlowski, and Zachary Young  
Department of Chemical Engineering, University of Virginia,  
Charlottesville, VA 22904

**Presentation Abstract**

Multiproduct steady-state isotopic transient kinetic analysis (SSITKA) of the ethanol coupling reaction was used over a stoichiometric calcium hydroxyapatite (HAP) catalyst and compared to the results obtained with magnesia (MgO), a standard solid base catalyst, in an attempt to evaluate important intrinsic kinetic parameters and benchmark the reaction. Results from surface characterization, reactivity testing, and isotopic transient studies were used to propose key structural and compositional properties that facilitate the Guerbet coupling reaction. The isotopic transient results revealed the surface coverage of reactive intermediates leading to butanol ( $N_{\text{BuOH}}$ ) relative to that leading to acetaldehyde ( $N_{\text{AcH}}$ ) was very high on HAP ( $N_{\text{BuOH}} \gg N_{\text{AcH}}$ ) whereas on MgO the opposite trend was observed ( $N_{\text{AcH}} > N_{\text{BuOH}}$ ). Given the generally understood mechanism for Guerbet coupling of ethanol, which involves aldol condensation, these results suggest that a higher fraction of surface acetaldehyde produced during the reaction of ethanol on MgO, desorbed into the gas-phase while the majority of adsorbed acetaldehyde on HAP remained on the surface to undergo sequential condensation reactions leading to butanol. Consistent with this idea, the surface density of adsorbed intermediates leading to butanol was orders of magnitude greater on HAP than on MgO at all conditions tested. Adsorption microcalorimetry of triethylamine and  $\text{CO}_2$  showed a significantly higher number of acid-base sites on the surface of HAP compared to MgO. Since the Guerbet coupling of ethanol likely occurs on acid-base site pairs, the high reactivity of ethanol on HAP compared to MgO appears to be related to a high surface density of acid-base site pairs along with a weak binding affinity for ethanol (revealed by IR spectroscopy) and for condensation products on HAP.

**DE-FG02-95ER14549: Structure and Function of  
Supported Base Catalysts**

**RECENT PROGRESS**

Over the last funding cycle, we completed and published our studies of transesterification catalyzed by Mg-Zr mixed oxides. Our work revealed a substantial promotional effect of adding small amounts of Zr to the solid base MgO as demonstrated by a several hundred percent increase in activity for transesterification. Our model for the unusual rate enhancement is that

the mixed oxide presents the appropriate number and location of Lewis acid sites (from Zr) adjacent to Lewis base sites (the O or OH on MgO) to accelerate the transesterification reaction.

We also started exploring the interesting Guerbet reaction of ethanol, which is a coupling reaction to produce butanol. Although Mg-Zr mixed oxides were excellent at catalyzing transesterification, we observed that the acid sites associated with Zr were too strong for ethanol coupling since excessive ethanol dehydration occurred. Thus, we started a detailed study of ethanol coupling on MgO, which eventually led us to investigate the unusually productive catalyst, hydroxyapatite.

## 1. Ethanol Coupling on Magnesia and Hydroxyapatite

The Guerbet coupling reaction has historically been used for the production of long chain branched alcohols due to the plethora of available primary and secondary alcohols that can be used as reactants. The reaction has received attention recently for the possible upgrading of short, readily available linear alcohols. The reaction is generally believed to occur through a series of elementary steps that include alcohol dehydrogenation to form an aldehyde or ketone intermediate, aldol condensation of the aldehyde or ketone intermediates to form a C-C bond, and hydrogenation of the resulting unsaturated product. Although alternative mechanisms have been proposed, the Guerbet reaction likely requires a catalyst that is multifunctional since O-H, C-H and C-C bonds are transformed in the sequence.

The stoichiometric form of hydroxyapatite (HAP,  $\text{Ca}_{10}(\text{PO}_4)_6(\text{OH})_2$ ) has a Ca/P molar ratio equal to 1.67, however, this ratio can vary substantially in synthetic materials. The surfaces of HAP can be acidic or basic in nature depending on the Ca/P molar ratio of the material, which in turn influences the catalytic behavior of HAP. The active sites on these materials have not been identified and therefore a detailed understanding of the reaction mechanism is lacking. In our work, we used steady-state isotopic transient kinetic analysis (SSITKA) of the ethanol coupling reaction over a stoichiometric calcium hydroxyapatite catalyst and compared the results to those obtained with magnesia, a standard solid base catalyst, in an effort to gain insight into the reaction mechanism at the active site level. Table 1 illustrates how HAP is significantly more active at ethanol conversion than MgO and much more selective at producing butanol. Notice that the temperature of the reaction over HAP that is reported in Table 1 is 40 K lower than that over MgO because the activity of HAP was so high.

**Table 1. Comparison of HAP and MgO in the Catalytic Conversion of Ethanol**

Catalyst	Ethanol conversion (%)	Rate of ethanol conversion ( $\text{mol m}^{-2} \text{s}^{-1}$ )	Selectivity (C%)		
			Ethene	Acetaldehyde	Butanol
<b>HAP (613 K)</b>	4.3	$4.4 \times 10^{-8}$	1	32	67
<b>MgO (653 K)</b>	3.7	$1.7 \times 10^{-8}$	13	67	20

## 2. Isotopic Transient Studies of Ethanol Coupling

The Steady-State Isotopic Transient Kinetic Analysis (SSITKA) technique is a well-established and powerful method that allows quantification of important kinetic parameters such as surface coverages of adsorbed reactant species and surface reaction intermediates, average surface lifetimes of those intermediates, and an upper bound of the turnover frequency. We have therefore performed a comparative study between stoichiometric HAP and MgO, using a modified SSITKA reactor system that allows the monitoring of multiple products formed during the reaction. Mean surface residence times as well as coverages of surface intermediates that led to acetaldehyde and butanol are summarized in Tables 2 and 3, respectively. For both HAP and MgO, the average surface lifetime of reactive intermediates leading to acetaldehyde was much shorter than that leading to butanol. Stated another way, it took a significantly longer time for butanol to exit the reactor compared to acetaldehyde. The surface coverage of reaction intermediates leading to acetaldehyde relative to butanol on the two catalysts also provides valuable information. On MgO, there was a higher number of intermediates that led to acetaldehyde compared to those that lead to butanol ( $N_{AcH} > N_{BuOH}$ ), whereas the opposite trend was observed over HAP ( $N_{BuOH} \gg N_{AcH}$ ). Moreover, Table 3 indicates the surface density of adsorbed intermediates leading to butanol was orders of magnitude greater on HAP than on MgO at all three flowrates investigated.

**Table 2. Time constants and surface coverages of reactive intermediates leading to acetaldehyde ( $N_{AcH}$ ) during the steady-state Guerbet coupling of ethanol over MgO and HAP at 653 and 613 K, respectively.**

Total Flow Rate ( $\text{cm}^3 \text{ min}^{-1}$ )	$\tau_{AcH}$ (s)		Coverage of intermediates to acetaldehyde $N_{AcH}$ ( $\text{mol m}^{-2}$ )	
	MgO (653 K)	HAP (613 K)	MgO (653 K)	HAP (613 K)
30	15	4.4	$1.1 \times 10^{-7}$	$4.3 \times 10^{-8}$
50	13	4.6	$1.2 \times 10^{-7}$	$6.5 \times 10^{-8}$
75	11	4.6	$1.2 \times 10^{-7}$	$8.2 \times 10^{-8}$

As mentioned earlier, a commonly-hypothesized reaction path for the Guerbet coupling of ethanol involves the aldol condensation of intermediate acetaldehyde which likely proceeds through a surface enolate species that produces coupled products that desorb as butanol. In this coupling path, surface acetaldehyde produced from ethanol dehydrogenation may desorb or undergo base-catalyzed abstraction of the  $\alpha$ -H to form an adsorbed enolate species. The isotopic transient results obtained during the steady-state conversion of ethanol over MgO revealed a significantly higher surface coverage of reactive intermediates leading to acetaldehyde than to butanol (Tables 2, 3:  $N_{AcH} > N_{BuOH}$ ) at all flow rates. These results suggest a higher fraction of surface acetaldehyde produced during the reaction of ethanol on MgO desorbed rather than coupled to form butanol. The coverages of intermediates leading to acetaldehyde and butanol on MgO are consistent with the low butanol selectivity observed on that material.

**Table 3. Time constants and surface coverages of reactive intermediates leading to butanol ( $N_{\text{butanol}}$ ) during the steady-state Guerbet coupling of ethanol over MgO and HAP at 653 and 613 K, respectively.**

Total Flow Rate ( $\text{cm}^3 \text{min}^{-1}$ )	$\tau_{\text{butanol}}$ (s)		Coverage of intermediates to butanol $N_{\text{butanol}}$ ( $\text{mol m}^{-2}$ )	
	MgO (653 K)	HAP (613 K)	MgO (653 K)	HAP (613 K)
30	93	310	$2.8 \times 10^{-7}$	$4.8 \times 10^{-6}$
50	53	117	$8.1 \times 10^{-8}$	$1.7 \times 10^{-6}$
75	27	69	$4.6 \times 10^{-8}$	$1.1 \times 10^{-6}$

It is likely that the high activity and selectivity observed during the Guerbet coupling of ethanol over HAP involves the proper balance of acid-base site pairs to facilitate all of the steps in the sequence, including alcohol dehydrogenation, aldol condensation and aldehyde hydrogenation. The relatively strong basicity of MgO retains adsorbed ethanol at higher temperatures compared to HAP, which is consistent with the idea that Guerbet coupling is facilitated by weak acid-base bifunctional catalysts.

#### **Publications Acknowledging this Grant in 2012-2015**

1. Hill, I.M.; Hanspal, S.; Young, Z.D.; Davis, R.J. "DRIFTS of Probe Molecules Adsorbed on Magnesia, Zirconia and Hydroxyapatite Catalysts" *J. Phys. Chem. C*, (2015) in press.
2. Hanspal, S.; Young, Z.D.; Shou, H.; Davis, R.J. "Multi-product steady-state isotopic transient kinetic analysis of the ethanol coupling reaction over hydroxyapatite and magnesia," *ACS Catal.* **2015**, *5*, 1737-1746.
3. Birky, T.W.; Kozlowski, J.T.; Davis, R.J. "Isotopic Transient Analysis of the Ethanol Coupling Reaction over Magnesia," *J. Catal.* **2013**, *298*, 130-137.
4. Kozlowski, J.T.; Davis, R.J.; "Sodium Modification of Zirconia Catalysts for Ethanol Coupling to 1-Butanol," *J. Energy Chemistry* **2013**, *22*, 58-64.
5. Kozlowski, J.T.; Behrens, M.; Schlögl, R.; Davis, R.J. "Influence of Precipitation Method on Acid-Base-Catalyzed Reactions over Mg-Zr Mixed Oxides," *ChemCatChem* **2013**, *5*, 1989-1997.
6. Kozlowski, J.T.; Davis, R.J. "Heterogeneous Catalysts for the Guerbet Coupling of Alcohols," *ACS Catal.* **2013**, *3*, 1588-1600.
7. Davis, S.E.; Zope, B.N.; Davis, R.J. "On the Mechanism of Selective Oxidation of 5-Hydroxymethylfurfural to 2,5-Furandicarboxylic Acid over Supported Pt and Au Catalysts," *Green Chem.* **2012**, *14*, 143-147.
8. B.N. Zope, S.E. Davis and R.J. Davis, "Influence of Reaction Conditions on Diacid Formation during Au-catalyzed Oxidation of Glycerol and Hydroxymethylfurfural," *Top. Catal.*, **2012**, *55*, 24-32.

**Mahdi M. Abu-Omar**

**Mechanistic Aspects of New C-H Activation Chemistries to Afford Bimetallic Complexes:  
Implication for Alkane Upgrading with Biorenewables**

Mahdi M. Abu-Omar, Kothanda Rama Pichaandi, and Michael Mazzotta  
Purdue University, Department of Chemistry and School of Chemical Engineering

**Presentation Abstract**

Conversion of natural gas (NG) into methanol or higher alkanes (paraffins) is of paramount importance because of its abundance; and recent developments in hydraulic fracturing has positioned the US as a leader in NG production that is rich in light hydrocarbons (LHC): C2-C5. Gas to liquid via syn gas (carbon monoxide and hydrogen) routes require high temperature and pressure, making it capital intensive. Therefore, direct partial oxidation of methane (and other light alkanes) at low temperature and low pressure is desirable. In this regard C-H activation followed by oxygen atom insertion into a metal alkyl bond (M-R) has attracted significant attention. A new approach to upgrading light hydrocarbons (LHC) with biorenewables will be described through the use of binuclear and bifunctional catalysts based on organometallic complexes. I will describe in the presentation C-H activation of the methyl group on methyltrioxorhenium (MTO) by iridium dihydride pincer complex to afford a novel bimetallic Ir-Re methylenidene complex. Investigation of the mechanism by a combination of experiment (NMR to characterize pertinent intermediates and kinetics) and theory (DFT) and how our understanding can lead to new investigations in catalysis will be discussed.

**DE-FG02-06ER15794: Oxo Rhenium and Molybdenum Catalysts for C-O Cleavage and  
Deoxygenation**

**PI:** Mahdi M. Abu-Omar

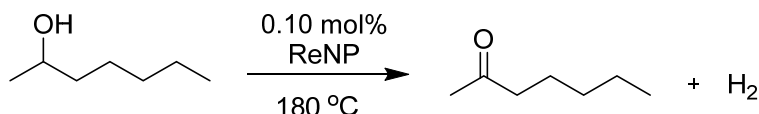
**Postdocs:** Kothanda Rama Pichaandi, Aysegul Senocak

**Students:** Isaac Corn, Michael Mazzotta, Jing Yi, Ms. Shuo Liu

**RECENT PROGRESS**

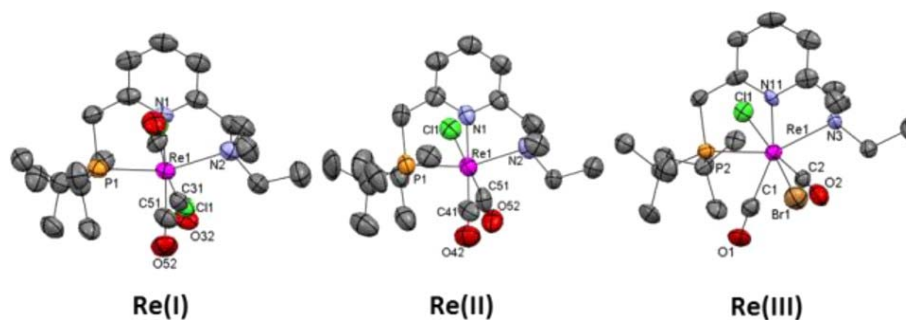
*Atomic Rhenium Nanoparticles (NP) as Catalysts in Alcohol Dehydrogenation.*

Small rhenium nanocrystalline particles (2 nm) are formed from  $\text{NH}_4\text{ReO}_4$  at 180 °C in neat aqueous-phase alcohol without any support. The Re NP catalyze the direct dehydrogenation of different secondary and benzyl alcohols to ketones or aldehydes. The NP catalyst can be employed at 0.10 mol % loading and is recyclable without loss of activity 9 times. The metallic Re nanocrystallines are formed by reduction of Re(VII) oxide by alcohols. The Re NPs were characterized by Re K-edge X-ray absorption near-edge spectroscopy (XANES). A fit of the XANES shows 45 % of the sample being  $\text{ReO}_2$  and 55 % metallic rhenium.



*Synthesis, Dynamics and DFT Studies of Rhenium Dicarbonyl PNN Pincer Complexes in Three Different Oxidation States.*

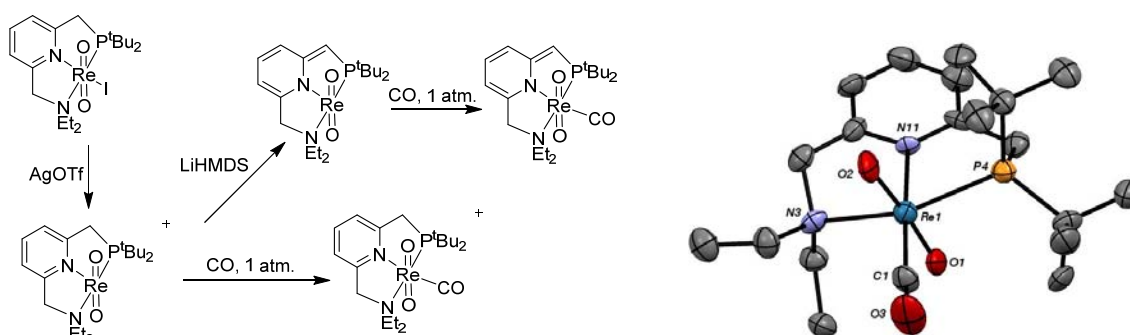
Three rhenium dicarbonyl halide complexes supported by PNN pincer ligands have been synthesized and fully characterized including single crystal X-ray structures (see figure below). One electron oxidation of the  $\text{Re}^{\text{I}}$  complex **1** by  $[(4\text{-BrC}_6\text{H}_4)_3\text{N}][\text{SbCl}_6]$  gave the  $\text{Re}^{\text{II}}$  complex **2**, which was further oxidized to  $\text{Re}^{\text{III}}$  (**3**) by PhIO. A systematic decrease in the pi-backbonding was observed as the oxidation state on rhenium was increased. The heptacoordinate complex **3** exhibited dynamic behavior in the NMR caused by pseudorotation of the rhenium center, which was supported by DFT calculations.



*Rhenium Oxo Carbonyl Complexes with PNN Pincer Ligands.*

Aromatized cationic  $[(\text{PNN})\text{Re}(\pi\text{-acid})(\text{O})_2]^+$  and dearomatized neutral  $(\text{PNN}^*)\text{Re}(\pi\text{-acid})(\text{O})_2$  (where,  $\pi\text{-acid} = \text{CO}$ ,  $^t\text{BuNC}$ , or  $(2,6\text{-Me}_2)\text{PhNC}$ ) complexes possessing both  $\pi$ -donor and  $\pi$ -acceptor ligands have been synthesized and fully characterized (see figure below). Metal complexes possessing both  $\pi$ -acids and  $\pi$ -bases are important in the context of green conversion of  $\text{CO}_2$  to  $\text{CO}$  as well as oxidation of  $\text{CO}$  by metal oxides. Recently, Donahue demonstrated the

utility of mono-oxo carbonyl tungsten complexes in a complete cycle of CO<sub>2</sub> reduction to CO and water. However, complexes with multiple oxo and carbonyl ligands such as M(O)<sub>2</sub>(CO)<sub>n</sub> (n = 1 or 2) have been isolated only in glass matrices from laser ablation of the reaction of CO<sub>2</sub> with metal oxides. Reaction of [(PNN)Re(O)<sub>2</sub>]<sup>+</sup> with lithiumhexamethyldisilazide (LiHMDS) yields the dearomatized [(PNN\*)Re(O)<sub>2</sub>]. [(PNN)Re(π-acid)(O)<sub>2</sub>]<sup>+</sup> and (PNN\*)Re(π-acid)(O)<sub>2</sub> were prepared from the reaction of precursors with CO or isocyanide (Scheme below). X-ray structures conform to the expected trans-dioxo structure, occupying the axial positions with the π-acid ligand in the equatorial plane in an overall octahedral geometry around rhenium(V) (ORTEP figure below). DFT studies revealed the stability of dioxo carbonyl complexes arises from a π-back bonding interaction between the d<sub>xy</sub> orbital of Re, π orbital of the oxo ligands, and π\* of CO/isocyanide.



Synthesis of PNN pincer oxorhenium carbonyl complexes. ORTEP drawing of (PNN)Re(O)<sub>2</sub>(CO)<sup>+</sup>.

### Publications Acknowledging this Grant in 2012-15

1. Basudeb Saha, Saikat Dutta, and Mahdi M. Abu-Omar, "Aerobic oxidation of 5-hydroxymethylfurfural with homogeneous and nanoparticulate catalysts " *Catal. Sci. Technol.* **2012**, 2, 79-81.
2. Kothanda Rama Pichaandi, Phillip E. Fanwick, and Mahdi M. Abu-Omar, "Trioxorhena(VII)carborane Anion and Its Methyl-Substituted Analogue: Synthesis, Structure, DFT, and Catalytic Studies" *Organometallics* **2012**, 31, 1888-1896.
3. Jing Yi, Shuo Liu, and Mahdi M. Abu-Omar, "Rhenium-Catalyzed Transfer Hydrogenation and Deoxygenation of Biomass-Derived Polyols to Small and Useful Organics" *ChemSusChem* **2012**, 5, 1401-1404.
4. Benjamin L. Wegenhart, Shuo Liu, Melanie Thom, David Stanley, and Mahdi M. Abu-Omar, "Solvent-Free Methods for Making Acetals Derived from Glycerol and Furfural and Their Use as a Biodiesel Fuel Component" *ACS Catal.* **2012**, 2, 2524-2530.

5. Basudeb Saha, Dinesh Gupta, Mahdi M. Abu-Omar, Arindam Modak, and Asim Bhaumik, "Porphyrin based porous organic polymer supported iron(III) catalyst for efficient aerobic oxidation of 5-hydroxymethylfurfural into 2,5-furandicarboxylic acid" *J. Cat.* **2013**, 299, 316-320.
6. Isaac R. Corn, Pablo D. Astudillo-Sánchez, Michael J. Zdilla, Phillip E. Fanwick, Michael J. Shaw, Jeffery T. Miller, Dennis H. Evans, and Mahdi M. Abu-Omar, "Synthesis and electrochemical reactivity of molybdenum dicarbonyl supported by redox active  $\pi$ -diimine ligand" *Inorg. Chem.* **2013**, 52, 5457-5463.
7. Shuo Liu, Aysegul Senocak, Jessica L. Smeltz, Linan Yang, Benjamin Wegenhart, Jing Yi, Hilka I. Kenttämä, Elon A. Ison, and Mahdi M. Abu-Omar, "Mechanism of MTO-catalyzed deoxydehydration (DODH) of diols to alkenes using sacrificial alcohols" *Organometallics* **2013**, 32, 3210-3219.
8. Jing Yi, Jeffrey T. Miller, Dmitry Y. Zemlyanov, Ruihong Zhang, Paul J. Dietrich, Fabio H. Ribeiro, Sergey Suslov, and Mahdi M. Abu-Omar, "A Reusable Unsupported Rhenium Nanocrystalline Catalyst for Acceptorless Dehydrogenation of Alcohols through gamma-C-H Activation" *Angew. Chem. Int. Ed.* **2014**, 53, 833-836.
9. Kothanda Rama Pichaandi, Michael G. Mazzotta, John S. Harwood, Phillip E. Fanwick, and Mahdi Abu-Omar, "Synthesis, Dynamics, and DFT Studies of Rhenium Dicarbonyl PNN Pincer Complexes in Three Different Oxidation States" *Organometallics* **2014**, 33, 1672-1677.
10. Michael G. Mazzotta, Kothanda R. Pichaandi, Phillip E. Fanwick, and Mahdi M. Abu-Omar, "Concurrent Stabilization of  $\pi$ -Acceptor and  $\pi$ -Donor Ligands in Aromatized and Dearomatized Pincer [(PNN)Re(CO)(O)<sub>2</sub>] Complexes" *Angew. Chem. Int. Ed.* **2014**, 53, 8320-8322.
11. Kothanda Rama Pichaandi, Phillip E. Fanwick, and Mahdi M. Abu-Omar, "C-H Activation of Methyltrioxorhenium by Pincer Iridium Hydride to Give Agile Ir-Re Bimetallic Compounds" *Organometallics*. **2014**, 33, 5089-5092.

## Catalytic deoxygenation on metal carbides

Aditya Bhan

Department of Chemical Engineering and Materials Science, University of Minnesota

### Abstract

The structure, site evolution, and mechanistic characteristics of self-supporting, high surface area ( $\sim 100 \text{ m}^2\text{g}^{-1}$ ) molybdenum-carbide ( $\text{Mo}_2\text{C}$ ) based catalytic formulations (i) for atmospheric pressure hydrodeoxygenation (HDO) of lignin-derived polyfunctional molecules to make aromatics, and (ii) upon exposure to oxygen that results in Brønsted acidity as inferred from probe molecule dehydration reactions and in situ chemical titration will be presented. These studies demonstrate that the oxophilic characteristics of  $\text{Mo}_2\text{C}$  make it both a selective and tunable catalyst for hydrodeoxygenation.

### **DE-SC000084818: One-pot catalytic conversion of biomass and alkanes: Kinetically coupling deoxygenation and dehydrogenation pathways**

Postdoc(s): Dr. Wen-Sheng Lee

Student(s): Mark Sullivan, Cha-Jung Chen, Anurag Kumar

Affiliation: University of Minnesota, 421 Washington Ave SE, Minneapolis, MN 55455;

### Recent Progress

#### *Hydrodeoxygenation of polyfunctional phenolic compounds on $\text{Mo}_2\text{C}$ catalysts:*

Selective deoxygenation of biomass-derived phenyl ethers (anisole, m-cresol, guaiacol, and dimethoxy benzene) to aromatics (>90% yield to benzene and toluene) over  $\text{Mo}_2\text{C}$  formulations at atmospheric pressure and 420-580 K occurs because sequential hydrogenation reactions of aromatic carbon-carbon bonds are absent on oxygen-modified  $\text{Mo}_2\text{C}$  catalysts as inferred from chemical transient and in situ chemical titration studies. Steady state kinetic measurements and  $\text{H}_2$ - $\text{D}_2$  isotopic switching experiments implicate the involvement of distinct sites for activation of the oxygenate and molecular  $\text{H}_2$  in HDO reactions. Selectivity towards  $\text{Ar-OCH}_3$  and  $\text{ArO-CH}_3$  bond cleavage on  $\text{Mo}_2\text{C}$  formulations can be systematically tuned by oxygen pre-treatment.

### ***Structure and site evolution of Mo<sub>2</sub>C upon exposure to oxygen:***

Acid site densities could be tuned by a factor of ~30 using an O<sub>2</sub> co-feed, which reversibly creates Brønsted acid sites, on the carbide surface without altering the bulk crystal structure of 2-5 nm Mo<sub>2</sub>C crystallites. Unimolecular isopropanol (IPA) dehydration at 415 K, a probe reaction, occurred on Brønsted acid sites of these oxygen-modified carbides with an intrinsic activation energy of ~93 kJ mole<sup>-1</sup> with a kinetically relevant step of β-hydrogen scission. Site densities were estimated via in situ 2,6-di-*tert*-butylpyridine (DTBP) titration and used to calculate a turnover frequency (TOF) of 0.1 s<sup>-1</sup>, which was independent of site density. Oxygen co-processing allows for facile in situ tunability of acidic and metallic sites on highly oxophilic metal carbides.

### **Publications (2012-2015)**

1. Bedard, J. W.; Hong, D-Y.; Bhan, A. CH<sub>4</sub> dehydroaromatization on Mo/H-ZSM-5: 1.Effects of co-processing H<sub>2</sub> and CH<sub>3</sub>COOH. *Journal of Catalysis* **2013**, *306*, 58-67.
2. Bedard, J. W.; Hong, D-Y.; Bhan, A. Co-processing CH<sub>4</sub> and oxygenates on Mo/H-ZSM-5: 2. CH<sub>4</sub>/CO<sub>2</sub> and CH<sub>4</sub>/HCOOH Mixtures. *Phys. Chem. Chem. Phys.* **2013**, *15*, 12173-12179.
3. Bedard, J. W.; Hong, D-Y.; Bhan, A. C to H effective ratio as a descriptor for co-processing light oxygenates and CH<sub>4</sub> on Mo/H-ZSM-5. *RSC Advances* **2014**, *4*, 49446-49448.
4. Lee, W-S.; Wang, Z.; Wu, R.; Bhan, A. Selective vapor phase hydrodeoxygenation of anisole to benzene on molybdenum carbide catalysts. *Journal of Catalysis* **2014**, *319*, 44-53.
5. Sullivan, M. M.; Held J. T.; Bhan, A. Structure and site evolution of molybdenum carbide catalysts upon exposure to oxygen. *Journal of Catalysis* **2015**, *326*, 82-91.
6. Lee, W-S.; Kumar, A.; Wang, Z.; Bhan, A. Chemical titration and transient kinetic studies of site requirements in Mo<sub>2</sub>C catalyzed vapor phase anisole hydrodeoxygenation. *ACS Catalysis* (to appear).

# Poster Presentations

This page is intentionally blank.

**Radoslav Adzic**

**Structure and Function in Electrocatalysis of Reactions for  
Direct Energy Conversion**

Radoslav R. Adzic<sup>1</sup>, Kurian A. Kuttiyiel<sup>1</sup>, Kotaro Sasaki<sup>1</sup>, Miomir Vukmirovic<sup>1</sup>, Jia X. Wang<sup>1</sup>,  
Meng Li<sup>1</sup>, Gu-Gon Park<sup>1</sup>, Dong Su<sup>2</sup>, Lijun Wu<sup>3</sup>, Yimei Zhu<sup>3</sup>

<sup>1</sup>Chemistry Department, <sup>2</sup>Center for Functional Nanomaterials, <sup>3</sup>Department of Condensed  
Matter Physics and Materials Science, Brookhaven National Laboratory

**Abstract**

We conduct studies of Pt monolayer electrocatalysts for the O<sub>2</sub> reduction reaction, oxidation of ethanol and methanol, hydrogen oxidation and evolution and CO<sub>2</sub> reduction aiming at producing ultimately low Pt content electrocatalysts with high activity and good stability. Our recent studies (i) showed a new route to obtain PtMN core-shell catalysts consisting of inexpensive M nitride cores covered with very thin Pt shells (M = Co, Ni, Fe) by annealing in a NH<sub>3</sub> gas. The experimental data and the DFT calculations indicate that the nitride cores (typically M<sub>4</sub>N with a diameter of 3~5 nm) improve the performance of the Pt shell (2~4 monolayer-thick) by inducing both the geometric and electronic effects. (ii) We demonstrated a simple method to synthesize core-shell-structured PdCo nanoparticles that can be transformed into ordered intermetallic phases by addition of Au atoms and subsequent annealing. The unusual ordering of PdCo atoms occurs along the [111] direction in the AuPdCo nanoparticles with twin boundaries and with stable {111}, {110} and {100} facets. These structurally ordered intermetallics AuPdCo tend to behave similar to Pt catalyst for ORR, but more interestingly have much better stability than Pt in alkaline media. A Pt monolayer deposited on the Au<sub>1</sub>Pd<sub>4</sub>Co<sub>5</sub> significantly increases the ORR activity and durability in acid media. (iii) We obtained a factor of about 4 enhanced Pt mass activities for the hydrogen evolution and oxidation reactions in alkalies using well-defined monolayer- and bilayer-thick Ru@Pt core-shell catalysts. The best catalysts is bilayer Pt for the HOR and monolayer Pt for the HER. We attribute enhanced activities to the weakening of the H binding energy by the interaction of Pt shell with the Ru core based on kinetic analysis and DFT calculations. (iv) We demonstrated that the Pt monolayer under tensile strain on Au substrates showed highly enhanced activity for methanol oxidation by precluding CO formation, and by inducing the C-C bond splitting in ethanol oxidation.

Grant Number: 2016-BNL-MA510MAEA-Budg

Grant Title: Structure and Function in Electrocatalysis of Reactions for Direct Energy  
Conversion

PI: Radoslav Adzic

Postdoc(s): Kurian Kuttiyiel, Meng Li

Student(s): Yu Zhang, Zhixiu Liang

## RECENT PROGRESS

### *Enhancement of the Oxygen Reduction on Nitride Stabilized Pt-M (M = Fe, Co and Ni) and Pt-PdNi Core-Shell Nanoparticle Electrocatalysts*

We have reported a new route to the development of PtMN core-shell catalysts consisting of inexpensive M nitride cores covered with very thin Pt shells (M = Co, Ni, Fe) by annealing in a NH<sub>3</sub> gas. Despite substantial reduction in Pt loading the catalysts retained considerably high ORR activity and stability. The experimental data and the DFT calculations indicate that the nitride cores (typically M<sub>4</sub>N with a diameter of 3~5 nm) improve the performance of the Pt shell (2~4 monolayer-thick) by inducing both the geometric and electronic effects. Adding metal nitride in the core increases the ORR activity in the order of PtNiN/C > PtFeN/C > PtCoN/C. DFT calculations have shown a volcano type behavior with PtNiN/C at the top of the curve revealing the fact that, among the catalysts investigated, it has the best combination of both the surface strain and d-band center shifts.

We also developed highly active and stable oxygen reduction catalysts by depositing Pt monolayer on a nitrated PdNi alloy core (Figs. 1a-1d). The prepared Pt<sub>ML</sub>PdNiN/C catalyst retains 89% of the initial electrochemical surface area after 50000 cycles between potentials 0.6 and 1.0 V (Fig. 1d). By correlating electron energy-loss spectroscopy and X-ray absorption spectroscopy analyses with electrochemical measurements, we found that stabilization of the Pt<sub>ML</sub>PdNiN/C catalyst exhibited a significant improvement by nitrogen doping while reducing the total precious metal loading.

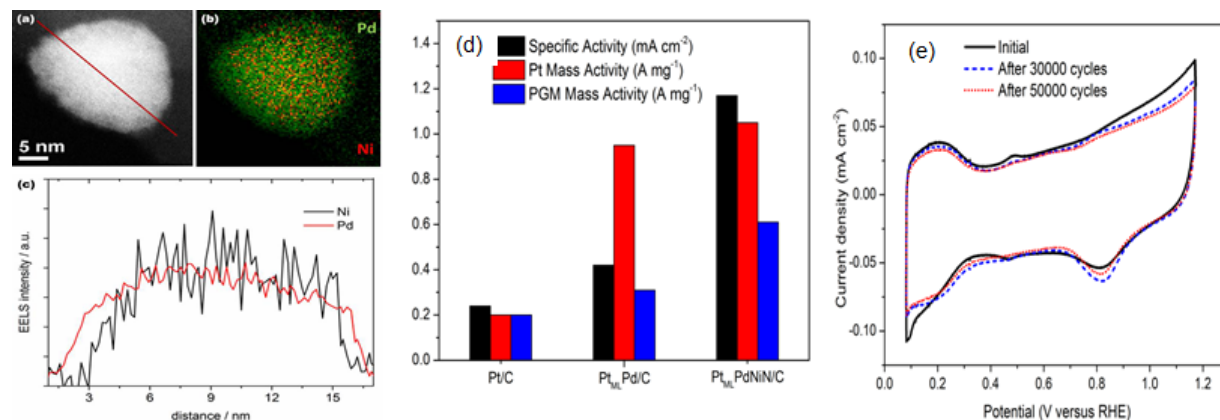


Fig. 1 (a) HAADF-STEM image of PdNiN core-shell nanoparticle. (b) Two dimensional EELS mapping of Ni L signal (red) and Pd M signal (green). (c) EELS line scan profile for Pd M-edge and Ni L-edge along the scanned line indicated in (a). (d) Specific and mass activities for the commercial Pt/C, Pt<sub>ML</sub>Pd/C and Pt<sub>ML</sub>PdNiN/C catalysts at 0.9 V. (e) Cyclic voltammograms of the obtained Pt<sub>ML</sub>PdNiN/C catalyst before and after 50000 cycles test between 0.6 and 1.0 V in 0.1 M HClO<sub>4</sub> solution.

## Gold-promoted structurally ordered intermetallic palladium cobalt nanoparticles for the oxygen reduction reaction

The study of ORR on Pd-based catalysts has received less attention than on Pt due to the lower activity and stability of the former. Previous studies have mainly been pursued on the Pd alloy catalysts with various shapes and structures, and little experimental studies have been focused on structurally ordered intermetallic Pd-based nanocatalysts. However, using certain material composition and structure, ordered intermetallic phases can be obtained at nanometer ranges. We demonstrated a simple method to synthesize core-shell-structured PdCo nanoparticles that can be further transformed into ordered intermetallic phases by addition of Au atoms and subsequent annealing. The discovery of unusual ordering of PdCo atoms along the [111] direction in the AuPdCo nanoparticles with twin boundaries and with stable {111}, {110} and {100} facets is revealed using high-resolution transmission electron microscope (HRTEM) (Fig. 2 a, b) and scanning transmission electron microscope (STEM) coupled with electron energy-loss spectroscopy (EELS) and electron diffraction patterns (EDPs). To our knowledge, no prior evidence of such intermetallic phases in nanoparticles of PdCo alloy has been reported. These structurally ordered intermetallic AuPdCo nanoparticles tend to behave similar to Pt catalyst for ORR (Figs. 2a & 2b), but more interestingly have much better stability than Pt in alkaline media (Fig. 2c). The superior stability of this catalyst compared with platinum after 10,000 potential cycles in alkaline media is attributed to the atomic structural order of PdCo nanoparticles along with protective effect of clusters of gold atoms on the surface. This strategy of making ordered palladium intermetallic alloy nanoparticles is considered to be a promising approach to solve the problems for the cathode in AEMFCs. We further found that a Pt monolayer deposited on the intermetallic  $\text{Au}_1\text{Pd}_4\text{Co}_5$  nanoparticle catalyst significantly increases the ORR activity and durability in acid media, and can be very suitable for the cathode material in PEMFCs.

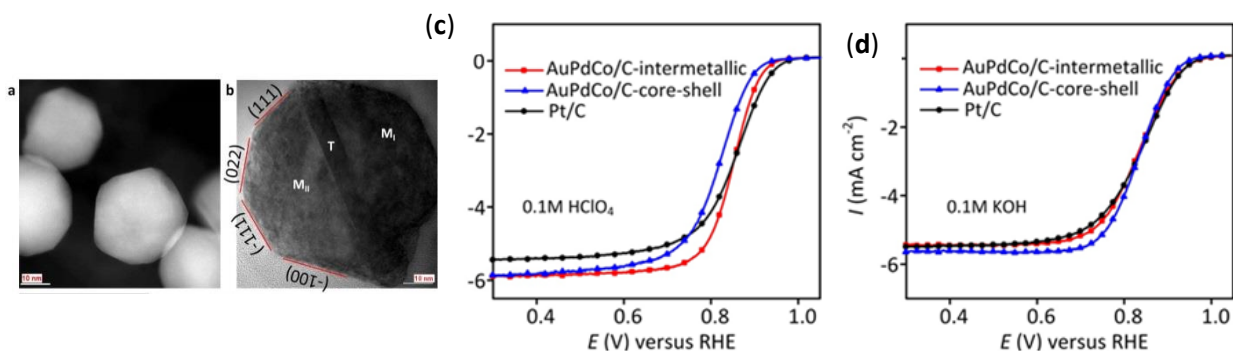


Fig. 2. (a) and (b) STEM and HRTEM image of AuPdCo-intermetallic nanoparticles showing multiple facets respectively; ORR Polarization curves for AuPdCo/C- intermetallic and core-shell catalyst along with Pt/C catalyst on an RDE electrode in (c) 0.1 M  $\text{HClO}_4$  and (d) 0.1 M  $\text{KOH}$ , respectively. Precious metal loading was  $7.65 \mu\text{g}/\text{cm}^2$  for AuPdCo catalysts and  $6.0 \mu\text{g}/\text{cm}^2$  for Pt catalyst.

## Enhanced catalytic activity of Pt monolayer under tensile strain on Au: Induced C-C bond splitting in ethanol oxidation and direct methanol oxidation to $\text{CO}_2$

We investigated the Pt monolayer electrocatalysts for alcohol electrooxidation, and demonstrated that the Pt monolayer under tensile strain on Au substrates (i.e. extended surface of Au(111))

single-crystal and Au nanoparticle) showed greatly enhanced activity for methanol and ethanol oxidation. The activity of Pt<sub>ML</sub>/Au can be further improved by incorporating active co-catalysts, and the Ru/Pt<sub>ML</sub>/Au/C and RhSnO<sub>2</sub>/Pt<sub>ML</sub>/Au/C electrocatalysts were designed and synthesized for practical application in a direct alcohol fuel cell (DAFC). Our attention was then focused on the selectivity of these Pt electrocatalysts, and *in situ* infrared spectroscopy studies (Fig. 3) were carried out with both single-crystal- and nanoparticle-based catalysts. Fig. 1a and 1b present IR spectra collected during methanol oxidation on Pt<sub>ML</sub>/Au(111) and Ru/Pt<sub>ML</sub>/Au/C surfaces. The absence of adsorbed CO band (~2090 cm<sup>-1</sup>) demonstrated that methanol oxidation on both surfaces proceeded via a direct mechanism wherein methanol was oxidized to CO<sub>2</sub> without forming a CO intermediate, and this observation was in agreement with theoretical prediction by density functional theory (DFT) calculation. Moreover, the addition of Ru co-catalyst in Ru/Pt<sub>ML</sub>/Au/C successfully moved onset of CO<sub>2</sub> band (~2343 cm<sup>-1</sup>) to around 0.3 V vs. RHE. During ethanol oxidation on Pt<sub>ML</sub>/Au(111) (Fig. 3c), the absence of both the CO<sub>ads</sub> and CO<sub>2</sub> bands suggested that ethanol dissociative adsorption did not occur and that the reaction followed partial oxidation pathway without cleavage of the C–C bond. However, the splitting of C–C bond was observed on Pt<sub>ML</sub>/Au/C and RhSO<sub>2</sub>/Pt<sub>ML</sub>/Au/C catalysts, as evidenced by the CO<sub>2</sub> band in Fig. 3d and 3e. Future work is needed to explain the difference and to further optimize the catalysts for a complete ethanol oxidation.

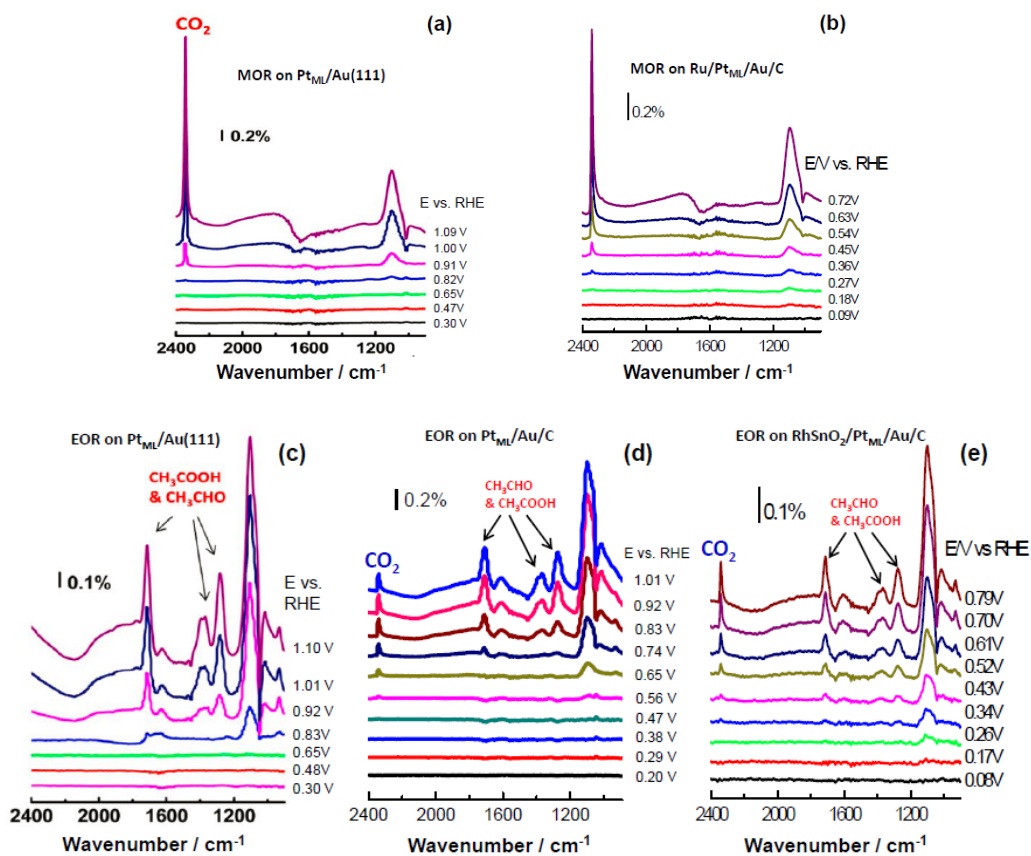


Figure 3. *In situ* infrared spectra recorded during methanol oxidation on: (a) Pt<sub>ML</sub>/Au(111), (b) Ru/Pt<sub>ML</sub>/Au/C; and during ethanol oxidation on: (c) Pt<sub>ML</sub>/Au(111), (d) Pt<sub>ML</sub>/Au/C, (e) RhSnO<sub>2</sub>/Pt<sub>ML</sub>/Au/C.

## Tuning Pt-Shell Thickness on Ru Core for Superior Activities for Hydrogen Evolution and Oxidation in Alkaline Electrolytes

Alkaline electrolytes enable use of non-Platinum-group-metals catalysts for oxygen reduction in anion exchange membrane (AEM) fuel cells and for oxygen evolution in AEM water electrolyzers. However, the challenge in reducing Pt loading remains because the activities for hydrogen oxidation reaction (HOR) and hydrogen evolution reaction (HER) on Pt are two-orders-of-magnitude lower in alkaline than in acid. Our approach for enhancing HER-HOR performance in alkalies involves synthesizing well-defined Ru@Pt<sub>1.0</sub> and Ru@Pt<sub>0.5</sub> core-shell nanocatalysts to optimize specific activity and to maximize Pt surface area. Performance test was carried out using hanging-strip gas-diffusion electrodes (GDEs) in 1 M KOH.

With gas-transport limitations alleviated by micro-porous channels in the GDEs, we obtained the iR-corrected HER-HOR polarization curves with currents up to  $\pm 600$  mA cm<sup>-2</sup> (Fig. 4a). The two Ru@Pt catalysts having Pt:Ru atomic ratios of 1.0 and 0.5 (corresponding to a Pt shell of mainly 2 and 1 monolayer, respectively) performed better than the commercial catalysts of Pt and Pt-Ru alloy. Figure 4b shows that the Pt mass activity at the HER-HOR reversible potential is enhanced by about a factor of 4 for the bilayer and monolayer Ru@Pt catalysts versus Pt nanoparticles.

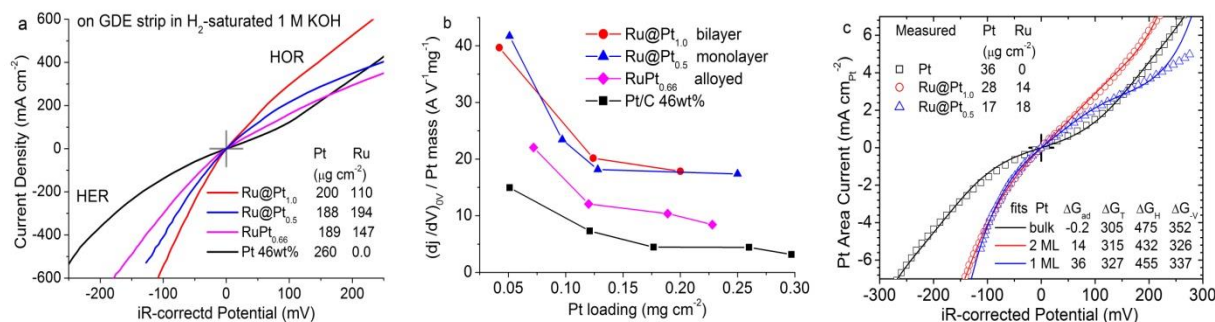


Figure 4. (a) Typical iR-corrected HER-HOR polarization curves for four catalysts on hanging strips of GDEs in 1 M KOH. (b) Pt mass activities for the HER and HOR measured by the current/voltage slope at 0 V as a function of Pt loading. (c) Fits of Pt-surface-area-normalized polarization curves using dual-path kinetic equation. Four fitted parameters with the unit of meV are the free energy of hydrogen adsorption,  $\Delta G_{ad}$ , and three activation free energies for the Tafel ( $\Delta G_T$ ), Heyrovsky ( $\Delta G_H$ ), and the reversed Volmer ( $\Delta G_v$ ) reactions.

To gain insight in the mechanism of enhanced specific activity, we fitted the Pt-area-normalized polarization curves using the dual-path kinetic equation developed based on the thermodynamic principles using the model involving Tafel, Heyrosky, and Volmer reactions as the three elementary steps. The obtained  $\Delta G_{ad}$  increased from -0.2 meV on Pt to 14 and to 36 meV, respectively, on bilayer and monolayer Pt on Ru; the trend is consistent with the DFT calculated hydrogen binding energy being weakened from Pt by 0.15 eV for the bilayer and 0.37 eV for the monolayer. A moderately weakened hydrogen adsorption on bilayer Pt is the optimum for the HOR, while more weakening in hydrogen binding on the monolayer Pt is favored for the HER. The new insight can guide future studies in optimizing Ru@Pt catalysts and developing the best catalysts for fuel cells and water electrolyzers.

## Publication Acknowledging this Grant 2012-2015

1. Tsai, H. C.; Hsieh, Y. C.; Yu, T. H.; Lee, Y. J.; Wu, Y. H.; Merinov, B. V.; Wu, P. W.; Chen, S. Y.; Adzic, R. R.; Goddard, W. A., DFT Study of Oxygen Reduction Reaction on Os/Pt Core-Shell Catalysts Validated by Electrochemical Experiment. *ACS Catalysis* 2015, 5 (3), 1568-1580.
2. Kuttiyiel, K. A.; Choi, Y.; Hwang, S.-M.; Park, G.-G.; Yang, T.-H.; Su, D.; Sasaki, K.; Liu, P.; Adzic, R. R., Enhancement of the oxygen reduction on nitride stabilized Pt-M (M=Fe, Co, and Ni) core-shell nanoparticle electrocatalysts. *Nano Energy* 2015, 13, 442-449.
3. Cao, B. F.; Neufeind, J. C.; Adzic, R. R.; Khalifah, P. G., Molybdenum Nitrides as Oxygen Reduction Reaction Catalysts: Structural and Electrochemical Studies. *Inorganic Chemistry* 2015, 54 (5), 2128-2136.
4. Zhang, Y.; Hsieh, Y. C.; Volkov, V.; Su, D.; An, W.; Si, R.; Zhu, Y. M.; Liu, P.; Wang, J. X.; Adzic, R. R., High Performance Pt Mono layer Catalysts Produced via Core-Catalyzed Coating in Ethanol. *Acs Catalysis* 2014, 4 (3), 738-742.
5. Roller, J.; Yu, H.; Vukmirovic, M. S.; Bliznakov, S.; Kotula, P. G.; Carter, C. B.; Adzic, R. R.; Maric, R., Flame-Based Synthesis of Core-Shell Structures Using Pd-Ru and Pd Cores. *Electrochim. Acta* 2014, 138, 341-352.
6. Liu, H. Q.; Koenigsmann, C.; Adzic, R. R.; Wong, S. S., Probing Ultrathin One-Dimensional Pd-Ni Nanostructures As Oxygen Reduction Reaction Catalysts. *Acs Catalysis* 2014, 4 (8), 2544-2555.
7. Kuttiyiel, K. A.; Sasaki, K.; Su, D.; Wu, L. J.; Zhu, Y. M.; Adzic, R. R., Gold-promoted structurally ordered intermetallic PdCo nanoparticles for the oxygen reduction reaction. *Nature Communications* 2014, 5.
8. Kuttiyiel, K. A.; Sasaki, K.; Chen, W. F.; Su, D.; Adzic, R. R., Core-shell, hollow-structured iridium-nickel nitride nanoparticles for the hydrogen evolution reaction. *J. Materials Chemistry A* 2014, 2 (3), 591-594.
9. Gong, K. P.; Park, J.; Su, D.; Adzic, R. R., Metalizing carbon nanotubes with Pd-Pt core-shell nanowires enhances electrocatalytic activity and stability in the oxygen reduction reaction. *Journal of Solid State Electrochemistry* 2014, 18 (5), 1171-1179.
10. Zhang, Y.; Ma, C.; Zhu, Y. M.; Si, R.; Cai, Y.; Wang, J. X.; Adzic, R. R., Hollow core supported Pt monolayer catalysts for oxygen reduction. *Catal. Today* 2013, 202, 50-54.
11. Yang, L. J.; Vukmirovic, M. B.; Su, D.; Sasaki, K.; Herron, J. A.; Mavrikakis, M.; Liao, S. J.; Adzic, R. R., Tuning the Catalytic Activity of Ru@Pt Core-Shell Nanoparticles for the Oxygen Reduction Reaction by Varying the Shell Thickness. *J. Phys. Chem. C* 2013, 117 (4), 1748-1753.
12. Vukmirovic, M. B.; Zhang, Y.; Wang, J. X.; Buceta, D.; Wu, L. J.; Adzic, R. R., Pt monolayer shell on hollow Pd core electrocatalysts: scale up synthesis, structure, and activity for the oxygen reduction reaction. *Journal of the Serbian Chemical Society* 2013, 78 (12), 1983-1992.
13. Li, M.; Zhou, W. P.; Marinkovic, N. S.; Sasaki, K.; Adzic, R. R., The role of rhodium and tin oxide in the platinum-based electrocatalysts for ethanol oxidation to CO<sub>2</sub>. *Electrochimica Acta* 2013, 104, 454-461.
14. Li, M.; Cullen, D. A.; Sasaki, K.; Marinkovic, N. S.; More, K.; Adzic, R. R., Ternary Electrocatalysts for Oxidizing Ethanol to Carbon Dioxide: Making Ir Capable of Splitting C-C Bond. *J Am Chem Soc* 2013, 135 (1), 132-141.
15. Kuttiyiel, K. A.; Sasaki, K.; Su, D.; Vukmirovic, M. B.; Marinkovic, N. S.; Adzic, R. R., Pt monolayer on Au-stabilized PdNi core-shell nanoparticles for oxygen reduction reaction. *Electrochimica Acta* 2013, 110, 267-272.
16. Kang, Y. J.; Ye, X. C.; Chen, J.; Cai, Y.; Diaz, R. E.; Adzic, R. R.; Stach, E. A.; Murray, C. B., Design of Pt-Pd Binary Superlattices Exploiting Shape Effects and Synergistic Effects for Oxygen Reduction Reactions. *J Am Chem Soc* 2013, 135 (1), 42-45.
17. Kang, Y.; Li, M.; Cai, Y.; Cargnello, M.; Diaz, R. E.; Gordon, T. R.; Wieder, N. L.; Adzic, R. R.; Gorte, R. J.; Stach, E. A.; Murray, C. B., Heterogeneous Catalysts Need Not Be so "Heterogeneous": Monodisperse Pt Nanocrystals by Combining Shape-Controlled Synthesis and Purification by Colloidal Recrystallization. *J Am Chem Soc* 2013, 135 (7), 2741-2747.

18. Hsieh, Y. C.; Zhang, Y.; Su, D.; Volkov, V.; Si, R.; Wu, L. J.; Zhu, Y. M.; An, W.; Liu, P.; He, P.; Ye, S. Y.; Adzic, R. R.; Wang, J. X., Ordered bilayer ruthenium-platinum core-shell nanoparticles as carbon monoxide-tolerant fuel cell catalysts. *Nature Communications* 2013, 4.
19. Choi, Y. M.; Kuttiyiel, K. A.; Labis, J. P.; Sasaki, K.; Park, G. G.; Yang, T. H.; Adzic, R. R., Enhanced Oxygen Reduction Activity of IrCu Core Platinum Monolayer Shell Nano-electrocatalysts. *Topics in Catalysis* 2013, 56 (12), 1059-1064.
20. Cheon, J. Y.; Kim, T.; Choi, Y.; Jeong, H. Y.; Kim, M. G.; Sa, Y. J.; Kim, J.; Lee, Z.; Yang, T. H.; Kwon, K.; Terasaki, O.; Park, G. G.; Adzic, R. R.; Joo, S. H., Ordered mesoporous porphyrinic carbons with very high electrocatalytic activity for the oxygen reduction reaction. *Scientific Reports* 2013, 3.
21. Chen, W. F.; Wang, C. H.; Sasaki, K.; Marinkovic, N.; Xu, W.; Muckerman, J. T.; Zhu, Y.; Adzic, R. R., Highly active and durable nanostructured molybdenum carbide electrocatalysts for hydrogen production. *Energy & Environmental Science* 2013, 6 (3), 943-951.
22. Cao, B. F.; Veith, G. M.; Neuefeind, J. C.; Adzic, R. R.; Khalifah, P. G., Mixed Close-Packed Cobalt Molybdenum Nitrides as Non-noble Metal Electrocatalysts for the Hydrogen Evolution Reaction. *J Am Chem Soc* 2013, 135 (51), 19186-19192.
23. Cao, B. F.; Veith, G. M.; Diaz, R. E.; Liu, J.; Stach, E. A.; Adzic, R. R.; Khalifah, P. G., Cobalt Molybdenum Oxynitrides: Synthesis, Structural Characterization, and Catalytic Activity for the Oxygen Reduction Reaction. *Angewandte Chemie-International Edition* 2013, 52 (41), 10753-10757.
24. Zhou, W. P.; An, W.; Su, D.; Palomino, R.; Liu, P.; White, M. G.; Adzic, R. R., Electrooxidation of Methanol at SnOx-Pt Interface: A Tunable Activity of Tin Oxide Nanoparticles. *Journal of Physical Chemistry Letters* 2012, 3 (22), 3286-3290.
25. Vukmirovic, M. B.; Cai, Y.; Bliznakov, S. T.; Sasaki, K.; Wang, J. X.; Adzic, R. R., Platinum Monolayer Electrocatalysts for the Oxygen Reduction Reaction. *Tutorials on Electrocatalysis in Low Temperature Fuel Cells* 2012, 45 (2), 15-23.
26. Sasaki, K.; Naohara, H.; Choi, Y. M.; Cai, Y.; Chen, W. F.; Liu, P.; Adzic, R. R., Highly stable Pt monolayer on PdAu nanoparticle electrocatalysts for the oxygen reduction reaction. *Nature Communications* 2012, 3.
27. Li, M.; Liu, P.; Adzic, R. R., Platinum Monolayer Electrocatalysts for Anodic Oxidation of Alcohols. *Journal of Physical Chemistry Letters* 2012, 3 (23), 3480-3485.
28. Kuttiyiel, K. A.; Sasaki, K.; Choi, Y. M.; Su, D.; Liu, P.; Adzic, R. R., Nitride Stabilized PtNi Core-Shell Nanocatalyst for high Oxygen Reduction Activity. *Nano Letters* 2012, 12 (12), 6266-6271.
29. Kuttiyiel, K. A.; Sasaki, K.; Choi, Y.; Su, D.; Liu, P.; Adzic, R. R., Bimetallic IrNi core platinum monolayer shell electrocatalysts for the oxygen reduction reaction. *Energy & Environmental Science* 2012, 5 (1), 5297-5304.
30. Koenigsmann, C.; Sutter, E.; Chiesa, T. A.; Adzic, R. R.; Wong, S. S., Highly Enhanced Electrocatalytic Oxygen Reduction Performance Observed in Bimetallic Palladium-Based Nanowires Prepared under Ambient, Surfactantless Conditions. *Nano Letters* 2012, 12 (4), 2013-2020.
31. Koenigsmann, C.; Sutter, E.; Adzic, R. R.; Wong, S. S., Size- and Composition-Dependent Enhancement of Electrocatalytic Oxygen Reduction Performance in Ultrathin Palladium-Gold (Pd1-xAu) Nanowires. *J. Phys. Chem. C* 2012, 116 (29), 15297-15306.
32. Karan, H. I.; Sasaki, K.; Kuttiyiel, K.; Farberow, C. A.; Mavrikakis, M.; Adzic, R. R., Catalytic Activity of Platinum Mono layer on Iridium and Rhenium Alloy Nanoparticles for the Oxygen Reduction Reaction. *Acc Catalysis* 2012, 2 (5), 817-824.
33. Kang, Y. J.; Qi, L.; Li, M.; Diaz, R. E.; Su, D.; Adzic, R. R.; Stach, E.; Li, J.; Murray, C. B., Highly Active Pt3Pb and Core-Shell Pt3Pb-Pt Electrocatalysts for Formic Acid Oxidation. *Acc Nano* 2012, 6 (3), 2818-2825.
34. Huang, K.; Sasaki, K.; Adzic, R. R.; Xing, Y. C., Increasing Pt oxygen reduction reaction activity and durability with a carbon-doped TiO2 nanocoating catalyst support. *J. Mater. Chem.* 2012, 22 (33), 16824-16832.
35. Herron, J. A.; Jiao, J.; Hahn, K.; Peng, G. W.; Adzic, R. R.; Mavrikakis, M., Oxygen Reduction Reaction on Platinum-Terminated "Onion-structured" Alloy Catalysts. *Electrocatalysis* 2012, 3 (3-4), 192-202.

36. Gong, K. P.; Cho, Y.; Vukmirovic, M. B.; Liu, P.; Ma, C.; Su, D.; Adzic, R. R., Tetrahedral Palladium Nanocrystals: A New Support for Platinum Monolayer Electrocatalysts with High Activity and Stability in the Oxygen Reduction Reaction. *Zeitschrift Fur Physikalische Chemie-International Journal of Research in Physical Chemistry & Chemical Physics* 2012, 226 (9-10), 1025-1038.
37. Chen, W. F.; Sasaki, K.; Ma, C.; Frenkel, A. I.; Marinkovic, N.; Muckerman, J. T.; Zhu, Y. M.; Adzic, R. R., Hydrogen-Evolution Catalysts Based on Non-Noble Metal Nickel-Molybdenum Nitride Nanosheets. *Angewandte Chemie-International Edition* 2012, 51 (25), 6131-6135.
38. Bliznakov, S. T.; Vukmirovic, M. B.; Yang, L.; Sutter, E. A.; Adzic, R. R., Pt Monolayer on Electrodeposited Pd Nanostructures: Advanced Cathode Catalysts for PEM Fuel Cells. *Journal of the Electrochemical Society* 2012, 159 (9), F501-F506.

**Increasing Catalytic Performance for the Reduction of CO<sub>2</sub>  
by Controlling Free Energies for Proton and Hydride Transfers**

**Aaron M. Appel**, John C. Linehan, Eric S. Wiedner,  
Brandon R. Galan, Christopher M. Zall, Samantha J. Connelly  
Pacific Northwest National Laboratory

Due to the intermittent and distributed nature of carbon-neutral energy production, the storage of energy in the form of chemical fuels is highly desirable. The catalytic reduction of CO<sub>2</sub> would allow the production of liquid fuels from this commonly available substrate. We seek to understand how to rationally design catalysts for the reduction of CO<sub>2</sub> and utilization of the corresponding fuels, using both electrocatalysis and hydrogenation.

One of the first steps in the reduction of CO<sub>2</sub> is the formation of the initial C-H bond by hydride transfer. For the hydrogenation of CO<sub>2</sub> to formate, we are using the free energy for transfer of a hydride as a specific focus in the design of first-row transition metal complexes. Nickel hydride complexes are typically unable to hydrogenate CO<sub>2</sub> due to inadequate hydricities, however, new design strategies are being used to enable nickel-based catalysts. The free energy for transferring a hydride from nickel to CO<sub>2</sub> can be shifted from unfavorable to spontaneous by improving the hydricity of the nickel hydride relative to formate. Two approaches will be presented: synthetic modification of the complexes using more strongly donating ligands, and the use of a change in solvent to bias the reaction energetics. Quantifying the role of solvent in controlling the reaction profile is critical to the second approach and will be discussed.

**Multiscale Imaging and DFT Analysis of Reactant Interactions on Single-Layer MoS<sub>2</sub> and related Molybdenum-Sulfur Nanomaterials**

Ludwig Bartels, Talat S. Rahman\*, Koichi Yamaguchi, Duy Le,\* Takat B. Rawal,\* Miguel Isarraraz, Joseph Martinez, Ariana Nguyen, Emily Li, Sampyo Hong\*

University of California at Riverside (\*=University of Central Florida)

**Presentation Abstract**

We present experimental and theoretical investigations of the structure and chemical interaction of single-layer films/islands of MoS<sub>2</sub> and related molybdenum-sulfur compounds on Cu(111) and SiO<sub>2</sub>/Si substrates. In particular, our work focuses on the properties of sub-stoichiometric sulfides and sulfur vacancies, which we find to have a significantly higher affinity for reactants than – unsurprisingly – the MoS<sub>2</sub> basal plane but also the brims/edges of MoS<sub>2</sub> islands. Our multipronged effort involves scanning tunneling microscopy imaging, density functional theory simulation, photoluminescence spectroscopy and submicron optical imaging. The latter two approaches required the setup of dedicated instrumentation; they offer a complementary approach to the properties of this catalyst material that permits probing at ambient pressures and above.

Additional work in this project addressed the role of the support in facilitating reactions on supported metal catalysts. This is described in a separate poster.

**DE-FG02-07ER15842: Controlling Structural, Electronic, and Energy Flow Dynamics of Catalytic Processes through Tailored Nanostructures**

PI: Talat S. Rahman, Ludwig Bartels

Postdocs: Duy Le, Sampyo Hong

Students: Wenhao Lu, Koichi Yamaguchi, Chen Wang, Quan Ma, Miguel Isarraraz, Michael Gomez, Cindy Merida, Emily Li, Ariana Nguyen, Gretel von Son, Joseph Martinez, Sahar Naghibi, Takat B. Rawal, Maral Aminpour, S. Islamuddin Shah, Ghazal Shafai

**RECENT PROGRESS**

***Large-Scale Growth of MoS<sub>2</sub> on Insulators***

**Beyond the Atomic Scale.** STM is the ideal tool for investigating atomic-scale interactions between reactants and substrates as long as they can be realized under UHV and low-temperature conditions. Yet crucial to our research project is obtaining knowledge beyond these limitations — i.e., under realistic reaction conditions of MoS<sub>2</sub> hydrogenation catalysis. Under higher temperature and pressure the spatial resolution is limited (depending on the technique) and larger-scale samples are required. Likewise, thermally-programmed desorption experiments demand cm-scale continuous film substrates. As we are interested in spatially-resolved understanding of the processes on MoS<sub>2</sub> nanostructures, we require single-layer material spread out over a substrate. To this end, we adapted and improved upon known growth methodologies for single-layer MoS<sub>2</sub> films. These techniques allow us to grow MoS<sub>2</sub> islands both of the typical triangular shape with straight edges and

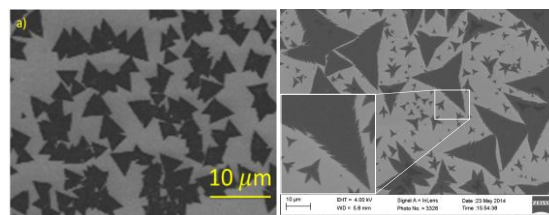


Fig. 1 SEM images of single-layer MoS<sub>2</sub> islands on SiO<sub>2</sub>/Si substrates. The left panel shows islands with straight edges: the right panel ones with ‘feathered’ edges, which increase total edge length.

of a type with concave sides, whose edges are “feathered,” maximizing edge length within the triangular footprint [Fig. 1].

### Activation of the MoS<sub>2</sub> Basal Plane:

**Sulfur-vacancies provide opportunity for catalytic activity.** An important result of the current funding period is that sulfur depletion of MoS<sub>2</sub> is possible via gentle Ar<sup>+</sup> sputtering without destabilization of the single-layer character of the material. This provides a facile route for making the basal plane of MoS<sub>2</sub> catalytically active. Creation of sulfur-vacancy on MoS<sub>2</sub> is also possible under electron irradiation. At sulfur-vacancy sites undercoordinated Mo atoms are exposed to the surface. This allows their *d*-states to form bonds with adsorbing species, thereby offering opportunities for chemical activity.

**Validation via HDS on Sputtered MoS<sub>2</sub>.** In order to characterize the activity of defects in the MoS<sub>2</sub> basal plane we turn to photoluminescence (PL) spectroscopy as a tool that can be applied over a wide temperature range. Fig. 2 shows the temperature-dependent PL intensity of single-layer MoS<sub>2</sub> films in UHV. Sputtering reduces the PL intensity significantly and annealing is not able to restore it to near its original value. Exposure of the sample to benzenethiol followed by renewed annealing to 600 K, in contrast, restores the PL intensity nearly to its original value, thereby a) ascertaining that benzenethiol inserts its sulfur into the sputter-induced vacancies and b) that the vacancies on the basal plane are capable of abstracting sulfur from an organic (albeit comparatively easy to desulfurize) reactant.

**Multi-Scale Imaging of MoS<sub>2</sub> Hydrogenation.** We have already begun with the investigation of high-pressure, high-temperature hydrogenation of MoS<sub>2</sub> as it may be expected under reactive conditions in the presence of hydrogen. We are developing a setup that allows us direct imaging of micron-scale MoS<sub>2</sub> islands via their photoluminescence. Fig. 3 shows (a) the PL signal of a set of triangular MoS<sub>2</sub> islands obtained at 150K and its evolution under 760 torr of H<sub>2</sub> at 350°C. Initially, the islands show enhanced PL yield near their edges and an overall bright luminescence. As they are exposed to hydrogen, their PL diminishes after a brief

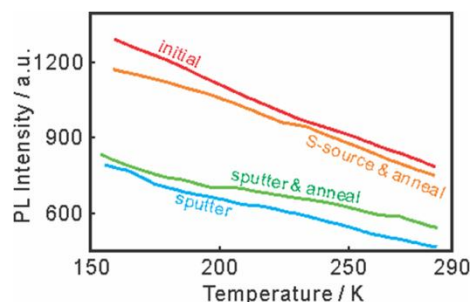


Fig. 2 Temperature dependent PL intensities of single-layer MoS<sub>2</sub> before (red) and after (blue) creation of sulfur-vacancies by sputtering; after (green) subsequent anneal, exposure to benzenethiol (BT) and renewed anneal. The significant recovery of the PL yield indicates desulfurization of BT and repair of the MoS<sub>2</sub> film to its almost pristine state.<sup>4</sup>

initiation period, during which it slightly increases. Moreover, we observe that internal structure develops inside the island, both from the edges moving inward and also on the inside of the islands. As the exposure progresses, the amount of structure increase suggesting that fronts of defects emerge starting from locations both at the edge and at initial basal plane defects. Tentatively, we attribute them to hydrogenation of the MoS<sub>2</sub> film and/or ensuing sulfur depletion.



Fig. 3 Spatially resolved photoluminescence of a population of single-layer islands of MoS<sub>2</sub> on SiO<sub>2</sub> after the indicated duration of exposure to H<sub>2</sub> at 760 torr and 350°C. PL was acquired at 150K and exclusively photons between 665 and 675 nm are displayed.

Anticipated computational results on the PL properties of hydrogenated MoS<sub>2</sub> will soon provide clarity.

**Real-Time *in-situ* Monitoring of HDS.** If the dimming of the PL yield of the MoS<sub>2</sub> single-layer island is associated with sulfur removal or the presence of surface hydrogen, then exposure of the islands to a sulfur source, such as benzenethiol, will be able to invert this trend. Moreover, a hydrogen/sulfur precursor mixing ratio may be found, at which the total brightness of an island remains constant. This may be interpreted as the optimal scenario for HDS. The results of such an experiment are shown in Fig. 4 which traces the PL intensity of a MoS<sub>2</sub> islands at 600 K while exposing it to 100 torr of H<sub>2</sub> and 600 torr

of  $N_2$ . After about 8h of exposure, we add a small amount ( $\sim 10^{-3}$  torr) of benzenethiol (BT) to the process gas mixture and observe over the following 15 min a steep increase of the PL yield. We interpret this as removal of hydrogen-induced modifications of the catalyst material by means of desulfurization of BT, i.e., real-time monitoring of the HDS reaction. Once the BT vapor is consumed, the PL yield of the islands decreases again until we established a constant concentration of BT and  $H_2$  in the process gas.

### Reaction Pathways on Defected $MoS_2$

#### Methanol synthesis on defect-laden single-layer $MoS_2$ supported on Cu(111):

Despite being found to be the preferred structure in single layer  $MoS_2$ , the sulfur vacancy row does not facilitate alcohol synthesis from syngas because its narrow size limits adsorption, diffusion, and formation of possible intermediates. On the Cu(111) surface, strong interactions between  $MoS_2$  and Cu are expected to reduce the corrugations caused by sulfur vacancy rows, resulting in a larger exposure of vacancies to adsorbates which could enhance the catalytic activity of the row towards alcohol synthesis from syngas. We investigated the alcohol synthesis from syngas ( $CO$ ,  $CO_2$ ,  $H_2$ ) on a single layer  $MoS_2$  with sulfur vacancy row grown on the Cu(111) surface by mean of DFT using PBE functional<sup>6,7</sup> together with DFT-D3 correction<sup>8</sup> for accounting the vdW interactions. We found that, as predicted, the  $MoS_2$  with sulfur vacancy row on Cu(111) does not exhibit strong reconstruction resulting in an almost-flat layer producing an ideal condition for enhancing the efficiency of alcohol synthesis. We show that: (1) there is significant charge transfer from the Cu(111) surface to  $MoS_2$ , enhancing its catalytic properties, (2) the binding energies of  $CO$  and dissociated  $H_2$  increase by 0.3 eV in comparison to that on unsupported  $MoS_2$ , indicating stronger interactions, and (3) the barriers for forming intermediate species in the alcohol synthesis process reduce significantly in comparison to that on unsupported  $MoS_2$ .

On the basis of these energetics, we conclude the Cu(111) substrate promotes methanol synthesis from syngas on single-layer  $MoS_2$  with a vacancy row. In addition, our preliminary results for water gas shift reaction indicate that  $H_2O$  may dissociate at a sulfur vacancy row of  $MoS_2$  on Cu(111) and that  $CO_2$  also dissociates here from  $CO$  and atomic oxygen adsorbed to the  $MoS_2/Cu(111)$  system.

**Atomic-Scale Validation of Computational Reaction Pathways.** Important for modeling reaction pathways (such as in Fig. 6) is a comprehensive understanding of the interaction of adsorbates with the S- and Mo-centers of defected  $MoS_2$ . The geometry of the vacancy patch determines reactant access to Mo-

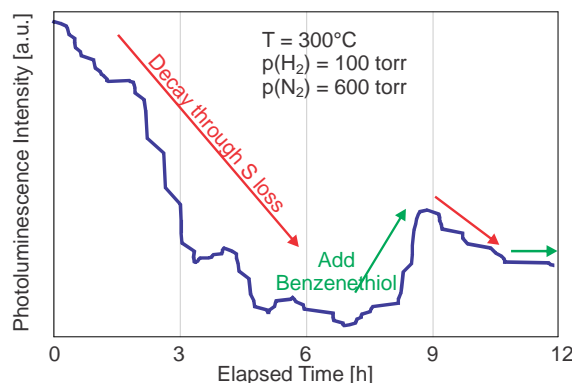


Fig. 4. PL intensity of a  $MoS_2$  island during exposure to 100 torr of  $H_2$  at 600 K. After a short initiation phase (not shown) a continuous decrease of PL intensity is visible, which is partially recovered when at 7h and 8h increasing bursts of benzenethiol are added to the process gas. Subsequently, the PL yield decreases again, until at 11h BT is leaked continuously into the process gas to stabilize film conditions. Images were acquired every minute, selected for focal quality and PL yield over an island was integrated to obtain this graph.

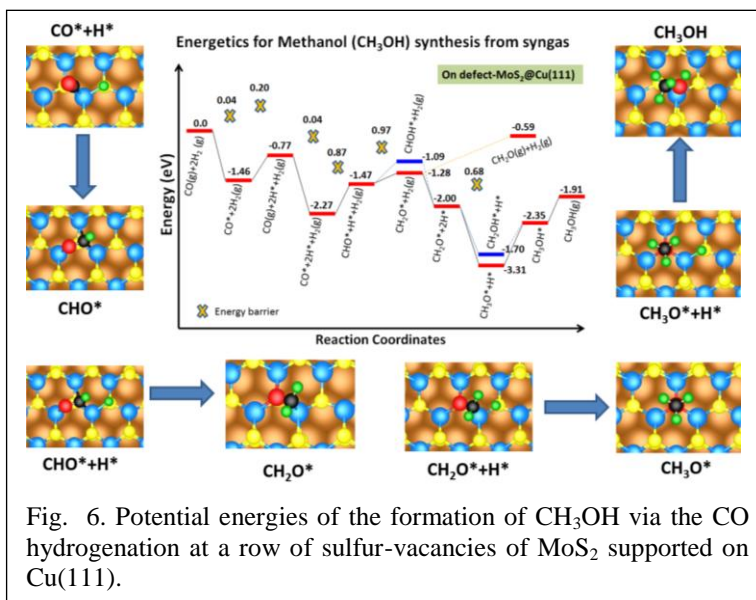


Fig. 6. Potential energies of the formation of  $CH_3OH$  via the  $CO$  hydrogenation at a row of sulfur-vacancies of  $MoS_2$  supported on Cu(111).

and S-centers via specific binding/coordination sites. In order to screen the affinities of different geometries to reactant binding, we have turned to experiments involving  $\text{Mo}_x\text{S}_y$  clusters in collaboration with Michael White of BNL<sup>9,10</sup>. Mass-selected deposition of clusters in the White group allows access to  $\text{Mo}_x\text{S}_y$  aggregates of known sulfur-to-molybdenum ratio.

We have carried out preliminary studies of well-defined  $\text{Mo}_x\text{S}_y$  clusters deposited onto a Cu(111) surface both on the basis of DFT (Fig. 7) and experimentally through TPD. These experiments started with the deposition of  $\text{Mo}_6\text{S}_8$ ,  $\text{Mo}_3\text{S}_7$  and  $\text{Mo}_4\text{S}_6$  onto Cu(111); the choice of substrate provides direct comparability to our growth of  $\text{MoS}_2$  inverted catalyst on the same substrate.

**Beyond Isolated Defects.** Foundational to the prevalent assignment of  $\text{MoS}_2$  activity to the edge locations is the presence of a charge density at the Fermi level there. Experimental and theoretical studies by Dowben's, Bartels' and Rahman's groups reveal other avenues to generate Fermi-level charge density on  $\text{MoS}_2$ . Alkali metal adsorption on  $\text{MoS}_2(0001)$  has significant influence on the catalytic properties of  $\text{MoS}_2$ . We have collaborated with Dowben et al. to investigate the influence of sodium on the occupied and unoccupied band structure of  $\text{MoS}_2$  utilizing angle-resolved photoemission and inverse photoemission spectroscopy (ARPES & ARIPES, respectively) experiments (Fig. 8). Starting with bulk  $\text{MoS}_2$  we have recently also obtained synchrotron data on single-layer  $\text{MoS}_2$  films grown in this collaboration. A comparison of the experimental band dispersion with DFT shows excellent agreement for the occupied states, and qualitative agreement for the unoccupied states. Na-adsorption leads to charge transfer to the  $\text{MoS}_2$  surface causing an effect similar to n-type doping of a semiconductor.

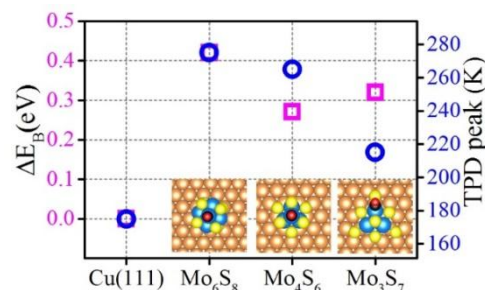


Fig. 7 Changes of binding energies (magenta squares) of CO on  $\text{Mo}_x\text{S}_y/\text{Cu}(111)$  with respect to that on the clean Cu(111) surface calculated from DFT ( $\Delta E_B$ ) and TPD peaks (blue circles) of the CO desorption from these systems (M. White et al.)

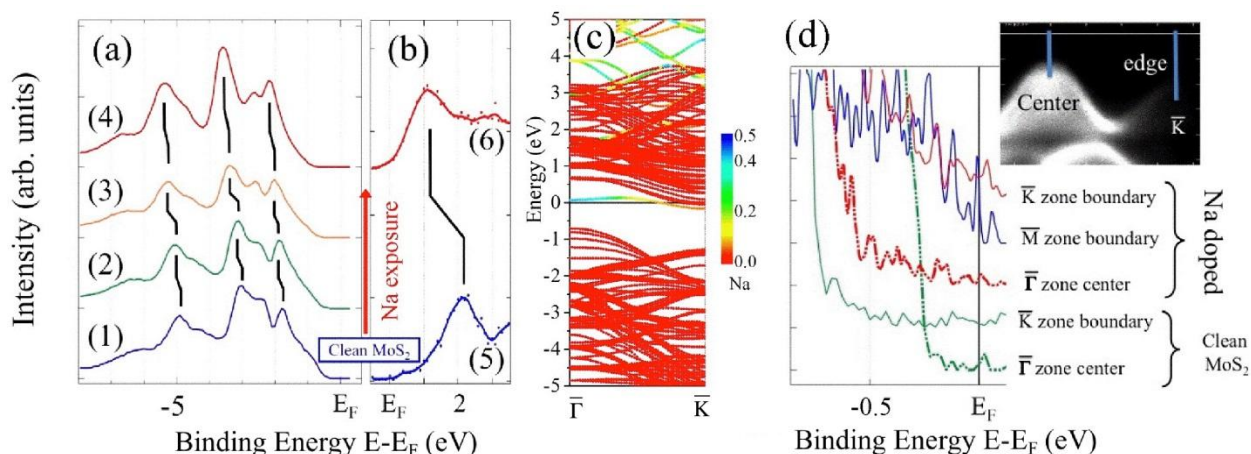


Fig. 8. A comparison of occupied density of states (DOS) near  $\bar{\Gamma}$  from photoemission (a), unoccupied DOS for normal incidence from inverse photoemission (b) and computation band structure for high coverages of Na on  $\text{MoS}_2$ (c). A rigid shift of the bands to lower energy (corresponding to n-doping) is observed, which is stronger for unoccupied than occupied states. While no DOS near  $E_F$  is found in the vicinity of  $\bar{\Gamma}$ , off-axis photoemission reveals its presence at the Brillouin zone boundary (in the vicinity of both K and M), thereby indicating that potentially-active frontier orbitals are created through alkali adsorption onto  $\text{MoS}_2$ . This preliminary result is consistent with (c) and highlights the importance of the DOS of  $\text{MoS}_2$  under environmental influences.

## Publications Acknowledging this Grant in 2012-2014<sup>1-29</sup>

1. S. Berciaud, V.V. Deshpande, R. Caldwell, Y. Miyauchi, C. Voisin, P. Kim, J. Hone, and T.F. Heinz, "All-optical structure assignment of individual single-walled carbon nanotubes from Rayleigh and Raman scattering measurements," *physica status solidi (b)* **249**, 2436-2441 (2012).
2. R.P. Galhenage, S.C. Ammal, H. Yan, A.S. Duke, S.A. Tenney, A. Heyden, and D.A. Chen, "Nucleation, Growth, and Adsorbate-Induced Changes in Composition for Co–Au Bimetallic Clusters on TiO<sub>2</sub>," *The Journal of Physical Chemistry C* **116**, 24616-24629 (2012).
3. L. Ge, F. Zuo, J. Liu, Q. Ma, C. Wang, D. Sun, L. Bartels, and P. Feng, "Synthesis and Efficient Visible Light Photocatalytic Hydrogen Evolution of Polymeric g-C<sub>3</sub>N<sub>4</sub> Coupled with CdS Quantum Dots," *The Journal of Physical Chemistry C* **116**, 13708-13714 (2012).
4. Y. Hou, F. Zuo, Q. Ma, C. Wang, L. Bartels, and P. Feng, "Ag<sub>3</sub>PO<sub>4</sub> Oxygen Evolution Photocatalyst Employing Synergistic Action of Ag/AgBr Nanoparticles and Graphene Sheets," *The Journal of Physical Chemistry C* **116**, 20132-20139 (2012).
5. D. Le, M. Aminpour, A. Kiejna, and T.S. Rahman, "The role of van der Waals interaction in the tilted binding of amine molecules to the Au(111) surface," *Journal of Physics: Condensed Matter* **24**, 222001 (2012).
6. D. Le, A. Kara, E. Schroder, P. Hyldgaard, and T.S. Rahman, "Physisorption of nucleobases on graphene: a comparative van der Waals study," *Journal of Physics: Condensed Matter* **24**, 424210 (2012).
7. D. Le, D.Z. Sun, W.H. Lu, L. Bartels, and T.S. Rahman, "Single layer MoS<sub>2</sub> on the Cu(111) surface: First-principles electronic structure calculations," *Physical Review B* **85**, 075429 (2012).
8. E.A. Lewis, D. Le, C.J. Murphy, A.D. Jewell, M.F.G. Mattera, M.L. Liriano, T.S. Rahman, and E.C.H. Sykes, "Dissociative Hydrogen Adsorption on Close-Packed Cobalt Nanoparticle Surfaces," *Journal of Physical Chemistry C* **116**, 25868-25873 (2012).
9. D. Sun, W. Lu, D. Le, Q. Ma, M. Aminpour, M. Alcantara Ortigoza, S. Bobek, J. Mann, J. Wyrick, T.S. Rahman, and L. Bartels, "An MoS<sub>x</sub> Structure with High Affinity for Adsorbate Interaction," *Angewandte Chemie International Edition* **51**, 10284-10288 (2012).
10. S.A. Tenney, B.A. Cagg, M.S. Levine, W. He, K. Manandhar, and D.A. Chen, "Enhanced activity for supported Au clusters: Methanol oxidation on Au/TiO<sub>2</sub>(110)," *Surface Science* **606**, 1233-1243 (2012).
11. V. Turkowski, S. Babu, D. Le, A. Kumar, M.K. Haldar, A.V. Wagh, Z. Hu, A.S. Karakoti, A.J. Gesquiere, B. Law, S. Mallik, T.S. Rahman, M.N. Leuenberger, and S. Seal, "Linker-induced anomalous emission of organic-molecule conjugated metal-oxide nanoparticles," *ACS Nano* **6**, 4854-4863 (2012).
12. Z. Yeming, W. Jonathan, D.C. Kamelia, M. Katie Marie, H. Connor, S. Daniel, M. Quan, S. Dezheng, and B. Ludwig, "Acetylene on Cu(111): imaging a molecular surface arrangement with a constantly rearranging tip," *Journal of Physics: Condensed Matter* **24**, 354005 (2012).
13. S. Hong, D. Le, and T. Rahman, "Deactivation of Cu<sub>2</sub>O(100) by CO Poisoning," *Topics in Catalysis* **56**, 1082-1087 (2013).
14. S. Hong and T.S. Rahman, "Rationale for the Higher Reactivity of Interfacial Sites in Methanol Decomposition on Au<sub>13</sub>/TiO<sub>2</sub>(110)," *Journal of the American Chemical Society* **135**, 7629-7635 (2013).
15. D. Le and T.S. Rahman, "Joined edges in MoS<sub>2</sub>: metallic and half-metallic wires," *Journal of Physics: Condensed Matter* **25**, 312201 (2013).
16. D. Le, D. Sun, W. Lu, M. Aminpour, C. Wang, Q. Ma, T.S. Rahman, and L. Bartels, "Growth of aligned Mo<sub>6</sub>S<sub>6</sub> nanowires on Cu(111)," *Surface Science* **611**, 1-4 (2013).
17. E.A. Lewis, D. Le, A.D. Jewell, C.J. Murphy, T.S. Rahman, and E.C.H. Sykes, "Visualization of Compression and Spillover in a Coadsorbed System: Syngas on Cobalt Nanoparticles," *ACS Nano* **7**, 4384-4392 (2013).

18. Q. Ma, P.M. Odenthal, J. Mann, D. Le, C.S. Wang, Y. Zhu, T. Chen, D. Sun, K. Yamaguchi, T. Tran, M. Wurch, J.L. McKinley, J. Wyrick, K. Magnone, T.F. Heinz, T.S. Rahman, R. Kawakami, and L. Bartels, "Controlled Argon Beam-Induced Desulfurization of Monolayer Molybdenum Disulfide," *Journal of Physics: Condensed Matter* **25**, 252201 (2013).
19. K.F. Mak, K. He, C. Lee, G.H. Lee, J. Hone, T.F. Heinz, and J. Shan, "Tightly bound trions in monolayer MoS<sub>2</sub>," *Nature Materials* **12**, 207-11 (2013).
20. J. Mann, D.Z. Sun, Q. Ma, J.R. Chen, E. Preciado, T. Ohta, B. Diaconescu, K. Yamaguchi, T. Tran, M. Wurch, K. Magnone, T.F. Heinz, G.L. Kellogg, R. Kawakami, and L. Bartels, "Facile growth of monolayer MoS<sub>2</sub> film areas on SiO<sub>2</sub>," *European Physical Journal B* **86**, 2261-4 (2013).
21. T. Komesu, D. Le, Q. Ma, E.F. Schwier, Y. Kojima, M. Zheng, H. Iwasawa, K. Shimada, M. Taniguchi, L. Bartels, T.S. Rahman, and P.A. Dowben, "Symmetry Resolved Surface-Derived Electronic Structure of MoS<sub>2</sub>(0001)," *Journal of Physics: Condensed Matter* **26**, 455501 (2014).
22. T. Komesu, D. Le, X. Zhang, Q. Ma, E.F. Schwier, Y. Kojima, M. Zheng, H. Iwasawa, K. Shimada, M. Taniguchi, L. Bartels, T.S. Rahman, and P.A. Dowben, "Occupied and unoccupied electronic structure of Na doped MoS<sub>2</sub>(0001)," *Applied Physics Letters* **105**, 241602 (2014).
23. D. Le, T.B. Rawal, and T.S. Rahman, "Single-Layer MoS<sub>2</sub> with Sulfur Vacancies: Structure and Catalytic Application," *The Journal of Physical Chemistry C* **118**, 5346-5351 (2014).
24. E.A. Lewis, D. Le, A.D. Jewell, C.J. Murphy, T.S. Rahman, and E.C.H. Sykes, "Segregation of Fischer-Tropsch reactants on cobalt nanoparticle surfaces," *Chemical Communications* **50**, 6537-9 (2014).
25. Q. Ma, M. Isarraraz, C.S. Wang, E. Preciado, V. Klee, S. Bobek, K. Yamaguchi, E. Li, P.M. Odenthal, A. Nguyen, D. Barroso, D. Sun, G. von Son Palacio, M. Gomez, A. Nguyen, D. Le, G. Pawin, J. Mann, T.F. Heinz, T.S. Rahman, and L. Bartels, "Post-Growth Tuning of the Bandgap of Single-Layer Molybdenum Disulfide Films by Sulfur/Selenium Exchange," *ACS Nano* **8**, 4672-7 (2014).
26. J. Mann, Q. Ma, P.M. Odenthal, M. Isarraraz, D. Le, E. Preciado, D. Barroso, K. Yamaguchi, G. von Son Palacio, A. Nguyen, T. Tran, M. Wurch, A. Nguyen, V. Klee, S. Bobek, D. Sun, T.F. Heinz, T.S. Rahman, R. Kawakami, and L. Bartels, "2-Dimensional Transition Metal Dichalcogenides with Tunable Direct Band Gaps: MoS<sub>2(1-x)</sub> Se<sub>2x</sub> Monolayers," *Advanced Materials* **26**, 1399-404 (2014).
27. S.I. Shah, S. Hong, and T.S. Rahman, "Combined Density Functional Theory and Kinetic Monte Carlo Study of Selective Oxidation of NH<sub>3</sub> on Rutile RuO<sub>2</sub>(110) at Ambient Pressures," *The Journal of Physical Chemistry C* **118**, 5226-5238 (2014).
28. D. Le, A. Barinov, E. Preciado, M. Isarraraz, I. Tanabe, T. Komesu, C. Troha, L. Bartels, T.S. Rahman, and P.A. Dowben, "Spin-Orbit Coupling in the Band Structure of Monolayer WSe<sub>2</sub>," *Journal of Physics: Condensed Matter* **27**, 182201 (2015).
29. D.T. Restrepo, K.E. Giesler, R.A. Penabe, M. Aminpour, D. Le, T.S. Rahman, and R.G. Blair, "Heterogeneous Metal-Free Hydrogenation Over Defect Hexagonal Boron Nitride," Submitted (2015).

## Catalysts for the Selective Synthesis of Fuels and Chemicals

Alexis T. Bell

Lawrence Berkeley National Laboratory  
Chemical Science Division  
Berkeley, CA 94720

### Abstract

This effort is devoted to establishing the role of composition on the activity and selectivity of both bulk and supported metal oxides on a variety of catalyzed reactions, including the oxidation of propene to acrolein, the ammoxidation of propene to acrylonitrile, the metathesis of propene, the conversion of ethanol to butanol, and the promotion of Fischer-Tropsch synthesis by metal oxides. The objectives of these studies are pursued through measurements of reaction kinetics complemented by spectroscopic measurements and high-resolution electron microscopy.

### FWP CH030201: Catalysis Research Program

**PI:** Alexis T. Bell

**Students:** Christopher Ho; John Howell; Gregory Johnson; Rachel Licht; Zheng Zhai

### RECENT PROGRESS

#### *Mechanism and Kinetics of Alkene Oxidation*

Bismuth molybdate is known to be active for the oxidation of propene to acrolein and its activity can be altered by substitution of other elements (e.g., Fe, V, W) into the scheelite phase of  $\alpha$ - $\text{Bi}_2\text{Mo}_3\text{O}_{12}$ . This work has further revealed that the apparent activation energy for propene formation correlates with the band gap of the catalyst measured at reaction temperature. It is, therefore, of interest to establish to how the crystal structure of the catalyst affects the activation energy. We report here an investigation of propene oxidation conducted over Bi, Mo, V oxides having the aurivillius structure with the composition  $\text{Bi}_4\text{V}_{2-x}\text{Mo}_x\text{O}_{11+x/2}$  ( $x = 0-1$ ) and compare the results those for oxides having the scheelite structure with the composition  $\text{Bi}_{2-x/3}\text{Mo}_x\text{V}_{1-x}\text{O}_{12}$  ( $x = 0-1$ ). The aurivillius-phase catalysts also show a correlation between the apparent activation energy and the band gap of the oxide, the only difference being that for a given band gap, the apparent activation energy for the aurivillius-phase catalysts is  $\sim 1.5$  kcal/mol higher than that for the scheelite-phase catalysts. This difference is attributed to the lower heat of propene adsorption on the aurivillius-phase catalysts (Fig. 1). A further finding is that for catalysts with band gaps greater than  $\sim 2.1$  eV, the acrolein selectivity is  $\sim 75\%$  for the conditions used and independent of the propene conversion (Fig. 1). When the band gap falls below  $\sim 2.1$  eV, the intrinsic selectivity to acrolein decreases rapidly and then decreases further with increasing propene conversion. This pattern shows that when the activity of oxygen atoms at the catalyst surface becomes very high, two processes become more rapid - the oxidation of the intermediate from which acrolein is formed and the sequential combustion of acrolein to  $\text{CO}_2$ . These findings

clearly indicate that there is no advantage to developing propene oxidation catalysts with band gaps below  $\sim 2.1$  eV.

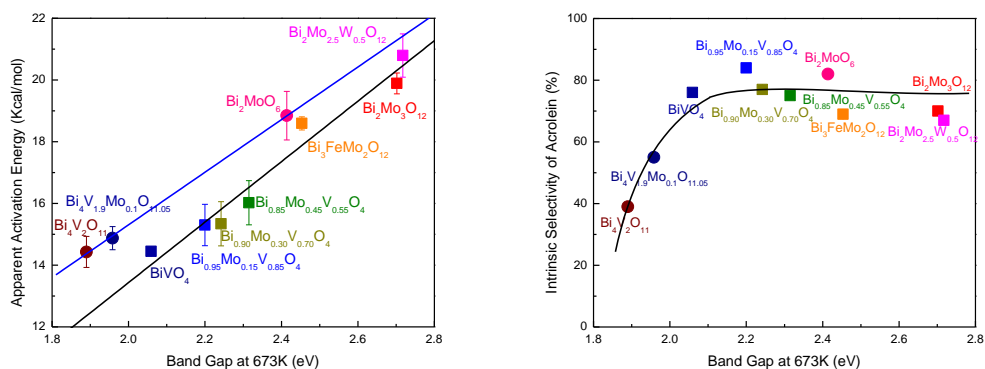


Fig. 1. Apparent activation energies (left) and intrinsic selectivity to acrolein (right) for propene oxidation to acrolein versus the band gap measured at 673K for catalysts having the scheelite (lower line) and aurivillius (upperline) structures. Reaction conditions:  $T = 673\text{K}$  and  $P_{\text{C}_3\text{H}_6} = P_{\text{O}_2} = 0.167$  atm.

### Mechanism and Kinetics of Propene Ammoxidation

The ammoxidation of propene to acrylonitrile occurs over bismuth-molybdate-based catalysts and requires a feed of ammonia and oxygen in addition to propene stoichiometry  $1\text{C}_3\text{H}_6:1\text{NH}_3:1.5\text{O}_2$ . The mechanism for this reaction is thought to be similar to that of the related oxidation of propene to acrolein that has been more extensively studied in the literature and by our group. However, there are still many open questions regarding the role of ammonia, the nature of the active site, and the mechanism for acrylonitrile formation. In this work, we investigate the properties of propene ammoxidation over  $\alpha\text{-Bi}_2\text{Mo}_3\text{O}_{12}$ , which produces four major carbon-containing products (acrylonitrile, HCN, acetonitrile and acrolein), as well as molecular nitrogen, over the temperature range of  $340^\circ\text{C}$ - $470^\circ\text{C}$ .

From the literature, the rate-determining step for acrylonitrile formation over  $\text{Bi}_2\text{Mo}_3\text{O}_{12}$  is known to be hydrogen abstraction from the methyl group of propene to produce a symmetric allyl radical. We found the propene consumption rate to be first order in propene partial pressure and zeroth order in both ammonia and oxygen partial pressures for ammonia:propene ratios from 0 to 2 (Fig. 2). However, the selectivities to the various products change significantly with the partial pressures of all three reactants. For example, the ratio of the rates of the major ammoxidation product to the major oxidation product increases linearly across a wide range of ammonia partial pressures at a fixed propene and oxygen partial pressure, as do the selectivities to the byproducts HCN, acetonitrile and  $\text{N}_2$  also increase with increased ammonia partial pressure.

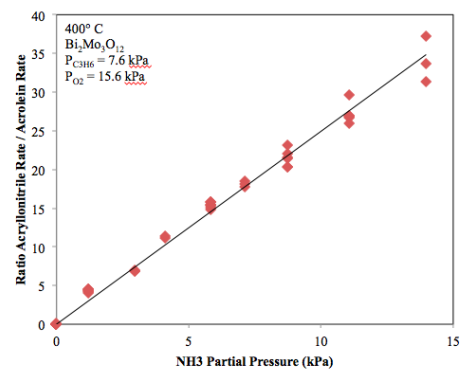


Fig. 2. Effect of  $\text{NH}_3$  partial pressure on the ratio of the rates of acrylonitrile to acrolein formation.

Co-fed acrolein reacted with ammonia and oxygen to produce acrylonitrile but co-fed acrylonitrile did not participate in significant secondary reaction. Using these results, we formulated a general reaction scheme that accounts for the all the major primary and secondary reaction pathways. By fitting our kinetic data to the reaction model, we extracted rate coefficients and activation energies for the major products. We have also observed that prolonged exposure to ammonia results in a permant 1.5 fold increase in the catalytic activity for both oxidation and ammoxidation. STEM EDS and XPS data indicate that nitrogen is present on the catalyst, leading us to hypothesize that the increased activity is due to improved hydrogen abstraction by surface imido groups compared to oxo groups.

### Investigation of Propene Metathesis

Alkene metathesis is known to occur over supported metal oxide moities. Our research has focused on defining the structure of the active species and elucidating the mechanism of their formation. To probe these questions, we have synthesized, and characterized, a range of silica-supported  $WO_x$  samples, and studied their catalytic performance for propene metathesis.

As-synthesized catalysts (pretreated in air at 550 °C) exhibit low activity at the onset of reaction, and gradually increase in activity over the first 200 min of time-on-stream (TOS), until reaching steady state, and becoming stable and highly selective for converting propene into stoichiometric a mixture of ethene and butene. During the activation period, acetone is formed as a transient product, which we attribute to the partial reduction of isolated  $WO_x$  surface species (Scheme 1a). The amount of acetone formed corresponds to reduction of approximately 5% of W-sites. Compared to air-pretreated samples, samples treated at high temperature in He (600 °C), or dilute concentrations of  $H_2$  in He (10 % by vol. at 550 °C), exhibit a two-fold increase in activity.

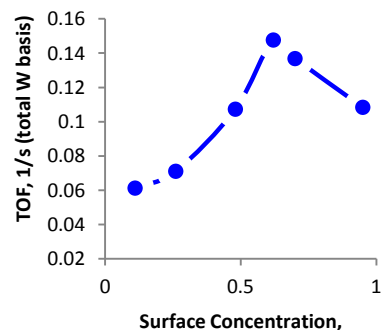


Fig. 4. Effect of  $WO_x$  surface concentration on the TOF for propene metathesis.

Additionally, these samples do not undergo the long activation period, quickly reaching steady state, and acetone formation is not observed. These observations suggest that pretreatment eliminates the slow formation of active sites (Scheme 1a).

A strong dependence of the TOF for propene activation on  $WO_x$  surface concentration has been identified (Fig. 4). This trend has been observed for catalyst samples prepared using different synthesis strategies and pretreatments, and suggests that a fundamental relationship exists between the interactions of  $WO_x$  with the silica surface and activity for alkene metathesis. Raman spectra reveal that the activity decrease seen at high loadings results from the formation of  $WO_3$

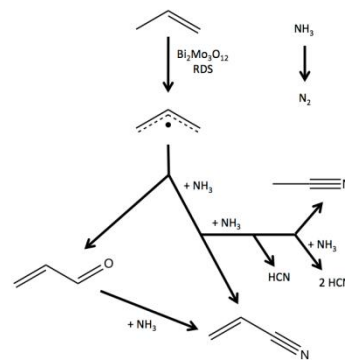
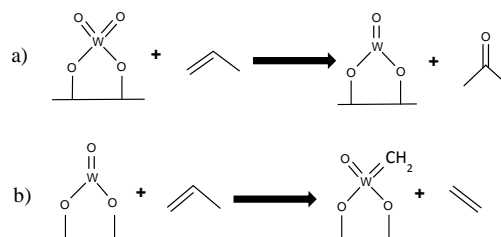


Fig. 3. Proposed mechanism for the ammoxidation of propene.



Scheme 1. Active Site Formation: a) Partial reduction of the tungsten oxide; b) formation of metallocarbene.

nanoparticles that are less active for propene metathesis. However, a definitive explanation for the increasing activity at lower W-loadings has proven more elusive, and is a focus of our current work. Interestingly, we observed the same activation energy for all  $\text{WO}_x/\text{SiO}_2$  samples for which spectroscopic evidence suggest that only isolated tungstate species are present. This suggests that the trend in TOF with W loading is due to an increase in the fraction of the tungstate sites that are catalytically active. Both experimental and theoretical efforts are currently in progress aimed defining the composition and structure of the activesites and the effects of W loading on the fraction of catalytically active sites.

### Defining the Role of Metal Oxide Promoters on Fischer-Tropsch Synthesis

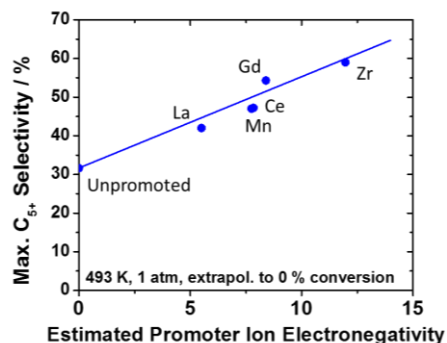


Fig. 5.  $\text{C}_{5+}$  selectivity versus promoter cation electronegativity, which serves as a proxy for Lewis acidity.

shift the  $\text{C}_2\text{-C}_4$  product fraction in favor of olefinic compounds. The reaction kinetics for the promoted catalysts were identical to those for the unpromoted catalyst, but the apparent rate constants and CO adsorption constants for the promoted catalysts were larger. Combined with results from CO TPD and in situ IR spectroscopy, these data are consistent with the hypothesis that CO binds more strongly and dissociates more readily at active sites near the interface between Co and the promoter oxide. Promoter oxidation states obtained from in situ XANES measurements were used to calculate promoter electronegativity, a proxy for promoter Lewis acidity. Fig. 5 shows how the increase in  $\text{C}_{5+}$  selectivity due to promotion increased with promoter electronegativity. These trends provide a basis for identifying candidate metal oxide promoters for our future work.

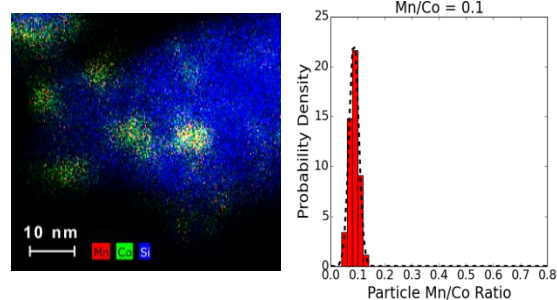


Fig. 6. STEM-EDS map of Co-Mn nanoparticles supported on silica (left) and distribution of particle Mn/Co ratios.

Co-containing Fischer-Tropsch synthesis catalysts exhibit high selectivities toward long-chain hydrocarbons, but also produce substantial amounts of methane as a byproduct. To suppress the formation of methane and shift the product distribution toward higher molecular weight hydrocarbons, metal oxide promoters are often used. While the effects on product distribution have been described, relatively few attempts have been undertaken to relate the promoter composition and its degree of association with Co to the

effects of the promoter on catalyst activity and selectivity. We have investigated these issues for metal oxides Mn, Zr, La, Ce, and Gd. Each of these promoters was found to decrease methane selectivity, increase  $\text{C}_{5+}$  selectivity, and shift the  $\text{C}_2\text{-C}_4$  product fraction in favor of olefinic compounds. The reaction kinetics for the promoted catalysts were identical to those for the unpromoted catalyst, but the apparent rate constants and CO adsorption constants for the promoted catalysts were larger. Combined with results from CO TPD and in situ IR spectroscopy, these data are consistent with the hypothesis that CO binds more strongly and dissociates more readily at active sites near the interface between Co and the promoter oxide. Promoter oxidation states obtained from in situ XANES measurements were used to calculate promoter electronegativity, a proxy for promoter Lewis acidity. Fig. 5 shows how the increase in  $\text{C}_{5+}$  selectivity due to promotion increased with promoter electronegativity. These trends provide a basis for identifying candidate metal oxide promoters for our future work.

STEM-EDS elemental mapping served as an effective technique for identifying the spatial distribution of Co and promoter and assessing the degree of spatial association between these two components. Statistical analysis of these data revealed that co-location of the Co and promoter is linked to product selectivity improvements. These results confirm that the Co and promoter must be in close contact to achieve the promotion effects, which suggests the interface of these two materials is responsible for the enhanced FTS reactivity. The dependence of nanoparticle composition on

promoter weight loading indicates that different promoter elements exhibit different affinities for co-locating with the Co. For example, MnO is found to saturate the surface of the Co nanoparticles before any segregation from the Co is observed, whereas Zr distributes randomly over the catalyst even at the lowest detectable loadings. These trends are directly related to the onset of promotion effects as promoter weight loading increased.

### Investigation of Ethanol Conversion to Butanol

Dramatic growth of U.S. ethanol production from biomass has led to a strong interest in developing efficient methods for converting ethanol to more valuable products, such as n-butanol. Various heterogeneous catalysts have been investigated for the ethanol-to-butanol reaction, but only hydroxyapatite (HAP;  $\text{Ca}_5(\text{PO}_4)_3\text{OH}$ ) has demonstrated a high activity and selectivity (>70%) towards butanol. Rational design of next generation of catalysts requires an understanding why hydroxyapatite is so efficient. To that end, we have investigated the mechanism and site requirements of ethanol coupling to butanol over HAP using a combination of catalytic screening, kinetic measurements, in-situ titrations, and FTIR experiments.

Butanol formation rates on HAP were determined over a range of ethanol (3.5 – 9.4 kPa) and acetaldehyde (0.055 – 0.12 kPa) partial pressures. A drastic rate enhancement was observed upon addition of acetaldehyde, demonstrating that the reaction is autocatalytic. For all reaction conditions tested, ethanol exhibits a negative order dependence while acetaldehyde exhibits a positive, first order dependence. These findings show that a direct coupling pathway involving two ethanol molecules does not play a major role over HAP catalysts. HAP was also screened for the occurrence of hydrogen transfer and condensation between acetaldehyde and 1-propanol. Ethanol was formed predominantly along with a small amount of C5 products. This shows that hydrogen transfer proceeds much more rapidly than aldol condensation. Taken together, the screening and kinetic rate data indicate that butanol is formed via a Guerbet-type mechanism involving sequential dehydrogenation, aldol condensation, and hydrogen transfer reactions with enolate formation being the rate-limiting step. In-situ pyridine titration revealed that HAP contains weak acid sites that catalyze the dehydrogenation and aldol condensation reactions. Poisoning experiments with  $\text{CO}_2$  and propionic acid reveal that acetaldehyde and butanol formation rates decrease to different extents, demonstrating that the sites for the two reactions are not equivalent. Combined with in-situ FTIR results, it was found that dehydrogenation is

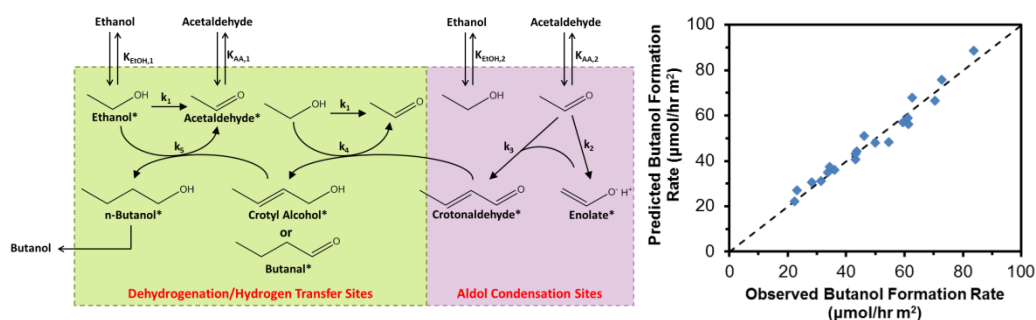


Fig. 6. Proposed reaction pathway for the Guerbet coupling of ethanol to butanol over HAP catalyst (left) and parity plot comparing the observed butanol formation rate with the predicted butanol formation rate derived from the proposed model. The dotted line represents a perfect fit.

is catalyzed by weakly basic hydroxyl groups while aldol condensation requires a combination of basic calcium oxide sites next to weakly acidic phosphate groups to

stabilize the enolate intermediate. These results can be summarized in the model presented in Fig. 6. A two-parameter rate equation that is consistent with all is also shown in Fig. 6.

### Publications acknowledging this grant in 2012-2015

1. Vining, J.; Strunk, J.; Bell, A. T. Investigation of the structure and activity of  $\text{VO}_x/\text{CeO}_2/\text{SiO}_2$  catalysts for methanol oxidation to formaldehyde, *J. Catal.* **2012**, *285*, 160-167.
2. Shapovalov, V.; Fievez, T.; Bell, A. T. A theoretical study of methanol oxidation catalyzed by isolated vanadia clusters supported on the (101) surface of anatase, *J. Phys. Chem. C* **2012**, *116*, 18728.
3. Zhai, Z.; Getsoian, A.; Bell, A. T. The kinetics of selective oxidation of propene on bismuth vanadium molybdenum oxide catalysts, *J. Catal.* **2013**, *305*, 25-36.
4. Getsoian, A.; Shapovalov, V.; Bell, A. T. DFT+U investigation of propene oxidation over bismuth molybdate; active sites, reaction intermediates, and the role of bismuth, *J. Phys. Chem. C* **2013**, *117*, 7123.
5. Rumberger, E. M.; Ahn, H. S.; Bell, A. T.; Tilley, T. D. Water oxidation via immobilization of the dimanganese complex  $[\text{Mn}_2(\mu\text{-O})(2)(\mu\text{-O}_2\text{CH}_3)\text{-}(\text{byp})(2)(\text{H}_2\text{O})]$  onto silica, *Dalton Trans.* **2013**, *42*, 12238-12247.
6. Getsoian, A.; Bell, A. T. The influence of functionals on density-functional theory calculation of reducible metal oxide catalysts, *J. Phys. Chem. C*, **2013**, *117*, 22562-22578.
7. Nell, A.; Getsoian, A.; Werner, S.; Kiwi, L.; Bell, A. T. Preparation and characterization of high surface areas  $\text{Bi}_{1-x/3}\text{V}_{1-x}\text{Mo}_x\text{O}_4$  catalysts, *Langmuir* **2014**, *30*, 873-880.
8. Getsoian, A.; Zhai, Z.; Bell, A. T. Band gap energy as a descriptor of catalytic activity for propene oxidation over mixed metal oxide catalysts, *J. Am. Chem. Soc.* **2014**, *XX*, XXX.
9. Zhai, Z.; Wüschert, M.; Bell, A. T. Effects of catalyst crystal structure on the oxidation of propene to acrolein, *Topics Catal.*, **2015**, submitted.
10. Ho, C. R.; Shylesh, S.; Bell, A. T. Kinetics and site requirements of ethanol coupling to butanol over a hydroxyapatite catalyst, *J. Catal.* **2015**, submitted.
11. Johnson, G.; Werner, S.; Bell, A. T. Evidence for enhanced CO adsorption and dissociation in Mn-promoted Co-based Fischer-Tropsch synthesis catalysts, *ACS Catal.*, **2015**, submitted.

**Adsorbate interactions in catalytic trend studies**

Xinyan Liu, Andrew J. Medford, Bo Yang, Max Hoffmann, Han-Jung Li, and Thomas Bligaard

SUNCAT Center for Interface Science and Catalysis, SLAC National Accelerator Laboratory

**Presentation Abstract**

There is a constant drive toward more energy- and resource-efficient technologies, for example related to the use of natural gas or biomass, and new sustainable energy processes. A key element in most novel energy technologies is the need for new, efficient catalysts made from Earth-abundant materials. The atomic-scale design of catalytic materials with tailored properties represents a scientific grand challenge. Computational catalyst search approaches leveraging electronic structure theory based atomic-scale simulations coupled with kinetic models constitute a promising avenue for future catalyst discovery efforts. To reliably address detailed catalytic properties, such as for example product selectivity, the simulation accuracy needs to be improved significantly. The absence of suitable models for reliably including interactions between adsorbates presents a leading contribution to the inaccuracy in computational catalysis trend studies. This project aims to improve the fundamental understanding of the interactions between adsorbed atoms and molecular fragments on transition metal surfaces and devise models to include these interactions in catalytic trend studies. The scientific insights and the set of tools established in this project aim to create a break-through in obtaining quantitative agreement between theoretical catalysis studies and experimental measurements and could potentially become a cornerstone in establishing an accurate and reliable “Catalyst Genome”. The tools will be applied to catalytic processes pertaining to the transformations and eventually the liquefaction (Fischer-Tropsch) of methane. This could ultimately lead to improved processes for utilization of natural gas resources.

**FWP-100167: Early Career Grant, Adsorbate-adsorbate interactions**

**PIs:** Thomas Bligaard

**Postdocs:** Bo Yang, Max Hoffmann, Han-Jung Li

**Students:** Xinyan Liu

**RECENT PROGRESS**

We have developed a method for calculating the uncertainties on adsorbate-adsorbate interaction parameters using Bayesian error estimation functionals. This allows us to establish Ensemble Kinetic Models including adsorbate interactions. It means that trend studies based on the BEEF-class of exchange correlation functionals now can be carried out with fully consistent uncertainty estimates of the combined DFT/kinetics model. The methodology allows one to give an error estimate that describes the

uncertainties from the quantum description on any scientific conclusion that can be drawn from coupling non-selfconsistent functional ensembles with kinetic models. We have then subsequently used this approach to analyze the methanation reaction and the anhydrous formation of formaldehyde from methanol. For the methanation reaction it has been possible to show that the uncertainty on which pure metals and alloys are active catalysts is very independent on which exchange-correlation functional is being used in the simulations, whereas for the anhydrous formation of formaldehyde, the selectivity of different alloys is quite sensitive on the exchange-correlation treatment. This means that for reliable conclusions on the formaldehyde selectivity one must utilize an ensemble approach. Since the selectivity is also quite sensitive to the inclusion of adsorbate-adsorbate interactions, we believe that we can now, with the implemented methodology, for the first time reliably predict from simulations which alloys might be active, stable and selective for anhydrous formaldehyde synthesis. We have analyzed the anhydrous formaldehyde synthesis over both close-packed and stepped facets of transition and noble metal surfaces, and come to the computational prediction that the close-packed facets should be significantly more selective. Finally, we have screened on the order of 1000 different alloy surfaces for the ability to catalyze the formaldehyde formation.

Additionally, we have implemented a multi-site integral adsorption energy model in the CatMAP kinetics package. This allows for the multisite integral adsorption model to be readily utilized by the SUNCAT group and by other research groups. Additionally, the model has been parameterized for a large set of adsorbates over catalytically interesting transition metal surfaces, such that one can include adsorbate-adsorbate interactions in many relevant catalytic reactions taking place on stepped transition and noble metal surfaces, without the necessity to calculate complex geometries for assessing adsorbate-adsorbate interactions and parameterizing models for these. The multi-site interaction model in CatMAP has been utilized to study the ammonia oxidation reaction over transition metals, and it has been shown that the high activity of Cu/Ru(0001) of this reaction is due to some intricacies in the adsorbate-adsorbate interactions.

Finally, the electrochemical evolution of chlorine has been studied, and it has been shown that the interactions between Ru and Ti atoms in the electrode material lead to interesting doping phenomena, where the material can be significantly optimized with respect to its chlorine evolution ability. These computational results, made in collaboration with researchers in Stockholm, have subsequently been verified experimentally by experiments in Stockholm.

### **Publications Acknowledging this Grant in 2012-2015**

1. Karlsson, R.K.B.; Hansen, H.A.; Bligaard, T.; Cornell, A.; Pettersson, L.G.M. Ti atoms in  $\text{Ru}_{0.3}\text{Ti}_{0.7}\text{O}_2$  mixed oxides form active and selective sites for electrochemical chlorine evolution. *Electrochimica Acta* **2014**, *146*, 733-740.
2. Li, H.J.; Lausche, A.C.; Peterson, A.A.; Hansen, H.A.; Studt, F.; Bligaard, T. Using microkinetic analysis to search for novel anhydrous formaldehyde production catalysts *Surf. Sci.* DOI: 10.1016/j.susc.2015.04.028
3. Medford, A.J.; Shi, C.; Hoffmann, M.J.; Lausche, A.C.; Fitzgibbon, S.R., Bligaard, T.; Norskov, J.K. CatMAP: A software package for descriptor-based micro-kinetic mapping of catalytic trends. *Catal. Lett.* **2015**, *145*, 794-807.

**Catalytic processing of levulinic acid: expanding applications while building fundamental insights**

Omar A. Abdelrahman, Anargyros Chatzidimitriou, and **Jesse Q. Bond**  
Syracuse University, Department of Biomedical and Chemical Engineering

**Presentation Abstract**

This poster summarizes recent progress in the upgrading of levulinic acid (4-oxopentanoic acid) for the production of bio-based chemicals, and it has two core focus areas.

First, we consider the hydrogenation of levulinic acid for the preparation of  $\gamma$ -valerolactone. This chemistry is of practical interest as valerolactone can enable production of lignocellulose-based biofuels and biochemicals.<sup>1</sup> Further, this reaction captures many challenges common to the broad class of hydrogenation reactions in biomass upgrading. As with most bio-based intermediates, levulinic acid has both low vapor pressure and high oxygen content, and its hydrogenation is generally carried out in liquid water at elevated temperatures and pressures. Because it partially dissociates, this reaction also occurs at low pH. In such media, both metals and their supports are frequently unstable, and catalysts often undergo profound structural changes under reaction conditions. In addition to presenting practical challenges, the transient nature of catalyst structures in aqueous media hinders a fundamental understanding of phenomena governing reaction kinetics. Here, we summarize our recent efforts to rigorously decouple the intrinsic kinetics of levulinic acid hydrogenation from confounding effects arising in condensed media. In parallel, we examine material properties that govern activity and stability in acidic water, guiding the design of new materials for biomass upgrading.<sup>2,3</sup>

Second, this presentation explores emerging applications of levulinic acid as a precursor to oxygenated chemicals. In general, biomass can be viewed as having a competitive advantage relative to oil and gas in applications where the oxygen content of the product is high relative to its carbon content. One may therefore potentially identify petrochemical commodities that have existing markets and for which biomass may be an economically viable feedstock. In this context, we outline recent progress in the selective production of C<sub>4</sub> diacids via vapor-phase oxidation of levulinic acid.<sup>4,5</sup> Diacids and diacid anhydrides offer higher sale prices than liquid fuels, and their markets are robust and growing. These targets might be appropriate for near-term commercial development of levulinic acid-based biorefineries.

**References**

1. J. Q. Bond, A. A. Upadhye, H. Olcay, et al., *Energy Environ. Sci.*, 2014, **7**, 1500-1523.
2. O. A. Abdelrahman, A. Heyden and J. Q. Bond, *ACS Catal.*, 2014, **4**, 1171 - 1181.
3. O. A. Abdelrahman, H. Y. Luo, A. Heyden, Y. Román-Leshkov and J. Q. Bond, *J. Catal.*, 2015, **329**, 10-21.
4. A.P. Dunlop, *US Pat.*, 2676186, 1954.
5. A. Chatzidimitriou and J. Q. Bond, *In Review*, 2015.

**Supported Metal Nanoparticles:  
Correlating Structure with Catalytic Function through Energetics**

Charles T. Campbell (PI), Trevor James, Stephanie Hemmingson, Jason Sellers, Gabriel Feeley  
University of Washington, Department of Chemistry

**Presentation Abstract**

Energy and environmental technologies require better catalysts and electrocatalysts, many involving nanoparticles of late transition metals supported on oxides and carbon. This experimental research program aims to provide the basic understanding needed to improve such catalysts. Specifically, we study well-defined model catalysts consisting of metal nanoparticles supported on single-crystalline oxide and carbon surfaces, structurally characterized using a variety of ultrahigh vacuum surface science techniques. We use calorimetry techniques invented here and available nowhere else in the world to measure the energies of the metal atoms in these particles, the metal/support adhesion energies ( $E_{\text{adh}}$ ) and the energy of adsorbed intermediates on these particles. Our results show that these energies depend strongly on the size of the particles and the nature of the support surface, and that they correlate with their catalytic properties (chemisorption strengths, elementary-step rates, net catalytic reaction rates and sintering kinetics). They further suggest that these catalytic properties correlate with the chemical potential of the metal atoms, which we measure directly by metal adsorption calorimetry and which we find to increase with decreasing particle size below 6 nm and with decreasing  $E_{\text{adh}}$ . We found predictive correlations trends that reveal how  $E_{\text{adh}}$  varies with intrinsic properties of the metal element for a given oxide, and how it varies from surface to surface for a given metal on five different oxides. These measured energies also serve as important benchmarks for developing more accurate computational tools for surface science, which could accelerate catalyst discovery and revolutionize research in many areas.

**Grant # DE-FG02-96ER14630: Supported Metal Nanoparticles:  
Correlating Structure with Catalytic Function through Energetics**

**Students:** Trevor James, Stephanie Hemmingson, and Gabe Feeley

**RECENT PROGRESS**

***Introduction***

This research program combines experiments with theory with the goal of providing the basic understanding needed to develop better catalyst materials for energy and environmental technologies. Our main focus has been on catalysts based on late transition metal nanoparticles anchored to oxide supports. Our results have helped clarify how metal particle size affects catalyst activity and selectivity, and how to maintain catalyst particles at their optimum size for extended periods while running chemical reactions. We have also elucidated several reaction mechanisms. We have done this by studying model catalysts involving well-defined metal nanoparticles on single-crystalline oxide supports, prepared under the clean conditions of ultrahigh vacuum (UHV). The structure of these materials was characterized using a variety of

state-of-the-art experimental techniques including surface spectroscopies (XPS, AES, LEIS, TPD) and surface microscopies (STM, AFM). Most importantly, we have used single-crystal adsorption calorimetry (SCAC) to measure the energies of the transition metal atoms in these catalytic materials and determine how their energy depends upon details of the catalyst structure (particle size and support). We have also measured surface reaction kinetics and catalytic reaction rates, both steady-state and transient (sometimes in UHV and sometimes at higher pressures). We have often interpreted our results using computational results provided by collaborations with theoreticians. Finally, we have also developed some semi-empirical theoretical methods for estimating rate constants in surface reactions.

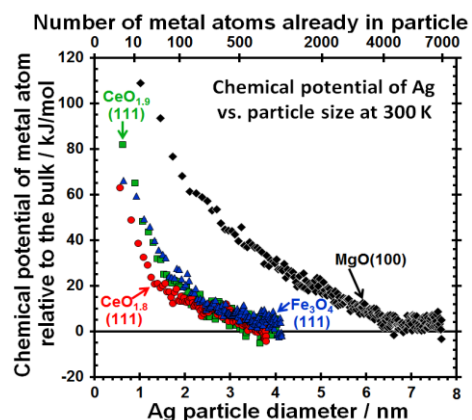
### ***Metal Adsorption / Adhesion Energies onto Catalyst Supports by Microcalorimetry***

We have completed a detailed systematic study of the adsorption of all three Group IB metals (Ag, Cu and Au) onto stoichiometric and reduced  $\text{CeO}_2(111)$  surfaces. In all cases, the vapor-deposited metal atoms stick with nearly unit probability on the oxide surface at temperatures between 100 K and 300 K. They diffuse rapidly as adatoms across the surface, and nucleate into 3-dimensional metal clusters. After a few percent of a monolayer, the number of these clusters stays constant, and they just grow in size with further metal deposition. Thus the adsorption energy generally increases with coverage, asymptotically approaching the bulk sublimation energy at high coverages. This is due to the formation of more metal-metal bonds per atom as the size grows toward the bulk limit.

Because the number of clusters stays constant (until they grow so large they overlap), and because we know the fraction of the surface they cover versus coverage from  $\text{He}^+$  low-energy ion scattering spectroscopy (LEIS) measurements, we can convert the coverage to average particle thickness, and from that to average diameter, if we assume they have the shape of hemispherical caps (an assumption approximately confirmed by quantitative X-ray Photoelectron Spectroscopy (XPS) and Auger Electron Spectroscopy (AES)). This allowed us to determine the chemical potential of these three metal atoms as a function of particle size on  $\text{CeO}_{2-x}(111)$  surfaces with different extents of reduction, assuming that entropic differences are negligible, since these have mainly vibrational entropy only. Example results are shown in Fig. 1 for the case of Ag, whose chemical potential decreases dramatically with size below 3 nm. This chemical potential is a direct measure of the thermodynamic driving force for catalyst deactivation by sintering. The differences between different oxide surfaces reflect differences in bonding strength (adhesion energy) at the metal nanoparticle / oxide interface. Stronger adhesion, as in the lower curves, greatly reduce the driving force and thus rate of sintering [4]. We observed trends in adhesion energies, as discussed below.

**Fig. 1.** Calorimetric measurements of the chemical potential of Ag atoms versus particle size on different oxide supports, from [4].

The results like in Fig. 1 for Ag, Cu and Au are all similar, but with some important differences. Most notably, Cu binds much more weakly to surfaces with more oxygen vacancies, whereas Ag and Au do just the opposite. The stronger binding to vacancy sites for Ag and Au is manifested as stronger adhesion energy and lower chemical potential for the more reduced surface at



the same size, as in Fig. 1. In contrast, Cu binds much more strongly to stoichiometric step edges and to stoichiometric terraces. We attribute this difference to the greater affinity of Cu to oxygen atoms compared to Ag and Au. Because of this, Cu nucleates clusters mainly on stoichiometric terrace sites at 100 K, whereas nuclei mainly grow at step edges for Ag and Au at 100 K (and Cu at 300 K). The number density of Cu nuclei is therefore 10-fold larger for Cu at 100 K also. Because of this, the particles are 10-fold smaller, which permitted us to measure the adsorption energy of Cu versus particle size all the way down to the monomer limit at 100 K on stoichiometric CeO<sub>2</sub>(111) terrace sites. *This is the first measurement of the adsorption energy for any late transition metal monomer on any oxide support.* Such monomer energies have been our long-sought goal, since they are much easier to compare to a quantum mechanical calculations (like DFT) than are the energies for metal clusters, and *thus this result will serve as a key benchmark for validating theory.* These measurements of Cu and Au adsorption energies were only possible due to recent calorimeter improvements [11].

Because Cu binds so strongly to stoichiometric step edge sites, we can also see its heat of adsorption at 300 K decrease to a minimum with coverage as those step sites are titrated. For Ag and Au, the binding to stoichiometric step edges is not so strong, so this minimum is completely masked by the stronger counter effect: the increase in adsorption energy with particle size as coverage increases.

In spite of these differences, all three metals increase the Ce<sup>3+</sup>:Ce<sup>4+</sup> ratio within the XPS probe depth upon adsorption onto CeO<sub>2-x</sub>(111) at 300 K (for all x), as if they are donating electron density to the oxide, but without themselves becoming measurably charged. We are still trying to understand this seemingly contradictory behavior (confirmed for Ag by another group) through quantitative measurements at different temperatures.

Our metal adsorption energy versus coverage results can also be integrated versus coverage to get the metal / oxide adhesion energy ( $E_{adh}$ ) in the large-particle limit. These, when combined with a few  $E_{adh}$  values obtained from measurements of the equilibrium particle shape, have revealed a systematic relationship between the adhesion energy (measured on clean oxide surfaces in ultrahigh vacuum) and the intrinsic properties of the metal element. We found that, for a given oxide surface,  $E_{adh}$  grows linearly with the heat of formation of the metal's most stable oxide from metal vapor plus O<sub>2</sub>(gas). (This is a measure of the strength of the chemical bonds which that metal atom can make to oxygen). The slope of this linear relationship is almost the same for CeO<sub>2</sub>(111) and MgO(100), but CeO<sub>2</sub>(111) lies 2.0 J/m<sup>2</sup> higher, a difference that is larger than the whole range between different late transition metals for one oxide. Assuming the same slope for different oxides for which only one metal's  $E_{adh}$  had been measured has allowed us also to make quantitative predictions of  $E_{adh}$  for many metals on all of these surfaces. These parallel lines are offset such that for a given metal,  $E_{adh}$  varies as: MgO(100)  $\approx$  TiO<sub>2</sub>(110) <  $\alpha$ -Al<sub>2</sub>O<sub>3</sub>(0001) < CeO<sub>2-x</sub>(111)  $\approx$  Fe<sub>3</sub>O<sub>4</sub>(111), with these last two oxides being  $\sim$ 0.6 J/m<sup>2</sup> higher than  $\alpha$ -Al<sub>2</sub>O<sub>3</sub>(0001), and the first two lower than it by  $\sim$ 2 J/m<sup>2</sup>. Qualitatively, metal atoms in the same size nanoparticle on these different supports will have a chemical potential that increases in the opposite order (i.e., with the highest chemical potential when on the oxide with the lowest  $E_{adh}$ ). *These trends will serve as important benchmarks for validating computational estimates of such bonding energetics using quantum mechanical calculations (like DFT).* There exist almost no other experimental measurements of this type at clean metal/oxide interfaces. We found that previous measurements of  $E_{adh}$  without ultrahigh vacuum and surface analysis to verify cleanliness systematically underestimated values by a factor of 2 to 3.

These predictive trends of adhesion energies are also very important for predicting sintering kinetics, since knowing  $E_{adh}$  allows us to also predict curves like Fig. 1 of chemical

potential versus size. This function in Fig. 1 is needed as direct input to make quantitative calculations of the rates of sintering using our kinetic model [4], which quantitatively includes the effects of both particle size and support. The mechanistic and quantitative details of that model led us to a new idea for making more sinter-resistant transition metal catalysts, which we implemented through collaboration with an expert in nanomaterials synthesis, Younan Xia, who developed a wet-chemical method for making this 3-phase material in high-surface-area form [9]. As with the similar structure previously prepared by Atomic Layer Deposition (ALD) by the group at Argonne National Labs (with PC Stair), we found this to sinter much more slowly than Pt on either pure silica or pure titania supports. Our synthesis method would be far easier to implement in making catalysts on an industrial scale than that prior ALD method.

### ***Quantitative Modelling of Electron Spectroscopy Intensities for Supported Nanoparticles: The Hemispherical Cap Model for Non-Normal Detection***

We mentioned above when discussing Ag, Cu and Au deposition onto CeO<sub>2</sub>(111) that the growing particles have the shape of hemispherical caps, and that this shape was confirmed by quantitative XPS and AES combined with He<sup>+</sup> LEIS. That confirmation was only made possible using the new theoretical method for such XPS and AES data analysis which we summarize in this section and published elsewhere [12].

Nanoparticles of one element or compound dispersed across the surface of another substrate element or compound form the basis for many materials of great technological importance, and also form during film growth by deposition in many fabrication processes. The average size and number density of such nanoparticles is often very important, and these can be estimated with electron microscopy or scanning tunneling microscopy. However, this is very time consuming and often unavailable with sufficient resolution when the particle size is ~1 nm. Because the probe depth of electron spectroscopies like XPS and AES is ~1 nm, these provide quantitative information on both the total amount of adsorbed material when it is in the form of such small nanoparticles, and the particle thickness. For electron spectroscopy conducted with electron detection normal to the surface, Diebold et al. derived analytical relationships between the signal intensities for the adsorbate and substrate and the particles' average size and number density, under the assumption that all the particles have hemispherical shape and the same radius U. Diebold, J.-M. Pan, and T.E. Madey, *Phys. Rev. B* 1993, 47, 3868-3876. We developed a simple angle- and particle-size-dependent correction factor that can be applied to these analytical expressions so that they can also be extended to measurements made at other detection angles away from the surface normal [12]. This correction factor was computed using numerical integration and published for use by future researchers [12]. This correction factor is large (>2) for angles beyond 60°, so comparing model predictions to measurements at both 0° and ≥60° will also provide a new means for testing the model's assumptions (hemispherical shape and fixed size particles). The ability to compare the hemispherical cap model at several angles simultaneously also should enable more accurate estimates of surface structural parameters when elastic diffraction effects cause strong peaks in the angular distributions of emitted electrons.

### ***Kinetic Modelling of Catalytic Reactions***

Predictive kinetic modelling of catalytic reaction mechanisms remains one of our central goals. Based on a trend in experimentally-measured entropies of adsorbates which we had discovered earlier under other funding, we also developed some new semi-empirical theoretical methods for estimating the pre-exponential factors in rate constants for elementary surface

reactions [8]. These prefactors are applicable to kinetics in heterogeneous catalysis and indeed much more generally in surface chemistry.

### Publications Acknowledging this Grant in 2012-2015

1. Campbell, C. T. Catalyst-Support Interactions: Electronic Perturbations, *Nature Chemistry* (News and Views) **2012**, *4*, 597-598.
2. Yang, Y.; Mims, C.A.; Mei, D.H.; Peden, C.H.F.; Campbell, C.T. Mechanistic Studies of Methanol Synthesis over Cu from CO/CO<sub>2</sub>/H<sub>2</sub>/H<sub>2</sub>O Mixtures: the Source of C in Methanol and the Role of Water, *J. Catalysis* **2013**, *298*, 10-17.
3. Campbell, C. T. The Energetics of Supported Metal Nanoparticles: Relationships to Sintering Rates and Catalytic Activity, *Accts. Chemical Research* **2013**, *46*, 1712-1719.
4. Campbell, C. T.; Sellers, J. R. V. Introductory Lecture: Anchored Metal Nanoparticles: Effects of Support and Size on Their Energy, Sintering Resistance and Reactivity, *Faraday Discussion* **2013**, *162*, 9–30.
5. Campbell, C. T.; Sellers, J. R. V. Enthalpies and Entropies of Adsorption on Well-Defined Oxide Surfaces: Experimental Measurements, *Chem. Reviews* **2013**, *113*, 4106–4135.
6. Campbell, C. T.; Sauer, J. Introduction: Surface Chemistry of Oxides, *Chemical Reviews* (special issue on Surface Chemistry of Oxides) **2013**, *113*, 3859–3862.
7. Sharp, J. C.; Yao, Y. X.; Campbell, C. T. Silver Nanoparticles on Fe<sub>3</sub>O<sub>4</sub>(111): Energetics by Ag Adsorption Calorimetry and Structure by Surface Spectroscopies, *J. Phys. Chem. C* **2013**, *117*, 24932–24936.
8. Campbell, C. T.; Árnadóttir, L.; Sellers, J. R. V. Kinetic Prefactors of Reactions on Solid Surfaces, *Z. Physikalische Chemie* (invited, for special issue celebrating famous Eyring / Polanyi paper introducing transition states) **2013**, *227*, 1435–1454
9. Lu, P.; Campbell, C. T.; Xia, Y. A Sinter-resistant Catalytic System Fabricated by Maneuvering the Selectivity of SiO<sub>2</sub> Deposition onto TiO<sub>2</sub> Surface versus Pt Nanoparticle Surface, *Nano Letts* **2013**, *13*, 4957-4962 (highlighted: IOP's *NanotechWeb.org* website).
10. Farmer, J. A.; Baricuatro, J. H.; Campbell, C. T. Correction to: Ag Adsorption on Reduced CeO<sub>2</sub>(111) Thin Films, *J. Physical Chemistry C* **2013**, *117*, 27167.
11. Sellers, J. R.V.; James, T. E.; Farmer, J. A.; Hemmingson, S. L.; Campbell, C. T. Adsorption Calorimetry during Metal Vapor Deposition on Single Crystal Surfaces: Increased Flux, Reduced Optical Radiation, and Real-Time Flux and Reflectivity Measurements, *Review of Scientific Instruments* **2013**, *84*, art. 123901 (9 pages).
12. Sharp, J. C., Campbell, C. T., Quantitative Modelling of Electron Spectroscopy Intensities for Supported Nanoparticles: The Hemispherical Cap Model for Non-Normal Detection, *Surface Science Letters* **2015**, *632*, L5-L8.

**Benchmarking active phases, supports and reaction conditions  
using monodisperse nanocrystals**

Matteo Cargnello

Stanford University, Department of Chemical Engineering  
and SUNCAT Center for Interface Science and Catalysis

Colloidal methods provide well-defined nanocrystals (NCs) that are monodisperse in size, shape and composition. Nanocrystals of metals, oxides, chalcogenides, and heterostructures (e.g. metal-oxide NCs) can be routinely prepared with size dispersions <10%, and in many cases with atomic precision (e.g.  $\pm 1$  atomic layer). Recent advances in ligand removal<sup>1,2</sup> and phase stabilization<sup>3,4</sup> provide access to clean and well-defined active phases and supports for catalytic studies.<sup>5</sup> These materials offer a unique opportunity for benchmarking, as pointed out in the breakout slides: “Homogeneity of sites seems critical if we want to correlate TOF/selectivity with structure.” (Breakout slides on Non-molecular catalysts). These materials can be used for benchmarking active phases, supports and more importantly reaction conditions (e.g. appropriate determination of active sites, structures, adsorption energies etc.) and to determine best practices for catalytic studies with well-defined materials, yet under relevant conditions.

In this contribution, recent efforts on using monodisperse nanocrystals for studying catalytic reactions and structure-activity relationships will be presented. Selected examples include: correlating size and selectivity for methane activation reactions; studying metal-support interactions; relating nanostructure, surface area and photoactivity in titania-based photocatalysts. Finally, emphasis will be placed on appropriate methods for determining active sites and structural parameters by taking advantage of the high uniformity of the systems, and on the appealing of these materials for computational studies.

<sup>1</sup>Cargnello, M.; Chen, C.; Diroll, B. T.; Doan-Nguyen, V. V. T.; Gorte, R. J.; Murray, C. B. *J. Am. Chem. Soc.* **2015**, asap, doi:10.1021/jacs.5b03333.

<sup>2</sup>Dong, A.; Ye, X.; Chen, J.; Kang, Y.; Gordon, T.; Kikkawa, J. M.; Murray, C. B. *J. Am. Chem. Soc.* 2011, 133, 998-1006.

<sup>3</sup>Cargnello, M.; Delgado Jaén, J. J.; Hernández Garrido, J. C.; Bakhmutsky, K.; Montini, T.; Calvino Gamez, J. J.; Gorte, R. J.; Fornasiero, P. *Science* **2012**, 337, 713-717.

<sup>4</sup>Joo, S. H.; Park, J. Y.; Tsung, C.-K.; Yamada, Y.; Yang, P.; Somorjai, G. A. *Nature Mater.* **2009**, 8, 126-131.

<sup>5</sup>Cargnello, M.; Doan-Nguyen, V.; Gordon, T. R.; Paik, T.; Diaz, R. E.; Stach, E. A.; Gorte, R. J.; Fornasiero, P.; Murray, C. B. *Science* **2013**, 341, 771-773.

**Research in the Celik Catalysis Group**

Fuat E. Celik

Department of Chemical and Biochemical Engineering,  
Rutgers, The State University of New Jersey

The Celik Catalysis Group is interested in combining experimental and theoretical techniques to elucidate the role of the structure and composition of the active site of a catalyst with its macroscopic activity and selectivity. Special emphasis is placed on in situ spectroscopy and density functional theory to gain insight into surface intermediates and transition states. This approach is used to develop new materials to produce renewable and alternative fuels and chemicals from a variety of carbon resources. A few example projects are given

**Density Functional Theory Investigation of Ethene Dehydrogenation and Coke Formation on Binary Metal Alloys: Effect of Surface Ensembles and Composition**

with Alec Hook, Jacob D. Massa

Through density functional theory (DFT), we have examined the effect of platinum tin alloy structure and composition on the kinetics and thermodynamics of dehydrogenation and coke formation pathways during light alkane dehydrogenation. Supported Pt catalysts are known to be active but show significant coke formation and deactivation, which can be alleviated by alloying with Sn and other main group elements. We aim to understand how the structure and composition of these alloys affect their ability to suppress coke formation. As compared to pure Pt, bond scission is more difficult on the alloys and desorption is more facile, and both effects are enhanced as three-fold hollow sites consisting of only Pt atoms are eliminated at higher Sn coverage. On Pt(111), the formation of atomic carbon is thermodynamically favorable and kinetically competitive with ethene formation. As the Sn loading increases, carbon formation becomes less kinetically and thermodynamically competitive with ethene formation and at high tin coverage cannot be considered likely as the source of coke.

**Oligomerization of Pentenes by Acid Zeolites**

with Atish Kulkarni, Longfei Chao

in collaboration with Akshai Kumar, Prof. Alan Goldman

The reactions of 1-pentene over acid zeolites were investigated in the liquid phase. The primary reactions were isomerization, dimerization, and subsequent cracking of the dimers. Zeolites consisting of only 10-membered (MFI) or 12-membered rings (FAU, BEA) behaved similarly, with dimerization and subsequent cracking competing with one another. Zeolites with 8-membered ring pores (MOR, FER) showed very different selectivity from each other and from

other zeolites. MOR showed almost complete conversion of C<sub>10</sub> olefins upon formation, such that cracking products were the dominant products. FER showed high activity and selectivity for dimerization, with very small amounts of cracking products observed.

The reactivity trends were reproduced in a fixed bed gas-phase flow reactor, with FER showing high dimerization selectivity, and MOR showing high cracking selectivity, especially to hexenes and butenes.

### **Low Temperature Continuous Gas-Phase Alkane Dehydrogenation Catalyzed by Supported Pincer-Iridium Complexes**

with Bo Li, Longfei Chao

in collaboration with Akshai Kumar, Prof. Alan Goldman

We have begun to develop gas-solid flow reactors capable of carrying out continuous transfer dehydrogenation of alkanes using propene as a sacrificial acceptor at 240 °C by supporting the conventionally homogenous pincer-ligated Ir complexes on silicon carbide. The highly reactive Ir complexes deactivate with any exposure to air (N<sub>2</sub> as well as O<sub>2</sub>) or H<sub>2</sub>O, and so a sealable reactor was developed to transport the reactor from the inert Ar atmosphere inside a glove box to a high-pressure gas manifold. The reactor is charged with excess olefin prior to reaction to prevent the loss of the olefin ligand from the 16 e<sup>-</sup> complex to generate the active but easily deactivated 14 e<sup>-</sup> complex. Preliminary results indicated that despite the high air and impurity sensitivity of the catalysts, careful selection of reactor design and reaction conditions resulted in three orders of magnitude improvement in reaction rates.

### **Alkyl-Aryl Coupling Catalyzed by Tandem Systems of Pincer-Ligated Iridium Complexes and Zeolites**

with Bo Li

in collaboration with Akshai Kumar, Prof. Alan Goldman

Organometallic-catalyzed alkane dehydrogenation to give olefins has been known since 1979, and was extensively developed over the years since then. Dehydrogenation catalysts in tandem with olefin metathesis catalysts were reported to afford catalytic systems for the metathesis of alkanes or alkyl-groups. Now we report a different tandem dehydrogenation-based system, in which the net reaction is the formation of an alkyl-aryl bond, with liberation of H<sub>2</sub>, from the coupling of alkyl-H and aryl-H units. In view of the importance of alkyl-aryl bonds in organic chemistry coupling reactions of this type have great potential applicability. No hydrogen acceptor is required so the system is highly atom-economical. Our approach to the development of a system for the catalysis of alkyl-aryl coupling was based on pincer-iridium-catalyzed acceptorless dehydrogenation of an alkyl group, followed by Friedel-Crafts coupling of the resulting olefin with arene, as show in the scheme below. Further dehydrogenation can give us more unsaturated products, such as dihydro-methylnaphthalene and methylnaphthalene.

## **Band-Gap Modification in TiO<sub>2</sub> Photocatalysts**

with Ashley M. Pennington, Katelyn A. Dagnall, Deniz A. Dindi

in collaboration with Prof. Stephen Tse

It is known that the lattice structure, particle size, dopant concentration, and supported metal nanoparticles may all affect the band gap of TiO<sub>2</sub>. The band gaps of anatase, rutile, and Degussa P25, were measured and compared TiO<sub>2</sub> samples synthesized and modified by a variety of techniques, such as flame-spray pyrolysis, high pressure reduction, and metal nanoparticle impregnation. In situ UV-visible spectrophotometry was carried out in a high-temperature reaction chamber (Harrick Scientific) equipped with a diffuse reflectance accessory. Absolute reflectance was calculated with respect to a Spectralon® disk. The band gaps of rutile and anatase were measured to be 2.98 eV and 3.26 eV, respectively, in close agreement with the cited fundamental optical values of 3.03 eV and 3.20 eV. Flame-synthesized C-doped anatase TiO<sub>2</sub> samples possessed band gaps smaller than rutile. The as-prepared, black material possessed a band gap of 2.75 eV, which increased to 2.96 eV as the material turned grey following calcination in air at 500 °C. Carbon loss during calcination was confirmed by GC and MS analysis during calcination. The band gap of P25 depended on particle size. After grinding and sieving, the largest particles ( $d_p > 53 \mu\text{m}$ ) exhibited the smallest band gap (3.23 eV), compared to as-received P25 (3.42eV). The addition of transition metals to P25 also decreased the measured band gap. 1% Cu-TiO<sub>2</sub> (P25) had an apparent band gap of 3.02 eV, and 1% Ni-TiO<sub>2</sub>(P25) had an apparent band gap of 3.06 eV. Supporting Cu on the calcined flame-synthesized anatase decreased the band gap into the visible region with a band gap of 2.75 eV, comparable to the as-prepared material.

**DHMF: A C<sub>12</sub> Building Block for Renewable Chemicals, Liquid Fuels, and Polymeric Materials**

Eugene Y. Chen

Department of Chemistry, Colorado State University, Fort Collins, CO 80523-1872.

**Presentation Abstract**

The direct coupling of 5-hydroxymethylfurfural (HMF) into higher-energy density C<sub>12</sub> 5,5'-di(hydroxymethyl)furoin (DHMF), first reported by the PI's group in 2012, proceeds through umpolung self-condensation of HMF catalyzed by an organic *N*-heterocyclic carbene (NHC) catalyst. This HMF upgrading method bears hallmarks of a green technology: organocatalytic approach, a solvent-free process, quantitative selectivity & yield, and 100% atom economy. Subsequently, DHMF has been catalytically transformed into diketones, polyols, oxygenated diesel fuels, C<sub>10</sub>–C<sub>12</sub> hydrocarbon transportation & jet fuels, polyesters, and polyurethanes. This presentation will update our recent progress in this area, including application of this organocatalytic self-condensation to other biomass furaldehydes, development of new molecular catalysts for this coupling reaction, design of fully recyclable supported heterogeneous catalysts for this upgrading process, and synthesis of new polymeric materials derived from DHMF.

**DE-FG02-10ER16193: Catalytic Upgrading of Key Biorefining Building Blocks to Renewable Chemicals, Polymeric Materials, and Liquid Fuels**

**PI:** Eugene Y. Chen  
**Postdoc:** Hongjun Zang  
**Students:** Eric Dunn, DJ Liu, Kelvin Feng

**RECENT PROGRESS**

**Organocatalytic upgrading of furfural and HMF to C<sub>10</sub> and C<sub>12</sub> furoins with quantitative yield and atom-efficiency:** There is increasing interest in upgrading of C<sub>5</sub> furfural (FF) and C<sub>6</sub> 5-hydroxymethyl furfural (HMF) into C<sub>10</sub> and C<sub>12</sub> furoins as higher energy-density intermediates for renewable chemicals, materials, and biofuels. This work utilizes the organocatalytic approach, using the *in situ* generated *N,S*-heterocyclic carbene catalyst derived from thiazolium ionic liquids (ILs), to achieve highly efficient self-coupling reactions of FF and HMF. Specifically, variations of the thiazolium IL structure have led to the most active and efficient catalyst system of the current series, which is derived from a new thiazolium IL carrying the electron-donating acetate group at the 5-ring position. For FF coupling by this IL (0.1 mol%, 60 °C, 1 h), when combined with Et<sub>3</sub>N, furoin was obtained in >99% yield. A 97% yield of the C<sub>12</sub> furoin was also achieved from the HMF coupling by this catalyst system. On the other hand, the thiazolium IL bearing the electron-withdrawing group at the 5-ring position is the least active

and efficient catalyst. The mechanistic aspects of the coupling reaction by the thiazolium catalyst system have also been examined and a mechanism has been proposed (Fig. 1).

**Organocatalytic polymerization of furfuryl methacrylate and post Diels-Alder click reaction to cross-linked materials:**

Biomass-derived furfuryl methacrylate (FMA) has been effectively polymerized at ambient temperature by the P<sub>4</sub>-phosphazene superbase, <sup>t</sup>Bu-P<sub>4</sub>, with or without <sup>i</sup>PrOH as the co-initiator, producing syndio-rich atactic poly(furfuryl methacrylate), PFMA. The Diels-Alder (DA) “click” reaction has been utilized to produce two types of cross-linked PFMA

materials. The first is PFMA-C<sub>60</sub>, prepared from the DA reaction between the furfuryl group of PFMA and polydienophile C<sub>60</sub>, and the second employs a bifunctional bismaleimide (BM) to construct the cross-linked network polymer PFMA-BM. When compared to the pristine PFMA, the cross-linked network polymers PFMA-C<sub>60</sub> and PFMA-BM, especially the PFMA-BM materials with a high crosslinking density, exhibit significantly enhanced thermal stability at temperatures above 600 °C and a much higher glass-transition temperature, as showed by thermal and thermomechanical analyses (Fig. 2).

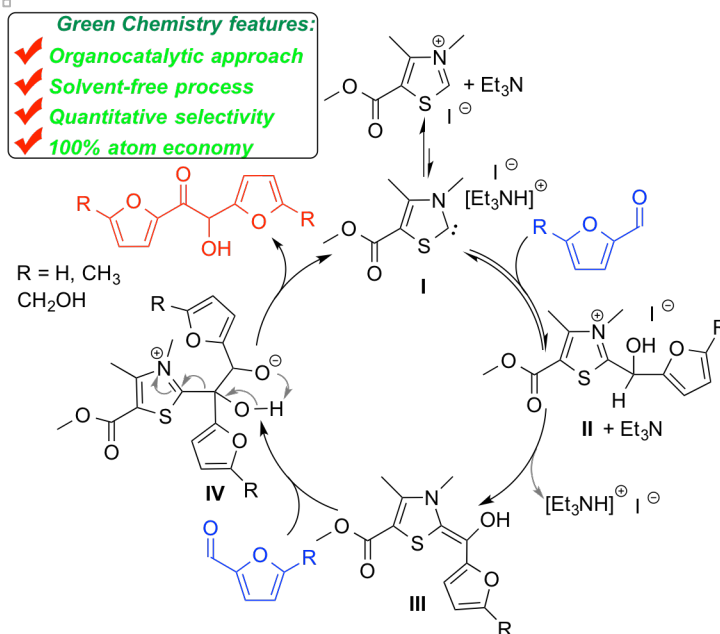


**Fig. 1.** Proposed mechanism for self-coupling of FF and HMF by <sup>Ac</sup>[TM]I/Et<sub>3</sub>N.

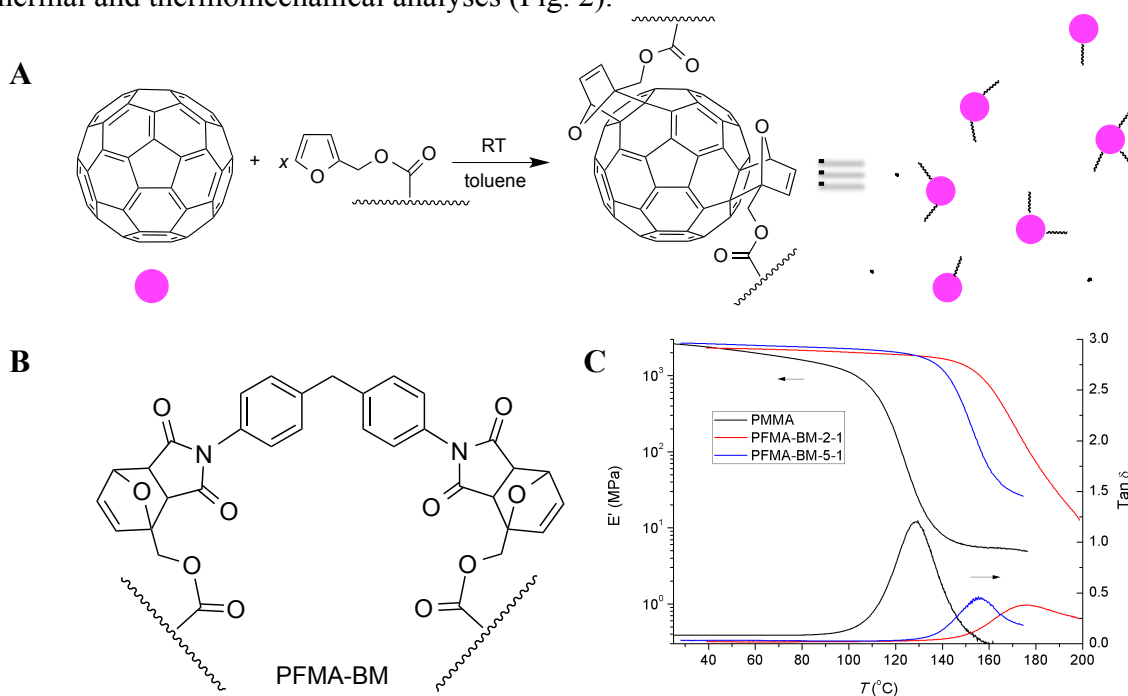


**Fig. 2.** Cross-linked PFMA-C<sub>60</sub> material (A) by the DA “click” reaction of PFMA with C<sub>60</sub>, cross-linked PFMA-BM polymers (B) through the DA “click” reaction, and dynamic mechanical analysis (DMA) curves of cross-linked PFMA materials (tension film mode): storage modulus (E') and tan δ as a function of temperature (C).

**Fully recyclable supported heterogeneous catalysts for quantitative upgrading of FF and HMF to C<sub>10</sub> and C<sub>12</sub> furoins:** N-heterocyclic carbene precatalysts have been successfully anchored onto silica, clay, and polymer supports to afford supported, heterogeneous catalysts that maintained near quantitative yield for each of the ten cycles performed in the catalytic upgrading of FF and HMF to the corresponding C<sub>10</sub> and C<sub>12</sub> furoins.

**DHMF-based polymeric materials:** The resulting HMF self-coupling product DHMF has been catalytic transformed into other derivatives, which have been utilized for polymerization into useful furan-based polymers.

### Publications Acknowledging this Grant (2012–2015)

1. Liu, D.; Zhang, Y.; Chen, E. Y.-X. “Organocatalytic Upgrading of the Key Biorefining Building Block by a Catalytic Ionic Liquid and N-heterocyclic Carbenes”, *Green Chem.* **2012**, *14*, 2738–2746 (cover article).
2. Liu, D.; Chen, E. Y.-X. “Ubiquitous Aluminum Alkyls and Alkoxides as Effective Catalysts for Glucose to HMF Conversion in Ionic Liquids”, *Appl. Catal. A: Gen.* **2012**, *435/436*, 78–85.
3. Dunn, E. F.; Liu, D.; Chen, E. Y.-X. “Role of N-Heterocyclic Carbenes in Glucose Conversion into HMF by Cr Catalysts in Ionic Liquids”, *Appl. Catal. A: Gen.* **2013**, *460-461*, 1–7.
4. Liu, D.; Chen, E. Y.-X. “Diesel and Alkane Fuels from Biomass by Organocatalysis and Metal-Acid Tandem Catalysis”, *ChemSusChem* **2013**, *6*, 2236–2239.
5. He, J.; Zhang, Y.; Chen, E. Y.-X. “Chromium(0) Nanoparticles as Effective Catalyst for the Conversion of Glucose into 5-Hydroxymethylfurfural”, *ChemSusChem* **2013**, *6*, 61–64.
6. Liu, D.; Chen, E. Y.-X. “Polymeric Ionic Liquid (PIL)-Supported Recyclable Catalysts for Biomass Conversion into HMF”, *Biomass & Bioenergy.* **2013**, *48*, 181–190.
7. Nakarit, C.; Kelland, M. A.; Liu, D.; Chen, E. Y.-X. “Cationic Kinetic Hydride Inhibitor Polymers and the Effect on Performance of Incorporating Cationic Monomers into N-Vinyl Lactam Copolymers”, *Chem. Eng. Sci.* **2013**, *102*, 424–431.

8. Zhang, Y.; Chen, E. Y.-X. “Polymerization of Nonfood Biomass-Derived Monomers to Sustainable Polymers”, *Top. Curr. Chem.* **2014**, *353*, 185–227 (*invited contribution to the topics volume on Selective Catalysis for Renewable Feedstocks and Chemicals*).
9. Chen, E. Y.-X.; Liu, D. “Biorefining Compounds and Organocatalytic Upgrading Methods”, PCT Int. Appl. WO 2014/008301; US2014/0007497 A1, **2014**.
10. Liu, D.; Chen, E. Y.-X. “Organocatalysis in Biorefining for Biomass Conversion and Upgrading”, *Green Chem.* **2014**, *16*, 964–981 (*invited review*).
11. Liu, D.; Chen, E. Y.-X. “An Integrated Catalytic Process for Biomass Conversion and Upgrading to C<sub>12</sub> Furoin and Alkane Fuel”, *ACS Catal.* **2014**, *4*, 1302–1310.
12. Zang, H.; Chen, E. Y.-X. “Organocatalytic Upgrading of Furfural and 5-Hydroxymethyl Furfural to C<sub>10</sub> and C<sub>12</sub> Furoins with Quantitative Yield and Atom-Efficiency”, *Int. J. Mol. Sci.* **2015**, *16*, 7143–7158 (*invited contribution to the Green Chemistry and Biorefinery issue*).
13. Magnusson, C. D.; Liu, D.; Chen, E. Y.-X.; Kelland, M. A. “Non-Amide Kinetic Hydrate Inhibitors: Investigation of the Performance of a Series of Polyvinylphosphonate Diesters”, *Energy & Fuels* **2015**, *29*, 2336–2341.
14. Feng, S.; Schmitt, M.; Chen, E. Y.-X. “Organocatalytic Polymerization of Furfuryl Methacrylate and Post Diels-Alder Click Reaction to Cross-linked Materials”, *Macromol. Chem. Phys.* **2015**, DOI: 10.1002/macp.201500079.

**Interaction of Na, water and CO<sub>2</sub> with MnO(100): Modeling a complex mixed oxide system for thermochemical water splitting**

Xu Feng, Han Chen and David F. Cox  
Virginia Tech, Chemical Engineering

**Presentation Abstract**

Our work in the past year has focused on developing a surface science model of a multicomponent catalyst system developed by the Davis group at Caltech that shows promise for the low-temperature (850 °C) thermochemical splitting of water.<sup>1</sup> The system is based on a mixture of Na<sub>2</sub>CO<sub>3</sub> and manganese oxides. We have succeeded in generating all the manganese oxides proposed in the catalytic cycle by oxidation and thermal reduction processes. For the critical water reduction step, an intimate mixture of MnO and Na<sub>2</sub>CO<sub>3</sub> is thought to be required. A surface science model of this mixture can be produced via the deposition of metallic sodium on MnO(100), oxidation of Na to Na<sub>2</sub>O, and reaction with CO<sub>2</sub> to generate Na<sub>2</sub>CO<sub>3</sub>. The details of the interaction of Na with MnO are critical to the preparation of the model system, and CO<sub>2</sub> can be used as a probe molecule to characterize different forms of Na at the interface. Details of these interactions will be described.

1. Xu, Bhawe and Davis. *PNAS* **2012**, *109*: 9260.

## DE-FG02-97ER14751: Hydrocarbon Oxidation, Dehydrogenation and Coupling over Model Metal Oxide Surfaces

Postdoc(s): n/a

Student(s): Xu Feng and Han Chen

### RECENT PROGRESS

#### *Interaction of Na with MnO(001)*

The deposition of Na on MnO(001) proceeds via a Stranski-Krastanov (SK) growth mode with metallic Na island formation following completion of the first monolayer of Na. Na within the first monolayer has an oxidic electronic structure, and is irreversibly adsorbed. Metallic Na present at coverages greater than 1 ML evaporates at 430 K in TPD, and irreversibly adsorbed Na in the first monolayer diffuses into the bulk of MnO at around 600 K. CO<sub>2</sub> can be used to probe the nature of the Na at the interface. CO<sub>2</sub> reacts strongly with metallic sodium, forming a non-metallic compound that decomposes in TPD at 735 K to give both CO<sub>2</sub> and CO. The interaction of CO<sub>2</sub> with oxidic Na in the first monolayer is slightly weaker, desorbing at 650 K. Heating above 600 K to drive Na into subsurface sites blocks the interaction of Na with CO<sub>2</sub>, and only the weak interaction of CO<sub>2</sub> seen with the clean MnO(100) surface is apparent as a desorption signal for CO<sub>2</sub> at 150 K.

#### *Na oxidation and Na<sub>2</sub>CO<sub>3</sub> formation*

For coverages of Na greater than 1 ML on MnO(100), O<sub>2</sub> exposures oxidize metallic Na to Na<sub>2</sub>O. Adsorption of CO<sub>2</sub> in the presence of Na<sub>2</sub>O forms a Na carbonate surface compound that is stable to 825 K in TPD.

### Publications Acknowledging this Grant in 2012-2015

1. Dong, Y.; Brooks, J. D.; Chen, T. L.; Mullins, D. R.; Cox, D. F. Reactions of methyl groups on a non-reducible metal oxide: the reaction of iodomethane on stoichiometric  $\alpha$ -Cr<sub>2</sub>O<sub>3</sub>(0001). *Surf. Sci.* **Submitted**.
2. Gibbs, G. V.; Ross, N. L.; Cox D. F. An estimation of bond lengths for oxide crystals with a simple molecular power law expression. *Phys. Chem. Minerals* **In Press**.
3. Dong, Y.; Brooks, J. D.; Chen, T. L.; Mullins, D. R.; Cox, D. F. Methylene migration and coupling on a non-reducible metal oxide: the reaction of dichloromethane on stoichiometric  $\alpha$ -Cr<sub>2</sub>O<sub>3</sub>(0001). *Surf. Sci.* **2015**, 632, 28-38.
4. Gibbs, G. V.; Ross, N. L.; Cox D. F.; Rosso K. M. Insights into the crystal chemistry of earth materials rendered by electron density distributions: Pauling's rules revisited, *American Mineralogist* **2014**, 99, 1071-1084.
5. Gibbs, G. V.; Ross, N. L.; Cox D. F.; Rosso K. M.; Iversen, B. B.; Spackman M. A. Pauling Bond Strength, Bond Length and Electron Density Distribution, *Phys. Chem. Minerals* **2014**, 41, 17-25.

6. Gibbs, G. V.; Ross, N. L.; Cox D. F.; Rosso K. M.; Iversen, B. B.; Spackman M. A. Bonded radii and the contraction of the electron density of the oxygen atom by bonded interactions. *J. Phys. Chem. A* **2013**, *117*, 1632-1640.
7. Gibbs, G. V.; Wang, D.; Hin, C.; Ross, N. L.; Cox, D. F.; Crawford, T. D.; Spackman, M. A.; Angel, R. J. Properties of atoms under pressure: Bonded interactions of the atoms in three perovskites. *J. Chem. Phys.* **2012**, *137*, 164313.

**Abhaya K. Datye and Yong Wang**

**Sub Nanometer Sized Clusters for Heterogeneous Catalysis**

Abhaya Datye<sup>1</sup> and Yong Wang<sup>2</sup>

<sup>1</sup>University of New Mexico and <sup>2</sup>Washington State University

**Presentation Abstract**

The focus of this project is the synthesis, characterization and reactivity of transition metal moieties ranging from single atoms to clusters of about 1 nm in diameter that are present on high surface area supports. A major barrier in the utilization of sub-nm clusters is that they are subject to Ostwald ripening, leading to growth in size to form nanoparticles. Previous work suggests that trapping single atoms on the support could help to slow the rates of ripening. Hence, one of the goals of this project is the creation of suitable anchoring sites on high surface area catalyst supports. Conventional (non-reducible) oxide supports provide only limited number of sites to anchor ionic species. Reducible oxides provide many more sites for anchoring due to the presence of defects, such as vacancies. But reducible oxides are often not available in high surface area form, and they may not be as robust (can react to form carbonates, for example, or sinter easily) compared to the commonly-used high surface area supports such as silica, alumina, or carbon. Increasing atomic trapping sites on conventional catalyst supports is therefore important for improving the stability of sub-nm metal clusters on a supported catalyst. Another goal of this project is to expand the applicability of single atom catalysts to a broader class of catalyzed reactions. Transition metals in ionic form are perfectly situated for further manipulation of their catalytic activity by use of ligands, as in homogeneous catalysis. Understanding the principles that help in the design of robust single atom catalysts is one of the research challenges that is addressed in this project.

**DOE grant # DE-FG02-05ER15712**

**Sub Nanometer Sized Clusters for Heterogeneous Catalysis**

Post-docs: Andrew DeLaRiva (UNM), Zhang He (WSU)  
Graduate Students: Angelica Benavidez (UNM), Eric Petersen (UNM), Monique Curley (UNM), Aaron Jenkins (UNM), Stephen Davison (WSU), Yongchun Hong (WSU), Xavier Isidro Pereira Hernández (WSU).

**RECENT PROGRESS**

**Low temperature CO oxidation on atomically dispersed Pd/Lanthana-modified alumina**

Low temperature CO oxidation performance is important for meeting DOE goals for more efficient combustion engines which have lower exhaust temperatures. Catalysts need to

provide low temperature reactivity in reactions important for eliminating exhaust gas pollutants. Metallic Pd is poisoned by CO at low temperatures. We have identified a novel pathway for CO oxidation on atomically dispersed ionic Pd sites which are present even on industrially-relevant gamma alumina. Aberration corrected STEM confirms the presence of isolated Pd species on alumina supports. The presence of La on the alumina, which is added to improve the hydrothermal stability of the alumina, results in enhanced stability of the ionic Pd species. Our proposed reaction mechanism involves oxygen coming from the lattice, as shown by DFT calculations. The ionic Pd bound to alumina activates CO which then picks up a lattice oxygen. The vacancy site then adsorbs dioxygen, a second CO picks up the extra O, and the cycle repeats itself. Atomically dispersed Pd species show a positive order of reaction in CO, very different from that on metallic Pd. (Published in Nature Communications, 5, 2014)

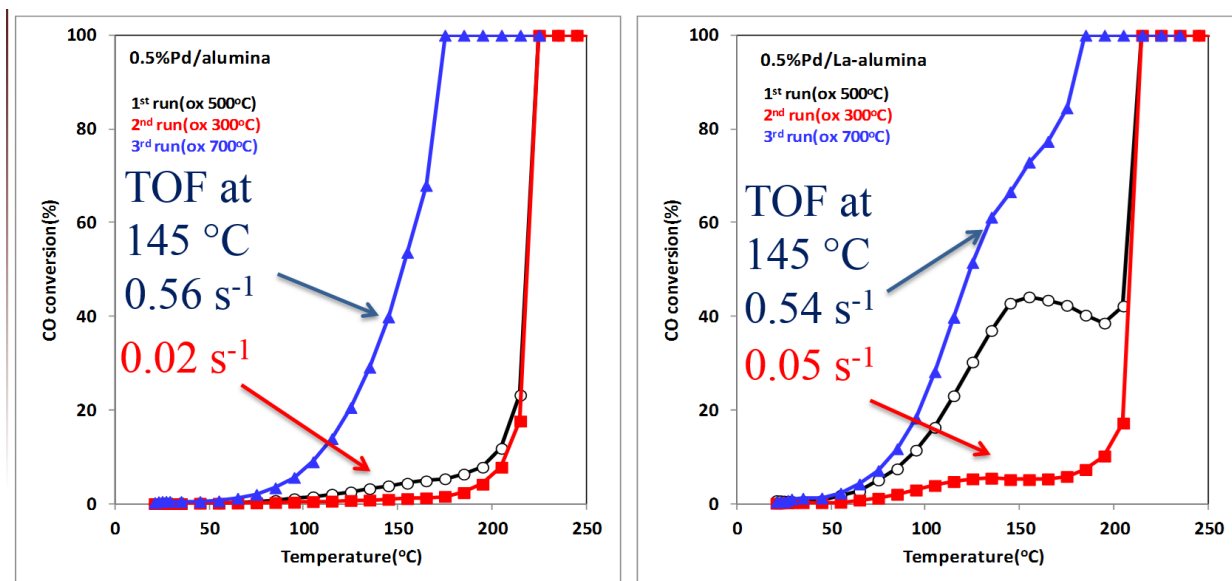


**Figure 1.** Lightoff curves of 0.5 wt% Pd/Al<sub>2</sub>O<sub>3</sub> and 0.5 wt% Pd/Lanthana-modified alumina. The high activity state is an oxidized Pd in the +1 state. This work shows that while metallic Pd gets poisoned by CO, the isolated Pd+1 is able to bind CO weakly to provide high turnover rates at low temperatures (Peterson et al., Nature Communications, 2014).

### Atomically dispersed Pd/CeO<sub>2</sub>

In our quest for stable, atomically dispersed species we explored the characteristics of Pd/CeO<sub>2</sub>. While most previous work has focused on the nature of the metal-support interface, we learnt that at low metal loadings the Pd is very well dispersed while providing very high catalytic activity. We studied the role of the support, CeO<sub>2</sub> rods, cubes and polyhedra. We find that the rods provide the best supports to yield high activity for CO oxidation, similar to the behavior seen in low loading Pd/alumina. However, in this case the Pd does not get reduced, but

survives repeated runs. Preliminary EXAFS data shows that the Pd is highly dispersed (CN ~7) and the key difference between rods and cubes is that the former provide a facile redox character to the Pd. This flexibility is very important in catalyzing CO oxidation. To apply this concept to industrial catalysis, we need to develop methods to stabilize the Pd in the size range that is most conducive to facile redox behavior.

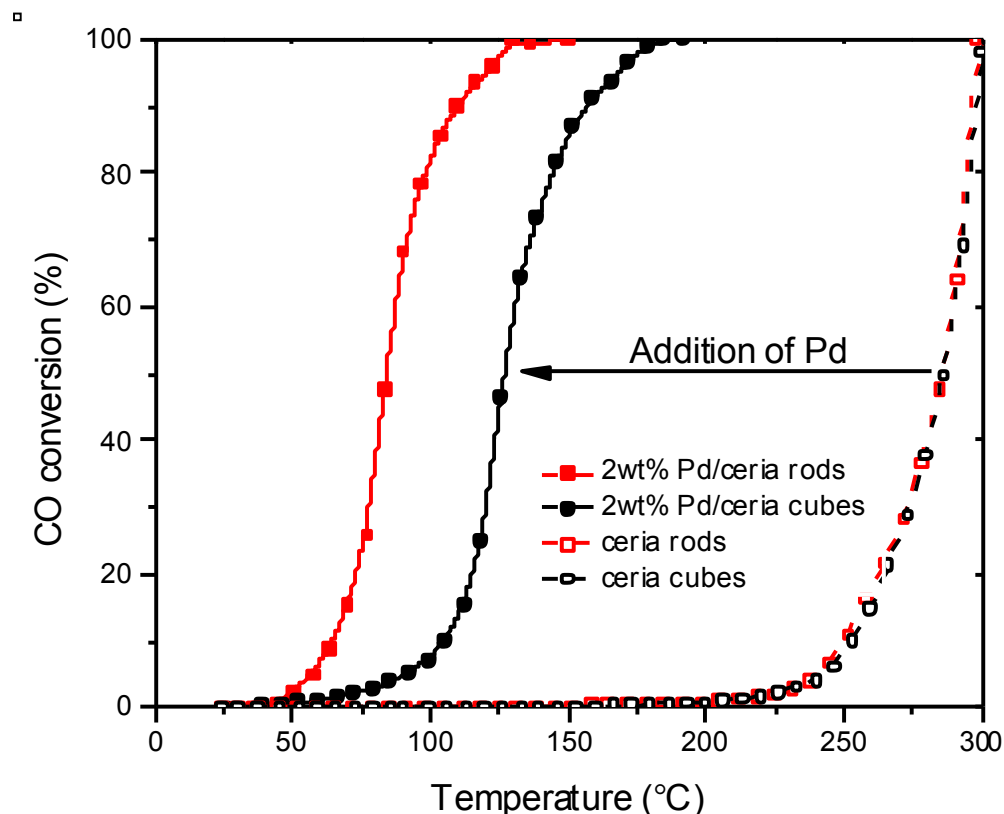
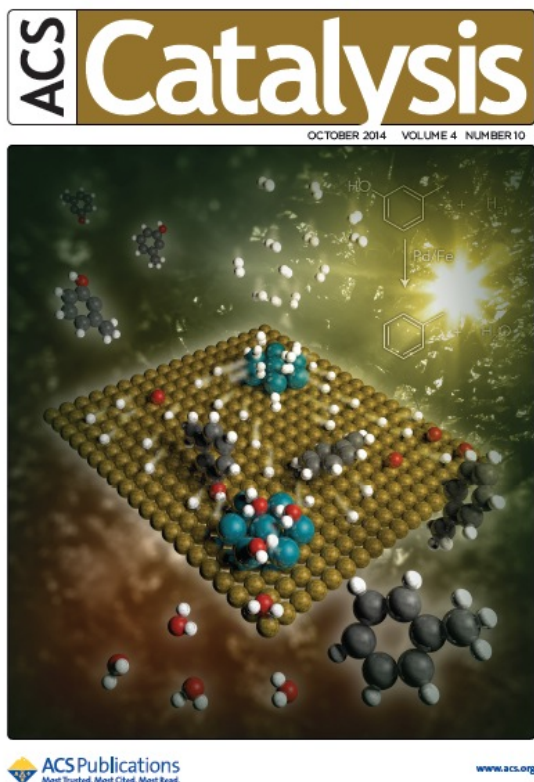


**Figure 2.** Addition of 2wt%Pd to ceria rods provides exceptional low temperature CO oxidation reactivity. Our XAS study shows that the key difference between the Pd/rods is the facile redox behavior of the Pd, which makes it easy for oxygen to compete with the CO for active sites. Further work is needed to understand fully the mechanism by which ceria modifies the redox properties of the metal phase.

### Pd modified Fe<sub>2</sub>O<sub>3</sub> catalysts

In a second project, we investigated the manipulation of Fe catalysts by the addition of Pd. A series of Pd/Fe<sub>2</sub>O<sub>3</sub> catalysts were synthesized, characterized, and evaluated for the hydrodeoxygenation (HDO) of *m*-cresol. It was found that the addition of Pd promotes the catalytic activity of Fe while the product distributions resemble those of monometallic Fe catalysts, showing high selectivity towards the production of toluene (C-O cleavage without

saturation of aromatic ring and C-C cleavage). A possible mechanism, including Pd assisted H<sub>2</sub> dissociation and Pd facilitated stabilization of metallic Fe surface via reducing barrier of water formation as well as Pd enhanced product desorption, was proposed to be responsible for the high activity and HDO selectivity in Pd-Fe catalysts (see the figure below). The synergistic catalysis derived from the Pd-Fe interaction proved to be applicable to other precious metal promoted Fe catalysts, providing a promising strategy for future design of highly active and selective HDO catalysts using earth abundant Fe. The figure on the right shows the cover page for the review of supported metal catalysts for alcohol/sugar steam reforming.



### Publications acknowledging this grant (2012-2015)

1. H. Xiong, A. DeLaRiva, Y. Wang, and A.K. Datye, Low-temperature aqueous-phase reforming of ethanol on bimetallic PdZn catalysts. *Catalysis Science & Technology*, 2015, 5(1): p. 254-263.
2. S.Davidson, J.Sun, H.Zhang, Y.Wang, “Bimetallic catalysts for alcohol reforming”, *Dalton Transactions* 2014, DOI:10.1039/c4dt00521j (invited perspective, cover of the issue 31 of 2014).
3. H.Zhang, V.Lebarbier, A.M.Karim, J.Sun, B.Halevi, A.DeLariva, A.Datye, J.Vohs, Y.Wang, “The influence of ZnO facets on Pd/ZnO catalysts for methanol steam reforming”, *ACS Catalysis*, 2014, 4, 2379-2386, doi: dx.doi.org/10.1021/cs500590t

4. J.Sun, A.Karim, D.Mei, M.Engelhard, Y.Wang, “New insight into reaction mechanisms of ethanol steam reforming on Co/ZrO<sub>2</sub>”, *Appl.Catal.B: Environmental*,2014, doi:10.1016/j.apcatb.2014.06.043
5. A.J.R.Hensley, Y.Hong, R.Zhang, H.Zhang, J.Sun, Y.Wang, J.S.McEwen\*, “Enhanced Fe<sub>2</sub>O<sub>3</sub> reducibility via surface modification with Pd: characterizing the synergy within Pd/Fe catalysts for hydrodeoxygenation reactions”, *ACS Catalysis*, 2014, doi: dx.doi.org/10.1021/cs500565e.
6. Y.Hong, A.J.R.Hensley, H.Zhang, J.Sun, J.S.McEwen, Y.Wang, “Synergistic catalysis between Pd and Fe in gas phase hydrodeoxygenation of m-cresol”, *ACS Catalysis*, 2014, doi: dx.doi.org/10.1021/cs500578g (cover of the Oct issue).
7. Z.Weil, A.Karim, Y.Li, D.L.King, Y.Wang, “Elucidation of the roles of Re in steam reforming of glycerol over Pt-Re/C catalysts”, *J.Catal.*, 2014, doi:10.1016/j.jcat.2014.11.006.
8. S.Davidson, J.Sun, Y.Wang, “The effect of ZnO addition on Co/C catalyst for vapor and aqueous phase reforming of ethanol”, *Catal.Today*, 2014, dx.doi.org/10.1016/j.cattod.2013.12.044.
9. C.Liu, H.Wang, A.Karim, J.Sun, Y.Wang, “Advances in catalytic pyrolysis of lignocellulosic biomass”, *Chem.Soc.Rev.* 2014, 43(22), 7594-7623 (inside cover of the Nov. issue)
10. J.Sun, Y.Wang\*, “Review of ethanol conversion to chemicals and fuels”, *ACS Catalysis*, 2014, dx.doi.org/10.1021/cs4011343. (cover art for the No.4 issue of 2014).
11. J.Kwak, R.Dagle, G.Tustin, J.Zoeller, L.Allard, Y.Wang, “Molecular active sites in heterogeneous Ir-La/C catalyzed carbonylation of methanol to acetates”, *J.Phy.Chem.Lett.* 2014, dx.doi.org/10.1021/jz402728e
12. A.J.Hensley, Y.Wang, J.S.McEwen, “Adsorption of Phenol on Fe (110) and Pd (111) from First Principles”, *Surface Science*, doi: 10.1016/j.susc.2014.08.003.
13. E.J. Peterson, A.T. DeLaRiva, S. Lin, R.S. Johnson, H. Guo, J.T. Miller, J. Hun Kwak, C.H.F. Peden, B. Kiefer, L.F. Allard, F.H. Ribeiro, and A.K. Datye, Low-temperature carbon monoxide oxidation catalysed by regenerable atomically dispersed palladium on alumina. *Nat Commun*, 2014. 5.
14. J. Paiz, J. Fitch, E. Peterson, T. Hough, W. Barnard, and A. Datye, Synthesis of PdO-ZnO mixed oxide precursors for PdZn intermetallic catalysts. *Crystal Research and Technology*, 2014. 49(9): p. 699-707.
15. A.D. Benavidez, P.D. Burton, J.L. Nogales, A.R. Jenkins, S.A. Ivanov, J.T. Miller, A.M. Karim, and A.K. Datye, Improved selectivity of carbon-supported palladium catalysts for the hydrogenation of acetylene in excess ethylene. *Applied Catalysis A-General*, 2014. 482: p. 108-115.
16. S.Davidson, J.Sun, Y.Wang, “Ethanol steam reforming on Co/CeO<sub>2</sub>: the effect of ZnO promoter”, *Topics in Catalysis*, 2013, doi: 10.1007/s11244-013-0103-5.
17. Z.Weil, J.Sun, H.Zhang, Y.Li, A.Datye, Y.Wang, “Bimetallic nanocatalysts hydrogen generation”, *Chem.Soc.Review* 2012, DOI:10.1039/C2CS35201J – invited review
18. B. Halevi, S. Lin, A. Roy, H. Zhang, E. Jeroro, J. Vohs, Y. Wang, H. Guo, and A.K. Datye, High CO<sub>2</sub> Selectivity of ZnO Powder Catalysts for Methanol Steam Reforming. *Journal of Physical Chemistry C*, 2013. 117(13): p. 6493-6503.
19. J.R. Gaudet, A. de la Riva, E.J. Peterson, T. Bolin, and A.K. Datye, Improved Low-Temperature CO Oxidation Performance of Pd Supported on La-Stabilized Alumina. *ACS Catalysis*, 2013: p. 846-855.

20. R.S. Johnson, A. DeLaRiva, V. Ashbacher, B. Halevi, C.J. Villanueva, G.K. Smith, S. Lin, A.K. Datye, and H. Guo, *The CO oxidation mechanism and reactivity on PdZn alloys*. Physical Chemistry Chemical Physics, 2013. 15: p. 7768-7776.
21. A.T. DeLaRiva, T.W. Hansen, S.R. Challa, and A.K. Datye, *In situ Transmission Electron Microscopy of catalyst sintering*. Journal of Catalysis, 2013. 308: p. 291-305, invited review for the 50<sup>th</sup> anniversary special edition of J. Catal.
22. A.K. Datye, *7.05 - Imaging of Heterogeneous Catalysts*, in *Comprehensive Inorganic Chemistry II (Second Edition)*, J. Reedijk and K. Poeppelmeier, Editors. 2013, Elsevier: Amsterdam. p. 103-129, invited book chapter.
23. B. Halevi, E.J. Peterson, A. Roy, A. Delariva, E. Jerero, F. Gao, Y. Wang, J.M. Vohs, B. Kiefer, E. Kunkes, M. Hävecker, M. Behrens, R. Schlögl, and A.K. Datye, Catalytic reactivity of face centered cubic PdZn  $\alpha$  for the steam reforming of methanol. *Journal of Catalysis*, 2012. 291: p. 44-54.
24. J.Sun, D.Mei, A.Karim, A.Datye, Y.Wang, “Minimizing the formation of coke and methane on Co nanoparticles in steam reforming of biomass-derived oxygenates”, *ChemCatChem*. 2013, DOI:10.1002/cctc.201300041.(cover page featured in the June issue).
25. A.J.Hensley, R.Zhang, Y.Wang, J.S.McEwen, “Energetic and electronic interactions between benzene and PdFe surfaces: a density functional theory study”, *J.Phy.Chem.C* 2013, 117, 24317-24328.
26. C.J.Liu, J.Sun, C.Smith, Y.Wang, “A study of Zn<sub>x</sub>Zr<sub>y</sub>O<sub>z</sub> mixed oxides for direct conversion of ethanol to isobutene”, *Appl.Catal.A: General*, 2013, doi:10.1016/j.apcata.2013.07.011.
27. J.Sun, A.M.Karim, H.Zhang, L.Kovarik, X.Li, J.S.McEwen, A.J.Hensley, Y.Wang, “Vapor phase hydrodeoxygenation of guaiacol on carbon supported metal catalysts”, *Journal of Catalysis*, 2013, doi:10.1016/j.jcat.2013.05.020.
28. A.D. Benavidez, L. Kovarik, A. Genc, N. Agrawal, E.M. Larsson, T.W. Hansen, A.M. Karim, and A.K. Datye, *Environmental transmission electron microscopy study of the origins of anomalous particle size distributions in supported metal catalysts*. ACS Catalysis, 2012. 2(11): p. 2349-2356.
29. B. Roy, U. Martinez, K. Loganathan, A.K. Datye, and C.A. Leclerc, *Effect of preparation methods on the performance of Ni/Al<sub>2</sub>O<sub>3</sub> catalysts for aqueous-phase reforming of ethanol: Part I-catalytic activity*. International Journal of Hydrogen Energy, 2012. 37(10): p. 8143-8153.
30. B. Roy, K. Artyushkova, H.N. Pham, L. Li, A.K. Datye, and C.A. Leclerc, *Effect of preparation method on the performance of the Ni/Al<sub>2</sub>O<sub>3</sub> catalysts for aqueous-phase reforming of ethanol: Part II-characterization*. International Journal of Hydrogen Energy, 2012. 37(24): p. 18815-18826.

**Computational Studies of Catalytic Reactions of Alcohols on Oxide Nanoclusters**

David A. Dixon,<sup>1</sup> Zdenek Dohnálek,<sup>2</sup> Roger Rousseau,<sup>2</sup> Bruce D. Kay<sup>2</sup>

<sup>1</sup> Department of Chemistry, The University of Alabama

<sup>2</sup>Fundamental and Computational Sciences Directorate and Institute for Integrated Catalysis,  
Pacific Northwest National Laboratory

**Presentation Abstract**

Our studies of the reactions of mono-alcohols on transition metal oxide (TMO) clusters have been extended to polyols and acids and from Group 6 TMOs to Group 4 TMO clusters and to an Al<sub>8</sub>O<sub>12</sub> cluster model of  $\gamma$ -Al<sub>2</sub>O<sub>3</sub>. Dehydration, dehydrogenation, and condensation reactions were studied to evaluate cluster reactivity. Geometries were optimized at the density functional theory level followed by single point coupled cluster CCSD(T) calculations to provide quantitative molecular-scale information of the reaction mechanisms. The dehydration and dehydrogenation probe both the Lewis/Brønsted acid/base and redox properties of the metal centers. Up to three alcohols per cluster have been studied computationally. The reactions of ethanol and 1,2-ethanediol on M<sub>3</sub>O<sub>9</sub> clusters for M = W and Mo, the reactions of ethanol on (MO<sub>2</sub>)<sub>n</sub> n = 1 – 4 for M = Ti, Zr, Hf, and the reactions of ethanol on Al<sub>8</sub>O<sub>12</sub> have been studied. All of the reactions proceed by a Lewis acid-base step of the alcohol interacting with the metal center with diol having an additional hydrogen bond to an adjacent oxygen. This initial addition step is followed by proton transfer to a M=O oxygen for the Group 4 and 6 nanoclusters. The dehydration reaction of ethanol on M<sub>3</sub>O<sub>9</sub> is through a dialkoxy intermediate with  $\beta$  hydrogen transfer to a terminal M=O. Dehydration on Al<sub>8</sub>O<sub>12</sub> begins with a stable physisorbed ethanol-cluster complex with a strong Lewis acid-base donor-acceptor bond followed by a  $\beta$ -H transfer to a bi-coordinated oxygen atom leading to the formation of ethylene. Dehydrogenation on M<sub>3</sub>O<sub>9</sub> takes place via an  $\alpha$  hydrogen transfer to an adjacent M<sup>VI</sup>=O atom or a W<sup>VI</sup> metal center with redox at the metal for M = Mo and no redox for M = W. Dehydrogenation on Al<sub>8</sub>O<sub>12</sub> takes place through a chemisorbed intermediate followed by an  $\alpha$ -H transfer to the active metal center, which is a proton coupled electron transfer reaction. For M<sub>3</sub>O<sub>9</sub>, ether formation requires the presence of three alcohol molecules with one alcohol sacrificed to form a metal hydroalkoxide, which is a strong gas phase Brønsted acid. The addition of a second ethanol on Al<sub>8</sub>O<sub>12</sub> forms two hydrogen bonds with the physisorbed intermediate from the first addition and diethyl ether is generated by an  $\alpha$ -C transfer from the first to the second ethanol. The computational results agree well with the available experimental data. An improved method for obtaining heats of formation of TMO clusters based on CCSD(T) will be shown.

This work is part of the PNNL FWP 47319, “Multifunctional Catalysis to Synthesize and Utilize Energy Carriers”.

**Postdoctoral Fellow:** Zongtang Fang (UA)

**Control of Reactivity in Nanoporous Metal/Ionic Liquid Composite Catalysts**

Jonah Erlebacher  
Johns Hopkins University  
Department of Materials Science and Engineering

**Presentation Abstract**

In this program, we have been exploring a new concept in nanostructured heterogeneous catalysis design – the nanoporous metal/ionic liquid (IL) composite. The idea behind this concept is to tailor the chemical environment within and near the pores of a metallic electrocatalyst in order to enhance the aggregate composite activity and selectivity. Most recent electrocatalyst design focuses upon lowering the activation barrier for a particular synthesis reaction. While we also try to minimize this quantity, one should also recognize that significant catalytic enhancements can be made by biasing the reaction to completion via control of the environment in which the reaction occurs. Specific ideas we are exploring in this program include (a) bias of mass transport of reactants to the surface and products away from it, and (b) corralling of reactants and products to spatially separate them and reduce side reactions. We are making a particular focus on electrocatalysis under kinetically limited conditions, and in which the catalyst is a nanoporous metal and the biasing environment is an ionic liquid impregnating the pores.

A notable achievement in this program has been the development and characterization of a dealloyed nanoporous nickel/platinum catalyst, whose intrinsic high activity in magnified via impregnation with hydrophobic ionic liquids (ILs) to make materials with some of the highest activity toward the electrochemical oxygen reduction reaction yet discovered. Fundamental electrochemical characterization of these materials indicates that the origin of the enhanced activity lies in the physico-chemical properties of the ILs, particularly their higher oxygen solubility relative to aqueous solution and their lower water solubility, both effects working synergistically to bias the reaction to completion.

By recognizing that proton transport through the ionic liquid can be slow relative to reactant (dissolved gas) transport, we have been exploring using the IL layer over nanoporous catalysts to tailor electrochemical reaction selectivity under unusual reaction conditions. For instance, by operating at a high electrochemical potential using an aprotic IL buffer layer, we are attempting to drive oxygen reduction, not to water, but to superoxide, at the same time kinetically suppressing hydrogen evolution. Similar strategies are being explored to synthesis highly reduced species of other simple gasses dissolved in the aqueous solution, and using multi-electrode systems to throttle the flux of protons to these reduced gasses.

## DE-FG02-12ER16355: Control of Reactivity in Nanoporous Metal/Ionic Liquid Composite Catalysts

**Student(s):** Joshua Snyder (graduated), Ellen Benn

### RECENT PROGRESS

***Ionic-Liquid Encapsulated Nanoporous NiPt Nanoparticles.*** In our previous program, we developed a highly active nanoporous NiPt (np-NiPt) composite catalyst comprised of the dealloyed nanoporous metal impregnated with the ionic liquid [MTBD][beti] (7-methyl-1,5,7-triazabicyclo[4.4.0]dec-5-ene, MTBD)[bis(perfluoroethylsulfonyl)imide, beti]) [J. Snyder, T. Fujita, M.W. Chen, J. Erlebacher, "Oxygen Reduction in Nanoporous Metal/Ionic Liquid Composite Electrocatalysts," *Nature Materials* **9** (2010), 940-907; , H. Luo, G. Baker, J. Lee, R. Pagni, S. Dai, "Ultrastable superbase-derived protic ionic liquids," *J. Phys. Chem. B*, **113** (2009), 4181-4183]. We also developed a method to produce monodisperse NiPt nanoparticles that could be dealloyed and turned porous [J. Snyder, I. McCue, K. Livi, J. Erlebacher, "Structure/Processing/Properties Relationships in Nanoporous Nanoparticles As Applied to Catalysis of the Cathodic Oxygen Reduction Reaction," *J. Amer. Chem. Soc.*, **134** (2012), 8633-8645.]. In our current program, we combined both ideas, encapsulating nanoporous nanoparticles with [MTBD][beti] [J. Snyder, K. Livi, J. Erlebacher, "Oxygen Reduction Reaction Performance of [MTBD][beti]-Encapsulated Nanoporous NiPt Alloy Nanoparticles," *Adv. Func. Mat.*, **23** (2013), 5494-5501.]. Micrographs of the composite are shown in Figure 1. The mass

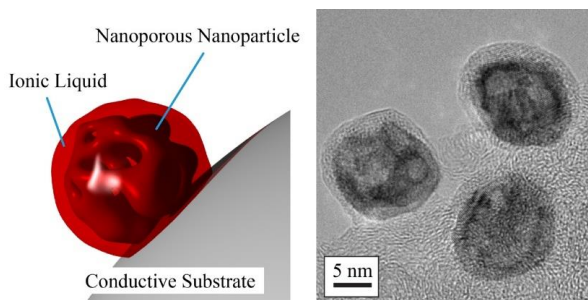


**Figure 1. Schematic and implementation of encapsulated nanoporous nanoparticle catalysts for high-performance PEMFC oxygen reduction:** (A) Cartoon illustrating the key components: The nucleus of the catalyst is a high surface area nanoporous nanoparticle, which allows the particle to be encapsulated by an ionic liquid (IL). The composite catalyst is attached to a conductive substrate to aid integration into a PEMFC cathode catalyst layer. (B) High resolution transmission electron micrograph (HRTEM) of nanoporous nickel-platinum (np-NiPt) nanoparticles encapsulated with [MTBD][beti] IL, supported on carbon. This protic, hydrophobic IL increases the residence time of oxygen near the catalyst surface, improving activity.

activities for oxygen reduction at 0.9 V and 0.95 V vs. RHE are 2.2 mA/ $\mu\text{g}_{\text{Pt}}$  and 0.54 mA/ $\mu\text{g}_{\text{Pt}}$ , respectively, and at the time of publication were the highest mass activities yet found for an oxygen reduction reaction (ORR) catalyst. More importantly, in our opinion, is that the strategy is based on magnifying the reactivity of the metal by controlling the properties of the ionic liquid encapsulant, with serves to confine reactants within the catalyst environment. This strategy has been recently adopted by the Yang and Stamenkovic groups [C. Chen, Y. Kang, Z. Huo, Z. Zhu, W. Huang, H.L. Xin, J.D. Snyder, D. Li, J.A. Herron, M. Mavrikakis, M. Chi, K.L. More, Y. Li, N.M. Markovic, G.A. Somorjai, P. Yang, V. Stamenkovic, "Highly crystalline

multimetallc nanoframes with three-dimensional electrocatalytic surfaces,” *Science*, **343** (2014), 1339-1343] greatly magnifying the activity of their Ni/Pt nanocage catalysts.

**Fundamental electrochemistry using nanoporous metal/ionic liquids composite catalysts.** In this segment of the program, we have been studying the fundamental electrochemical response of nanoporous metal/ionic liquid catalysts, primarily using a dealloyed nanoporous Pt/Ni electrode impregnated with IL, and using the oxygen reduction reaction as a model system. We have been looking at a variety of ionic liquids, particularly the response of protic versus aprotic ionic liquids, with more or less hydrophobicity (water solubility). We have also surmounted many technical challenges associated with this system and are in a data-gathering phase of the program.

The primarily technical challenge we have needed to address is that the thickness of the IL layer between the electrode and electrolyte is not controlled in traditional rotating disk electrode (RDE) measurements. More specifically, to incorporate the IL into a porous electrode disk in a rotating disk electrode, a drop of desired IL is added to the surface of the disk, then placed in a room temperature vacuum oven for 30 minutes in an attempt to have the IL penetrate deep into the pores, before the excess is spun off and the experiment carried out. However, with this technique, we have no way to control the precise volume of IL, which we expect to have a significant impact on the performance especially in comparing different ILs with very different viscosities and reactant/product solubilities.

To address this issue, we re-considered the standard apparatus to measure the ORR. Instead of rotating our working electrode, it needs to remain stationary and inverted relative to the RDE arrangement to allow for control over the volume of IL added, yet still allow electrolyte flow in order to replenish oxygen to the surface of the electrode. To address these requirements, we adapted the flow-cell design of Heller-Ling et al. [N. Heller-Ling, G. Poillerat, J.F. Koenig, J.L. Gautier, P. Chartier, *Electrochimica Acta*, **39** (1994), 1669-1674].

Switching to a flow cell allows for more control of IL volume, but also requires the optimization of other parameters. Experimental parameters have now been optimized, and have submitted a publication with our results. As shown in Figure 2, we have identified the key physical properties of the IL that determine reductions in ORR overpotential to be higher oxygen solubility and lower water solubility, a figure-of-merit that should lead to the identification or synthesis of even better candidate ILs in future work.

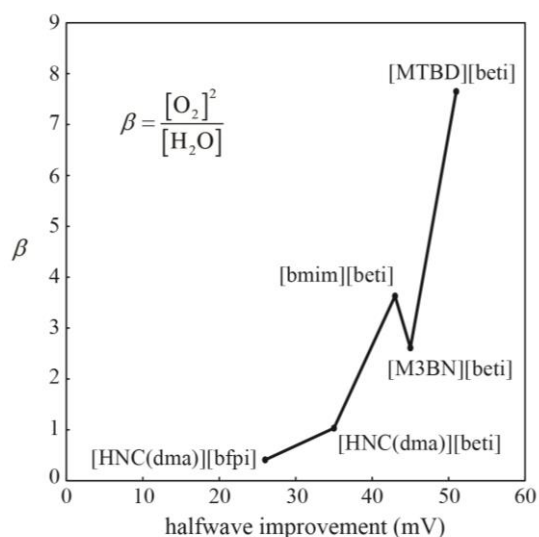


**Figure 2.** Improvement figure-of-merit in the half-wave potential for electrochemical oxygen reduction associated with IL oxygen and water solubility.

Our primary result at this point is this: our hypothesis that an IL can mediate proton, reactant, and product transport between an acidic aqueous electrolyte and a catalytic metal surface so as to enhance the activity is so far being upheld. More recently, we have been exploiting how ionic liquid layers can simultaneously mediate proton and reactant transport to catalytic surfaces. This has led us to identify experimental conditions under which, for instance, oxygen reduction is proton-diffusion limited. This effectively suppresses hydrogen evolution, so oxygen reduction can be driven to extremely reducing potentials, allowing oxygen to be reduced to superoxide and other unusual reduction products.

### **Publications Acknowledging this Grant in 2012-2015**

1. E. Benn, H. Uvegi, J. Erlebacher, “Characterization of Nanoporous Metal-Ionic Liquid Composites for the Electrochemical Oxygen Reduction Reaction,” under revision to *J. Electrochem. Soc.*, 2014.
2. J. Snyder, K. Livi, J. Erlebacher, “Oxygen Reduction Reaction Performance of [MTBD][beti]-Encapsulated Nanoporous NiPt Alloy Nanoparticles,” *Adv. Func. Mat.*, **2013**, 23, 5494-5501.
3. “Encapsulated Nanoporous Metal Nanoparticle Catalysts,” United State Patent Application 20140113218, published 4/24/2014.

**Mechanism of CO<sub>2</sub> Reductive Disproportionation by Base Metal Isocyanometalates**

Joshua S. Figueroa (PI), Douglas W. Agnew, Charles C. Mokhtarzadeh and Matthew D. Sampson

*Department of Chemistry and Biochemistry, University of California, San Diego*

**ABSTRACT**

Isocyanometalates represent a class of anionic, electron-rich transition metal complexes that are formally related to classic carbonylmetalates (*i.e.*  $[M(\text{CO})_n]^{m-}$ ). However, the stronger  $\sigma$ -donation abilities and weaker  $\pi$ -acidic capacity of isocyanides relative to carbon monoxide impart isocyanometalates with enhanced nucleophilic properties relative to the carbonylmetalates. Accordingly, this enhanced nucleophilicity allows isocyanometalates to be active in small molecule activation and transformation reactions, especially when nucleophilic attack is the primary step of the activation processes. In addition, the steric and electronic profile of organic isocyanides (CNR) can be readily manipulated in a manner that allows for the isolation of reactive intermediates in a small-molecule transformation process and/or the interrogation of discrete mechanistic steps during such transformations. Based on these concepts, new synthetic and mechanistic aspects of CO<sub>2</sub> reductive disproportionation by manganese and iron isocyanometalates are presented. These systems feature encumbering *m*-terphenyl isocyanide ligands, which have been established to allow the kinetic isolation of reactive transition metal complexes. For manganese, the bis-isocyanide complexes  $\text{XMn}(\text{CO})_3(\text{CNAr}^{\text{Dipp}2})_2$  ( $X = \text{Cl, Br, I}$  and  $\text{OSO}_2\text{CF}_3$ ;  $\text{Ar}^{\text{Dipp}2} = 2,6-(2,6-(i\text{-Pr})_2\text{C}_6\text{H}_3)_2\text{C}_6\text{H}_3$ ) are shown to reduce CO<sub>2</sub> to carbon monoxide (CO) and carbonate ( $[\text{CO}_2]^{2-}$ ) under electrolytic conditions and in the presence of stoichiometric reductants. Mechanistic investigations show that the neutral monoradical complex  $\text{Mn}(\text{CO})_3(\text{CNAr}^{\text{Dipp}2})_2$  is an intermediate in this process. Furthermore, the precursor complexes  $\text{XMn}(\text{CO})_3(\text{CNAr}^{\text{Dipp}2})_2$  ( $X = \text{halide}$ ) are shown to exhibit a dramatically different electrochemical profile than that of the triflate species  $(\text{OTf})\text{Mn}(\text{CO})_3(\text{CNAr}^{\text{Dipp}2})_2$ . The origin of this difference is traced to ion-solvation effects that are significantly influenced by the steric profile of the  $\text{CNAr}^{\text{Dipp}2}$  ligands. In related work, the iron isocyanometalate dianion  $[\text{Fe}(\text{CNAr}^{\text{Mes}2})_4]^{2-}$  ( $\text{Ar}^{\text{Mes}2} = 2,6-(2,4,6\text{-Me}_3\text{C}_6\text{H}_2)_2\text{C}_6\text{H}_3$ ) is also shown to effect CO<sub>2</sub> reductive disproportionation. However, the encumbering  $\text{CNAr}^{\text{Mes}2}$  ligands allow for the critical intermediates in this process to be trapped and isolated. Presented are silane trapping experiments showing that both the Fe center and the isocyanide ligands in  $[\text{Fe}(\text{CNAr}^{\text{Mes}2})_4]^{2-}$  work cooperatively to bind and activate CO<sub>2</sub>. This finding has allowed the traditional CO<sub>2</sub> reductive disproportionation pathway to be redirected toward the formation of organic carbonyl compounds.

## DE-SC0008058: Bond-Formation and Catalysis by Base-Metal Unsaturated Isocyanides

Student(s): Douglas W. Agnew, Charles C. Mokhtarzadeh and Alex E. Carpenter

### RECENT PROGRESS

*Elucidation of the Electrocatalytic Mechanism of CO<sub>2</sub> Reduction by [XMn(CO)<sub>3</sub>(CNAr<sup>Dipp2</sup>)<sub>2</sub>] complexes:* Following our isolation of the neutral species Mn(CO)<sub>3</sub>(CNAr<sup>Mes2</sup>)<sub>2</sub>, we spent significant effort to determine the efficiency and mechanism of electrocatalytic CO<sub>2</sub> reduction by [XMn(CO)<sub>3</sub>(CNAr<sup>Mes2</sup>)<sub>2</sub>] precursor complexes (X = Cl, Br, I, O<sub>3</sub>SCF<sub>3</sub>). We have already established that reduction of [XMn(CO)<sub>3</sub>(CNAr<sup>Dipp2</sup>)<sub>2</sub>] complexes generates the monoanion [Mn(CO)<sub>3</sub>(CNAr<sup>Dipp2</sup>)<sub>2</sub>]<sup>-</sup>, which interacts with CO<sub>2</sub>. Accordingly, over the past several months, we have sought to establish the exact nature of this interaction under catalytically relevant conditions.

As shown in Figure 1, cyclic voltammograms (CVs) were collected for the halide series XMn(CO)<sub>3</sub>(CNAr<sup>Dipp2</sup>)<sub>2</sub> (X = Cl (**1**), Br (**2**), I (**3**)) and the cationic complex [Mn(CO)<sub>3</sub>(CNAr<sup>Dipp2</sup>)<sub>2</sub>(THF)]OTf (OTf

= CF<sub>3</sub>SO<sub>3</sub><sup>-</sup>) (**4**) in dry THF under an atmosphere of dry dinitrogen. The three halides each show a similar, non-reversible reduction centered at -2.7 V vs. Fc<sup>+</sup>/Fc, with the larger halides trending to slightly more negative potentials. This reduction for the halide complexes corresponds to two electrons, as evidenced by infrared spectroelectrochemistry (IR-SEC) experiments (not shown). In strong contrast, the cationic complex **4** exhibits two one-electron reduction waves, an irreversible reduction at -1.56 V vs. Fc<sup>+</sup>/Fc and a reversible reduction at -1.75 V vs. Fc<sup>+</sup>/Fc. These reductions occur at a significantly more positive potential than the reductions of the halides, by over 1 V. Most notably, the magnitude of this discrepancy in cathodic waves between **4** and the halides **1-3** is to our knowledge unparalleled in other low-valent homoleptic or heteroleptic manganese systems. However, we are confident this observation arises from the fact that THF is a weakly bound and weakly donating ligand to Mn in this system. Furthermore, we believe that -1.5 V reduction represents a one-electron

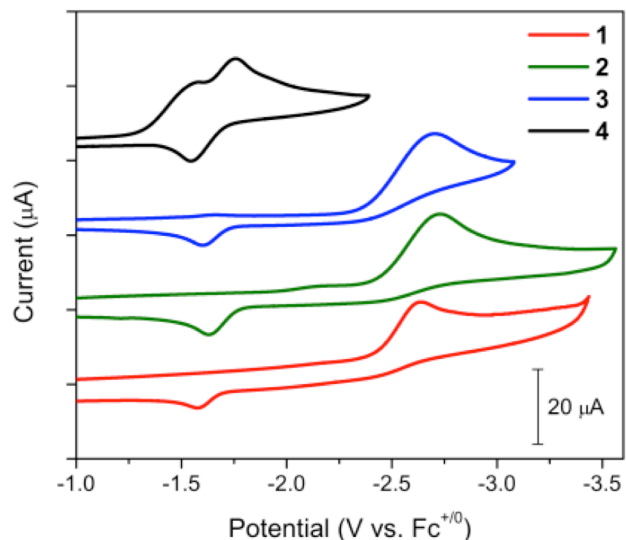


**Figure 1.** Cyclic voltammograms of XMn(CO)<sub>3</sub>(CNAr<sup>Dipp2</sup>)<sub>2</sub> complexes (X = Cl, **1** (red); Br, **2** (green); I, **3** (blue); OTf, **4** (black)) in THF with 0.1 M TBAPF<sub>6</sub> under N<sub>2</sub>. Conditions: 1 mM complex, scan rate = 100 mV/s, glassy carbon working electrode, Ag/AgCl reference electrode, Pt wire counter electrode.

$[\text{Mn}(\text{CO})_3(\text{CNAr}^{\text{Dipp}2})_2(\text{THF})]^+/\text{Mn}(\text{CO})_3(\text{CNAr}^{\text{Dipp}2})_2$  couple, with irreversibility arising from rapid formation of the hydride complex  $\square$   $\text{HMn}(\text{CO})_3(\text{CNAr}^{\text{Dipp}2})_2$  via H-atom abstraction of THF by  $\text{Mn}(\text{CO})_3(\text{CNAr}^{\text{Dipp}2})_2$ . The  $-1.75$  V wave is also quite clearly the reversible couple between neutral  $\text{Mn}(\text{CO})_3(\text{CNAr}^{\text{Dipp}2})_2$  and monoanionic  $[\text{Mn}(\text{CO})_3(\text{CNAr}^{\text{Dipp}2})_2]^-$  (as demonstrated by IR-SEC). Most importantly, this data indicates that halide coordination *significantly increases the overpotential for catalyst formation* in these  $[\text{Mn}(\text{CO})_3(\text{CNAr}^{\text{Dipp}2})_2]$ -based reduction systems. This is a major contrast with the more traditional Group 7  $[\text{M}(\text{CO})_3(\text{bipy})]$  systems, where the redox non-innocence of the bipy ligands mitigate such influence of the halide ligands.

In order to further compare the catalytic competency of  $[\text{XMn}(\text{CO})_3(\text{CNAr}^{\text{Dipp}2})_2]$  complexes with the Group 7  $[\text{M}(\text{CO})_3(\text{bipy})]$  systems, we investigated the ability of complexes **2** and **4** to reduce  $\text{CO}_2$  by monitoring the CVs of these species in  $\text{CO}_2$ -saturated THF. Under  $\text{CO}_2$ , the CV of **2** reveals a slight anodic shift and slight current increase of the two-electron reduction wave in addition to complete disappearance of the oxidative feature at  $-1.6$  V vs  $\text{Fc}^+/\text{Fc}$  (Figure 2, top). These electrochemical features under  $\text{CO}_2$  are consistent with reactivity of anionic  $[\text{Mn}(\text{CO})_3(\text{CNAr}^{\text{Dipp}2})_2]^-$  with  $\text{CO}_2$ . The current responses of **2** under  $\text{CO}_2$  do not appear catalytic, since the current enhancements are quite minor. The CV of **4** under  $\text{CO}_2$  displays slight anodic shifts of the two reduction waves (Figure 2, bottom), a slight change in the oxidative wave at  $-1.6$  V vs  $\text{Fc}^+/\text{Fc}$ , and very small current enhancement observed between  $-2.4$  and  $-2.6$  V vs.  $\text{Fc}^+/\text{Fc}$  (Figure 6). All of these features in the CV of **4** under  $\text{CO}_2$  are much less pronounced than in the CV of **2**, despite the formation of **6** in both cases. As such, we undertook the direct reaction of  $\text{CO}_2$  with  $\text{Na}[\text{Mn}(\text{CO})_3(\text{CNAr}^{\text{Dipp}2})_2]$  to clarify its reactivity with  $\text{CO}_2$ .

Stoichiometric addition of  $\text{CO}_2$  to  $\text{Na}[\text{Mn}(\text{CO})_3(\text{CNAr}^{\text{Dipp}2})_2]$  in THF produces a light orange solution with a green precipitate. Analysis of the product mixture revealed the formation of the zerovalent complex **5** and the decomposition products  $\text{HMn}(\text{CO})_3(\text{CNAr}^{\text{Dipp}2})_2$ ,  $\text{Mn}_2(\text{CO})_7(\text{CNAr}^{\text{Dipp}2})_3$ ,  $\text{Mn}_2(\text{CO})_8(\text{CNAr}^{\text{Dipp}2})_2$ , and free isocyanide  $\text{CNAr}^{\text{Dipp}2}$ . Performing the

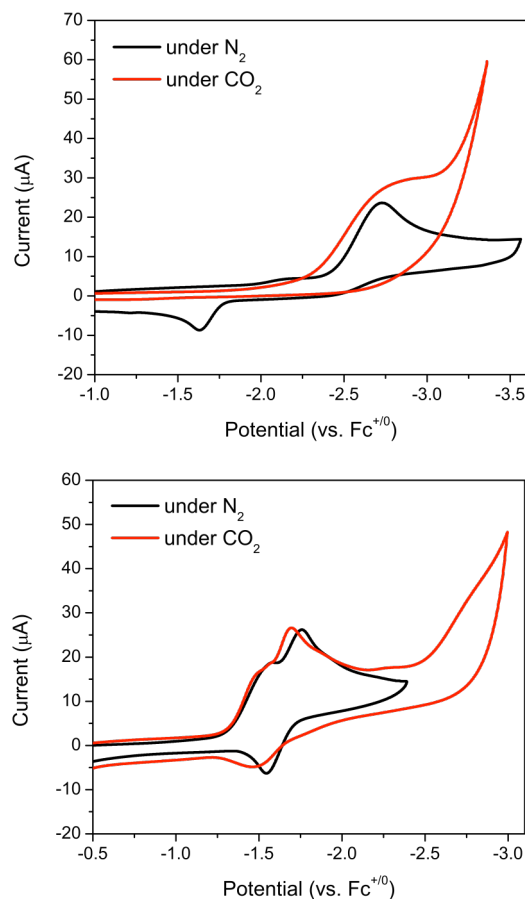


**Figure 2.** (Top) CV of **2** in THF with 0.1 M TBAPF<sub>6</sub> under N<sub>2</sub> (black) and CO<sub>2</sub> (red). (Bottom) CV of **4** in THF with 0.1 M TBAPF<sub>6</sub> under N<sub>2</sub> (black) and CO<sub>2</sub> (red). Conditions: 1 mM complex, scan rate = 100 mV/s, glassy carbon working electrode, Ag/AgCl reference electrode, Pt wire counter electrode.

reaction with isotopically-labeled  $^{13}\text{CO}_2$  demonstrated CO incorporation into the dimeric manganese species with concomitant formation of  $\text{Na}_2^{13}\text{CO}_3$ . These data suggest that  $\text{Na}[\text{Mn}(\text{CO})_3(\text{CNAr}^{\text{Dipp}2})_2]$  performs as a one-electron reductant toward  $\text{CO}_2$ , resulting in the initial formation of **5** and sodium oxalate, which rapidly disproportionates to CO and  $\text{Na}_2\text{CO}_3$  under reducing conditions (Figure 3). However, we have some evidence for a direct  $\text{CO}_2$  reductive disproportionation pathway stemming from the unobserved metalcarboxylate species  $[(\text{O}_2\text{C})\text{Mn}(\text{CO})_3(\text{CNAr}^{\text{Dipp}2})_2]^-$ .

Nevertheless, this behavior is in marked contrast to  $[\text{M}(\text{CO})_3(\text{bipy})]$  catalysts, in which the reductive route to CO involves a discrete metalcarboxylate intermediate. We attribute this behavior as well as the divergent electrochemical behavior under variation of the apical X ligand to the substantial differences in redox-innocence between the isocyanide and bipyridine ligands. Accordingly, this study, along with elucidation of the electronic influence of substituted *m*-terphenyl isocyanides, puts us in the position to rationally change the molecular architecture of  $[\text{XMn}(\text{CO})_3(\text{CNAr}^{\text{R}2})_2]$  complexes to i) disfavor one-electron  $\text{CO}_2$  reduction pathways and ii) further lower the overpotential for catalyst formation and operation.

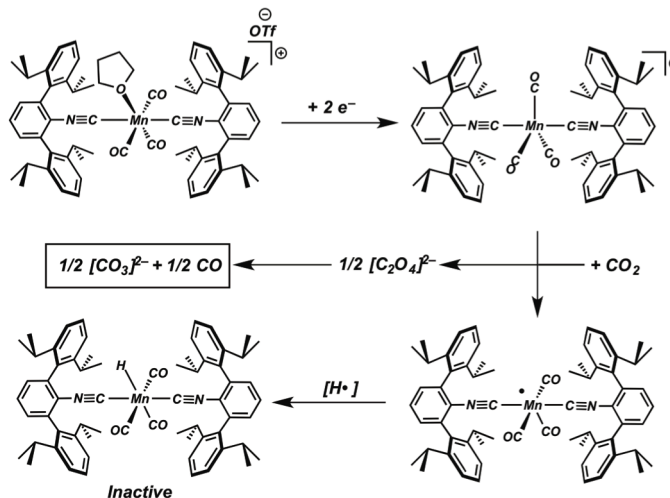


**Figure 3.** Proposed mechanism for stoichiometric  $\text{CO}_2$  disproportionation by  $[\text{Mn}(\text{CO})_3(\text{CNAr}^{\text{Dipp}2})_2]$  complexes.

### Publications Acknowledging this Grant:

- 1) "Chloro- and Trifluoromethyl-Substituted Flanking-Ring *m*-Terphenyl Isocyanides:  $\eta^6$ -Arene Binding to Zero-Valent Molybdenum Centers and Comparison to Alkyl-Substituted Derivatives" Ditri, T. B.; Carpenter, A. E.; Ripatti, D. S.; Moore, C. E.; Rheingold, A. L.; Figueroa, J. S. *Inorg. Chem.* **2013**, *52*, 13216–13229.
- 2) "Comparative Measure of the Electronic Influence of Highly Substituted Aryl Isocyanides" Carpenter, A. E.; Mokhtarzadeh, C. C.; Ripatti, D. S.; Havrylyuk, I. Kamezawa, R.; Moore, C. E.; Rheingold, A. L.; Figueroa, J. S. *Inorg. Chem.* **2015**, *54*, 2936–2944.
- 3) "Synthesis and Protonation of an Encumbered Iron Tetraisocyanide Dianion" Mokhtarzadeh, C. C.; Margulieux, G. W.; Carpenter, A. E.; Weidemann, N.; Moore, C. E.; Rheingold, A. L.; Figueroa, J. S. *Inorg. Chem.* **2015**, *54*, ASAP.

**Agglomerative Sintering of an Atomically Dispersed Ir<sub>1</sub>/Zeolite Y Catalyst: Compelling Evidence Against Ostwald Ripening But for Bimolecular and Autocatalytic Agglomeration Catalyst Sintering Steps**

Richard G. Finke<sup>1</sup>, Bruce C. Gates,<sup>2</sup> Ercan Bayram,<sup>1</sup> Jing Lu,<sup>2</sup> Ceren Aydin,<sup>2</sup> Nigel D. Browning,<sup>2,3</sup> Saim Özkar,<sup>4</sup> Eric Finney<sup>1</sup>

<sup>1</sup> Department of Chemistry, Colorado State University, Fort Collins, CO 80523 USA, <sup>2</sup> Department of Chemical Engineering and Materials Science, University of California, One Shields Avenue, Davis, CA 95616 USA, <sup>3</sup> Physical and Life Sciences Directorate, Lawrence Livermore National Laboratory, 700 East Avenue, Livermore, CA 94550 USA, <sup>4</sup> Department of Chemistry, Middle East Technical University, 06800 Ankara, Turkey.

**Abstract**

Agglomerative sintering of an atomically dispersed, zeolite Y-supported catalyst, Ir<sub>1</sub>/zeolite Y, formed initially from the well-characterized precatalyst [Ir(C<sub>2</sub>H<sub>4</sub>)<sub>2</sub>]/zeolite Y, and in the presence of liquid-phase reactants, was monitored over three cycles of 3800 turnovers (TTOs) of cyclohexene hydrogenation at 72 °C. Post each of the three cycles of catalysis, the resultant sintered catalyst was characterized by extended X-ray absorption fine structure spectroscopy and atomic-resolution high-angle annular dark-field scanning transmission electron microscopy. The results—the first quantitative investigation of sintering of an atomically dispersed catalyst—show that higher-nuclearity iridium species, Ir<sub>n</sub>, are formed during each successive cycle. The progression from the starting mononuclear precursor, Ir<sub>1</sub>, is first to Ir<sub>~4-6</sub>, then, on average, Ir<sub>~40</sub>, and, finally, on average, Ir<sub>~70</sub>, the latter more accurately described as a bimodal dispersion of on-average Ir<sub>~40-50</sub> and on-average Ir<sub>~1600</sub> nanoparticles. The size distribution and other data disprove Ostwald Ripening during the initial and final stages of the observed catalyst sintering. Instead, the diameter-dispersion data plus quantitative fits to the cluster or nanoparticle diameter vs. time data provide good evidence for the underlying, pseudo-elementary steps of bimolecular agglomeration, B + B → C, and autocatalytic agglomeration, B + C → 1.5C, where B represents the smaller, formally Ir(0) nanoparticles, and C is the larger (more highly agglomerated) nanoparticles. These two specific, balanced chemical reactions are of significance in going beyond the present state-of-the-art, but word-only, “mechanism” for catalyst sintering of “Particle Migration and Coalescence”. The steps of bimolecular plus autocatalytic agglomeration provide two specific, balanced chemical equations useful for fitting sintering kinetics data, thereby quantitatively testing proposed sintering mechanisms.

**DE-FG02-03ER15453: Supported-Nanoparticle Catalyst Formation in Contact With Solution: Kinetic, Mechanistic and Synthetic Fundamental Studies**

**PI:** Professor Richard G. Finke

**Students:** Ercan Bayram, Eric Finney

**RECENT PROGRESS**

***Overview of Publications.***

Fifteen publications to date have been produced under our DOE support; a list of their titles follows [1-15] and provides a concise description of their contents. All but the last 2014 publication and the 2015 publications have been described in past DOE annual reports, so only those latest publications are detailed briefly in what follows.

***Supported-Nanoparticle Catalyst Formation and Subsequent Sintering***

We published an important paper in 2014 entitled [12] “A Four-Step Mechanism for the Formation of Supported-Nanoparticle Heterogeneous Catalysts in Contact with Solution: The Conversion of Ir(1,5-COD)Cl/ $\gamma$ -Al<sub>2</sub>O<sub>3</sub> to Ir(0)<sub>-170</sub>/ $\gamma$ -Al<sub>2</sub>O<sub>3</sub>”. As our abstract of that paper notes, “The significance of this work is at least four-fold: first, this is the first documentation of a 4-step mechanism for supported-nanoparticle formation in contact with solution. Second, the proposed 4-step mechanism—which was obtained following the disproof of 18 alternative mechanisms—is a new 4-step mechanism in which the new 4<sup>th</sup> step is  $A + C \rightarrow 1.5C$  in the presence of the solid,  $\gamma$ -Al<sub>2</sub>O<sub>3</sub> support. Third, the 4-step mechanism provides rare, precise chemical and kinetic precedent for metal particle nucleation, growth and now agglomeration ( $B + B \rightarrow C$ ) and secondary surface autocatalytic growth ( $A + C \rightarrow 1.5C$ ) involved in supported-nanoparticle heterogeneous catalyst formation in contact with solution. Fourth, one now has firm, disproof-based chemical-mechanism precedent for two specific, balanced pseudoelementary kinetic steps and their precise chemical descriptors of bimolecular particle agglomeration,  $B + B \rightarrow C$ , and autocatalytic agglomeration,  $B + C \rightarrow 1.5C$  involved in, for example, nanoparticle catalyst sintering.”

We also published a paper in 2015 which provides additional for the underlying steps of sintering, a paper entitled [13] “Agglomerative Sintering of an Atomically Dispersed Ir<sub>1</sub>/Zeolite Y Catalyst: Compelling Evidence Against Ostwald Ripening But for Bimolecular and

Autocatalytic Agglomeration Catalyst Sintering Steps”. This is the paper whose abstract is presented above for the poster that will be presented at the DOE Contractor’s meeting.

***The “Who’s The True Catalyst?” and “Is It Homogeneous or Heterogeneous Catalysis?” Problems***

We were also able to complete what is likely the final paper in a series of studies supported by our DOE grant, “Determining the True Catalyst Derived from the  $[\text{RhCp}^*\text{Cl}_2]_2$  Precatalyst System: Is it Single-Metal  $\text{RhCp}^*$ -Based, or a Sub-nanometer  $\text{Rh}_4$  Cluster-Based, Cyclohexene Hydrogenation Catalysis at Room Temperature and Mild Pressures?” [14]. Ten lines of evidence are provided in that paper addressing the nature of the kinetically dominant room temperature cyclohexene hydrogenation catalyst derived from  $[\text{RhCp}^*\text{Cl}_2]_2$ . The resultant methodology—especially the quantitative catalyst poisoning experiments in combination with *in operando* spectroscopy—are expected to be more broadly applicable to the study of other systems and the important “who’s the true catalyst?” question.

***Addressing the Problem of Reproducibility in Precatalyst and Catalyst Syntheses***

Finally, we also published a paper entitled “The Story of a Mechanism-Based Solution to an Irreproducible Synthesis Resulting in an Unexpected Closed-System Requirement for the  $\text{LiBEt}_3\text{H}$ -Based Reduction: the Case of the Novel Subnanometer Cluster,  $[\text{Ir}(1,5\text{-COD})(\mu\text{-H})_4]$ , and the Resulting Improved, Independently Repeatable, Reliable Synthesis” [15]. Interested readers are referred to this paper for its contents and details.

**Publications Acknowledging this Grant in 2012-2015**

1. Mondloch, J. E.; Finke, R. G., Kinetic Evidence for Bimolecular Nucleation In Supported-Transition-Metal-Nanoparticle Catalyst Formation In Contact With Solution: The Prototype  $\text{Ir}(1,5\text{-COD})\text{Cl}/\gamma\text{-Al}_2\text{O}_3$  to  $\text{Ir}(0)\text{-}_{900}/\gamma\text{-Al}_2\text{O}_3$  System, *ACS Catalysis*, **2012**, 2, 298-305.
2. Bayram, E.; Lu, J.; Aydin, C.; Uzun, A.; Browning, N. D.; Gates, B. C.; Finke, R. G., Mononuclear Zeolite-Supported Iridium: Kinetic, Spectroscopic, Electron Microscopic, and Size-Selective Poisoning Evidence for an Atomically Dispersed True Catalyst at 22 °C, *ACS Catalysis*, **2012**, 2, 1947-1957.
3. Mondloch, J. E.; Bayram, E.; Finke, R. G., A Review of the Kinetics and Mechanisms of Formation of Supported-Nanoparticle Heterogeneous Catalysts, *J. Mol. Catal. A* **2012**, 355, 1-38. (“Editor’s Choice” selection).
4. Shields, S., Buhro, W. E., Finney, E. E.; Finke, R. G., Gold Nanocluster Agglomeration Kinetic Studies: Evidence for Parallel Bimolecular Plus Autocatalytic Agglomeration

Pathways as a Mechanistic Alternative to an Avrami-Based Analysis, *Chemistry of Materials*, **2012**, *24*, 1718-1725.

5. Bayram, E.; Finke, R. G., Quantitative 1,10-Phenanthroline Catalyst-Poisoning Kinetic Studies of Rh(0)<sub>n</sub> Nanoparticle and Rh<sub>4</sub> Cluster Benzene Hydrogenation Catalysts: Estimates of the Poison  $K_{\text{association}}$  Binding Constants, of the Equivalents of Poison Bound and of the Number of Catalytically Active Sites for Each Catalyst, *ACS Catalysis*, **2012**, *2*, 1967-1975.

6. Stracke, J. J.; Finke, R. G., Water oxidation catalysis beginning with 2.5  $\mu\text{M}$   $[\text{Co}_4(\text{H}_2\text{O})_2(\text{PW}_9\text{O}_{34})_2]^{10-}$ : Investigation of the true electrochemically driven catalyst at  $\geq 600$  mV overpotential at a glassy carbon electrode, *ACS Catalysis*, **2013**, *3*, 1209-1219

7. Jordan Stracke, Ph.D Dissertation, Distinguishing Homogeneous and Heterogeneous Water Oxidation Catalysis When Beginning with Cobalt Polyoxometalates, Colorado State University, November 2013.

8. Stracke, J. J.; Finke, R. G., Water Oxidation Catalysis Beginning with  $\text{Co}_4(\text{H}_2\text{O})_2(\text{PW}_9\text{O}_{34})^{10-}$  when Driven by the Chemical Oxidant Ruthenium(III)tris(2,2'-bipyridine): Stoichiometry, Kinetic, and Mechanistic Studies En Route to Identifying the True Catalyst, *ACS Catalysis*, **2014**, *4*, 79-89.

9. Stracke, J. J.; Finke, R. G., Distinguishing Homogeneous from Heterogeneous Water Oxidation Catalysis When Beginning with Polyoxometalates, *ACS Catalysis*, **2014**, *4*, 909-933.

10. Laxson, W. W.; Özkar, S.; Finke, R. G., The Tri-Niobium, Wells-Dawson Type Polyoxoanion,  $[(n\text{-C}_4\text{H}_9)_4\text{N}]_9\text{P}_2\text{W}_{15}\text{Nb}_3\text{O}_{62}$ : Improvements in the Synthesis, Its Reliability, the Purity of the Product and the Detailed Synthetic Procedure, *Inorg. Chem.* **2014**, *53*, 2666-2676.

11. Laxson, W. W.; Finke, R. G., Nucleation is Second Order: An Apparent Kinetically Effective Nucleus of Two for Ir(0)<sub>n</sub> Nanoparticle Formation From  $[(1,5\text{-COD})\text{Ir}^I\text{-P}_2\text{W}_{15}\text{Nb}_3\text{O}_{62}]^{8-}$  Plus Hydrogen, *J. Am. Chem. Soc.* **2014**, *136*, 17601-17615.

12. Kent, P. D.; Mondloch, J. E.; Finke, R. G., A Four-Step Mechanism for the Formation of Supported-Nanoparticle Heterogeneous Catalysts in Contact with Solution: The Conversion of Ir(1,5-COD)Cl/ $\gamma\text{-Al}_2\text{O}_3$  to Ir(0)<sub>-170</sub>/ $\gamma\text{-Al}_2\text{O}_3$ , *J. Am. Chem. Soc.* **2014**, *136*, 1930-1941.

13. Bayram, E.; Lu, J.; Aydin, C.; Browning, N. D.; Özkar, S.; Finney, E. E.; Gates, B. C.; Finke, R. G., Agglomerative Sintering of an Atomically Dispersed Ir<sub>1</sub>/Zeolite Y Catalyst: Compelling Evidence Against Ostwald Ripening But for Bimolecular and Autocatalytic Agglomeration Catalyst Sintering Steps, *ACS Catalysis*, **2015**, in press.

14. Bayram, E.; Linehan, J. C.; Fulton, J. L.; Szymczak, N. K.; Finke, R. G., Determining the True Catalyst Derived from the  $[\text{RhCp}^*\text{Cl}_2]_2$  Precatalyst System: Is it Single-Metal RhCp\*-Based, or a Sub-nanometer Rh<sub>4</sub> Cluster-Based, Cyclohexene Hydrogenation Catalysis at Room Temperature and Mild Pressures?, *ACS Catalysis*, **2015**, in press.

15. Laxson, W. W.; Özkar, S.; Folkman, S.; Finke, R. G., The Story of a Mechanism-Based Solution to an Irreproducible Synthesis Resulting in an Unexpected Closed-System Requirement for the LiBEt<sub>3</sub>H-Based Reduction: the Case of the Novel Subnanometer Cluster,  $[\text{Ir}(1,5\text{-COD})(\mu\text{-H})_4]$ , and the Resulting Improved, Independently Repeatable, Reliable Synthesis, *Inorg. Chim. Acta.*, **2015**, in press.

## The Reduction of Inorganic Anions: Ligand Redox Tautomerism Supports Base Metal Reactivity

Alison R. Fout, Ellen M. Matson, Yun Ji Park, Zachary Gordon,  
and Courtney L. Ford

University of Illinois at Urbana-Champaign  
School of Chemical Sciences

Transition metal complexes featuring inorganic oxyanions have long been touted for their inertness since these species are generally considered to be non-complexing anions, poor nucleophiles, and kinetically inert to oxidation or reduction. Interested in exploring the reduction of oxyanions we have developed a ligand system to facilitate these transformations. A series of redox-active, multi-dentate ligand frameworks containing both hydrogen bond donating and accepting moieties in the secondary coordination sphere have been synthesized. The reactivity of base metals with the inorganic oxyanions will be described, highlighting the variety of coordination modes of this electronically diverse ligand framework through both spectroscopic and DFT studies. Characterization of complexes described herein will include  $^1\text{H}$  NMR, IR, Electronic Absorption, and EPR spectroscopies as well as X-ray crystallography.

### Publications:

- a. Matson, E. M.; Bertke, J. A.; Fout, A. R. "Isolation of Fe(II)-Aqua and Hydroxyl Complexes Featuring a Tripodal Hydrogen-Bond Donor and Acceptor Ligand." *Inorg. Chem.* **2014**, *53*, 4450-4458. *Selected as newsworthy article May 6-19, 2014.*
- b. Matson, E. M.; Gordon, Z.; Lin, B. L.; Nilges, M. J.; Fout, A. R. "Meridional vs. Facial Coordination Geometries of a Dipodal Ligand Framework Featuring a Secondary Coordination Sphere." *Dalton Trans.* **2014**, *43*, 16992-16995.
- c. Park, Y.; Matson, E. M.; Fout, A. R. "Exploring Mn-O Bonding in the Context of an Electronically Flexible Secondary Coordination Sphere: Synthesis of a Mn(III)-Oxo." *Chem Comm.* **2015**, *51*, 5310-5313.
- d. Matson, E. M.; Park, Y.; Bertke, J. A.; Fout, A. R. "Facile Nitrite Reduction in a Non-Heme System: Formation of an Fe(III)-Oxo." *J. Am. Chem. Soc.* **2014**, *136*, 17398-17401.
- e. Matson, E. M.; Park, Y.; Bertke, J. A.; Fout, A. R. "Synthesis and Characterization of M(II) (M = Mn, Fe and Co) azafulvene complexes and their  $\text{X}_3^-$  derivatives." *Dalton Trans.* **2015**, Ahead of Print.

## Well-Defined Molecular Single-Site Catalysts on Crystalline Supports

Bruce C. Gates

Chemical Engineering & Materials Science, University of California, Davis

### Presentation Abstract

Recent advances in the synthesis and characterization of small, essentially molecular metal complexes on support surfaces have brought new insights to catalysis and point the way to systematic catalyst design. We summarize recent work unraveling effects of key design variables of site-isolated catalysts: the metal, metal nuclearity, support, and other ligands on the metals, also considering catalysts with separate, complementary functions on supports. The catalysts were synthesized with the goal of structural simplicity and uniformity to facilitate incisive characterization. Thus, they are essentially molecular species bonded to porous supports chosen that are crystalline, chosen for their high degree of uniformity; the supports are zeolites and MgO. The catalytic species are synthesized in reactions of organometallic precursors with the support surfaces; the precursors include  $M(L)_2(\text{acetylacetonate})_{1-2}$ , with  $M = \text{Ru, Rh, Ir, or Au}$  and the ligands  $L = \text{C}_2\text{H}_4, \text{CO, or CH}_3$ . The simplicity and uniformity of the supported catalysts facilitate precise structure determinations, even in reactive atmospheres and during catalysis. The methods of characterizing catalysts in reactive atmospheres include IR, EXAFS, XANES, and NMR spectroscopies, and complementary methods include density functional theory and atomic-resolution aberration-corrected STEM for imaging of individual metal atoms. IR, NMR, XANES, and microscopy data demonstrate the high degrees of uniformity of well-prepared supported species. The characterizations determine the compositions of surface metal complexes, including the ligands and the metal-support bonding and structure, which identify the supports as ligands with electron-donor properties that influence reactivity and catalysis. Each of the catalyst design variables has been varied independently, illustrated by isostructural rhodium and iridium (diethylene or dicarbonyl) complexes on these supports. The data provide examples resolving the roles of the catalyst design variables and place the catalysis science on a firm foundation of organometallic chemistry linked with surface science. Supported molecular catalysts offer the advantages of characterization in the absence of solvents and with surface-science methods that do not require ultrahigh vacuum. The approach was illustrated with the discovery of a highly active and selective MgO-supported rhodium carbonyl dimer catalyst for hydrogenation of 1,3-butadiene to give butenes.

### RECENT PROGRESS

With D. A. Dixon, N. D. Browning, M. Chen, C. Y. Chen, S.-J. Hwang, and P. Praserttham we investigated families of zeolite and MgO-supported metal complex catalysts. Triosmium carbonyls were prepared by the reaction of  $\text{Os}_3(\text{CO})_{12}$  with calcined MgO and fragmented to give  $\text{Os}^{2+}(\text{CO})_2$  complexes by treatment in helium and fully decarbonylated in flowing helium at 623 K. IR, XANES, and EXAFS spectroscopies were used to characterize the supported species and their transformations in various flowing gases. The samples were imaged with dark-field HAADF STEM. Electronic structure calculations on cluster models of the site-isolated catalysts were done with density functional theory. EXAFS spectra show that each isolated Os atom was bonded, on average, to approximately 2 support oxygen and 2 doubly bonded oxygen ligands; the average surface species is represented as  $\text{Os}^{5+}(\text{=O})_2\{-\text{O}_{\text{support}}\}_2$ . STEM images confirm that the Os atoms were site isolated. IR spectra show that the supported  $\text{Os}^{5+}(\text{=O})_2\{-\text{O}_{\text{support}}\}_2$  species react readily

with C<sub>2</sub>H<sub>4</sub> at 298 K to form osmium glycol species formulated as Os<sup>5+</sup>(OCH<sub>2</sub>CH<sub>2</sub>O){-O<sub>support</sub>}<sub>2</sub>. We infer that the reactivity of the surface Os(=O)<sub>2</sub> species with C<sub>2</sub>H<sub>4</sub> is similar to that of OsO<sub>4</sub>. When the Os<sup>5+</sup>(=O)<sub>2</sub>{-O<sub>support</sub>}<sub>2</sub> species was exposed to flowing CO, bands arose in the IR spectrum, assigned to various single-atom osmium carbonyls with osmium in various oxidation states. The reactivities these osmium carbonyls with O<sub>2</sub> were in the order of (Os<sup>3+</sup>) ≈ (Os<sup>3+</sup> a separate species) > (Os<sup>4+</sup>) >> (Os on Lewis acid sites) > (Os<sup>4+</sup>) = (Os<sup>2+</sup>(CO)<sub>2</sub>) (which was not reactive); these were characterized by the following respective CO stretching frequencies: 1917, 1938, 1962, 1893, 1981, and 2012 cm<sup>-1</sup>. This set of supported metal complexes is the first with systematically varied metal oxidation states and offers numerous opportunities to investigate the influence of metal oxidation states and ligands on catalyst performance. We tested the supported Os<sup>5+</sup>(=O)<sub>2</sub>{-O<sub>support</sub>}<sub>2</sub> for CO oxidation catalysis in a plug flow reactor at 473 K at CO and O<sub>2</sub> partial pressures of 10 mbar. The catalyst was active and stable, characterized by a TOF of 4.0 × 10<sup>-3</sup> (mol CO)/(Os atom × s). Only Os<sup>4+</sup> carbonyl species (with IR bands at 1981 and 1962 cm<sup>-1</sup>) were detected by IR spectroscopy during catalysis. Because the Os<sup>4+</sup> carbonyl at 1981 cm<sup>-1</sup> was not reactive with O<sub>2</sub>, we infer that Os<sup>4+</sup> (with a carbonyl ligand having a band at 1962 cm<sup>-1</sup>) was the active species. The calculations agree with the spectral assignments. The supported osmium complexes are among the best-defined single-site supported metal catalysts, offering a rich new chemistry with the metal in a range of oxidation states and related to Sharpless chemistry in solution; this is the first work demonstrating the identities of the oxygen ligands bonded to a noble metal in a supported site-isolated catalyst.

With Dixon and Chen we investigated HY zeolite-supported cationic organoiridium carbonyl complexes formed by reaction of Ir(CO)<sub>2</sub>(acac) (acac = acetylacetonate) to form supported Ir(CO)<sub>2</sub> complexes, which were treated at 298 K and 1 atm with flowing gas-phase reactants, including C<sub>2</sub>H<sub>4</sub>, H<sub>2</sub>, <sup>12</sup>CO, <sup>13</sup>CO, and D<sub>2</sub>O. Mass spectrometry was used to identify effluent gases, and IR and X-ray absorption spectroscopies were used to characterize the supported species, with the results bolstered by DFT calculations. Because the support is crystalline and presents a nearly uniform array of bonding sites for the iridium species, these were characterized by a high degree of uniformity, which allowed a precise determination of the species involved in the replacement, for example, of one CO ligand of each Ir(CO)<sub>2</sub> complex with ethylene. The supported species include the following: Ir(CO)<sub>2</sub>, Ir(CO)(C<sub>2</sub>H<sub>4</sub>)<sub>2</sub>, Ir(CO)(C<sub>2</sub>H<sub>4</sub>), Ir(CO)(C<sub>2</sub>H<sub>5</sub>), and (tentatively) Ir(CO)(H). The data determine a reaction network involving all of these species. The zeolite-supported Ir(CO)<sub>2</sub> species, with each Ir atom bonded to 2 oxygen atoms of the support as shown by EXAFS spectra, were characterized by atomic-resolution STEM images (Figure 1), which confirm the IR and EXAFS data demonstrating the presence of mononuclear site-isolated iridium complexes. STEM also allowed observations of the amorphous regions of the zeolite and showed that iridium in these regions was more susceptible to aggregation than that confined in the crystalline pores.

We also prepared a stable site-isolated mononuclear platinum catalyst with a well-defined structure. Platinum complexes supported in zeolite KLTL were synthesized from Pt(NH<sub>3</sub>)<sub>4</sub>(NO<sub>3</sub>)<sub>2</sub>, oxidized at 633 K, and used to catalyze CO oxidation. IR and X-ray absorption spectra and electron micrographs determine the structures and locations of the Pt complexes in the zeolite pores, demonstrate the platinum-support bonding, and show that the platinum remained site isolated after oxidation and catalysis. These are among the most stable site-isolated noble metal catalysts. This work was collaborative with C. Y. Chen of Chevron

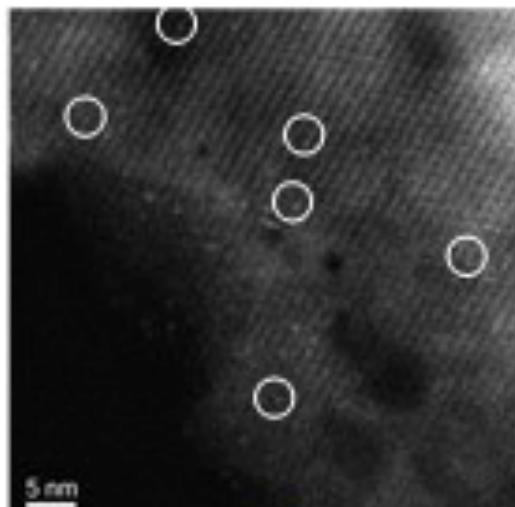


**Figure 1.** Aberration-corrected HAADF-STEM image of HY zeolite containing  $\text{Ir}(\text{CO})_2$  (1 wt% iridium) showing the zeolite framework in the [110] direction. Bright features in white circles are examples of site-isolated mononuclear iridium complexes in the zeolite framework.

We also prepared a stable site-isolated mononuclear platinum catalyst with a well-defined structure. Platinum complexes supported in zeolite KLTL were synthesized from  $\text{Pt}(\text{NH}_3)_4(\text{NO}_3)_2$ , oxidized at 633 K, and used to catalyze CO oxidation. IR and X-ray absorption spectra and electron micrographs determine the structures and locations of the Pt complexes in the zeolite pores, demonstrate the platinum–support bonding, and show that the platinum remained site isolated after oxidation and catalysis. These are among the most stable site-isolated noble metal catalysts.

### Publications Acknowledging this Grant in 2012-2015

1. Flytzani-Stephanopoulos, M.; Gates B. C. Atomically Dispersed Supported Metal Catalysts. *Ann. Rev. Chem. Biomol. Eng.* **2012**, *3*, 545.
2. Lu, J.; Aydin, C.; Browning, N. D.; Gates, B. C. Imaging Isolated Gold Atom Catalytic Sites on Zeolite NaY. *Angew. Chem. Int. Ed.* **2012**, *51*, 5842.
3. Lu, J.; Aydin, C.; Liang, A. J.; Chen, C.-Y.; Browning, N. D.; Gates, B. C. Site-isolated Molecular Iridium Complex Catalyst Supported in the 1-Dimensional Channels of Zeolite HSSZ-53: Characterization by Spectroscopy and Aberration-Corrected Scanning Transmission Electron Microscopy. *ACS Catal.* **2012**, *2*, 1002.
4. Yardimci, D.; Serna, P.; Gates, B. C. A Highly Selective Catalyst for Partial Hydrogenation of 1,3-Butadiene: MgO-Supported Rhodium Clusters Selectively Poisoned with CO. *ChemCatChem* **2012**, *4*, 1547.
5. Aydin, C.; Kulkarni, A.; Chi, M.; Browning, N. D.; Gates, B. C. Atomically Resolved Site-Isolated Catalyst on MgO: Mononuclear Osmium Dicarboxyls formed from  $\text{Os}_3(\text{CO})_{12}$ . *J. Phys. Chem. Lett.* **2012**, *3*, 1865.
6. Bayram, E.; Lu, J.; Aydin, C.; Uzun, A.; Browning, N. D.; Gates, B. C.; Finke, R. G. Mononuclear Zeolite-Supported Iridium Catalyst: Kinetic, Spectroscopic, Electron Microscopic, and Size-Selective Poisoning Evidence for an Atomically Dispersed True Catalyst at 22°C. *ACS Catal.* **2012**, *2*, 1947.
7. Lu, J.; Aydin, C.; Browning, N. D.; Gates, B. C. Oxide- and Zeolite-Supported Isostructural  $\text{Ir}(\text{C}_2\text{H}_4)_2$  Complexes: Molecular-level Observations of Electronic Effects of Supports as Ligands, *Langmuir* **2012**, *28*, 12806.

8. Yardimci, D.; Serna, P.; Gates, B. C. Tuning Catalytic Selectivity: Zeolite- and Magnesium Oxide-Supported Molecular Rhodium Catalysts for Hydrogenation of 1,3-Butadiene. *ACS Catal.* **2012**, *2*, 2100.
9. Gates, B. C.; Marks, T. J. Defragmenting Catalysis (editorial). *Angew. Chem. Int. Ed.* **2012**, *51*, 11644.
10. Yardimci, D.; Serna, P.; Gates, B. C. Surface-Mediated Synthesis of Dimeric Rhodium Catalysts on MgO: Tracking Changes in Nuclearity and Ligand Environment of the Catalytically Active Sites by X-Ray Absorption and Infrared Spectroscopies. *Chem. Eur. J.* **2013**, *19*, 1235.
11. Khabuanchalad, S.; Wittayakun, J.; Lobo, R. J.; Stoll, S.; Britt, R. D.; Gates, B. C. Formation of MgO-Supported Manganese Carbonyl Complexes by Chemisorption of  $\text{Mn}(\text{CO})_5\text{CH}_3$ . *Langmuir* **2013**, *27*, 6279.
12. Lu, J.; Martinez Macias, C.; Aydin, C.; Browning, N. D.; Gates, B. C. Zeolite-Supported Bimetallic Catalyst: Controlling Selectivity of Rhodium Complexes by Nearby Iridium Complexes. *Catal. Sci. Technol.* **2013**, *3*, 2199.
13. Browning, N. D.; Aydin, C.; Lu, J.; Kulkarni, A.; Okamoto, N. L.; Ortalan, V.; Reed, B. W.; Uzun, A.; Gates, B. C. Quantitative Z-Contrast Imaging of Supported Metal Complexes and Clusters – A Gateway to Understanding Catalysis on the Atomic Scale. *ChemCatChem* **2013**, *5*, 2673.
14. Serna, P.; Gates, B. C. Zeolite- and MgO-Supported Rhodium Complexes and Rhodium Clusters: Tuning Catalytic Properties to Control Carbon–Carbon vs. Carbon–Hydrogen Bond Formation Reactions of Ethene in the Presence of  $\text{H}_2$ . *J. Catal.* **2013**, *308*, 201.
15. Serna, P.; Yardimci, D.; Kistler, J. D.; Gates, B. C. Formation of supported rhodium clusters from mononuclear rhodium complexes controlled by the support and ligands on rhodium. *Phys Chem Chem Phys* **2014**, *16*, 1262.
16. Martinez Macias, C.; Xu, P.; Hwang, S.-H.; Lu, J.; Chen, C.-Y.; Browning, N. D.; Gates, B. C. Iridium complexes and Clusters in Dealuminated Zeolite HY: Distribution between Crystalline and Impurity Amorphous Regions. *ACS Catal.* **2014**, *4*, 2662.
17. Kistler, J. D.; Chotigkrai, N.; Xu, P.; Enderle, B.; Praserthdam, P.; Chen, C.-Y.; Browning, N. D.; Gates, B. C. A Single-Site Platinum CO Oxidation Catalyst in Zeolite KLTL: Microscopic and Spectroscopic Determination of the Locations of the Platinum Atoms. *Angew. Chem. Int. Ed.* **2014**, *53*, 8904.
18. Serna, P.; Gates, B. C. Molecular Metal Catalysis: Organometallic Chemistry Meets Surface Science. *Acc. Chem. Res.* **2014**, *47*, 2612.
19. Yang, D.; Chen, M.; Martinez Macias, C.; Dixon, D. A.; Gates, B. C. Mononuclear iridium dinitrogen complexes bonded to zeolite HY. *Chem. Eur. J.* **2015**, *21*, 631.
20. Gates, B. C. From Catalyst Preparation toward Catalyst Synthesis. *J. Catal.* **2015**, in press.
21. Kistler, J. D.; Serna, P.; Asakura, K.; Gates, B. C. Surface Metal Complexes and their Applications, in XAS and XES: Theory and Applications, J. van Bokhoven and C. Lamberti, editors, Wiley, **2015**, in press.
22. Xu, P.; Lu, J.; Aydin, C.; Debeve, L.; Browning, N. D.; Chen, C.-Y.; Gates, B. C. Imaging Individual Lanthanum Atoms in Zeolite Y by Scanning Transmission Electron Microscopy: Evidence of Lanthanum Pair Sites. *Micropor. Mesopor. Matl.* **2015**, *213*, 95.

**Surface Structure Sensitive Enantioselectivity  
in Surface Explosion Reactions**

Andrew J. Gellman, Aaron Reinicker  
Dept. of Chemical Engineering, Carnegie Mellon University

**Presentation Abstract**

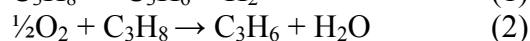
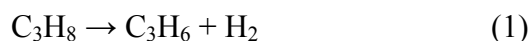
The origin of the enantioselective chemistry chiral adsorbates lies in the asymmetric structure of high Miller index naturally chiral crystal surfaces. Developing a comprehensive understanding of the surface structural origins of enantioselectivity by traditional means would require the study of chiral adsorbate reaction kinetics on many naturally chiral single crystal surfaces. We have broached this seemingly intractable problem by using curved Surface Structure Spread Single Crystals ( $S^4Cs$ ) that expose a continuous distribution of single crystal surfaces spanning a continuous region of the stereographic projection. The decomposition of tartaric acid (TA) and Aspartic acid (Asp) on Cu surfaces occurs via an explosive vacancy mediated decomposition reaction to yield  $CO_2$  and other products. On naturally chiral Cu surfaces, the highly non-linear rate law for the explosive decomposition reaction results in extremely high enantiospecificity during isothermal heating. Using Cu  $S^4Cs$  it has been possible to anneal adsorbed monolayers of TA and Asp for different periods of time to cause the surface reaction to progress to various extents of reaction. XPS has been used to map the surface and image measure the extent of reaction as a function of surface orientation. On a  $Cu(111)\pm 10^\circ S^4C$  after heating at 450 K for long enough to decompose ~ 50% of the adsorbed TA the map reveals the three-fold symmetry of the surface, and shows that the decomposition reaction occurs preferentially on the regions of the surface that are stepped and much more prevalently on the surfaces with (100) step edges than on surfaces with (110) step edges.

## Unconventional Oxidants & Reaction Schemes for Propane Dehydrogenation

Alan Derk<sup>1</sup>, Ches Upham<sup>2</sup>, Chang Huang<sup>2</sup>, Henrik Kristoffersen<sup>2</sup>,  
 Horia Metiu<sup>2</sup>, Eric McFarland<sup>1</sup>, and Michael Gordon<sup>1</sup>  
*Dept. of Chemical Engineering<sup>1</sup> and Chemistry<sup>2</sup>, University of California Santa Barbara*

### Presentation Abstract

Oxidative dehydrogenation (ODH) of propane has the potential to solve the coking and separations problems that accompany commercially practiced thermal dehydrogenation of propane (1) by removing the equilibrium limitation. This potential has not been realized because ODH using O<sub>2</sub> (2) and heterogeneous catalysts suffer from low conversion and selectivity [F. Cavani *et al.*, *Catal. Today* **127**, 113–131 (2007)].



In this work, we consider ODH with alternative oxidants (than O<sub>2</sub>), catalysts, and reaction schemes to increase propane to propylene yield:

(i) V<sub>2</sub>O<sub>5</sub>, a major component of ODH catalysts, was modified computationally to compare the reactivity of single-layer and bulk V<sub>2</sub>O<sub>5</sub>; surprisingly, single layer V<sub>2</sub>O<sub>5</sub> appears much less reactive than the bulk, which may ultimately inhibit combustion.

(ii) Solid oxides (Bi<sub>2</sub>O<sub>3</sub> and CuO) were combined with thermal dehydrogenation catalysts to combust H<sub>2</sub>, produce heat and pull the reaction forward. Bi<sub>2</sub>O<sub>3</sub> added to Pt-based dehydrogenation catalysts selectively combusted H<sub>2</sub> and increased propylene yield. However, Bi metal poisons the Pt-based dehydrogenation catalyst, resulting in poor long term performance. CuO was encapsulated in a coke-resistant SiO<sub>2</sub> shell with H<sub>2</sub> permeability. Unfortunately, the CuO@SiO<sub>2</sub> system was found to be unstable in propylene because of Cu aggregate formation outside the shells, leading to non-selective combustion.

(iii) Iodine radical chemistry was used to extract hydrogen from propane. I<sub>2</sub> was supplied directly or via reaction between molten LiI salt and O<sub>2</sub>. The recovery of I<sub>2</sub> was achieved by co-feeding O<sub>2</sub> without compromising selectivity (i.e., 2HI + ½O<sub>2</sub> → H<sub>2</sub>O + I<sub>2</sub> is very fast). Yields obtained with I<sub>2</sub>-mediated ODH were among the best ever reported for oxidative dehydrogenation.

DE-FG02-89ER14048

### Investigations of the Reactivity of Doped Metal Oxide Catalysts

**PIs:** Eric W. McFarland<sup>1,3</sup> (lead), Michael J. Gordon<sup>1</sup>, Horia Metiu<sup>2</sup>

**Postdocs:** Henrik H. Kristoffersen<sup>2</sup>, Ru Fen Liu<sup>1,2</sup>, Louis Jones<sup>1</sup>

**Graduate students:** Alan R. Derk<sup>1</sup>, D. Chester Upham<sup>2</sup>

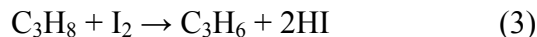
**Undergraduate students:** Andrew Dawson<sup>2</sup>, Zach Snodgrass<sup>1</sup>, Brian Owen<sup>1</sup>

**Affiliations:** Dept. of Chemical Engineering<sup>1</sup> and Chemistry<sup>2</sup>, University of California, Santa Barbara. DOW Centre for Sustainable Engineering Innovation, Department of Chemical Engineering, University of Queensland, Brisbane, Australia<sup>3</sup>

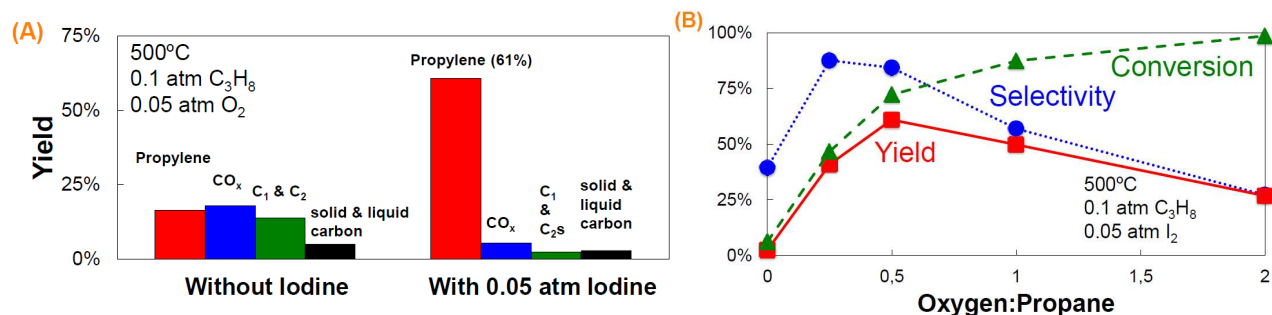
## RECENT PROGRESS

### Iodine Mediated ODH

Propane ODH with gaseous I<sub>2</sub> (3) and with *in-situ* HI recovery (4) was explored.

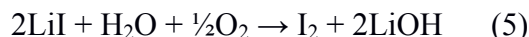


Propylene yield was seen to increase (~3 times) when co-feeding I<sub>2</sub>, O<sub>2</sub> and propane gas without significant CO<sub>x</sub> formation, compared to the non-I<sub>2</sub> case (see Figure A). In the former, HI is converted back to I<sub>2</sub> in the same reactor as the I<sub>2</sub> + C<sub>3</sub>H<sub>8</sub> reaction without significant hydrocarbon combustion. Single-pot recovery of I<sub>2</sub> with O<sub>2</sub> (4) increased propylene yield by improving the equilibrium conversion (Figure B). Maximum yield was obtained at stoichiometric O<sub>2</sub>:propane ratio (0.5), while selectivity and yield suffers with higher amounts of oxygen.

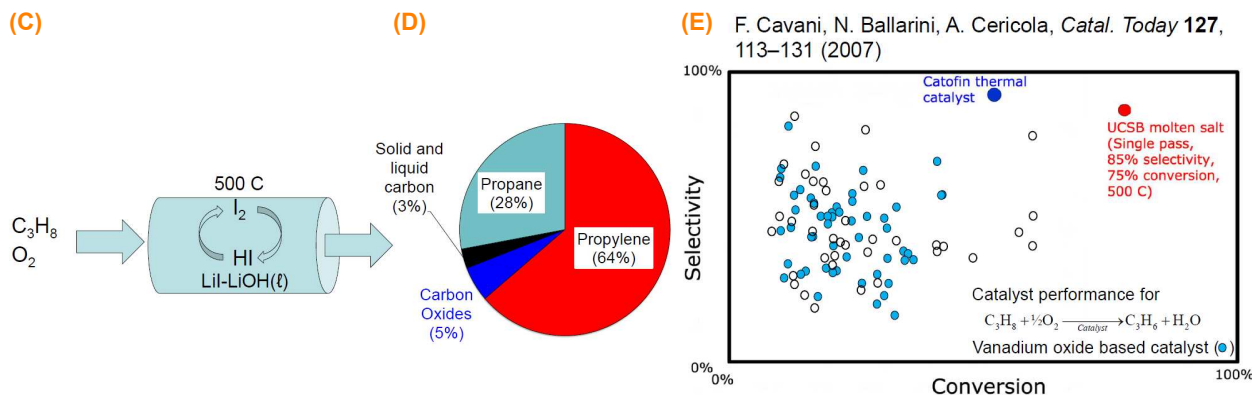


### Molten LiI Mediated ODH

We have also used molten LiI-LiOH and O<sub>2</sub> to generate I<sub>2</sub> and recover HI in a single pot without having to recycle I<sub>2</sub> in the gas phase (Figure C). Molecular dynamics simulations indicate that I<sub>2</sub> gas is produced by reaction (5).



High yields to propylene (64%) were achieved with molten salt mediated I<sub>2</sub> generation and recovery (Figure D). The yields obtained are among the highest reported in the literature (Figure E).



## Publications Acknowledging this Grant in 2012-2015

1. Kristoffersen, H. H.; Shea, J.-E.; Metiu, H. Catechol and HCl Adsorption on TiO<sub>2</sub>(110) in Vacuum and at the Water-TiO<sub>2</sub> Interface. *J. Phys. Chem. Lett.* **2015**, *6*, 2277-2281
2. Kristoffersen, H. H.; Metiu, H. Reconstruction Of Low-Index  $\alpha$ -V<sub>2</sub>O<sub>5</sub> Surfaces. *J. Phys. Chem. C* **2015**, *119*, 10500-10506
3. Kristoffersen, H. H.; Metiu, H. Molten LiCl Layer Supported on MgO: Its Possible Role in Enhancing the Oxidative Dehydrogenation of Ethane. *J. Phys. Chem. C* **2015**, *119*, 8681-8691
4. Upham, D. C.; Derk, A. R.; Sharma, S.; Metiu, H.; McFarland, E. W. CO<sub>2</sub> Methanation By Ru-Doped Ceria: The Role Of The Oxidation State Of The Surface. *Catal. Sci. Tech.* **2015**, *5*, 1783-1791
5. Chretien, S.; Metiu, H. Acid-Base Interaction And Its Role In Alkane Dissociative Chemisorption On Oxide Surfaces. *J. Phys. Chem. C* **2014**, *118*, 27336-27342
6. Singh, N.; Upham, D. C.; Liu, R-F.; Burk, J. J.; Economou, N. J.; Metiu, H.; McFarland, E. W. Investigation Of The Active Sites Of Rhodium Sulfide For Hydrogen Evolution/Oxidation Using Carbon Monoxide As A Probe. *Langmuir* **2014**, *30*, 5663-5668
7. Chretien, S.; Metiu, H. Oxygen Adsorption On Irreducible Oxides Doped With Higher-Valence Ions: O<sub>2</sub> Binding To The Dopant. *J. Phys. Chem. C* **2014**, *118*, 23070-23802
8. Derk, A. R.; Moore, G. M.; Sharma, S.; McFarland, E.W.; Metiu, H. Catalytic Dry Reforming Of Methane On Ruthenium-Doped Ceria And Ruthenium Supported On Ceria. *Top. Catal.* **2014**, *57*, 118-124
9. Sun, X. Y.; Li, B.; Metiu, H. Ethane Activation By Nb-Doped NiO. *J. Phys. Chem. C* **2013**, *117*, 23597-23608
10. Yu, J.; Scheffler, M.; Metiu, H. Oxidative Dehydrogenation Of Methane By Isolated Vanadium Oxide Clusters Supported On Au (111) and Ag (111) Surfaces. *J. Phys. Chem. C* **2013**, *117*, 18475-184883
11. Ding, K.; Metiu, H.; Stucky, G. D. Interplay Between Bromine And Iodine In Oxidative Dehydrogenation. *Chem Cat Chem* **2013**, *5*, 1906-1910
12. Derk, A. R.; Li, B.; Sharma, S.; Moore, G. M.; McFarland, E. W.; Metiu, H. Methane Oxidation By Lanthanum Oxide Doped With Cu, Zn, Mg, Fe, Nb, Ti, Zr, Or Ta: The Connection Between The Activation Energy And The Energy Of Oxygen-Vacancy Formation. *Catalysis Letters* **2013**, *143*, 406-410
13. Singh, N.; Upham, D. C.; Metiu, H.; McFarland, E.W.; Gas-Phase Chemistry To Understand Electrochemical Hydrogen Evolution And Oxidation On Doped Transition Metal Sulfides. *J. Electrochemical Soc.* **2013**, *160*, A1902-A1906
14. Ding, K.; Metiu, H.; Stucky, G. D. The Selective High-Yield Conversion Of Methane Using Iodine-Catalyzed Methane Bromination. *ACS Catalysis* **2013**, *3*, 474-477

15. McFarland, E. W.; Metiu, H. Catalysis By Doped Oxides. *Chemical Reviews* **2013**, *113*, 4391-4427
16. Ding, K.; Derk, A. R.; Zhang, A.; Hu, Z.; Stoimenov, P. K.; Stucky, G. D.; Metiu, H.; McFarland, E. W. Hydrodebromination And Oligomerization Of Dibromomethane. *ACS Catalysis* **2012**, *2*, 479-486
17. Metiu, H.; Chretien, S.; Li, B.; Hu, Z.; Sun, X.Y. Chemistry Of Lewis Acid-Base Pairs On Oxide Surfaces (Feature Article). *J. Phys. Chem. C* **2012**, *116*, 10439-10450
18. Hu, Z.; Metiu, H. Halogen Adsorption On CeO<sub>2</sub>: The Role Of Lewis Acid-Base Pairing. *J. Phys. Chem. C* **2012**, *116*, 6664-6671
19. Li, B.; Metiu, H. Does Halogen Adsorption Activate The Oxygen Atom On An Oxide Surface? I. A Study Of Br<sub>2</sub> And Hbr Adsorption On La<sub>2</sub>O<sub>3</sub> And La<sub>2</sub>O<sub>3</sub> Doped With Mg Or Zr. *J. Phys. Chem. C* **2012**, *116*, 4137-4148
20. Chretien, S.; Metiu, H. DFT Study Of The Electronic Properties Of LaOCl Surfaces. *J. Phys. Chem. C* **2012**, *116*, 681-691

**Oxide-Metal Interactions Studied on Core-Shell Catalysts**

Students: Chen Chen, Lisandra Arroyo  
Collaborators: J. M. Vohs (Penn), C. B. Murray (Penn), P. Fornasiero (Trieste), Mahmoud Khader (Qatar), M. Cargnello (Stanford)  
Contact: Department of Chemical & Biomolecular Engineering, 311 Towne Building, 220 S. 33rd Street, University of Pennsylvania, Philadelphia, PA 19104 Ph: 215-898-4439; Fax: 215-573-2093, [gorte@seas.upenn.edu](mailto:gorte@seas.upenn.edu)  
Yearly Budget: \$180,000  
Period: March 1, 2013 through February 26, 2016

**Goals:**

We are trying to maximize interactions between oxides and metals for improved catalytic performance. A main approach involves synthesizing and characterizing core-shell catalysts in which the metal core is surrounded by a thin porous shell of a catalytically active oxide. We are interested in understanding how the oxide shell can modify the activity and stability of metal catalysts.

**DOE Interest:**

Precious metal catalysts are widely applied for pollution control in gasoline and diesel exhausts, as well as many other chemical processes. Catalyst stability and activity are serious issues that are not completely resolved, especially with new regulations planned for CH<sub>4</sub> emissions. Developing catalysts with improved stability and activity remains an important goal that could have a very large commercial impact.

## Recent Progress:

### *The Effect of Water on Methane Combustion Over Pd@Ceia:*

The influence of water vapor on methane catalytic combustion was studied over Pd@CeO<sub>2</sub>/Si-Al<sub>2</sub>O<sub>3</sub> catalysts and compared to results on a conventional impregnated catalyst with identical chemical composition. While the nanostructured Pd@CeO<sub>2</sub>/Si-Al<sub>2</sub>O<sub>3</sub> catalyst is thermally stable, the addition of water to the reaction feed leads to a transient deactivation at low temperatures, consistent with well documented competitive adsorption of water on PdO. In addition to this, the hierarchically structured, core-shell catalyst exhibits an additional severe deactivation after methane oxidation in the presence of water vapor at 600°C that can be reversed only by heating the catalyst above 700°C. The presence of water in the reaction feed deactivates the conventional impregnated catalyst less severely and the activity largely returns upon water removal. Catalytic, FTIR, and CO-chemisorption data indicate that the severe deactivation process in the hierarchical catalyst is due to the ceria shell transforming to Ce(OH)<sub>3</sub>. This significantly inhibits the oxygen spillover from the CeO<sub>2</sub> nanoparticles to Pd, preventing the efficient re-oxidation of Pd, as observed by *operando* XANES experiments in which the Pd is observed to transform from PdO to Pd under methane oxidation conditions when water is added. At the same time, the presence of the hydroxyls can limit the accessibility of Pd to gas-phase reactants, as indicated by the decrease of CO chemisorption capability. The presence of hydroxyls plays a relatively minor role in the deactivation of conventional catalysts at 600°C.

### *Methane Oxidation on Pd@ZrO<sub>2</sub>:*

The catalytic properties of Pd@ZrO<sub>2</sub> core-shell catalysts supported on Si-modified alumina were studied for application to methane oxidation and compared to the analogous Pd@CeO<sub>2</sub> catalysts. In the absence of water (dry conditions), both Pd@ZrO<sub>2</sub> and Pd@CeO<sub>2</sub> were highly active and showed nearly identical reaction rates and thermal stabilities. However, unlike catalysts based on Pd@CeO<sub>2</sub>, the Pd@ZrO<sub>2</sub> catalysts were also very stable in the presence of high concentrations of water vapor. By means of Coulometric titration and pulse-reactor studies, we demonstrated that ZrO<sub>2</sub> in contact with Pd can be reduced. Additionally, Coulometric titration showed that the Pd-PdO equilibrium at 600°C is shifted to much lower P(O<sub>2</sub>) in the Pd@ZrO<sub>2</sub> catalyst compared to conventional Pd/ZrO<sub>2</sub> or Pd/Al<sub>2</sub>O<sub>3</sub> catalysts. Because PdO is more active for methane oxidation, this observation provides a possible explanation for the superior performance of the Pd@ZrO<sub>2</sub> catalyst.

### *Stabilization of Au Catalysts Through Formation of Core-Shell Structures:*

A catalyst system consisting of core-shell nanostructures with Au cores and porous TiO<sub>2</sub> shells was synthesized and characterized for room temperature CO oxidation. The core-shell structures were prepared by colloidal methods starting from pre-formed 3-nm Au particles in solution and then adsorbed onto high-surface-area, functionalized, hydrophobic Al<sub>2</sub>O<sub>3</sub> supports. The Au@TiO<sub>2</sub>/Si-Al<sub>2</sub>O<sub>3</sub> catalysts prepared in this way showed higher activity and thermal stability than conventional Au/TiO<sub>2</sub> samples prepared by impregnation of the same Au particles onto commercial titania P25. The core-shell catalyst was able to maintain its activity and 3-nm Au particles size upon calcination up to 600 °C, whereas the Au/TiO<sub>2</sub> sample was found to sinter. Furthermore, it was found that the crystallization of TiO<sub>2</sub> was suppressed in the core-shell structure, resulting in a thin layer of small TiO<sub>2</sub> particles, which is favorable for the dispersion and thermal stability of Au nanoparticles.

#### *Supported Pt-Zn and Pd-Zn Nanoparticles for Methanol Steam Reforming:*

Platinum-zinc oxide (Pt@ZnO) and palladium-zinc oxide (Pd@ZnO) core-shell nanoparticles were synthesized in solution using a method based on self-assembly and deposited onto a functionalized alumina (Si-Al<sub>2</sub>O<sub>3</sub>) support. TEM investigations of the samples confirm the formation of core-shell structures of approximately 6 nm of diameter following calcination to remove the ligands. In-situ TEM and coulometric titration experiments suggest that Pt-Zn alloys are formed upon reduction and that these are highly tunable in size. While methanol-steam reforming (MSR) measurements on conventional Pt/Al<sub>2</sub>O<sub>3</sub> and Pd/Al<sub>2</sub>O<sub>3</sub> catalysts show poor CO<sub>2</sub> selectivities, a Pt(1-wt.%)@ZnO(9-wt.+)/Si-Al<sub>2</sub>O<sub>3</sub> system showed comparable activity and selectivity for CO<sub>2</sub> as a conventional Pt/ZnO catalyst, providing further indication that Pt@ZnO forms a Pt-Zn alloy upon reduction due to the intimate contact between the two materials. The Pd@ZnO/Si-Al<sub>2</sub>O<sub>3</sub> exhibited lower CO<sub>2</sub> selectivities than Pt@ZnO/Si-Al<sub>2</sub>O<sub>3</sub>.

#### *A Comparison of Hierarchical Pt@CeO<sub>2</sub>/Si-Al<sub>2</sub>O<sub>3</sub> and Pd@CeO<sub>2</sub>/Si-Al<sub>2</sub>O<sub>3</sub>*

The catalytic properties of Pt@CeO<sub>2</sub>/Si-Al<sub>2</sub>O<sub>3</sub> and Pd@CeO<sub>2</sub>/Si-Al<sub>2</sub>O<sub>3</sub> core-shell catalysts were compared. For calcination at 773 K, Pt@CeO<sub>2</sub>/Si-Al<sub>2</sub>O<sub>3</sub> exhibits Water-Gas-Shift (WGS) rates that are similar to rates found on conventional Pt/CeO<sub>2</sub>, suggesting that there is good contact between the Pt and CeO<sub>2</sub> phases. While WGS rates over Pd@CeO<sub>2</sub>/Si-Al<sub>2</sub>O<sub>3</sub> declined rapidly due to reduction of CeO<sub>2</sub>, rates over Pt@CeO<sub>2</sub>/Si-Al<sub>2</sub>O<sub>3</sub> were reasonably stable with time indicating a different interaction between metal and CeO<sub>2</sub> phases. Reduction of CeO<sub>2</sub> also greatly suppresses CO adsorption capacities on Pd@CeO<sub>2</sub>/Si-Al<sub>2</sub>O<sub>3</sub> but has minimal effect on Pt@CeO<sub>2</sub>/Si-Al<sub>2</sub>O<sub>3</sub>, suggesting that these interactions with CeO<sub>2</sub> are stronger with Pd than with Pt. After calcination to 1073 K, large metal particles were observed with Pt@CeO<sub>2</sub>/Si-Al<sub>2</sub>O<sub>3</sub>, but not on Pd@CeO<sub>2</sub>/Si-Al<sub>2</sub>O<sub>3</sub>. Coulometric titration measurements on these two materials also suggest stronger interactions between CeO<sub>2</sub> and Pd.

#### **Future Work:**

##### *Influence of Core-Shell Structures on the Redox Properties of Pd Catalysts:*

Maintaining Pd in the form of PdO is extremely important for achieving high activity for methane oxidation and other reactions. We have seen indications that interactions with the support can affect the P(O<sub>2</sub>) at which reduction of PdO occurs. Therefore, we are continuing to study the thermodynamic properties of core-shell catalysts for which a very large fraction of the Pd is in direct contact with the oxide shell in order to understand how this contact affects the equilibrium properties. The primary tool for this characterization is Coulometric Titration, an electrochemical method for measuring equilibrium properties, together with pulse and reactor studies.

##### *Alternative Oxide Shells/Metal Particles:*

We are preparing Pd catalysts with mixed oxide shells, especially ceria-zirconia, to see how that influences the catalytic and redox properties of the catalyst. We are also preparing alloy nanoparticles for use in alternative reactions where alloy catalysts might exhibit better properties.

##### *Metal Catalysts Stabilized by ZrO<sub>2</sub> ALD:*

We are preparing Pd and Pt/alumina catalysts that have been stabilized by a thin covering of zirconia, added by ALD. A small ALD system has been assembled and the coverage per ALD layer has been calibrated. Catalysts with and without the ALD layer will be tested for methane

oxidation activity. Accelerated aging tests will be performed to determine whether the ALD layer help stabilize the Pd particles.

**Publications Acknowledging Either DE-FG02-85ER13350 or DE-FG02-13ER16380, from 1/1/2011 to present.**

1. "A Comparison of Hierarchical Pt@CeO<sub>2</sub>/Si-Al<sub>2</sub>O<sub>3</sub> and Pd@CeO<sub>2</sub>/Si-Al<sub>2</sub>O<sub>3</sub>", L. Arroyo-Ramírez, C. Chen, M. Cargnello, C. B. Murray, and R. J. Gorte, *Catalysis Today*, accepted.
2. "Supported Platinum-Zinc Oxide Core-Shell Nanoparticle Catalysts for Methanol Steam Reforming", L. Arroyo-Ramírez, Chen Chen, M. Cargnello, C. B. Murray, P. Fornasiero, and R. J. Gorte, *Journal of Materials Chemistry A*, 2 (2014)19509-14.
3. "Methane catalytic combustion over hierarchical Pd@CeO<sub>2</sub>/Si-Al<sub>2</sub>O<sub>3</sub>: Effect of the presence of water", M. Monai, T. Montini, Chen Chen, E. Fonda, R. J. Gorte, P. Fornasiero, *ChemCatChem*, accepted.
4. "Thermodynamic and catalytic properties of Pd@ZrO<sub>2</sub>/Si-Al<sub>2</sub>O<sub>3</sub> core-shell catalysts", Chen Chen, Yu-Hao Yeh, Matteo Cargnello, Christopher B. Murray, Paolo Fornasiero, Raymond. J. Gorte, *ACS Catalysis*, 4 (2014) 3902-09.
5. "Au@TiO<sub>2</sub> core-shell nanostructures with high thermal stability", Chen Chen, Mengxue Shi, Matteo Cargnello, Paolo Fornasiero, Christopher B. Murray, and Raymond. J. Gorte, *Catalysis Letters*, 144 (2014) 1939-45.
6. "Playing with structures at the nanoscale: designing catalysts by manipulation of the component building blocks", M. Cargnello, P. Fornasiero, and R. J. Gorte, *ChemPhysChem*, 14 (2013) 3869-77.
7. "High Temperature Calcination Improves the Catalytic Properties of Alumina-Supported Pd@Ceria Prepared by Self Assembly", Chen Chen, J. Cao, M. Cargnello, P. Fornasiero, and R. J. Gorte, *Journal of Catalysis*, 306 (2013) 109-115.
8. "Exceptional Thermal Stability of Monolayer Films of Pd@Ceria Core-Shell Catalyst Nanostructures Grafted onto an Oxide Surface", L. Adijanto, D. Bennett, C. Chen, A. S. Yu, M. Cargnello, P. Fornasiero, R. J. Gorte, John M. Vohs, *Nanoletters*, 13 (2013) 2252-2257.
9. "Core-Shell-Type Materials Based on Ceria", M. Cargnello, R. J. Gorte, and P. Fornasiero, in "Catalysis by Ceria and Related Materials, 2cnd Edition", A. Trovarelli and P. Fornasiero, Editors, Imperial College Press (2013) pp 361-396, DOI: 10.1142/9781848169647\_0007.
10. "Opportunities for Tailoring Catalytic Properties Through Metal-Support Interactions", M. Cargnello, P. Fornasiero, and R. J. Gorte, *Catalysis Letters*, 142 (2012) 1043-48.
11. "A Thermodynamic Study of the Redox Properties of Supported Co particles", K. Bakhtmutsky, N. L. Wieder, T. Baldassare, M. A. Smith, and R. J. Gorte, *Applied Catalysis A*, 397 (2011) 266-271.
12. "A Comparison of Redox Properties of Molybdenum-Based Mixed Oxides", I. Baldychev, A. Javadekar, D. J. Buttrey, J. M. Vohs, and R. J. Gorte, *Applied Catalysis A*, 394 (2011) 287-93.

13. "The Effect of Support on Redox Properties and Methanol-Oxidation Activity of Vanadia Catalysts", I. Baldychev, J. M. Vohs, and R. J. Gorte, *Applied Catalysis A*, 391 (2011) 86-91.

**Hydrodeoxygenation of furan on oxygen vacancy sites of MoO<sub>3</sub>(010):  
A DFT investigation**

Lars C. Grabow and Sashank Kasiraju

University of Houston, Department of Chemical and Biochemical Engineering

**Presentation Abstract**

MoO<sub>3</sub> is a promising candidate with high reactivity and selectivity for bio-oil upgrade via catalytic hydrodeoxygenation (HDO) [1]. Its sulfur counterpart, MoS<sub>2</sub>, is used in the well-studied hydrodesulfurization process (HDS). Here, we attempt an atomic-level comparison between the two related chemistries based on a prominent density functional theory (DFT) study of thiophene HDS on MoS<sub>2</sub> [2].

Similar to HDS, HDO requires the initial creation of an oxygen-vacancy site where the feed molecule can adsorb. We assessed the thermodynamic stability of three distinct oxygen vacancy sites on the MoO<sub>3</sub>(010) surface using a detailed ab-initio thermodynamic phase diagram under typical reaction conditions. Next, we used this most stable MoO<sub>3</sub>(010) facet to investigate the elementary reaction steps for furan HDO. The potential energy diagram based on the thermodynamic stability of reaction intermediates suggests that the reaction pathways for thiophene HDS and furan HDO are similar. Activation barriers for elementary reactions further indicate that furan HDO on MoO<sub>3</sub> is facile. However, the oxygen vacancy formation on MoO<sub>3</sub>(010) is slow. For HDS on MoS<sub>2</sub>, Cobalt promotion facilitates sulfur vacancy formation, leading to increased activity of the industrially used CoMoS catalyst. Our DFT results for Cobalt promoted MoO<sub>3</sub> provide valuable insights regarding the extent to which existing HDS knowledge can be translated to HDO catalysis. Unraveling the similarities and differences between the two processes (HDO and HDS) will ultimately let us design a novel HDO catalyst for the commercial use of biomass for the production of chemicals and fuels.

[1] Prasomsri, T.; Nimmanwudipong, T.; Román-Leshkov, Y. *Energy Environ. Sci.* **2013**, *6*, 1732.

[2] Moses, P. G.; Hinnemann, B.; Topsøe, H.; Nørskov, J. K. *J. Catal.* **2007**, *248*, 188–203.

**DE-SC0011983: Unifying Principles for Catalytic Hydrotreating Processes**

**PI: Lars C. Grabow**

**Postdoc(s): N/A**

**Student(s): Byeongjin Baek, Sashank Kasiraju, Charlie Chirino (undergraduate)**

**RECENT PROGRESS**

***Active site location for hydrodeoxygenation of phenolic compounds over Ru/TiO<sub>2</sub>(110)***

Catalytic conversion of oxygenated aromatic compounds into oxygen-free compounds suffers from both poor selectivity and low conversion, because the direct deoxygenation

(DDO) is harder to activate than decarbonylation (DCN) or hydrogenation (HYD). A promising catalyst with good activity and selectivity towards DDO is Ru/TiO<sub>2</sub>, according to recent studies. However, the nature of the active site and roles of the Ru cluster and TiO<sub>2</sub> support remain by and large unknown.

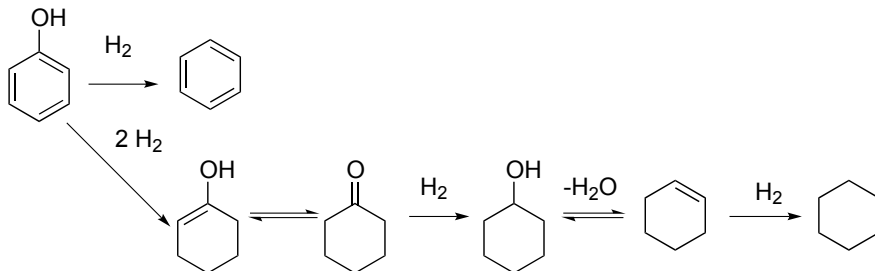


*Figure 1 The direct deoxygenation (DDO) and hydrogenation (HYD) pathways for phenol.*

Using density functional theory (DFT) we have explored the hydrodeoxygenation (HDO) pathways of phenol and *m*-cresol over supported Ru/TiO<sub>2</sub>. The catalyst was modeled as Ru(0001) surface and a 10-atom Ru cluster supported on TiO<sub>2</sub>(110). The comparison of the HYD vs. DDO pathways for phenol on Ru(0001) indicates that HYD is fast and kinetically preferred over DDO, suggesting that metallic Ru is unselective for direct C-O scission. For the Ru<sub>10</sub>/TiO<sub>2</sub> interface our results suggest that the presence of Ru on TiO<sub>2</sub> facilitates hydrogen delivery to TiO<sub>2</sub>(110) and facilitates oxygen vacancy formation at the Ru/TiO<sub>2</sub> interface. Phenol and *m*-cresol subsequently adsorb via their hydroxyl groups to the formed vacancy, and energy barriers for the following C-O scissions in phenol and *m*-cresol are 0.78 eV and 0.71 eV, respectively. The eliminated OH group heals the TiO<sub>2</sub> vacancy, and the aromatic rings of phenol and *m*-cresol remain on the Ru cluster. Metallic Ru has known hydrogenation activity and the formation of benzene and toluene is assumed to be quasi-equilibrated. Because of the strong interaction of the aromatic ring with the Ru cluster desorption of benzene and toluene is ca. 1.4 eV endothermic. Based on our theoretical analysis and in agreement with experimental observations, the role of Ru is to activate hydrogen, while C-O scission requires an oxygen vacancy site near the Ru/TiO<sub>2</sub> interface.

### ***Comparison of hydrotreating pathways for thiophene (HDS) and furan (HDO) on metal-sulfides and metal-oxides***

The main hypothesis of our project is that HDS and HDO are similar at the atomic level. The most detailed theoretical HDS studies are available for thiophene on MoS<sub>2</sub>. Similar to HDS, HDO requires the initial creation of a vacancy site where the feed molecule can adsorb. We assessed the thermodynamic stability of three distinct oxygen vacancy sites on the MoO<sub>3</sub>(010) surface using a detailed *ab-initio* thermodynamic phase diagram under

typical reaction conditions. In our analysis we predict an asymmetric oxygen vacancy with two subsurface hydrogen atoms as the most stable surface termination.

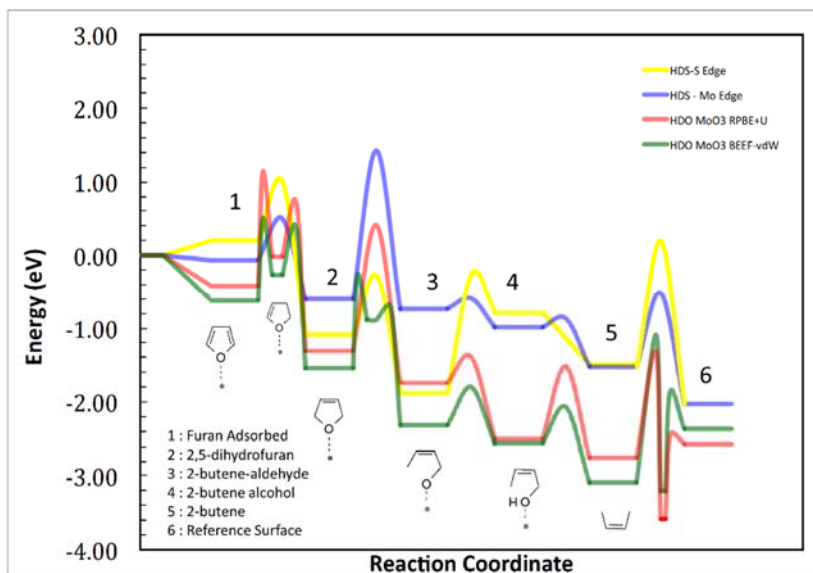


Figure 2 Comparison of potential energy diagrams for HDS of thiophene (yellow and blue) and HDO of furan (green and red).

We reproduce literature data from Nørskov's group for the HDS pathways on the sulfur-edge (yellow) and molybdenum-edge (blue) of  $\text{MoS}_2$  in Figure 2. In the same figure we provide the reaction pathway for furan HDO on the  $\text{MoO}_3(010)$  surface calculated with the more accurate BEEF-vdW functional (green).

For better comparison with the HDS data, we also include non-self-consistent results using the RPBE functional, which was used in the HDS work. The potential energy diagram based on the thermodynamic stability of reaction intermediates suggests that the reaction pathways for thiophene HDS and furan HDO are similar, but not identical. In particular, the initial part of the HDO process up to intermediate state 3 is similar to HDS on the S-edge. The remainder of the path is more similar to the Mo-edge. This is interesting, because it has been speculated that different HDS steps on  $\text{MoS}_2$  occur on different edges. The barriers for elementary steps along the furan HDO path on  $\text{MoO}_3$  indicated that the reaction is facile. However, the oxygen vacancy formation on  $\text{MoO}_3(010)$  is slow, but could be promoted by Co and Ni, just as the S-edge of  $\text{MoS}_2$ .

### Publications Acknowledging this Grant in 2012-2015

1. Ghorbanpour, A.; Gumidyala, A.; Grabow, L. C.; Crossley, S. P.; Rimer, J. D. Epitaxial Growth of ZSM-5@Silicalite-1: A Core-Shell Zeolite Designed with Passivated Surface Acidity. *ACS Nano* **2015**, *9*, 4006–4016.

**Michael A. Henderson**

**Photodesorption of Molecular Hydrogen from the Surface of RuO<sub>2</sub>(110)**

Michael A Henderson, Rentao Mu, Zdenek Dohnálek, Igor Lyubinetsky,  
Roger Rousseau and Vassiliki-Alexandra Glezakou  
Physical Sciences Division, Fundamental and Computational Sciences Directorate,  
and Institute for Integrated Catalysis, Pacific Northwest National Laboratory

Using thin films of RuO<sub>2</sub>(110) grown by oxidation on the Ru(0001) single crystal surface, we have investigated the adsorption, desorption and photochemistry of molecular hydrogen using temperature programmed desorption (TPD), photon stimulated desorption (PSD), scanning tunneling microscopy (STM) and density functional theory (DFT). Preparation of uniform RuO<sub>2</sub>(110) films without the presence of other phases (e.g., O-covered Ru metal or RuO<sub>x</sub> suboxides) constituted a major experimental challenge. Nonetheless, we have refined literature growth procedures to produce films with minimal contributions from undesired phases. Their presence on the surface is marked in the TPD (of D<sub>2</sub> or Kr) by appearance of multiple desorption features that grown in simultaneously with exposure. D<sub>2</sub> adsorbs on clean RuO<sub>2</sub>(110) with an initial sticking coefficient of ~0.4 at 40 K, which diminishes significantly with increasing coverage. The initial sticking drops to <<0.01 as the temperature is raised above 125 K. STM results indicate that D<sub>2</sub> binds preferentially at undercoordinated Ru sites (aka Ru<sub>cus</sub>) with a tendency first to form (2xn) arrays before generating a saturated surface. D<sub>2</sub> binding is predominately molecular on the RuO<sub>2</sub>(110) surface based on TPD, with dissociation constituting a minor pathway of chemistry. Some D<sub>2</sub>O is generated, but at levels (>0.1 ML) that suggest involvement of defects or secondary surface phases. The most favored adsorption geometry based on DFT is the Kubas structure with a binding energy of ~0.4 eV. This Ru<sub>cus</sub>-(D<sub>2</sub>) complex on RuO<sub>2</sub>(110) decomposes to liberate D<sub>2</sub> in TPD at 125 K. Irradiation of the D<sub>2</sub>-covered surface with light results in PSD of D<sub>2</sub>, concomitant with attenuation of the 125 K D<sub>2</sub> TPD state and disappearance of the associated STM features, with little evidence for photodissociation. Interestingly, there is a strong wavelength dependence in this process, peaked in the visible, which suggests photodesorption involves local excitation of the Kubas complex.

This work was supported by the US Department of Energy, Office of Science, Office of Basic Energy Sciences, Division of Chemical Sciences, Geosciences & Biosciences. Pacific Northwest National Laboratory (PNNL) is a multiprogram national laboratory operated for DOE by Battelle. The research was performed using EMSL, a national scientific user facility sponsored by the Department of Energy's Office of Biological and Environmental Research and located at Pacific Northwest National Laboratory.

**DE-AC05-76RL0 1830:  
Multifunctional Catalysis to Synthesize  
and Utilize Energy Carriers  
PI: Johannes Lercher**

## A Theoretical and Experimental Approach for Correlating Nanoparticle Structure and Electrocatalytic Activity

Richard M. Crooks, Graeme Henkelman, Long Luo, Liang Zhang  
The University of Texas at Austin, Department of Chemistry

### Presentation Abstract

The objective of the research described in this poster is the development of high-throughput computational-based screening methods for discovery of catalyst candidates and subsequent experimental validation using appropriate catalytic nanoparticles. Dendrimer-encapsulated nanoparticles (DENs), which are well-defined 1-2 nm diameter metal nanoparticles, fulfill the role of model electrocatalysts. Effective comparison of theory and experiment requires that the theoretical and experimental models map onto one-another perfectly. We use novel synthetic methods, advanced characterization techniques, and density functional theory (DFT) calculations to approach this ideal. Theory is also used to learn more about structure than can be determined by analytical characterization alone. The second principal focus of the work described here is correlating structure and catalytic function through the combined use of theory and experiment. For instance, DFT was used to determine the optimal composition of the alloy-core in AuPd@Pt DENs for the ORR. This prediction was subsequently confirmed experimentally. This study highlights the major theme of our research: the progression of using theory to rationalize experimental results to the more advanced goal of using theory to predict catalyst function *a priori*. Overall, We demonstrate that iteration between theory and experiment can facilitate an understanding of nanoparticle catalysts and reduce the time and effort involved in the design of new catalysts.

### DE-FG02-13ER16428 Testing the Predictive Power of Theory for Determining the Structure and Activity of Nanoparticle Electrocatalysts

**PI:** Richard M. Crooks

**Co-PI:** Graeme Henkelman

**Postdoc(s):** Zhiyao Duan, Long Luo, Liang Zhang

**Graduate Student(s):** Rachel M. Andersen

**Multistep Galvanic Exchange Synthesis of Pt Dendrimer-Encapsulated Nanoparticles.** In this study we outline a new method for synthesizing fully reduced Pt dendrimer-encapsulated nanoparticles (DENs). This is significant because of the importance of studying Pt electrocatalysts on a fundamental level, as Pt is one of the most important catalytic metals. Previously, direct chemical reduction of the Pt<sup>2+</sup>-dendrimer complex led to a bimodal distribution of reduced DENs and fully unreduced complex due to the strong interaction of the Pt<sup>2+</sup> salt and the dendrimer. Building off previous work from our group, fully reduced Pt DENs were achieved by first synthesizing Cu DENs of the appropriate size through sequential dendrimer loading and reduction steps, and then galvanically exchanging the zerovalent Cu DENs for Pt as shown in **Figure 1**. The

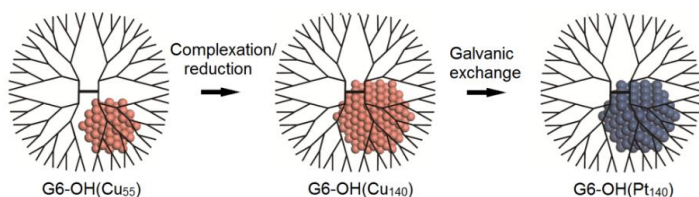


**Figure 1.** Scheme showing the sequential  $\text{Cu}^{2+}$  complexation/reduction steps that form a larger Cu DEN which can then undergo galvanic exchange for  $\text{Pt}^{2+}$  to form a fully reduced Pt DENs.

properties of Pt DENs having an average of 55, 140, and 225 atoms prepared by direct chemical reduction and by galvanic exchange are compared. Data obtained by UV-vis spectroscopy, X-ray absorption spectroscopy (XAS), X-ray photoelectron spectroscopy, and high-resolution electron microscopy confirm only the presence of fully reduced Pt DENs when synthesized by galvanic exchange while chemical

reduction leads to a mixture of reduced DENs and unreduced precursor. These results are significant because Pt DENs are good models for developing a better understanding of the effects of finite size on catalytic reactions. Until now, however, the results of such studies have been complicated by a heterogeneous mixture of Pt catalysts.

**Computational design of alloy-core@shell nanoparticles.** Our previous finding shows that alloy-core@shell nanoparticles are promising geometry for new nanoparticle catalysis. One successful case was  $\text{Au}_{0.28}\text{Pd}_{0.72}@\text{Pt}$  nanoparticle for oxygen reduction reaction, where predictions made by first principal calculations lead to a perfect agreement of experimental results. Alloy-core@shell nanoparticles has a homogenous noble metal shell around a random alloy core of tunable composition. The noble shell enhances the durability of nanoparticles for catalysis and the alloy-core composition allows for fine tuning of the catalytic properties. In this work, we provide general design rules of alloy-core@shell metal nanoparticles for catalysis.

As one of the most important properties of alloy-core@shell nanoparticles, the linear correlation between the binding of adsorbate to the shell and the alloy core composition was tested and found to be valid for a range of nanoparticle composition, size and adsorbate. This systematic tunability allows for a simple approach to design of this type of catalyst. As shown in **Figure 4**, tuning the alloy-core composition allows us to achieve high activity region and the optimal composition can be theoretically predicted. Calculations of candidate structures for the hydrogen evolution reaction (HER) predict a high activity for the  $\text{PtRu}@\text{Pd}$  structure, in good agreement with what has been reported previously. Calculations of alloy-core@Pt 140-atoms nanoparticles reveal new candidate structures for CO oxidation at high temperature, including  $\text{Au}_{0.65}\text{Pd}_{0.35}@\text{Pt}$  and  $\text{Au}_{0.73}\text{Pt}_{0.27}@\text{Pt}$ , which are predicted to have reaction rates 200 times higher than Pt(111). Segregation energy of single-core@shell nanoparticles were calculated in vacuum and with presence of adsorbates as an evaluation of the nanoparticles' stability. While our demonstration is only for the HER and CO oxidation reactions, this method of tuning catalytic activity provides a general framework for computational optimization of alloy-core@shell nanoparticles for other reactions of interest. Promoted by this work, we are also conducting further studies on alloy-core@shell nanoparticles, including the correlation between theory and experiment, optimization of catalytic function and enhanced stability gain from alloy-core.

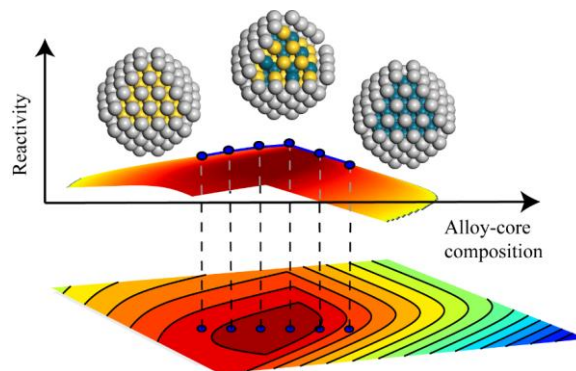


**Figure 4.** Tuning of alloy-core composition to improve activity.

**Unusual electrocatalytic activity trend core@shell nanoparticles for CO oxidation.** In this study, we found an unusual electrocatalytic activity trend of  $\text{Pd}_x\text{Au}_{140-x}\text{@Pt}$  ( $x$ : 0-140) dendrimer-encapsulated core@shell nanoparticles for adsorbed CO oxidation. These nanoparticles are comprised of a core having an average of 140 atoms and a Pt monolayer shell, which results in a diameter of about 2 nm. During the synthesis of these particles, intermediate products ( $\text{Pd}_x\text{Au}_{140-x}$  and  $\text{Pd}_x\text{Au}_{140-x}\text{@Cu}$ ) were characterized, and the results suggest random alloy core configurations. The final product,  $\text{Pd}_x\text{Au}_{140-x}\text{@Pt}$ , shows a “ $\zeta$ (koppa)-shaped” electrocatalytic activity trend (Figure 5) for adsorbed CO oxidation as  $x$ -the average number of Pd atoms in the core-was continuously varied from 0 to 140. Calculations based on density functional theory (DFT) suggest that the trend is caused by the change of core@shell particle structures as a function of core composition, altering the CO binding energy on the surface. A pure Au core leads to the deformation of Pt shell and a compressed Pt lattice, while pure Pd core tends to segregate on the surface, forming an inverted configuration. In contrast, an alloyed PdAu core stabilizes the core@shell structures by keeping Au or Pd from escaping the core. Notably, this example provides a novel means for designing nanoparticle catalysts with the consideration of both stability and reactivity. Most importantly, this study shows the critical role of the structural effect in influencing the catalytic activity in addition to electronic effects for nanosized alloy or core@shell multimetallic electrocatalysts.

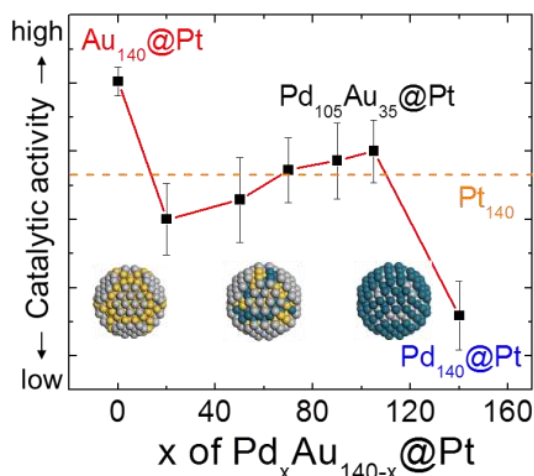


**Figure 5.** “ $\zeta$ (koppa)-shaped” electrocatalytic trend for adsorbed CO oxidation as related to the amount of Pd in the core of PdAu@Pt nanoparticles.

### Publications Acknowledging this Grant in 2012-2015

1. Myers, V. S.; Frenkel, A. I.; Crooks, R. M. In-situ Structural Characterization of Platinum Dendrimer-Encapsulated Oxygen Reduction Electrocatalysts. *Langmuir* 2012, 28, 1596-1603.\*
2. Dumitrescu, I.; Yancey, D. F.; Crooks, R. M. Dual-Electrode Microfluidic Cell for Characterizing Electrocatalysts. *Lab Chip* 2012, 12, 986-993.\*
3. Yancey, D. F.; Zhang, L.; Crooks, R. M.; Henkelman, G. Au@Pt Dendrimer Encapsulated Nanoparticles as Model Electrocatalysts for Comparison of Experiment and Theory. *Chem. Sci.* 2012, 3, 1033-1040.\*
4. Carino, E. V.; Kim, H. Y.; Henkelman, G.; Crooks, R. M. Site-Selective Cu Deposition on Pt Dendrimer-Encapsulated Nanoparticles: Correlation of Theory and Experiment. *J. Am. Chem. Soc.* 2012, 134, 4153-4162.\*
5. Dumitrescu, I.; Crooks, R. M. Effect of Mass Transfer on the Oxygen Reduction Reaction Catalyzed by Platinum Dendrimer Encapsulated Nanoparticles. *Proc. Natl. Acad. Sci., USA*

- 2012, 109, 11493-11497.\*
- Anderson, R. M.; Zhang, L.; Loussaert, J. A.; Frenkel, A. I.; Henkelman, G.; Crooks, R. M. An Experimental and Theoretical Investigation of the Inversion of Pd@Pt Core@Shell Dendrimer-Encapsulated Nanoparticles. *ACS Nano* **2013**, *7*, 9345-9353.
  - Zhang, L.; Iyyamperumal, R.; Crooks, R. M.; Henkelman, G. Design of Pt-shell Nanoparticles with Alloy Cores for the Oxygen Reduction Reaction. *ACS Nano* **2013**, *7*, 9168-9172.
  - Yancey, D. F.; Chill, S. T.; Zhang, L.; Frenkel, A. I.; Henkelman, G.; Crooks, R. M. Systematic Ligand-Induced Disorder in Au<sub>147</sub> Dendrimer-Encapsulated Nanoparticles. *Chem. Sci.* **2013**, *4*, 2912-2921.
  - Iyyamperumal, R.; Zhang, L.; Henkelman, G.; Crooks, R. M. Efficient Electrocatalytic Oxidation of Formic Acid using Au@Pt Dendrimer-Encapsulated Nanoparticles. *J. Am. Chem. Soc.* **2013**, *135*, 5521-5524.
  - Kim, H.-Y.; Henkelman, G. CO Adsorption-driven Surface Segregation of Pd on Au/Pd Bimetallic Surfaces: Role of Defects and Effect on CO Oxidation. *ACS Catal.* **2013**, *3*, 2541-2546.
  - Zhang, L.; Kim, H.-Y.; Henkelman, G. CO Oxidation at the Au–Cu Interface of Bimetallic Nanoclusters Supported on CeO<sub>2</sub>(111). *J. Phys. Chem. Lett.* **2013**, *4*, 2943-2947.
  - Anderson, R. M.; Yancey, D. F.; Loussaert, J. A.; Crooks, R. M. Multistep Galvanic Exchange Synthesis Yielding Fully Reduced Pt Dendrimer-Encapsulated Nanoparticles. *Langmuir* **2014**, *30*, 15009-15015.
  - Loussaert, J. A.; Fosdick, S. E.; Crooks, R. M. Electrochemical Properties of Metal-Oxide-Coated Electrodes Prepared by Atomic Layer Deposition. *Langmuir* **2014**, *30*, 13707-13715.
  - Duan, Z.; Henkelman, G. CO Oxidation on the Pd(111) Surface. *ACS Catal.* **2014**, *4*, 3435-3443.
  - Anderson, M.; Crooks, R. M. High-Efficiency Generation-Collection Microelectrochemical Platform for Interrogating Electroactive Thin Films. *Anal. Chem.* **2014**, *86*, 9962-9969.
  - Zhang, L.; Henkelman, G. Computational Design of Alloy-Core@Shell Metal Nanoparticle Catalyst. *ACS Catal.* **2015**, *5*, 655-660.
  - Duan, Z.; Henkelman, G. CO Oxidation at the Au/TiO<sub>2</sub> Boundary: The Role of the Au/Ti<sub>5c</sub> Site. *ACS Catal.* **2015**, *5*, 1589-1595.
  - Zhang, L.; Anderson, R. M.; Crooks, R. M.; Henkelman, G. Correlating Structure and Function of Metal Nanoparticles for Catalysis. *Surf. Sci.*, **2015** (in press).
  - Chill, S. T.; Anderson, R. M.; Yancey, D. F.; Frenkel, A. I.; Crooks, R. M.; Henkelman, G. Probing the Limits of Conventional EXAFS Analysis using Thiolated Au Nanoparticles. *ACS Nano* **2015**, *9*, 4036-4042.
  - Anderson, R. M.; Yancey, D. F.; Zhang, L.; Chill, S. T.; Henkelman, G.; Crooks, R. M. A Theoretical and Experimental Approach for Correlating Nanoparticle Structure and

Electrocatalytic Activity. *Acc. Chem. Res.*, **2015**, Published on web, DOI:  
10.1021/acsnano.5b00090

21. Luo, L.; Zhang, L.; Henkelman, G.; Crooks, R. M. Unusual Electrocatalytic Activity Trend of Pd<sub>x</sub>Au<sub>(140-x)</sub>@Pt (x: 0-140) Core@shell Nanoparticles for CO Oxidation. *J. Phys. Chem. Lett.* (submitted, **2015**).

\*Indicates that these publications cite an earlier DOE BES Catalysis Program grant number:  
DE-FG02-09ER16090



## FWP # 59066: New Single-atom Catalysts for Activation and Selective Reaction of Small Molecules, Including Alkanes

**PI:** Emilio E. Bunel<sup>1</sup>, Larry Curtiss<sup>2</sup>, Adam S. Hock<sup>1,3</sup>, Christopher L. Marshall,<sup>1</sup> Jeffrey T. Miller<sup>1,4</sup>, SonBinh T. Nguyen<sup>1,5</sup>, Peter C. Stair<sup>1,5</sup>

**Postdoc(s):** Andrew Getsoian<sup>1</sup>, Kristine Tanabe<sup>1</sup>, Theodore Helgert<sup>1</sup>, Jeffrey Camacho-Bunquin<sup>1</sup>, Casey Larsen<sup>1</sup> (Former), Debabrata Mukherjee<sup>1</sup> (Former), Steven Kraft<sup>1</sup> (Former), Nathan Siladke<sup>1</sup> (Former), Neil Schweitzer<sup>1</sup> (Former)

**Student(s):** Bo Hu<sup>3</sup>

**Affiliations(s):** <sup>1</sup>Chemical Sciences and Engineering, Argonne National Laboratory, <sup>2</sup>Material Sciences Divisions, Argonne National Laboratory, <sup>3</sup>Department of Chemistry, Illinois Institute of Technology, <sup>4</sup>Department of Chemical Engineering, Purdue University, <sup>5</sup>Department of Chemistry, Northwestern University

### *Goals*

The objective of this research is to develop new surface structures with low-coordinate coordination environments that are thermally stable single-atom heterogeneous catalysts. These materials combine the best properties of heterogeneous and homogeneous catalysts. One goal is to demonstrate that single atom catalysts offer the design control and structural uniformity of homogeneous catalysts, and the thermal stability and robustness of heterogeneous catalysts. We utilize both traditional hard supports like SiO<sub>2</sub> as well as a new class of tailorable porous organic polymers (POPs) to produce well-defined metal binding sites. A second goal is to show that these catalysts perform new chemistry; e.g. activating small molecules by different mechanisms and reaction pathways than supported nano-particles. In particular, we have found that these catalysts function through a heterolytic bond dissociation mechanism for the functionalization of alkanes, rather than by oxidative addition/reductive elimination chemistry. The project combines precise application of organometallic grafting and atomic layer deposition to prepare and stabilize the single atom sites; state-of-the-art characterization of the active sites at reaction conditions; and quantum mechanical modeling to provide insight into the mechanisms of molecular activation and reaction pathways. The catalyst targets selected are those that offer the potential to activate C-H bonds which may lead to new selective catalyst systems for the conversion of light alkanes to liquid fuels.

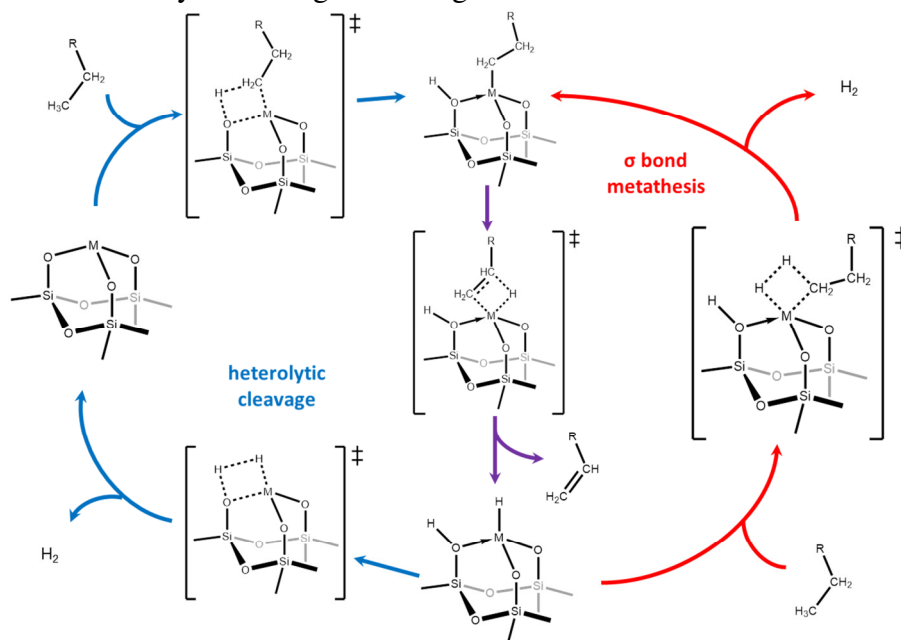
### *DOE Interest*

Combining the tunability options of homogeneous catalyst architectures with the robust nature of heterogeneous catalysts remains an unsolved problem. Furthermore, understanding and controlling the site or ensemble of sites at the molecular level is a “grand challenge” of catalysis science. We are studying thermodynamically limited reactions and their low-temperature microscopic reverse reactions to understand the key steps in C-H, C-C, and other bond activations relevant to the conversion of light alkanes to liquid fuels.

### *Recent Progress*

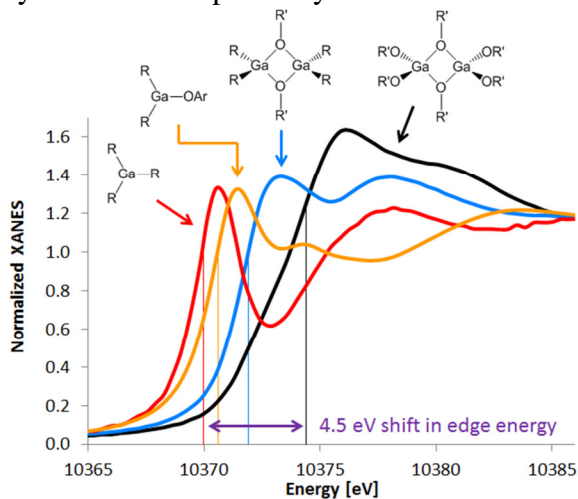
During the past year we have focused in on understanding the mechanism of our catalyst systems, in particular whether the mechanisms of precatalyst activation differ from catalyst turnover. In particular, we have explored the role of heterolytic C-H bond dissociation and activation as a catalyst initiation step in both catechol POP and SiO<sub>2</sub>-supported hydrogenation catalysts, as well as in Cu oxidation catalysts supported by POPs.

We have developed a variety of isolated metal catalysts that are highly selective for nonoxidative propane dehydrogenation. During the course of this work we have advanced synthetic routes including aqueous impregnation, surface organometallic chemistry, and high throughput atomic layer deposition in order to understand the interplay between synthesis, precatalyst structure, and initiation. In the case of precatalysts that do not contain metal-carbon or metal-hydride bonds, we believe that a Lewis acid-catalyzed heterolytic C-H cleavage of propane to produce a metal-carbon bond is the key initiation step for dehydrogenation. What is not clear at this point is whether catalytic turnover occurs through continuous heterolytic cleavage or through a  $\sigma$  bond metathesis mechanism.



To address this question we prepared a variety of very Lewis acidic isolated sites of Zn<sup>2+</sup>, Ga<sup>3+</sup>, Sc<sup>3+</sup>, and Y<sup>3+</sup> and assessed their activity for propane dehydrogenation. Zinc and gallium on SiO<sub>2</sub> catalysts are highly active and selective, but scandium and yttrium are not. Calculations show that the high strengths of Sc-O and Y-O bonds render the catalyst initiation step prohibitively endergonic. We have shown that surface-bound Sc and Y alkyl complexes are active hydrogenation catalysts, consistent with the hypothesis that it is catalyst initiation, not turnover, that is limited by the choice of precatalyst.

We have also used a variety of techniques to identify the structures of silica-supported zinc and gallium catalysts under reaction conditions. For gallium, conflicting reports have argued for [GaH<sub>x</sub>]<sup>(3-x)+</sup> or reduced Ga<sup>+</sup> species in various systems. We found single site Ga<sup>3+</sup> could be prepared as tetrahedral sites in high abundance. This Ga/SiO<sub>2</sub> catalyst, which is very active for propane dehydrogenation, shows an edge shift in the XANES spectrum at high temperatures when exposed to H<sub>2</sub> or propane. We prepared a series of model complexes using gallium alkoxides, halides,



and alkyls. The edge shifts of these model complexes establish that gallium is present as  $\text{Ga}^{3+}$  during catalysis, and that XANES edge shifts arise not from reduction, but from changes to the ligand environment around Ga. Computational analysis supports these conclusions and the same effects are also observed for  $\text{Zn}/\text{SiO}_2$ .

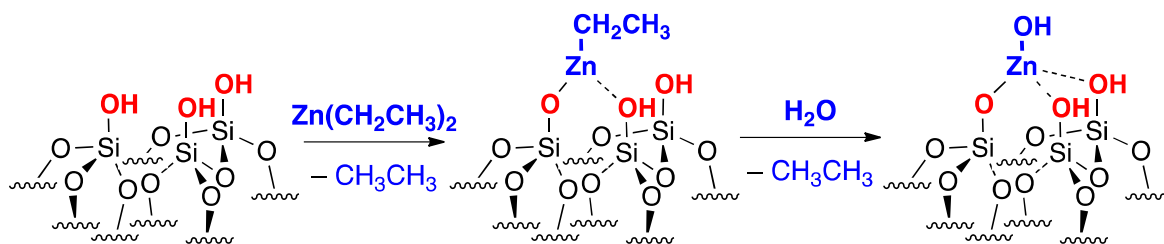
#### *High Throughput Atomic Layer Deposition (HT-ALD)*

In principle Atomic Layer Deposition (ALD) is a high-precision, vapor phase grafting technique that can synthesize a variety of supported catalytic sites (e.g., single atoms or clusters) at the atomic/monolayer level. ALD relies on a stoichiometric and thus self-limiting reaction of chemical precursors with substrate surface functionalities. The self-limiting nature of the ALD process presents a number of synthetic advantages that include (1) uniform active site dispersion, (2) high conformity to surface features which, in certain cases, allows for maximum utilization of the support surface area, and (3) high level of reproducibility. The initial nucleation of sites during an ALD should consist of isolated sites. However, the evolution of the coordination geometry about that metal site from isolated nuclei to sub-monolayer particles and on to a film are poorly understood. Thus ALD as a catalyst synthesis tool has been applied mainly for the controlled synthesis of supported bulk structures such as metal particles, films, alloys and core-shell nanoparticles, as well as in the application of protective and functional oxide over coatings. These materials are nanoscale in size and few reports of ALD for single-atom catalysts have appeared. Hence, improved understanding of synthesis mechanisms and optimization of key factors for the design of effective ALD synthesis methods is warranted. Some of the critical factors for the development of efficient ALD methods include (1) the nature of the ALD precursors, (2) substrate preparation and (3) deposition conditions (e.g. temperature, dose).



The HT-ALD-CAT developed by the Argonne Catalysis group in collaboration with ARRadiance, Inc.

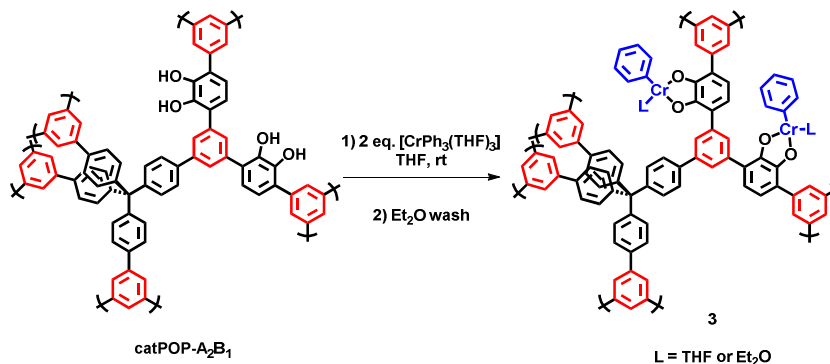
Our initial use of this HT-ALD-CAT combinatorial and catalyst reaction testing tool was for the systematic study of the transformations that these supported active sites undergo at the atomic-scale/monolayer level during catalysis of Zn sites similar to our previous  $\text{Zn}/\text{SiO}_2$  catalyst.<sup>11</sup> The HT-ALD tool<sup>2</sup> – *the first of its kind* – has the capability of (1) ALD synthesis and (2) *in situ* catalyst performance evaluation under plug-flow conditions



Zinc surface species prepared *in situ* using the HT-ALD-CAT

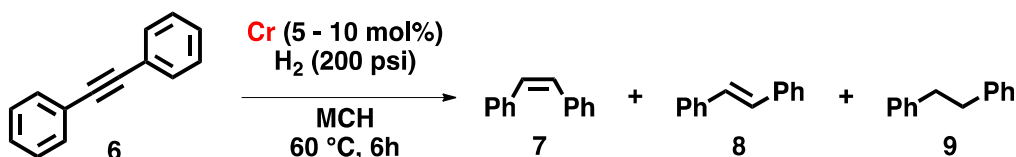
Zinc oxide and organozinc active sites were synthesized by atomic layer deposition on high-surface-area silica using the HT-ALD-CAT (see above). One-cycle ALD experiments using diethylzinc (DEZ) afforded Zn/SiO<sub>2</sub> systems that provided key insights into the reactivity and stability of Zn sites as a function of dispersion at the sub-monolayer level. The HT-ALD tool design allowed for systematic comparison of the reactivity of different grafted zinc sites. Open-shell 16-electron, tricoordinate ethyl zinc-silica sites exhibit higher activity in propane hydrogenation-dehydrogenation compared to 18-electron, tetracoordinate zinc oxide-type centers. Silica surface saturation with Zn(II) sites (~75% of a monolayer) results in facile zinc agglomeration and catalyst deactivation under reaction conditions. Reduced DEZ dosing and substrate pretreatment (e.g., dehydration under vacuum) resulted in increased Zn dispersion and produced Zn/SiO<sub>2</sub> catalysts with improved activity and stability under propylene hydrogenation (200°C) and propane dehydrogenation (550°C) conditions. The HT-ALD-CAT tool is now being utilized to develop new materials for catalyst testing in the group.

Last year we reported<sup>9</sup> a variety of catechol-supported metal complexes that are active catalysts for selective alkyne semi-hydrogenation. Since the reactive catecholate coordination sites are already integrated into the polymer backbone, the catPOP architecture allows for nucleation of isolated low-coordinate, monomeric species that are typically unstable in solution. In contrast to inorganic oxide supports, the bidentate catecholate site on catPOP provides a unique ligand coordination environment that can impart unique and unprecedented reactivity to low-coordinate organometallic chromium species. While chromium has been primarily studied for polymerization and oxidation catalysis, its reactivity for reduction remains relatively unexplored. In our original report complete structural assignment of the Cr active sites was unsuccessful due to the complicated reaction between catPOP and the organometallic precursor [Cr(CH<sub>2</sub>SiMe<sub>3</sub>)<sub>4</sub>]. The slow and complicated metallation reaction is a consequence of (1) the low reactivity of it for protonolysis and presumably, by (2) competing Cr-alkyl decomposition pathways (i.e.  $\alpha$ -H abstraction). Thus in a follow-up study we employed the aryl-chromium reagent [CrPh<sub>3</sub>(THF)<sub>3</sub>] as a well-defined precursor for the synthesis of a Cr-catPOP catalyst. We



Metallation reaction between [CrPh<sub>3</sub>(THF)<sub>3</sub>] **1** and catPOP A<sub>2</sub>B<sub>1</sub> **2**.

have found that it is far more susceptible to protonolysis and less vulnerable to Cr-alkyl decomposition pathways and leads to a well-defined Cr precatalyst (scheme 1). This well-defined Cr precatalyst was more active for hydrogenation of nonpolar unsaturated organic substrates under mild conditions.<sup>6</sup>



Entry	Cat	mol% Cr	Time (h)	Conversion (%)			TOF (h <sup>-1</sup> ) <sup>a</sup>
				7	8	9	
1	3	5	6	35	1	6	1.4
2		5	18	55	9	20	1.0
3		10	18	0	6	94	--

Through the reaction of [Cu(Mes)]<sub>n</sub> with our catechol-containing porous organic polymer (catPOP), we were able to fully incorporate Cu<sup>I</sup> into catPOP in a 2:1 Cu:catechol stoichiometry. In contrast to the previously reported Cu<sup>II</sup>-catPOP<sup>1</sup> where the Cu<sup>II</sup> center was bound to the catechol ligand in a 1:1 stoichiometry, each Cu<sup>I</sup> atom is bound to one oxygen of the catechol functionality in this new material. This Cu<sup>I</sup>-catPOP is a rare example of a coordination environment where two copper centers are stabilized next to each other in a monodentate dinuclear fashion and each Cu is two-coordinate with one anionic O<sup>-</sup> ligand and one neutral solvent-like ligand. Preliminary data suggested that this Cu<sup>I</sup>-catPOP is much more active than Cu<sup>II</sup>-catPOP in the TEMPO-mediated aerobic selective oxidation of primary and secondary alcohol to aldehyde and ketone, possibly due to its ability to better activate O<sub>2</sub> via a bimetallic mechanism. In-situ EXAFS characterization suggests that the two-coordinate Cu<sup>I</sup> centers in Cu<sup>I</sup>-catPOP readily converted to four-coordinate Cu<sup>II</sup> centers potentially resembling the dicopper motif in the tricopper cluster reported by Chan and coworkers<sup>2</sup> that can bind and activate O<sub>2</sub> for methane oxidation.

As a further illustration that the catPOP environment can stabilize monomeric Cu<sup>I</sup> species, the reaction of [Cu(Mes)]<sub>n</sub> with 3,6-di-tert-butylcatechol (3,6-DBcat), a sterically encumbered homogeneous analog of the catechol derivative in catPOP, only afforded Cu<sup>0</sup> colloids and the semiquinone (SQ) derivative (3,6-DBSQ)<sub>2</sub>Cu<sup>II</sup> as isolable products. Presumably, the (3,6-DBcat)Cu<sup>I</sup><sub>2</sub> intermediate is too unstable in solution and readily undergo disproportionation. Attempt to stabilize this intermediate with donor ligands only resulted in a variety of multinuclear complexes and clusters where the Cu centers are either three- or four-coordinate.

## Publications Acknowledging this Grant in 2012-2015

1. Getsoian A; Hu B; Miller J.T.; Hock A.S. "Supported single site Sc and Y alkyl catalysts for olefin hydrogenation" **2015**, *submitted*
2. Camacho-Bunquin, J.; Shou, H.; Aich, P.; Beaulieu, D. R.; Klotzsch, H.; Bachman, S.; Marshall, C. L.; Hock, A. S.; Stair, P. C. "Catalyst Synthesis and Evaluation Using A High-Throughput Atomic Layer Deposition–Catalysis Testing Tool" **2015**, *submitted*
3. Getsoian, A.; Das, U.; Camacho-Bunquin, J.; Zhang, G.; Gallagher, J. Hu, B; Schaidle, J.; Ruddy, D. A.; Kraft, S. J.; Henley, J.; Curtiss, L. A. Miller, J. T.; Hock, A.S. "Oxidation State and Ligand Field Effects in Ga K-edge XANES: Mechanistic Implications for Alkane Dehydrogenation by Ga-Zeolite Catalysts" **2015** *submitted*
4. Camacho-Bunquin, J.; Aich, P.; Ferrandon, M.; Getsoian A.; Das, U; Curtiss L. A.; Miller, J. T.; Marshall, C. L.; Hock, A. S; Stair, P. C. "Single-Site Zinc on Silica Catalysts for Propylene Hydrogenation and Propane Dehydrogenation. Synthesis and Reactivity Evaluation Via High-Throughput Atomic Layer Deposition-Catalysis Experimentation" **2015**, *submitted*
5. Hu, B.; Schweitzer, N. M.; Zhange, G.; Kraft, S. J.; Childers, D. J; Lanci, M. P.; Miller, J. T.; Hock, A. S. "Isolated Fe<sup>II</sup> on Silica As a Selective Propane Dehydrogenation Catalyst" *ACS Catalysis*, **2015**, 5, 3494-3503
6. Camacho-Bunquin, J.; Siladke, N. A.; Zhang, G.; Niklas, J.; Poluektov, O. G.; Nguyen, S. T.; Miller, J. T.; Hock, A. S. "Synthesis and Catalytic Hydrogenation Reactivity of a Chromium Catecholate Porous Organic Polymer" *Organometallics* **2015**, 34, 947-952.
7. Hu, B., Schweitzer, N. M., Das, U., Kim, H. K., Stair, P. C., Curtiss, L., Hock, A. S., and Miller, J. T. "Selective Propane Dehydrogenation with Single Site Co<sup>II</sup> on SiO<sub>2</sub> by a Non-redox Mechanism" *J. Catal.* **2015**, 322, 24-37
8. Krogman, J. P.; Gallagher, J. R.; Zhang, G.; Hock, A. S.; Miller, J. T.; Thomas C. "Definitive Assignment of the Oxidation States of Zr and Co in a Highly Reactive Heterobimetallic Zr/Co Complex Using X-ray Absorption Spectroscopy (XANES)" *Dalton Trans.* **2014**, 13852-13857
9. Tanabe, K. K.; Ferrandon, M. S.; Siladke, N. A.; Kraft, S. J.; Zhang, G.; Niklas, J.; Poluektov, O. G.; Lopykinski, S. J.; Bunel, E. E.; Krause, T. R.; Miller, J. T.; Hock, A. S.; Nguyen, S. T. "Discovery of highly selective alkyne semi-hydrogenation catalysts based on 1<sup>st</sup>-row transition metallated porous organic polymers" *Angew. Chem. Int. Ed.* **2014**, 53, 12055.
10. Kraft, S. J.; Zhang, G.; Childers, D.; Dogan, F.; Miller, J. T.; Nguyen, S. T.; Hock, A. S., "Rhodium Catechol Containing Porous Organic Polymers: Defined Catalysis for Single-Site and Supported Nanoparticulate Materials." *Organometallics* **2014**, 33, 2517-2522
11. Schweitzer, N. M.; Hu, B.; Das, U.; Kim, H.; Greeley, J.; Curtiss, L. A.; Stair, P. C.; Miller, J. T.; Hock, A. S., "Propylene Hydrogenation and Propane Dehydrogenation by a Single-Site Zn<sup>2+</sup> on Silica Catalyst." *ACS Catalysis* **2014**, 4 (4), 1091.
12. Kraft, S. J.; Hu, B.; Zhang, G.; Miller, J. T.; Hock, A. S., "In Situ X-ray Absorption Spectroscopy and Nonclassical Catalytic Hydrogenation with an Iron(II) Catecholate Immobilized on a Porous Organic Polymer." *European Journal of Inorganic Chemistry* **2013**, 2013 (22-23), 3972.
13. Kraft, S. J.; Sánchez, R. H.; Hock, A. S., A Remarkably Active Iron Catecholate Catalyst Immobilized in a Porous Organic Polymer. *ACS Catalysis* **2013**, 826-830.
14. Schweitzer, N. M.; Hu, B.; Miller, J. T.; Hock, A. S. "Selective Alkane Activation with Single Site Atoms on Amorphous Supports" *patent application filed*, **2013**

15. Maria, S.; Poli, R.; Gallagher, K. J.; Hock, A. S.; Johnson, M. J. A.; “*Ether Complexes Of Molybdenum(III) And (IV) Chloride.*” *Inorg. Synth.* **2013**, *36*, 15.
16. Broderick, E. M.; Browne, S. C.; Johnson, M. J. A.; Hitt, T. A.; Girolami, G. S. “*Dimolybdenum and Ditungsten Hexa(Alkoxides).*” *Inorg. Synth.* **2013**, *36*, 96.
17. Tanabe, K. K.; Siladke, N. A.; Broderick, E. M.; Kobayashi, T.; Goldston, J. F.; Weston, M. H.; Farha, O. K.; Hupp, J. T.; Pruski, M.; Mader, E. A.; Johnson, M. J. A.; Nguyen, S. T., Stabilizing unstable species through single-site isolation: a catalytically active TaV trialkyl in a porous organic polymer. *Chemical Science* **2013**, *4*, 2483.
18. Nelson, R. C.; Miller, J. T. “An Introduction to X-ray Absorption Spectroscopy and Its In Situ Application to Organometallic Compounds and Homogeneous Catalysts,” *Catalysis Science and Technology*, *2*, 461-470 (2012). Lu, J., Fu, B., Kung, M.C., Xiao, G., Elam, J.W., Kung, H.H., Stair, P.C., Coking and Sintering Resistant Palladium Catalysts Achieved through Atomic Layer Deposition. *Science* **2012**, *335*, 1205.
19. Lu, J., Liu, B., Greeley, J.P., Feng, Z., Libera, J.A., Lei, Y., Bedzyk, M.J., Stair, P.C., Elam, J.W., Porous Alumina Protective Coatings on Palladium Nanoparticles by Self-Poisoned Atomic Layer Deposition, *Chemistry of Materials* **2012**, *24*, 2047.
20. Mehmood, F., Rankin, R.B., Greeley, J.P., and Curtiss, L.A., Trends in Methanol Decomposition on Transition Metal Alloy Clusters from Scaling and Bronsted-Evans-Polyani Relationships, *Physical Chemistry Chemical Physics* **2012**, *14*, 8644.

### Atomically Precise Metal Nanoclusters for Catalytic Application

Postdoc: Gao Li  
 Student: Yuxiang Chen  
 Collaborators: Prof. De-en Jiang (University of California at Riverside); Dr. Qingjie Ge (Dalian Inst. of Chemical Physics)  
 Contact: Carnegie Mellon University, Department of Chemistry, Pittsburgh, PA 15213;  
 Email: [rongchao@andrew.cmu.edu](mailto:rongchao@andrew.cmu.edu)

#### Goal

Develop atomically precise metal nanoclusters ranging from tens to hundreds of atoms in size for catalytic application

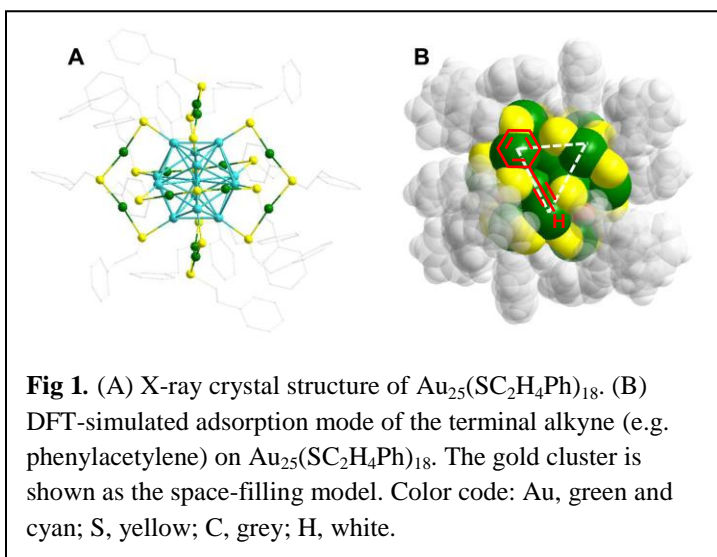
#### DOE Interest

Atomically precise metal nanoclusters provide some exciting opportunities for fundamental catalysis research, such as the tuning of catalytic activity/selectivity at the single-atom level through controlled doping of nanoclusters, the study of structure-reactivity relationships of nanoclusters in solution or supported on solids, as well as the identification of catalytic sites at the atomic level. The crystallographic characterization reveals the atomic structure of nanoclusters, which permits the identification of the molecular adsorption geometry and elementary steps of catalytic reaction mechanisms through a combination of experiment and theory. Such information is important for fundamental understanding of catalytic processes and rational catalyst design.

#### Recent Progress

##### 1. Semihydrogenation of terminal alkynes to alkenes (work published in *J. Am. Chem. Soc.* 2014)

The olefin (-C=C-) is typically synthesized by semihydrogenation of the alkyne. In the previous catalytic work, semihydrogenation of alkynes was mainly catalyzed by palladium, but the selectivity was poor. We explored the ultras-small, *non-metallic* Au<sub>25</sub>(SR)<sub>18</sub> nanocluster supported on oxides for the semihydrogenation of terminal alkynes to alkenes using H<sub>2</sub> as the hydrogen source under relatively mild conditions (100 °C, 20 bar H<sub>2</sub>, ethanol/H<sub>2</sub>O as solvent and pyridine as base). High conversion of a wide range of terminal alkynes (up to ~100%) and excellent selectivity for alkene products (~100%) were achieved. The TOF is ~200 h<sup>-1</sup> (comparable to nano-Pd). The nanocluster catalyst showed excellent recyclability.



The well-defined structure of  $\text{Au}_{25}(\text{SR})_{18}$  (Fig 1A) provides an important clue as to the catalytic active-site. Specifically, the open triangular facet (Fig 1B) was identified to be the active site for alkyne adsorption. The facet comprises three surface gold atoms ( $\text{Au}_3$ ) from three separate “staple”-like  $-\text{S}(\text{R})-\text{Au}-\text{S}(\text{R})-\text{Au}-\text{S}(\text{R})-$  surface motifs, and this open facet allows easy access of reactants. Density functional theory (DFT) modeling (in collaboration with Prof. De-en Jiang) of the reactant adsorption shows that phenylacetylene prefers to adsorb on the open facet with the phenyl ring facing one gold atom of the  $\text{Au}_3$  facet (adsorption energy  $-0.40$  eV).

## 2. Nanocluster structures and sizes (published in *Angew. Chem. Int. Ed. & Nano Lett.* 2015)

Unravelling the total structures of small gold clusters is the key to understanding the origin of catalytic reactivity. The crystal structure of a new nanocluster formulated as  $\text{Au}_{18}(\text{SC}_6\text{H}_{11})_{14}$  has been solved (Fig 2). The structure comprises an unprecedented hexagonal close pack (hcp)  $\text{Au}_9$  kernel (Fig 2), which is protected by various staples including three  $-\text{SR}-\text{Au}-\text{SR}-$  monomer staples, one dimeric staple and one tetrameric staple. Until the present, the  $\text{Au}_{18}(\text{SC}_6\text{H}_{11})_{14}$  cluster is the smallest crystallographically characterized gold cluster protected by thiolates and provides important insight into the structural evolution with size. Theoretical calculations indicate charge transfer from surface to kernel for the HOMO-LUMO transition. The distinct kernel and staple motifs offer new opportunities for investigating their catalytic reactivity (ongoing work).

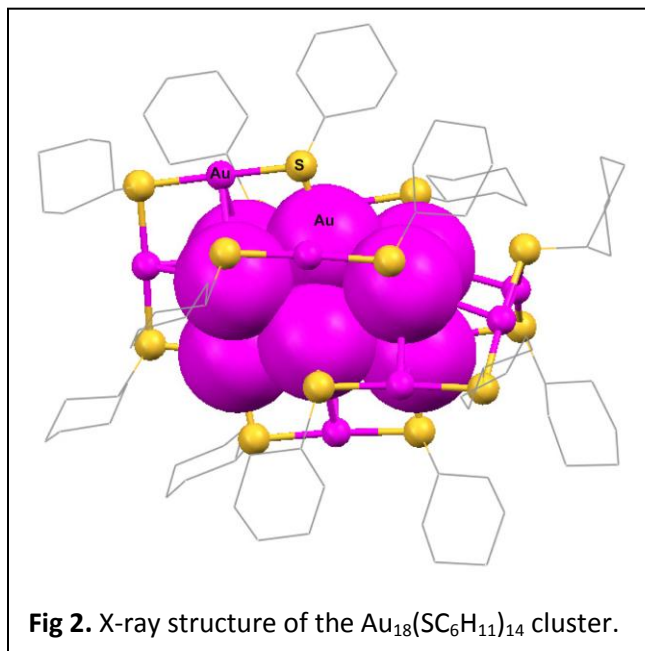


**Fig 2.** X-ray structure of the  $\text{Au}_{18}(\text{SC}_6\text{H}_{11})_{14}$  cluster.

Toward controlling the size of atomically precise gold nanoclusters, we have devised a

new strategy by exploring the *para*-, *meta*-, *ortho*-methylbenzenethiol (MBT) and successfully prepared  $\text{Au}_{130}(p\text{-MBT})_{50}$ ,  $\text{Au}_{104}(m\text{-MBT})_{41}$  and  $\text{Au}_{40}(o\text{-MBT})_{24}$  nanoclusters. The decreasing size sequence is in line with the increasing hindrance of the methyl group to the interfacial Au-S bond (Fig 3). That the subtle change of ligand structure can result in drastically different magic sizes under otherwise similar reaction conditions is indeed for the first time observed in the synthesis of thiolate-protected gold nanoclusters.

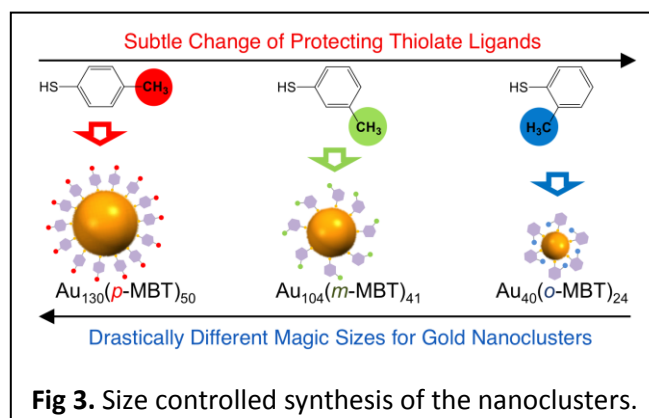


**Fig 3.** Size controlled synthesis of the nanoclusters.

## Future Plans

Detailed mechanistic studies on the activation pathway of terminal alkynes over ligand-on gold nanoclusters: Our hypothesis is that it may follow a deprotonation activation pathway via

the formation of a  $R'-C\equiv C-[Au_nL_m]$  intermediate. We will also investigate the reactivity difference between terminal and internal alkynes based upon our hypothesis is that it may involve the steric effect of surface ligands.

Based upon the obtained  $Au_{18}$ ,  $Au_{40}$ ,  $Au_{104}$  and  $Au_{130}$  nanoclusters, we will study the potential size effect of nanoclusters in the catalytic hydrogenation of  $C\equiv C$  or  $C=C$  substrates, as well as catalytic oxidation reactions. In addition, we will carry out doping gold nanoclusters with a precise number of heteroatoms (Ag, Cu, Pt, Pd, etc) and investigate the effect of doping on the structure and catalytic reactivity.

## Publications

1. Gold Nanocluster-Catalyzed Semihydrogenation: A Unique Activation Pathway for Terminal Alkynes. G. Li and R. Jin. *J. Am. Chem. Soc.* **2014**, *136*, 11347–11354.
2. Size Dependence of Atomically Precise Gold Nanoclusters in Chemoselective Hydrogenation and Active Site Structure. G. Li, D.-e. Jiang, S. Kumar, Y. Chen, and R. Jin. *ACS Catal.* **2014**, *4*, 2463–2469.
3. Structure Determination of  $[Au_{18}(SR)_{14}]$ . A. Das, C. Liu, H. Y. Byun, S. Zhao, N. L. Rosi, R. Jin, *Angew. Chem. Int. Ed.* **2015**, *54*, DOI: 10.1002/anie.201410161.
4. Tuning the magic size of atomically precise gold nanoclusters via isomeric methylbenzenethiols. Y. Chen, C. Zeng, D. R. Kauffman and R. Jin. *Nano Lett.* **2015**, *15*, 3603-3609.
5. Chemoselective Hydrogenation of Nitrobenzaldehyde to Nitrobenzyl Alcohol with Unsupported Au Nanorod Catalysts in Water. G. Li, C. Zeng, and R. Jin, *J. Phys. Chem. C*, **2015**, *119*, 11143–11147.
6. Probing active site chemistry with differently charged  $Au_{25}^q$  nanoclusters ( $q = 1, 0, +1$ ). D. R. Kauffman, D. Alfonso, C. Matranga, P. Ohodnicki, X. Deng, R. C. Siva, C. Zeng, and R. Jin. *Chem. Sci.* **2014**, *5*, 3151-3157.
7. (Book chapter) Y. Chen, G. Li, H. Qian, and R. Jin. Catalysis by Atomically Precise Gold Nanoclusters. In *Catalysis by Materials with Well-defined structures* (Zili Wu et al Eds. 2015)
8. (Review) Atomically Precise Metal Nanoclusters: Stable Sizes and Optical Properties. R. Jin, *Nanoscale*, **2015**, *7*, 1549–1565.
9. Experimental and Mechanistic Understanding of  $C=O$  Hydrogenation Using  $Au_{25}$  Nanoclusters with Lewis-Acids: Unique Sites for Catalytic Reactions. G. Li, H. Abroshan, Y. Chen, R. Jin, H. Kim (*submitted*).

**Selectivity of Intermolecular C-H Activation at [Tp'Rh(PMe<sub>3</sub>)]:  
How Does the Ancillary Ligand Affect the Metal-Carbon Bond Strength?**

William D. Jones, Yunzhe Jiao, Meagan E. Evans, and James Morris  
Department of Chemistry, University of Rochester, Rochester, NY 14627

**Poster Abstract**

The thermal precursors Tp'RhL(Me)H where L = CNneopentyl, PMe<sub>3</sub>, or P(OMe)<sub>3</sub> were used to generate the active [Tp'RhL] fragment, which activates C-H bonds of various hydrocarbons to form products of the type Tp'RhL(R)H (Tp'=tris-(3,5-dimethylpyrazolyl)borate). Only one single activation product was observed in each case. The structures of Tp'RhL(R)X (X= H, Br, Cl) have been characterized by NMR spectroscopy, elemental analysis, and X-ray crystallography. The kinetics of reductive elimination of RH from Tp'RhL(R)H as well as competition experiments between substrates allow measurement of the Rh-C bond strengths relative to the Rh-Ph bond strength. Two separate linear correlations of the Rh-C bond energies versus H-C bond energies were found based on whether the alkyl group is  $\alpha$ -substituted or not. The correlations for  $\alpha$ -substituted substrates give slopes of 1.40-1.71, similar to the slopes seen for unsubstituted hydrocarbons, 1.38-1.54. The two Rh-C bond energy correlations are parallel, with the products with  $\alpha$ -substituents higher by 7 kcal mol<sup>-1</sup>. From these studies we conclude that replacing the spectator ligand with a more electronic donating group slightly increases the range of metal-carbon bond strengths as the trend in slopes of the correlations follows an order of CNneopentyl < P(OMe)<sub>3</sub> < PMe<sub>3</sub>.

**FG02-86ER-13569: Transition Metal Activation and Functionalization of  
Carbon-Hydrogen and Carbon-Carbon Bonds**

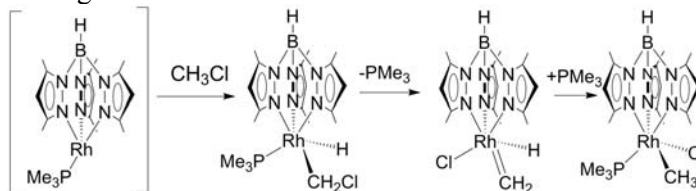
**PI:** William D. Jones

**Students:** Yunzhe Jiao, Meagan E. Evans, and James Morris

**RECENT PROGRESS**

*C-Cl vs. C-H activation*

The reactive fragment [Tp'Rh(PMe<sub>3</sub>)], generated from the thermal precursor Tp'Rh(PMe<sub>3</sub>)(Me)H, is found to cleave the C-Cl bonds of chlorohydrocarbons under mild conditions. Reaction with chloromethane gives clean formation of an initial C-H activation product, which rearranges to form the C-Cl activation product at 30 °C. The rearrangement is found to occur via a carbene intermediate.



*C-H vs. B-H vs. Si-H vs. C-F activation*

The photochemical reactions of Tp' Rh(PMe<sub>3</sub>)H<sub>2</sub> and thermal reactions of Tp' Rh(PMe<sub>3</sub>)(CH<sub>3</sub>)H (Tp' = tris(3,5-dimethylpyrazolyl)borate) with substrates containing B-H, Si-H, C-F, and C-H bonds have been examined. We are able to establish intermolecular selectivities that follow the order: H-SiPh<sub>3</sub> (2.3); H-CHF<sub>2</sub> (1.6); C<sub>6</sub>H<sub>6</sub> (1.0); H-C≡CPh (0.47); pentane (0.41); H-CH<sub>3</sub> (0.39); H-Bpin (0.36); H-CH<sub>2</sub>CF<sub>3</sub> (0.20); H-CH<sub>2</sub>C(O)CH<sub>3</sub> (0.16); F-C<sub>3</sub>NF<sub>4</sub> (0.07); H-c-C<sub>3</sub>H<sub>9</sub> (0.063).

### Publications Acknowledging this Grant in 2012-2015:

1. "C-H Activation of Terminal Alkynes by tris-(3,5-dimethylpyrazolyl)boraterhodium-neopentylisocyanide: New Metal-Carbon Bond Strengths," Gyeongshin Choi, James Morris, William W. Brennessel, and William D. Jones, *J. Am. Chem. Soc.* **2012**, *134*, 9276–9284. (DOE)
2. "Rhodium-Carbon Bond Energies in Tp'Rh(CNneopentyl)(CH<sub>2</sub>X)H: Quantifying Stabilization Effects in M-C Bonds," Yunzhe Jiao, Meagan E. Evans, James Morris, William W. Brennessel, and William D. Jones. *J. Am. Chem. Soc.* **2013**, *135*, 6994–7004. (DOE)
3. "A Trispyrazolylboraterhodium Phosphite Complex that Undergoes an Arbusov-Like Rearrangement," Yunzhe Jiao, William W. Brennessel, and William D. Jones, *Acta Cryst. C*, **2013**, *C69*, 939-942. doi:10.1107/S0108270113015953 (DOE)
4. "Kinetic and Thermodynamic Selectivity of Intermolecular C-H Activation at [Tp'Rh(PMe<sub>3</sub>)]. How Does the Ancillary Ligand Affect the Metal-Carbon Bond Strength?" Yunzhe Jiao, James Morris, William W. Brennessel, and William D. Jones, *J. Am. Chem. Soc.* **2013**, *135*, 16198–16212. (DOE)
5. "Nickel(0) Addition to a Disulfide Bond," Juanjuan Li, James Morris, William W. Brennessel, William D. Jones, *J. Chem. Cryst.* **2013**, *44*, 15-19. (DOE)
6. "Synthesis and energetics of Tp'Rh[P(OMe)<sub>3</sub>](R)H: A systematic investigation of ligand effects on C-H activation at rhodium," Yunzhe Jiao, William W. Brennessel, and William D. Jones, *Chem. Sci.* **2014**, *4*, 804-812. (DOE, NSF-CENTC)
7. "Addition of C-C and C-H Bonds by Pincer-Iridium Complexes: A Combined Experimental and Computational Study," David A. Laviska, Changjian Guan, Thomas J. Emge, Miles Marnell, William W. Brennessel, William D. Jones, Karsten Krogh-Jespersen, Alan S. Goldman, *Dalton Trans.* **2014**, *43*, 16354-16365. (DOE)
8. "Investigation of C-C Bond Activation of sp-sp<sup>3</sup> C-C Bonds of Acetylene Derivatives via Photolysis of Pt Complexes," Ahmet Gunay, William W. Brennessel, and William D. Jones, *Organometallics* **2015**, in press, DOI: 10.1021/om500999u. (DOE)
9. "Activation of B-H, Si-H, and C-F bonds with Tp'Rh(PMe<sub>3</sub>): Kinetics, Mechanism and Selectivity," Barbara Procacci, Yunzhe Jiao, Meagan E. Evans, William D. Jones, Robin N. Perutz, Adrian C. Whitwood, *J. Am. Chem. Soc.* **2015**, *137*, 1258–1272. (DOE)
10. "Oxidative Addition of Chlorohydrocarbons to a Rhodiumtrispyrazolylborate Complex," Yunzhe Jiao, William W. Brennessel, and William D. Jones, *Organometallics*, **2015**, *34*, just accepted. (DOE)

## Immobilized Molecular Catalysts in Cooperative Catalysis and Cascade Reactions

Marcus Weck,<sup>1</sup> Seung Soon Jang,<sup>2</sup> C. David Sherrill<sup>2</sup>

<sup>1</sup>New York University, <sup>2</sup>Georgia Institute of Technology

### Presentation Abstract

The team of Jones, Sherrill, Jang (GT) and Weck (NYU) are working on cooperative catalytic reactions and cascade/tandem reactions using combinations of organocatalysts and transition metal complex catalysts. Building on past work on cooperative reactions, the current emphasis is on tandem reactions using distinct, sometimes incompatible active sites by designing oxide and polymeric catalysts that contain well-defined active sites contained within specific locales or domains within their structures.

### DE-FG02-03ER15459: Immobilized Molecular Catalysts:

#### Cooperative Catalysis to Cascade Reactions

**Postdocs:** Jonas Dimroth (NYU), Niels ten Brummelhuis (NYU), Lori Burns (GT), Nicholas Brunelli (GT), Yan Feng (GT), Eric Moschetta (GT), Li-Chen Lee (GT)

**Students:** Michael Kahn (NYU), Jie Lu (NYU), Aaron Cohen (NYU), Byeong Jae Chun (GT), Matthew Kennedy (GT), Brandon Bakr (GT), Caroline Hoyt (GT), Wei Long (GT)

### RECENT PROGRESS

This collaborative research program has focused on the design and understanding of cooperative catalysts that combine two distinct catalytic sites (e.g. acid and base) into a single material or molecule to effect catalytic reactions that are accelerated by cooperative interactions with the two sites, relative to catalysis by a single site. In a new direction within the team, these cooperative reactions are being extended to tandem and cascade reactions, whereby multiple individual catalytic steps are catalyzed in a series using different active centers. Cooperative catalysis and cascade catalysis are two examples of the use of designed, multi-functional

catalysts, with both sites interacting with a substrate(s) simultaneously to effect a reaction in the former case, and with different sites working independently in a series in the latter case.

A major initiative in the past years has been the development of cooperative Co-Salen catalysts for epoxide ring-opening reactions (Weck, Jones), whereby some of the most efficient catalysts known have been synthesized and characterized. In recent work, the team has sought to understand on the molecular level the catalytic reaction pathway (Sherrill, Ludovice, Weck, Jones), which was proposed by Jacobsen and Blackmond ten years ago based on kinetic studies.

We (Sherrill) have used density functional theory (DFT) to study the rate-determining step for the hydrolytic kinetic resolution (HKR) of terminal epoxides as catalyzed by Co(III)-Salen-X, with X a counterion. The rate-determining step is thought to involve activation of the epoxide through its coordination to one Co(III)-Salen-X catalyst, concomitant with a ring-opening attack by activated OH<sup>-</sup> from Co(III)-Salen-OH [*in-situ* generated by loss of counterion from Co(III)-Salen-X]. Our previous studies of Metal-Salen complexes suggest an intricate electronic structure, hence we have used both the B3LYP and BP86 functionals to test variation in DFT results. These two functionals yield quantitative differences but overall similar qualitative trends. Co(III)-Salen-OH by itself, without the presence of Co(III)-Salen-X (X being some other counterion), is not active in HKR. Contrary to expectations that this results from Co(III)-Salen-OH being insufficiently Lewis acidic to activate the epoxide, our computations indicate that X=OH<sup>-</sup> binds epoxide nearly as well as X=Cl<sup>-</sup> (gas-phase or with implicit solvent correction). Instead, the inactivity of Co(III)-Salen-OH as the sole catalytic species results from an increased barrier height in the ring-opening step. Barrier heights for chloride, acetate, and tosylate counterions are similar, consistent with their similar peak reaction rates. The different reaction profiles found for these counterions therefore seems to be a result of different rates of reaction with epoxide to form the activated Co(III)-Salen-OH species required for the bimetallic reaction mechanism. Barrier heights were computed using propylene oxide, 1-hexene oxide, and epichlorohydrin as reactants. Propylene oxide and 1-hexene oxide exhibit similar barrier heights, while epichlorohydrin has a significantly lower barrier, qualitatively consistent with experiments showing faster reactions for epichlorohydrin than propylene oxide when catalyzed by Co(III)-Salen-OAc. Overall, the computational studies have provided new insight into the mechanistic details of HKR catalysis by Co(III)-Salen-X and have resolved some questions previously raised in the literature.

Building on the above work, which involves cooperative activation of substrates by electrophilic and nucleophilic centers, we (Jones, Weck) are working on silica-supported and polymer-supported organocatalytic acid-base catalyzed (aldol, nitroaldol) reactions. Having determined that weakly acidic silanols were better cooperative partners than carboxylic acids in aldol reactions, we elucidated the optimal distance between the amines and silanols for aldol and nitroaldol reactions, showing they depend on the pore curvature and nature of the coupling partners in the reaction (ketone/aldol vs. nitroalkane/nitroaldol). By synthesizing a homologous series of aminosilanes (C1-C5 linkers), we showed that we could alter the catalytic activity by an order of magnitude by changing only the pore curvature and linker length in the nitroaldol reaction. In contrast, the aldol reaction was much less sensitive to linker length, suggesting significant differences in reaction pathway of these seemingly similar reactions. In addition to our linker length and pore size studies, we also examined the effect of incorporating heteroatoms (B, Al, Ga, Ti, Zr, and Ce) into the framework of the silica support for amine-silanol bifunctional catalysts. For the nitroaldol condensation, four of the six heteroatoms (B, Al, Ga, and Ti) increased the catalytic activity compared to the supported amine-silanol catalyst with no heteroatom substitution. We observed a decrease in catalytic activity for the aldol condensation for all heteroatom substitutions compared to the catalyst with no heteroatom substitution. We also initiated an international collaboration with researchers at the University of Ghent in Belgium, exploring the role of alcohols vs. silanols as co-catalysts with amines in aldol reactions. These differences will be the subject of future theoretical/computational investigations by the team (Sherrill, Jang).

Moving from cooperative reactions to consecutive, tandem reactions, a major initiative within the team is the design of well-defined reaction environments to promote or control tandem reactions (Weck, Jang, Jones). Operation of multiple catalytic reactions in one pot is often limited by incompatibilities of the catalysts and reaction conditions. Inspired by nature where the compartmentalization of cells enables metabolism pathways to proceed simultaneously, we have designed and synthesized metal catalyst containing shell cross-linked micelles (SCMs) as well as multi compartment micelles (MCMs) that enable the site isolation of two or more incompatible catalytic systems. Our first compartmentalization strategy is based on shell-cross-linked micelles that have been introduced by Wooley and coworkers. The micelle structure contains a hydrophobic core and a hydrophilic shell. This core-shell domain structure should

provide perfect site-isolation and compartmentalization of incompatible transformations, making it an excellent platform to combine two incompatible transition metal complexes for a multistep sequential reaction. A requirement for our polymer micelle support strategy is the introduction of orthogonal functional handles located in the core and shell domains to attach two different metal catalysts. Our target tandem reaction is the synthesis of chiral secondary alcohols that are used as building blocks in the production of pharmaceuticals and fine chemicals. Starting from commercially available alkynes, Co-catalyzed hydration was used to form the corresponding methyl ketones that were then transformed by Rh-catalyzed asymmetric transfer hydrogenation (ATH) into the chiral secondary alcohols. Methyl ketones can be prepared by the catalytic hydration of terminal alkynes using a variety of catalysts including cobalt porphyrin (Co-Por) complexes. ATH is a powerful method for the preparation of enantioenriched chiral alcohols from ketones, and transition metal complexes based on N-tosylated 1,2-diphenyl-1,2-ethylenediamine (TsDPEN) derivatives are among the most efficient catalysts for this reaction. We demonstrated that this non-orthogonal two-step catalytic tandem reaction proceeds in one pot with high yields and enantioselectivities. While the tandem reaction worked in principle even when the two catalysts were immobilized in different micelles separately, the multicompartmentalized micelle containing both catalysts gave significantly better results. This strategy will pave the way for unforeseen tandem reactions that involve incompatible catalytic transformations. The number of catalytic steps that can be combined using this strategy is currently limited by the number of functionalized domains within a micelle. The use of multicompartment micelles will allow to expand this strategy to three or four non-orthogonal transformations.

Multicompartment micelles are a particular type of supramolecular assembly, which features an additional level of microphase separation within a micellar core. Such a phenomenon is accessible using a triblock copolymer consisting of hydrophilic, hydrophobic, and fluorophilic blocks. The former of these three blocks solubilizes the polymer in an aqueous environment while the latter two are both internalized into the micellar core, where they phase separate to form discrete hydrophobic and fluorophilic domains. To date multicompartment micelles have been prepared and visualized but their applied uses remain non-existent. We are preparing multicompartment micelles based on styrene-derivatives where each block possesses a functional "handle," through which a series of modified catalysts can be covalently attached to during post-

polymerization functionalization. Such a modified multicompartment micelle can be viewed as a nano-reactor, capable of carrying out a wide variety of multistep tandem reactions.

To characterize the transport of reactant/product molecules through the multicompartment micelles as a function of the molecular structures (Jang, Weck), we first investigated the molecular interaction of reactants/products with the each compartment. For this purpose, the Flory-Huggins interaction parameters ( $\chi$ ) were calculated for every reactant-block and product-block pair using a full-atomistic molecular dynamics (MD) simulation method since thermodynamic molecular miscibility should correlate with the molecular diffusivity of the reactants/products through the multicompartment micelles. From our simulation results, it was found that our MD simulation method can be used to narrow down the reactant/product candidates for given multicompartment micelles consisting of multiblock copolymers. Building on this, using such Flory-Huggins interaction parameters ( $\chi$ ), we can design multiblock copolymers to create desirable multicompartment micelles for given reactant/product pairs. For this, the dissipative particle dynamics (DPD) simulation method has been used to investigate the internal structure of a multicompartment micelles via phase segregation as well as the molecular association of reactants/products with the designed micelles. The major tasks of this simulation study were to 1) calculate  $\chi$  parameters for reactant-block, product-block and block-block pairs using MD simulations, 2) design multiblock copolymer chain architectures (such as linear, branched and so on) and 3) obtain a multicompartment micelle using DPD simulation method. To design a good micelle, critical variables are i)  $\chi$  parameters (chemical structures) and ii) length of the blocks (composition). For direct assessment of the transport properties of reactants/products, the energy barriers for molecular diffusion are being estimated using the umbrella sampling method as well as the potential of mean force approach.

### **Publications Acknowledging this Grant in 2012-2015**

1. Kahn M. G. C.; Weck, M.; Highly Crosslinked Polycyclooctyl-Salen Cobalt (III) for the Hydrolytic Kinetic Resolution of Terminal Epoxides. *Catal. Sci. Tech.* **2012**, 2, 386-389.
2. Kahn, M. G. C.; Stenlid, J. H.; Weck, M.; Poly(styrene) Resin-Supported Co (III) Salen Cyclic Oligomers: Highly Active and Easily Recycled HKR Catalysts. *Adv. Synth. Catal.* **2012**, 354, 3016-3024.
3. Brunelli, N. A.; Didas, S. A.; Venkatasubbaiah, K.; Jones, C. W.; Tuning Cooperativity by Controlling the Linker Length of Silica-Supported Amines in Catalysis and CO<sub>2</sub> Capture. *J. Am. Chem. Soc.* **2012**, 134, 13950-13953.

4. Brunelli, N. A.; Venkatasubbaiah, K.; Jones, C. W.; Cooperative Catalysis with Acid-Base Bifunctional Mesoporous Silica: Impact of Grafting and Co-condensation Synthesis Methods on Material Structure and Catalytic Properties. *Chem. Mater.* **2012**, *24*, 2433-2442.
5. Brunelli, N. A.; Long, W.; Venkatasubbaiah, K.; Jones, C. W.; Catalytic Regioselective Epoxide Ring Opening with Phenol using Homogeneous and Supported Analogues of Dimethylaminopyridine. *Top. Catal.* **2012**, *55*, 432-438.
6. Brunelli, N. A.; Jones, C. W.; Tuning Acid-Base Cooperativity to Create Next Generation Silica-Supported Organocatalysts. *J. Catal.* **2013**, *308*, 60-72.
- 7.. Key, R. E.; Venkatasubbaiah, K.; Jones, C. W.; Evaluation of Enantiopure and Non-Enantiopure Co(III)-Salen Catalysts and their Counter-ion Effects in the Hydrolytic Kinetic Resolution (HKR) of Racemic Epichlorohydrin. *J. Mol. Catal. A. Chem.* **2013**, *366*, 1-7. Editor's Choice Paper.
- 8.. Long, W.; Brunelli, N. A.; Didas, S. A.; Ping, E. W.; Jones, C. W.; Aminopolymer-Silica Composite Supported Pd Catalysts for Selective Hydrogenation of Alkynes. *ACS. Catal.* **2013**, *3*, 1700-1708.
- 9.. Feng, Y.; Lydon, M. E.; Jones, C. W.; Cobalt Salen Catalysts Supported on a Highly Cross-linked Polymer Resin: Role of Co(II) Salen species in the Heterogeneous Cooperative Regioselective Ring Opening of 1,2-Epoxyhexane with Methanol. *ChemCatChem* **2013**, *5*, 3636-3643.
10. Brummelheis, N. T.; Weck, M.; RAFT Polymerization of Alternating Styrene-Pentafluorostyrene Copolymers. *J. Polym. Sci. Polym. Chem.* **2014**, *52*, 1555-1559.
11. Lu, J.; Brummelheis, N. T.; Weck, M.; Intramolecular Folding of Triblock Copolymers via Quadrupole Interactions between Poly(styrene) and Poly(pentafluorostyrene) Blocks. *Chem. Commun.* **2014**, *50*, 6225-6227.
12. Dimroth, J.; Weck, M. Co-Salen Complexes as Catalysts for the Asymmetric Henry Reaction - Reversed Enantioselectivity through Simple Ligand Modification *RSC Adv.* **2015**, *5*, 29108-29113.
13. Moschetta, E.; Brunelli, N.A.; Jones, C. W.; Reaction-Dependent Heteroatom Modification of Acid-Base Catalytic Cooperativity in Aminosilica Materials. *Appl. Catal. A. Gen.* **2015**, in press.
14. Feng, Y.; Burns, L. A.; Lee, L.-C.; Murdock, C. R.; Sherrill, C. D.; Jones, C. W.; Co(III) Complexes of Tetradentate X<sub>3</sub>L Type Ligands: Synthesis, Electronic Structure, and Reactivity. *Inorg. Chim. Acta* **2015**, *430*, 30-35.
15. Kennedy, M. R.; Burns, L. A.; Sherrill, C. D. Counterion and Substrate Effects on Barrier Heights of the Hydrolytic Kinetic Resolution of Terminal Epoxides Catalyzed by Co(III)-salen. *J. Phys. Chem. A* **2015**, *119*, 403-409.
16. Lauwaert, J.; Moschetta, E. G.; Van Der Voort, P.; Thybaut, J.W.; Jones, C. W.; Marin, G. B.; Spatial Arrangement and Acid Strength Effects on Acid-Base Cooperatively-Catalyzed Aldol Condensation on Aminosilica Materials. *J. Catal.* **2015**, *325*, 19-25.
17. Moschetta, E. G.; Sakwa-Novak, M. A.; Greenfield, J. L.; Jones, C. W.; Post-Grafting Amination of Alkylhalide-Functionalized Silica for Applications in Catalysis, Adsorption and <sup>15</sup>N NMR Spectroscopy. *Langmuir* **2015**, *31*, 2218-2227.
18. Chun, B. J.; Kim, K. C.; Jang, S. S.; Molecular Dynamics Simulation Study of Sodium Dodecyl Sulfate Micelle: Water Penetration and Sodium Dodecyl Sulfate dissociation. *Colloids Surf. A.* **2015**, *474*, 36-43.

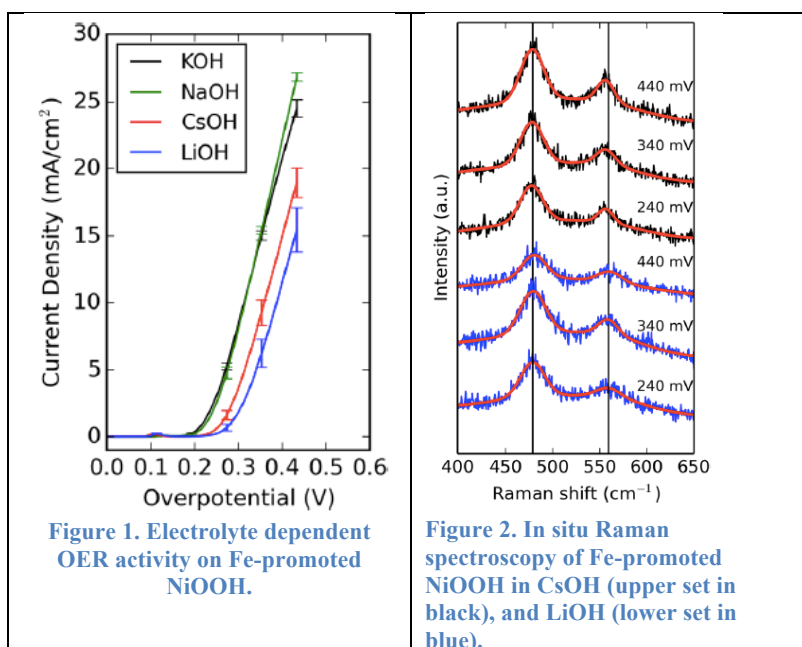
## Electrolyte dependent oxygen evolution catalysis on Ni-based electrocatalysts

John R. Kitchin

Department of Chemical Engineering, Carnegie Mellon University

**Poster Abstract**

Fe-promoted Ni hydroxide based electrocatalysts are among the best known for the oxygen evolution reaction in alkaline electrolytes. We found the activity of these electrocatalysts is also dependent on the electrolyte. LiOH consistently suppresses OER activity. Fe-promoted NiOOH had the highest activity in NaOH and KOH. Purified NiOOH in electrolytes purified of Fe showed the highest activity in CsOH at large overpotentials, and the lowest activity in LiOH. We used in situ Raman spectroscopy to probe the structure of the electrocatalysts under electrochemical oxygen evolution conditions. We find a subtle shift in the vibrational modes of the metal-oxygen bonds to lower wavenumbers in CsOH than in LiOH. We interpret this as a softening and lengthening of these bonds, which likely weakens them and makes them more active. Overall, the electrolyte is small compared to the effects of Fe-promotion, but they point to a new approach to improving electrocatalytic activity.



DESC0004031: Multifunctional Oxygen Evolution Electrocatalyst Design and Synthesis

PI: John Kitchin

Students: John Michael

RECENT PROGRESS

### Effect of DFT+U on trends in OER activity

It is known that standard DFT has some errors in it that are particularly notable in calculating oxide properties. Previous studies have shown scaling relations in the OER on metal oxides using standard DFT calculations. We investigated (Publication 5) whether using DFT+U would change those observations. We found that the scaling relations are preserved using DFT+U, but that U moves the calculations up and down the scaled correlation. We illustrated how a linear response approach to calculating U could reduce the ambiguity of which U value should be used.

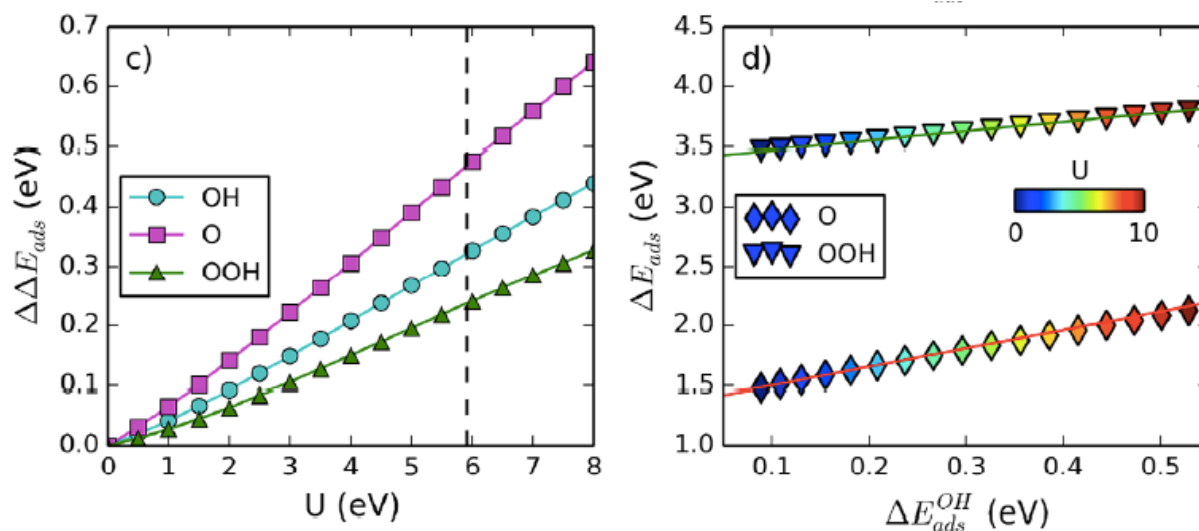


Figure 3. Illustration of the effect of U on adsorption energies of O, OH, and OOH on an oxide surface. On the right, these results are overlaid on the existing known scaling relations.

### Reproducible Research Tools

We have made significant progress in developing tools for documenting and sharing research methods and results. We now document all of our work in a plain text-based format called org-mode. This format enables one to embed source code into documents, run the code and capture the output. Additionally, one can embed images, links, and export the format to a variety of different formats including HTML and PDF. We published two perspectives on this approach recently (Publications 1 and 2).

### Publications Acknowledging this Grant in 2012-2015

1. John R. Kitchin, Examples of effective data sharing in scientific publishing, ACS Catalysis, accepted May 2015.
2. John R. Kitchin, Data sharing in Surface Science, Surface Science, Accepted May 2015.
3. John Michael, Ethan L. Demeter, Steven M. Illes, Qingqi Fan, Jacob R. boes, and John R. Kitchin, *Alkaline Electrolyte and Fe Impurity Effects on the Performance and Active-Phase*

*Structure of NiOOH Thin Films for OER Catalysis Applications*, J. Phys. Chem. C, Accepted May 2015. <http://pubs.acs.org/doi/abs/10.1021/acs.jpcc.5b02458>.

4. Zhongnan Xu, John R. Kitchin, *Relationships between the surface electronic and chemical properties of doped 4d and 5d late transition metal dioxides*, J. Chem. Phys. 142, 104703 (2015). <http://scitation.aip.org/content/aip/journal/jcp/142/10/10.1063/1.4914093>

5. Zhongnan Xu , Jan Rossmeisl , and John R. Kitchin, *A Linear Response, DFT+U Study of Trends in the Oxygen Evolution Activity of Transition Metal Rutile Dioxides*, Accepted J. Phys. Chem. C 119(9) 4827-4833 (2015). <http://pubs.acs.org/doi/abs/10.1021/jp511426q>.

6. Ethan L. Demeter , Shayna L. Hilburg , Newell R. Washburn , Terrence J. Collins , and John R. Kitchin, *Electrocatalytic Oxygen Evolution with an Immobilized TAML Activator*, Journal of the American Chemical Society, Accepted March 2014. <http://dx.doi.org/10.1021/ja5015986>

7. Mehta, Prateek; Salvador, Paul; Kitchin, John, *Identifying Potential BO<sub>2</sub> Oxide Polymorphs for Epitaxial Growth Candidates*", ACS Applied Materials and Interfaces, accepted 1/27/2014. <http://pubs.acs.org/doi/full/10.1021/am4059149>.

8. Zhongnan Xu and John R Kitchin, *Relating the Electronic Structure and Reactivity of the 3d Transition Metal Monoxide Surfaces*, Catalysis Communications, Accepted Oct 2013. <http://dx.doi.org/10.1016/j.catcom.2013.10.028>

9. Spencer D. Miller, Vladimir V. Pushkarev, Andrew J. Gellman and John R. Kitchin, *Simulating Temperature Programmed Desorption of Oxygen on Pt(111) Using DFT Derived Coverage Dependent Desorption Barriers*, Topics In Catalysis, 57(1), 106-117 (2013). <http://link.springer.com/article/10.1007%2Fs11244-013-0166-3>

10. Sneha A. Akhade and John R. Kitchin\*, *Effects of strain, d-band filling and oxidation state on the surface electronic structure and reactivity of 3d perovskite surfaces*, J. Chem. Phys. 137, 084703 (2012). <http://dx.doi.org/10.1063/1.4746117>

11. James Landon, Ethan Demeter, Nilay İnođlu, Chris Keturakis, Israel E. Wachs, Relja Vasić, Anatoly I. Frenkel, John R. Kitchin, *Spectroscopic characterization of mixed Fe-Ni oxide electrocatalysts for the oxygen evolution reaction in alkaline electrolytes*, ACS Catalysis, 2, 1793-1801 (2012). <http://dx.doi.org/10.1021/cs3002644>.

Ping Liu

**Promoting the activity and selectivity of catalysts towards CO<sub>2</sub> activation:  
mechanistic understanding and rational catalyst optimization**

Ping Liu, Jose A. Rodriguez, and Mike G. White

Brookhaven National Laboratory

**Presentation Abstract**

Optimization of catalyst behaviors in a rational way is of great importance in catalysis. Here, we made a coordinated experimental and theoretical effort to better understand promising Cu-based nanostructured catalysts, and to develop concepts to improve the CO<sub>2</sub> hydrogenation to methanol ( $\text{CO}_2 + 3\text{H}_2 \rightarrow \text{CH}_3\text{OH} + \text{H}_2\text{O}$ ). The combined density functional theory (DFT) and Kinetic Monte Carlo (KMC) simulation was able to well describe the catalytic behaviors of Cu catalysts observed experimentally. In addition, the descriptors that were able to control the overall conversion and selectivity to methanol were identified. Finally, on the basis of the descriptors, the catalyst optimization by forming alloys or depositing oxides was performed at a theoretical level. Our results not only pinpoint the effects of doping on the optimal reaction pathways, the possible intermediates and transition states, but also provide the guidance for rational design of better of Cu-based catalysts for methanol synthesis.

**FWP: CO-027**

**Mechanisms for the Water Gas Shift Reaction**

**PI:** Jose A. Rodriguez

**Co-PI:** Ping Liu, Senjaya Senanayake, Dario Stacchiola

**Postdoc(s):** Wenqian Xu (partly), Liang Yu (partly)

**Student(s):** Dimitriy Vovchok (Stony Brook University)

**Affiliations(s):** Brookhaven National Laboratory; Stony Brook University; Xiamen University

## RECENT PROGRESS

We made a coordinated experimental and theoretical effort to better understand promising transition metal catalysts supported on oxides or carbides, and to develop concepts for their improvement for the water gas shift (WGS,  $\text{CO} + \text{H}_2\text{O} \rightarrow \text{H}_2 + \text{CO}_2$ ) reaction. It combines three thrusts: (i) *in-situ* studies to determine catalyst structure, oxidation state and chemistry under reaction conditions; (ii) studies of relevant model systems, primarily based on nanoparticles supported on single crystal substrates; and (iii) computational modeling.

### *In-situ studies of WGS catalysts with XRD, PDF, XAFS and TEM*

The active phase of a series of metal/oxide powder catalysts (Pt/CeO<sub>2</sub>, Pt-Ru/CeO<sub>2</sub>, Pt/CeO<sub>x</sub>/TiO<sub>2</sub>, Au/CeO<sub>x</sub>/TiO<sub>2</sub>, Ce<sub>1-x</sub>Ni<sub>x</sub>O<sub>2-y</sub>, CeO<sub>x</sub>/CuO) was investigated using a combination of *in-situ* time-resolved X-ray diffraction (XRD), Pair-distribution function (PDF) analysis, X-ray absorption fine structure (XAFS) and environmental transmission electron microscopy (TEM). Under reaction conditions most of these WGS catalysts underwent chemical transformations that drastically modified their composition with respect to that obtained during the synthesis process. The active phase of catalysts which combine Cu, Ni, Au or Pt with oxides such as CeO<sub>2</sub>, TiO<sub>2</sub> and CeO<sub>x</sub>/TiO<sub>2</sub> essentially involved reduced oxides, which were not simple spectators, but facilitated the dissociation of water and in some cases modified the chemical properties of the supported metal. Therefore, to optimize the performance of these catalysts one must take into consideration the properties of the metal and oxide phases.

The ability to understand the role of morphology and structure on chemical reactivity is critical to further the understanding of structure-function relationships. We have studied the behavior of catalysts generated by depositing Cu upon nanostructured ceria (CeO<sub>x</sub>) supports (spheres, rods and cubes), see Figure 1. We

have discovered a distinct selectivity towards the water-gas shift and CO oxidation reactions likely driven through unique surface chemistries, metal-support interactions and faceting behavior of the supports that are prevalent in the structure of the support under reaction conditions.

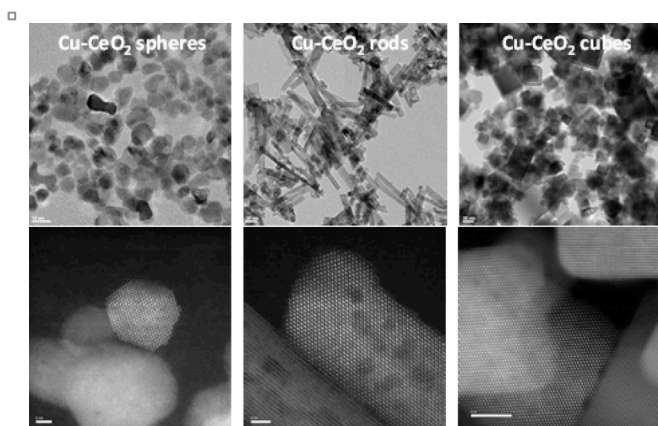


Fig. 1: Microscopy images of catalysts generated by the deposition of Cu on nanospheres, nanorods and nanocubes of ceria.

After performing pulse experiments for the WGS on these catalysts, we found a strong effect of the support morphology on the performance and behavior of these systems. The results showed that CuO/CeO<sub>2</sub> nanospheres exhibited a substantially better activity than CuO/CeO<sub>2</sub> nanocubes.

The higher activity was associated with the unique properties of CuO/CeO<sub>2</sub> nanospheres, such as the easier reduction of highly dispersed CuO to metallic Cu, the stability of metallic Cu and a larger concentration of Ce<sup>3+</sup> in the CeO<sub>2</sub> nanospheres.

Previous studies at BNL indicated that the Au/CeO<sub>x</sub>/TiO<sub>2</sub>(110) and Pt/CeO<sub>x</sub>/TiO<sub>2</sub>(110) model surfaces are excellent catalysts for the WGS. For powder catalysts, the activity measurements indicate that the Au/CeO<sub>x</sub>/TiO<sub>2</sub> catalysts are more active than plain Au/TiO<sub>2</sub>. The improvement in activity is very pronounced at 300°C. The ceria nanoparticles deposited on the titania powder act as anchoring sites for Au, reducing the sintering of the admetal and, thus, improving the long term stability of the Au/CeO<sub>x</sub>/TiO<sub>2</sub> catalysts. Powders of Pt/CeO<sub>x</sub>/TiO<sub>2</sub> were also excellent catalysts for the WGS. As a result of complex Pt↔ceria and ceria↔titania interactions, Pt/CeO<sub>x</sub>/TiO<sub>2</sub> catalysts are much more active and stable than Pt/CeO<sub>2</sub> or Pt/TiO<sub>2</sub> catalysts. The characterizations using a combination of TEM, XAFS or NEXAFS, and EELS point to the existence of a mixed-oxide interface in which the

$\text{Ce}^{3+}$  is trapped. Furthermore, *in situ* measurements with XANES indicate that the  $\text{Ce}^{4+}$  cations in the ceria nanoparticles are much easier to reduce than in bulk ceria. The Pt L<sub>3</sub>-edge spectra pointed to the initial presence of a  $\text{PtO}_x$  that got reduced to Pt under WGS reaction conditions at temperatures as low as 100°C. The ceria nanoparticles in contact with titania do have special electronic and spatial properties that contribute to the very high catalytic activity of Pt/CeO<sub>x</sub>/TiO<sub>2</sub>.

#### *Mechanistic study of WGS on well-defined model Catalysts*

A series of model catalysts (Cu surfaces, Metal (Pt, Cu, Ni, Au)/Oxide surface [CeO<sub>2</sub>(111), CeO<sub>x</sub>/TiO<sub>2</sub>(110), TiC(001)]) was used to study fundamental aspects of the WGS reaction. These studies revealed that the support can affect the reaction process in two different ways (Figure 2). First, the presence of vacancies greatly facilitates the water dissociation and the rest of reactions occur at the metal-support interface (bifunctional effect). And second, the electronic properties of the metal can be affected by interactions with the support producing special chemical properties to catalyze the WGS reaction (electronic effect).

The DFT calculations show that the electronic effect plays an essential role for the WGS reaction on Pt/CeO<sub>2</sub>(111) and Pt/CeO<sub>x</sub>/TiO<sub>2</sub>(110). The large electronic perturbations seen for small Pt particles in contact with ceria significantly enhanced the ability of the admetal to promote the bottleneck water dissociation, which was eventually used to oxidize CO via carboxyl (HOCO) intermediate. As a result, Pt/CeO<sub>2</sub>(111) is a highly active catalyst for the WGS reaction (Figure 3). When going from Pt(111) to Pt<sub>8</sub>/CeO<sub>2</sub>(111), the dissociation of water becomes a very exothermic process. The ceria-supported Pts appears as a fluxional system that can change geometry and charge distribution to better accommodate adsorbates.



Fig. 2: Water-gas shift reaction at a Pt/CeO<sub>2</sub> interface.

The reducibility of Pt/CeO<sub>2</sub> was greatly enhanced by the incorporation of Ga<sup>3+</sup> cations in the form of Pt/Ce<sub>80</sub>Ga<sub>20</sub>. These characteristics allowed the comparison of the formation of oxygen vacancies and the step water activation concerning the WGS mechanism on these systems. A series of experimental in situ and operando

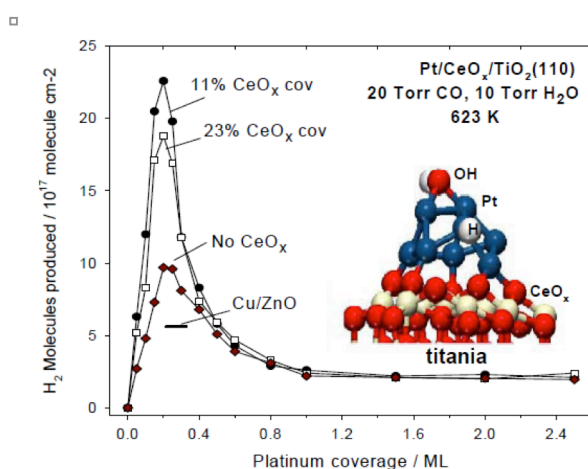


Fig. 3: Water-gas shift activity of Pt/TiO<sub>2</sub>(110) and Pt/CeO<sub>x</sub>/TiO<sub>2</sub>(111) as a function of Pt coverage. Inset: DFT-optimized structures for water dissociation on Pt<sub>8</sub>/CeO<sub>2</sub>.

techniques, combined with theoretical calculations allowed to gain information on the role of the oxygen vacancies in the WGS mechanism. The higher activity found on the Pt/CeO<sub>2</sub> cannot be correlated with the enhanced reducibility and reactivity with H<sub>2</sub>O of the Pt/Ce<sub>80</sub>Ga<sub>20</sub>. Therefore, the activation of water molecules in the WGS mechanism is not the rate limiting step in this system. The c-MES results suggest that the low

temperature WGS activity exhibited by Pt catalysts could be governed by another step in the “associative mechanism”, where monodentate formate (m-HCOO) and carboxylate (CO<sub>2</sub><sup>δ-</sup>) species at the metal-support interface could be the main reaction intermediates.

The electronic effect was also observed to play an essential role in accelerating the WGS reaction on Au/TiC(001). Experimentally, we found that the clean TiC(001) surface was able to catalyze the WGS. In fact, at 450 K, TiC(001) displays a WGS activity larger than that of Cu(111), a typical benchmark in WGS studies (Figure 4). Metallic Au does not catalyze the WGS, due to the hindered water dissociation. However, the addition of Au to TiC(001) produces a drastic increase in the WGS activity of the system. A maximum in the production of H<sub>2</sub> and CO<sub>2</sub> was observed at  $\theta_{Au} \approx 0.15$  ML. DFT calculations indicates that the active sites for the

WGS on Au/TiC(001) are small metal clusters in close contact with the support, similar to that observed for Au/oxide catalysts. The WGS reaction occurs preferentially at the Au sites, where the bottleneck water dissociation is greatly facilitated and the rest of the reaction follows an associative mechanism via HOCO species. The origin of promotion is associated with the electronic effect induced by the strong Au-TiC(001) interaction, which results in charge polarization and the enhancement of its chemical activity. As a result, the interaction of Au with TiC produces a large number of active  $\text{Au(OH)}_x$  species that are not present on surfaces of pure gold, and the other reaction steps for the WGS proceed on the admetal at a reasonable speed. The generation of a high concentration of active  $\text{Au(OH)}_x$  species probably proceeds faster on TiC(001) than on oxide surfaces, such as  $\text{TiO}_2(110)$  or  $\text{MgO}(001)$ . Furthermore, the 1:1 metal-to-carbon ratio in TiC provides stability and prevents the transformation of CO into methane. Thus, Au/TiC(001) is a highly active and selective catalyst for the low-temperature WGS reaction.

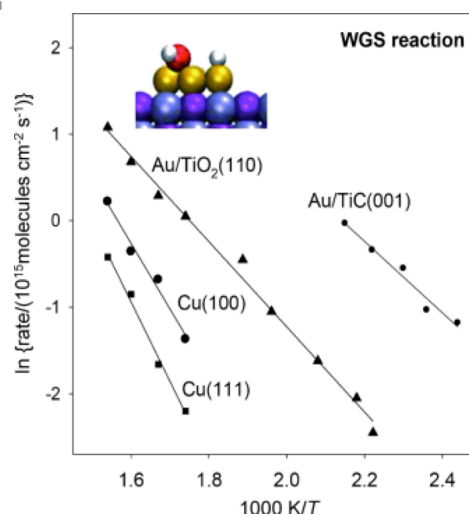


Fig. 4: Arrhenius plots for the WGS on Cu(111), Cu(100), Au/TiO<sub>2</sub>(110), and Au/TiC(001) catalysts (CO: 20 Torr; H<sub>2</sub>O: 10 Torr). Inset: structures for water dissociation on Au<sub>4</sub>/TiC(001) based on DFT.

#### *Theory-guided catalyst design for the WGS reaction*

What we learn from our studies of the WGS catalysts is that a good catalyst should be active enough to dissociate H<sub>2</sub>O, but still being able to oxidize and remove CO efficiently. Our previous theoretical studies show that the DFT-calculated reaction energy and activation barrier for H<sub>2</sub>O dissociation on pure metal (Au, Cu) and metal (Au,Cu)-oxide correlates with the WGS activity measured experimentally. By using oxides, an enhanced WGS activity should be observed due to the fact that

the oxides, in particular the reduced oxides, help the rate-limiting H<sub>2</sub>O dissociation via bifunctional effects. The strong metal-oxide interaction is likely to result in the reduction of oxides and therefore promote the WGS reaction at the interface.

Size-selected niobium oxide nanoclusters (Nb<sub>3</sub>O<sub>5</sub>, Nb<sub>3</sub>O<sub>7</sub>, Nb<sub>4</sub>O<sub>7</sub>, and Nb<sub>4</sub>O<sub>10</sub>) were deposited onto a Cu(111) surface and a thin film of Cu<sub>2</sub>O on Cu(111). According to TPD experiments with D<sub>2</sub>O, water dissociation occurred on all the clusters with Cu(111) support, while on the Cu<sub>2</sub>O film it was only observed for the reduced Nb<sub>3</sub>O<sub>5</sub> and Nb<sub>4</sub>O<sub>7</sub> clusters rather than the oxidized Nb<sub>3</sub>O<sub>7</sub> and Nb<sub>4</sub>O<sub>10</sub> clusters (Figure 5). Therefore, the promotion of NbO<sub>x</sub> clusters for the WGS activity of Cu is expected. The DFT calculations showed that this was due to the stronger Cu-NbO<sub>x</sub> interaction than that of Cu<sub>2</sub>O-NbO<sub>x</sub>. As a result, the oxidized Nb<sub>3</sub>O<sub>7</sub> cluster was reduced due to the charge transfer from Cu and therefore water dissociation was facilitated, while it stayed as the oxidized form on Cu<sub>2</sub>O support and no O-H bond cleavage was observed (Figure 5). That is, the strong metal-oxide interaction is able to produce and stabilize the reduced oxides, which is not stable in bulk, but is the key for promoting the WGS reaction at metal-oxide interfaces.

Overall, our systematic study using combined in-situ measurements of real catalysts with experimental and theoretical studies on well-defined model systems takes advantage of unique capabilities for in-situ studies in the BNL catalysis programs and at BNL facilities. Our approach allows more insight into the active sites and reaction mechanism for the WGS on promising metal-oxide catalysts.

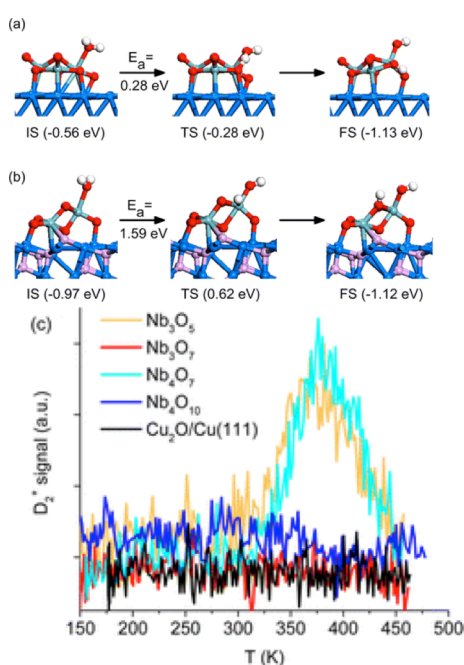


Fig. 5: (a,b) DFT optimized water dissociation on Nb<sub>3</sub>O<sub>7</sub>/Cu(111) and Nb<sub>3</sub>O<sub>7</sub>/Cu<sub>2</sub>O(111); (c) The D<sub>2</sub> signal from D<sub>2</sub>O TPD experiments for the clusters on Cu<sub>2</sub>O/Cu(111).

## Publications Acknowledging this Grant in 2012-2015

### 2012

1. Barrio, L.; Zhou, G.; González, I. D.; Estrella, M.; Hanson, J.; Rodriguez, J. A.; Navarro R. M.; Fierro J. L. G. In situ characterization of Pt catalysts supported on ceria modified TiO<sub>2</sub> for the WGS reaction: influence of ceria loading on catalytic behavior, *Phys. Chem. Chem. Phys.*, **2012**, *14*, 2192-2202.
2. Senanayake, S. D.; Sadowski, J.; Evans, J.; Kundu, S.; Agnoli, S.; Yang, F.; Stacchiola, D.; Flege, J.I.; Hrbek, J.; Rodriguez, J.A. Nanopatterning in CeO<sub>x</sub>/Cu(111): A New Mechanism for Surface Reconstruction and Enhancement of Catalytic Activity, *J. Phys. Chem. Lett.*, **2012**, *3*, 839-843.
3. Vidal, A.B.; Liu, P. Density Functional Study of Water-gas Shift Reaction on M<sub>3</sub>O(3x)/Cu(111), *Phys. Chem. Chem. Phys.* **2012**, *14*, 16626-16632.
4. Bruix, A.; Rodriguez, J.A.; Ramirez, P.J.; Senanayake, S.D.; Evans, J.; Park, J.B.; Stacchiola, D.; Liu, P.; Hrbek, J.; Illas, F. A New Type of Strong Metal-Support Interaction and the Production of H<sub>2</sub> through the Transformation of Water on Pt/CeO<sub>2</sub>(111) and Pt/CeO<sub>x</sub>/TiO<sub>2</sub>(110) Catalysts, *J. Am. Chem. Soc.* **2012**, *134*, 8968-8974.
5. Xu, W.; Si, R.; Senanayake, S. D.; Llorca, J.; Idriss, H.; Stacchiola, D.; Hanson, J. C.; Rodriguez, J.A. In situ Studies of CeO<sub>2</sub>-supported Pt, Ru, and Pt-Ru Alloy Catalysts for the Water-gas Shift Reaction: Active Phases and Reaction Intermediates, *J. Catal.* **2012**, *291*, 117-126.
6. Kubacka, A.; Si, R.; Michorczyk, P.; Martínez-Arias, A.; Xu, W.; Hanson, J. C.; Rodriguez, J. A.; Fernández-García, M. Tungsten as an Interface Agent Leading to Highly Active and Stable Cu-Ce Water Gas Shift Catalyst, *Applied Catal. B: Environmental*, **2012**, *132/133*, 423-432.

7. Si, R.; Tao, J.; Evans, J.; Park, J. B.; Barrio, L.; Hanson, J. C.; Zhu, Y.; Hrbek J.; Rodriguez, J.A. Effect of Ceria on Gold-Titania Catalysts for the Water-Gas Shift Reaction: Fundamental Studies for Au/CeO<sub>x</sub>/TiO<sub>2</sub>(110) and Au/CeO<sub>x</sub>/TiO<sub>2</sub> Powders, *J. Phys. Chem. C*, **2012**, *116*, 23547-23555.
8. Rodriguez, J.A. Supported Gold in CO Oxidation, the Water-gas Shift, and DeSO<sub>x</sub> Reactions, book chapter for *Supported Metals in Catalysis*, 2<sup>nd</sup> Edition (Editors: James Anderson and Marcos Fernandez-Garcia), Imperial College Press, London, 2012 (**invited book chapter**).

### **2013**

9. Ramírez Reina, T.; Xu, W.; Ivanova, S.; Centeno, M. A.; Hanson, J.; Rodriguez, J. A.; Odriozola, J. A. Operando Characterization of Iron-promoted Ceria-alumina Gold Catalysts during the Water-gas Shift Reaction, *Catal. Today*, **2013**, *205*, 41- 48.
10. Rodriguez, J.A.; Hanson, J. C.; Stacchiola D.; Senanayake S., In-situ/Operando Studies for the Production of Hydrogen through the Water-Gas Shift on Metal Oxide/Catalysts, *Phys. Chem. Chem. Phys.* **2013**, *15*, 12004-12025 (**invited**).
11. Mudiyansele, K.; Senanayake, S. D.; Feria, L.; Kundu, S.; Baber, A. E.; Graciani, J.; Vidal, A. B.; Agnoli, S.; Evans, J.; Chang, R.; Axnanda, S.; Liu, Z.; Sanz, J. F.; Liu, P.; Rodriguez, J. A.; Stacchiola D. J. Importance of the Metal–Oxide Interface in Catalysis: In Situ Studies of the Water–Gas Shift Reaction by Ambient-Pressure X-ray Photoelectron Spectroscopy, *Angew. Chem. Intl. Ed.* **2013**, *52*, 5101-5105.
12. Johnston-Peck, A.C.; Senanayake, S. D.; Plata, J. J.; Kundu, S.; Xu, W.; Barrio, L.; Graciani, J.; Fdez. Sanz, J.; Navarro, R. M.; Fierro, J.L.G.; Stach, E. A.; Rodriguez, J. A., Nature of the mixed-oxide interface in Ceria–Titania

- catalysts: clusters, chains, and nanoparticles, *J. Phys. Chem. C*, **2013**, *117*, 14463-14471.
13. Senanayake, S.D.; Rodriguez J.A.; Stacchiola, D. Electronic Metal–Support interactions and the production of hydrogen through the Water-Gas Shift reaction and ethanol steam reforming: fundamental studies with well-defined model catalysts, *Top. Catal.* **2013**, *56*, 1488-1498.
  14. Senanayake, S.D.; Stacchiola, D.; Rodriguez, J. A. Unique Properties of Ceria Nanoparticles Supported on Metals: Novel Inverse Ceria/Copper catalysts for CO Oxidation and the Water-Gas Shift Reaction, *Acc. Chem. Res.*, **2013**, *46*, 1702–1711 (**invited**).
  15. Mudiyansele, K.; Kim, H-Y.; Senanayake, S.D.; Baber, A.E.; Liu, P.; Stacchiola, D. Probing adsorption sites for CO on ceria, *Phys. Chem. Chem. Phys.*, **2013**, *15*, 15856-15862.
  16. Liu, P. Synergistic Effect of metal/oxide catalysts in the water-gas shift reactions: a theory-guided rational design of better catalysts” in *New and Future Developments in Catalysis: Hybrid Materials, Composites, and Organocatalysts*, 1st Edition, S. Suib (Ed.), Elsevier (2013) 213-241132 (**invited book chapter**).

## **2014**

17. Rodriguez, J. A.; Senanayake, S. D.; Stacchiola, D.; Liu, P.; Hrbek, J. The Activation of Gold and the Water-Gas Shift Reaction: Insights from Studies with Model Catalysts, *Acc. Chem. Res.*, **2014**, *47*, 773–782 (**invited**).
18. Zhao, F.; Liu, Z.; Xu, W.; Yao, S.; Kubacka, A.; Johnston-Peck, A. C.; Senanayake, S. D.; Zhang, A.-Q.; Stach, E.A.; Fernández-García, M.; Rodriguez, J.A. Water Gas Shift Reaction on Ni-W-Ce Catalysts: Catalytic Activity and Structural Characterization, *J. Phys. Chem. C*, **2014**, *118*, 2528–2538.

19. Rodriguez, J. A.; Ramirez, P. J.; Asara, G. G.; Viñes, F.; Evans, J.; Liu, P.; Ricart, J. M.; Illas, F. Charge Polarization at a Au-TiC Interface and the Generation of Highly Active and Selective Catalysts for the Low-Temperature Water Gas Shift Reaction, *Angew. Chem. Int. Ed.*, **2014**, *53*, 11270-11274.
20. Yao, S. Y.; Xu, W. Q.; Johnston-Peck, A. C.; Zhao, F. Z.; Liu, Z. Y.; Lou, S.; Senanayake, S. D.; Martines-Arias, A.; Liu, W. J.; Rodriguez, J. A. Morphological Effects of the Nanostructured Ceria Support on the Activity and Stability of CuO/CeO<sub>2</sub> Catalysts for the Water-gas Shift Reaction, *Phys. Chem. Chem. Phys.* **2014**, *16*, 17183-17195.
21. Vecchiotti, J. Bonivardi, A.; Xu, W.; Stacchiola, D. Delgado, J. J.; Calatayud, M.; Collins, S, Understanding the role of oxygen vacancies in the water gas shift reaction on ceria-supported platinum catalysts, *ACS Catal.* **2014**, *4*, 2088–209.

## **2015**

1. Zhao, F. Z.; Liu, Z. Y.; Xu, W. Q.; Yao, S. Y.; Si, R.; Johnston-Peck, A. C.; Martines-Arias, A.; Hanson, J. C.; Senanayake, S. D.; Rodriguez, J. A. Pulse Studies to Decipher the Role of Surface Morphology in CuO/CeO<sub>2</sub> Nanocatalysts for the Water Gas Shift Reaction, *Catal. Lett.* **2015**, *145*, 808-815.
2. Mudiyansele, K.; Senanayake, S. D.; Ramirez, P. J.; Kundu, S.; Baber, A. E.; Yang, F.; Agnoli, S.; Axnanda, S.; Liu, Z.; Hrbek, J.; Evans, J.; Rodriguez, J. A.; Stacchiola, D. Intermediates arising from the Water-Gas Shift Reaction over Cu Surfaces: From UHV to Near Atmospheric Pressures” *Top. Catal.* **2015**, *58*, 271–280.
3. Mudiyansele, K.; Baber, A. E.; Liu, Z.; Senanayake, S. D.; Stacchiola, D. Isolation and Characterization of Formates on CeO<sub>x</sub>-Cu<sub>y</sub>O/Cu(111), *Catal. Today* **2015**, *240*, 190–200.

4. Nakayama, M.; Xue, M.; An, W.; Liu, P.; White, M. G. Influence of Cluster-Support Interactions on Reactivity of Size-Selected Nb<sub>x</sub>O<sub>y</sub> Clusters, *J. Phys. Chem. C*, **DOI:** 10.1021/acs.jpcc.5b00691.

## Neutron Spectroscopy in Catalysis

Daniel A. Lutterman,<sup>†</sup> Michelle K. Kidder,<sup>†</sup> Luke L. Daemen<sup>‡</sup>

Chemical Sciences Division<sup>†</sup> and Chemical and Engineering Materials Division<sup>‡</sup>  
Oak Ridge National Laboratory

### Presentation Abstract

Heterogeneous catalysis remains a critical area of research, both at the fundamental and industrial levels. At a basic level, great strides have been made in understanding the molecule-surface interaction in simple system but there is still a lack of understanding of the mechanisms and dynamics of catalyzed reactions. We have begun utilizing neutron scattering techniques to understanding the surface chemistry of small organic molecules on catalyst surfaces, thanks to its great sensitivity to hydrogen. Recently, we have used quasielastic neutron scattering to probe the motion of tethered organic molecules in the pores of mesoporous silicas, and explored the effects of intermolecular hydrogen bonding between the tethered molecules and the silica surface and intramolecular hydrogen bonding within the tethered molecules. These studies have shown both the local geometry and timescale of the motion, and revealed how the molecular motion is dependent on grafting density and pore diameter.

Attention is now turning toward (1) the elucidation of reaction mechanisms and the identification of reactive intermediates, and (2) the study of reaction kinetics *in situ*. Traditionally, reaction mechanisms have been inferred indirectly from kinetic or thermodynamic data. The ability to follow a chemical reaction in real time and identify intermediates with neutron spectroscopy is enabled for the first time on VISION thanks to the extremely large flux and event mode data collection (which permits data reslicing after the experiment). With a new catalysis sample environment being developed at VISION, we will have the ability to conduct kinetic measurements simultaneously with the use of a microscopic level probe (inelastic neutron scattering), thereby coupling macroscopic kinetics with a microscopic view of catalytic chemistry. The simplicity of the neutron-nucleus interaction permits the quantitative computation of the neutron vibrational spectrum of an adsorbed species. Both mode frequencies and symmetry (intensities) can be computed exactly and routinely by means of simple density functional theory (DFT). This is emphatically more difficult to do with optical vibrational spectroscopies which rely on the more complex electron-photon interaction. The ability to predict vibrational spectra quantitatively for direct comparison with neutron experimental data provides an exquisitely sensitive test of the validity of the model (and therefore microscopic picture/understanding) of the system under consideration. No other technique permits such a potent degree of validation of structural/dynamic modeling of an adsorbate/adsorbent system.

**Elucidating the Mechanism for the Catalytic Hydrodeoxygenation of Phenols**

Alyssa J. R. Hensley<sup>a</sup>, Yong Wang<sup>a,b</sup>, Donghai Mei<sup>b</sup>, Jean-Sabin McEwen<sup>a\*</sup>

<sup>a</sup>Washington State University (WSU), Voiland School of Chemical Engineering and Bioengineering, Pullman, WA 99164

<sup>b</sup>Pacific Northwest National Laboratory, Institute for Integrated Catalysis, Richland, WA 99354

**Presentation Abstract**

One aspect crucial to the design of effective catalysts is knowledge of the elementary reaction mechanism, which is difficult to divine from experiment alone. However, first principle modeling techniques can be used to address this knowledge gap. An area currently in need of such fundamental insight is the hydrodeoxygenation (HDO) of bio-oil to create useable biofuels. Recent work has shown that Fe-based bimetallic catalysts are highly active for the HDO of phenolic and furanic compounds. In order to better design and optimize these bimetallic catalysts, we use density functional theory to quantify the metal-metal and surface-adsorbate interactions. Here, we present a study of the conversion of phenol to benzene on Fe (110) and Pd (111). We studied five different mechanisms which fell under the three typical HDO mechanism categories: hydrogenation, where the hybridization of the oxygen bonded carbon is altered from  $sp^2$  to  $sp^3$  prior to oxygen removal; direct deoxygenation, where the oxygen group is removed without altering the carbon backbone; and tautomerization, where the phenol converts to its respective ketone before being hydrogenated and the oxygen group removed. Under ultra-high vacuum (UHV) conditions, the deoxygenation of phenol was found to be highly unfavorable on Pd (111) while on Fe (110), all mechanisms were exothermic and the direct deoxygenation mechanism was found to be most favorable. While these UHV studies provide significant insight into the reactions occurring on the catalyst surface under typical experimental conditions, liquid bio-oil has a high concentration of water which can significantly affect the surface species and reaction mechanisms. In order to understand how water could affect the HDO mechanisms of phenol on Fe (110), we re-examined the HDO mechanisms under an aqueous environment and the results show that the presence of water only significantly affects elementary reactions involving the movement of hydrogen, promoting the hydrogenation and tautomerization mechanisms. Furthermore, the presence of hydroxyl on the Fe (110) surface was found to be crucial in hydrogenating the aromatic ring with the surface hydroxyl acting as Brønsted acid sites. The results provide significant insight into the deoxygenation of phenols on promoted Fe bimetallic catalysts by elucidating the catalytic function of noble and base metal surfaces, as well as the effect of water on the Fe surface and HDO mechanism. This information will allow for the further tailoring of the catalyst surface for the promotion of the deoxygenation reaction.

## Grant: Nanostructured Catalysts for Hydrogen Generation from Renewable Feedstocks

**PI:** Abhaya Datye (UNM) and Yong Wang (WSU)

**Postdoc(s):** Zhang He (WSU), Junming Sun (WSU), Barr Halevi (UNM)

**Student(s):** Jonathan Paiz (UNM), Angelica Benavidez (UNM), Eric Petersen (UNM), Stephen Davison (WSU), Yongchun Hong (WSU), Johnny Nogales (UNM), Aaron Jenkins (UNM), Monique Cordova (UNM)

**Affiliations(s):** University of New Mexico (UNM) Dept. of Chemical & Nuclear Engineering Albuquerque, NM 87131-0001

### Publications Acknowledging this Grant in 2012-2015

1. Sun, J.; Karim, A. M.; Zhang, H.; Kovarik, L.; Li, X.; Hensley, A. J. R.; McEwen, J.-S.; Wang, Y. Carbon Supported Bimetallic Pd-Fe Catalysts for Vapor-Phase Hydrodeoxygenation of Guaiacol J. Catal. 2013, 306, 47-57.
2. Hensley, A. J. R.; Hong, Y.; Zhang, R.; Zhang, H.; Sun, J.; Wang, Y.; McEwen, J.-S. Enhanced Fe<sub>2</sub>O<sub>3</sub> Reducibility via Surface Modification with Pd: Characterizing the Synergy within Pd/Fe Catalysts for Hydrodeoxygenation Reactions ACS Catal. 2014, 4, 3381-3392.
3. Hong, Y.; Zhang, H.; Sun, J.; Ayman, K. M.; Hensley, A. J. R.; Gu, M.; Engelhard, M. H.; McEwen, J.-S.; Wang, Y. Synergistic Catalysis between Pd and Fe in Gas Phase Hydrodeoxygenation of *m*-Cresol ACS Catal. 2014, 4, 3335-3345.
4. Hensley, A. J. R.; Wang, Y.; McEwen, J.-S. Adsorption of Phenol on Fe (110) and Pd (111) from First Principles Surf. Sci. 2014, 630, 244-253.
5. Hensley, A. J. R.; Wang, Y.; McEwen, J.-S. Phenol Deoxygenation Mechanisms on Fe (110) and Pd (111) ACS Catal. 2015, 5, 523-536.
6. Hensley, A. J. R.; Wang, Y.; McEwen, J.-S. Adsorption of Guaiacol on Fe (110) and Pd (111) from First Principles Surf. Sci. 2015, submitted.

## RECENT PROGRESS

### *Aqueous Phase Mechanistic Studies*

*Ab initio* studies were performed to determine the dominant phenol deoxygenation mechanism on Fe (110) in the aqueous environment. *Ab initio* molecular dynamics simulations were run on the high concentration, liquid water, system with phenol in order to optimize the aqueous, hydrogen bonding network in preparation for the mechanistic studies. Each of the three probable mechanisms identified based on our ultra-high vacuum work (Figure 1) were examined under the aqueous environment. Specifically, in the aqueous environment, we examined the reaction steps that were identical to those under ultra-high vacuum, as well as new mechanisms that could only occur in the presence of water due to the hydrogen bonding network of the aqueous system. Based on these studies, we came to four major conclusions concerning the dominant deoxygenation mechanism and the effect of water on said mechanism on the Fe (110) surface.

First, for reactions that did not directly involve the water molecules surrounding the phenol adsorbate, the presence of the aqueous environment had only a minor effect on the activation and reaction energies. This is shown in Figure 2 where we present the DHOx mechanism under both the ultra-high vacuum and aqueous environments. These results show that the addition of the aqueous environment slightly increases the activation energies for both elementary steps while the reaction energy is slightly increased for the C-O cleavage step (Figure 5A-C) and slightly decreased for the benzene formation step (Figure 5C-E). The maximum energy change for both the activation and reaction energies with the addition of water to the system in 0.25 eV, which is small compared to the activation energies involved in the reaction mechanisms that were examined.

Second, the presence of the aqueous environment greatly reduced the activation energies for reactions involving the movement of hydrogen, e.g. hydrogenation reactions, by moving the hydrogen through the hydrogen bonding network. As our proposed mechanisms (Figure 1) involved a total of seven steps requiring the movement of hydrogen, only an example of the hydrogenation reaction acceleration via the hydrogen bonding network is shown in Figure 3 for the Taut. & DHOx mechanism. Here, we can see that the addition of the liquid water around the adsorbed phenol significantly reduces the barrier for the tautomerization reaction by passing hydrogen through the hydrogen bonding network (Figure 3A-C). This result is consistent with previous work by Yoon, et al. on Pt and Ni (111).<sup>3</sup> Furthermore, we found that hydrogenation reactions (Figure 3G-I) have significantly smaller barriers when a hydrogen atom is moved from a surface hydroxyl through the hydrogen bonding network before being added to the aromatic ring. This result shows that hydroxyl groups on the Fe (110) surface can act as Brønsted acid sites, donating hydrogen to the hydrogen bonding network to greatly accelerate hydrogenation reactions. Overall, hydrogenation reactions via the movement of hydrogen through the hydrogen bonding network (e.g. tautomerization and Brønsted acid sites) decreases the activation barrier for the hydrogenation reaction by 0.6-1.0 eV as compared to hydrogenation reactions involving surface hydrogen directly.

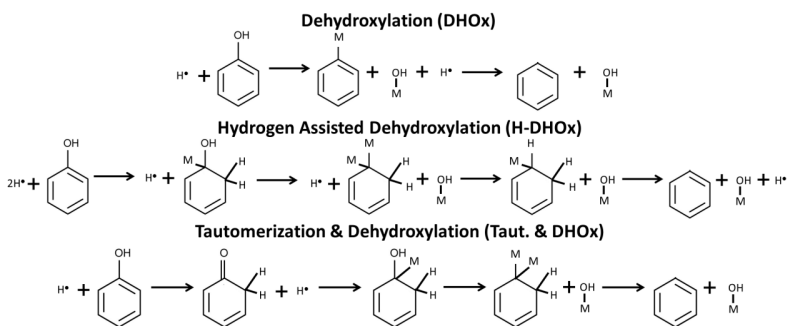


**Figure 1.** Proposed possible reaction mechanisms by which phenol could be deoxygenated on a catalyst surface. We note that M denotes a metallic site.

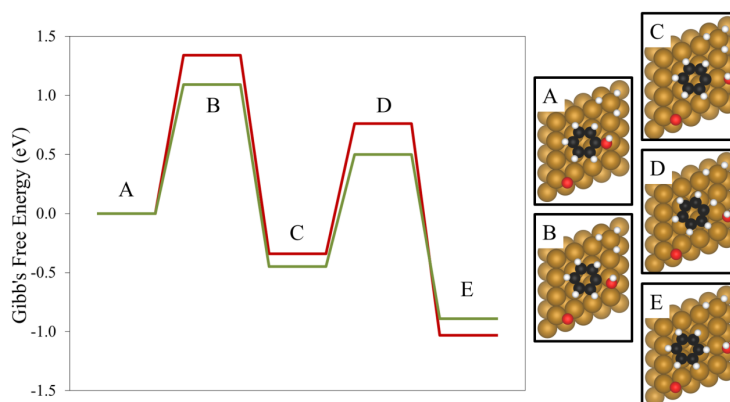


**Figure 2.** Gibb's free energy profile for phenol's DHOx mechanism under the ultra-high vacuum (green) and aqueous (red) environments on Fe (110). The structures shown on the right are for the aqueous environment with all water molecules uninvolved in the reaction removed for clarity. The gold, black, white, and red spheres represent Fe, C, H, and O, respectively.

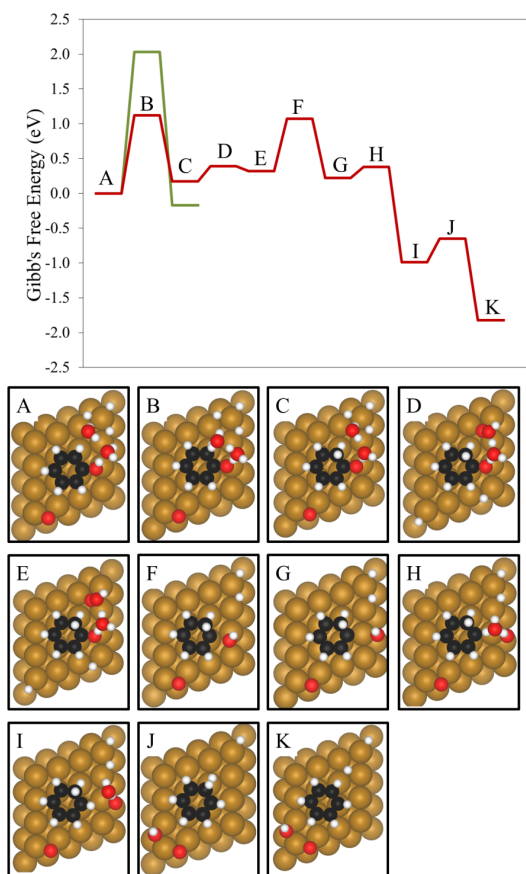


**Figure 3.** Gibb's free energy profile for phenol's Taut. &DHOx mechanism under the ultra-high vacuum (green) and aqueous (red) environments on Fe (110). The structures shown on the bottom are for the aqueous environment with all water molecules uninvolved in the reaction removed for clarity. Sphere coloring is identical to Figure 2. For the ultra-high vacuum system, only the tautomerization reaction was examined (first step) due the large activation barrier of this reaction.

higher thermodynamic driving force as compared with the other mechanisms. However, the rate limiting steps for all three mechanisms is the first step and all mechanisms have similar energy barriers, making each mechanism competitive under the aqueous environment.

Fourth, our work shows that the most likely rate limiting step in the deoxygenation of phenol is the hydrogenation of surface oxygen to hydroxyl. As Fe surfaces are known to be easily oxidized and our previous work has shown that surface hydroxyl groups are crucial to accelerating hydrogenation reactions on Fe (110), it is crucial to hydrogenate surface oxygen to hydroxyl groups in order to keep the Fe surface active for the adsorption and deoxygenation of phenols.

This more recent theoretical work in the aqueous phase was supported by the U.S. Department of Energy, Office of Science, Office of Workforce Development for Teachers and Scientists, Office of Science Graduate Student Research (SCGSR) program. The SCGSR program is administered by the Oak Ridge Institute for Science and Education for the DOE under contract number DE-AC05-06OR23100.

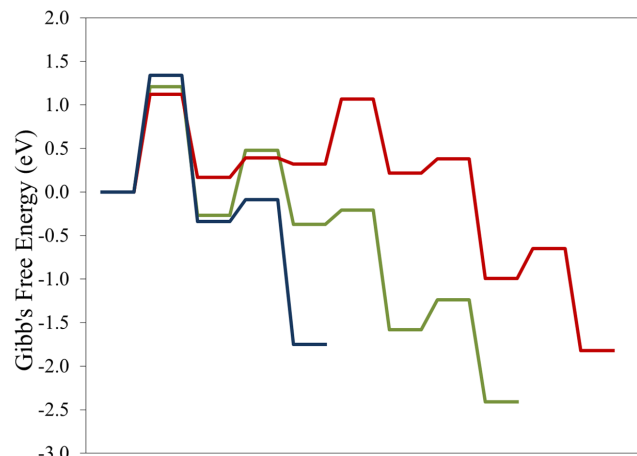


**Figure 4.** Gibb's free energy profile for the most energetically favorable pathways for phenol's deoxygenation via the DHOx (blue), H-DHOx (green), and Taut. &DHOx (red) mechanisms under the aqueous environment on Fe (110).

Third, we have compared the overall most favorable pathways for the three proposed reactions (Figure 1) and have found that the addition of both Brønsted acid sites on the Fe (110) surface and the hydrogen bonding network decreases the energy barriers for the tautomerization and hydrogenation reactions, making it clear that all three of the proposed mechanisms occur simultaneously on the Fe (110) surface under an aqueous environment. The Gibb's free energy profiles for each of the proposed mechanisms are shown in Figure 4. These results show that the H-DHOx mechanism has the most exothermic, overall reaction energy, making this the most likely mechanism to occur on Fe (110) in an aqueous environment due to the

**C. Buddie Mullins**

**Pd-Au Surface Chemistry - Effects of Water on Ethanol Oxidation over Au/TiO<sub>2</sub>**

G. M. Mullen, W.-Y. Yu, L. Zhang, E. J. Evans, Jr., G. Henkelman, C. B. Mullins  
University of Texas at Austin, Departments of Chemical Engineering and Chemistry

**Presentation Abstract**

Pd–Au catalysts are promising regarding the selective production of hydrogen via formic acid (HCOOH). Yet, the key factors controlling the catalytic performance (e.g., activity and selectivity) of Pd–Au bimetallic catalysts for HCOOH decomposition remain under debate. In order to explore the factors governing the catalytic properties of Pd–Au bimetallic catalyst, we have conducted model catalyst studies employing temperature-programmed desorption (TPD) and reactive molecular beam scattering (RMBS). Our results have revealed that Pd atoms at the Pd–Au surface are responsible for activating HCOOH molecules. Furthermore, the selectivity of the reaction is influenced by the atoms adjacent to the active Pd site. Pd atoms residing at Pd–Au interface sites tend to favor dehydrogenation of HCOOH, whereas Pd atoms that lack neighboring Au atoms favor dehydration of HCOOH. These observations suggest that the reactivity and selectivity of HCOOH decomposition on Pd–Au catalysts could be optimized by controlling the arrangement of surface Pd and Au ensembles.

Water has been shown to have a significant enhancement effect on gold catalyzed CO oxidation. Incorporation of water into the reactant feed stream in just ppm quantities can enhance CO oxidation activity by several orders of magnitude for some gold catalysts. Despite the widespread acceptance of this phenomenon for the CO oxidation reaction, the effects of water have been largely ignored for other catalytic reactions. Model catalyst studies from our group have shown that hydroxyl species on the gold surface generated in the presence of water can partake in the partial oxidation of alcohols and may play a role in dictating the selectivity of these processes. We are currently studying the effects of water on partial oxidation of ethanol over Au/TiO<sub>2</sub> in an attempt to extend the observations made in our model catalyst studies to high surface area, ambient pressure conditions.

**Grant # DE-FG02-04ER15587: Surface Chemistry of Gold Model Catalysts**

**PI:** Charles Buddie Mullins

**Postdocs:** N/A

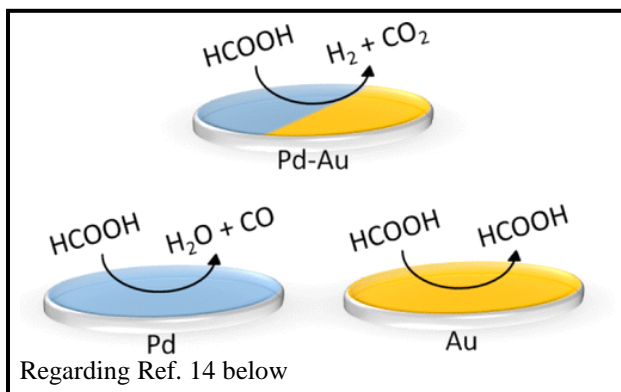
**Students:** Gregory M. Mullen, Adrian J. Brush, Wen-Yueh Yu, Edward J. Evans, Jr.

**RECENT PROGRESS**

***Selective Hydrogen Production from Formic Acid Decomposition on Pd–Au Bimetallic Surfaces***

Pd–Au catalysts have shown exceptional performance for selective hydrogen production via HCOOH decomposition, a promising alternative to solve issues associated with hydrogen storage and distribution. In this study, we have utilized temperature-programmed desorption (TPD) and reactive molecular beam scattering (RMBS) in an attempt to unravel the factors governing the catalytic properties of Pd–Au bimetallic

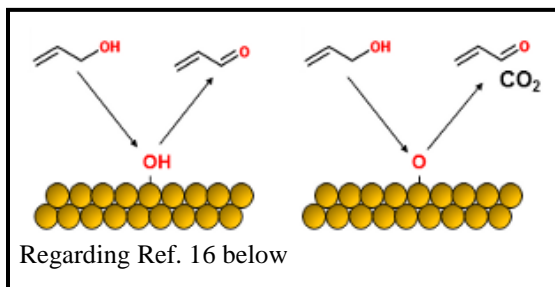
surfaces for HCOOH decomposition. Our results show that Pd atoms at the Pd-Au surface are responsible for activating HCOOH molecules; however, the selectivity of the reaction is dictated by the identity of the surface metal atoms adjacent to the Pd atoms. Pd atoms that reside at Pd-Au interface sites tend to favor dehydrogenation of HCOOH; whereas, Pd atoms in Pd(111)-like sites, which lack neighboring Au atoms, favor dehydration of HCOOH. These observations suggest that the reactivity and selectivity of HCOOH



decomposition on Pd-Au catalysts can be tailored by controlling the arrangement of surface Pd and Au atoms.

### ***Control of Selectivity in Allylic Alcohol Oxidation on Gold Surfaces: The Role of Oxygen Adatoms and Hydroxyl Species***

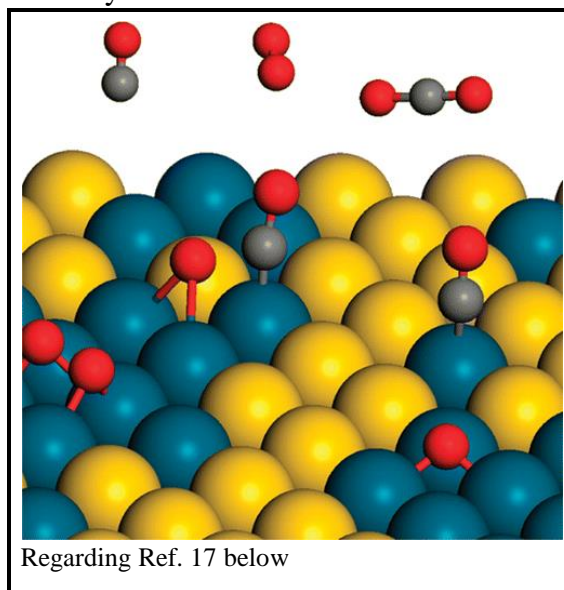
Gold catalysts display high activity and good selectivity for partial oxidation of a number of alcohol species. In this work, we discuss the effects of oxygen adatoms and surface hydroxyls on the selectivity for oxidation of allylic alcohols (allyl alcohol and crotyl alcohol) on gold surfaces. Utilizing temperature programmed desorption (TPD), reactive molecular beam scattering (RMBS), and density functional theory (DFT) techniques, we provide evidence to suggest that the selectivity displayed towards partial oxidation versus combustion pathways is dependent on the type of oxidant species present on the gold surface. TPD and RMBS results suggest that surface hydroxyls promote partial oxidation of allylic alcohols to their corresponding aldehydes with very high selectivity, while oxygen adatoms promote both partial oxidation and combustion pathways. DFT calculations indicate that oxygen adatoms can react with acrolein to promote the formation of a bidentate surface intermediate, similar to structures that have been shown to decompose to generate combustion products over other transition metal surfaces. Surface hydroxyls do not readily promote such a process.



### ***Oxygen Activation and Reaction on Pd–Au Bimetallic Surfaces***

Pd–Au bimetallic catalysts have shown promising performance for a number of oxidative reactions. The present study utilizes reactive molecular beam scattering (RMBS), reflection-absorption infrared spectroscopy (RAIRS), temperature-programmed desorption (TPD) and density functional theory (DFT) techniques in attempt to enhance fundamental understanding of oxygen activation and reaction with CO on Pd–Au surfaces. Our results reveal that the presence of contiguous Pd sites is

crucial for adsorption of oxygen molecules on Pd/Au(111) surfaces at 77 K. Upon heating, oxygen admolecules desorbed molecularly without detectable dissociation in O<sub>2</sub>-TPD measurements. CO-RMBS experiments indicate that at lower temperatures (77-150 K), oxygen admolecules were readily displaced by CO due to competitive adsorption. Oxygen admolecules can be thermally activated at higher temperatures (180-250 K) to react with CO to form CO<sub>2</sub>. DFT calculations show that the Pd–Au surface containing larger Pd ensembles favors dissociative CO oxidation, whereas associative CO oxidation and O<sub>2</sub> desorption are the two main competing processes for the Pd–Au surface containing small Pd ensembles. An associative CO oxidation pathway was not experimentally observed, which is likely due to facile CO-induced O<sub>2</sub> desorption.



### Publications Acknowledging this Grant in 2012-2015

1. Pan, M.; Pozun, Z. D.; Yu, W.-Y.; Henkelman, G.; Mullins, C. B. Structure revealing H/D exchange with co-adsorbed hydrogen and water on gold. *J. Phys. Chem. Lett.* **2012**, *3*, 1894-1899. <http://dx.doi.org/10.1021/jz3007707>
2. Pan, M.; Pozun, Z. D.; Brush, A. J.; Henkelman, G.; Mullins, C. B. Low-temperature chemoselective gold-surface-mediated hydrogenation of acetone and propionaldehyde. *ChemCatChem* **4**, 1241-1244 (2012). <http://dx.doi.org/10.1002/cctc.201200311>
3. Yan, T.; Redman, D. W.; Yu, W.-Y.; Flaherty, D. W.; Rodriguez, J. A.; Mullins, C. B. CO oxidation on inverse Fe<sub>2</sub>O<sub>3</sub>/Au(111) model catalysts. *J. Catal.* **2012**, *294*, 216-222. <http://dx.doi.org/10.1016/j.jcat.2012.07.024>
4. Pan, M.; Brush, A. J.; Dong, G.; Mullins, C. B. Tunable ether production via coupling of aldehydes or aldehyde/alcohol over hydrogen-modified gold catalysts at low temperature. *J. Phys. Chem. Lett.* **2012**, *3*, 2512-2516. <http://dx.doi.org/10.1021/jz301105e>
5. Brush, A. J.; Pan, M.; Mullins, C. B. Methanol O-H bond dissociation on H-precovered gold originating from a structure with a wide range of surface stability. *J. Phys. Chem. C* **2012**, *116*, 20982-20989. <http://dx.doi.org/10.1021/jp308099y>
6. Pan, M.; Ham, H. C.; Yu, W.-Y.; Hwang, G. S.; Mullins, C. B. Highly selective, facile NO<sub>2</sub> reduction to NO at cryogenic temperatures on H precovered gold. *J. Am. Chem. Soc.* **2013**, *135*, 436-442. <http://dx.doi.org/10.1021/ja3096575>

7. Pan, M.; Brush, A. J.; Pozun, Z. D.; Ham, H. C.; Yu, W.-Y.; Henkelman, G.; Hwang, G. S.; Mullins, C. B. Model studies of heterogeneous catalytic hydrogenation reactions with gold. *Chem. Soc. Rev.* **2013**, *42*, 5002-5013. <http://dx.doi.org/10.1039/c3cs35523c>
8. Mullen, G. M.; Pan, M.; Yan, T.; Gong, J.; Mullins, C. B. The effects of adsorbed water on gold catalysis and surface chemistry. *Top. Catal.* **2013**, *56*, 1499-1511. <http://dx.doi.org/10.1007/s11244-013-0143-x>
9. Yu, W.-Y.; Mullen, G. M.; Mullins, C. B. Hydrogen adsorption and absorption with Pd-Au bimetallic surfaces. *J. Phys. Chem. C* **2013**, *117*, 19535-119543. <http://dx.doi.org/10.1021/jp406736b>
10. Pan, M.; Yan, T.; Gong, J.; Dong, G.; Mullins, C. B. Model studies with gold: A versatile oxidation and hydrogenation catalyst. *Acc. Chem. Res.* **2014**, *47*, 750-760. <http://dx.doi.org/10.1021/ar400172u>
11. Yu, W.-Y.; Mullen, G. M.; Mullins, C. B. Interactions of hydrogen and carbon monoxide on Pd-Au bimetallic surfaces. *J. Phys. Chem. C* **2014**, *118*, 2129-2137. <http://dx.doi.org/10.1021/jp411299e>
12. Fosdick, S. E.; Berglund, S. P.; Mullins, C. B.; Crooks, R. M. Evaluating electrocatalysts for the hydrogen evolution reaction based on bi- and trimetallic combinations of Co, Fe, Ni, Mo, and W using bipolar electrode arrays. *ACS Catal.* **2014**, *4*, 1332-1339. <http://dx.doi.org/10.1021/cs400168t>
13. Mullen, G. M.; Zhang, L.; Evans Jr., E. J.; Yan, T.; Henkelman, G.; Mullins, C. B. Oxygen and hydroxyl species induce multiple reaction pathways for the partial oxidation of allyl alcohol on gold. *J. Am. Chem. Soc.* **2014**, *136*, 6489-6498. <http://dx.doi.org/10.1021/ja502347d>
14. Yu, W.-Y.; Mullen, G. M.; Flaherty, D. W.; Mullins, C. B. Selective hydrogen production from formic acid decomposition on Pd-Au bimetallic surfaces. *J. Am. Chem. Soc.* **2014**, *136*, 11070-11078. <http://dx.doi.org/10.1021/ja505192v>
15. Mullen, G. M.; Mullins, C. B. Water's place in Au catalysis. *Science* **2014**, *345*, 1564-1565. <http://www.sciencemag.org/content/345/6204/1564.short>
16. Mullen, G. M.; Zhang, L.; Evans Jr., E. J.; Yan, T.; Henkelman, G.; Mullins, C. B. Control of selectivity in allylic alcohol oxidation on gold surfaces: the role of oxygen adatoms and hydroxyl species. *Phys. Chem. Chem. Phys.* **2015**, *17*, 4730-4738. <http://dx.doi.org/10.1039/C4CP04739G>
17. Yu, W.-Y.; Zhang, L.; Mullen, G. M.; Henkelman, G.; Mullins, C. B. Oxygen Activation and Reaction on Pd-Au Bimetallic Surfaces. accepted by *J. Phys. Chem. C*. <http://dx.doi.org/10.1021/acs.jpcc.5b02970>

**DE-FOA-0001204: Institute for Catalysis in Energy Processes**

**Lead PI:** Peter C. Stair<sup>1</sup>

**ICEP PIs:** Michael J. Bedzyk,<sup>3</sup> Linda J. Broadbelt,<sup>2</sup> Massimiliano Delferro,<sup>1</sup> Omar K. Farha,<sup>1</sup> Franz M. Geiger,<sup>1</sup> Joseph T. Hupp,<sup>1</sup> Harold H. Kung,<sup>2</sup> Laurence D. Marks,<sup>3</sup> Tobin J. Marks,<sup>1</sup> SonBinh T. Nguyen,<sup>1</sup> Justin M. Notestein,<sup>2</sup> Kenneth R. Poeppelmeier,<sup>1</sup> George C. Schatz,<sup>1</sup> Neil Schweitzer,<sup>2</sup> Randall Q. Snurr,<sup>2</sup> Richard P. Van Duyne,<sup>1</sup> Eric Weitz,<sup>1</sup>

**Affiliations(s):** <sup>1</sup>Department of Chemistry, <sup>2</sup>Department of Chemical & Biological Engineering, <sup>3</sup>Department of Materials Science & Engineering, all of Northwestern University

**Goals.** The Institute for Catalysis in Energy Processes (ICEP) is multi-investigator program located in the Northwestern University (NU) Center for Catalysis and Surface Science (CCSS). It is organized into two highly integrated thrusts that address fundamental questions about how the atomic-level nature of solid catalytic materials controls catalytic function: *Understanding and Control of Catalyst Performance by Metal-Oxide Nanoparticle System Design* and *Atom-Scale Control of Critical Oxide-Oxide Interfaces*. Over the last three years, ICEP research focused on understanding dioxygen and hydrogen peroxide activation, C-H bond scission, and O-insertion into C-C and C-H bonds by deliberate design of catalyst structures at the atomic and nanoscale.

An overarching ICEP goal is targeted research to address *the inhomogeneity challenge in heterogeneous catalysis*. Almost all commercial or research-level catalysts are inhomogeneous, containing numerous different possible active sites. Some of these are spectators, playing no role; some are active for desirable reactions, others lead to undesirable side products. Since direct interrogation of individual active sites in an inhomogeneous system is rarely possible, in almost all cases only indirect evidence about the key sites and steps can be gleaned from experimental and theoretical models. More than this will be required to achieve disruptive advances in our understanding of catalysts and their catalysis.

The ICEP vision is that we can *create catalysts with unique types of active sites in an atomistically controlled fashion* so that we can move beyond indirect evidence to definitive, control-oriented science. This directly addresses the two Grand Challenges identified in the 2007 report *Basic Research Needs: Catalysis for Energy*

*Challenge 1: Understanding mechanisms and dynamics of catalyzed reactions* where the reactions occur on only a few isolated sites and in the presence of highly complex mixtures of molecules interacting with the surface in myriad ways.

*Challenge 2: Design and controlled synthesis of catalyst structures* to test ideas and to provide the necessary foundation for the synthesis of improved catalysts.

**DOE Interest.** The scientific questions addressed by the aforementioned three thrusts are directly relevant to the efficient use of the nation's resources, to reducing its reliance on overseas sources of energy for transportation fuels, to reducing energy consumption and waste in chemicals production, and to reducing carbon dioxide emissions. Major ICEP strengths are in catalytic materials synthesis, in measurements that elucidate catalyst properties, reaction mechanisms, and kinetics, and in theory and modeling to understand the properties, measurements, and chemical pathways, as well as to suggest new experiments. In many cases

ICEP researchers are the inventors or developers of the materials and methods that can be brought to bear on the Institute's catalytic systems. The ICEP organization and emphasis continues to evolve in order to optimize the contributions of its world-class participants.

**Recent Progress.** A major aspect of ICEP research, since its inception, has been the preparation and characterization of new materials with the goal of advancing our understanding of heterogeneous catalysis. Some of these included wholly new materials systems, such as metal organic frameworks (MOFs). Some were prepared with new methodologies, such as atomic layer deposition (ALD), and possessed novel structures or enhanced uniformity. Prior to 2012 both *Chemical Catalytic* and *Photocatalytic* processes were studied in ICEP. During the current funding period, from September 2012, ICEP transitioned away from *Photocatalysis* and focused on the understanding and advancement of heterogeneous catalytic oxidation by supported late transition metals and supported early transition metal oxides. This work emphasized atomic-scale understanding of the chemical nature of active surface oxygen species, the process of surface oxidation and reduction, and how the catalyst surface composition and structure influence O-insertion into C-C and C-H bonds. Below, we summarize some of our major achievements to date.

*1. Understanding and Control of Catalyst Performance by Metal-Oxide Nanoparticle System Design.* The support plays a critical role in catalysis effected by metal nanoparticle (NP). It imparts stability to metallic NPs; it can influence their shape and electronic properties; it can participate directly as part of the active site. During the past three years, we employed three approaches to investigate how support structure and composition influence metal NPs: (i) using crystalline oxide nanoparticles of well-defined surface atomic structure and composition; (ii) creating the support-metal interface using well-defined ligands for the metal NPs; and (iii) grafting stable organometallic compounds onto a support, followed by encapsulation with a porous ALD-deposited oxide. Our accomplishments include:

- A unique approach was developed that uses SrTiO<sub>3</sub> nanocuboids as supports for which both the surface composition and atomic positions are determined and controlled. Specifically, crystalline nanocuboids with support surface terminations of TiO<sub>2</sub> and SrO or BaO were prepared, the role of termination in determining the shape of supported Pt and Pd NPs was elucidated (Figure 1), and differences in the activity for CO oxidation for Pt and Pd supported on these surfaces were observed.
- Detailed work was performed to understand the formation of Pt and Pd NPs by ALD on the SrTiO<sub>3</sub> nanocuboids and to probe their catalytic activity for CO oxidation.
- In another oxide support system, the surface atomic positions were determined for all the major surface facets of CeO<sub>2</sub> nanocuboids.

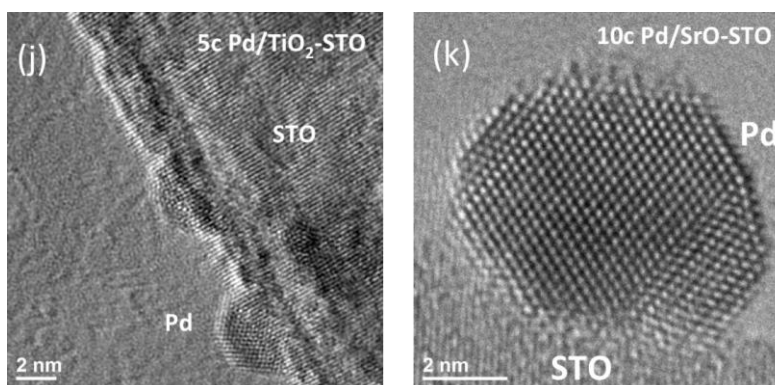
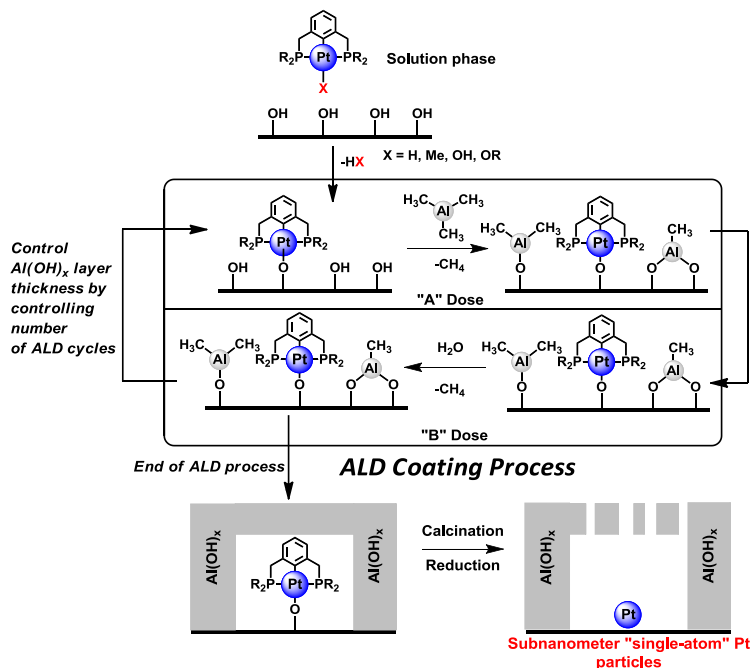


**Figure 1.** Shape of Pd nanoparticles supported on TiO<sub>2</sub>-terminated SrTiO<sub>3</sub> (left) and SrO-terminated SrTiO<sub>3</sub> (right).

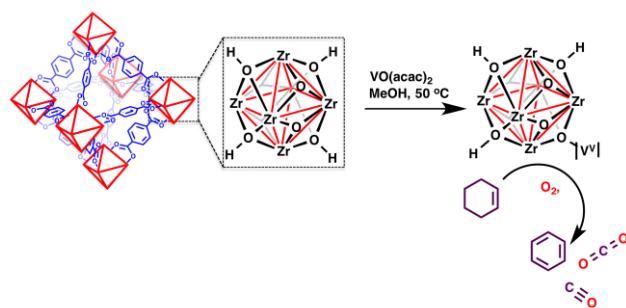
- An ALD procedure was developed for the synthesis of supported Ag nanoparticle catalysts. Catalysis by supported Ag and Pd nanoparticles was compared.
- A procedure was developed to prepare inverse catalysts by decorating Au nanoparticles with  $\text{TiO}_x$  clusters, and these materials were employed to emphasize the role of  $\text{TiO}_2/\text{Au}$  interactions in catalytic oxidation.
- Supported, single-atom Pd and Pt species were prepared by: 1) surface grafting of organometallic precursors, 2) stabilizing the grafted species by overcoating with ALD alumina and titania, and removing the ligands by mild oxidation (Scheme 1).



**Scheme 1.** Strategy to control the size of Pt(Pd) supported nanoparticles.

**2. Atom-Scale Control of Critical Oxide-Oxide Interfaces.** Vanadium oxide, molybdenum oxide, titanium oxide, chromium oxide, manganese oxide, and other early transition metals in the form of monolayer or isolated molecular species supported on a high surface area refractory oxide are active and selective oxidation catalysts. During this funding period, ICEP targeted the synthesis of vanadium oxide on novel support materials that are expected to afford novel molecular vanadia structures, as well as the preparation of mixed oxide monolayers of vanadium and molybdenum, and of titanium oxide. In analogy to the metal-oxide interactions described above, the detailed atomic structure of an oxide support has a strong influence on the molecular structure and properties of catalytic oxide overlayers on the support. For example, the geometry of support oxygen atoms that bind an isolated  $\text{VO}_4$  vanadyl to the surface determines whether one, two, or three surface bonds are formed to anchor the vanadyl. When the oxide overlayer contains two or more early transition metal cations (V, W, Mo) the interactions between these cations and their interaction with the support give rise to new and unexpected structures and chemical properties. The following are some examples of our major accomplishments in this area:

- $\text{SrTiO}_3$  nanocuboid-supported vanadium oxide was prepared by ALD, which is active for the oxidative dehydrogenation (ODH) of cyclohexane.
- Successful grafting of vanadyl groups to zirconium oxide nodes of MOF UiO-66 to form catalysts that are also active for the ODH of cyclohexane



**Scheme 2.** Synthesis of VUiO-66 and its catalytic activity in the oxidative dehydrogenation of cyclohexane using molecular oxygen as oxidant.

(Scheme 2). The catalyst exhibits high activity for the ODH of cyclohexene at 350 °C. At low conversion (<2%), benzene is the sole product. At higher conversions the selectivity to benzene decreases to 83% with the remaining products being CO and CO<sub>2</sub>. While gas-phase catalysis is an underexplored territory in MOF-based catalysis, our results demonstrate the potential of MOFs as a versatile and robust class of supports for heterogeneous gas-phase chemical reactions.

- A silica layer over the top of low loading TiO<sub>2</sub>/SBA-15 increases the selectivity in propylene oxidation towards propylene oxide by almost 100 fold.
- ALD of molybdenum oxide species on alumina was developed and the resulting materials are active catalysts for the epoxidation of cyclooctene in liquid phase using *tert*-butylhydroperoxide
- The structure and reactivity of V-W mixed oxide monolayers on TiO<sub>2</sub> have been determined with atomic precision for the first time using XSW, and show dramatically different behavior depending on the substrate and composition.
- The mechanisms of catalytic cyclohexene oxidation by ALD-derived supported VO<sub>x</sub> catalysts have been investigated using in situ FTIR. Surprisingly, using O<sub>2</sub> as the oxidant, the formation of diol and 2-cyclohexene-1-one are detected using vanadium oxide supported on SiO<sub>2</sub>, Al<sub>2</sub>O<sub>3</sub>, TiO<sub>2</sub>, and ZrO<sub>2</sub> (Figure 2), whereas oxygenates are not detectable in conventional catalytic reaction experiments.

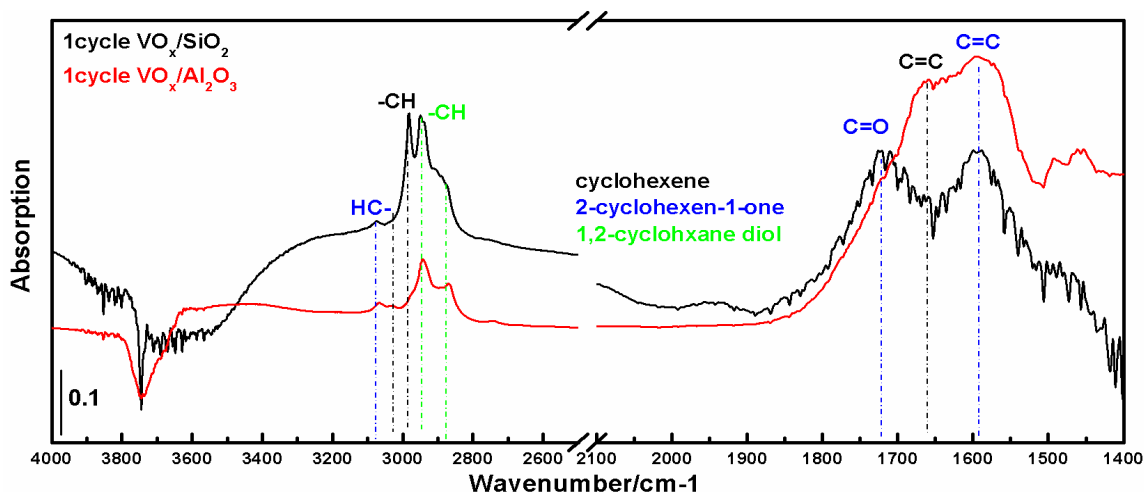


**Figure 2.** Infrared spectra of 1 cycle VO<sub>x</sub>/SiO<sub>2</sub> (black trace) and 1 cycle VO<sub>x</sub>/Al<sub>2</sub>O<sub>3</sub> (red trace) showing an absorption for the 1,2 cyclohexane diol product (labeled in green) and absorptions for the 2-cyclohexene-1-one (labeled in blue) product as a result of the reaction of cyclohexene (absorptions labeled in black) with oxygen.

*Development of a gas-phase H<sub>2</sub>O<sub>2</sub> reactor:* An achievement in the realm of catalysis methodology is a newly acquired ability to employ gas phase H<sub>2</sub>O<sub>2</sub> in reaction experiments. We have successfully constructed a gas-phase plug flow reactor capable of feeding either H<sub>2</sub>O<sub>2</sub> or O<sub>2</sub> as the oxidant and determining the kinetics of hydrocarbon oxidation reactions (Figure 3). Decomposition of the H<sub>2</sub>O<sub>2</sub> feed is minimized by using quartz and Teflon for construction materials, wrapping the

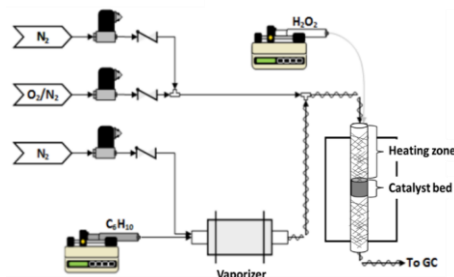


**Figure D-4** Reactor system for vapor-phase catalytic studies with H<sub>2</sub>O<sub>2</sub>.

feed lines with Al foil to prevent light-initiated decomposition, and shortening the peroxide residence time upstream of the catalyst bed as much as possible.

### ***Publications Acknowledging this Grant in 2012-2015***

1. Allotta, P.M. and P.C. Stair, Time-Resolved Studies of Ethylene and Propylene Reactions in Zeolite H-MFI by In-Situ Fast IR Heating and UV Raman Spectroscopy. *ACS Catal.*, 2012. **2**(11): p. 2424-2432.
2. Bao, X.Y., C.-Y. Sung, R.Q. Snurr, and L.J. Broadbelt, Rate-determining step in the NO<sub>x</sub> reduction mechanism on BaY zeolites and the importance of long-range lattice effects. *ACS Catalysis*, 2012. **2**: p. 350-359.
3. Becerra-Toledo, A.E., J.A. Enterkin, D.M. Kienzle, and L.D. Marks, Water adsorption on SrTiO<sub>3</sub>(001): II. Water, water, everywhere. *Surface Science*, 2012. **606**(9-10): p. 791-802.
4. Canlas, C.P., J. Lu, N.A. Ray, N.A. Grosso-Giordano, S. Lee, J.W. Elam, R.E. Winans, R.P. Van Duyne, P.C. Stair, and J.M. Notestein, Shape-selective sieving layers on an oxide catalyst surface. *Nat. Chem.*, 2012. **4**(12): p. 1030-1036.
5. Danon, A., K. Bhattacharyya, B.K. Vijayan, J. Lu, D.J. Sauter, K.A. Gray, P.C. Stair, and E. Weitz, Effect of Reactor Materials on the Properties of Titanium Oxide Nanotubes. *ACS Catal.*, 2012. **2**(1): p. 45-49.
6. Danon, A., E. Weitz, and P.C. Stair, Molecular nature and site requirements of adsorbed CO<sub>2</sub>. *Prepr. Symp. - Am. Chem. Soc., Div. Fuel Chem.*, 2012. **57**(1): p. 310.
7. DeSario, P.A., J.S. Wu, M.E. Grahm, and K.A. Gray, Nanoscale structure of Ti<sub>1-x</sub>Nb<sub>y</sub>O<sub>2</sub> mixed-phase thin films: Distribution of crystal phase and dopants. *Journal of Materials Research*, 2012. **27**(6): p. 944-950.
8. Enterkin, J.A., K.R. Poeppelmeier, and L.D. Marks, A Chemical Approach to Understanding Oxide Surfaces. *Surf. Sci.*, 2012. **606**: p. 334-355.
9. Feng, Z.X., L. Cheng, C.Y. Kim, J.W. Elam, Z. Zhang, L.A. Curtiss, P. Zapol, and M.J. Bedzyk, Atomic-Scale Study of Ambient-Pressure Redox-Induced Changes for an Oxide-Supported Submonolayer Catalyst: VO<sub>x</sub>/alpha-TiO<sub>2</sub>(110). *Journal of Physical Chemistry Letters*, 2012. **3**(19): p. 2845-2850.
10. Finkelstein-Shapiro, D., C.Y.H. Tsai, S.Y. Li, and K.A. Gray, Synthesis of high-energy anatase nanorods via an intermediate nanotube morphology. *Chemical Physics Letters*, 2012. **546**: p. 106-108.
11. Frontiera, R.R., N.L. Gruenke, and R.P. Van Duyne, Fano-Like Resonances Arising from Long-Lived Molecule-Plasmon Interactions in Colloidal Nanoantennas. *Nano Letters*, 2012. **12**(11): p. 5989-5994.
12. Hayner, C.M., X. Zhao, and H.H. Kung, Materials for rechargeable lithium-ion batteries. *Annu. Rev. Chem. Biomol. Eng.*, 2012. **3**: p. 445-471.
13. Jiang, N., E.T. Foley, J.M. Klingsporn, M.D. Sonntag, N.A. Valley, J.A. Dieringer, T. Seideman, G.C. Schatz, M.C. Hersam, and R.P. Van Duyne, Observation of Multiple Vibrational Modes in Ultrahigh Vacuum Tip-Enhanced Raman Spectroscopy Combined with Molecular-Resolution Scanning Tunneling Microscopy. *Nano Letters*, 2012. **12**(10): p. 5061-5067.
14. Kang, B., R.K. Totten, M.H. Weston, J.T. Hupp, and S.T. Nguyen, Cyclic metalloporphyrin dimers and tetramers: tunable shape-selective hosts for fullerenes. *Dalton Transactions*, 2012. **41**(39): p. 12156-12162.
15. Liang, Y.T. and M.C. Hersam, Towards Rationally Designed Graphene-Based Materials and Devices. *Macromolecular Chemistry and Physics*, 2012. **213**(10-11): p. 1091-1100.
16. Liang, Y.T., B.K. Vijayan, O. Lyandres, K.A. Gray, and M.C. Hersam, Effect of Dimensionality on the Photocatalytic Behavior of Carbon-Titania Nanosheet Composites: Charge Transfer at Nanomaterial Interfaces. *Journal of Physical Chemistry Letters*, 2012. **3**(13): p. 1760-1765.
17. Lin, S.S.Y., J. Yang, and H.H. Kung, Transition metal-decorated activated carbon catalysts for dehydrogenation of NaAlH<sub>4</sub>. *Int. J. Hydrogen Energy*, 2012. **37**(3): p. 2737-2741.
18. Lu, J., B. Liu, J.P. Greeley, Z. Feng, J.A. Libera, Y. Lei, M.J. Bedzyk, P.C. Stair, and J.W. Elam, Porous Alumina Protective Coatings on Palladium Nanoparticles by Self-Poisoned Atomic Layer Deposition. *Chemistry of Materials*, 2012. **24**(11): p. 2047-2055.
19. Luo, J., X. Zhao, J. Wu, H.D. Jang, H.H. Kung, and J. Huang, Crumpled Graphene-Encapsulated Si Nanoparticles for Lithium Ion Battery Anodes. *J. Phys. Chem. Lett.*, 2012. **3**(13): p. 1824-1829.
20. Lyandres, O., P. Chakhranont, D.F. Shapiro, M. Graham, and K. Gray, The effects of preferred orientation in sputtered TiO<sub>2</sub> thin films on the photooxidation efficiency of acetaldehyde. *Chemistry of Materials*, 2012. **24**(17): p. 3355-3362.
21. Mashayekhi, N.A., Y.Y. Wu, M.C. Kung, and H.H. Kung, Metal nanoparticle catalysts decorated with metal oxide clusters. *Chem. Commun.*, 2012. **48**(81): p. 10096-10098.
22. McBriarty, M.E., M.J. Bedzyk, and D.E. Ellis, Structure and properties of a model oxide-supported catalyst under redox conditions: WO<sub>x</sub>/alpha-Fe<sub>2</sub>O<sub>3</sub> (0001). *Surface Science*, 2012. **606**(17-18): p. 1367-1381.

23. Missaghi, M.N., M.C. Kung, and H.H. Kung, Polysiloxanes in Catalysis and Catalyst Preparation: Opportunities for Control of Catalytic Processes. *Topics in Catalysis*, 2012. **55**(1-2): p. 99-107.
24. Nguyen, H.G.T., M.H. Weston, O.K. Farha, J.T. Hupp, and S.T. Nguyen, A catalytically active vanadyl(catecholate)-decorated metal organic framework via post-synthesis modifications. *CrystEngComm*, 2012. **14**(12): p. 4115-4118.
25. Ostojic, G.N. and M.C. Hersam, Biomolecule-Directed Assembly of Self-Supported, Nanoporous, Conductive, and Luminescent Single-Walled Carbon Nanotube Scaffolds. *Small*, 2012. **8**(12): p. 1840-1845.
26. Prieto-Centurion, D., A.M. Boston, and J.M. Notestein, Structural and electronic promotion with alkali cations of silica-supported Fe(III) sites for alkane oxidation. *Journal of Catalysis*, 2012. **296**: p. 77-85.
27. Ray, N.A., R.P. Van Duyne, and P.C. Stair, Synthesis Strategy for Protected Metal Nanoparticles. *J. Phys. Chem. C*, 2012. **116**(14): p. 7748-7756.
28. Ryan, P., I. Konstantinov, R.Q. Snurr, and L.J. Broadbelt, DFT investigation of hydroperoxide decomposition over copper and cobalt sites within metal-organic frameworks. *Journal of Catalysis*, 2012. **286**: p. 95-102.
29. Schwartzberg, K.C. and K.A. Gray, Nanostructured Titania: the current and future promise of Titania nanotubes. *Catalysis Science & Technology*, 2012. **2**(8): p. 1617-1624.
30. Sharma, B., R.R. Frontiera, A.-I. Henry, E. Ringe, and R.P. Van Duyne, SERS: Materials, Applications, and the Future. *Materials Today*, 2012(15): p. 16-25.
31. Song, K., D.J. Sauter, J. Wu, V.P. Dravid, and P.C. Stair, Evolution of High-Energy Electron Beam Irradiation Effects on Zeolite Supported Catalyst: Metal Nanoprecipitation. *ACS Catal.*, 2012. **2**(3): p. 384-390.
32. Sonntag, M.D., J.M. Klingsporn, L.K. Garibay, J.M. Roberts, J.A. Dieringer, T. Seideman, K.A. Scheidt, L. Jensen, G.C. Schatz, and R.P. Van Duyne, Single-Molecule Tip-Enhanced Raman Spectroscopy. *The Journal of Physical Chemistry C*, 2012. **116**(1): p. 478-483.
33. Stair, P.C., Synthesis of supported catalysts by atomic layer deposition. *Topics in Catalysis*, 2012. **55**(1-2): p. 93-98.
34. Totten, R.K., P. Ryan, B. Kang, S.J. Lee, L.J. Broadbelt, R.Q. Snurr, J.T. Hupp, and S.T. Nguyen, Enhanced catalytic decomposition of a phosphate triester by modularly accessible bimetallic porphyrin dyads and dimers. *Chemical Communications*, 2012. **48**(35): p. 4178-4180.
35. Vijayan, B.K., N.M. Dimitrijevic, D. Finkelstein-Shapiro, J.S. Wu, and K.A. Gray, Coupling Titania Nanotubes and Carbon Nanotubes To Create Photocatalytic Nanocomposites. *Acs Catalysis*, 2012. **2**(2): p. 223-229.
36. Wegener, S.L., T.J. Marks, and P.C. Stair, Design Strategies for the Molecular Level Synthesis of Supported Catalysts. *Accounts of Chemical Research*, 2012. **45**: p. 206-214.
37. Zhao, X., C.M. Hayner, M.C. Kung, and H.H. Kung, Photothermal-assisted fabrication of iron fluoride-graphene composite paper cathodes for high-energy lithium-ion batteries. *Chem. Commun.*, 2012. **48**(79): p. 9909-9911.
38. Bhattacharyya, K., A. Danon, B.K. Vijayan, K.A. Gray, P.C. Stair, and E. Weitz, Role of the Surface Lewis Acid and Base Sites in the Adsorption of CO<sub>2</sub> on Titania Nanotubes and Platinized Titania Nanotubes: An in Situ FT-IR Study. *Journal of Physical Chemistry C*, 2013. **117**(24): p. 12661-12678.
39. Enterkin, J.A., R.M. Kennedy, J.L. Lu, J.W. Elam, R.E. Cook, L.D. Marks, P.C. Stair, C.L. Marshall, and K.R. Poepelmeier, Epitaxial Stabilization of Face Selective Catalysts. *Topics in Catalysis*, 2013. **56**(18-20): p. 1829-1834.
40. Feng, Z., J. Lu, H. Feng, P.C. Stair, J.W. Elam, and M.J. Bedzyk, Catalysts Transform While Molecules React: An Atomic-Scale View. *The Journal of Physical Chemistry Letters*, 2013. **4**(2): p. 285-291.
41. Finkelstein-Shapiro, D., S.J. Hurst, K.A. Gray, N. Dimitrijevic, T. Rajh, P. Tarakeshwar, and V. Mujica, CO<sub>2</sub> pre-activation via charge transfer states of TiO<sub>2</sub>-aminosalicylic acid complexes. *Journal of Physical Chemistry Letters*, 2013. **4**(3): p. 475-479.
42. Fu, B., J. Lu, P.C. Stair, G. Xiao, M.C. Kung, and H.H. Kung, Oxidative dehydrogenation of ethane over alumina-supported Pd catalysts. Effect of alumina overlayer. *J. Catal.*, 2013. **297**: p. 289-295.
43. Hu, L.H., C.D. Wang, S. Lee, R.E. Winans, L.D. Marks, and K.R. Poepelmeier, SrTiO<sub>3</sub> Nanocuboids from a Lamellar Microemulsion. *Chemistry of Materials*, 2013. **25**(3): p. 378-384.
44. Kleinman, S.L., R.R. Frontiera, A.I. Henry, J.A. Dieringer, and R.P. Van Duyne, Creating, characterizing, and controlling chemistry with SERS hot spots. *Physical Chemistry Chemical Physics*, 2013. **15**(1): p. 21-36.
45. Lalonde, M., W. Bury, O. Karagiari, Z. Brown, J.T. Hupp, and O.K. Farha, Transmetalation: routes to metal exchange within metal-organic frameworks. *Journal of Materials Chemistry A*, 2013. **1**(18): p. 5453-5468.
46. Mondloch, J.E., W. Bury, D. Fairen-Jimenez, S. Kwon, E.J. DeMarco, M.H. Weston, A.A. Sarjeant, S.T. Nguyen, P.C. Stair, R.Q. Snurr, O.K. Farha, and J.T. Hupp, Vapor-Phase Metalation by Atomic Layer

- Deposition in a Metal–Organic Framework. *Journal of the American Chemical Society*, 2013. **135**(28): p. 10294-10297.
47. Nguyen, H.G.T., M.H. Weston, A.A. Sarjeant, D.M. Gardner, Z. An, R. Carmieli, M.R. Wasielewski, O.K. Farha, J.T. Hupp, and S.T. Nguyen, Design, Synthesis, Characterization, and Catalytic Properties of a Large-Pore Metal-Organic Framework Possessing Single-Site Vanadyl(monocatecholate) Moieties. *Crystal Growth & Design*, 2013. **13**(8): p. 3528-3534.
  48. Shen, Z., J. Kim, J. Shen, C.M. Downing, S. Lee, H.H. Kung, and M.C. Kung, Spherosilicates with peripheral malonic acid and vinyl end groups. *Chem. Commun.*, 2013. **49**(32): p. 3357-3359.
  49. Weiqiang Wu, Kaustava Bhattacharyya, Kimberly Gray, and E. Weitz, Photo-Induced Reactions of Surface Bound Species on the Titania Nanotubes and Platinized Titania Nanotubes: An in-situ FTIR study *The Journal of Physical Chemistry C* 2013. **117**: p. 20643-20655.
  50. Aditya Savara and Eric Weitz, Elucidation of Intermediates and Mechanisms in Heterogeneous Catalysis Using Infrared Spectroscopy. *Annual Review of Physical Chemistry*, 2014. **65** p. 249-273.
  51. Childers, D.J., N.M. Schweitzer, S.M.K. Shahari, R.M. Rioux, J.T. Miller, and R.J. Meyer, Modifying structure-sensitive reactions by addition of Zn to Pd. *Journal of Catalysis*, 2014. **318**: p. 75-84.
  52. Crosby, L., J. Enterkin, and L.D. Marks, Wulff-shape of SrTiO<sub>3</sub>. *Surface Science*, 2014. doi:10.1016/j.susc.2014.10.014.
  53. Feng, Z., M.E. McBriarty, A.U. Mane, J. Lu, P.C. Stair, J.W. Elam, and M.J. Bedzyk, Redox-driven atomic-scale changes in mixed catalysts: VOX / WOX /  $\alpha$ -TiO<sub>2</sub>(110). *RSC Adv*, 2014. **4**: p. 64608-64616.
  54. Hu, L., C. Wang, R.M. Kennedy, L. D. Marks, and K.R. Poeppelmeier, The Role of Oleic Acid: From Synthesis to Assembly of Perovskite Nanocuboid Two-Dimensional Arrays. *Inorganic Chemistry*, 2014. ACS ASAP.
  55. Johnson, A.M., B.R. Quezada, L.D. Marks, and P.C. Stair, Influence of the Metal Oxide Substrate Structure on Vanadium Oxide Monomer Formation. *Topics in Catalysis*, 2014. **57**(1-4): p. 177-187.
  56. Kwon, S., N.M. Schweitzer, S.Y. Park, P.C. Stair, and R.Q.i.p. Snurr, A Kinetic Study of Vapor-Phase Cyclohexene Epoxidation by H<sub>2</sub>O<sub>2</sub> over Mesoporous TS-1. *J. Catalysis*, Submitted.
  57. Lin, Y., J.A. McCarthy, K.R. Poeppelmeier, and L.D. Marks, Applications of Electron Microscopy in Heterogeneous Catalysis. *Catalysis by Materials with Well-Defined Structures*, Z. Wu, Editor. 2014, Elsevier.
  58. Lin, Y., Z. Wu, J. Wen, K.R. Poeppelmeier, and L.D. Marks, Imaging the Atomic Surface Structures of CeO<sub>2</sub> Nanoparticles. *Nano Letters*, 2014. **14**(1): p. 191-196.
  59. Masango, S.S., L. Peng, L.D. Marks, R.P. Van Duyne, and P.C. Stair, Nucleation and Growth of Silver Nanoparticles by AB and ABC-Type Atomic Layer Deposition. *The Journal of Physical Chemistry C*, 2014.
  60. Mashayekhi, N.A., M.C. Kung, and H.H. Kung, Selective oxidation of hydrocarbons on supported Au catalysts. *Catalysis Today*, 2014. **238**: p. 74-79.
  61. McBriarty, M.E., Atomic Scale Structure-Chemistry Relationships at Oxide Catalyst Surfaces and Interfaces in *Materials Science and Engineering*. 2014, Northwestern University Evanston.
  62. Nguyen, H.G.T., N.M. Schweitzer, C.Y. Chang, T.L. Drake, M.C. So, P.C. Stair, O.K. Farha, J.T. Hupp, and S.T. Nguyen, Vanadium-Node-Functionalized UiO-66: A Thermally Stable MOF-Supported Catalyst for the Gas-Phase Oxidative Dehydrogenation of Cyclohexene. *Acs Catalysis*, 2014. **4**(8): p. 2496-2500.
  63. Paddock, R.L., D. Adhikari, R.L. Lord, M.-H. Baik, and S.T. Nguyen, Catalyzed Synthesis of N-Aryl-Substituted Oxazolidinones from Epoxides and Aryl Isocyanates. *Chem. Commun.*, 2014. **50**: p. 15187-15190.
  64. Pan, Q., B.H. Liu, M.E. McBriarty, Y. Martynova, I.M.N. Groot, S. Wang, M.J. Bedzyk, S. Shaikhutdinov, and H.J. Freund, Reactivity of Ultra-Thin ZnO Films Supported by Ag(111) and Cu(111): A Comparison to ZnO/Pt(111). *Catalysis Letters*, 2014. **144**(4): p. 648-655.
  65. Stoltz, S.E., D.E. Ellis, and M.J. Bedzyk, Structure and reactivity of zero-, two- and three-dimensional Pd supported on SrTiO<sub>3</sub>(001). *Surface Science*, 2014. **630**: p. 46-63.
  66. Stoltz, S.E., D.E. Ellis, and M.J. Bedzyk, Interface of Pt with SrTiO<sub>3</sub>(001); A combined theoretical and experimental study. *Surface Science*, 2014.
  67. Tuci, G., G. Giambastiani, S. Kwon, P.C. Stair, R.Q. Snurr, and A. Rossin, Chiral Co(II) Metal-Organic Framework in the Heterogeneous Catalytic Oxidation of Alkenes under Aerobic and Anaerobic Conditions. *Acs Catalysis*, 2014. **4**(3): p. 1032-1039.
  68. Wu, W.Q. and E. Weitz, Modification of acid sites in ZSM-5 by ion-exchange: An in-situ FTIR study. *Applied Surface Science*, 2014. **316**: p. 405-415.
  69. Lin, Y., J. Wen, L. Hu, J.A. McCarthy, S. Wang, K.R. Poeppelmeier, and L.D. Marks, Electron-induced Ti-rich surface segregation on SrTiO<sub>3</sub> nanoparticles. *Micron*, 2015. **68**: p. 152-7.

**DE-FG02-01ER15264: Catalytic Growth of Molecular Scale Wiring**

Prof. Colin Nuckolls

Columbia University, Department of Chemistry

This poster will present the catalytic methods for the synthesis of carbon-based nanoelectronic materials. This is a field that is currently limited by the dearth of methods available to cleanly produce atomically defined materials such as carbon nanotubes and graphene ribbons. We utilize ring-opening alkyne metathesis polymerization (ROAMP) as the basis for creating an entire class of new electronic materials. The presentation is comprised of three integrated areas: (1) monomer design, (2) catalyst design, and (3) post-polymerization reactivity. These studies promise state of the art catalysts and monomers to create advanced materials.

We have developed the first example of a living ROAMP reaction, and further shown that multidentate ligands in the form of salicylimine ligands create more well-behaved living polymerizations. Building from these studies, we recently discovered the first new bench stable catalytic system that is able to effect the ROAMP reactions in protic solvents such as methanol and water. We have also begun a detailed mechanistic study of the ROAMP reaction of a dibenzocyclooctadiyne derivative reaction and have identified a metallotetrahedrane intermediate in the reaction.

**DE-FG02-01ER15264: Catalytic Growth of Molecular Scale Wiring**

**Publications Acknowledging this Grant in 2012-2015**

1. Sedbrook, D. F.; Paley, D. W.; Steigerwald, M. L.; Nuckolls, C.; Fischer, F. R. Bidentate Phenoxides as Ideal Activating Ligands for Living Ring Opening Alkyne Metathesis Polymerization *Macromol.*, **2012**, *45*, (12), 5040-5044.

2. Paley, D.W.; Sedbrook, D. F.; Decatur, J.; Fischer, F.R.; Steigerwald, M.L.; Nuckolls, C. Alcohol-Promoted Ring-Opening Alkyne Metathesis Polymerization *Angew. Chemie. Int. Ed.*, **2013**, 52, 17, 4491-4594.
3. Chen, Z.; Paley, D.; Wei, L.; Weisman, A.; Friesner, R.; Nuckolls, C.; Min, W. Multicolor Live-Cell Chemical Imaging by Isotopically Edited Alkyne Vibrational Palette *J. Am. Chem. Soc.*, **2014**, 136 (22), 8027–8033
4. Zhong, Y.; Trinh, M.; Chen, R.; Wang, W.; Khlyabich, P. P.; Kumar, B.; Zhu, Q.; Nam, C.-Y.; Sfeir, M.; Black, C.; Steigerwald, M.; Xiao, S.; Ng, F.; Zhu, X.-Y.; Nuckolls, C. Efficient Organic Solar Cells with Helical Perylene Diimide Electron Acceptors *J. Am. Chem. Soc.*, **2014**, 136 (43), 15215–15221
5. Ball, M.; Zhong, Y.; Wu, Y.; Schenck, C.; Ng, F.; Steigerwald, M.; Xiao, S.; Nuckolls, C. Contorted Polycyclic Aromatics *Acc. Chem. Res.*, **2015**, 48 (2), 267–276

**In situ/Operando Investigations of Structural Dynamics of Supported Metal Catalysts**

S. Zhao,<sup>1</sup> U. Jung,<sup>1</sup> A. Elsen,<sup>1</sup> R. G. Nuzzo,<sup>1</sup> Y. Li,<sup>2</sup> A. I. Frenkel,<sup>2</sup> E. A. Stach,<sup>3</sup> J. Kas,<sup>4</sup> F. Vila,<sup>4</sup> J. J. Rehr,<sup>4</sup> C. Bonifacio,<sup>5</sup> J. C. Yang,<sup>5</sup>

<sup>1</sup>Dept. of Chemistry, Univ. of Illinois, Urbana-Champaign, <sup>2</sup>Dept. of Physics, Yeshiva University, <sup>3</sup>Center for Functional Nanomater., Brookhaven National Lab. <sup>4</sup>Dept. of Physics, Univ. of Washington  
<sup>5</sup>Dept. of Mat. Science and Eng. and Dept. of Chem. Eng., Univ. of Pittsburgh

**Presentation Abstract**

The heterogeneity of catalytic materials poses significant challenges to characterization due, in large part, to the ensemble-averaging nature of most structural probes. This, in turn, hinders identification of the structural features of catalytically active sites and ensembles, with consequences for understandings of mechanisms. In previous cycles of our research program we used a combination of XAFS, TEM, and theory for quantitative characterization of model catalysts. Surprisingly, we discovered that the “model” catalysts, always believed to have “well-defined” structures of specific and distinctly different polyhedral architectures, turned out to possess a plethora of coexisting structural motifs, sizes, shapes, compositions, degrees of crystalline order as well as fluctuations of structure over multiple temporal scales. These findings, coupled with recently emerging results by us and others, show that catalytic species restructure in the course of chemical reaction, calling for new approaches to characterization that are capable of capturing the heterogeneity of the catalytic species and their structural and dynamic attributes in real time during a reaction. In the present work, we developed an integrated, experimental and theoretical approach that synergistically combines three attributes of characterization: 1) a multi-mode form of analysis in operando conditions that rely on average and local probes; 2) high energy resolution spectroscopy measurements; and 3) the enabling power of advanced forms theory that provides the interpretation of these experimental data. Our multi-technique, *operando* characterization of catalytic process is enabled by using a portable micro-reactor made compatible with structure-sensitive techniques (XAFS, TEM and micro-IR) that give a balanced view on the intra-particle structure, and on the ensemble properties (e.g., average particle size and the distribution of sizes and shapes), as well as the interactions occurring with adsorbates and the support material. When applied to the test case of ethylene hydrogenation over SiO<sub>2</sub>-supported Pt and Pd catalysts, it was possible to investigate multiple types of bond forming and breaking processes occurring during the course of the reaction (M-M, M-O, M-C, M-H, C-C, C-H) by correlating the data of several probes in *operando* conditions—to explicitly link structural changes in the catalyst to a particular mechanistic aspects of the reaction. These data were measured at the NSLS, CFN, SSRL and ALS facilities. Using high-energy resolution X-ray absorption and emission spectroscopies (XAS and XES), measured at the ESRF and SLS synchrotrons, we focused on another form of heterogeneity, here the intra-particle heterogeneity of atomic and electronic structure. Aided by the first principle theoretical modeling of XAS and XES spectra and real-time DFT/MD simulations, we demonstrated the striking consequences of charge heterogeneity and its fluxional nature. In response to the increasing adsorbate coverage (CO or H<sub>2</sub>), the clusters transform from having negatively charged bare cluster surface (positive interior) to a positive one (negative interior) in the fully covered case. This study illustrates a complexity of bulk and surface structures and their dynamic, responsive transformations throughout changing reaction conditions.

**Grant Number: DE FG02-03ER15476**

**Grant Title: The Reactivity and Structural Dynamics of Supported Metal Nanoclusters Using Electron Microscopy, *in situ* X-Ray Spectroscopy, Electronic Structure Theories, and Molecular Dynamics Simulations.**

**PIs:** Ralph G. Nuzzo, Anatoly I. Frenkel, Judith C. Yang, John J. Rehr  
**Postdocs:** A. Elsen, C. Bonifacio, U. Jung, S. Zhao, J. Kas, Y. Li, F. Vila

## RECENT PROGRESS

### 1. Complex structural dynamics of nanocatalysts revealed in operando conditions by correlated imaging and spectroscopy probes

A major goal of our work is to better understand the mechanisms of catalytic reactions. This interest is being addressed foremost through efforts that seek to provide and exploit new multi-modal means of characterization—ones that will make it possible to explore catalytic materials with multiple techniques, with the hope of using this combined data to elucidate the complex structure-property-rate relationships of catalysis with unprecedented clarity. While it is well established that the size, shape, composition and atomic structure of supported metal catalysts impact reactivity, quantitative understandings of these attributes and the environmental influences that modify them in *operando* conditions remain limited. This reflects limitations due to the paucity of *operando* methods that can assess atomistic nature of composition and bonding present in complex heterogeneous systems. In 2014 we completed a three-year project, in which we developed a new methodology that can provide quantitative descriptions of the atomic and electronic structural attributes that underpin the complex structural dynamics exhibited by catalysts in real reaction conditions. The current work exploits a microfabricated catalytic reactor designed for correlated use with both synchrotron x-ray absorption spectroscopy and scanning transmission electron microscopy. The power of the method is illustrated in recent results that demonstrate the dynamic transformations that are manifested in an ensemble of Pt clusters during an exemplary catalytic reaction—the hydrogenation of ethylene. We find a complex functionality exists that spans sizes ranging from single atoms to large agglomerates throughout changing reaction conditions (Fig. 1, left). In each experiment (at the focusing XAS beamline X27A at NSLS and the Titan E-TEM at CFN) we used an identical setup: a micro-cell for sample analysis by XAS and TEM (Fig. 1, right), and a coupled quartz capillary plug-flow cell placed downstream from the micro-cell for product analysis. The new results emerging from this work revealed that the changes in the SiO<sub>2</sub> support evidenced in Si EELS data correlate with the atomistic changes evidenced in the bonding environment of Pt atoms before, during and after the reaction. These impacts are highly responsive to the reactant atmosphere composition and conversion regime of the reaction (Fig. 2). This method is generalizable to quantitative *operando* studies of complex systems using a wide variety of x-ray and electron based experimental probes.

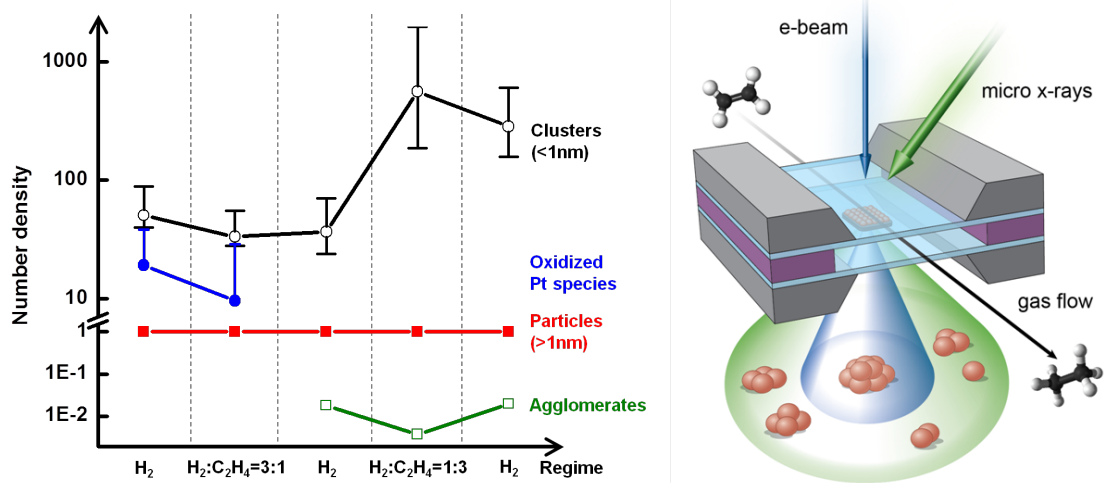


**Figure 1 (Left) Evolution in number density of Pt species (schematic).** Combination of XAFS and STEM analyses accounts for the following components, and for their evolution in reaction conditions: oxidized Pt species (blue), clusters smaller than 1nm in size (black), agglomerated clusters, or “agglomerates” (green), and particles larger than 1nm in size (red). **(Right) Schematic of experimental cell.** The catalyst is confined between two silicon

nitride windows with the reacting gas mixture flowing through the system. Arrows show the direction of the electron beam and incident X-ray beam. In the X-ray absorption experiment, all types of Pt species are probed (shown by a green cone). In the STEM experiment, only particles larger than  $\sim 1$  nm are detectable (shown by a dark blue cone).

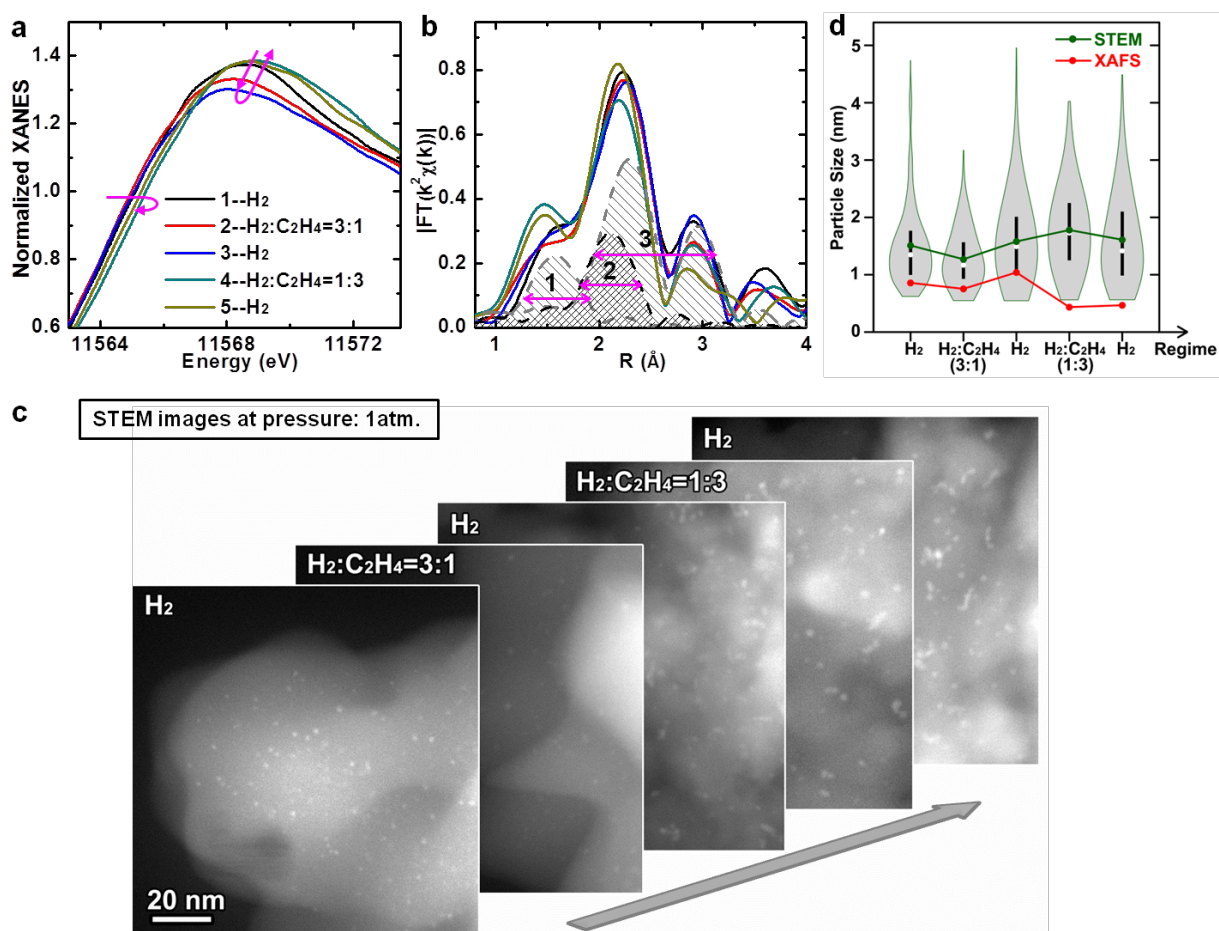


**Figure 2 | The experimental results from XAFS and STEM.** (a) The XANES spectra, (b) the Fourier transform magnitudes of Pt L<sub>3</sub> edge EXAFS spectra, and (c) the STEM images are shown as measured in the *operando* mode, during different reaction regimes. Theoretical fits to EXAFS data included three contributions between Pt and their nearest neighbors. Combined EXAFS and STEM results are displayed in (d) for all regimes. The green line indicates the mean particle sizes, as obtained by the STEM image analysis. The red line shows the change in the average particle size obtained from XAFS analysis, assuming that all particles are identical and adopt a truncated cuboctahedron geometry.

## 2. Structural and charge heterogeneities of supported nanoscale metal catalysts

We recently completed a study based on a synergistic combination of experiment and theory to answer the following questions: (1) *What are the distributions of atoms and charges present in supported metal clusters, and* (2) *how are they affected by the interaction with adsorbates and supports?* The concerns about inter and intra cluster heterogeneity are tightly related and central to understanding how mechanisms of reaction operate most fundamentally at atomistic levels. In the section above, we described methods that probe the heterogeneity of different forms of metal species comprising a catalytic sample, i.e., inter-particle heterogeneity. In this part of our work, we have examined a model system in both experiment and theory and quantified the inherent heterogeneity in the structure and charge distribution present in a single metal particle—the intra-particle heterogeneity. We show that the distributions of atoms and charges are strongly coupled to both structural and dynamic perturbations, and this fact helps clarify the nature of dynamic bonding of nano-scale catalytic systems with supports, and the role the

presence of adsorbates plays in mediating these effects. Exemplary results, supported by theoretical modeling and experimental data obtained for supported Pt catalysts using *in-situ*, high energy resolution X-ray absorption and emission spectroscopies, *in-situ* diffuse reflectance infrared Fourier transform spectroscopy, and *ex-situ* scanning transmission electron microscopy, are shown in Figures 3 and 4.

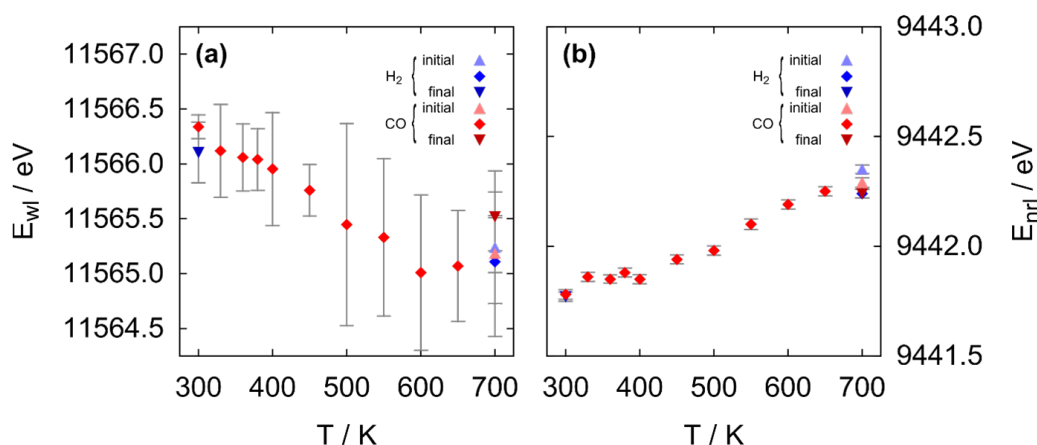


**Figure 3** Temperature dependence of the (a) white line energy measured in the High Energy Resolution Fluorescence Detection (HERFD) XANES experiment of Pt/SiO<sub>2</sub> nanoparticles under H<sub>2</sub> and CO flow conditions and (b) non-resonant emission line energy measured in the RIXS experiment in the same experimental conditions.

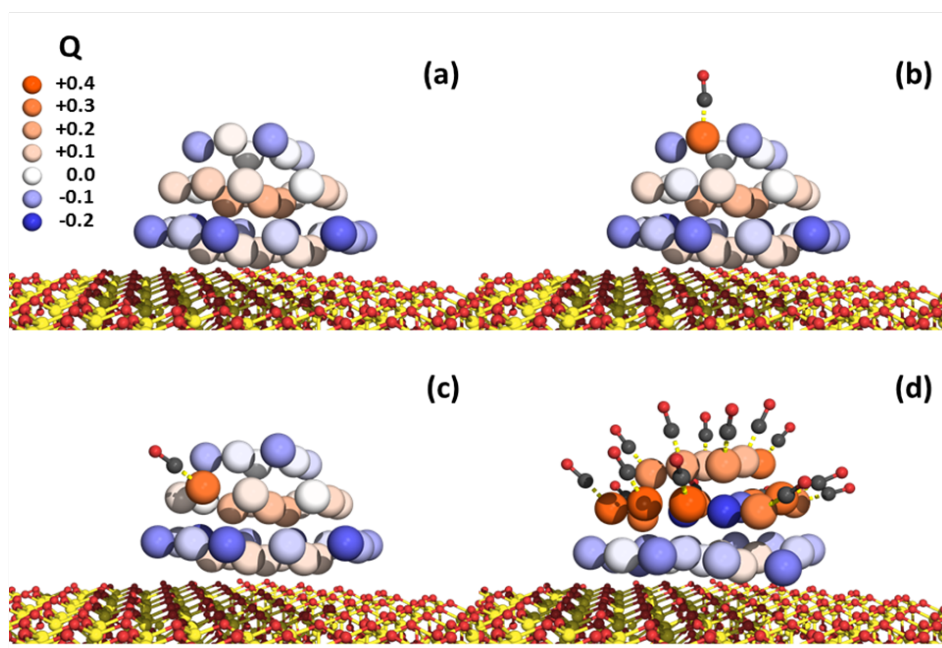


**Figure 4** Theoretical calculations of charge transfer upon CO adsorption on a Pt<sub>37</sub> cluster on SiO<sub>2</sub> support. The explanation of the experimental observation is given in terms of temperature-dependent coverage of adsorbates that increases from (a) through (d) and causes redistribution of atoms and charges within the cluster.

### Publications Acknowledging this Grant in 2012-2015

1. A. Elsen, U. Jung, F. D. Vila, Y. Li, O. Safonova, R. Thomas, M. Tromp, J. J. Rehr, R. G. Nuzzo, A. I. Frenkel Structural and charge heterogeneities of supported nanoscale metal catalysts *J. Am. Chem. Soc.* **submitted**
2. S. Zhao, Y. Li, D. Zakharov, R. Tappero, E. Stavitski, M. Castaldi, R. G. Nuzzo, A. I. Frenkel, E. A. Stach Correlative studies of catalytic mechanisms by spectroscopy, microscopy and scattering methods in operando conditions (Invited) *Chem. Cat. Chem.* **submitted**
3. A. I. Frenkel Two views at strained nanocrystals from the opposite sides of spatial resolution limit (Invited) *Physica Scripta*, **Submitted**
4. H. Liu, W. An, Y. Li, A. I. Frenkel, K. Sasaki, C. Koenigsmann, D. Su, R. M. Anderson, R. M. Crooks, R. R. Adzic, P. Liu, S. S. Wong Combining theory and experiment to deduce the active structure geometry of ultrathin nanowires analyzed in situ for the oxygen reduction reaction *Nature Communications*, **submitted**.
5. Y. Li and A. I. Frenkel Metal nanocatalysts, in: XAFS techniques for catalysts, nanomaterials and surfaces, Y. Iwasawa, K. Asakura, M. Tada, Eds., **submitted**
6. J. J. Rehr Theoretical modeling, in: XAFS techniques for catalysts, nanomaterials and surfaces, Y. Iwasawa, K. Asakura, M. Tada, Eds., **submitted**
7. F. Tao, J. Shan, S. Zhang, T. Choksi, C. Fittz, L. Nguyen, W. Zhu, Y. Li, Y. Zhang, J. C. Yang, J. Greeley, A. I. Frenkel, Tuning catalytic performance through single or sequential post-synthesis reaction in a gas phase *Nature Communications*, **submitted**
8. S. Zhang, L. Nguyen, J.-X. Liang, J. Shan, J. Liu, A. I. Frenkel, A. Patlolla, J. Li, F. Tao Catalysis on singly dispersed bimetallic sites on oxide support, *Nature Communications*, **submitted**
9. B. D. Briggs, N. M. Bedford, S. Seifert, H. Koerner, H. Ramezani-Dakhel, H. Heinz, R. R. Naik, A. I. Frenkel, M. R. Knecht Atomic-scale identification of Pd leaching in nanoparticle catalyzed C-C coupling: Effects of particle surface disorder *Chem. Science*, **submitted**
10. L. Nguyen, S. Zhang, L. Wang, Y. Li, H. Yoshida, J.-J. Shan, A. Patlolla, A. I. Frenkel, S. Takeda, F. Tao Reaction on single site bimetallic catalysts Pt<sub>1</sub>Co<sub>4</sub> and Pd<sub>1</sub>Co<sub>5</sub> *ACS Catalysis*, **submitted**
11. Y. Li, D. Zakharov, S. Zhao, R. Tappero, U. Jung, A. Elsen, Ph. Baumann, R. G. Nuzzo, E. A. Stach, A. I. Frenkel  
Complex structural dynamics of nanocatalysts revealed in operando conditions by correlated imaging and spectroscopy probes, *Nature Communications*, **2015, in press**
12. N. M. Bedford, H. Ramezani-Dakhel, J. M. Slocik, B. D. Briggs, Y. Ren, A. I. Frenkel, V. G. Petkov, H. Heinz, R. R. Naik, M. R. Knecht, Elucidation of peptide-directed palladium surface structure for biologically-tunable nanocatalysts *ACS Nano*, **2015**, ASAP Article, DOI: 10.1021/acsnano.5b00168
13. U. Jung, A. Elsen, Y. Li, J. G. Smith, M. W. Small, E. A. Stach, A. I. Frenkel, R. G. Nuzzo, Comparative in operando studies in heterogeneous catalysis: Atomic and electronic structural features in the hydrogenation of ethylene over supported Pd and Pt catalysts, *ACS Catalysis (Perspective)* **2015**, *5*, 1539-1551
14. Zhu, Q.; Saidi, W. A.; Yang, J. C. Step-induced oxygen upward diffusion on stepped Cu(100) surface. *J. Phys. Chem. C* **2015**, *119*, 251-261
15. S. Lwin, C. Keturakis, J. Handzlik, P. Sautet, Y. Li, A. I. Frenkel, I. E. Wachs Surface ReOx sites on Al<sub>2</sub>O<sub>3</sub> and their molecular structure-reactivity relationships for olefin methathesis, *ACS Catalysis* **2015**, *5*, 1452-1444
16. R. Korobko, A. Lerner, Y. Li, E. Wachtel, A. I. Frenkel, I. Lubomirsky In-situ Extended X-ray Absorption Fine Structure study of electrostriction in Gd doped ceria, *App. Phys. Lett.* **2015**, *106*, 042904
17. J. Wang, Q. Wang, X. Jiang, Z. Liu, W. Yang, A. I. Frenkel Determination of nanoparticle size by measuring the metal-metal bond length: The case of palladium hydride, *J. Phys. Chem. C* **2015**, *119*, 854-861
18. He, L.;Liu, F.;Hautier, G.;Oliveira, M. J. T.;Marques, M. A. L.;Vila, F. D.;Rehr, J. J.;Rignanese, G.-M.;Zhou, A., Accuracy of generalized gradient approximation functionals for density-functional perturbation theory calculations. *Phys. Rev. B.* **2014**, *89*, 64305.
19. Zhu, Q.; Fleck, C.; Saidi, W. A.; McGaughey, A.; Yang, J. C.. TFOx: A versatile kinetic Monte Carlo program for simulations of island growth in three dimensions *Comp. Mat. Sci.* **2014**, *91*, 292-302.
20. Erickson, E. M.;Oruc, M. E.;Wetzel, D. J.;Cason, M. W.;Hoang, T. T. H.;Small, M. W.;Li, D.;Frenkel, A. I.;Gewirth, A. A.;Nuzzo, R. G., A Comparison of Atomistic and Continuum Approaches to the Study of Bonding Dynamics in Electrocatalysis: Microcantilever Stress and in Situ EXAFS Observations of Platinum Bond Expansion Due to Oxygen Adsorption during the Oxygen Reduction Reaction. *Anal. Chem.* **2014**, *86*, 8368-8375.
21. Frenkel, A. I.;Cason, M. W.;Elsen, A.;Jung, U.;Small, M. W.;Nuzzo, R. G.;Vila, F. D.;Rehr, J. J.;Stach, E. A.;Yang, J. C., Critical review: Effects of complex interactions on structure and dynamics of supported metal catalysts. *J. Vac. Sci. Technol., A* **2014**, *32*, 020801.

22. Frenkel, A. I.; van Bokhoven, J. A., X-ray spectroscopy for chemical and energy sciences: the case of heterogeneous catalysis. *J. Synchrotron Radiat.* **2014**, *21*, 1084-1089.
23. Patete, J. M.; Han, J.; Tiano, A. L.; Liu, H.; Han, M.-G.; Simonson, J. W.; Li, Y.; Santulli, A. C.; Aronson, M. C.; Frenkel, A. I.; Zhu, Y.; Wong, S. S., Observation of Ferroelectricity and Structure-Dependent Magnetic Behavior in Novel One-Dimensional Motifs of Pure, Crystalline Yttrium Manganese Oxides. *J. Phys. Chem. C* **2014**, *118*, 21695-21705.
24. Rehr, J. J.; Vila, F. D., Dynamic structural disorder in supported nanoscale catalysts. *J. Chem. Phys.* **2014**, *140*, 134701.
25. Shan, J.; Huang, W.; Nguyen, L.; Yu, Y.; Zhang, S.; Li, Y.; Frenkel, A. I.; Tao, F., Conversion of Methane to Methanol with a Bent Mono( $\mu$ -oxo)nickel Anchored on the Internal Surfaces of Micropores. *Langmuir* **2014**, *30*, 8558-8569.
26. Small, M. W.; Kas, J. J.; Kvashnina, K. O.; Rehr, J. J.; Nuzzo, R. G.; Tromp, M.; Frenkel, A. I., Effects of Adsorbate Coverage and Bond-Length Disorder on the d-Band Center of Carbon-Supported Pt Catalysts. *ChemPhysChem* **2014**, *15*, 1569-1572.
27. Zhang, L.; Yang, C.; Frenkel, A. I.; Wang, S.; Xiao, G.; Brinkman, K.; Chen, F., Co-generation of electricity and chemicals from propane fuel in solid oxide fuel cells with anode containing nano-bimetallic catalyst. *J. Power Sources* **2014**, *262*, 421-428.
28. Spanjers, C. S.; Senf, T. P.; van Duin, A. C. T.; Janik, M. J.; Frenkel, A. I.; Rioux, R. M., Illuminating surface atoms in nanoclusters by differential X-ray absorption spectroscopy. *Phys. Chem. Chem. Phys.* **2014**, *16*, 26528-26538.
29. Wu, L.-b.; Wu, L.-h.; Yang, W.-m.; Frenkel, A. I., Study of the local structure and oxidation state of iron in complex oxide catalysts for propylene ammoxidation. *Catal. Sci. Technol.* **2014**, *4*, 2512-2519.
30. Frenkel, A.I.; Small, M.W.; Smith, J.G.; Nuzzo, R.G.; Kvashnina, K.O.; Tromp, M. An In-Situ Study of Bond Strains in 1 nm Pt Catalysts and Their Sensitivities to Cluster-Support and Cluster-Adsorbate Interactions. *J. Phys. Chem. C* **2013**, *117*, 23286-23294.
31. Anderson, R. M.; Zhang, L.; Loussaert, J. A.; Frenkel, A. I.; Henkelman, G.; Crooks, R. M., An Experimental and Theoretical Investigation of the Inversion of Pd@Pt Core@Shell Dendrimer-Encapsulated Nanoparticles. *ACS Nano* **2013**, *7*, 9345-9353.
32. Frenkel, A.I.; Wang, Q.; Sanchez, S.I.; Small, M.W.; Nuzzo, R.G. Short range order in bimetallic nanoalloys: An extended X-ray absorption fine structure study. *J. Chem. Phys.* **2013**, *138*, 064202.
33. Zhang, Z.; Li, L.; Yang, J.C. Adhesion of Pt nanoparticles supported on  $\gamma$ -Al<sub>2</sub>O<sub>3</sub> single crystal. *J. Phys. Chem. C* **2013**, *117*, 21407-21412.
34. Li, L.; Wang, L.-L.; Johnson, D.D.; Zhang, Z.; Sanchez, S.I.; Kang, J.H.; Nuzzo, R.G.; Wang, Q.; Frenkel, A.I.; Ciston, J.; Stach, E.A.; Yang, J.C. Noncrystalline-to-crystalline transformations in Pt nanoparticles. *J. Am. Chem. Soc.* **2013**, *135*, 13062-13072.
35. Stach, E.A.; Zakharov, D.; Akatay, M.C.; Baumann, P.; Ribeiro, F.; Zvienevich, Y.; Li, Y.; Frenkel, A.I. Developments in environmental transmission electron microscopy for catalysis research *Microsc. Microanal.* **2013**, *19*, Suppl. 2, 1174-1175.
36. Zhang, S.; Tao, F.; Frenkel, A.I.; Takeda, S. Singly anchored Pt and Pd atoms on Co<sub>3</sub>O<sub>4</sub> and their catalytic performance. *Microsc. Microanal.* **2013**, *19*, Suppl. 2, 1620-1621.
37. Stach, E.A.; Baumann, P.; Li, Y.; Zakharov, D.; Frenkel, A.I. Using operando methods to characterize working catalysts with TEM, XAS, EXAFS and Raman Spectroscopy. *Microsc. Microanal.* **2013**, *19*, Suppl. 2, 1674-1675.
38. Zhang, S.; Shan, J.-J.; Zhu, Y.; Frenkel, A.I.; Patlolla, A.; Huang, W.; Yoon, S.; Wang, L.; Yoshida, H.; Takeda, S.; Tao, F. WGS Catalysis and in-situ studies of CoO(1-x)PtCo(n)/Co<sub>3</sub>O<sub>4</sub> and Pt(m)Co(m')/CoO(1-x) nanorod catalysts. *J. Am. Chem. Soc.* **2013**, *135*, 8283-8293.
39. Merte, L.R.; Ahmadi, M.; Behafarid, F.; Ono, L.K.; Lira, E.; Matos, J.; Li, L.; Yang, J.C.; Cuenya, B.R. Correlatign Catalytic Methanol Oxidation with the Structure and Oxidation State of Size-Selected Pt Nanoparticles. *ACS Catal.* **2013**, *3*, 1460-1468.
40. Frenkel, A.I.; Khalid, S.; Hanson, J.C.; Nachtegaal, M. QEXAFS in Catalysis Research: Principles, Data Analysis and Applications. In *In-situ Characterization of Heterogeneous Catalysts*, Chupas, P.; Hanson, J.; Rodriguez, J.A., Eds., John Wiley and Sons **2013**.
41. Frenkel, A.I.; Hanson, J.C. Combined XAFS-XRD methods in Catalysis Research. In *In-situ Characterization of Heterogeneous Catalysts*, Chupas, P.; Hanson, J.; Rodriguez, J. A., Eds., John Wiley and Sons **2013**.
42. Kossov, A.; Wang, Q.; Korobko, R.; Grover, V.; Feldman, Y.; Wachtel, E.; Tyagi, A.K.; Frenkel, A.I.; Lubomirsky, I. Evolution of the local structure at the phase transition in CeO<sub>2</sub>-Gd<sub>2</sub>O<sub>3</sub> solid solutions. *Phys. Rev. B* **2013**, *87*, 054101.

43. Perelshtein, I.; Ruderman, E.; Perkas, N.; Tzanov, T.; Beddow, J.; Joyce, E.; Mason, T.; Blanes, M.; Molla, K.; Patlolla, A.; Frenkel, A.I.; Gedanken, A., Chitosan and chitosan-ZnO-based complex nanoparticles: formation, characterization, and antibacterial activity. *J. Mater. Chem. B* **2013**, *1*, 1968-1976.
44. Sanchez, S.I.; Small, M.W.; Bozin, E.S.; Wen, J.-G.; Zuo, J.-M.; Nuzzo, R.G., Metastability and Structural Polymorphism in Noble Metals: the Role of Composition and Metal Atom Coordination in Mono- and Bimetallic Nanoclusters. *ACS Nano* **2013**, *7*, 1542-1557.
45. Amit, Y.; Eshet, H.; Faust, A.; Patlolla, A.; Rabani, E.; Banin, U.; Frenkel, A.I. Unraveling the Impurity Location and Binding in Heavily Doped Semiconductor Nanocrystals: The Case of Cu in InAs Nanocrystals. *J. Phys. Chem. C* **2013**, *117*, 13688-13696.
46. Amit, Y.; Eshet, H.; Milo, O.; Rabani, E.; Frenkel, A.I.; Banin, U. How to dope a semiconductor nanocrystal. *ECS Trans.* **2013**, *58*, 127-133.
47. Yancey, D.F.; Chill, S.T.; Zhang, L.; Frenkel, A.I.; Henkelman, G.; Crooks, R.M. A theoretical and experimental examination of systematic ligand-induced disorder in Au dendrimer-encapsulated nanoparticles. *Chem. Science* **2013**, *4*, 2912-2921.
48. Wang, L.; Zhang, S.; Zhu, Y.; Patlolla, A.; Shan, J.-J.; Yoshida, H.; Takeda, S.; Frenkel, A.I.; Tao, F. Catalysis and In-situ Studies of Rh/Co<sub>3</sub>O<sub>4</sub> Nanorods in Reduction of NO with H<sub>2</sub>. *ACS Catalysis* **2013**, *3*, 1011-1019.
49. Patlolla, A.; Baumann, P.; Xu, W.; Senanayake, S.; Rodriguez, J.A.; Frenkel, A.I. Characterization of Metal-Oxide Catalysts in Operando Conditions by Combining X-Ray Absorption and Raman Spectroscopies in the Same Experiment. *Top. Catal.* **2013**, *56*, 896-904.
50. Amakawa, K.; Sun, L.; Guo, C.; Havecker, M.; Kube, P.; Wachs, I.E.; Lwin, S.; Frenkel, A.I.; Patlolla, A.; Hermann, K.; Schlogl, R.; Trunschke A. *How strain affects the reactivity of surface metal oxide catalysts. Angew. Chem. Int. Ed.* **2013**, *52*, 13553-13557.
51. Frenkel, A.I., Applications of extended X-ray absorption fine-structure spectroscopy to studies of bimetallic nanoparticle catalysts. *Chem. Soc. Rev.* **2012**, *41*, 8163-8178.
52. Yang, J.C.; Small, M.W.; Grieshaber, R.V.; Nuzzo, R.G., Recent Developments and Applications of Electron Microscopy to Heterogeneous Catalysis. *Chem. Soc. Rev.* **2012**, *41*, 8179-8194.
53. Zhang, Z.; Gleeson, B.; Jung, K.; Li, L.; Yang, J.C., A Diffusion Analysis of Transient Subsurface gamma-Ni<sub>3</sub>Al Formation During beta-NiAl Oxidation, *Acta. Mater.* **2012**, *60*, 5273-5283.
54. Zhang, Z.; Jung, K.; Li, L.; Yang, J.C., Kinetic Aspects of Initial Stage Thin gamma-Al<sub>2</sub>O<sub>3</sub> Film Formation on Single Crystalline beta-NiAl (110). *J. Appl. Phys.* **2012**, *111*, 34312.
55. Erickson, E. M.; Thorum, M. S.; Vasic, R.; Marinkovic, N.; Frenkel, A. I.; Gewirth, A. A.; Nuzzo, R. G., In-Situ Electrochemical X-ray Absorbance Spectroscopy Oxygen Reduction Catalysis with High Oxygen Flux. *J. Am. Chem. Soc.* **2012**, *134*, 197-200.
56. Small, M. W.; Sanchez, S. I.; Marinkovic, N. S.; Frenkel, A. I.; Nuzzo, R. G., Influence of Adsorbates on the Electronic Structure, Bond Strain, and Thermal Properties of an Alumina-Supported Pt Catalyst. *ACS Nano*, **2012**, *6*, 5583-5595.
57. Yan, W.; Vasic, R.; Frenkel, A. I.; Koel, B. E., Intra-particle reduction of arsenite (As(III)) by nanoscale zerovalent iron (nZVI) investigated with *in-situ* X-ray absorption spectroscopy. *Environ. Sci. & Technology* **2012**, *46*, 7018-7026.
58. Patlolla, A.; Zunino III, J.; Frenkel, A. I.; Iqbal, Z., Thermochromism in Polydiacetylene-metal oxide nanocomposites *J. Mater. Chem.* **2012**, *22*, 7028-7035.
59. Myers, S. V.; Frenkel, A. I.; Crooks, R. M., In Situ Structural Characterization of Platinum Dendrimer-Encapsulated Oxygen Reduction Electrocatalysts. *Langmuir* **2012**, *28*(2), 1596-1603.
60. Ryu, H.; Lei, H.; Frenkel, A. I.; Petrovic, C., Local structural disorder-induced superconductivity in K(x)Fe(2-y)Se(2) materials *Phys. Rev. Lett.* **2012**, *85*, 224515.
61. Chen, W.-F.; Sasaki, K.; Ma, C.; Frenkel, A. I.; Marinkovic, N.; Muckerman, J. T.; Zhu, Y.; Adzic, R. R., Noble metal-free hydrogen-evolution catalysts based on NiMo nitride nanosheets. *Angew. Chemie Int. Ed.* **2012**, *51*, 6131-6135.
62. Yadgarov, L.; Rosentsveig, R.; Leitun, G.; Albu-Yaron, A.; Moshkovitz, A.; Perfiliev, V.; Vasic, R.; Frenkel, A. I.; Enyashin, A. N.; Seifert, G.; Rapoport, L.; Tenne, R., Controlled doping of MS<sub>2</sub> (M=W, Mo) nanotubes and fullerene-like nanoparticles *Ang. Chemie, Int. Ed.* **2012**, *51*, 1148-1151.
63. Yih, K.; Hamdemir, I.K.; Mondoch, J.E.; Bayrem, E.; Ozkar, S.; Vasic, R.; Frenkel, A.I.; Anderson, O.P.; Finke, R.G., Synthesis and Characterization of [Ir(1,5-Cyclooctadiene)(μ-H)]<sub>4</sub>: A Tetrametallic Ir<sub>4</sub>H<sub>4</sub>-core, Coordinatively Unsaturated Cluster. *Inorg. Chem.* **2012**, *51*, 3186-3193.
64. Frenkel, A.I.; Vasic, R.; Dukesz, B.; Li, D.; Chen, M.; Zhang, L.; Fujita, T.; Thermal Properties of Nanoporous Gold. *Phys. Rev. B* **2012**, *85*, 195419.

65. Landon, J.; Demeter, E.; Inoglu, N.; Keturakis, C.; Wachs, I.E.; Vasic R.; Frenkel, A.I.; Kitchin, J.R., Spectroscopic Characterization of Mixed Fe-Ni Oxide Electrocatalysts for the Oxygen Evolution Reaction in Alkaline Electrolytes. *ACS Catalysis* **2012**, *2*, 1793-1801.
66. Korobko, R.; Patlolla, A.; Kossoy, A.; Wachtel, E.; Tuller, H.L.; Frenkel, A.I.; Lubomirsky, I., Giant Electrostriction in Gd-doped Ceria. *Adv. Mater.* **2012**, *24*, 5857-5861.
67. Lyahovitskaya, V.; Feldman, Y.; Zon, I.; Yoffe, A.; Frenkel, A.I., Strain-arranged structure in amorphous films. *J. Mater. Res.* **2012**, *27*, 2819-2828.
68. Copping, R.; Slocik, J. M.; Briggs, B. D.; Frenkel, A. I.; Naik, R. R.; Knecht, M. R., Determining peptide sequence effects that control the size, structure and function of nanoparticles. *ACS Nano* **2012**, *6*, 1625-1636.
69. Patlolla, A.; Carino, E.V.; Ehrlich, S.N.; Stavitski, E.; Frenkel, A.I., Application of Operando XAS, XRD, and Raman Spectroscopy for Phase Speciation in Water Gas Shift Reaction Catalysts. *ACS Catalysis* **2012**, *2*, 2216-2223.
70. Lei, H.; Ryu, H.; Ivanovski, V.; Warren, J.B.; Frenkel, A.I.; Cekic, B.; Yin, W.-G.; Petrovic, C., Structure and physical properties of the layered iron oxychalcogenide BaFe<sub>2</sub>Se<sub>2</sub>O. *Phys. Rev. B* **2012**, *86*, 195133.

## **Solid-State Chemistry Production and Property of Platinum Group Metal Nanoparticle Catalysts with Tailored Particle Morphology**

Changlin Zhang, Sang Youp Hwang, Shirin Norooz Oliaee, Zhenmeng Peng  
Department of Chemical and Biomolecular Engineering, University of Akron, Akron, OH 44325

### **Poster Presentation Abstract**

Catalytic property of platinum group metal (PGM) nanoparticles can be altered significantly by the nature of facets exposed. For example, Pt (100) plane excels in activity/selectivity compared to other planes in many reactions, including ring-opening hydrogenation of pyrroles, benzene hydrogenation, methanol oxidation (MOR), and electro-oxidation of ammonia (AOR). Pt-Ni (111) surface can exhibit exceptionally high activity towards oxygen reduction reaction (ORR) for polymer electrolyte membrane fuel cells (PEMFCs). The findings have stimulated the exploration of new methods for preparing PGM catalysts with tailored particle morphology, because the usage of PGMs and thus the cost can be largely decreased. However, to date, there have been no feasible methods for cost-effective and mass production of the shaped PGM nanoparticle catalysts.

We realize scalable production of PGM nanoparticle catalysts with tailored particle morphology by developing a green and low manufacturing cost solid-state chemistry approach. A variety of shaped PGM nanoparticle catalysts, including cubic Pt/SiO<sub>2</sub>, cubic Pt/C, tetrahedral Pd/C, octahedral Pt-Ni/C, and cubic Pt-Cu/C, have been demonstrated for preparation. The experiments suggest that the formation of shaped PGM nanoparticles is resultant of employing both CO and H<sub>2</sub> gases, wherein H<sub>2</sub> aids transportation and reduction of the metal precursors on support and CO is responsible for the particle morphology formation. Several catalytic reactions, including preferential CO oxidation, hydrazine decomposition, ORR, and AOR, have been studied using the prepared catalysts. The octahedral Pt<sub>1.5</sub>Ni/C catalyst exhibits high ORR activities of 3.99 mA/cm<sup>2</sup> Pt and 1.96 A/mg Pt at 0.90 V vs. RHE, which are about 20 and 10 times the values for commercial Pt/C specifically. The cubic Pt/C catalyst shows 1.44 mA/cm<sup>2</sup> at 0.6 V vs. RHE in AOR, which is five times that of 0.30 mA/cm<sup>2</sup> using commercial Pt/C.

### **Grant or FWP Number: Grant Title**

N/A (I was invited as new investigator.)

## Characterization of Catalytic Materials by DNP-Enhanced Solid-State NMR

Takeshi Kobayashi, Aaron D. Sadow, Igor I. Slowing, Marek Pruski  
Ames Laboratory, U.S. DOE, Iowa State University, Ames, IA 50011-3111

### Presentation Abstract

Characterization of heterogeneous catalysts by solid-state (SS)NMR for decades suffered because of the intrinsically low sensitivity, especially in structural elucidations of minute concentrations of catalytic sites, fast screening of new materials and identification of short-lived intermediates. Recent developments in dynamic nuclear polarization (DNP) afforded remarkable signal enhancements, enabling measurements that are off-limits to traditional SSNMR. We will report several novel applications of these methods to the studies of catalytic materials in our laboratory, which indeed demonstrate that the DNP-driven hyperpolarization opens an unprecedented range of opportunities in surface science and catalysis. The studies commenced in collaboration with O. Lafon and G. Bodenhausen using an instrument located in Lausanne (Switzerland), but most of the results were recently obtained at the Ames Laboratory on a newly installed 400 MHz DNP NMR spectrometer funded by DOE Basic Energy Sciences.

**(AL-03-380-011: Homogeneous and Interfacial Catalysis in 3D Controlled Environment)**

### Recent Progress

We systematically studied the enhancement factor (per scan) and the sensitivity enhancement (per unit time) in  $^{13}\text{C}$  and  $^{29}\text{Si}$  cross-polarization magic angle spinning (CPMAS) NMR boosted by DNP of functionalized mesoporous silica nanoparticles (MSNs). We separated contributions due to: (i) microwave irradiation, (ii) quenching by paramagnetic effects, (iii) the presence of frozen water, (iv) the temperature, as well as changes in (v) relaxation and (vi) cross-polarization behaviour. Notwithstanding a significant signal reduction due to quenching by TOTAPOL radicals, DNP CPMAS at 100 K provided global sensitivity enhancements of 23 and 45 for  $^{13}\text{C}$  and  $^{29}\text{Si}$ , respectively, relative to standard CPMAS measurements at room temperature.<sup>1</sup> The most recently developed biradical polarizing agents (AMUPol, TEKPol) provided further boost to sensitivity affording enhancements of 100-150 in our laboratory.

We demonstrated that DNP can be used to enhance NMR signals of  $^{13}\text{C}$ ,  $^{15}\text{N}$  and  $^{29}\text{Si}$  nuclei located in mesoporous organic/inorganic hybrid materials, at several hundreds of nanometers from stable radicals trapped in the surrounding frozen disordered water. The approach was used to study the MSNs functionalized with 3-(N-phenylureido)propyl (PUP) groups, filled with the surfactant cetyltrimethylammonium bromide (CTAB), where the DNP-enhanced proton magnetization was transported into the mesopores via  $^1\text{H}$ - $^1\text{H}$  spin diffusion and transferred to rare spins by cross-polarization.<sup>2</sup> We explored the same approach to study the host-guest interaction between metal ions ( $\text{Pt}^{2+}$  and  $\text{Cu}^{2+}$ ) and a zirconium metal-organic framework (MOF, UiO-66-NH<sub>2</sub>) using DNP-enhanced  $^{15}\text{N}\{^1\text{H}\}$  CPMAS NMR supported by X-ray absorption spectroscopy and density-functional theory.<sup>3</sup> The combined experimental results conclude that

each  $\text{Pt}^{2+}$  coordinates with two  $-\text{NH}_2$  groups from the MOF and two  $\text{Cl}^-$  from the metal precursor, whereas  $\text{Cu}^{2+}$  do not form chemical bonds with the  $-\text{NH}_2$  groups of the MOF framework. Density-functional theory calculations reveal that  $\text{Pt}^{2+}$  prefers a square-planar structure with the four ligands and resides in the octahedral cage of the MOF in either *cis*- or *trans*- configurations.

We demonstrated that the elimination of solvent-derived signals in DNP-enhanced 2D  $^1\text{H}$ -X heteronuclear correlation (HETCOR) experiments may be simply accomplished by using proton-less solvents.<sup>4</sup> In fact, the use of such solvents affords an additional sensitivity gain when studying naturally abundant surface species. This approach notably prevented HETCOR spectra of surface-bound catalytic groups from being obfuscated by the unwanted signals originating from the correlations to the solvent. We also explored the feasibility of indirect detection in DNP-enhanced HETCOR experiments.

Due to its extremely low natural abundance and quadrupolar nature, the  $^{17}\text{O}$  nuclide is very rarely used for spectroscopic investigation of solids by NMR without isotope enrichment. We recently demonstrated new DNP-based measurements that extend  $^{17}\text{O}$  SSNMR beyond its current capabilities. The use of the PRESTO technique instead of conventional  $^1\text{H}$ - $^{17}\text{O}$  cross-polarization greatly improved the sensitivity and enabled the facile measurement of undistorted lineshapes, two-dimensional  $^1\text{H}$ - $^{17}\text{O}$  HETCOR NMR spectra, as well as accurate internuclear distance measurements at natural abundance. This was applied for distinguishing hydrogen-bonded and non-hydrogen-bonded  $^{17}\text{O}$  sites on the surface of silica gel; the 1D spectrum of which could not be used to extract such detail. Lastly, this greatly enhanced sensitivity has enabled, for the first time, the detection of surface hydroxyl sites on mesoporous silica at natural abundance, thereby extending the concept of DNP surface-enhanced NMR spectroscopy (DNP-SENS) of catalytic materials to the  $^{17}\text{O}$  nuclide.<sup>5</sup>

We will also present DNP-enhanced spectra of other challenging systems, including natural abundance  $^{15}\text{N}$  spectra of a new silica-supported zirconium  $\text{Zr}(\text{NMe}_2)_n@MSN$  catalyst for hydroboration of aldehydes and ketones developed in our catalysis program. Until now, such catalytic sites were undetectable by conventional  $^{15}\text{N}$  SSNMR. Similarly,  $^{29}\text{Si}$  and  $^{27}\text{Al}$  DNP NMR was used to characterize isolated  $(-\text{AlO})_3\text{Si}(\text{OH})$  sites deposited on the  $\gamma\text{-Al}_2\text{O}_3$  surface via atomic layer deposition (in collaboration with T.J. Marks and P.C. Stair, from Northwestern University). We also identified, for the first time, the molecular binding intermediates on metal nanoparticles by DNP NMR (in collaboration with J. Dumesic, from UW-Madison and B. Shanks from Iowa State University). Finally, we acquired  $^{27}\text{Al}\{^1\text{H}\}$  CPMAS spectra small surface  $\text{Al}_x\text{O}_y$  films deposited on silicon wafers (in collaboration with S. Hayes from Washington University). In this case, the MAS rotor contained only a few  $\text{cm}^2$  of studied surface (!), thereby raising the prospects of eliciting detectable NMR signals from the surfaces of single crystals. These capabilities will provide new catalytic insights never before revealed in low surface catalytic materials.

This work is part of Ames Laboratory research on "Homogeneous and Interfacial Catalysis in 3D Controlled Environment", described in detail elsewhere.

## Publications

1. Kobayashi, T.; Lafon, O.; Lilly Thankamony, A. S.; Slowing, I. I.; Kandel, K.; Carnavale, D. Vitzthum, V.; Vezin, H.; Amoureux, J.-P.; Bodenhausen G.; Pruski M. Analysis of sensitivity enhancement by dynamic nuclear polarization in solid-state NMR: a case

- study of functionalized mesoporous materials. *Phys. Chem. Chem. Phys.*, **2013**, *15*, 5553-5562.
2. Lafon, O.; Lilly Thankamony, A. S.; Kobayashi, T.; Carnavale, D.; Vitzthum, V.; Slowing, I. I.; Kandel, K.; Vezin, H.; Amoureux, J.-P.; Bodenhausen G.; Pruski M. Mesoporous silica nanoparticles loaded with surfactant: low temperature magic angle spinning  $^{13}\text{C}$  and  $^{29}\text{Si}$  NMR enhanced by dynamic nuclear polarization. *J. Phys. Chem. C*, **2013**, *117*, 1375-1382.
  3. Guo, Z.; Kobayashi, T.; Wang, L.-L.; Goh, T. W.; Xiao, C.; Caporini, M. A.; Rosay, M.; Johnson, D. D.; Pruski, M.; Huang W. Selective host-guest interaction between metal ions and metal organic framework using dynamic nuclear polarization enhanced solid-state NMR spectroscopy. *Chem-Eur. J.*, **2014**, *20*, 16308-16313.
  4. Kobayashi, T.; Perras, F. A.; Slowing, I. I.; Huang, W.; Sadow, A. D.; Pruski, M., DNP-enhanced 2D  $^1\text{H}$ -X heteronuclear correlation spectroscopy using proton-less solvent for eliminating the solvent-derived signals, *submitted*.
  5. Perras, F. A.; Kobayashi, T.; Pruski, M., Natural abundance  $^{17}\text{O}$  DNP two-dimensional and surface enhanced NMR spectroscopy, *submitted*.

**Reactivity of oxide and sulfide supported metal nanoparticles: role of the interface**

Talat S. Rahman, Ludwig Bartels,\* Duy Le, Takat Rawal and Sampyo Hong

University of Central Florida

\*University of California, Riverside

**Presentation Abstract**

While the reactivity of metallic nanoparticles, as function of shape, size, and composition has been the subject of many investigations, more recently attention has focused on the role of interfacial and perimeter sites. This is not surprising as the interface can provide a better and stronger mixing of the wave functions of the reactants, nanoparticle, and the substrate atoms. However, not all supported metal nanoparticles nor all chemical reactions exhibit such interface effect. Given the recent interest in single layer MoS<sub>2</sub> and the large number of studies already carried out on titania, in this presentation we will compare and contrast the microscopic details of CO oxidation and methanol decomposition on sub-nanometer sized metallic nanoparticles (Au, Ag, Pt), supported on vacancy-laden single layer MoS<sub>2</sub> and TiO<sub>2</sub>(110). Activation energy barriers and reaction pathways will be calculated using density functional theory and the nudged elastic band method. We will pay attention to the role of charge transfer at the interface and its impact on the formation and scission of specific bonds. In particular, an activation mechanism which is applicable for both CO and methanol oxidation reactions in the interface of Au/TiO<sub>2</sub> will be discussed [1] and its validity with MoS<sub>2</sub> as the substrate will be tested.

[1] S. Hong and T. S. Rahman, J. Am. Chem. Soc. 135, 7629 (2013).

Work supported in part by DOE grant DE-FG02-07ER15842.

**DE-FG02-07ER46354: Controlling Structural, Electronic, and Energy Flow Dynamics of Catalytic Processes through Tailored Nanostructures**

**PI:** Talat S. Rahman ; **Co PI :** Ludwig Bartels

**Postdocs:** Duy Le, Sampyo Hong

**Students:** Wenhao Lu, Koichi Yamaguchi, Chen Wang, Quan Ma, Miguel Isarraraz, Michael Gomez, Cindy Merida, Ariana Nguyen, Gretel von Son, Sahar Naghibi, Takat B. Rawal, Maral Aminpour, S. Islamuddin Shah, Ghazal Shafai

**Affiliations:** University of Central Florida and University of California, Riverside

**RECENT PROGRESS**

(See main abstract with Bartels as presenter)

## **Influence of Support Effects on CO Oxidation by Graphene–Pt<sub>13</sub> Nanocomposites**

Ashwin Ramasubramaniam, Ioanna Fampiou  
Department of Mechanical & Industrial Engineering, University of Massachusetts Amherst

### **Presentation Abstract**

Pt nanoclusters on carbon supports have been shown to possess superior catalytic activity and increased selectivity in a variety of electrochemical reactions as compared to bulk Pt electrodes; however, the underlying mechanisms remain poorly understood. As a step towards unraveling the critical role of cluster–support interactions in these systems, we study as a model system the CO oxidation reaction on graphene–supported Pt<sub>13</sub> nanoclusters using first-principles density functional theory calculations. As CO adsorption on Pt<sub>13</sub> clusters is found to be substantially stronger than O adsorption, we focus on understanding CO oxidation kinetics on CO-saturated Pt nanoclusters. For this high CO coverage regime, the relevant kinetic mechanism is shown to proceed via a CO\*-assisted activation of the O<sub>2</sub> molecule, resulting in the formation of an O\*–O–C\*–O transition state that eventually forms a CO<sub>2</sub> molecule and a chemisorbed O\* species. By sampling this particular reaction pathway at various surface sites on unsupported Pt<sub>13</sub> nanoclusters as well as clusters bound at support point defects (vacancies/divacancies) in graphene, we show that strong support–cluster interactions substantially reduce the CO oxidation reaction barrier, on average, by about 0.5 eV. Our results suggest that defect engineering of carbon supports could serve to enhance the catalytic activity of ultrasmall Pt nanoclusters, opening up another dimension for rational design of catalytic materials.

### **DE-SC0010610: Computational Design of Graphene–Nanoparticle Catalysts**

**PI:** Dr. Ashwin Ramasubramaniam

**Students:** Dr. Ioanna Fampiou, Mr. Raymond Gasper, Mr. Hongbo Shi

### **RECENT PROGRESS**

#### ***CO Adsorption and Oxidation on Graphene-Supported Pt Nanoclusters:***

We systematically investigated CO binding on unsupported and graphene-supported clusters. [1, 2] For defective graphene supports, in particular, we showed that the cluster–support interaction leads to an appreciable downshift of the cluster *d*-band center. This, in turn, leads to weaker CO adsorption on the cluster and provides a possibility for defect engineering of supports as a means of controlling cluster catalytic activity. While reduced strength of adsorbate binding provides a possible explanation for improved CO tolerance of Pt-graphene nanocomposites, it does not furnish *direct* proof of a reduced reaction barrier for CO oxidation. To conclusively establish this, we performed systematic DFT studies of the CO oxidation reaction on supported and unsupported Pt<sub>13</sub> nanoclusters. [3] In general, CO adsorption energies and oxidation barriers depend sensitively upon the coordination of catalyst atom(s) at the binding site. Unlike

crystalline facets, the local coordination on a nanocluster is highly variable and requires expensive DFT-based statistical sampling. Site-to-site variations in adsorption energies and reaction barriers are nevertheless sufficiently small such that signatures of cluster–substrate interactions can still be identified and systematically analyzed.

Given that CO\* binding to Pt<sub>13</sub> clusters is substantially stronger (by 0.7-0.8 eV) than O\*, the Pt cluster is expected to be *fully saturated* by CO under normal operating conditions. Therefore, in departure from most studies in the literature, we went beyond single-CO oxidation studies and studied CO oxidation on fully saturated clusters. We examined reaction pathways that proceed via CO\*-assisted O<sub>2</sub> activation without the involvement of adsorbed O<sub>2</sub>\* precursors, which was shown recently by Neurock, Iglesia, and coworkers to be favored over the Langmuir-Hinshelwood mechanism. Using the Climbing Nudged Elastic Band Method, we sampled multiple reaction sites and trajectories on supported as well as unsupported Pt<sub>13</sub> clusters, examples of which are displayed in Fig. 1. The reaction initiates via CO\*-assisted O<sub>2</sub> activation in the vicinity of the CO-covered Pt<sub>13</sub> cluster and proceeds with the formation of an O\*-O-C\*-O complex, which subsequently decomposes to CO<sub>2</sub> and an adsorbed O\* species. The mechanism is similar to that proposed by Neurock, Iglesia, and coworkers for CO oxidation at an unsupported cuboctahedral Pt<sub>201</sub> cluster: neither the involvement of adsorbed O<sub>2</sub>\* precursors nor O<sub>2</sub> dissociation are necessary; instead, there is direct reaction of O<sub>2</sub> with pre-adsorbed CO\* on the cluster. Typically, the O\*-O-C\*-O complex dissociates exothermically to CO<sub>2</sub> and O\*. The support effect in these reactions is appreciable: CO oxidation on unsupported Pt<sub>13</sub> clusters requires significantly higher activation energies (~1.22-1.97 eV) as compared to CO-covered Pt<sub>13</sub> clusters bound at point defects in graphene (~0.3-0.9 eV). The fundamental cause of this large difference in energy barriers can be attributed to the downshift of the *d*-levels for clusters bound at graphene point defects. The normally strong CO binding is then weakened and, in keeping with the Sabatier principle, the barrier for CO oxidation is lowered. Defective-graphene-supported Pt<sub>13</sub> nanoclusters are thus identified as effective catalysts for CO reduction with significantly lower activation energies than unsupported clusters. In the course of our studies, we also identified an oxidation pathway (hitherto only reported on Au) wherein, after the CO\*-assisted O<sub>2</sub> activation, the system falls into a stable minimum forming a carbonate-like CO<sub>3</sub>\* intermediate, which then endothermically dissociates into O\* and CO<sub>2</sub>. The apparent activation energy for this pathway is typically higher than the exothermic pathway discussed above though, and is expected to be less kinetically relevant.

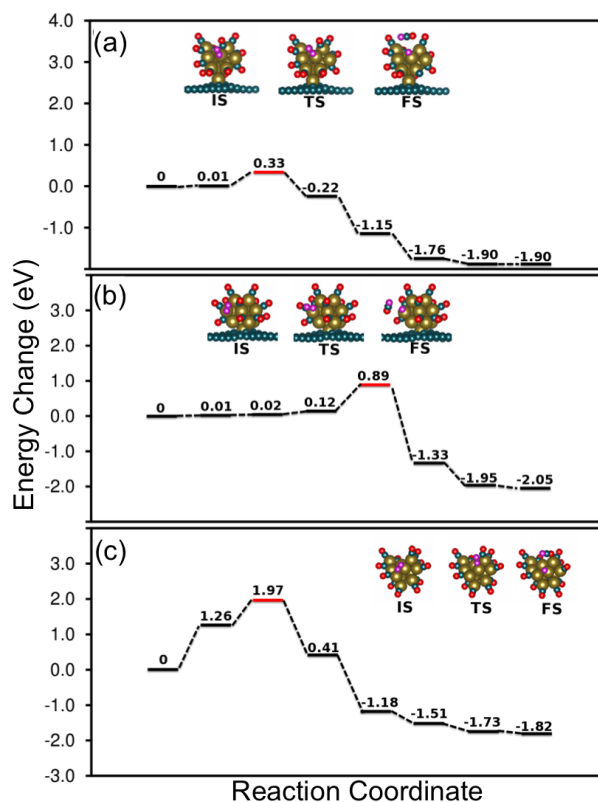


**Figure 1:** Sample energy profiles for CO oxidation on Pt<sub>13</sub> clusters (a) at a vacancy on graphene, (b) at a divacancy on graphene, and (c) without a support.

### **References:**

- [1] Fampiou, I.; Ramasubramaniam, A. CO Adsorption on Defective Graphene-Supported Pt<sub>13</sub> Nanoclusters, *J. Phys. Chem. C* **2013**, 117 (39), 19927-19933.
- [2] Fampiou, I.; Ramasubramaniam, A. Binding of Pt nanoclusters to defects in graphene: adsorption, morphology, and electronic structure, *J. Phys. Chem. C* **2012**, 116 (11), 6543-6555.
- [3] Fampiou, I.; Ramasubramaniam, A. The Influence of Support Effects on CO Oxidation Kinetics on Graphene-Supported Pt<sub>13</sub> Nanoclusters, *J. Phys. Chem. C* **2015**, 119 (16), 8703-8710.

### **Publications Acknowledging this Grant in 2013-2015**

1. Fampiou, I.; Ramasubramaniam, A. CO Adsorption on Defective Graphene-Supported Pt<sub>13</sub> Nanoclusters, *J. Phys. Chem. C* **2013**, 117, 19927.
2. Fampiou, I.; Ramasubramaniam, A. The Influence of Support Effects on CO Oxidation Kinetics on Graphene-Supported Pt<sub>13</sub> Nanoclusters, *J. Phys. Chem. C* **2015**, 119 (16), 8703-8710.

**Andrew M. Rappe**

**Synergistic Oxygen Evolving Activity of  
a TiO<sub>2</sub>-Rich Reconstructed SrTiO<sub>3</sub>(001) Surface**

John Mark P. Martirez, Seungchul Kim, Erie H. Morales,  
Benjamin T. Diroll, Matteo Cargnello, Thomas R. Gordon,  
Christopher B. Murray, Dawn A. Bonnell, and Andrew M. Rappe

The Makineni Theoretical Laboratories,  
Department of Chemistry, and  
Department of Materials Science and Engineering,  
University of Pennsylvania,  
Philadelphia, Pennsylvania 19104-6323 United States

Center for Computational Science,  
Korea Institute of Science and Technology,  
Seoul 136-791, Republic of Korea

**Presentation Abstract**

In addition to composition, the structure of a catalyst is another fundamental determinant of its catalytic reactivity. Recently, anomalous Ti oxide-rich surface phases of ternary oxides have been stabilized as nonstoichiometric epitaxial overlayers. These structures give rise to different modes of oxygen binding, which may lead to different oxidative chemistry. Through density functional theory investigations and electrochemical measurements, we predict and subsequently show that such a TiO<sub>2</sub> double-layer surface reconstruction enhances the oxygen evolving activity of the perovskite-type oxide SrTiO<sub>3</sub>. Our theoretical work suggests that the improved activity of the restructured TiO<sub>2</sub> (001) surface toward oxygen formation stems from (i) having two Ti sites with distinct oxidation activity and (ii) being able to form a strong O–O moiety (which reduces overbonding at Ti sites), which is a direct consequence of (iii) having a labile lattice O that is able to directly participate in the reaction. Here, we demonstrate the improvement of the catalytic performance of a well-known and well-studied oxide catalyst through more modern methods of materials processing, predicted through first-principles theoretical modeling.

**DE-FG02-07ER15920: Exploring the flexibility and the polarization of ferroelectric perovskite surfaces to achieve efficient photochemistry and enantiospecificity**

**Postdoc(s):** Dr. Seungchul Kim, Dr. Jianmin Tao, Dr. Liang Tan

**Student(s):** John Mark P. Martirez (now postdoc with Emily Carter); Rob Wexler

**Undergrad(s):** Nathan Koocher, Kevin Scanlan

### Recent Progress:

- Examination of graphene chemistry, including graphene growth (#1) and electrostatic doping with oxides (#9)
- Control of surface chemistry and surface oxide composition by changing ferroelectric polarization (#2)
- New accurate methodology to model van der Waals interactions between molecules and metal surface (#3)
- First principles approach to exactly and unambiguously to calculate oxidation state from first principles (#4)
- Study of charge ordering metal-insulator transition and its modification with doping (#5)
- First demonstration of chemical activity of nonstoichiometric epitaxial perovskite oxide surfaces (#6, subject of this poster abstract)
- Examination of nonstoichiometric surface phase transitions (#8,#11) and their interactions with water (#7)
- Studies of octahedral rotations in oxide superlattices (#10)
- Oxide/metal interfaces and the coupling of oxide structure to interfacial charge transfer (#12)
- Control of catalytic metal particle morphology via oxide surface dipole (#13)

### Publications Acknowledging this Grant in 2012-2015:

**13 publications, including Nat. Comm., JACS, 3PRL, 2ACSNano, NanoLett, JPCL, 3PRB**

1. Han, Gang Hee, Julio A. Rodríguez-Manzo, Chan-Woo Lee, Nicholas J. Kybert, Mitchell B. Lerner, Zhengqing John Qi, Eric N. Dattoli, Andrew M. Rappe, Marija Drndic, and AT Charlie Johnson. "Continuous growth of hexagonal graphene and boron nitride in-plane heterostructures by atmospheric pressure chemical vapor deposition." *ACS nano* 7, no. 11 (2013): 10129-10138.
2. Saidi, Wissam A., John Mark P. Martirez, and Andrew M. Rappe. "Strong reciprocal interaction between polarization and surface stoichiometry in oxide ferroelectrics." *Nano letters* 14, no. 11 (2014): 6711-6717.
3. Tao, Jianmin, and Andrew M. Rappe. "Physical Adsorption: Theory of van der Waals Interactions between Particles and Clean Surfaces." *Physical review letters* 112, no. 10 (2014): 106101.
4. Jiang, Lai, Sergey V. Levchenko, and Andrew M. Rappe. "Rigorous definition of oxidation states of ions in solids." *Physical review letters* 108, no. 16 (2012): 166403.
5. Jiang, Lai, Diomedes Saldana-Greco, Joseph T. Schick, and Andrew M. Rappe. "Enhanced charge ordering transition in doped  $\text{CaFeO}_3$  through steric templating." *Physical Review B* 89, no. 23 (2014): 235106.

6. Martirez, John Mark P., Seungchul Kim, Erie H. Morales, Benjamin T. Diroll, Matteo Cargnello, Thomas R. Gordon, Christopher B. Murray, Dawn A. Bonnell, and Andrew M. Rappe. "Synergistic Oxygen Evolving Activity of a TiO<sub>2</sub>-Rich Reconstructed SrTiO<sub>3</sub> (001) Surface." *Journal of the American Chemical Society* 137, no. 8 (2015): 2939-2947.
7. Koocher, Nathan Z., John Mark P. Martirez, and Andrew M. Rappe. "Theoretical Model of Oxidative Adsorption of Water on a Highly Reduced Reconstructed Oxide Surface." *The Journal of Physical Chemistry Letters* 5, no. 19 (2014): 3408-3414.
8. Martirez, John Mark P., Erie H. Morales, Wissam A. Saidi, Dawn A. Bonnell, and Andrew M. Rappe. "Atomic and Electronic Structure of the BaTiO<sub>3</sub> (001)( $\sqrt{5}\times\sqrt{5}$ ) R 26.6° Surface Reconstruction." *Physical review letters* 109, no. 25 (2012): 256802.
9. Baeumer, Christoph, Diomedes Saldana-Greco, John Mark P. Martirez, Andrew M. Rappe, Moonsub Shim, and Lane W. Martin. "Ferroelectrically driven spatial carrier density modulation in graphene." *Nature Communications* 6 (2015).
10. Schick, Joseph T., Lai Jiang, Diomedes Saldana-Greco, and Andrew M. Rappe. "Coupling between octahedral rotations and local polar displacements in WO<sub>3</sub>/ReO<sub>3</sub> superlattices." *Physical Review B* 89, no. 19 (2014): 195304.
11. Morales, Erie H., John Mark P. Martirez, Wissam A. Saidi, Andrew M. Rappe, and Dawn A. Bonnell. "Coexisting Surface Phases and Coherent One-Dimensional Interfaces on BaTiO<sub>3</sub> (001)." *ACS nano* 8, no. 5 (2014): 4465-4473.
12. Polanco, Miguel Angel Méndez, Ilya Grinberg, Alexie M. Kolpak, Sergey V. Levchenko, Christopher Pynn, and Andrew M. Rappe. "Stabilization of highly polarized PbTiO<sub>3</sub> nanoscale capacitors due to in-plane symmetry breaking at the interface." *Physical Review B* 85, no. 21 (2012): 214107.
13. Kim, Seungchul, Michael Rutenberg Schoenberg, and Andrew M. Rappe. "Kinetics of palladium particles on LiNbO<sub>3</sub>: an origin of the polarization-dependent catalysis." In *MRS Proceedings*, vol. 1397, pp. mrsf11-1397. Cambridge University Press, 2012.

**Fundamental Studies of Oxidation Reactions on Model Catalysts  
Catalytic Sites for Propylene Epoxidation by O<sub>2</sub> and H<sub>2</sub> over Au/ titanium silicalite-1**

Fabio H. Ribeiro and W. Nicholas Delgass  
School of Chemical Engineering, 480 Stadium Mall Drive, West Lafayette, IN 47907

**Presentation Abstract**

The discovery by Haruta more than a decade ago that by co-feeding H<sub>2</sub> with propylene and O<sub>2</sub> and using Au/TiO<sub>2</sub> as the catalyst, one can produce PO with high selectivity provides the potential for a single-step, direct and green solution to this long standing catalytic partial oxidation challenge. We have focused on Au/TS-1 catalysts and probed the nature and location of the active Au. Since proximity of Au and Ti is required for the catalysis, the activity of Au on a support made by coating TS-1 with an S-1 shell showed that Au clusters small enough to enter the MFI pore structure are active for PO production. Addition of Au to uncalcined TS-1, the pores of which were still blocked by the template, led to an unprecedented 20 hour activation period. Correlated changes in apparent surface area and other supported data showed that peroxide generated from H<sub>2</sub> and O<sub>2</sub> over the Au particles burned some of the template out of the pores, allowing Au migration to the Ti anchor points that create the active sites in the pores. Analysis of the most active catalysts yet reported, 300 g<sub>POH</sub><sup>-1</sup>kg<sub>cat</sub><sup>-1</sup>, showed that the Cs salt used in deposition precipitation of the Au in these catalysts helps to stabilize the small Au particles in the TS-1 pores, thus maximizing the number of stable Au sites. These studies all confirm the importance of Au clusters small enough to enter the TS-1 pore structure as active sites for propylene epoxidation. Our planned work for the coming year will focus on (i) further understanding the *site requirements* for the PO reaction (H<sub>2</sub>O<sub>2</sub> production) via kinetic studies including isotopic switch experiments, titration experiments, periodic Density Functional Theory calculations, and using specially designed materials combined with various characterization techniques, (ii) studying the *origin of the catalyst deactivation* in the Au/TS-1 system via *operando* IR experiments, (iii) further exploring the higher *H<sub>2</sub> selectivity* observed in the Au/Uncalcined-TS-1 system, and (iv) participating in the *development of the new technique* of X-ray emission spectroscopy.

**Grant title: Fundamental Studies of Oxidation Reactions on Model Catalysts**

**Grant number:** DE-FG02-03ER15408

**PI:** Fabio H. Ribeiro and W. Nicholas Delgass

**Student(s):** Viktor J. Cybulskis, Wen-Sheng Lee

**RECENT PROGRESS**

Recent work has focused three areas. The first is closure of the work on Au supported on uncalcined TS-1 supports, Au/U-TS-1. The motivation for that work was to force the gold to be deposited on the outer surface of the TS-1 crystallites by blocking the interior pore structure by not removing the template around which the TS-1 structure grows during its synthesis. Second is elaboration of the discovery that the reaction rate of Au/TS-1 can be dramatically enhanced by using Cs<sub>2</sub>CO<sub>3</sub> instead of our standard Na<sub>2</sub>CO<sub>3</sub> as the pH control agent during the deposition precipitation (DP) of the Au. The third is examination of the effects of the residual Na left from the standard DP process, the Cl left from the chloroauric acid gold precursor, and the method of activation.

**Au/U-TS-1:** The preliminary results of this approach given in last year's annual report have now been published in the *Journal of Catalysis*. The unique feature of this catalyst is its slow activation, taking nearly 20 hours to reach full activation. In contrast, Au/TS-1 with the same Au loading rises almost

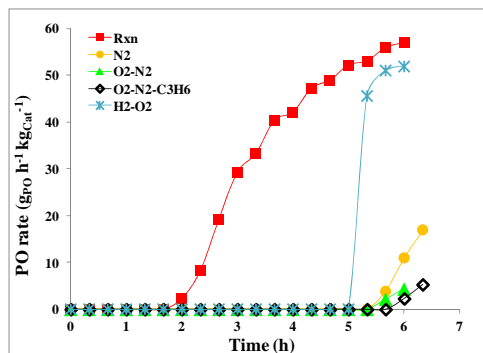


Figure 2 PO rate per gram of catalyst as a function of time for 0.05Au/UTS-1(119) samples first pretreated under different conditions for 5 h at  $\sim 200$  °C (including the time for temperature ramping with a ramping rate  $\sim 1$  °C  $\text{min}^{-1}$ ): (■) normal reaction conditions (10 vol% each of  $\text{H}_2, \text{O}_2, \text{C}_3\text{H}_6$  in  $\text{N}_2$ ), (●) pure  $\text{N}_2$  (▲) 10 vol%  $\text{O}_2$  in  $\text{N}_2$  (◊) 10 vol% each of  $\text{O}_2$  and  $\text{C}_3\text{H}_6$  in  $\text{N}_2$  (×) 10% each of  $\text{H}_2$  and  $\text{O}_2$  in  $\text{N}_2$ , and then tested under normal conditions for another 1-2 h. For reference, the BET apparent surface area of UTS-1(119) was  $21 \pm 1$   $\text{m}^2$   $\text{g}^{-1}$ .

hydrogen selectivity may well be the deciding factor on whether this catalyst will ever be applied commercially. We note that the sample 0.01Au/U-TS-1(119) showed the  $\text{H}_2$  selectivity at the level of  $\sim 55\%$  with PO rate  $\sim 60$   $\text{gPO h}^{-1} \text{kgCat}^{-1}$  at 200 °C, which is the highest  $\text{H}_2$  selectivity yet reported at similar conditions.

**Effects of Cs on Au/TS-1:** We have known for some time that Au efficiency for the PO reaction is highest at the lowest loadings, an observation consistent with need for small, isolated Au clusters. Thus an optimal gold loading can be expected at a point where the increase in the number of sites with increasing loading is offset by the decrease in Au efficiency. This effect is illustrated in Fig 3. Fig 3b show clearly that the efficiency drops with loading regardless of the method of catalyst preparation. Fig 3a, however, shows a surprising effect of Cs vs. other alkali metals as the cation of the DP agent. With Cs the drop in efficiency is delayed as the rate increases, allowing the rate to continue increasing to higher Au loading. The net effect is a doubling of the rate to the highest value yet recorded for PO production over Au catalysts.

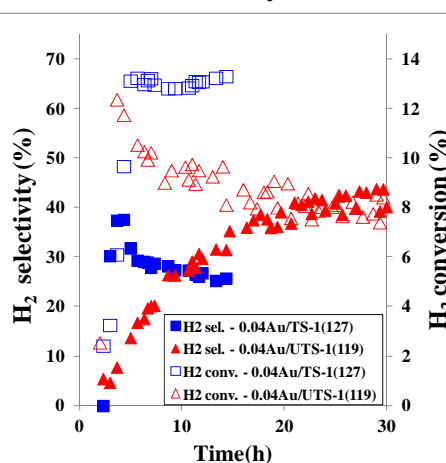
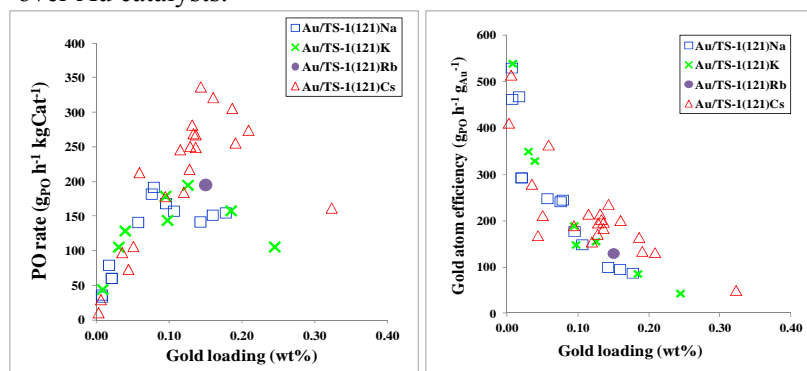


Figure 1.  $\text{H}_2$  selectivity/conversion as a function of time

Figure 3. a) (left) PO rate per gram of catalyst and b) (right) PO rate per gram of gold for Au/TS-1(121) with different gold loadings prepared by using different precipitation agents:  $\text{Na}_2\text{CO}_3$ ,  $\text{K}_2\text{CO}_3$ ,  $\text{Rb}_2\text{CO}_3$ , and  $\text{Cs}_2\text{CO}_3$ . The data were taken as the average values of the first 1–2 h at 200 °C. The circled data points were the rates right at 200 °C (reacted at 200 °C for less than 0.5 h).

As shown in Figure 4, there is some deactivation of these high rate catalysts, but they still level out at well above 200  $\text{g}_{\text{PO}}\text{h}^{-1}\text{g}_{\text{cat}}^{-1}$ . It is also interesting to note that we have found that the Cs enhances the catalyst performance even if it is added after DP with Na, provided the Au loading is high enough. At

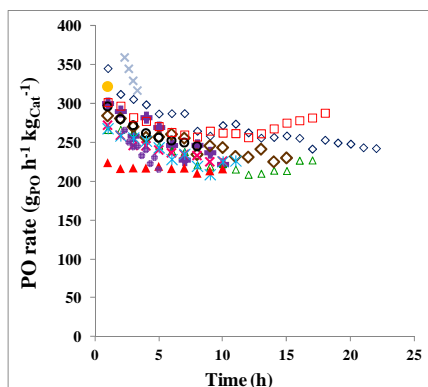


Figure 4. PO rates for 12 Au/TS-1 (121)Cs catalysts as a function of time on stream

very low Au loading, sintering is not a problem and Cs is not needed. This can be seen in the low loading portion of Fig 3a, where the slopes are about the same for the Na and Cs samples. At higher loading, however, the presence of Cs retards sintering and preserves the population of optimal sites. The small Au clusters associated with those sites show a slightly higher hydrogen selectivity relative to the Na analogs (~20% vs. 12-15%), but not as high as that found for the uncalcined catalysts discussed above. There is clearly some chemical interaction of the Cs with both the TS-1 and the Au. With Cs DP, the Au capture onto the catalyst is enhanced by about a factor of 4 relative to that with Na and XPS of the Ti 2p region of the fresh catalyst shows some  $\text{Ti}^{3+}$ . Nevertheless, the activation energies and orders of reaction are independent of the alkali used, indicating that the chemistry of the Au sites is unchanged. We conclude, therefore, that the role of the Cs is to increase the number, but not the nature of the Au sites.

**Effects of Residual Alkali, Chlorine and Activation Method on the PO Rate:** Effects of both Na and particularly Cl might be expected for these catalysts, but as shown in Figs 5 and 6 they are not important descriptors of performance. In Fig. 5, a four times increase in the Na/Au ratio does not affect the Au efficiency. Fig. 6 shows that post impregnation of additional NaCl or  $\text{NaNO}_3$  also has little effect on the rate.

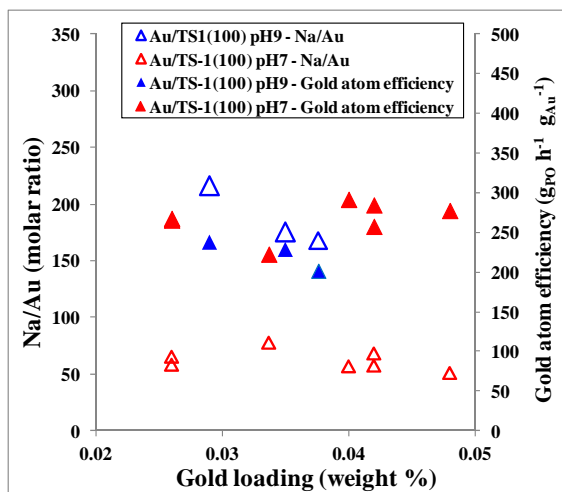


Figure 5. Na/Au molar ratio and the gold atom efficiency of the Au/TS-1(100) samples prepared at pH~7 and pH~9. The samples are prepared at different pH with different Na/Au molar ratios but have similar gold atom efficiency at  $\sim 250 \text{ g}_{\text{PO}} \text{ h}^{-1} \text{ g}_{\text{Au}}^{-1}$ .

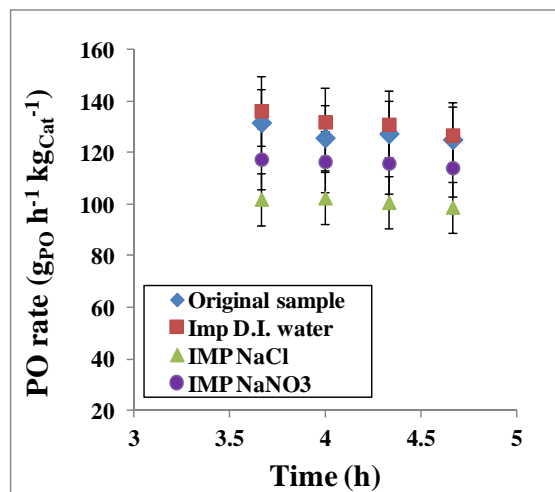


Figure 6. PO rate per gram of catalyst vs. time on stream

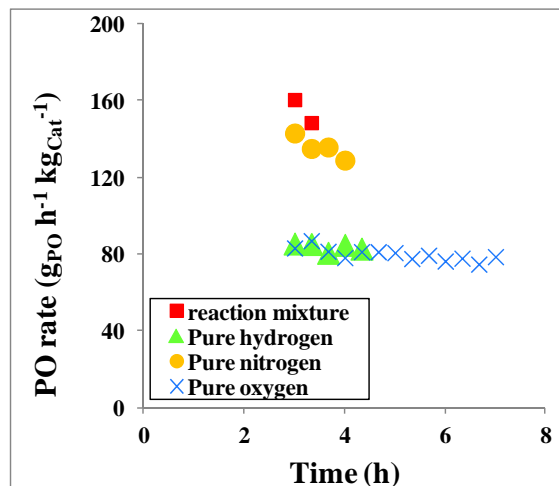


Figure 7. PO rate (gPO h<sup>-1</sup> kgCat<sup>-1</sup>) vs. time on stream for the 0.11Au/TS-1(121) samples activated in different environments: (triangle) pure H<sub>2</sub>, (round) pure N<sub>2</sub>, (cross) pure O<sub>2</sub>, and (square) reaction mixture from RT to ~200 °C with ramping rate ~1-1.5 °C min<sup>-1</sup>.

To study the effects the activation procedure on the rate of reaction, we compare H<sub>2</sub>, N<sub>2</sub>, and O<sub>2</sub> individually to the standard activation in the reaction mixture in Fig. 7. Pure hydrogen and oxygen are clearly poorer choices, while N<sub>2</sub> is only slightly below the reaction mixture activation. TEM analysis of the activated samples showed that in hydrogen and oxygen the average particle sizes were 3.91 and 3.68 nm respectively, compared to 3.29 nm for activation in the reaction mixture. While the change is relatively small, coupled with the broadening of the distribution, it is in keeping with our findings that loss of the smallest particles is most detrimental. A complete study of the effects of the size of the particles that can be seen by TEM, i.e. larger than 1 nm, shows that the rate does not correlate with particle size or with the number of edge, corner, or surface sites. This finding again confirms that the TEM invisible small particles in the pores are the important active sites.

#### Publications Acknowledging this Grant in 2012-2015

1. Lee, W.-S.; Akatay, M. C.; Stach, E. A.; Ribeiro, F. H.; Delgass, W. N. Reproducible Preparation of Au/TS-1 with High Reaction Rate for Gas Phase Epoxidation of Propylene. *J. Catal.* **2012**, 287, 178-189.
2. Lee, W.-S.; Lai, L.-C.; Akatay, M. C.; Stach, E. A.; Ribeiro, F. H.; Delgass, W. N. Probing the Gold Active Sites in Au/TS-1 for Gas Phase Epoxidation of Propylene in the Presence of Hydrogen and Oxygen. *J. Catal.* **2012**, 296, 31-42.
3. Lee, W.-S.; Akatay, M. C.; Stach, E. A.; Ribeiro, F. H.; Delgass, W. N. Enhanced Reaction Rate for Gas Phase Epoxidation of Propylene using H<sub>2</sub> and O<sub>2</sub> by Cs Promotion of Au/TS-1. *J. Catal.* **2013**, 308, 98-113.
4. Zemlyanov, D.; Klötzer, B.; Gabasch, H.; Smeltz, A.; Ribeiro, F. H.; Zafeiratos, S.; Teschner, D.; Schnörrch, P.; Vass, E.; Hävecker, M.; Knop-Gericke, A.; Schlögl, R. Kinetics of Palladium Oxidation in the mbar Pressure Range: Ambient Pressure XPS Study. *Top. Catal.* **2013**, 56, 885-895.
5. Lee, W.-S.; Akatay, M. C.; Stach, E. A.; Ribeiro, F. H.; Delgass, W. N. Gas Phase Epoxidation of Propylene in the Presence of H<sub>2</sub> and O<sub>2</sub> over Small Gold Ensembles in Uncalcined TS-1. *J. Catal.* **2014**, 313, 104-112.

## Heterogeneous and Homogeneous Catalyst Design by Discovery Informatics

Fabio H. Ribeiro, Mahdi M. Abu Omar, and William F. Schneider

Purdue University, School of Chemical Engineering, Department of Chemistry  
Notre Dame University, Department of Chemical and Biomolecular Engineering

### Abstract

Work on an informatics protocol for design of heterogeneous catalysts is currently focused on the metal-support interface of catalysts for the water gas shift reaction. Effects of removal of Co from PtCo/MWCNT, studies of Pt on Mo<sub>2</sub>C supports, and DFT theory on Au/MgO and Au, Ag, Pt and Pd on Al<sub>2</sub>O<sub>3</sub> all show the importance of the metal support interface for promoting activity by improving activation of water. Homogeneous catalyst studies have shown structure/activity relations for Group IV amine bis(phenolate) catalysts, illustrated the dynamic behavior of these catalysts and how sterics can affect dormancy, and the unique behavior of the ZrNEt<sub>2</sub> catalyst to form both oligomers and branched polymers made from those oligomers.

**DOE Grant No. DE-FG02-03ER15466 CATALYSIS SCIENCE INITIATIVE:**

### Catalyst Design by Discovery Informatics

**PI:** W. N. Delgass **Co-PIs:** M. Abu-Omar (Chemistry), J. M. Caruthers, F. H. Ribeiro, K. T. Thomson, W. F. Schneider (University of Notre Dame), **Research Associate:** G. Medvedev, **Postdocs:** Z. Zhao and Houyu Zhu (Notre Dame), **Students:** J. Clay (N. D.), Y. Cui, T. Gunanska (Chem.), J. Kim, P. Majumdar, P. Pletcher (Chem.), S. Pradhan, A. Preston (Chem.), S. McDonough (N. D.), P. Mehta (N.D.), K. Sabnis, K. Steelman (Chem.), J. Switzer, S. Xiong, **Collaborators:** J. P. Greeley, Purdue; J. T. Miller, Purdue.; E. A. Stach, Brookhaven Nat. Lab.; M. Neurock, University of Minnesota; Volkan Ortolan, School of Materials Engineering, Purdue

### Recent Progress

**Water Gas Shift Reaction: Pt-Co bimetallic catalysts:** The WGS rate per mole of surface Pt (measured

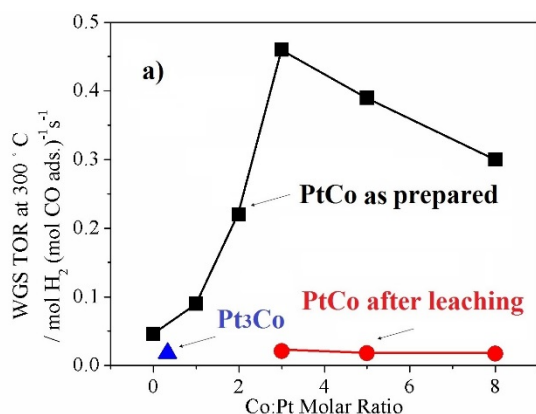


**Figure-1.** Variation of WGS rate per mole of Pt at 300 °C with respect to the Co loading.

with 6.8% CO, 21.9% H<sub>2</sub>O, 8.5% CO<sub>2</sub>, 37.4% H<sub>2</sub>, and balance Argon) for a series of Pt-Co catalysts supported on multi-wall carbon nanotubes (MWCNT) was observed to increase with Co loading to a maximum promotion of 12 times the rate on Co-free Pt/MWCNT and showed a maximum at a Co:Pt atomic ratio of about 3:1, Fig-1.

EXAFS showed that the Pt in all Pt/Co/MWCNT samples was alloyed with Co when the samples were reduced in 25% H<sub>2</sub>/Ar at 450°C. The Co-edge EXAFS data showed that in addition to reduced Co, a significant

fraction of the Co remained partially oxidized. To selectively remove the excess CoO<sub>x</sub> species, we leached them with 5 wt% Acetic acid solution in water. EXAFS confirmed the existence of Pt-Co alloy after leaching. The leached sample showed comparable WGS rates and kinetics with Co-free Pt/MWCNT sample and with Pt<sub>3</sub>Co alloy nanoparticles loaded onto MWCNT. These data confirm the importance of the Pt-CoO<sub>x</sub> interface as a promoter to the Pt rate rather than the Pt-Co alloy.

**Metals Supported on Molybdenum Carbide (Mo<sub>2</sub>C):** Two papers in progress show that the high rates of the WGS reaction over Pt/Mo<sub>2</sub>C and PtMo/MWCNT can be attributed to active sites that are formed by Pt-Mo alloy nanoparticles in contact with Mo<sub>2</sub>C, not by the formation of the alloy alone. Water activation on Mo<sub>2</sub>C is suggested to be the cause for the higher WGS rate over Pt/Mo<sub>2</sub>C. Our most recent work on this system is aimed at low temperature activation. From TPR experiments, low surface oxygen content was

observed to be crucial for the activity of Mo<sub>2</sub>C catalysts. The extent of oxygen removal by 300°C reduction after passivation was significantly higher for Pt/Mo<sub>2</sub>C (0.44 ML residual oxygen, 0.98 ML oxygen removed) compared to Mo<sub>2</sub>C alone (0.83 ML residual oxygen, 0.69 ML oxygen removed). The finding that Pt/Mo<sub>2</sub>C catalyst can be activated by a mild reduction pretreatment improves the prospects of this catalyst for commercial application.

**Au/MgO:** We have successfully synthesized Au/MgO and Au/Mg(OH)<sub>2</sub> using a deposition-precipitation method with urea. Both Au/MgO and Au/Mg(OH)<sub>2</sub> showed similar kinetics except for the apparent order with respect to H<sub>2</sub>O. Au/MgO showed a lower apparent H<sub>2</sub>O order of 0.7±0.1 while Au/Mg(OH)<sub>2</sub> showed H<sub>2</sub>O order 1.0±0.1. This implies a higher H<sub>2</sub>O/OH coverage over the Au/MgO compared with Au/Mg(OH)<sub>2</sub>, and corresponds to the higher rate found on Au/MgO. A kinetic isotope effect (KIE) of 2.0±0.3 for both catalysts implies the same reaction mechanism on both, and that the breaking of a covalent hydrogen bond is involved in the rate-determining step. Detailed Density Functional Theory (DFT) calculations underway on this system reveal a decrease of about 0.7 eV in the energy barrier for H<sub>2</sub>O dissociation at Au/MgO interface compared with pure MgO and pure Au. The objective of this work is to quantify the importance of H<sub>2</sub>O dissociation in WGS activity.

**Operando IR and Isotopic Transient Techniques:** To further study water activation we are also using time-resolved, transient infrared (IR) and mass spectrometry (MS) data obtained during H<sub>2</sub>O/D<sub>2</sub>O isotope switching. Initial experiments have shown that the coverage of deuterium-containing active intermediates can range from 0.03 (mole D) (mole surface Pt)<sup>-1</sup> on Pt/Al<sub>2</sub>O<sub>3</sub> up to 2.7 (mol D) (mole surface Pt)<sup>-1</sup> on Pt/CeO<sub>2</sub> at 250 °C and 7% CO, 11% H<sub>2</sub>O, 9% CO<sub>2</sub>, 37% H<sub>2</sub>. Time-resolved IR spectra collected during H<sub>2</sub>O/D<sub>2</sub>O switches revealed that linear and bridging (including tri-bonded) surface OH groups correlate with the WGS TOR, while formates are spectator species for all supported Pt catalysts tested under these WGS conditions.

**DFT studies of WGS at metal-support interfaces:** To investigate WGS intermediates on models of supported quasi-two-dimensional transition metal nanowires, we have systematically varied the type of metal (Au, Ag, Pd, Pt), the oxide (MgO(100), α-Al<sub>2</sub>O<sub>3</sub>(0001) ), and the number of layers in the nanowire. We have found that the metal support interactions are limited to near the interface region, and metal-like behavior is recovered at the top of the nanowire with as few as 2-3 layers, see Fig 2(a). The one layer surface shows different behavior due to quantum size effects. The interface sites have a modest stabilizing influence on the adsorbates, shown for the case of H in Fig 2(b-c). On the oxide, we find that binding of molecular intermediates (CO, H<sub>2</sub>O) is unaffected by the presence of the metal. However, a dramatic metal-dependent stabilization of redox-active intermediates (H, OH and COOH) is seen, caused by to electron tunneling

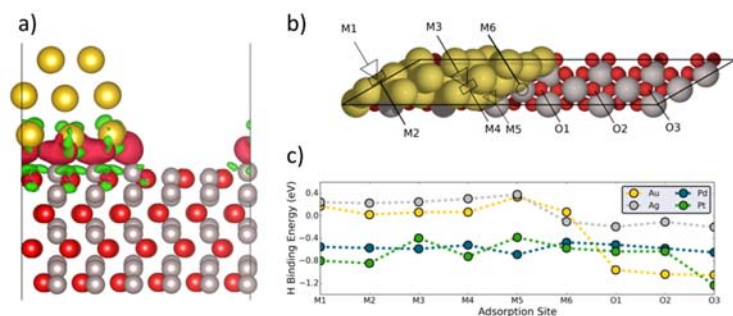


**Figure 2:** (a) Charge density difference plot of 3-ML Au nanowire on α-Al<sub>2</sub>O<sub>3</sub>(0001) (side view) . (b) Top view of the nanowire model. Atop, bridge and hollow sites are shown as circles, rectangles and triangles respectively. (c) H binding energies referenced to ½ H<sub>2</sub> vs. adsorption sites on Au, Ag, Pd, Pt.

between the metal and the adsorbate, Fig. 2(b-c). This electron transfer is closely coupled with large structural relaxations of the oxide surface, more pronounced in the case of α-Al<sub>2</sub>O<sub>3</sub>(0001) than MgO(100). This behavior of odd-electron adsorbates offers opportunities for tuning catalytic properties based on the choice of oxide and the choice of metal. Isolating different energetic contributions that affect the binding of such adsorbates and their catalytic implications is the focus of our study. Comparison of potential energy diagrams of H<sub>2</sub>O dissociation at or near the

interface of the 3-ML Pd-Al<sub>2</sub>O<sub>3</sub> system to that of the isolated metal and oxide shows that H<sub>2</sub>O dissociation is slow on Pd and rapid on the oxide; only near the interface can the H and OH fragments be separated. This illustrates the “dual” nature of the interface, i.e., the combined metal oxide system can be catalytically active, even though the individual components are inactive. We are also using Monte Carlo simulation of cluster expansion (CE) models to represent the configuration-dependent CO binding on Pd(111) with the objective of exploring both empirical and physically motivated fits to coverage-dependent binding energy functions for use in mean field models.

**Single Site Olefin Polymerization: Structure Activity Studies of Group IV Amine Bis(phenolate) Complexes:** Continuing the analysis of the kinetics of the six-coordinate, amine bis(phenolate) complexes first introduced by the Kol group in 2001, we followed studies of Zr and Hf with those on Ti. Fig. 3 shows how different parts of the precatalyst structure influence the overall polymerization mechanism in a piecewise fashion: ligand sterics control chain termination while ligand and metal electronics influence the

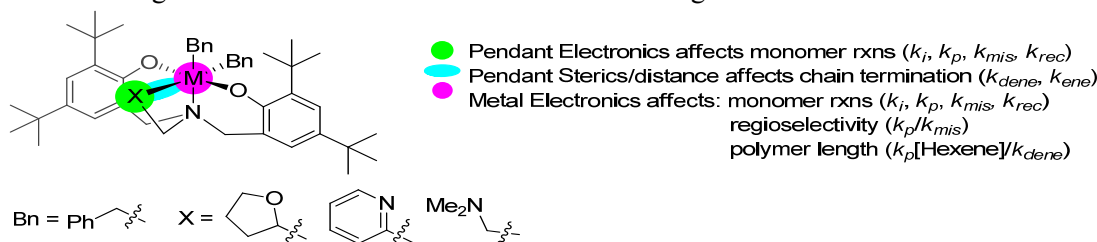


**Figure 3.** Group IV catalysts studied with metal center and ligand pendant group changes reactions between monomer and catalyst. Most interesting, we were able to show a decrease in  $k_p/k_{mis}$  as the electron density of the metal center was increased, a relationship controlling the appearance of regioerrors in the polymer structure. This has implications for designing copolymerization systems as well as offering a key method in reducing the appearance of regioerrors in the product structure. Fundamental structure-activity studies such as this are instrumental in the rational design of next generation catalysts.

**Observation of Dynamic Behavior and Structure-Activity Relationships in a Series of Group IV Amine bis(phenolate) Polymerization Catalysts:** For this study, four Zr-based salan catalysts (Fig. 4) were examined, and the rate constants for elementary steps in the catalytic mechanism showed a steric dependence. We have been able to experimentally prove the theorized dormancy states studied by Macchioni group. Salan compounds have been hypothesized to possess dynamic behavior upon activation with a number of cocatalysts. For olefin polymerization, the catalyst can exist in two form: the active form wherein the open coordination site is cis to the growing polymeryl (cis-active polymerization species or CAPS) and an inactive or dormant form wherein the coordination site and polymeryl are trans (trans-inactive polymerization species or TIPS). Furthermore, the effect is most prevalent in **1**, and is diminished as one increases the steric bulk of the ortho substituent, until it is completely absent in catalyst **4**. This was attributed

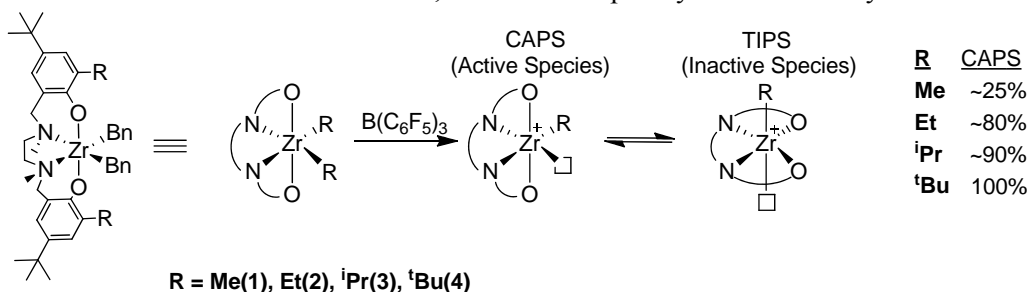
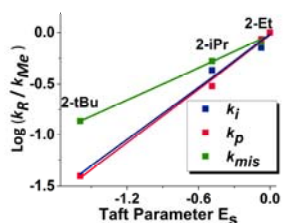


**Figure 4.** Four Zr-based ONNO-type catalysts active in the polymerization of 1-hexene to the destabilization of the TIPS form through steric crowding, as the ortho substituents begin to repel each other from the close proximity. This allows the CAPS form to be more favored as the size of the ortho



position increases. Once this dynamic behavior was incorporated into the model, we were able to successfully explain each facet of catalyst behavior. Upon examination of the subsequently calculated rate constants, it was observed that each step involving monomer insertion (initiation, propagation, and misinsertion) possessed a dependence on sterics at the ortho position of the phenolates, which was examined using a Taft plot (Figure left)

**Simultaneous Oligomerization and Polymerization of 1-hexene by a Group IV Amine Bis(phenolate) complex:** In this study, we investigated the “dual behavior” of the amine bis(phenolate) **Zr-NEt<sub>2</sub>** catalyst using our quantitative kinetic modeling approach. Some of the most notable findings are: The reaction between pre-catalyst and activator forms the oligomer active catalyst (Zr\*) only. The oligomer active catalyst then converts into a polymer active site (M\*) by virtue of the labile pendant arm. The polymer active site is more reactive towards oligomers than 1-hexene. The polymer produced was found to be structurally different from poly(1-hexene), with the polymer chain partially made up of vinyl terminated oligomers. Further experiments proved that free oligomers in the solution do not re-insert into the polymer active site. A number of chemical and kinetic models are being investigated to explain all of the features of this system. Surprisingly, it was found that the oligomer site, in concert with the rather less active polymer site, is able to produce highly branched dendritic polymers of 1-hexene, similar to LDPE. The ratio of polymer to oligomer formed could also be tuned by specific aging of the **Zr-NEt<sub>2</sub>/B(C<sub>6</sub>F<sub>5</sub>)<sub>3</sub>** mixture.

#### Publications Acknowledging this Grant in 2012-2015

- Pazmiño, J. H.; Shekhar, M.; Williams, W. D.; Akatay, M. C.; Miller, J. T.; Delgass, W. N.; Ribeiro, F. H. Metallic Pt as active sites for the Water-Gas Shift reaction on alkali-promoted supported catalysts. *J. Catal.* **2012**, *286*, 279–286.
- Shekhar, M.; Wang, J.; Lee, W.-S.; Williams, W. D.; Kim, S. M.; Stach, E. A.; Miller, J. T.; Delgass, W. N.; Ribeiro, F. H. Size and Support Effects for the Water-Gas Shift Catalysis over Gold Nanoparticles Supported on Model Al<sub>2</sub>O<sub>3</sub> and TiO<sub>2</sub>. *J. Am. Chem. Soc.* **2012**, *134*, 4700–4708.
- Wang, J.; Kispersky, V. F.; Delgass, W. N.; Ribeiro, F. H. Determination of the Au active site and surface active species via *operando* transmission FTIR and isotopic transient experiments on 2.3 wt% Au/TiO<sub>2</sub> for the WGS reaction, *J. Catal.* **2012**, *289*, 171–178.
- Switzer, J.; Travia, N.; Steelman, D. K.; Medvedev, G.; Thomson, K.; Delgass, W. N.; Abu-Omar, M. M.; Caruthers, J. M. Kinetic Modeling of 1-Hexene Polymerization Catalyzed by Zr(tBu-ONNMe<sub>2</sub>O)Bn<sub>2</sub>/B(C<sub>6</sub>F<sub>5</sub>)<sub>3</sub>. *Macromolecules* **2012**, *45*, 4978–4988.
- Williams, W. D.; Bollmann, L.; Miller, J. T.; Delgass, W. N.; Ribeiro, F. H. Effect of Molybdenum Addition on Supported Platinum Catalysts for the Water–Gas Shift Reaction. *Appl. Cat. B* **2012**, *125*, 206–214.
- Shekhar, M.; Wang, J.; Lee, W.-S.; Akatay, M. C.; Stach, E. A.; Delgass, W. N.; Ribeiro, F. H. Counting Au Catalytic Sites for the Water–Gas Shift Reaction. *J. Catal.* **2012**, *293*, 94–102.
- Manz, T. A.; Caruthers, J. M.; Sharma, S.; Phomphrai, K.; Thomson, K. T.; Delgass, W. N.; Abu-Omar, M. M. Structure-Activity Correlation for Relative Chain Initiation to Propagation Rates in Single-Site Olefin Polymerization Catalysis. *Organometallics* **2012**, *31*, 602–618.
- Stelman, D. K.; Xiong, S.; Pletcher, P. D.; Smith, E.; Switzer, J. M.; Medvedev, G. A.; Delgass, W. N.; Caruthers, J. M.; Abu-Omar, M. M. Effects of pendant ligand binding affinity on chain transfer for 1-hexene polymerization catalyzed by single-site zirconium amine bis-phenolate complexes. *J. Am. Chem. Soc.* **2013**, *135*, 6280–6288.
- Stelman, D. K.; Pletcher, P. D.; Switzer, J. M.; Xiong, S.; Medvedev, G. A.; Delgass, W. N.; Caruthers, J. M.; Abu-Omar, M. M. Comparison of Selected Zirconium and Hafnium Amine Bis(phenolate) Catalysts for 1-Hexene Polymerization. *Organometallics* **2013**, *32*, 4862–4867.
- Xiong, S.; Steelman, D. K.; Medvedev, G. A.; Delgass, W. N.; Abu-Omar, M. M.; Caruthers, J. M. Selective Degenerative Benzyl Group Transfer in Olefin Polymerization. *ACS Catal.* **2014**, *4*, 1162–1170.
- Brown, H. A.; Silei Xiong, S.; Medvedev, G. A.; Chang, Y. A.; Abu Omar, M. M.; Caruthers, J. M.; Waymouth, R. M. Zwitterionic Ring-Opening Polymerization: Kinetic Models for the Synthesis of Cyclic Poly(caprolactones). *Macromolecules*, **2014**, *47*, 2055–2963.
- Clay, John P., Jeffery P. Greeley, Fabio H. Ribeiro, W. Nicholas Delgass, William F. Schneider, “DFT Comparison of Intrinsic WGS Kinetics over Pd and Pt”, *J. Catal.* **2014**, *320*, 106–117.

Aaron D. Sadow and Igor I. Slowing

**Hybrid organic-inorganic-organometallic catalysts for reactions of oxygenates:  
characterization, catalytic activity and reaction mechanisms**

Aaron D. Sadow, Igor I. Slowing, Takeshi Kobayashi, Marek Pruski  
Ames Laboratory, U.S. DOE, Iowa State University, Ames, IA 50011-3111

**Presentation Abstract**

The overarching goal of this collaborative research project is to develop new catalytic principles for bringing together the best features of homogeneous and heterogeneous catalysis and ultimately enable the design of efficient catalysts with molecular-scale control of conversions, particularly those relevant to highly oxygenated compounds. The substantial challenges for rational design of catalysts for selective chemical conversions require understanding and control of the catalytic environment and reaction mechanisms. These requirements are addressed through the design of 3D, mesoporous interfacial catalysts. Doing so provides advantages in catalyst recovery, reaction control, sensitivity and efficiency. Our efforts combine expertise in mesoporous catalyst synthesis, transition metal chemistry, mechanisms of catalytic reactions, and solid-state (SS)NMR. Here, we specifically highlight tandem catalysis, cooperative effects of amines, and related mechanistic studies of carbon-carbon coupling reactions catalyzed by amine-modified silica surfaces, the development of new heterogeneous catalysts for the conversion of oxygenates to hydrocarbons, environmental effects on stereoselectivity in asymmetric catalytic conversions, and reductive catalysis employing oxophilic early transition metal centers.<sup>1-52</sup> Our studies of catalytic materials utilizing the emerging SSNMR methodologies that employ dynamic nuclear polarization (DNP) are shown in a separate presentation.

**AL-03-380-011: Homogeneous and Interfacial Catalysis in 3D Controlled Environment**

PI: Marek Pruski

Postdocs: Naftali Opembe

Students: Naresh Eedugurala, Jacob Fleckenstein, Zachary Weinstein, Zhuoran Wang

**Recent Progress**

**(1) Single pot tandem catalytic conversions.** The controlled functionalization of nanostructured materials enables the design of efficient multicatalytic systems to conduct tandem multistep reaction sequences. A control over attachment sites of each component is critical to enable simultaneous incorporation of mutually incompatible catalysts. The versatility of this approach was demonstrated and highlighted by synthesizing hybrid organic, inorganic and biocatalysts.

In one example aminoalkyl silanes were co-condensed with tetraethoxysilane in

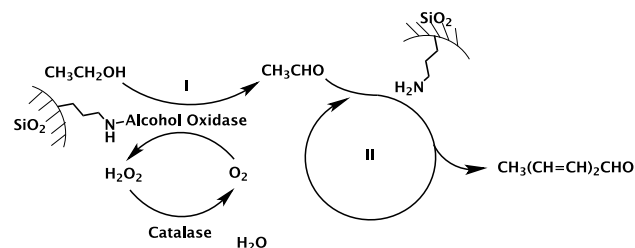


**Fig. 1.** Tandem conversion of ethanol into 2,4-hexadienal catalyzed by alcohol oxidase and aminopropyl groups anchored on mesoporous silica nanoparticles.

presence of surfactant to give aminoalkyl-functionalized mesoporous silica nanoparticles (MSNs), with the groups located mainly inside of the pores due to template-amine interactions. The material was then grafted with glycidoxypopyl silane, which served as a linker to immobilize alcohol oxidase on the external surface of the MSNs. The enzyme catalyzed the oxidation of ethanol to acetaldehyde by air (Fig. 1 catalytic reaction I), hydrogen peroxide byproduct was decomposed back to oxygen by catalase. The intermediate acetaldehyde went through three cycles of self-aldol condensation catalyzed by aminopropyl groups inside the pores to give 2,4-hexadienal as the only oligomerization product (Fig. 1, catalytic cycle II). Site separation of enzyme and organocatalyst prevented poisoning of the former by the amine, and oxidation of the latter by the enzyme.<sup>29</sup> A second system was developed by coupling Pd nanoparticle catalyzed oxidation of furfuryl alcohol with aldol condensation using acetone and secondary amine catalysts supported on MSNs (Fig. 2). Suitable adjustment of reaction conditions led to 71% yield of the product of the tandem reaction, with 100% selectivity for the monocondensation product.<sup>12</sup> Future work will involve increasing the number of consecutive reaction steps and attaining further control on active site localization.

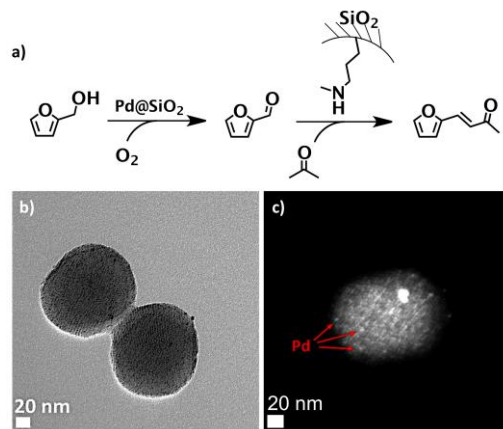


**Fig. 2.** Tandem single-pot conversion of furfuryl alcohol into furanylbutenone catalyzed by MSN-based hybrid inorganic-organic multicatalyst system.

**(2) Exploring the effect of organic groups on the activity of metal nanoparticle catalysts.** It is well known in homogeneous catalysis that the molecular environment of active sites can dramatically affect their performance and selectivity for a particular process. For example, the catalytic activity of metal cations can be fine tuned by complexation with ligands of varying electronic properties. The closest analogy to such control in heterogeneous catalysis is probably the use of different supports: the activity of metal catalysts frequently changes due to the nature and extent of their interaction with the support. Thus, it is common practice to select and evaluate the best possible support for a catalyst in a particular reaction. A potential way to explore how the properties of supports can affect the behavior of a catalyst is to modify its surface properties via introduction of organic moieties. These may interact and tune the local environment of the supported catalysts. In an effort to understand the potential effect of organic functionalization on the activity and selectivity of metal catalysts, the surface of MSNs containing catalytic Ni nanoparticles was modified with three different organosilanes. While the reaction rates of oleic acid hydrogenation decreased in the order non-functionalized > aminopropyl > cyanopropyl > hexyl, the selectivity of the reaction changed dramatically: in absence of organic groups the hydrogenation led primarily to cracking, while the organic groups tended to favor hydrodecarbonylation preserving the hydrocarbon chain (Fig. 3).<sup>28</sup> The largest ratio of decarbonylation to cracking was obtained

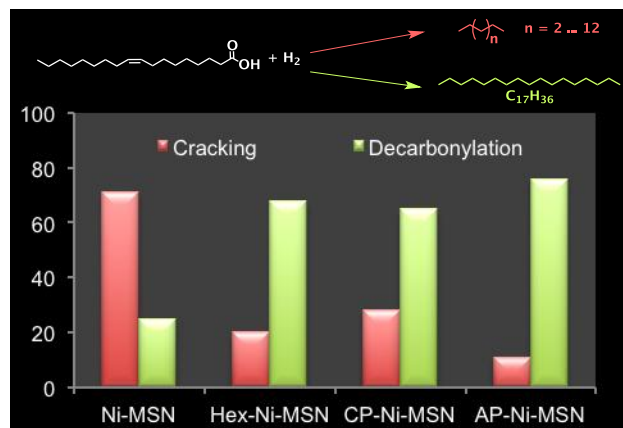


**Fig. 3.** Effect of organic functionalization on the selectivity of oleic acid hydrogenation.

with amine groups, and the selectivity was proportional to the amount of organic modifier bound to the surface of the material. These initial results set the basis for further structure activity studies to understand in depth the fundamental nature of these behaviors.

### (3) Investigating binding of reactants in the hydrotreatment of fatty acids (FA). Three different

systems involving separate binding sites for each reactant were investigated for the catalytic hydrogenation of FAs. The first system involved Ni supported on MSNs modified with amine groups.<sup>28</sup> While H<sub>2</sub> binds and is activated at the surface of the metal, the FAs are bound by the amine groups. Because of this, reaction progress depends on the proximity between the two binding sites. This was confirmed with control experiments using physical mixtures of Ni supported on bare MSNs and amine-modified MSNs, in which, despite the high reaction temperatures most FAs were adsorbed and retained by the amine-MSNs and the conversion decreased almost tenfold. The combination of FA-binding amines and Ni catalyst provides dual selectivity to the system, in

terms of the amine groups being able to selectively isolate FAs from complex feedstocks (microalgal oil) and the organic environment of Ni nanoparticles directing the reaction selectivity towards decarbonylation rather than hydrocracking (Fig. 4a). The second system consisted of Fe nanoparticles supported on MSNs (Fig 4b). When the catalyst is exposed to air, partial oxidation of Fe takes place leading to a mixed system containing metallic and oxidic phases of iron. Upon setting in hydrogen atmosphere, oxygen vacancies are formed in the oxidic phase, which then serve as binding sites for FAs. H<sub>2</sub> is bound and activated in the metallic phase. Reduction of the FA leads to formation of water and regeneration of oxygen vacancies with the overall process likely following a reverse Mars-Van Krevelen mechanism (Fig. 4c). Experiments with catalysts containing different proportions of oxidic to metallic phase (controlled by catalyst activation temperature and probed by XPS) showed the selectivity for hydrodeoxygenation decreases with increasing oxidic character of Fe.<sup>13</sup> A third system consisted of a partially oxidized bimetallic catalyst of Fe and Cu (Fig. 5).

Synergistic action between the metals led to halting the hydrogenation of FAs at the alcohol stage. The reaction proceeded with high selectivity and significantly lower reaction temperatures than typical FA hydrogenations. Further studies in each of these systems will include kinetic modeling and investigation of the effects of active site distribution

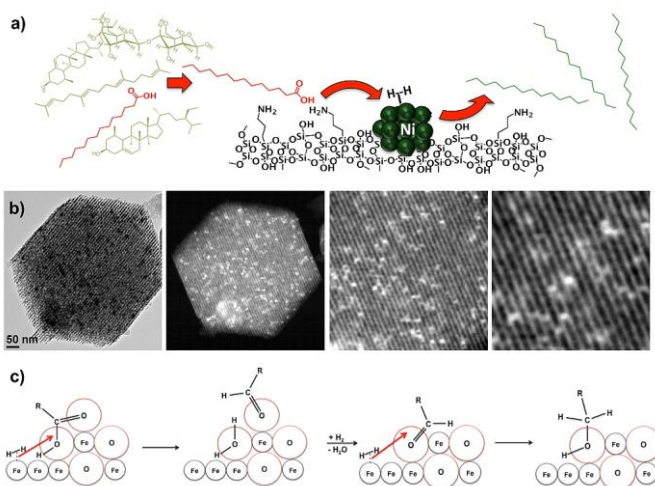


**Fig. 4.** a) Binding of fatty acids in complex mixtures by amine groups and of H<sub>2</sub> by Ni nanoparticles in a hybrid catalytic system to selectively yield liquid hydrocarbons from algal oil; b) iron nanoparticles grown within the pores of MSNs; c) catalytic hydrodeoxygenation of fatty acids by biphasic iron catalyst.

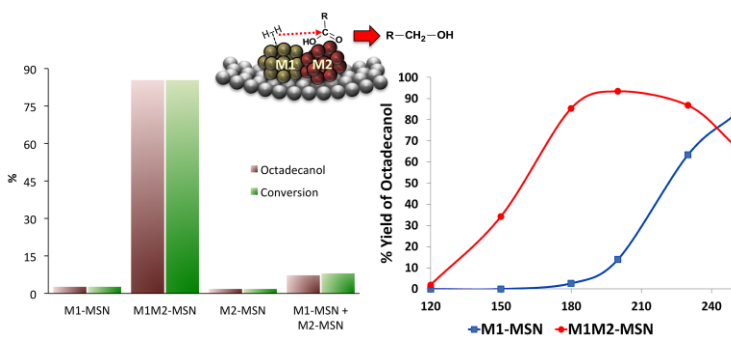


**Fig. 5.** Synergistic catalytic reduction of fatty acids by Fe and Cu oxides to selectively produce fatty alcohols.

to better understand the fundamental mechanism of the processes.

**(4) Environmental control over selectivity in catalytic asymmetric hydroamination.** A long-term goal of our catalysis program is to discover and understand the effect of 3D environment on catalytic conversions. Toward this goal, we have studied the effect of concentration of amine on the diastereoselectivity of a hydroamination/cyclization reaction of dialkene and dialkyne amines.<sup>3,23</sup> The catalytic addition of unsaturated alkenes and amines (hydroamination) typically

provides  $\alpha$ - or  $\beta$ -amino stereocenters directly through C–N or C–H bond formation. Alternatively, desymmetrization reactions of symmetrical aminodialkenes or aminodialkynes provide access to stereogenic centers with the position controlled by the substrate's structure. In the study of an enantioselective zirconium-catalyzed hydroamination, stereocenters resulting from C–N addition and desymmetrization of a prochiral quaternary center are independently controlled by the catalyst and reaction conditions. Using a single catalyst, the method provides selective access to either diastereomer of optically enriched 5-, 6-, and 7-membered cyclic amines from aminodialkenes and enantioselective synthesis of 5-, 6-, and 7-membered cyclic imines from aminodialkynes. Experiments on hydroamination of aminodialkenes testing the effects of the catalyst:substrate ratio, the absolute concentration of the catalyst, and the absolute initial concentration of the primary amine substrate show that the latter parameter strongly influences the stereoselectivity of the desymmetrization process, whereas the absolute configuration of the  $\alpha$ -amino stereocenter generated by C–N bond formation is not affected by these parameters. Interestingly, isotopic substitution ( $\text{H}_2\text{NR}$  vs.  $\text{D}_2\text{NR}$ ) of the substrate enhances the stereoselectivity of the enantioselective and diastereoselective processes in aminodialkene cyclization and the peripheral stereocenter in aminodialkyne desymmetrization/cyclization.

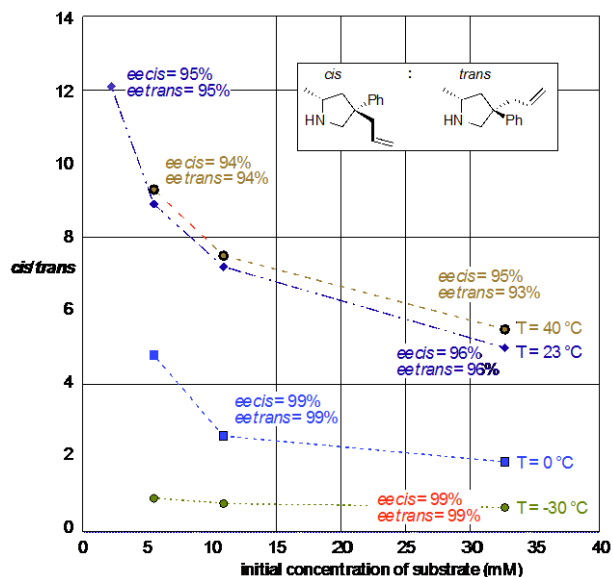


**Fig. 6.** Effect of reaction concentration on diastereoselectivity in a catalytic CN bond formation.

provides  $\alpha$ - or  $\beta$ -amino stereocenters directly through C–N or C–H bond formation. Alternatively, desymmetrization reactions of symmetrical aminodialkenes or aminodialkynes provide access to stereogenic centers with the position controlled by the substrate's structure. In the study of an enantioselective zirconium-catalyzed hydroamination, stereocenters resulting from C–N addition and desymmetrization of a prochiral quaternary center are independently controlled by the catalyst and reaction conditions. Using a single catalyst, the method provides selective access to either diastereomer of optically enriched 5-, 6-, and 7-membered cyclic amines from aminodialkenes and enantioselective synthesis of 5-, 6-, and 7-membered cyclic imines from aminodialkynes. Experiments on hydroamination of aminodialkenes testing the effects of the catalyst:substrate ratio, the absolute concentration of the catalyst, and the absolute initial concentration of the primary amine substrate show that the latter parameter strongly influences the stereoselectivity of the desymmetrization process, whereas the absolute configuration of the  $\alpha$ -amino stereocenter generated by C–N bond formation is not affected by these parameters. Interestingly, isotopic substitution ( $\text{H}_2\text{NR}$  vs.  $\text{D}_2\text{NR}$ ) of the substrate enhances the stereoselectivity of the enantioselective and diastereoselective processes in aminodialkene cyclization and the peripheral stereocenter in aminodialkyne desymmetrization/cyclization.

**(5) Rhodium-silylene catalyzed partial deoxygenation of esters, amides, and carbonyls.**

Selective partial catalytic reduction and deoxygenation chemistry in the conversion of biologically-derived chemical streams is the counterpart to selective partial oxidation, which has been long studied for the conversion of petroleum feedstocks into fuels and chemicals. In order to facilitate oxidative addition chemistry of *fac*-coordinated rhodium(I) and iridium(I) compounds, carbene-bis(oxazolonyl)phenylborate proligands have been synthesized and reacted with organometallic precursors. Photochemical reactions of dicarbonyl compounds  $\{\text{PhB}(\text{Ox}^{\text{Me}2})_2\text{Im}^{\text{Mes}}\}\text{Rh}(\text{CO})_2$  or  $\{\text{PhB}(\text{Ox}^{\text{Me}2})_2\text{Im}^{\text{Mes}}\}\text{Ir}(\text{CO})_2$  result in C–H bond oxidative addition in compounds  $\{\kappa^4\text{-PhB}(\text{Ox}^{\text{Me}2})_2\text{Im}^{\text{Mes}'}\text{CH}_2\}\text{RhH}(\text{CO})$  or  $\{\text{PhB}(\text{Ox}^{\text{Me}2})_2\text{Im}^{\text{Mes}}\}\text{IrH}(\text{Ph})\text{CO}$ . In the former, oxidative addition results in cyclometalation of the mesityl *ortho*-methyl whereas the iridium compound reacts with the benzene solvent to give a rare crystallographically characterized *cis*-[Ir](H)(Ph) complex. Alternatively, the rhodium

carbonyl reacts with  $\text{PhSiH}_3$  in the dark to form the silyl compound  $\{\text{PhB}(\text{Ox}^{\text{Me}_2})_2\text{Im}^{\text{Mes}}\}\text{RhH}(\text{SiH}_2\text{Ph})$ . These examples demonstrate the enhanced thermal reactivity of  $\{\text{PhB}(\text{Ox}^{\text{Me}_2})_2\text{Im}^{\text{Mes}}\}$ -supported iridium and rhodium compounds in comparison to tris(oxazolynyl)borate, tris(pyrazolyl)borate, and cyclopentadienyl-supported compounds.

This enhanced reactivity was studied in an electrophilic, coordinatively unsaturated rhodium complex supported by borate-linked oxazoline, oxazoline-coordinated silylene, and *N*-heterocyclic carbene donors  $[\{\kappa^3\text{-}N,\text{Si},\text{C}\text{-PhB}(\text{Ox}^{\text{Me}_2})(\text{Ox}^{\text{Me}_2}\text{SiHPh})\text{Im}^{\text{Mes}}\}\text{Rh}(\text{H})\text{CO}][\text{HB}(\text{C}_6\text{F}_5)_3]$  ( $\text{Ox}^{\text{Me}_2}$  = 4,4-dimethyl-2-oxazoline;  $\text{Im}^{\text{Mes}}$  = 1-mesitylimidazole) is synthesized from the neutral rhodium silyl  $\{\text{PhB}(\text{Ox}^{\text{Me}_2})_2\text{Im}^{\text{Mes}}\}\text{RhH}(\text{SiH}_2\text{Ph})\text{CO}$  and  $\text{B}(\text{C}_6\text{F}_5)_3$ . The unusual oxazoline-coordinated silylene structure in  $[\{\kappa^3\text{-}N,\text{Si},\text{C}\text{-PhB}(\text{Ox}^{\text{Me}_2})(\text{Ox}^{\text{Me}_2}\text{SiHPh})\text{Im}^{\text{Mes}}\}\text{Rh}(\text{H})\text{CO}]^+$  is proposed to form by rearrangement of an unobserved isomeric cationic rhodium silylene species

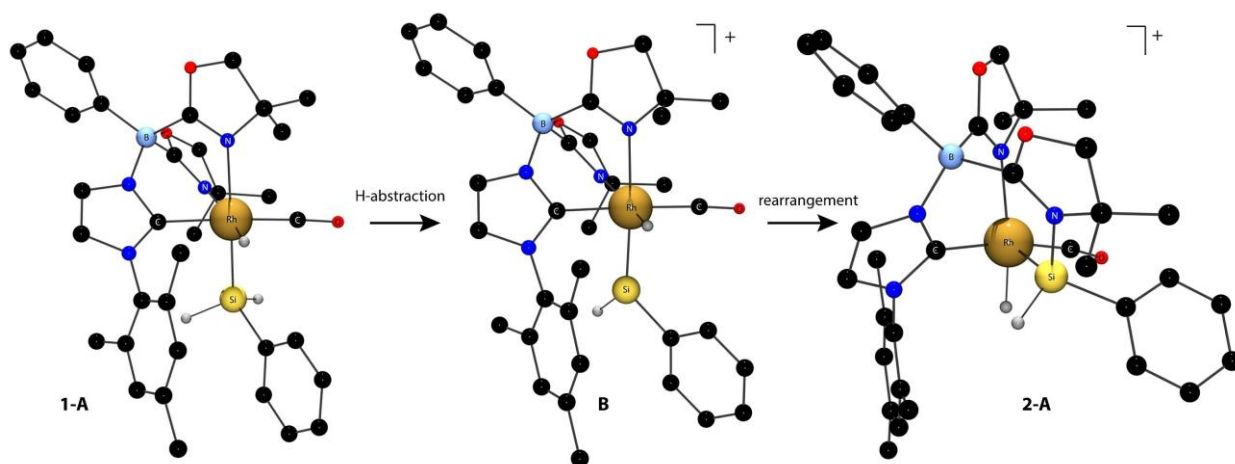
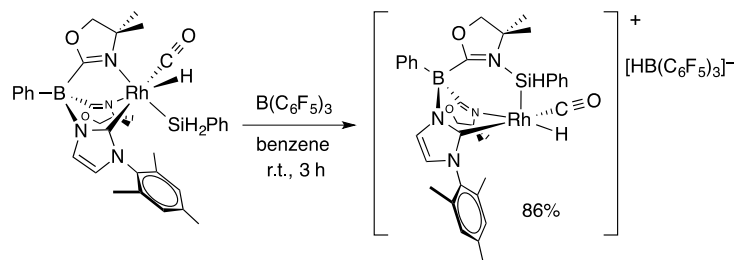
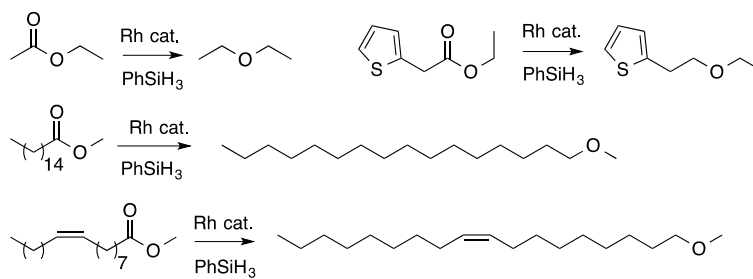


**Fig. 7.** DFT calculated rearrangement of a rhodium silylene into its oxazoline-coordinated isomer.

$[\{\text{PhB}(\text{Ox}^{\text{Me}_2})_2\text{Im}^{\text{Mes}}\}\text{RhH}(\text{SiHPh})\text{CO}][\text{HB}(\text{C}_6\text{F}_5)_3]$  generated by H abstraction. This assignment is based on DFT calculations that show the bridging silylene structure is 17 kcal/mol more stable than the terminal rhodium silylene.  $[\{\kappa^3\text{-}N,\text{Si},\text{C}\text{-PhB}(\text{Ox}^{\text{Me}_2})(\text{Ox}^{\text{Me}_2}\text{SiHPh})\text{Im}^{\text{Mes}}\}\text{Rh}(\text{H})\text{CO}]^+$  catalyzes reductions of organic carbonyl compounds with silanes to give hydrosilylation products or deoxygenation products. The pathway to these reactions is primarily influenced by the degree of substitution of the organosilane.

Reactions with primary silanes give deoxygenation of esters to ethers, amides to amines, and ketones and aldehydes to hydrocarbons, whereas tertiary silanes react to give 1,2-hydrosilylation of the carbonyl functionality. In contrast, the strong



Lewis acid  $B(C_6F_5)_3$  catalyzes the complete deoxygenation of carbonyl compounds to hydrocarbons with  $PhSiH_3$  as the reducing agent.

**(6) Catalytic hydroboration of carbonyls with a oxophilic surface-supported zirconium catalyst.**

The hydroboration of aldehydes and ketones using a silica-supported zirconium catalyst is reported. Reaction of  $Zr(NMe_2)_4$  and Mesoporous Silica Nanoparticles (MSN) provides the catalytic material  $Zr(NMe_2)_n@MSN$ .

Characterization of  $Zr(NMe_2)_n@MSN$  with solid-state NMR and infrared spectroscopy, elemental analysis, powder X-ray diffraction, electron microscopy, and reactivity studies suggests its surface structure is primarily the monopodal  $\equiv SiO-Zr(NMe_2)_3$ .

This material reacts with pinacolborane (HBpin) to provide  $Me_2N-Bpin$  and a surface bonded zirconium hydride, which was characterized by solid-state NMR spectroscopy and infrared spectroscopy and through its reactivity with  $D_2$ . The zirconium hydride material or the zirconium amide precursor  $Zr(NMe_2)_n@MSN$  catalyze the hydroboration of aldehydes and ketones with HBpin. This catalytic material may be recycled without loss of activity at least eight times, and air-exposed materials are catalytically active, showing that these single-site zirconium centers are robust catalytic sites for carbonyl reduction. Note that the Zr center is bonded to the surface by Zr-O interactions, and these are not disrupted by the HBpin reagent. In contrast, the  $[Zr]-OCHR_2$  catalytic intermediate reacts rapidly with HBpin to give the product and catalytic turnover.

**Publications (2012-present).**

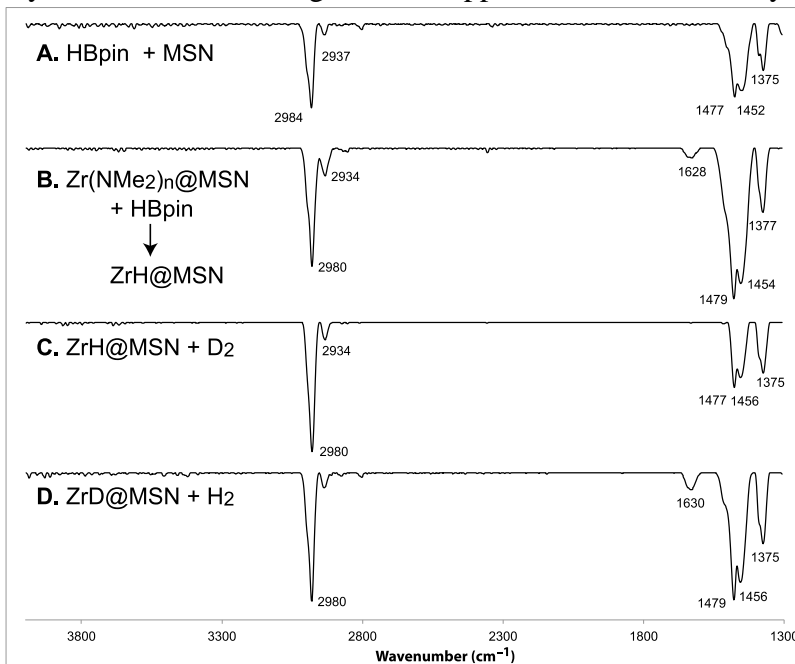


**Fig. 8.** IR spectra of  $ZrH@MSN$  and its exchange with  $D_2$ .

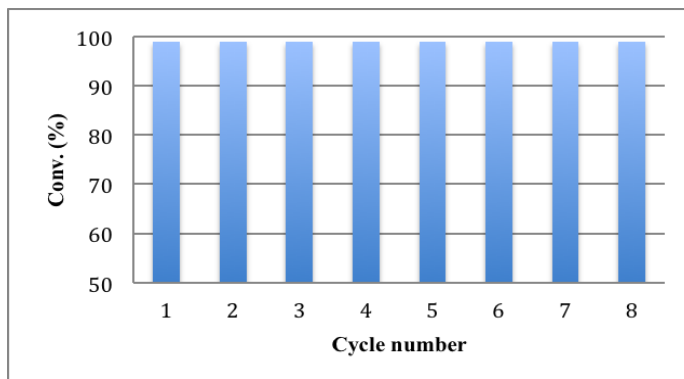
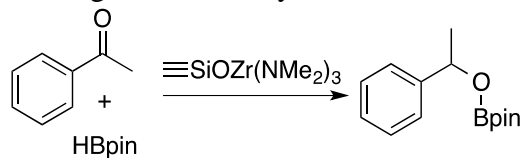


**Fig. 9.** Yields of the hydroboration product after recycling 8 times.

1. Webb, J. D.; Seki, T.; Goldston, J. F.; Pruski, M.; Crudden, C. M., Selective functionalization of the mesopores of SBA-15. *Microporous and Mesoporous Materials* **2015**, *203*, 123-131. doi: 10.1016/j.micromeso.2014.10.032.
2. Nishiyama, Y.; Kobayashi, T.; Malon, M.; Singappuli-Arachchige, D.; Slowing, I. I.; Pruski, M., Studies of minute quantities of natural abundance molecules using 2D heteronuclear correlation spectroscopy under 100 kHz MAS. *Solid State Nuclear Magnetic Resonance* **2015**, *66-67*, 56-61. doi: 10.1016/j.ssnmr.2015.02.001.
3. Manna, K.; Eedugurala, N.; Sadow, A. D., Zirconium-Catalyzed Desymmetrization of Aminodialkenes and Aminodialkynes through Enantioselective Hydroamination. *Journal of the American Chemical Society* **2015**, *137*, 425-435. doi: 10.1021/ja511250m.
4. Hull, E. A.; West, A. C.; Pestovsky, O.; Kristian, K. E.; Ellern, A.; Dunne, J. F.; Carraher, J. M.; Bakac, A.; Windus, T. L., UV-visible spectroscopy of macrocyclic alkyl, nitrosyl and halide complexes of cobalt and rhodium. Experiment and calculation. *Dalton Transactions* **2015**, *44*, 3811-3816. doi: 10.1039/c4dt03143a.
5. Gu, W.; Stalzer, M. M.; Nicholas, C. P.; Bhattacharyya, A.; Motta, A.; Gallagher, J. R.; Zhang, G.; Miller, J. T.; Kobayashi, T.; Pruski, M.; Delferro, M.; Marks, T. J., Benzene Selectivity in Competitive Arene Hydrogenation: Effects of Single-Site Catalyst...Acidic Oxide Surface Binding Geometry. *Journal of the American Chemical Society* **2015**. doi: 10.1021/jacs.5b03254.
6. Bataineh, H.; Pestovsky, O.; Bakac, A., Iron(II) Catalysis in Oxidation of Hydrocarbons with Ozone in Acetonitrile. *ACS Catalysis* **2015**, *5*, 1629-1637. doi: 10.1021/cs501962m.
7. Xu, S. C.; Manna, K.; Ellern, A.; Sadow, A. D., Mixed N-Heterocyclic Carbene-Bis(oxazolanyl)borato Rhodium and Iridium Complexes in Photochemical and Thermal Oxidative Addition Reactions. *Organometallics* **2014**, *33*, 6840-6860. doi: 10.1021/om500891h.
8. Xu, S.; Everett, W. C.; Ellern, A.; Windus, T. L.; Sadow, A. D., Oxygen insertion reactions of mixed N-heterocyclic carbene-oxazolanylborato zinc alkyl complexes. *Dalton Transactions* **2014**, *43*, 14368-14376. doi: 10.1039/C4DT01011F.
9. Wang, C. J.; Ackerman, D. M.; Slowing, I. I.; Evans, J. W., Langevin and Fokker-Planck Analyses of Inhibited Molecular Passing Processes Controlling Transport and Reactivity in Nanoporous Materials. *Physical Review Letters* **2014**, *113*, 038301. doi: 10.1103/PhysRevLett.113.038301.
10. Reichert, M. D.; Lin, C. C.; Vela, J., How Robust are Semiconductor Nanorods? Investigating the Stability and Chemical Decomposition Pathways of Photoactive Nanocrystals. *Chemistry of Materials* **2014**, *26*, 3900-3908. doi: 10.1021/cm500896n.
11. Opembe, N. N.; Guild, C.; King'ondou, C.; Nelson, N. C.; Slowing, I. I.; Suib, S. L., Vapor-Phase Oxidation of Benzyl Alcohol Using Manganese Oxide Octahedral Molecular Sieves (OMS-2). *Industrial & Engineering Chemistry Research* **2014**, *53*, 19044-19051. doi: 10.1021/ie5024639.

12. Nelson, N.; Chaudhary, U.; Kandel, K.; Slowing, I., Heterogeneous Multicatalytic System for Single-Pot Oxidation and C–C Coupling Reaction Sequences. *Topics in Catalysis* **2014**, *57*, 1000-1006. doi: 10.1007/s11244-014-0263-y.
13. Kandel, K.; Anderegg, J. W.; Nelson, N. C.; Chaudhary, U.; Slowing, I. I., Supported iron nanoparticles for the hydrodeoxygenation of microalgal oil to green diesel. *Journal of Catalysis* **2014**, *314*, 142-148. doi: 10.1016/j.jcat.2014.04.009.
14. Guo, Z. Y.; Kobayashi, T.; Wang, L. L.; Goh, T. W.; Xiao, C. X.; Caporini, M. A.; Rosay, M.; Johnson, D. D.; Pruski, M.; Huang, W. Y., Selective Host-Guest Interaction between Metal Ions and Metal-Organic Frameworks Using Dynamic Nuclear Polarization Enhanced Solid-State NMR Spectroscopy. *Chemistry-A European Journal* **2014**, *20*, 16308-16313. doi: 10.1002/chem.201403884.
15. Carraher, J. M.; Ellern, A.; Bakac, A., Preparation and reactivity of macrocyclic rhodium(III) alkyl complexes. *Inorganica Chimica Acta* **2014**, *409*, 254-258. doi: 10.1016/j.ica.2013.09.022.
16. Carraher, J. M.; Bakac, A., Generation of free oxygen atoms O(P-3) in solution by photolysis of 4-benzoylpyridine N-oxide. *Physical Chemistry Chemical Physics* **2014**, *16*, 19429-19436. doi: 10.1039/c4cp02751e.
17. Alvarado, S. R.; Guo, Y. J.; Ruberu, T. P. A.; Tavasoli, E.; Vela, J., Inorganic chemistry solutions to semiconductor nanocrystal problems. *Coordination Chemistry Reviews* **2014**, *263*, 182-196. doi: 10.1016/j.ccr.2013.09.001.
18. Althaus, S. M.; Mao, K. M.; Stringer, J. A.; Kobayashi, T.; Pruski, M., Indirectly detected heteronuclear correlation solid-state NMR spectroscopy of naturally abundant N-15 nuclei. *Solid State Nuclear Magnetic Resonance* **2014**, *57-58*, 17-21. doi: 10.1016/j.ssnmr.2013.11.001.
19. Wang, J.; Ackerman, D. M.; Lin, V. S. Y.; Pruski, M.; Evans, J. W., Controlling reactivity of nanoporous catalyst materials by tuning reaction product-pore interior interactions: Statistical mechanical modeling. *Journal of Chemical Physics* **2013**, *138*, 134705. doi: 10.1063/1.4798463.
20. Vela, J., Molecular Chemistry to the Fore: New Insights into the Fascinating World of Photoactive Colloidal Semiconductor Nanocrystals. *Journal of Physical Chemistry Letters* **2013**, *4*, 653-668. doi: 10.1021/jz302100r.
21. Tanabe, K. K.; Siladke, N. A.; Broderick, E. M.; Kobayashi, T.; Goldston, J. F.; Weston, M. H.; Farha, O. K.; Hupp, J. T.; Pruski, M.; Mader, E. A.; Johnson, M. J. A.; Nguyen, S. T., Stabilizing unstable species through single-site isolation: A catalytically active Ta-V trialkyl in a porous organic polymer. *Chemical Science* **2013**, *4*, 2483-2489. doi: 10.1039/c3sc22268c.
22. Mao, K. M.; Kennedy, G. J.; Althaus, S. M.; Pruski, M., Determination of the Average Aromatic Cluster Size of Fossil Fuels by Solid-State NMR at High Magnetic Field. *Energy & Fuels* **2013**, *27*, 760-763. doi: 10.1021/ef301804p.

23. Manna, K.; Everett, W. C.; Schoendorff, G.; Ellern, A.; Windus, T. L.; Sadow, A. D., Highly Enantioselective Zirconium-Catalyzed Cyclization of Aminoalkenes. *Journal of the American Chemical Society* **2013**, *135*, 7235-7250. doi: 10.1021/ja4000189.
24. Lesoine, M. D.; Bhattacharjee, U.; Guo, Y. J.; Vela, J.; Petrich, J. W.; Smith, E. A., Subdiffraction, Luminescence-Depletion Imaging of Isolated, Giant, CdSe/CdS Nanocrystal Quantum Dots. *Journal of Physical Chemistry C* **2013**, *117*, 3662-3667. doi: 10.1021/jp312231k.
25. Lafon, O.; Thankamony, A. S. L.; Kobayashi, T.; Carnevale, D.; Vitzthum, V.; Slowing, II; Kandel, K.; Vezin, H.; Amoureux, J. P.; Bodenhausen, G.; Pruski, M., Mesoporous Silica Nanoparticles Loaded with Surfactant: Low Temperature Magic Angle Spinning C-13 and Si-29 NMR Enhanced by Dynamic Nuclear Polarization. *Journal of Physical Chemistry C* **2013**, *117*, 1375-1382. doi: 10.1021/jp310109s.
26. Kobayashi, T.; Mao, K.; Paluch, P.; Nowak-Krol, A.; Sniechowska, J.; Nishiyama, Y.; Gryko, D. T.; Potrzebowski, M. J.; Pruski, M., Study of Intermolecular Interactions in the Corrole Matrix by Solid-State NMR under 100 kHz MAS and Theoretical Calculations. *Angewandte Chemie-International Edition* **2013**, *52*, 14108-14111. doi: 10.1002/anie.201305475.
27. Kobayashi, T.; Lafon, O.; Thankamony, A. S. L.; Slowing, II; Kandel, K.; Carnevale, D.; Vitzthum, V.; Vezin, H.; Amoureux, J. P.; Bodenhausen, G.; Pruski, M., Analysis of sensitivity enhancement by dynamic nuclear polarization in solid-state NMR: a case study of functionalized mesoporous materials. *Physical Chemistry Chemical Physics* **2013**, *15*, 5553-5562. doi: 10.1039/c3cp00039g.
28. Kandel, K.; Frederickson, C.; Smith, E. A.; Lee, Y. J.; Slowing, II, Bifunctional Adsorbent-Catalytic Nanoparticles for the Refining of Renewable Feedstocks. *ACS Catalysis* **2013**, *3*, 2750-2758. doi: 10.1021/cs4008039.
29. Kandel, K.; Althaus, S. M.; Pruski, M.; Slowing, I. I., Supported Hybrid Enzyme-Organocatalysts for Upgrading the Carbon Content of Alcohols. In *Novel Materials for Catalysis and Fuels Processing*, American Chemical Society: 2013; Vol. 1132, pp 261-271.
30. Kandel, K.; Althaus, S. M.; Peeraphatdit, C.; Kobayashi, T.; Trewyn, B. G.; Pruski, M.; Slowing, II, Solvent-Induced Reversal of Activities between Two Closely Related Heterogeneous Catalysts in the Aldol Reaction. *ACS Catalysis* **2013**, *3*, 265-271. doi: 10.1021/cs300748g.
31. Fang, X. K.; Hansen, L.; Haso, F.; Yin, P. C.; Pandey, A.; Engelhardt, L.; Slowing, I.; Li, T.; Liu, T. B.; Luban, M.; Johnston, D. C., {Mo<sub>24</sub>Fe<sub>12</sub>} Macrocycles: Anion Templatation with Large Polyoxometalate Guests. *Angewandte Chemie-International Edition* **2013**, *52*, 10500-10504. doi: 10.1002/anie.201304887.
32. Carraher, J. M.; Bakac, A., Alkyl group versus hydrogen atom transfer from metal alkyls to macrocyclic rhodium complexes. *Chemical Communications* **2013**, *49*, 6099-6101. doi: 10.1039/c3cc43472a.

33. Bakac, A.; Pestovsky, O.; Durfey, B. L.; Kristian, K. E., Kinetics and thermodynamics of nitric oxide binding to transition metal complexes. Relationship to dioxygen binding. *Chemical Science* **2013**, *4*, 2185-2192. doi: 10.1039/c3sc50157d.
34. Bakac, A.; Pestovsky, O. Selective oxidation of organic substrates to partially oxidized products. US Patent 8507730. **2013**.
35. Wang, C. J.; Liu, D. J.; Evans, J. W., Schloegl's second model for autocatalysis on hypercubic lattices: Dimension dependence of generic two-phase coexistence. *Physical Review E* **2012**, *85*, 041109. doi: 10.1103/PhysRevE.85.041109.
36. Ruberu, T. P. A.; Nelson, N. C.; Slowing, II; Vela, J., Selective Alcohol Dehydrogenation and Hydrogenolysis with Semiconductor-Metal Photocatalysts: Toward Solar-to-Chemical Energy Conversion of Biomass-Relevant Substrates. *Journal of Physical Chemistry Letters* **2012**, *3*, 2798-2802. doi: 10.1021/jz301309d.
37. Ruberu, T. P. A.; Albright, H. R.; Callis, B.; Ward, B.; Cisneros, J.; Fan, H. J.; Vela, J., Molecular Control of the Nanoscale: Effect of Phosphine-Chalcogenide Reactivity on CdS-CdSe Nanocrystal Composition and Morphology. *ACS Nano* **2012**, *6*, 5348-5359. doi: 10.1021/nn301182h.
38. Mukherjee, D.; Ellern, A.; Sadow, A. D., Remarkably Robust Monomeric Alkylperoxyzinc Compounds from Tris(oxazoliny)boratozinc Alkyls and O-2. *Journal of the American Chemical Society* **2012**, *134*, 13018-13026. doi: 10.1021/ja303440n.
39. Marchuk, K.; Guo, Y. J.; Sun, W.; Vela, J.; Fang, N., High-Precision Tracking with Non-blinking Quantum Dots Resolves Nanoscale Vertical Displacement. *Journal of the American Chemical Society* **2012**, *134*, 6108-6111. doi: 10.1021/ja301332t.
40. Mao, K. M.; Kennedy, G. J.; Althaus, S. M.; Pruski, M., Spectral editing in C-13 solid-state NMR at high magnetic field using fast MAS and spin-echo dephasing. *Solid State Nuclear Magnetic Resonance* **2012**, *47-48*, 19-22. doi: 10.1016/j.ssnmr.2012.07.003.
41. Klobukowski, E. R.; Angelici, R. J.; Woo, L. K., Bulk Gold-Catalyzed Reactions of Isocyanides, Amines, and Amine N-Oxides. *Organometallics* **2012**, *31*, 2785-2792. doi: 10.1021/om201068g.
42. Klobukowski, E. R.; Angelici, R. J.; Woo, L. K., Bulk Gold-Catalyzed Oxidations of Amines and Benzyl Alcohol Using Amine N-Oxides as Oxidants. *Catalysis Letters* **2012**, *142*, 161-167. doi: 10.1007/s10562-011-0758-0.
43. Kandel, K.; Althaus, S. M.; Peeraphatdit, C.; Kobayashi, T.; Trewyn, B. G.; Pruski, M.; Slowing, II, Substrate inhibition in the heterogeneous catalyzed aldol condensation: A mechanistic study of supported organocatalysts. *Journal of Catalysis* **2012**, *291*, 63-68. doi: 10.1016/j.jcat.2012.04.005.

44. Jana, B.; Hovey, M.; Ellern, A.; Pestovsky, O.; Sadow, A. D.; Bakac, A., Unusual structural motif in a zwitterionic Fe(II) complex of a tetradentate phosphine. *Dalton Transactions* **2012**, *41*, 12781-12785. doi: 10.1039/c2dt31437a.
45. Huang, Y. L.; Deng, W. H.; Guo, E. R.; Chung, P. W.; Chen, S.; Trewyn, B. G.; Brown, R. C.; Lin, V. S. Y., Mesoporous Silica Nanoparticle-Stabilized and Manganese-Modified Rhodium Nanoparticles as Catalysts for Highly Selective Synthesis of Ethanol and Acetaldehyde from Syngas. *Chemcatchem* **2012**, *4*, 674-680. doi: 10.1002/cctc.201100460.
46. Ho, H. A.; Manna, K.; Sadow, A. D., Acceptorless Photocatalytic Dehydrogenation for Alcohol Decarbonylation and Imine Synthesis. *Angewandte Chemie-International Edition* **2012**, *51*, 8607-8610. doi: 10.1002/anie.201203556.
47. Hara, K.; Akahane, S.; Wiench, J. W.; Burgin, B. R.; Ishito, N.; Lin, V. S. Y.; Fukuoka, A.; Pruski, M., Selective and Efficient Silylation of Mesoporous Silica: A Quantitative Assessment of Synthetic Strategies by Solid-State NMR. *Journal of Physical Chemistry C* **2012**, *116*, 7083-7090. doi: 10.1021/jp300580f.
48. Fernandez, C.; Pruski, M., Probing Quadrupolar Nuclei by Solid-State NMR Spectroscopy: Recent Advances. In *Solid State NMR*, Chan, J. C. C., Ed. Springer-Verlag Berlin: Berlin, 2012; Vol. 306, pp 119-188.
49. Carraher, J. M.; Pestovsky, O.; Bakac, A., Transition metal ion-assisted photochemical generation of alkyl halides and hydrocarbons from carboxylic acids. *Dalton Transactions* **2012**, *41*, 5974-5980. doi: 10.1039/c2dt30210a.
50. Bataineh, H.; Pestovsky, O.; Bakac, A., pH-induced mechanistic changeover from hydroxyl radicals to iron(IV) in the Fenton reaction. *Chemical Science* **2012**, *3*, 1594-1599. doi: 10.1039/c2sc20099f.
51. Alvarado, S. R.; Guo, Y. J.; Ruberu, T. P. A.; Bakac, A.; Vela, J., Photochemical versus Thermal Synthesis of Cobalt Oxyhydroxide Nanocrystals. *Journal of Physical Chemistry C* **2012**, *116*, 10382-10389. doi: 10.1021/jp301459s.
52. Althaus, S. M.; Mao, K. M.; Kennedy, G. J.; Pruski, M., Solid-State NMR Studies of Fossil Fuels using One- and Two-Dimensional Methods at High Magnetic Field. *Energy & Fuels* **2012**, *26*, 4405-4412. doi: 10.1021/ef3004637.

**Simulation of Temperature Programmed Reactions:  
TPR Mechanism Following Adsorption of Methanol on CeO<sub>2</sub>(111).**

Aditya (Ashi) Savara, David R. Mullins, Steven H. Overbury.  
Chemical Sciences Division, Oak Ridge National Laboratory

One of the objectives of our research is to connect the kinetics and mechanisms of catalytic surface chemistry under ultrahigh vacuum conditions (on  $\sim 1 \text{ cm}^2$  flat crystals) to that under molecular flow conditions on nanoparticles with known surface terminations. Here, we establish a general methodology for simulating and fitting the kinetics of temperature programmed reactions (TPR) to gain insight about reaction mechanisms and kinetics in complex reaction networks. Consideration of the response surfaces of possible objective functions (i.e., the functional forms of the residuals during fitting), in the context of reaction rates going through peaks, has led us to the conclusion that integrated production should be utilized rather than the rate of reaction. This response surface is monotonic, suppresses effects from experimental noise, requires fewer points to capture the response behavior, and can be simulated numerically with small errors. It is recommended that experimental datapoints be weighted by the experimental error, as well as the magnitude of the response at that datapoint. It is important to employ stiffness mediation to prevent numerical errors. There are multiple possible methods and technologies for the subsequent parameter optimization.

This methodology is then applied to simulate and fit the kinetics and mechanism of TPR following adsorption of methanol on a CeO<sub>2</sub>(111) thin film under ultrahigh vacuum conditions. The gaseous products observed experimentally are CH<sub>3</sub>OH, CH<sub>2</sub>O, H<sub>2</sub>, H<sub>2</sub>O, CO, and CO<sub>2</sub>. The appearance of these products can be divided into roughly two temperature regions: above 500 K and below 500 K. Most of the H<sub>2</sub>O production (and possibly some H<sub>2</sub> production) occurs at  $< 500 \text{ K}$ . Various features of the experimental results were reproduced by simulation, including gas phase production of each of the six gases (CH<sub>3</sub>OH, CH<sub>2</sub>O, H<sub>2</sub>, H<sub>2</sub>O, CO, and CO<sub>2</sub>), and also the observation of methoxies being the dominant C-containing surface species at temperatures  $< 500 \text{ K}$ . The simulations were unable to discriminate between several possible mechanisms for CH<sub>2</sub>O formation (which occurs primarily at  $> 500 \text{ K}$ ), and thus our insights focus on the kinetics and mechanism below 500 K.

In the kinetics model used here, the production of H<sub>2</sub>O and H<sub>2</sub> at  $< 500 \text{ K}$  can be explained by a mechanism that involves an intermediate (excited) metastable state of hydrogen on the surface, (H\*), which may be a radical state. Initially, the alcohol deprotonates on the surface to produce anionic methoxies and protons (CH<sub>3</sub>O<sup>-</sup> and H<sup>+</sup>). Based on the assumption that there is no low activation energy route for CH bond breaking, low temperature water production is interpreted as occurring via H\* production from H<sup>+</sup> by electron transfer from CH<sub>3</sub>O<sup>-</sup>/V species, where CH<sub>3</sub>O<sup>-</sup>/V represents an anionic methoxy absorbed in an oxygen vacancy (V) (which appears as an intermediate during the reaction mechanism). The reactions involving water and methoxies are shown in the figure below, which denotes the dominant reactions below 500 K. This model suggests that a small amount of vacancies must be present initially (e.g.,  $< 1\%$  of the surface oxygen lattice sites) to initiate the reactions depicted, which then produces additional vacancies and propagates until the “net reaction” shown is achieved. To produce low temperature gas phase H<sub>2</sub>O (at  $< 500 \text{ K}$ ), as observed experimentally, it was found to be critical

that H<sub>2</sub>O cannot dissociate directly on oxygen vacancies. Instead, the water dissociates on terrace sites and the OH groups produced can then jump into the oxygen vacancies: such an overall mechanism is consistent with density functional theory calculations. In the kinetic model that currently is the most representative of the experimental observations, CH<sub>3</sub>O<sup>-</sup> and CH<sub>3</sub>O<sup>\*</sup>/V (anionic methoxies on terraces and neutral methoxies in vacancies) are the major carbon containing species present, in virtually equal stoichiometries, directly subsequent to H<sub>2</sub>O production at <500 K.

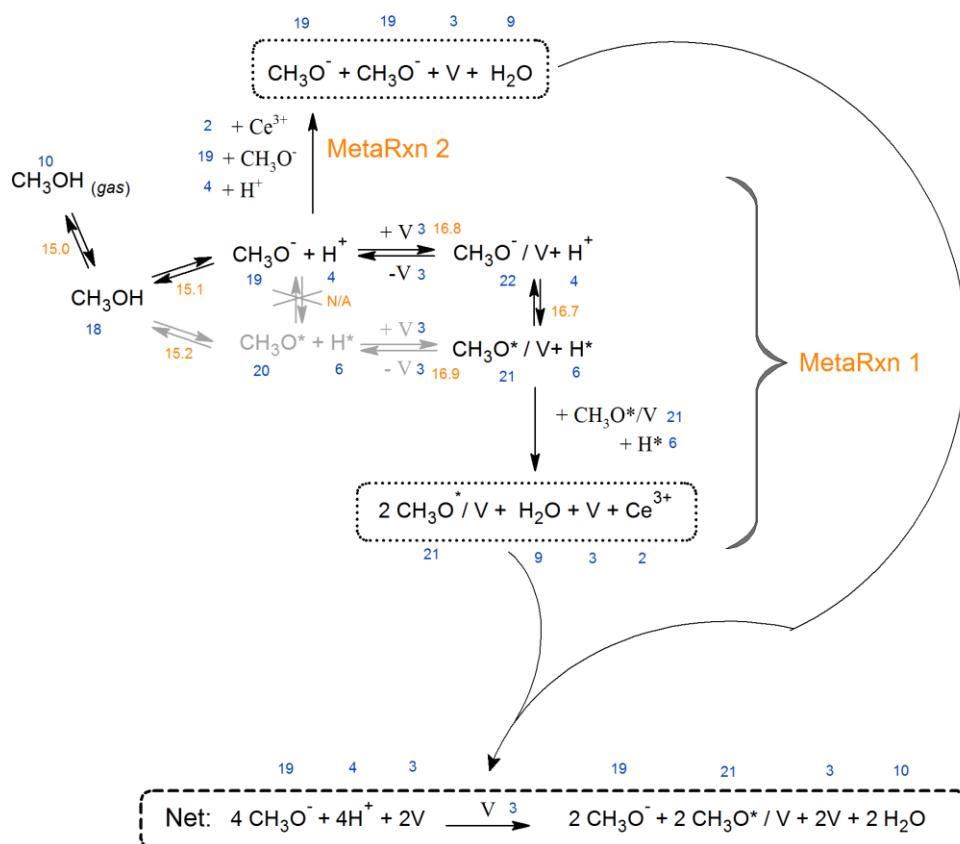
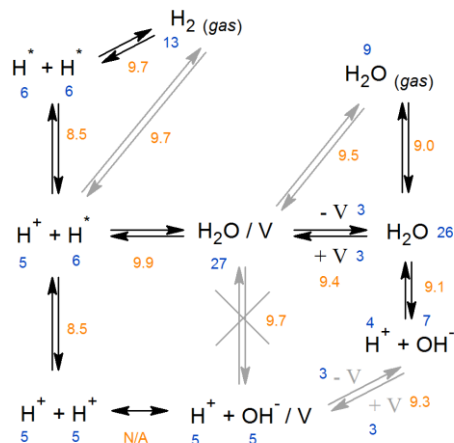


**Figure 1:** Possible reaction pathways for temperatures < 500 K. Reactions involving methoxy groups are shown above and reactions involving water and surface hydrogen are shown to the right. The black arrows designate dominant reaction pathways in the kinetic model currently believed to be most representative of experiments. All species are surface species, unless they are labelled as gas-phase species. Blue numbers correspond to the species numbers, while orange numbers correspond to reaction numbers (see poster for further details).



Research supported by the U.S. Department of Energy, Office of Science, Basic Energy Sciences, Chemical Sciences, Geosciences, and Biosciences Division. This research is part of FWP ERKCC96. For a full description of recent progress see Extended Abstract for ERKCC96.

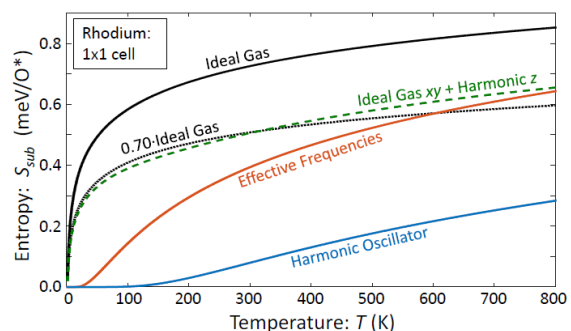
**New Approaches to Non-Ideal Surface Adsorption and Reaction**

William F. Schneider

University of Notre Dame, Dept. of Chemical and Biomolecular Engineering

**Presentation Abstract**

Free energies of adsorption are arguably the most elementary quantities in heterogeneous catalysis. These free energies depend on the surface and adsorbate (reactant, intermediate, or product) of interest, system temperature and adsorbate coverage. The free energy represents a balance between the energetic driving force for creating bonds between an adsorbate and a surface and the entropic cost of moving an adsorbate from a fluid phase to a surface. Standard density functional theory (DFT) approaches generally begin by optimizing the location of an adsorbate on a surface, computing a binding energy, and approximating the internal, translational, and configurational contributions to the free energy. In this contribution we compare standard harmonic approximations with more detailed methods, based on DFT-quantified potential energy surfaces and enumeration of surface densities of states. We recover results consistent with recent inference from experiment. Further, we propose a simple approach for extracting free energies from DFT models.



**DE-FG02-06ER15839: Towards Realistic Models of Heterogeneous Catalysis: Simulations of Oxidation Catalysis from First Principles**

Post-docs: Dr. Kurt Frey

Students: Laura Herder, Anshuman Bajpai

**RECENT PROGRESS**

***DFT-Based Adsorbate Free Energies***

We are developing a computationally inexpensive approach for estimating the translational free energies of adsorbates and comparing it with the standard approaches that corrects the deficiencies of the common harmonic oscillator approximations with no additional computational cost. We write

$$G(\text{M-ads}) = G(\text{M}) + (G(\text{M-ads}) - G(\text{M}))$$

and estimate the difference from the potential energy experienced by an adsorbate translating across the surface. Figure 1 compares the DFT-computed potential energy surface experienced by an O adsorbate on Rh(111) when the surface is frozen vs. relaxed. Results are obtained by rastering the adsorbate across the symmetry-unique grid of density  $\sim 0.2 \text{ \AA}$ . The relaxed surface is clearly much flatter. We solved the single particle Schrödinger equation on the PES using the

DE-FG02-06ER15839

shooting method to obtain in-plane densities of states, partition functions and free energy contributions. We found the out-of-plane potential to be well described by a harmonic potential. The in-plane potential is non-harmonic and gives much more negative free energies (and more positive) entropies than would be extracted from the rigid surface or a standard harmonic oscillator model. The computed in-plane free energies can be fit to good precision using a harmonic oscillator model with a fitted “effective harmonic” (EH) frequency. Extracted adsorption entropies are summarized in the Figure on page 1. The harmonic oscillator model grossly underestimates entropies. The full EH model predicts entropies larger by about a factor of three. The EH model is consistent with the predictions of a scaled ideal gas model as proposed by Campbell at temperatures above about 500 K. At lower  $T$ , this scaled result appears to exaggerate entropies.

Computation and solution of the full PES is relatively expensive. We found that very good estimates to the EH frequencies could be obtained through a simple finite difference approximation in which the adsorbate was displaced  $\pm 0.2 \text{ \AA}$  from its minimum energy position, the surface relaxed, and the result forces used to estimate a spring constant. This approximate method gave force constants within 5-10% of those computed using the full method. Figure 2 summarizes results for an O adsorbate on all the late transition metals. In general the effective frequencies are found to scale with the inverse of the corresponding binding energy with separate intercepts for the out-of-plane and in-plane modes.

### Coverage-aware kinetic models

Over the last several years we have explored this influence of lateral adsorbate interactions on surface reaction rates based on a cluster expansion (CE) approach. The CE is parameterized against DFT calculations and represents the energy of any arbitrary arrangement of adsorbates as an expansion in two- or higher-body terms. The CE captures both the energetic influences of lateral interactions as might be expressed as a coverage-dependent adsorption energy  $E(\theta)$  and the configurational influences of interactions. We used this approach to compare the “volcano” of predicted NO oxidation activity across the late transition metals (Figure 3) assuming  $O_2$  dissociation as the rate determining step. A model that neglects lateral interactions gives the familiar broad volcano. Including coverage-dependent energies collapses the volcano to a much narrower range.

DE-FG02-06ER15839

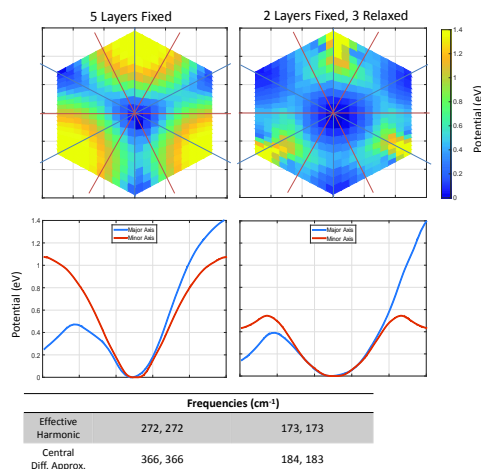


**Figure 1:** Potential energy surface of  $\frac{1}{4}$  ML O adsorbate on Rh(111) assuming the surface is frozen (left) and relaxed (right).

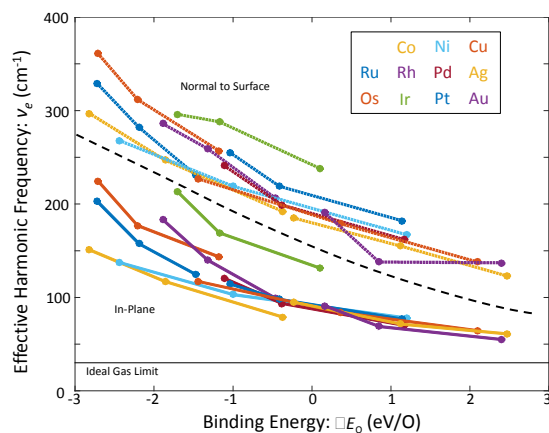


**Figure 2:** Scaling of effective harmonic frequencies with differential binding energies of O on the late transition metals at three coverages.

Further, configuration effects cause the points to deviate from a correlation with the O binding energy. The results illustrate the importance of both energy and ordering to surface reaction rates.

These models assume O to be the most-abundant and only relevant surface intermediate. We recently extended the CE to NO and O co-adsorbates on Pt(111). Central to the task of developing a dual-adsorbate CE was identifying the measures of predictive accuracy and optimizing the number and nature of adsorbate interactions that gives us a CE model versatile for various applications. We used conventional leave one out cross validation (LOOCV) score, 5-fold cross validation and root means square error (RMSE) comparisons to optimize the number of parameters. The obtained CE was also tested for its ability to predict the low coverage binding energy of both NO and O as these binding energies impact the kinetic parameters of the reaction. The model with optimized interaction parameters reveal that NO outbids O, that interactions among the adsorbates are repulsive and follow  $\text{NO-NO} > \text{NO-O} > \text{O-O}$ . These balance of factor cause the most abundant surface species to be sensitive to reaction conditions.

The parameterized CE is used in Grand Canonical Monte Carlo (GCMC) simulations to predict adsorbate coverages and energies vs. reaction conditions. Oxygen outcompetes NO at high temperatures while NO dominates the catalyst surface at lower temperatures. The specific temperature range depends on the ratio  $\frac{P_{\text{NO}_2}}{P_{\text{NO}}}$  as shown in Figure 4. The equilibrated surface is used to calculate reaction rates and obtain the kinetic parameters for NO oxidation on Pt (111). Our aim is to compare the results obtained from this NO-O co-adsorbate model with the oxygen only and the mean field model results to understand the complexity of the model needed to capture the critical parameters of catalytic NO oxidation reaction on Pt (111).

The parameterized CE is used in Grand Canonical Monte Carlo (GCMC) simulations to predict adsorbate coverages and energies vs. reaction conditions. Oxygen outcompetes NO at high temperatures while NO dominates the catalyst surface at lower temperatures. The specific temperature range depends on the ratio  $\frac{P_{\text{NO}_2}}{P_{\text{NO}}}$  as shown in Figure 4. The equilibrated surface is used to calculate reaction rates and obtain the kinetic parameters for NO oxidation on Pt (111). Our aim is to compare the results obtained from this NO-O co-adsorbate model with the oxygen only and the mean field model results to understand the complexity of the model needed to capture the critical parameters of catalytic NO oxidation reaction on Pt (111).

Our aim is to compare the results obtained from this NO-O co-adsorbate model with the oxygen only and the mean field model results to understand the complexity of the model needed to capture the critical parameters of catalytic NO oxidation reaction on Pt (111).

### Surface oxidations

The models above neglect any restructuring of the metal surface caused by adsorbates, but all the late metals are known to reconstruct in the presence of oxygen under some conditions. We have used DFT models to (1) determine the adsorbate conditions leading to development of surface reconstruction and buckling of Pt(111) by O and (2) understand the microscopic steps leading to the initiation of surface oxide formation and growth.

We first showed that particular arrangements of O around a surface Pt, in particular a first nearest neighbor fcc-hcp oxygen pair, result in relaxation of the Pt out of the surface and a partial

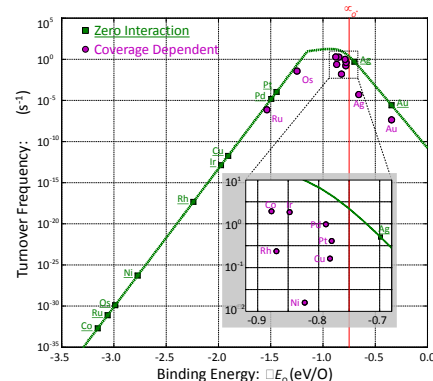


**Figure 3:** NO oxidation rates vs. O binding energy neglecting interaction effects (green) and including them through a CE model (purple).

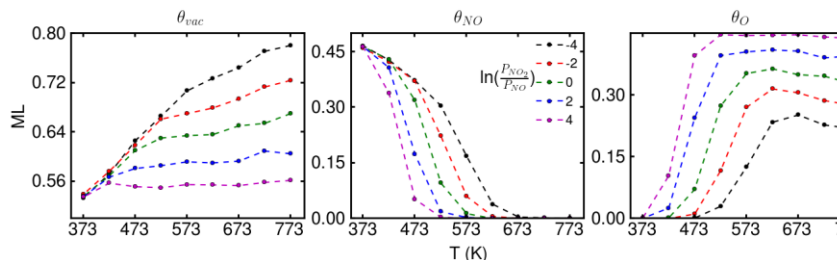


**Figure 4:** Vacancy, NO, and O coverage as a function of temperature ( $T$ ) for various  $\ln\left(\frac{P_{\text{NO}_2}}{P_{\text{NO}}}\right)$  using a NO-O dual adsorbate CE model.  $P_{\text{NO}} = 100$  ppm.

oxidation. Further, as shown in Figure 5, we explored the pathways by which such restructurings happen. Nucleation of a reconstruction involves barriers both for two O to approach one another and a larger barrier to simultaneously assume fcc-hcp positions and reconstruct the Pt. Once the reconstruction is nucleated, however, further chain growth has more modest barriers. The result is a preferential growth of oxide along an fcc row.

To understand the intermediate stages of surface oxide formation, we used the CE approach to model co-adsorption of O in fcc and hcp sites. This CE takes advantage of a “steepest descents” fitting procedure we developed. We find a strong tendency for parallel alignment of oxide chains. Through this approach we are able to recover known and discover previously unknown low-energy partially oxidized surface structures.

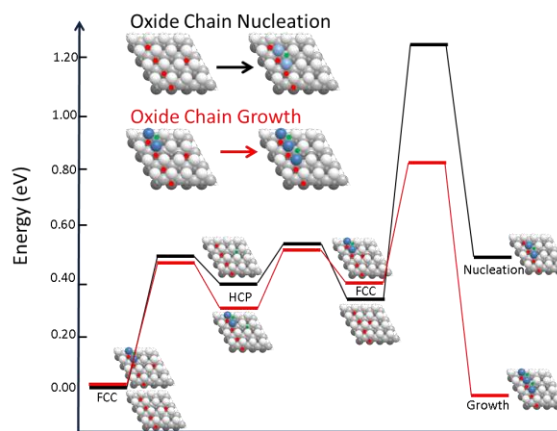


**Figure 5:** Potential energy surfaces for nucleation and growth of an oxidized Pt chain on Pt(111).

### Future Plans

We plan to explore more broadly adsorption free energy models, consider effects of adsorbate type and crystal facet, in particular to identify simple yet reliable models and correlations to parameterize kinetic models. We plan to extend our investigations of coverage-dependent kinetic models informed by DFT, with the goal of leveraging the reliability of the CE approach with the expediency of simpler mean field models.

### Publications Acknowledging this Grant in 2012-2015

C. Wu, D. J. Schmidt, C. Wolverton, and W. F. Schneider, “Accurate coverage-dependence incorporated into first-principles kinetic models: Catalytic NO oxidation on Pt(111),” *J. Catal.* **2012**, 286, 88-94.

H. Wang and W. F. Schneider, “Comparative chemistries of CO and NO oxidation over RuO<sub>2</sub>(110): Insights from first principles thermodynamics and kinetics,” *Molec. Sim.* **2012**, 38, 615-630.

J.-S. McEwen, J. Bray, C. Wu, and W. F. Schneider, “How low can you go? Minimum energy pathways for O<sub>2</sub> dissociation on Pt(111),” *Phys. Chem. Chem. Phys.*, **2012**, 14, 16677-16685.

J. M. Bray and W. F. Schneider, “First-Principles Thermodynamic Models In Heterogeneous Catalysis,” in *Computational Catalysis*, M. Janik and A. Asthagiri, eds., Royal Society of Chemistry: Cambridge (2013).

J. M. Bray and W. F. Schneider, “Coverage-dependent adsorption at a low symmetry surface: DFT and statistical analysis of oxygen chemistry on kinked Pt(321),” *Topics Catal.* **2014**, 57, 89-105.

J. M. Bray, I. Skavdahl, J.-S. McEwen, and W. F. Schneider, “First-principles Reaction Site Model for Coverage-Sensitive Surface Reactions: Pt(111)-O Temperature-Programmed Desorption,” *Surf. Sci. Lett.*, **2014**, 622, L1-L6.

K. Frey, D. J. Schmidt, C. Wolverton and W. F. Schneider, "Implications of coverage-dependent O adsorption for catalytic NO oxidation on the late transition metals," *Catal. Sci. Technol.*, **2014**, *4*, 4356-4365.

J. M. Bray and W. F. Schneider, "First-Principles Analysis of Structure Sensitivity in NO Oxidation on Pt," *ACS Catal.*, **2015**, *5*, 1087-1099.

L. M. Herder, J. M. Bray, and W. F. Schneider, "Comparison of Cluster Expansion Fitting Algorithms for Interactions at Surfaces," *Surf. Sci.* **2015**, in press.

Wendy J. Shaw

## Enhancing the Performance of Hydrogenase Mimics with An Enzyme-Inspired Outer Coordination Sphere

Wendy Shaw, Arnab Dutta, Sheri Lense, John Roberts, Bojana Ginovska-Pangovska  
Pacific Northwest National Laboratory

### Presentation Abstract

The outer coordination sphere of enzymes is essential to their superior function and our program focuses on trying to capture the desirable traits of the enzyme scaffold in homogeneous catalysts, catalysts which often focus on the impact of the first and second coordination spheres. We are developing redox active catalysts which oxidize and produce H<sub>2</sub>, mimicking the hydrogenase enzyme. Like other enzymes, hydrogenase enzymes use many outer coordination sphere features to very efficiently convert H<sup>+</sup> to H<sub>2</sub> and back again, providing inspiration for the development of molecular catalysts. Recent work on H<sub>2</sub> oxidation catalysts show the amino acids render the complexes water soluble, and the resulting catalysts have faster rates and significantly lower overpotentials than the unmodified complexes. Reminiscent of enzymes, reversibility is achieved while fast rates are maintained, although acidic conditions are needed for the complex in contrast to the enzyme. We have demonstrated that the carboxylic acid groups facilitate rapid proton movement resulting in lower overpotentials, and that side chain functional groups can influence the structure of the active site enhancing catalytic rates. Experiments at high temperature and high H<sub>2</sub> pressure have resulted in unprecedented rates of H<sub>2</sub> oxidation, as high as 1.5 x 10<sup>6</sup> s<sup>-1</sup>, at overpotentials below 300 mV. These observations demonstrate that outer coordination sphere amino acids work in synergy with the active site and can play an equally important role for synthetic molecular electrocatalysts as the protein scaffold does for redox active enzymes. Despite these phenomenal results, there is still evidence of limiting proton and/or electron transfer, suggesting that even faster rates and/or lower overpotentials can be achieved. To realize or exceed the combination of enzyme-like rates and overpotentials, future studies will include investigating additional amino acids to understand contributions of other side chains in structural roles, as well as the role of the pK<sub>a</sub> of the side chain in aiding proton movement. The addition of larger peptides to further enhance proton movement and control the positioning of functional groups to influence catalytic properties is also planned, building upon successes achieved attaching peptides to H<sub>2</sub> production catalysts. Combining these approaches allows us to explore and develop a mechanistic understanding of the role of the OCS on molecular catalysts, and may also serve as a model system for enzymes, offering insight into the function of their outer coordination sphere.

### DE-AC05-76RL0 1830: Early Career: Catalyst Biomimics: A novel approach in catalyst design

**Postdocs and Junior Staff:** Arnab Dutta  
Nilusha Borolugodage  
Bojana Ginovska-Pangovska (PNNL)

### RECENT PROGRESS

*1) Achieving Reversibility for H<sub>2</sub> Oxidation/H<sub>2</sub> production. Summary: A complex for H<sub>2</sub> oxidation, Ni(P<sup>Cy</sup><sub>2</sub>N<sup>Arginine</sup><sub>2</sub>)<sub>2</sub><sup>2+</sup>, was designed and synthesized. The resulting complex demonstrates true reversibility; i.e., operating in both directions at the equilibrium potential (Figure 1), while maintaining fast rates—a behavior reminiscent of hydrogenase enzymes and*

the first demonstration for hydrogenase mimics.<sup>37</sup> Reversible behavior is proposed to be caused by a combination of features in the outer coordination sphere. The COOH group facilitates proton movement, while interactions between the guanidinium groups in the outer coordination sphere (Figure 1, inset; reference<sup>87</sup>) facilitate H<sub>2</sub> addition possibly by altering the Ni•••N distance.<sup>37,39</sup>

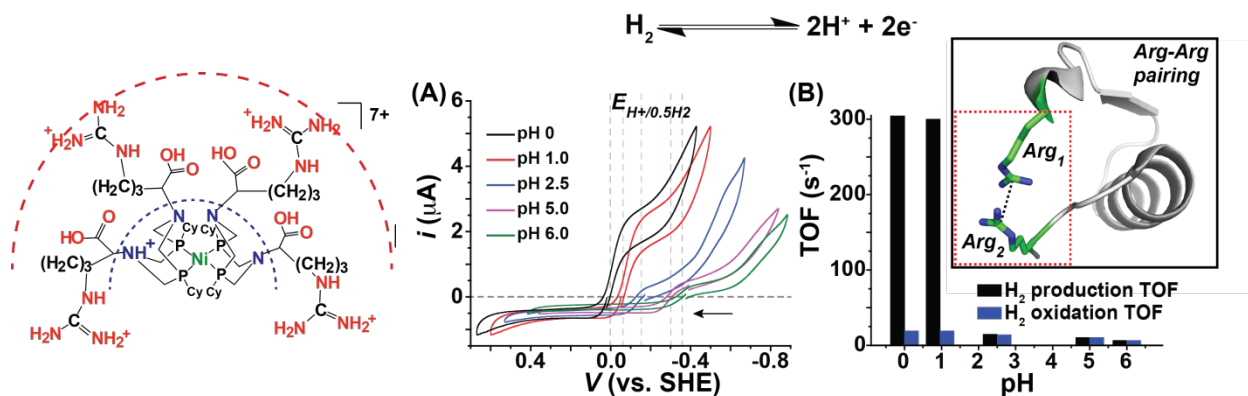
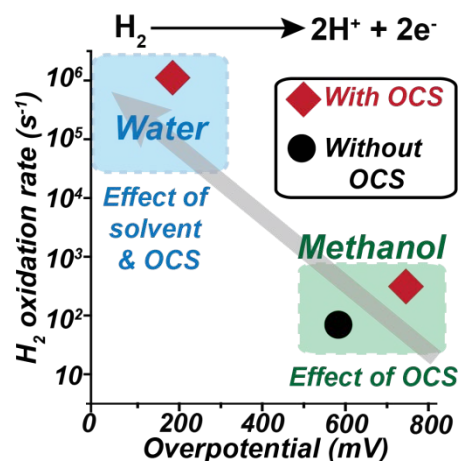


**Figure 1.** Arginine in the outer coordination sphere reproduces enzyme-like reversibility above 45 °C as shown in electrochemical traces (left) and with high TOFs for both H<sub>2</sub> oxidation and production (right). Inset: pairing between two arginines (shown from Zhang, *JPCB*, 2013<sup>87</sup>) proposed to assist reversibility by enhancing H<sub>2</sub> addition by changing the Ni•••N distance.

2) *The role of water and an amino acid outer coordination sphere in achieving unprecedented H<sub>2</sub> oxidation rates at low overpotentials.* Summary: A Ni-based complex with an appended arginine, [Ni(P<sup>Cy</sup><sub>2</sub>N<sup>arginine</sup><sub>2</sub>)<sub>2</sub>]<sup>7+</sup>, exhibits the fastest H<sub>2</sub> oxidation reported for any homogeneous electrocatalyst to date (TOF 1.1×10<sup>6</sup> s<sup>-1</sup>) operating at a moderate overpotential (240 mV). Control experiments demonstrate that both the outer coordination sphere and water are critical for this impressive catalytic performance. This work has been submitted to *Chemical Communications*.

**Table 1 and Figure 2.** Turnover frequencies (TOF) and overpotentials of H<sub>2</sub> oxidation by CyArg and CyBn (Bn=benzyl)in: i) water (pH=1) or ii) methanol with 25 mM [HTFSI], 0.28 M water, as a function of temperature and pressure. RT: 25 °C; HT: 55 °C (for methanol) or 72 °C (for water); <sup>c</sup>reported in reference<sup>8b</sup>. Data summarized in Figure 2, right.

Conditions (Temp./H <sub>2</sub> pressure) Catalyst (solvent)	TOF (s <sup>-1</sup> )			Overpotential (mV)		
	RT	RT	HT	RT	RT	HT
	1	100	100	1	100	100
	atm	atm	atm	atm	atm	atm
CyArg (H <sub>2</sub> O)	210 <sup>c</sup>	1.25×10 <sup>5c</sup>	1.1×10 <sup>6</sup>	120	380	240
CyArg (MeOH)	35	280	280	550	900	750
CyBn (MeOH)	10	80	80	225	650	550



### 3) Single Amino Acid Modifications Reveal Additional Controls of [FeFe]-hydrogenase activity.

**Summary:** The proton pathway of [FeFe]-hydrogenase is critical to the efficiency of the enzyme, and has previously been identified to have four residues and one water molecule based on experimental mutation studies. A computational analysis of this pathway revealed that the residue proposed to be at the mouth of the pathway (Glu282) was hydrogen bound to two residues outside the pathway (Arg286 and Ser320), raising a question of their functional role. Substituting Arg286 with leucine eliminates this hydrogen bond and results in a 2.5-fold enhancement in H<sub>2</sub> production activity, suggesting that Arg286 serves an important role in controlling the rate of proton delivery. Substitution of Ser320 with alanine reduces the rate 10-fold, suggesting that it is a member of the pathway. Its position relative to the rest of the pathway suggests that it may be the true pathway entrance. QM/MM and molecular dynamics results provide evidence consistent with these interpretations, by demonstrating that Ser320 does not play an electronic or structural role. Collectively, these data show the complexity and intricate nature of proton delivery and its dependence on the nearby protein scaffold. This work is being prepared for submission to *Biochemistry*.

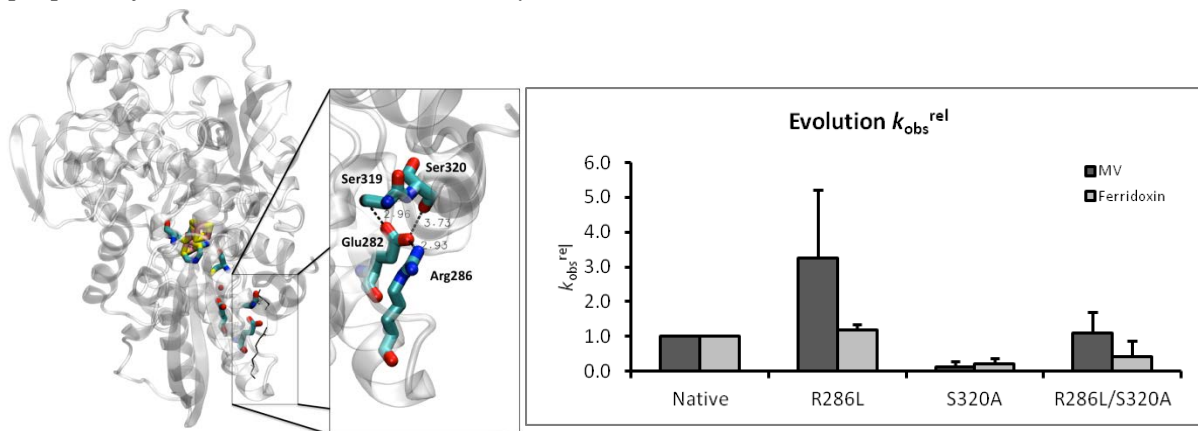


**Figure 3.** Proton pathway and active site in [FeFe]-Hydrogenase. The insert shows the proposed mouth of the proton pathway of [FeFe]-hydrogenase, and the relative orientations of Ser320, Arg286, Glu282 to each other and to the surface of the protein. Right: relative rates of the mutants relative to the parent complex.

### Publications Acknowledging this Grant in 2012-2015

1. Rodriguez-Macia, Arnab Dutta, Wolfgang Lubitz, Wendy J. Shaw, Olaf Rudiger, "Direct comparison of the performance of a bio-inspired synthetic Ni-catalyst and a [NiFe]-hydrogenase covalently attached to electrodes." *Angewandte Chemie International Edition*, **2015** Accepted.
2. Ming-Hsun Ho, Molly O'Hagan, Michel Dupuis, Daniel L. DuBois, R. Morris Bullock, Wendy J. Shaw, and Simone Raugei, "Water-Assisted Proton Delivery and Removal in Bio-inspired Hydrogen Production Catalysts", *Dalton Transactions*, **2015**, Accepted.

3. Arnab Dutta, Daniel L. DuBois, John A. S. Roberts, and Wendy J. Shaw, "Amino Acid Modified Ni Catalyst Exhibits Reversible H<sub>2</sub> Oxidation/Production over a Broad pH Range at Elevated Temperatures", *Proceedings of the National Academy of Sciences*, **2014**, *111*, 16286-16291.
4. J. Timothy Bays, Nilusha Priyadarshani, Matthew S. Jeletic, Elliott B. Hulley, Deanna L. Miller, John C. Linehan, Wendy J. Shaw. "The Influence of the Second and Outer Coordination Spheres on Rh(diphosphine)<sub>2</sub> CO<sub>2</sub> Hydrogenation Catalysts", *ACS Catalysis* **2014**, *4*, 3663-70.
5. (Invited) Bojana Ginovska-Pangovska, Arnab Dutta, Matthew L. Reback, John C. Linehan, Wendy J. Shaw, "Beyond the Active Site: The Impact of the Outer Coordination Sphere on Electrocatalysts for Hydrogen Production and Oxidation", *Accounts of Chemical Research*, **2014**, *47*, 2621-2630.
6. Arnab Dutta, Sheri Lense, John A. S. Roberts, Wendy J. Shaw, "Learning from Nature: Arg-Arg Pairing Enhances H<sub>2</sub> Oxidation Catalyst", *Angewandte Chemie*, **2014**, *53*, 6487-6491.
7. Jianbo Hou, Ming Fang, Allan J.P. Cardenas, Wendy J. Shaw, Monte L. Helm, R. Morris Bullock, John A.S. Roberts, Molly O'Hagan, "Electrocatalytic H<sub>2</sub> production with a turnover frequency >10<sup>7</sup> s<sup>-1</sup>: Medium provides increase in rate but not overpotential," *Energy and Environmental Science*, **2014**, *7*, 4013-4017.
8. Matthew L. Reback, Garry W. Buchko, Brandon L. Kier, Bojana Ginovska-Pangovska, Yijia Xiong, John A.S. Roberts, Christina M. Sorensen, Simone Rauegi, Thomas C. Squier, Wendy J. Shaw, "Enzyme Design from the Bottom-Up: An Active Nickel Electrocatalyst with a Peptide Outer Coordination Sphere," *Chemistry: A European Journal*, **2014**, *20*, 1510-1514.
9. Sheri Lense, Arnab Dutta, John A. S. Roberts, Wendy J. Shaw, "A Proton Channel Allows a Hydrogen Oxidation Catalyst to Operate at a Moderate Overpotential with Water Acting as a Base", *Chemical Communications*, **2014**, *50*, 792-795.
10. Bojana Ginovska-Pangovska, Ming-Hsun Ho, Yuhui Cheng, Michel Dupuis, Simone Rauegi, Wendy J. Shaw. "Molecular Dynamics Study of the Proposed Proton Transport Channels in [FeFe]-Hydrogenase", *Biochimica Et Biophysica Acta:Bioenergetics*, **2014**, *1837*, 131-138.
11. Arnab Dutta, Sheri Lense, Jianbo Hou, Mark H. Engelhard, John A. S. Roberts, Wendy J. Shaw, "Proton Channel Enables H<sub>2</sub> Oxidation and Production for a Water-Soluble Ni Catalyst", *Journal of the American Chemical Society*, **2013**, *135*, 18490-18496.
12. Brandon R. Galan, Matthew L. Reback, Avijita Jain, Aaron M. Appel, Wendy J. Shaw. "Electrocatalytic Oxidation of Formate Using [Ni(P<sup>R</sup><sub>2</sub>N<sup>R'</sup><sub>2</sub>)<sub>2</sub>]<sup>2+</sup> Complexes: Effect of Ligands Modified with Amino Acids", *European Journal of Inorganic Chemistry*, **2013**, 5366-5371.
13. Garry W. Buchko, Avijita Jain, Matthew L. Reback, Wendy J. Shaw. "Structural Characterization of the Model Amphipathic Peptide Ac-LKKLLKLLKLLKL-NH<sub>2</sub> in Aqueous Solution and with 2,2,2-trifluoroethanol and 1,1,1,3,3,3-hexafluoroisopropanol", *Canadian Journal of Chemistry*, **2013**, *91*, 406-413.

14. Sheri Lense, Ming-Hsun Ho, Shentan Chen, Avijita Jain, Simone Raugei, John C. Linehan, John Roberts, Aaron M. Appel, Wendy J. Shaw. "Investigating Steric and Electronic Effects through the Addition of Amino Acid Esters, and the Use of Water as a Base, for Hydrogen Oxidation Catalysts", *Organometallics*, **2012**, *31*, 6719-6731.
15. Avijita Jain, Garry W. Buchko, Matthew L. Reback, Molly O'Hagan, Bojana Ginovska-Pangovska, John C. Linehan, Wendy J. Shaw. "Active Hydrogenation Catalyst with a Structured, Peptide-Based Outer-Coordination Sphere", *ACS Catalysis*, **2012**, *2*, 2114-2118.
16. Wendy J. Shaw. "The Outer-Coordination Sphere: Incorporating Amino Acids and Peptides as Ligands for Homogeneous Catalysts to Mimic Enzyme Function", *Catalysis Reviews*, **2012**, *54*, 489-550.
17. Avijita Jain, Matthew L. Reback, Mary Lou Lindstrom, Colleen E. Thogerson, Monte L. Helm, Aaron M. Appel, Wendy J. Shaw. "Investigating the Role of the Outer-Coordination Sphere in  $[\text{Ni}(\text{P}^{\text{Ph}}_2\text{N}^{\text{Ph-R}}_2)_2]^{2+}$  Hydrogenase Mimics", *Inorganic Chemistry*, **2012**, *51*, 6592-6602.
18. Avijita Jain, Monte L. Helm, John C. Linehan, Daniel L. DuBois, Wendy J. Shaw. "Biologically Inspired Phosphine Platinum Complexes", *Inorganic Chemistry Communications*, **2012**, *22*, 65-67.
19. James A. Franz, Molly O'Hagan, Ming-Hsun Ho, Tianbio Liu, Monte Helm, Sheri Lense, Daniel L. DuBois, Wendy J. Shaw, Aaron M. Appel, Simone Raugei, R. Morris Bullock, "Conformational Dynamics of  $[\text{Ni}(\text{P}^{\text{R}}_2\text{N}^{\text{R}'_2})^{n+}$  Hydrogen Production and Oxidation Catalysts." *Organometallics*, **2013**, *32*, 7034-7042.
20. Wendy J. Shaw, Monte L. Helm, Daniel L. DuBois. "A Modular, Energy-Based Approach to the Development of Nickel Containing Molecular Electrocatalysts for Hydrogen Production and Oxidation." *Biochimica et Biophysica Acta*, **2013**, *1827*, 1123-1139.
21. **(Selected VIP and cover art)** Matthew L. Reback, Bojana Ginovska-Pangovska, Ming-Hsun Ho, Avijita Jain, Thomas C. Squier, Simone Raugei, John A. S. Roberts, Wendy J. Shaw. "The Role of a Dipeptide Outer-Coordination Sphere on  $\text{H}_2$  Production Catalysts: Influence on Catalytic Rates and Electron Transfer." *Chemistry: A European Journal*. **2013**, *19*, 1928-1941.
22. Molly O'Hagan, Ming-Hsun Ho, Jenny Y. Yang, Aaron M. Appel, M. Rakowski DuBois, Simone Raugei, Wendy J. Shaw, Daniel L. DuBois, and R. Morris Bullock. "Proton Delivery and Removal in  $[\text{Ni}(\text{P}^{\text{R}}_2\text{N}^{\text{R}'_2})_2]^{2+}$  Hydrogen Production and Oxidation Catalysts." *Journal of the American Chemical Society*. **2012**. *134*, 19409-19424

Darío J. Stacchiola

**The catalytic power of interfaces in catalysts determined by *In-situ* studies**

Darío J. Stacchiola, José A. Rodriguez, Mike White, Sanjaya Senanayake, Ping Liu  
Department of Chemistry, Brookhaven National Laboratory, Upton, NY 11973

The traditional approach to the optimization of metal/oxide catalysts has focused on the properties of the metal phase. A low concentration of chemically active sites in the oxide support may be blocked by the anchoring of metal nanoparticles. By using a second oxide as a support (host), one can create a multifunctional configuration in which both metal and oxide nanoparticles are exposed to the reactants [1]. As an example, depositing ceria on TiO<sub>2</sub>(110) leads to the formation of ceria dimers [1]. Atoms with properties ranging from metallic to ionic are available at the metal–oxide interface and create unique reaction sites. We show the creation of an efficient pathway for the water–gas shift reaction at the oxide–metal interface of ceria nanoparticles deposited on Cu(111) or Au(111). *In situ* experiments demonstrated that a carboxy species formed at the interface is the critical intermediate in the reaction [2]. A similar associative mechanism is observed even when the oxide is replaced by a carbide, creating an efficient multifunctional active site at the metal/carbide interface for the WGSR.[3] Using this knowledge, we show how to create a new multifunctional active site for the conversion of CO<sub>2</sub> to methanol.[4]

- [1] *Chem. Rev* **113**, 4373–4390 (2013)
- [2] *Angew. Chem. Int. Ed.* **52**, 5101–5105 (2013)
- [3] *Top. Catal.* **58**, 271–280 (2015)
- [4] *Science*, **345**, 546-550 (2014)

**FWP: BNL CO-009 – CATALYSIS SCIENCE FOR ADVANCED FUELS**

**Postdocs:** Ashleigh Baber, Kumudu Mudiyansele

**Students:** Fang Xu

Steven L. Suib

**POROUS TRANSITION METAL OXIDES: SYNTHESIS, CHARACTERIZATION, AND CATALYTIC ACTIVITY**

Steven L. Suib

University of Connecticut, Department of Chemistry

**Presentation**

**Abstract**

The goals of this project are to synthesize well ordered crystalline mesoporous transition metal oxide (MTMO) materials with monomodal uniform pore sizes; to prepare and characterize ordered mesoporous thin films; to optimize catalytic activity, selectivity, and stability in oxidation catalysis using amorphous porous oxides and crystalline microporous and mesoporous materials; to investigate the role of mesoporous materials in battery systems; and to develop novel *in situ* characterization methods for syntheses, selective oxidations, and battery studies. The assembly of these materials involves inverted micelles. Characterization of the nucleation process has been done with UV-Visible and Fourier transform infrared spectroscopy. Morphological studies have been done with a combination of scanning and transmission electron microscopy methods. A unique feature of these MTMO materials is that various compositions can be prepared such as CoO, Co<sub>3</sub>O<sub>4</sub> and other known structures of metal oxides. This in turn allows enhanced thermal stability of such materials that are most often made by preparations similar to MCM-41 or by replica methods, both of which are rather limiting. Various metal oxides of titanium, manganese, iron, cobalt, nickel, copper, zinc, zirconium, aluminum, silicon, tin, cerium, and many others have been made. Taking advantage of the control of pore size has led to enhanced activity in coupling reactions as well as oxidation reactions. The adsorptive properties of these materials are enhanced since the synthesis process allows numerous ordered pores greater in void volume than typical mesoporous materials. This period we have successfully made uniform monomodal pore sized crystalline walled mesoporous metal oxides that show excellent adsorption and catalytic properties. These materials have been expanded to systems throughout the periodic table that have outstanding thermal stabilities. There are now 65 families of new University of Connecticut (UCT) materials that have been made including sulfide materials.

**DE-FG02-86ER13622.A000: POROUS TRANSITION METAL OXIDES: SYNTHESIS, CHARACTERIZATION, AND CATALYTIC ACTIVITY**

**PI:** Steven L. Suib

**Postdoc(s):**

**Student(s):** Sourav Biswas, Saminda Dharmarathna, Curt Guild, David Kriz, Zhu Luo, Ehsan Moharerri, Lakshitha Pahalagedara, Altug Poyraz, Wenqiao Song, Wei Zhong

**Affiliations(s):** UCONN, Institute of Materials Science, Chemical Biomolecular Engineering Department.

## RECENT PROGRESS

### (1) Synthesis of Materials.

Several materials have been produced in this period such as porous nano-size particles of copper oxide,<sup>1,27</sup> various manganese oxides,<sup>2,4-7,9,12,13,16, 18,20-23,25-26</sup> doped mixed metal oxides,<sup>10,24,29</sup> zinc oxide,<sup>11</sup> titania,<sup>14,28</sup> mesoporous silica,<sup>17</sup> and hydroxyapatite materials.<sup>30</sup> Some unique synthetic methods that were used in such studies included microwave activation,<sup>1</sup>

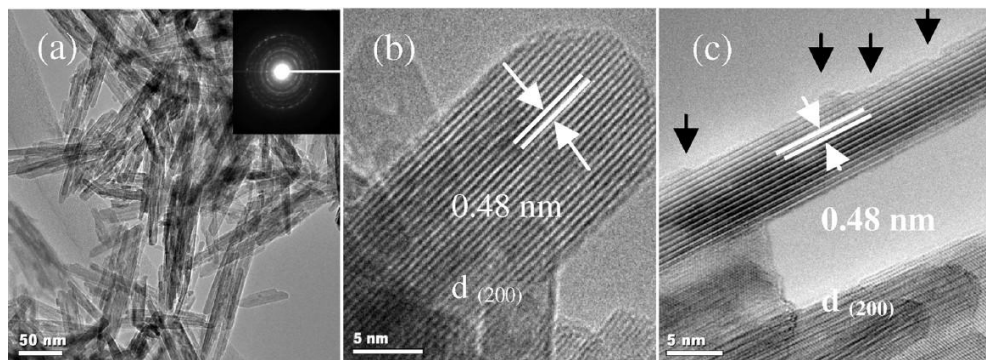


**Figure 1, TEM and HRTEM images of as synthesized OMS-2 materials after 12 h. (a) Low magnification image showing a morphology of short nanorods. (b) Nanofiber showing lattice fringes of (200) plane. (c) Nanofiber showing defects and lattice fringes.**

sonochemical activation,<sup>4</sup> combined ultraviolet and microwave methods,<sup>14</sup> hydrothermal methods,<sup>23</sup> heteroepitaxial growth,<sup>25</sup> sol-gel,<sup>29</sup> and ion-exchange.<sup>30</sup> Sonochemical activation is one of the more unusual activation methods used to synthesize porous manganese oxides and this resulted in defect structures as evidenced by TEM data of **Figure 1**.

Another unique method of synthesis involved heteroepitaxial growth of porous manganese oxides on SrTiO<sub>3</sub>.<sup>25</sup> TEM data have been used to study this heteroepitaxy and

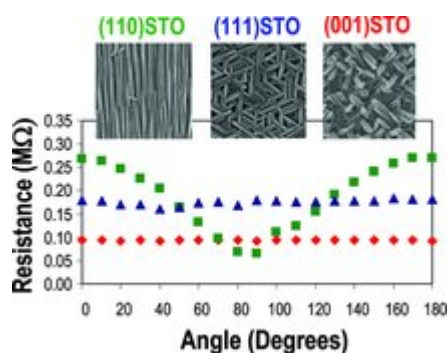


**Figure 2, Plot of Porous Manganese Oxides Grown on Different Planes of SrTiO<sub>3</sub> and Correlated Resistivity Measurements.**<sup>25</sup>

very low resistivity values measured parallel to the fibers and similar to the highest conductivity value ever reported (**Figure 2**).

In this past year, our primary focus has been synthesis, characterization, and applications of UCT materials.<sup>38,43,46,49,51,57-8,60</sup> The first publication<sup>38</sup> is a general article on the synthesis, unique characterization, and applications of mesoporous UCT materials. This paper covers mechanisms of the formation of nano-size particles of UCT systems, unique

adsorption, and catalytic data resulting from the monomodal pore sizes, high thermal stability, and crystalline walls of these oxides. Examples are given of various transition metal oxides, nonmetal oxides, and lanthanide oxide systems, showing the generality and uniqueness of this synthetic approach. Mesoporous  $\text{Co}_3\text{O}_4$  systems,<sup>43</sup> tungsten promoted group IV mesoporous materials,<sup>46</sup> mixed metal oxides,<sup>49</sup> and crystalline microporous/mesoporous OMS-2 systems<sup>51</sup> have also been reported in detail. These latter materials<sup>49,51</sup> are of key significance because mixed metal systems have been prepared and these synthetic methods open the door to make other mesoporous materials of great importance such as perovskites, spinels, and others heretofore unknown.

Other synthetic studies have focused on heteroepitaxial nanostructured arrays of OMS-2 materials,<sup>25</sup> nano-size zeolite ZK-5,<sup>45</sup> microwave assisted hydrothermal synthesis of OMS-2,<sup>54</sup> and  $\text{Co}_3\text{O}_4$ @CNT materials.<sup>50</sup> A unique set of basic UCT materials have been prepared by doping small amounts of alkali ions into UCT manganese oxide based materials.<sup>60</sup>

### Publications Acknowledging this Grant in 2012-2015

1. Qiu, G.; Dharmarathna, S.; Zhang, Y.; Opembe, N.; Huang, H.; Suib, S., Facile Microwave-Assisted Hydrothermal Synthesis of CuO Nanomaterials and Their Catalytic and Electrochemical Properties, *J. Phys. Chem. C*, 2012, **116**, 468-477.
2. Chen, C. H.; Suib, S. L., Control of Catalytic Activity Via Porosity, Chemical Composition, And Morphology of Nanostructured Porous Manganese Oxide Materials, *J. Ch. Chem. Soc.*, 2012, **2012**, 59, 465-472.
3. Genuino, H. C.; Horvath, D. T.; King'ondeu, C. K.; Hoag, G. E.; Collins, J. B.; Suib, S. L., Effects of visible and UV light on the characteristics and properties of crude oil-in-water emulsions, *Photochem. Photobiol. Sci.*, 2012, **11**, 692-702.
4. Dharmarathna, S.; King'ondeu, C. K.; Pedrick, W.; Pahalagedara, L.; Suib, S. L., Direct Sonochemical Synthesis of Manganese Octahedral Molecular Sieve (OMS-2) Nanomaterials Using Co-solvent Systems, Their Characterization, and Catalytic Applications, *Chem. Mat.*, 2012, **24**, 705-712.
5. Njagi, E. C.; Genuino, H. C.; King'ondeu, C. K.; Dharmarathna, S.; Suib, S. L., Catalytic Oxidation of Ethylene at Low Temperatures Using Porous Copper Manganese Oxides, *Appl. Catal. A*, 2012, **421-422**, 154-160.
6. Opembe, N. N.; King'ondeu, C. K.; Suib, S. L., Efficient Oxidation of 2,3,6-Trimethyl Phenol Non-Exchanged and  $\text{H}^+$  Exchanged Manganese Oxide Octahedral Molecular Sieves (K-OMS-2 and H-K-OMS-2) as Catalysts, *Catal. Lett.*, 2012, **142**, 427-432.
7. Iyer, A.; Del-Pilar, J.; King'ondeu, C.; Kissel, E.; Garces, H.; Huang, H.; El-Sawy, A.; Dutta, P.; Suib, S., Water Oxidation Catalysis using Amorphous Manganese Oxides, Octahedral Molecular Sieves (OMS-2) and Octahedral Layered (OL-1) Manganese Oxide Structures, *J. Phys. Chem. C*, 2012, **116(10)**, 6474-6483.
8. Genuino, H.; Opembe, N.; Njagi, E.; McClain, S.; Suib, S., A Review of Hydrofluoric Acid and Its Use in the Car Wash Industry, *J. Industr. Eng. Chem.*, 2012, **18**, 1529-1539.
9. Suib, S. L., Novel Catalysts for Oxidations, Biomass Conversion, and Alternative Fuels, *Preprints – American Chemical Society, Division of Petroleum Chemistry*, 2012, **57**, 173-174.
10. Liu, Y.; Cao, F.; Chen, B.; Zhao, X.; Suib, S. L.; Chan, L. W. H.; Yuan, J., High Performance of  $\text{LiNi}_{0.5}\text{Mn}_{0.5}\text{O}_2$  Positive Electrode Boosted by Ordered Three-Dimensional Nanostructures, *J. Power Sources*, 2012, **206**, 230-235.
11. Garces, H. F.; Espinal, A. E.; Suib, S. L., Tunable Shape Microwave Synthesis of Zinc Oxide Nanospheres and Their Desulfurization Performance Compared with Nanorods and Platelet-Like Morphologies for the Removal of Hydrogen Sulfide, *J. Phys. Chem. C*, 2012, **116**, 8465-8474.
12. Espinal, L.; Wong-Ng, W.; Kaduk, J. A.; Allen, A. J.; Snyder, C. R.; Chiu, C.; Siderius, D. W.; Li, L.; Cockayne, E.; Espinal, A. E.; Suib, S. L., Time Dependent  $\text{CO}_2$  Sorption Hysteresis by Octahedral Molecular Sieves with Manganese Oxide Framework, *J. Am. Chem. Soc.*, 2012, **134**, 7944-7951.
13. Genuino, H.; Dharmarathna, S.; Njagi, E.; Mei, M.; Suib, S., Gas-Phase Total Oxidation of Benzene, Toluene, Ethylbenzene, and Xylenes Using Shape-Selective Manganese Oxide and Copper Manganese Oxide Catalysts, *J. Phys. Chem. C*, 2012, **116**, 12066-12078.

14. Genuino, H.; Hamal, D.; Fu, Y. J.; Suib, S., Synergetic Effects of Ultraviolet and Microwave Radiation for Enhanced Activity of TiO<sub>2</sub> Nanoparticles in Degrading Organic Dyes Using a Continuous-Flow Reactor, *J. Phys. Chem. C*, 2012, **116**, 14040-14051.
15. Genuino, H.; Huang, H.; Njagi, E.; Stafford, L.; Suib, S. L., A Review of Green Synthesis of Nanophase Inorganic Materials for Chemistry Applications, in Handbook of Green Chemistry, Anastas, P. T., Ed., **Volume 8**, Perosa, A., Selva, M., Eds., Wiley-VCH, 2013, pp. 217-244.
16. Najafpour, M. M.; Sedigh, D. J.; King'onde, C. K.; Suib, S. L., Nano-Sized Manganese Oxide–Bovine Serum Albumin as a Promising and Biomimetic Catalyst for Water Oxidation, *RSC Adv.*, 2012, **2**, 11253-11257.
17. Poyraz, A. S.; Biswas, S.; Genuino, H. C.; Dharmarathna, S.; Kuo, C. H.; Suib, S. L., Bimodification of Mesoporous Silicon Oxide by Coupled “*In Situ* Oxidation at the Interface and Ion Exchange” and its Catalytic Activity in the Gas-Phase Toluene Oxidation, *ChemCatChem*, 2013, **5**, 920-930.
18. Hu, B.; Frueh, S.; Garces, H. F.; Zhang, L.; Aindow, M.; Brooks, C.; Kreidler, E.; Suib, S. L., Selective Hydrogenation of CO<sub>2</sub> and CO to Useful Light Olefins over Octahedral Molecular Sieve Manganese Oxide Supported Iron Catalysts, *Appl. Catal. B*, 2012, **132-133**, 54-61.
19. Hu, B.; Suib, S. L., Synthesis of Useful Compounds from CO<sub>2</sub>, in *Green CO<sub>2</sub>: Advances in CO<sub>2</sub> Utilization*, G. Centi, S. Perathoner, Eds., John Wiley and Sons, Inc., NY, Chapter 3, 2014, 51-97.
20. Najafpour, M. M.; Leonard, K. C.; Fan, F. F.; Tabrizi, M. A.; Bard, A. J.; King'onde, C.; Suib, S. L.; Haghighi, B.; Allakhverdiev, S. I.; Nano-Size Layered Manganese–Calcium Oxide as an Efficient and Biomimetic Catalyst for Water Oxidation Under Acidic Conditions Comparable to Platinum, *Dalton Trans.*, 2013, **42**, 5085-5091.
21. Genuino, H.; Meng, Y.; Horvath, D. T.; Kuo, C. H.; Seraji, M. S.; Morey, A. M.; Joesten, R.; Suib, S. L., Enhancement of Catalytic Activities of Octahedral Molecular Sieve Manganese Oxide for Total and Preferential CO Oxidation via Vanadium Ion Framework Substitution, *ChemCatChem*, 2013, **5**, 2306-2317.
22. Hu, B.; Guild, C.; Suib, S. L., Thermal, Electrochemical, and Photochemical Conversion of CO<sub>2</sub> to Fuels and Value-added Products, *J. of CO<sub>2</sub> Util.*, 2013, **1**, 18-27.
23. Meng, Y.; Genuino, H.; Kuo, C. H.; Huang, H.; Chen, S. Y.; Zhang, L.; Rossi, A.; Suib, S., One Step Hydrothermal Synthesis of Manganese Containing MFI-Type Zeolite Mn-ZSM-5, Characterization, and Catalytic Oxidation of Hydrocarbons, *J. Am. Chem. Soc.*, 2013, **135**, 8594-8605.
24. Noshadi, I.; Du, S.; Kanjilal, B.; Bollas, G. M.; Suib, S.; Provatas, A.; Liu, F.; Parnas, R. S., Biofuels from Brown Grease Using a New Catalyst and a New Process, *Appl. Energy*, 2-14, **129**, 112–122.
25. Espinal, A. E.; Yan, Y.; Zhang, L.; Espinal, L.; Morey, A.; Wells, B. O.; Aindow, M.; Suib, S. L., Substrate Control of Anisotropic Resistivity in Heteroepitaxial Nanostructured Arrays of Cryptomelane Manganese Oxide on Strontium Titanate, *Small*, 2013, **10**, 66-72.
26. Ozacar, M.T.; Poyraz, A. S.; Genuino, H. C.; Kuo, C. H.; Meng, Y.; Suib, S. L., Influence of Silver on the Catalytic Properties of the Cryptomelane and Ag-Hollandite Types of Manganese Oxides OMS-2 in the Low-Temperature CO Oxidation, *Appl. Catal., A: General*, 2013, **462-463**, 64-74.
27. Zhang, Y.; Liu, Y.; Huang, H.; Su, L.; Huo, D.; Suib, S. L.; Hou, C.; Lei, Y., Three - Dimensional CuO Nanoflowers for Electrochemical Detection of Glucose and Other Carbohydrates in Neutral Medium, *Chem. Sens.*, 2013, **3**, 19/1-19/6.
28. Hire, C. C.; Genuino, H. C.; Suib, S. L.; Adamson, D. H., Titania Condensation by a Bio-Inspired Synthetic Block Copolymer, *Chem. Mat.*, 2013, **25**, 2056-2063.
29. Iyer, A.; Garofano, J. K. M.; Reutenaur, J.; Suib, S. L.; Aindow, M.; Gell, M.; Jordan, E. H., A Sucrose-Mediated Sol-Gel Technique for the Synthesis of MgO-Y<sub>2</sub>O<sub>3</sub> Nanocomposites, *J. Am. Cer. Soc.*, 2013, **96**, 346-350.
30. Kramer, E. R.; Morey, A. M.; Staruch, M.; Suib, S. L.; Jain, M.; Budnick, J. I.; Wei, M., Synthesis and Characterization of Iron-Substituted Hydroxyapatite via a Simple Ion-Exchange procedure, *J. Mat. Sci.*, 2013, **48**, 665-673.
31. Sharma, H.; Suib, S. L.; Mhadeshwar, A., Interactions of Sulfur Oxides with Diesel Oxidation Catalysts (DOCs), in ACS Symposium Series, Novel Materials for Catalysis and Fuels Processing, 2013, **1132**, 117-155.
32. Suib, S. L., Some Grand Challenges in Environmental Chemistry, Specialty Grand Challenge Article, *Frontiers in Green and Environmental Chemistry*, 2013, **1**, 1-2.
33. Dharmarathna, S., Suib, S.L., Manganese Octahedral Molecular Sieve (OMS-2) Catalysts for Selective Aerobic Oxidation of Thiols to Disulfides, *Appl. Catal. B: Env.*, 2014, **147**, 124-131.

34. Kuo, C. H.; Poyraz, A. S.; Jin, L.; Meng, Y.; Pahalagedara, L.; Chen, S. Y.; Kriz, D. A.; Guild, C.; Guduz, A.; Suib, S. L., Heterogeneous Acidic TiO<sub>2</sub> Nanoparticles for Efficient Conversion of Biomass Derived Carbohydrates, *Green Chem.*, 2013, **16**, 785 - 791.
35. Owalude, S. O.; Odebunmi, E. O.; Eke, U. B.; Tella, A. C.; Rheingold, A. L.; Suib, S. L., The Synthesis and Structure of Hexakis(dimethylphenylphosphonite)ruthenium(II) bis[tetraphenylborate(-1)], *Zeit. Allg. Chem.*, 2014, **640**, 275-377.
36. Garces, H.; Roller, J.; King'onde, C.; Dharmarathna, S.; Ristau, R.; Jain, R.; Suib, S. L.; Maric, R., Formation of Platinum (Pt) Nanocluster Coatings on K-OMS-2 Manganese Oxide Membranes by Reactive Spray Deposition Technique (RSDT) for Extended Stability during CO Oxidation, *Adv. Chem. Eng.Sci.*, 2014, **4**, 23-35.
37. Huang, H.; Meng, Y.; Labonte, A.; Doble, A.; Suib, S. L., Large Scale Synthesis of Silver Manganese Oxide Nanofibers and Their Oxygen Reduction Properties, *J. Phys. Chem. C*, 2013, **117**, 25352-25359.
38. Poyraz, A.; Kuo, C. H., Biswas, S.; King'onde, C. K.; Suib, S. L., A General Approach to Crystalline and Monomodal Pore Size Mesoporous Materials, *Nature Comm.*, 2013, **4**, 3952, 1-10.
39. Sun, X.; Liu, Y.; Mopidevi, S.; Meng, Y.; Huang, F.; Parisi, J.; Nieh, M. P.; Cornelius, C.; Suib, S. L.; Lei, Y.; Super-hydrophobic "smart" sand for buried explosive detection, *Sensors & Actuators: B. Chemical*, 2014, **195**, 52-57.
40. Kuo, C. H.; Mosa, I. M.; Thanneeru, S.; Sharma, V.; Zhang, L.; Biswas, S.; Aindow, M.; Alpay, S. P.; Rusling, J. F.; Suib, S. L.; He, J. Facet-dependent Catalytic Activity of MnO Electrocatalysts for Oxygen Reduction and Oxygen Evolution Reactions, *Chem. Comm.*, 2015, **51**, 5951-5954.
41. Garces, L. J.; Hincapie, B.; Zenger, R.; Suib, S. L., The Effect of Temperature and Support on the Reduction of Cobalt Oxide: An *In Situ* X-ray Diffraction Study, *J. Phys. Chem. C*, 2015, **119**, 5484-5490.
42. Kona, J. R.; Kingonde, C. K.; Howell, A. R.; Suib, S. L., OMS-2 for Aerobic, Catalytic, One-pot Alcohol Oxidation-Wittig Reactions: Efficient Access to Unsaturated Esters, *Chem. Cat. Chem.*, 2014, **6**, 749-752.
43. Poyraz, A. S.; Hines, W. A.; Kuo, C. H.; Li, N.; Perry, D. M.; Suib, S. L., Mesoporous Co<sub>3</sub>O<sub>4</sub> Nanostructured Material Synthesized by One-Step Soft Templating: A Magnetic Study, *J. Appl. Phys.*, 2014, **115**, 114309/1-114309/10.
44. Zou, Jianping; Ma, J.; Huang, Q.; Luo, S. L.; Yu, J.; Luo, X. B.; Dai, W. L.; Sun, J.; Guo, G. C.; Au, C. T.; Suib, S. L., Graphene oxide as structure-directing and morphology-controlling agent for the syntheses of heterostructured graphene-Bi<sub>2</sub>MoO<sub>6</sub>/Bi<sub>3.64</sub>Mo<sub>0.36</sub>O<sub>6.55</sub> composites, *Appl. Catal. B*, 2014, **156-7**, 447-455.
45. Garces, L.; Hincapie, B.; Shen, X.; Makwana, V. D.; Corbin, D. R.; Sacco, A.; Suib, S. L., Influence of Tetrahydrofuran (THF) in the Synthesis of Zeolite ZK-5, *Micropor. Mesopor. Mat.*, 2014, **198**, 9-14.
46. Poyraz, A.; Kuo, C. H.; Kim, E.; Meng, Y.; Seraji, M.; Suib, S. L., Tungsten Promoted Mesoporous Group 4 (Ti, Zr, & Hf) Transition Metal Oxides for Room Temperature, Solvent Free Acetalization and Ketalization Reactions, *Chem. Mat.*, 2014, **26**, 2803-2813.
47. Guild, C.; Biswas, S.; Meng, Y.; Jafari, T.; Gaffney, A. M.; Suib, S. L., Perspectives of spray pyrolysis for facile synthesis of catalysts and thin films: An introduction and summary of recent directions, *Cat. Today*, 2014, **238**, 87-94.
48. Suib, S. L., Frontiers in chemistry grand challenge: open communication to the world, *Frontier in Chemistry*, 2014, **2**, 42, doi:10.3389/fchem.2014.00042.
49. Pahalagedara, M.; Pahalagedara, L.; Kuo, C. H. ; Dharmarathna, S.; Suib, S. L., Ordered mesoporous mixed metal oxides: Remarkable effect of pore size on the catalytic activity, *Langmuir*, 2014, **30**, 8228-8237.
50. Kuo, C. H.; Li, W.; ; Song, W.; Luo, Z.; Poyraz, A.; Guo, Y.; Ma, A.; Suib, S. L.; He, J., Facile synthesis of Co<sub>3</sub>O<sub>4</sub>@CNT with high catalytic activity for CO oxidation under moisture-rich conditions, *ACS Appl. Mat. & Interf.*, 2014, **6**, 11311-11317.
51. Poyraz, A.; Song, W.; Kriz, D.; Kuo, C. H.; Seraji, M.; Suib, S. L., Crystalline Mesoporous K<sub>2-x</sub>Mn<sub>8</sub>O<sub>16</sub> and ε-MnO<sub>2</sub> by Mild Transformations of Amorphous Mesoporous Manganese Oxides and Their Enhanced Redox Properties, *ACS Appl. Mat. & Interf.*, 2014, **6**, 10986-10991.
52. Pahalagedara, M.; Samaraweera, M.; Dharmarathna, S.; Kuo, C. H.; Pahalagedara, L.; Gascón, J.; Suib, S. L., Removal of Azo Dyes: Intercalation into Sonochemically Synthesized NiAl Layered Double Hydroxide, *J. Phys. Chem. C*, 2014, **118**, 17801-17809.

53. Meng, Y.; Song, W.; Huang, H.; Ren, Z.; Chen, S. Y.; Suib, S. L., Structure-Property Relationship of Bifunctional MnO<sub>2</sub> Nanostructures: Highly Efficient, Ultra-Stable Electrochemical Water Oxidation and Oxygen Reduction Reaction Catalysts Identified in Alkaline Media, *J. Am. Chem. Soc.*, 2014, **136**, 11452-11464.
54. Pahalagedara, L.; Dharmarathna, S.; King'onde, C.; Pahalagedara, M.; Meng, Y.; Kuo, C. H.; Suib, S. L., Microwave Assisted Hydrothermal Synthesis of  $\alpha$ -MnO<sub>2</sub>: Lattice Expansion via Rapid Temperature Ramping and Framework Substitution, *J. Phys. Chem.*, 2014, **118**, 20363-20373.
55. Genuino, H.; Seraji, M. S.; Meng, Y.; Valencia, D.; Suib, S. L., Combined Experimental and Computational Study of CO Oxidation Promoted by Nb in Manganese Oxide Octahedral Molecular Sieves, *Appl. Catal. B: Environmental*, 2015, **163**, 361-369.
56. Song, W. O.; Poyraz, A. S.; Meng, Y.; Ren, Z.; Chen, S. Y.; Suib, S. L., Mesoporous Co<sub>3</sub>O<sub>4</sub> with Controlled porosity: Inverse Micelle Synthesis and High Performance Catalytic CO Oxidation at -60°C, *Chem. Mat.*, 2014, **26**, 4629-4639.
57. El-Sawy, A.; King'onde, C.; Kuo, C. H.; Kriz, D.; Guild, C.; Meng, Y.; Frueh, S.; Dharmarathna, S.; Ehrlich, S.; Suib, S. L., An X-ray Absorption Spectroscopic Study of a Highly Thermally Stable Manganese Oxide Octahedral Molecular Sieve (OMS-2) with High Oxygen Reduction Reaction Activity, *Chem. Mat.*, 2014, **26**, 5752-5760.
58. Pahalagedara, L.; Poyraz, A.; Song, W.; Kuo, C. H.; Pahalagedara, M.; Meng, Y.; Suib, S. L., Low temperature Desulfurization of H<sub>2</sub>S: High sorption capacities by mesoporous cobalt oxide via increased H<sub>2</sub>S diffusion, *Chem. Mat.*, 2014, **26**, 6613-6621.
59. Dharmarathna, S.; Suib, S. L., Porous cryptomelane-type manganese oxide octahedral molecular sieves (OMS-2); synthesis, characterization and applications in catalysis, *RSC Catalysis Series*, 2014, **17**, (Metal Nanoparticles for Catalysis), 235-250.
60. Biswas, S.; Poyraz, A. S.; Meng, Y.; Kuo, C. H.; Guild, C.; Tripp, H.; Suib, S. L., Ion induced promotion of activity enhancement of mesoporous manganese oxides for aerobic oxidation reactions, *Appl. Catal., B: Env.*, 2015, **165**, 731-741.
61. Kuo, C. H.; Mosa, I.; Poyraz, A. S.; Biswas, S.; El-Sawy, A.; Song, W.; Luo, Z.; Chen, S. Y.; Rusling, J.; He, J.; Suib, S. L., Robust Mesoporous Manganese Oxide Catalysts for Water Oxidation, *ACS Catalysis*, 2015, **5**, 1693-1699.
62. Kuo, C. H.; Li, W.; Pahalagedara, L.; El-Sawy, A. M.; Kriz, D.; Genz, N.; Guild, C.; Ressler, T.; Suib, S. L.; He, J., Understanding the Role of Gold Nanoparticles in Enhancing the Catalytic Activity of Manganese Oxides in Water Oxidation Reactions, *Ang. Chem. Int. Ed.*, 2015, **54**, 2345 –2350.
63. Wasalathanthri, N.; Poyraz, A. S.; Biswas, S.; Meng, Y.; Kuo, C. H.; Kriz, D.; Suib, S. L., High-Performance Catalytic CH<sub>4</sub> Oxidation at Low Temperatures: Inverse Micelle Synthesis of Amorphous Mesoporous Manganese Oxides and Mild Transformation to K<sub>2-x</sub>Mn<sub>8</sub>O<sub>16</sub> and  $\epsilon$ -MnO<sub>2</sub>, *J. Phys. Chem. C*, (2015), **119**, 1473-1482.
64. Luo, Z.; Poyraz, A. S.; Kuo, C. H.; Miao, R.; Meng, Y.; Chen, S. Y.; Jiang, T.; Wenos, C.; Suib, S. L.; Crystalline Mixed Phase (Anatase/Rutile) Mesoporous Titanium Dioxides for Visible Light Photocatalytic Activity, *Chem. Mat.*, 2015, **27**, 6-17.

## C=O Bond Cleavage Reactions Facilitated by Early/Late Heterobimetallic Complexes

Christine M. Thomas\*, Bing Wu, Seth L. Marquard, Jeremy P. Krogman, Mark W. Bezpalko,  
Bruce M. Foxman  
Brandeis University, Department of Chemistry

### Presentation Abstract

Our group has been using bridging phosphinoamide ligands to investigate early/late heterobimetallic complexes. The metal-metal interactions in these compounds provide a unique method for tuning redox potentials and promoting  $\sigma$  and  $\pi$  bond activation processes across polar metal-metal bonds. In our most well-studied example to date, the reduced  $Zr^{IV}/Co^{-I}$  complex (THF)Zr(MesNP<sup>i</sup>Pr<sub>2</sub>)<sub>3</sub>CoN<sub>2</sub> (Mes = 2,4,6-trimethylphenyl) is accessible at relatively mild potentials (-1.9 V vs ferrocene) and has been shown to undergo one-, two-, and four-electron transfer processes, activating a wide variety of  $\sigma$  bonds (e.g. O-H, N-H, C-X) and  $\pi$  bonds (e.g. the C=O bond in CO<sub>2</sub> and ketones). Recently, we have been exploring the analogy between the activation of the C=O bond in CO<sub>2</sub>, which proceeds rapidly even at low temperature, and the cleavage of the C=O bond in diaryl ketones, which proceeds much more slowly through a series of observable intermediates. Using this analogous reactivity, we are able to suggest a mechanism for CO<sub>2</sub> activation in alignment of the substrate C=O bond with the polar metal-metal bond is crucial to the C=O oxidative addition step. We have, thus, extended our family of heterobimetallic complexes to bis(phosphino)amide-linked bimetallic frameworks that are more open, leaving the metal-metal bond more accessible to substrates. Bis(phosphinoamide) Ti/Co complexes of this type have been studied, revealing that strong metal-metal interactions can form in the absence of three supporting ligands. These Ti/Co complexes, and their reactivity towards C=O bonds will be presented.

### DE-SC0004019: Early-Late Heterobimetallic Complexes Linked by Phosphinoamide Ligands: Tuning Redox Potentials and Small Molecule Activation

**PI:** Christine M. Thomas

**Postdoc(s):** Subramaniam Kuppuswamy, Seth L. Marquard, Claudia M. Fafard

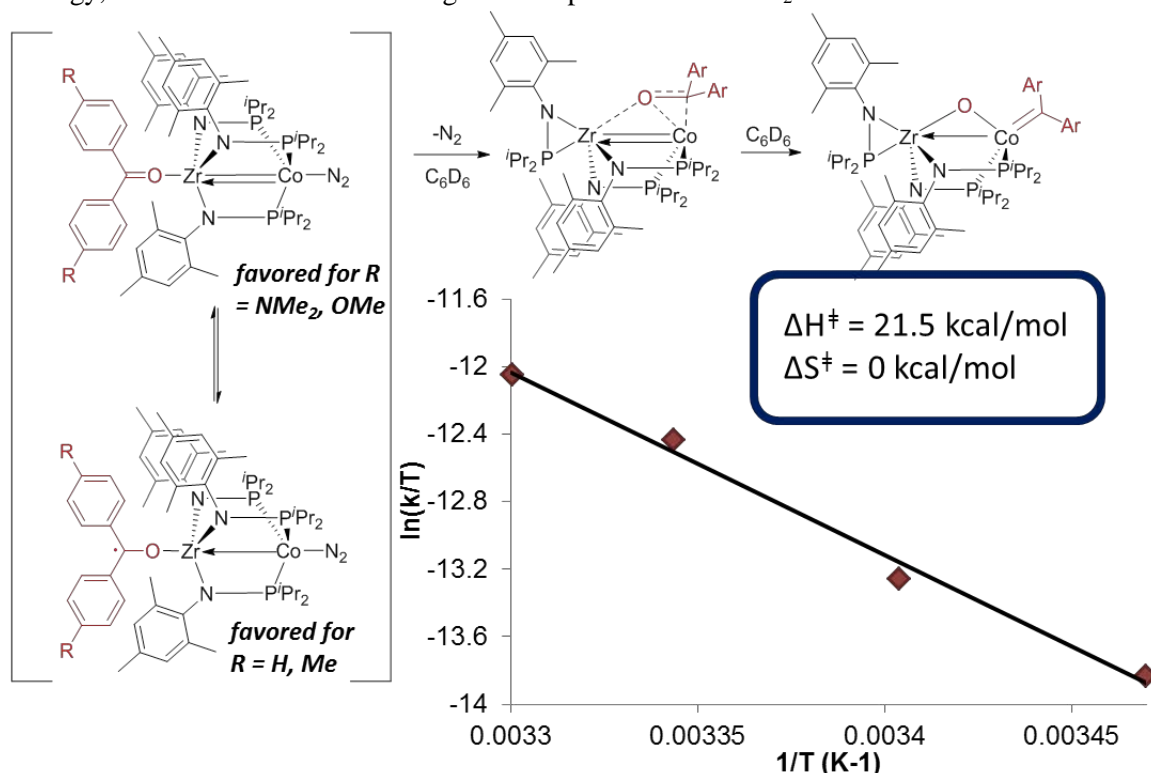
**Student(s):** Jeremy P. Krogman, J. Wesley Napoline, Bing Wu, Wen Zhou, Ramyaa Mathialagan, Bennett P. Greenwood, Kathryn Gramigna

### RECENT PROGRESS

#### *Mechanistic Insight into the Facile Cleavage of C=O Bonds in CO<sub>2</sub> and Ketones by Zr/Co Tris(phosphinoamide) Complexes*

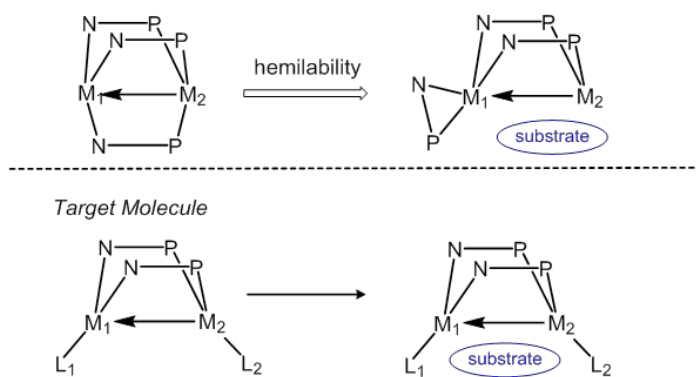
Both CO<sub>2</sub> and diaryl ketones are oxidatively added across the Zr-Co bond in (THF)Zr(MesNP<sup>i</sup>Pr<sub>2</sub>)<sub>3</sub>CoN<sub>2</sub> to afford products of the general form (MesNP<sup>i</sup>Pr<sub>2</sub>)<sub>2</sub>Zr(MesNP<sup>i</sup>Pr<sub>2</sub>)<sub>2</sub>( $\mu$ -O)CoL (L = CO, CAR<sub>2</sub>), such as the complex shown in the Scheme below (right). In the case of diaryl ketones, a series of isolable and/or observable intermediates are observed along the way, allowing detailed mechanistic study of the C=O bond cleavage process. When O=CAR<sub>2</sub> is added to (THF)Zr(MesNP<sup>i</sup>Pr<sub>2</sub>)<sub>3</sub>CoN<sub>2</sub>, the initial product formed is either a  $Zr^{IV}Co^{-I}$  ketone adduct (favored for

electron-rich ketones) or a  $\text{Zr}^{\text{IV}}\text{Co}^0$  ketyl radical complex in which a single electron has been transferred to the bound ketone (favored for electron-poor ketones). Regardless the initial product, removal of  $\text{N}_2$  from the reaction mixture in vacuo affords a diamagnetic species, assigned as the side-bound ketone adduct, which gradually converts at room temperature to the  $(\text{MesNP}^i\text{Pr}_2)_2\text{Zr}(\text{MesNP}^i\text{Pr}_2)_2(\mu\text{-O})\text{Co}=\text{C}(\text{Ar})_2$  complex via  $\text{C}=\text{O}$  bond cleavage, as shown below. Monitoring the latter part of this transformation at various temperatures reveals the Eyring plot and thermodynamic activation parameters shown below. By analogy, a similar mechanism is thought to be operative in the  $\text{CO}_2$  activation reaction.

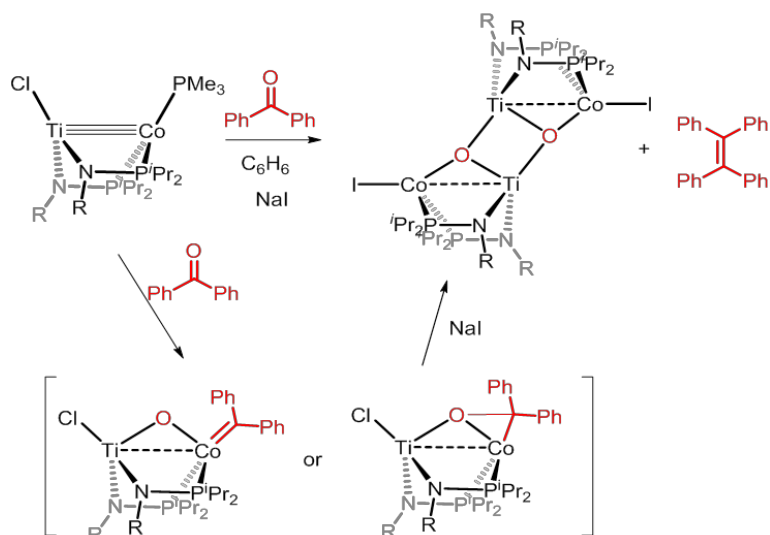


### New Ti/Co Bis(Phosphinoamide) Complexes

The activation of polar bonds by heterobimetallic complexes appears to require access of substrates to both metal centers. In the tris(phosphinoamide) system, this is accomplished via ligand hemilability; however, we posited that a more direct strategy might be to simply use a more accessible bis(phosphinoamide) framework (see Scheme on the right). Bis(phosphinoamide) complexes proved difficult to access using Zr in the early metal site, so we took this opportunity to investigate Ti-based heterobimetallic complexes.



A series of bis(phosphinoamide) Ti/Co complexes was synthesized through sequential metalation steps, followed by sequential one-electron reduction reactions. The reduced  $\text{ClTi}(\text{XylNP}^i\text{Pr}_2)_2\text{Co}(\text{PMe}_3)$  complex was shown to have a very short Ti-Co distance of 2.02 Å as a result of a formal triple bond between Ti and Co, demonstrating that the presence of three linking ligands is not a necessary requisite to multiple bonding between the early and late metals



in compounds of this type. Investigation of the reactivity of  $\text{ClTi}(\text{XylNP}^i\text{Pr}_2)_2\text{Co}(\text{PMe}_3)$  revealed a rapid reaction with aryl ketones, similar to the Zr/Co analogues discussed above. However, in this case, C=O bond cleavage is accompanied by C=C bond formation in a McMurry-type coupling reaction. This reaction is thought to proceed via either a carbene or an activated side-bound ketone adduct, with both metals playing a pivotal role in C=O bond cleavage (see Scheme on the left).

### Publications Acknowledging this Grant in 2012-2015

1. Wu, B.; Bezpalko, M. W.; Foxman, B. M.; Thomas, C. M. A Heterobimetallic Complex Featuring a Ti-Co Multiple Bond and Its Application to the Reductive Coupling of Ketones to Alkenes. *Chem. Sci.* **2015**, *6*, 2044-2049.
2. Lee, K. H.; Napoline, J. W.; Bezpalko, M. W.; Foxman, B. M.; Thomas, C. M. Probing Substituent Effects in Phosphinoamine Ligands Using  $\text{Mo}(\text{CO})_5\text{L}$  Complexes. *Polyhedron* **2015**, *87*, 354-360.
3. Wu, B.; Hernandez Sanchez, R.; Bezpalko, M. W.; Foxman, B. M.; Thomas, C. M. Formation of Heterobimetallic Zirconium/Cobalt Diimido Complexes via a Four-Electron Transformation. *Inorg. Chem.* **2014**, *53*, 10021-10023.
4. Kuppuswamy, S.; Cass, T. R.; Bezpalko, M. W.; Foxman, B. M.; Thomas, C. M. Synthesis and Investigation of the Metal-Metal Interactions in Heterobimetallic Cr/Rh and Cr/Ir Complexes. *Inorg. Chim. Acta* **2015**, *424*, 167-172.
5. Krogman, J. P.; Gallagher, J. R.; Zhang, G.; Hock, A. S.; Miller, J. T.; Thomas, C. M. Assignment of the Oxidation States of Zr and Co in a Highly Reactive Heterobimetallic Zr/Co Complex Using X-ray Absorption Spectroscopy (XANES). *Dalton Trans.* **2014**, *43*, 13852-13857.
6. Kuppuswamy, S.; Powers, T. M.; Johnson, B. M.; Brozek, C. K.; Krogman, J. P.; Bezpalko, M. W.; Berben, L. A.; Keith, J. M.; Foxman, B. M.; Thomas, C. M. One-electron Oxidation Chemistry and Subsequent Reactivity of Diiron Imido Complexes. *Inorg. Chem.* **2014**, *53*, 5429-5437.
7. Marquard, S. L.; Bezpalko, M. W.; Foxman, B. M.; Thomas, C. M. Interaction and Activation of Carbon-Heteroatom  $\pi$  Bonds with a Zr/Co Heterobimetallic Complex. *Organometallics* **2014**, *33*, 2071-2079.
8. Kuppuswamy, S.; Bezpalko, M. W.; Powers, T. M.; Wilding, M. J. T.; Brozek, C. K.; Foxman, B. M.; Thomas, C. M. A Series of  $C_3$ -Symmetric Heterobimetallic Cr/M (M = Fe, Co, and Cu) Complexes. *Chem. Sci.* **2014**, *5*, 1617-1626.

9. Zhou, W.; Saper, N. I.; Krogman, J. P.; Foxman, B. M.; Thomas, C. M. Effect of Ligand Modification on the Reactivity of Phosphinoamide-Bridged Heterobimetallic Zr/Co Complexes. *Dalton Trans.* **2014**, *43*, 1984-1989.
10. Napoline, J. W.; Kraft, S. J.; Matson, E. M.; Fanwick, P. E.; Bart, S. C.; Thomas, C. M. Tris(phosphinoamide)-supported Uranium-Cobalt Heterobimetallic Complexes Featuring Co→U Dative Interactions. *Inorg. Chem.* **2013**, *52*, 12170-12177.
11. Kuppuswamy, S.; Powers, T. M.; Krogman, J. P.; Bezpalko, M. W.; Foxman, B. M.; Thomas, C. M. Vanadium-Iron Complexes Featuring Metal-Metal Multiple Bonds. *Chem. Sci.* **2013**, *4*, 3557-3565.
12. Marquard, S. L.; Bezpalko, M. W.; Foxman, B. M.; Thomas, C. M. Stoichiometric C=O Bond Oxidative Addition of Benzophenone by a Discrete Radical Intermediate to Form a Cobalt(I) Carbene. *J. Am. Chem. Soc.* **2013**, *135*, 6018-6021.
13. Napoline, J. W.; Krogman, J. P.; Shi, R.; Kuppuswamy, S.; Bezpalko, M. W.; Foxman, B. M.; Thomas, C. M. Activation of E-H and E-E (E = S, O) Bonds by Heterobimetallic Zr/Co Complexes: Evidence for both One- and Two-Electron Processes. *Eur. J. Inorg. Chem.* **2013**, *2013*, 3874-3882.
14. Krogman, J. P.; Bezpalko, M. W.; Foxman, B. M.; Thomas, C. M. Synthesis, Structure, and Reactivity of an Anionic Zr-Oxo Relevant to CO<sub>2</sub> Reduction by a Zr/Co Heterobimetallic Complex. *Inorg. Chem.* **2013**, *52*, 3022-3031.
15. Zhou, W.; Marquard, S. L.; Bezpalko, M. W.; Foxman, B. M.; Thomas, C. M. Catalytic Hydrosilylation of Ketones Using a Co/Zr Heterobimetallic Complex: Evidence for an Unusual Mechanism Involving Ketyl Radicals. *Organometallics* **2013**, *32*, 1766-1772.
16. Mathialagan, R.; Kuppuswamy, S.; De Denko, A. T.; Bezpalko, M. W.; Foxman, B. M.; Thomas, C. M. Metal-Metal Bonding in Low Coordinate Dicobalt Complexes Supported by Phosphinoamide Ligands. *Inorg. Chem.* **2013**, *52*, 701-706.
17. Kuppuswamy, S.; Powers, T. M.; Johnson, B. M.; Bezpalko, M. W.; Brozek, C. K.; Foxman, B. M.; Berben, L. A.; Thomas, C. M. Metal-Metal Interactions in C<sub>3</sub>-Symmetric Diiron Imido Complexes Linked by Phosphinoamide Ligands. *Inorg. Chem.* **2013**, *52*, 4802-4811.
18. Napoline, J. W.; Bezpalko, M. W.; Foxman, B. M.; Thomas, C. M. N-H Activation of Hydrazines by a heterobimetallic Zr-Co Complex: Promotion of One-Electron Chemistry at Zr. *Chem. Commun.* **2013**, *49*, 4388-4390.
19. Kuppuswamy, S.; Bezpalko, M. W.; Powers, T. M.; Turnbull, M. M.; Foxman, B. M.; Thomas, C. M. Utilization of Phosphinoamide Ligands in Homobimetallic Fe and Mn Complexes: The Effect of Disparate Coordination Environments on Metal-Metal Interactions and Magnetic and Redox Properties. *Inorg. Chem.* **2012**, *51*, 8225-8240.
20. Evers, D. A.; Bluestein, A. H.; Foxman, B. M.; Thomas, C. M. Synthesis and investigations of Metal-Metal Interactions in Early/Late Heterobimetallic Complexes Linking Group 5 Imido Fragments to Co(I). *Dalton Trans.* **2012**, *41*, 8111-8115.
21. Kuppuswamy, S.; Cooper, B. G.; Bezpalko, M. W.; Foxman, B. M.; Powers, T. M.; Thomas, C. M. Synthesis and Structural Characterization of High Spin M/Cu (M = Mn, Fe) Heterobimetallic and Fe/Cu<sub>2</sub> Trimetallic Phosphinoamides. *Inorg. Chem.* **2012**, *51*, 1866-1873.

## Catalytic Formal [2+2+1] Synthesis of Pyrroles from Alkynes and Diazenes via Ti<sup>II</sup>/Ti<sup>IV</sup> Redox Catalysis

Zachary W. Gilbert, Ryan J. Hue and Ian A. Tonks\*

Pyrroles are structurally important heterocycles in materials science and pharmaceuticals; however, the synthesis of polysubstituted pyrroles is often challenging. Herein we report a multicomponent, Ti-catalyzed formal [2+2+1] reaction of alkynes and diazenes for the oxidative synthesis of penta- and trisubstituted pyrroles: a nitrenoid analogue to classical Pauson-Khand-type syntheses of cyclopentenones. Given the scarcity of early transition metal redox catalysis, preliminary mechanistic studies are presented. Initial stoichiometric and kinetic studies indicate that the mechanism of this reaction proceeds through a formally Ti<sup>II</sup>/Ti<sup>IV</sup> redox catalytic cycle, wherein an azatitanacyclobutene intermediate, resulting from [2+2] alkyne + Ti imido coupling, undergoes a second alkyne insertion followed by reductive elimination to yield pyrrole and a Ti<sup>II</sup> species. The key component for catalytic turnover is the reoxidation of the Ti<sup>II</sup> species to a Ti<sup>IV</sup> imido *via* the disproportionation of an  $\eta^2$ -diazene-Ti<sup>II</sup> complex.

**David A. Vivic**

**Accessing Nickel(II), (III), and (IV) Complexes Bearing a Readily Attached [C<sub>4</sub>F<sub>8</sub>] Ligand**

Siqi Yu, Yulia Dudkina, and David A. Vivic\*

Department of Chemistry, Lehigh University, 6 E. Packer Ave., Bethlehem, PA 18015 USA

**Presentation Abstract**

Nickel-catalyzed chemical bond forming reactions have remarkable potential. There is an emerging importance of understanding the Ni(III) and the Ni(IV) redox states in synthetic chemistry, and the research outlined in this project seeks to understand at the molecular level the details of transformations that would help replace the use of precious metals like palladium in catalysis with nickel. Mechanistic proposals for nickel-catalyzed coupling reactions often invoke five-coordinate alkyl- or aryl-bound Ni(II) and/or high valent nickel(III) species, but due to their reactive nature, they have been difficult to study and fingerprint. Here, we invoke the stabilizing properties of fluoroalkyl ligands to access such nickel species bearing ligands that are commonplace in organic coupling reactions. We show that the [C<sub>4</sub>F<sub>8</sub>] ligand is suitable for supporting well-defined terpyridyl nickel complexes in the +2 and +3 oxidation states. Notably, a cyclic voltammetry study of the nickel(III) species indicates that an additional oxidation is accessible, providing a family of related fluoroalkyl nickel complexes spanning the +2 to +4 oxidation states.

**DE-FG02-13ER16369: Development of Catalytic Alkylation and Fluoroalkylation Methods.**

**(Previous project number: DE-FG02-07ER15885)**

**PI: David A. Vivic**

**Postdocs:** Cheng Pan Zhang, Huan Wang, and Bo Chen

**Students:** Peter T. Kaplan, Long Xu, Siqi Yu

**Collaborators:** Axel Klein (Cologne, Germany) and Yulia Budnikova (Kazan, Russia)

## RECENT PROGRESS

**Background and DOE Interest:** Reducing our nation's dependence on precious metals for catalysis is an important goal in chemical research. This topic was discussed heavily at the 2014 Meeting of the Catalysis Science Program of the DOE in Annapolis, where the breakout sessions discussed existing challenges and future trends in the area of catalysis. Among the bullet points for the "Tandem/Parallel Reactions Session" were:

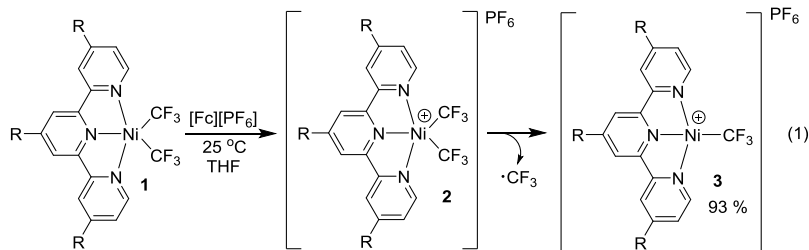
*Characterizations of paramagnetic intermediates and products require advanced physical methods and DFT. Opportunities exist for new mechanisms in catalysis. There are opportunities for utilization of more abundant metals in catalysis.*

*Can we design and isolate analogues to reactive compounds? Once isolated, can we use these compounds to learn more about catalysis? Can we discover new bond-activation processes, especially those with "unnatural" catalytic substrates?*

In order to understand how to use the more naturally abundant first-row metals in catalysis, a more detailed knowledge of the reactivity patterns of *all* accessible oxidation states is required. Nickel and copper are two metals which show great promise in chemical bond forming reactions, and the ability to control redox transformations with these metals will impact many areas of basic science. We have a program aimed at developing the higher oxidation states of these metals for alkylation and fluoroalkylation technologies with a focus of understanding at the molecular level the details of transformations that not only would help lead to the replacement of palladium with nickel and copper in widely-used methods, but would also enable reactions that are unique to the earth abundant metals. The main components of this project are: 1) To obtain a broader fundamental knowledge of chemical bond forming reactions at well-defined organonickel(III) and organonickel(IV) complexes, and 2) to exploit the redox stability of zinc for developing new reagents for nickel- and copper-catalyzed difluoromethylation, difluoromethylenation, and polydifluoromethylenation methodologies. The two components are highly complementary, and we have already demonstrated that advances in the zinc chemistry have enabled unique access to new terpyridyl organonickel(III) and potentially organonickel(IV) complexes that are amenable for systematic reactivity studies.

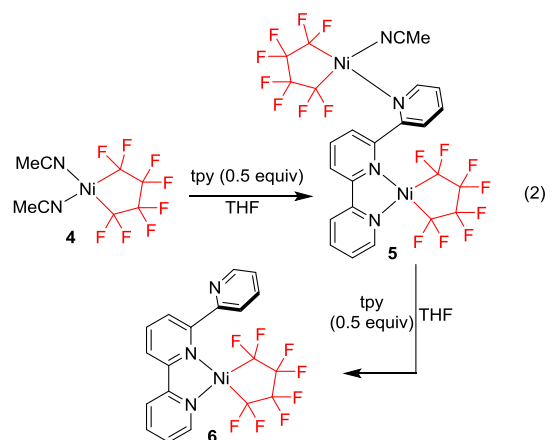
**Goal:** To develop new methods for alkyl and fluoroalkyl bond forming reactions based on a mechanistic understanding of the basic organometallic chemistry involved therein.

**Highlights:** While many examples of well-defined organo-Ni(III) complexes are now known, there has been only one example of an isolable and structurally characterized fluoroalkyl-Ni(III) species.<sup>1</sup> Such high valent fluoroalkyl complexes of nickel are desirable targets for understanding how to coax fluoroalkyl ligands into participating in synthetically useful transformations. Understanding how to access and manipulate the higher oxidation states of first row metals is especially important for fluoroalkylation chemistry, where reductive eliminations are considered to be the

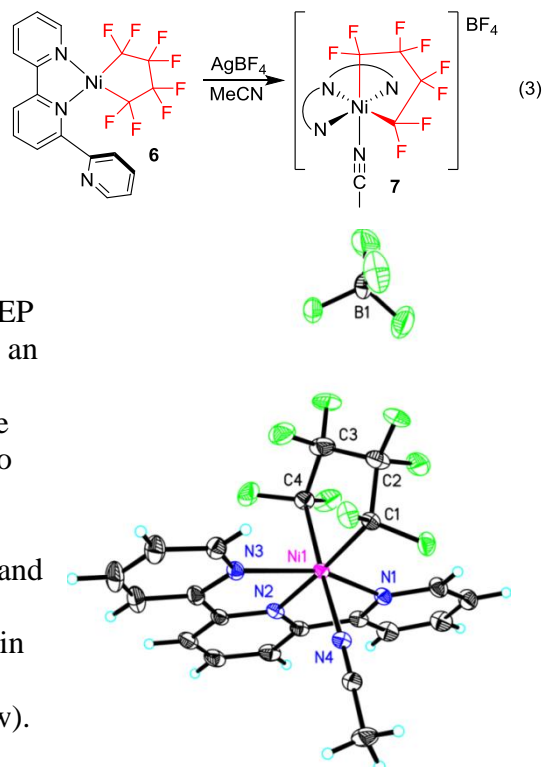


troublesome steps. We have previously shown that trifluoromethyl ligands can support the five-coordinate nickel(II) species **1**, and that **1** can be chemically oxidized with [ferrocenium][PF<sub>6</sub>] to generate the transient nickel(III) species **2** (eq 1). Once formed, however, **2** undergoes a reductive homolysis of a trifluoromethyl ligand to afford the cationic nickel(II) species **3**. Spectroelectrochemical EPR studies supported the intermediacy of **2**, but its short-lived nature precluded any fundamental studies of its reactivity.

In order to increase the stability of a terpyridine nickel(III) perfluoroalkyl complex, we decided to replace the two trifluoromethyl ligands in **2** with a chelating [C<sub>4</sub>F<sub>8</sub>] unit. This modification first involved developing a synthesis for a terpyridine and [C<sub>4</sub>F<sub>8</sub>]-containing nickel(II) precursor. We found that the addition of terpyridine to [(MeCN)<sub>2</sub>Ni(C<sub>4</sub>F<sub>8</sub>)] (**4**) led cleanly to the formation of [(tpy)Ni(C<sub>4</sub>F<sub>8</sub>)] (**6**, eq 2). Surprisingly, in the solid state, the terpyridine ligand in **6** coordinates to nickel in a K<sup>2</sup>-fashion. Solutions of **6** are paramagnetic, however, supporting an equilibrium with the K<sup>3</sup>-binding mode. Interestingly, when 0.5 equiv of terpyridine is added to **4**, the unusual bimetallic species **5** can be isolated reproducibly, thus providing a snapshot of the ligand substitution reaction. Terpyridine is known to bind to more than one metal center, however such nickel adducts are unknown.



With [(tpy)Ni(C<sub>4</sub>F<sub>8</sub>)] in hand, we explored its oxidation chemistry. Gratifyingly, upon addition of Ag[BF<sub>4</sub>], yellow solutions of **6** turn bluish/purple affording the stable Ni(III) species **7** (eq 3). Unlike complex **2** which readily loses a trifluoromethyl radical, we found no evidence that **7** loses a perfluoroalkyl radical, even upon standing for hours in MeCN solution. The stability of **7** facilitated its characterization by X-ray crystallography, and an ORTEP diagram is shown below. The X-ray structure confirms an octahedral nickel center where the terpyridine binds K<sup>3</sup> and an acetonitrile ligand becomes incorporated into the coordination sphere. The nickel-nitrogen bonds *trans* to the fluoroalkyl ligands in **7** (1.966(3) and 1.964(3) Å) were found to be much shorter than the nickel-nitrogen bonds that were *cis* to the fluoroalkyl groups (2.163(3) and 2.172(3) Å), similar to that seen for the only known Ni(III) bis(trifluoromethyl) complex. This may be due in part to the residual spin density accumulated at the *cis* nitrogen atoms in the paramagnetic molecule (see below).



Complex **7** is indeed paramagnetic and its magnetic moment was determined to be 1.77 μ<sub>B</sub>, corresponding to one unpaired electron. Variable

temperature EPR spectra were recorded both in the solid state and solution, and selected spectra are shown in Figure 1. The  $\langle g \rangle = 2.122$  in the solid state is almost coincident with the  $g$ -factors of the complex in acetonitrile solution, indicating that when dissolved, the first coordination sphere remains the same. A pseudo-axial spectrum was recorded in a frozen solution. Simulation of both the solid state and solution spectra reveal contributions from two nitrogen atoms to the super hyperfine splitting patterns. This assignment is supported by density functional theory (DFT) calculations, which reveal that the central nitrogen of the terpyridyl ligand and the nitrogen atom of the acetonitrile ligand bear very little spin density (Figure 2).

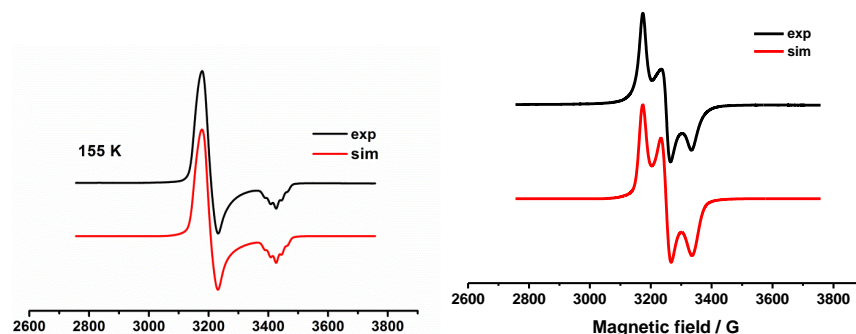


**Figure 1.** Top: Solution EPR spectrum of **7** in MeCN at 155K.  $\langle g \rangle = 2.117$ ,  $g_{\parallel} = 2.017$ ;  $a_N = 19$  G (two N atoms);  $\Delta H = 14$  G,  $g_{\perp} = 2.166$ ;  $a_N = 15$  G (two N atoms);  $\Delta H = 21$  G. Bottom: Solid state EPR spectra of **7**.  $g_1 = 2.175$ ,  $\Delta H_1 = 21$  G,  $g_2 = 2.123$ ,  $\Delta H_2 = 25$  G,  $g_3 = 2.067$ ,  $\Delta H_3 = 35$  G.

The cyclic voltammogram of **7** is shown below. The low redox potential of  $-0.57$  V observed for the Ni(II)/Ni(III) couple in **7** relative to those seen in  $S=0$  square planar fluoroalkyl complexes of nickel is consistent with the preorganization of the terpyridine ligand in a  $K^3$ -binding mode leading to an  $S=1$  nickel(II) species. Interestingly, another redox couple with good reversibility was detected, centered at  $+1.34$  V. We propose that this wave represents the Ni(III)/Ni(IV) redox couple. Sanford and co-workers recently demonstrated the first example of chemical bond forming reactions from well-defined Ni(IV) species, supported by a trifluoromethyl ligand.<sup>2</sup> The Ni(IV) species in that case were prepared by two-electron oxidations of Ni(II) species, thus excluding reactivity comparisons to the intermediate Ni(III) state.

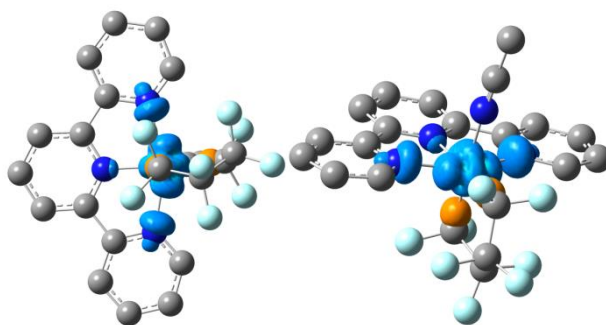
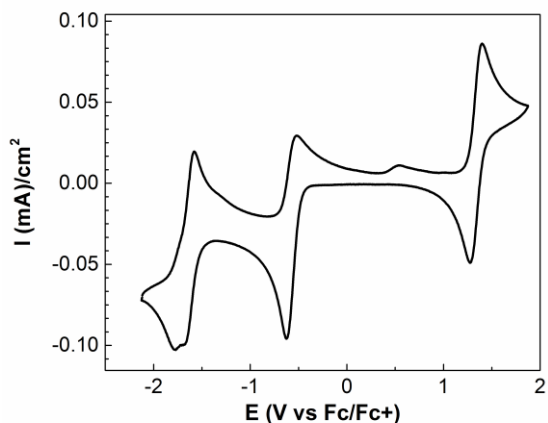


**Figure 2.** Calculated ( $m6-31g^*$ )<sup>[8]</sup> spin density of **7**. Hydrogens are omitted for clarity. Isovalues set at 0.004. The Mulliken spin densities are: Ni (0.905924), N1<sub>TPY</sub> (0.082329), N2<sub>TPY</sub> (0.019285), N3<sub>TPY</sub> (0.079219), and N4<sub>MeCN</sub> (0.012877).

Because of the emerging importance of understanding the Ni(IV) redox state in synthetic chemistry, we are currently pursuing modifications of the terpyridine ligand in hopes of lowering the redox potential of the Ni(III)/Ni(IV) couple to more reasonable potentials. Redox potentials of terpyridine metal complexes are highly dependent on the substitution pattern of the terpyridine ligands.<sup>38,39</sup> For instance, the replacement of a single hydrogen in terpyridine with an NMe<sub>2</sub> substituent in [Ru(tpy-X)<sub>2</sub>][PF<sub>6</sub>] complexes made the oxidation of the NMe<sub>2</sub> complex 0.5 V more negative than the unsubstituted derivative. This bodes well for our ability to tune the electronics so we can explore the preparation of new stable and well-defined terpyridine Ni(IV) complexes. Such studies are currently underway.



**Conclusions:** The [C<sub>4</sub>F<sub>8</sub>] ligand is exceptionally suitable at stabilizing high valent nickel. Unlike [(tpy)Ni(CF<sub>3</sub>)<sub>2</sub>]<sup>+</sup> complexes, which readily lose [CF<sub>3</sub>] radicals, the [(tpy)Ni(C<sub>4</sub>F<sub>8</sub>)]<sup>+</sup> analogue can be isolated in the solid state. Furthermore, electrochemical experiments demonstrate that a Ni(IV) species is accessible, providing a family of related fluoroalkyl nickel complexes spanning the +2 to +4 oxidation states.

#### References:

1. B. Zheng, F. Tang, J. Luo, J. W. Schultz, N. P. Rath and L. M. Mirica, *J. Amer. Chem. Soc.*, 2014, **136**, 6499-6504.
2. N. M. Camasso and M. S. Sanford, *Science*, 2015, **347**, 1218-1220.

### Publications from 2012 - 2015 citing DOE support

- 1) "Nickel-Catalyzed Synthesis of Aryl Trifluoromethyl Sulfides at Room Temperature" Zhang, C. P.; Vicic, D. A. *J. Am. Chem. Soc.* **2012**, *134*, 183-185. (Sole DOE support)
- 2) "Linear Bis-Perfluoroalkyl Complexes of Nickel Bipyridine" Yamaguchi, Y; Ichioka, I.; Klein, A.; Brennessel, W. W.; Vicic, D. A. *Organometallics* **2012**, *31*, 1477-1483. (Sole DOE support)
- 3) "Binuclear Arylnickel Complexes with Bis(arylimino)-1,4-Pyrazine Bridging Ligands" Klein, A.; Biewer, C.; Hamacher, C.; Hurkes, N.; Perez Outeiral, J.; Mora Paniagua, E.; Schmieder, A.-K.; Schuren, A. O.; Burma, P. R.; Ciszewski, J. T.; Vicic, D. A. *Eur J. Inorg. Chem.* **2012**, 2444-2455. (Sole DOE support for US PI; the German collaborator cited his support)
- 4) "Synthesis and Electronic Properties of a Pentafluoroethyl-Derivatized Nickel Pincer Complex" Madhira, V. N.; Ren, P.; Vechorkin, O.; Hu, X., and Vicic, D. A. *Dalton Trans.* **2012**, *41*, 7915-7919. (Sole DOE support for US PI; the Swiss collaborator cited his support)
- 5) "Oxygen-Bound Trifluoromethoxide Complexes of Copper and Gold" Zhang, C. P.; Vicic, D. A. *Organometallics* **2012**, *31*, 7812-7815. (Sole DOE support)
- 6) "Oxidative Trifluoromethylthiolations of Aryl Boronic Acids Using a Copper/O<sub>2</sub> -Based Protocol" Zhang, C. P.; Vicic, D. A. *Chem. Asian J.* **2012**, *7*, 1756-1758. (Sole DOE support)
- 7) "Synthesis and Structure of a Bis-Trifluoromethylthiolate Complex of Nickel" Zhang, C. P.; Vicic, D. A. *J. Fluorine Chem.* **2012**, *140*, 112-115. (Sole DOE support)
- 8) "Oxidative Cleavage of CH<sub>3</sub> and CF<sub>3</sub> Radicals from BOXAM Nickel Complexes" Klein, A.; Vicic, D. A.; Biewer, C.; Kieltsch, I.; Stirnat, K.; Hamacher, C. *Organometallics* **2012**, *31*, 5334-5341. (Sole DOE support for US PI; the German collaborator cited his support)
- 9) "Lithium Bromide-Induced Structural Changes in a Nickel Bis-Alkoxide Complex" Ichioka, H. and Vicic, D. A. *Acta Chim. Slov.* **2013**, *60*, 190-192. (Sole DOE support)
- 10) "A Five-Coordinate Nickel(II) Fluoroalkyl Complex as a Precursor to a Spectroscopically Detectable Ni(III) Species" Zhang, C. P.; Wang, H.; Klein, A.; Biewer, C.; Stirnat, K.; Yamaguchi, Y.; Gomez-Benitez, V.; Vicic, D. A. *J. Am. Chem. Soc.* **2013**, *135*, 8141-8144. (Sole DOE support for US PI; the German collaborator cited his support)
- 11) "Organometallic Aspects of Fluoroalkylation Reactions with Copper and Nickel" Wang, H.; Vicic, D. A. *Synlett* **2013**, *24*, 1887-1898. (joint DOE and NSF support cited)
- 12) "Mild, Safe, and Versatile Reagents for (CF<sub>2</sub>)<sub>n</sub> Transfer and the Construction of Fluoroalkyl-Containing Rings" Kaplan, P. T.; Xu, L.; Chen, B.; McGarry, K. R.; Yu, S.; Wang, H.; Vicic, D. A. *Organometallics* **2013**, *32*, 7552-7558. (Sole DOE support)
- 13) "Improved Synthesis, Structure, and Reactivity of 1,4-Bis(trimethylsilyl)octafluorobutane" Chen, B.; Vicic, D. A. *J. Fluorine Chem.* **2014**, *167*, 139-142. (Sole DOE support)
- 14) "Synthesis and Reactivity of New Aminophenolate Complexes of Nickel" Yu, S.; Wang, H.; Sledziewski, J. E.; Madhira, V. N.; Takahashi, C. G.; Leon, M. K.; Budnikova, Y. H.; Vicic, D. A. *Molecules* **2014**, *19*, 13603-13613. (Sole DOE support for US PI; the Russian collaborator cited her support)

- 15) "Synthetic Utility of Dizinc Reagents Derived from 1,4-Diiodo- and 1,4-Dibromooctafluorobutane" Kaplan, P. T.; Chen, B.; Vivic, D. A. *J. Fluorine Chem.* **2014**, *168*, 158-162. (Sole DOE support)
- 16) "Nanoheterogeneous Catalysis in Electrochemically Induced Olefin Perfluoroalkylation" Dudkina, Y. B.; Gryaznova, T. V.; Davydov, N. A.; Mustafina, A. R.; Vivic, D. A.; Budnikova, Y. B. *Dalton Trans.* **2015**, DOI: 10.1039/C5DT00269A. (Sole DOE support for US PI; the Russian collaborator cited her support)
- 17) "Stepwise Conversion of a Platinum Dimethyl Complex to a Perfluorometallacyclobutane Derivative" Xu, L.; Solowey, D. P.; Vivic, D. A. *Organometallics* **2015**, DOI: 10.1021/acs.organomet.5b00045. (Sole DOE support)
- 18) "An Unusual Example of Halogen Bonding to Potassium t-Butoxide" Xu, L.; Cramer, R. E.; Vivic, D. A. *J. Fluorine Chem.* **2015**, DOI:10.1016/j.jfluchem.2015.04.008 (Sole DOE support)
- 19) "Iron-Catalyzed Electrochemical C-H Perfluoroalkylation of Arenes" Khrizanforov, M.; Strelakova, S.; Khrizanforova, V.; Grinenko, V.; Kholin, K.; Gryaznova, T.; Sinyashin, O.; Xu, L.; Vivic, D. A.; Budnikova, Y. **2015**, *submitted*. (Sole DOE support for US PI; the Russian collaborator cited her support)

**Characterization of propane  $\sigma$ -complexes on PdO(101) using vibrational spectroscopy**

F. Zhang<sup>1</sup>, L. Pan<sup>2</sup>, J. Choi<sup>1</sup>, V. Mehar<sup>1</sup>, J.T. Diulus<sup>1</sup>, A. Asthagiri<sup>2</sup> and J.F. Weaver<sup>1</sup>

- 1) Department of Chemical Engineering, University of Florida
- 2) William G. Lowrie Department of Chemical and Biomolecular Engineering, The Ohio State University

We characterized propane  $\sigma$ -complexes adsorbed on the PdO(101) surface using reflection absorption infrared spectroscopy (RAIRS) and density functional theory (DFT) calculations. RAIR spectra obtained from propane-saturated PdO(101) at 90 K exhibit two broad C-H stretch bands ( $\sim 2530$  and  $2620\text{ cm}^{-1}$ ) that are redshifted by 300 to  $400\text{ cm}^{-1}$  from gas-phase values. DFT calculations predict that these soft C-H stretch modes arise from Pd-coordinated C-H bonds of adsorbed propane  $\sigma$ -complexes on PdO(101). Disappearance of the soft C-H stretch bands with increasing surface temperature to 250 K coincides with initial C-H bond cleavage and the formation of adsorbed 1-propyl species, thus demonstrating that adsorbed  $\sigma$ -complexes serve as precursors to propane C-H bond cleavage on the PdO(101) surface. RAIRS measurements using propane isotopologues in combination with DFT further demonstrate that the propane complexes undergo a change in preferred bonding configuration with increasing propane surface coverage. We find that the propane complexes preferentially adopt a bidentate geometry at low coverage in which a single H-Pd  $\eta^1$  bond forms at each CH<sub>3</sub> group. At higher coverage, the adsorbed propane complexes adopt both  $\eta^2$  and  $\eta^1$  configurations but coordinate to the surface Pd atoms only through the CH<sub>2</sub> group. The tendency for propane complexes to coordinate to PdO(101) through the CH<sub>3</sub> groups at low coverage is a key factor in determining the strong preference for propane to dissociate on PdO(101) via primary C-H bond cleavage that we have previously reported.

**DE-FG02-03ER15478: Alkane Activation and Oxidation on Pd and Pd-Pt Oxide Surfaces**

PIs: Jason F. Weaver, Aravind Asthagiri

Students: Feng Zhang, Li Pan, Juhee Choi, Abbin Antony, Can Hakanoglu

**RECENT PROGRESS**

In this project, we have been investigating the growth and surface chemistry of oxide phases that are prepared on Pd and Pt surfaces in UHV using oxygen atom beams. In 2008, we discovered that a high-quality PdO(101) thin film can be grown on Pd(111) by oxidizing the metal with atomic oxygen. We have since been investigating the surface chemical properties of the PdO(101) thin film both experimentally and computationally,

focusing particularly on the activation and oxidation of alkanes. This focus was inspired originally by experiments which showed that propane undergoes facile C-H bond activation on the PdO(101) surface and that a strongly-bound molecularly adsorbed state acts as the precursor for initial propane dissociation. Through both UHV experiments and DFT calculations, we have shown that the formation of strongly-bound  $\sigma$ -complexes is a general feature of *n*-alkane adsorption on PdO(101), and that these species serve as precursors for alkane C-H bond cleavage on PdO(101). We have also recently reported DFT calculations which predict that the formation and facile C-H bond activation of alkane  $\sigma$ -complexes occurs on RuO<sub>2</sub> and IrO<sub>2</sub> surfaces as well. Indeed, these findings suggest that the formation of  $\sigma$ -complexes and facile C-H bond activation is a common aspect of alkane adsorption on the surfaces of late TM oxides that expose cus-metal/oxygen pairs.

Over the last few years we have been performing RAIRS measurements in combination with DFT calculations to investigate the adsorption and oxidation of small molecules on the PdO(101) surface, including CO, NO and propane. These investigations have provided new insights for understanding the mechanisms for reaction on PdO(101) and the dynamic coupling between the surface reaction kinetics and the oxide surface structure.

### ***Vacancy-mediated processes in the oxidation of CO on PdO(101)***

We have investigated CO oxidation on PdO(101) extensively, and find that surface oxygen vacancies play a central role in mediating this reaction. Our results show that CO binds selectively to atop-Pd<sub>cus</sub> sites of the PdO(101) surface, producing a peak at ~2135 cm<sup>-1</sup> in RAIR spectra (Figure 1a). During CO oxidation, a fraction of the adsorbed CO molecules bind to Pd<sub>cus</sub> sites located next to O<sub>cus</sub> vacancies (O<sub>v</sub> sites) and generate a feature at ~2085 cm<sup>-1</sup> in RAIRS. Figure 1a shows CO RAIR spectra obtained at different temperatures during temperature programmed reaction spectroscopy (TPRS) measurements in which CO<sub>2</sub> evolves from the surface in distinct peaks centered at 330 and 525 K, and Figure 1b shows the integrated intensities of the peaks at 2135 cm<sup>-1</sup> and 2085 cm<sup>-1</sup> as a function of the temperature, where the peaks arise from CO adsorbed on Pd<sub>cus</sub>/O<sub>cus</sub> and Pd<sub>cus</sub>/O<sub>v</sub> sites, respectively. The RAIRS data reveals that the low temperature CO<sub>2</sub> peak results from the oxidation of CO-Pd<sub>cus</sub>/O<sub>cus</sub> species, and that CO molecules concurrently diffuse to Pd<sub>cus</sub>/O<sub>v</sub> sites as vacancies are created during reaction. Oxidation of the CO-Pd<sub>cus</sub>/O<sub>v</sub> species generates the higher temperature CO<sub>2</sub> TPRS peak at 525 K, as evidenced by the diminution of the peak at 2085 cm<sup>-1</sup> at temperatures above about 450 K (Figure 1b). DFT calculations support these interpretations and indeed predict that both CO-Pd<sub>cus</sub>/O<sub>cus</sub> and CO-Pd<sub>cus</sub>/O<sub>v</sub> species can access facile pathways for oxidation on PdO(101) wherein the barriers for reaction are ~75 kJ/mol lower than the barriers for desorption for both CO species, yet the absolute barriers are higher for the CO-Pd<sub>cus</sub>/O<sub>v</sub> species. The predicted energetics suggest that higher temperatures are required for the CO-Pd<sub>cus</sub>/O<sub>v</sub> species to react at similar rates as the CO-Pd<sub>cus</sub>/O<sub>cus</sub> species, while the nearly identical values of the apparent reaction barriers suggest that reaction of each CO species could produce similar CO<sub>2</sub> yields, which is consistent with experimental observations.

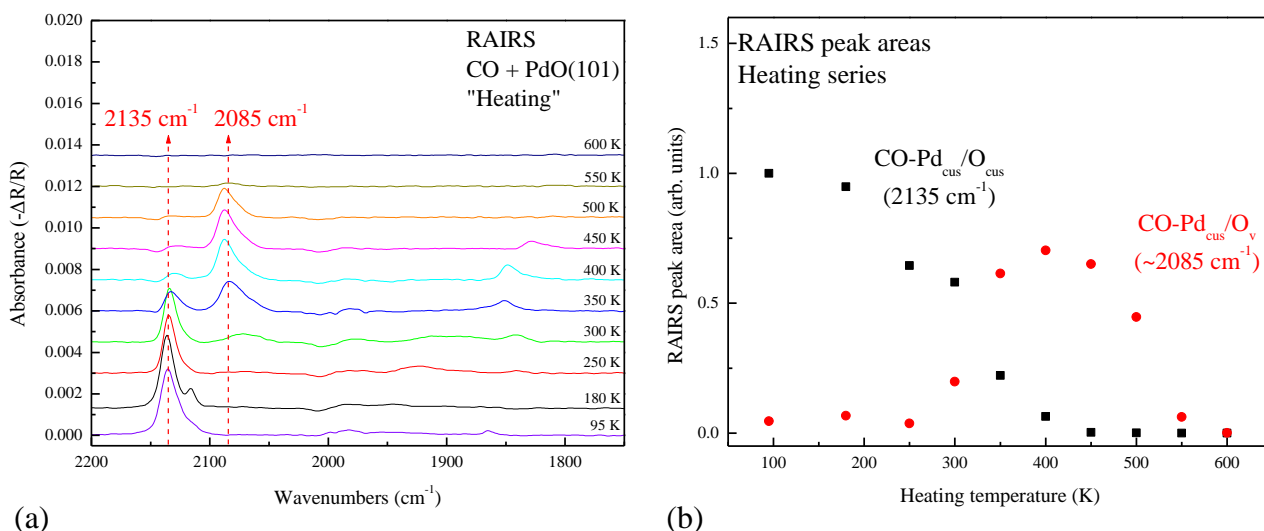


**Figure 1:** “Heating” series of RAIR spectra (a) and integrated area of atop CO peak at  $2135\text{ cm}^{-1}$  and  $2085\text{ cm}^{-1}$  as a function of heating temperature (b). Each RAIR spectrum was obtained at 95 K after heating CO-saturated PdO(101) to the temperatures indicated.

Our investigations also demonstrate that surface  $\text{O}_{\text{cus}}$  atoms are efficiently regenerated during CO oxidation on PdO(101) at temperatures above about 450 K via the migration of subsurface oxygen to the surface. After heating CO-saturated PdO(101) to selected temperatures, followed by re-saturating the surface with CO at 95 K, we find that the concentration of  $\text{O}_{\text{cus}}$  atoms begins increasing while the concentration of surface  $\text{O}_{\text{v}}$  sites concurrently decreases at temperatures at which the  $\text{CO-Pd}_{\text{cus}}/\text{O}_{\text{v}}$  species start to react and desorb. At the end of a TPRS experiment at  $\sim 600\text{ K}$ , our RAIRS data shows that the concentration of  $\text{O}_{\text{cus}}$  atoms is nearly restored to its value on the initial PdO(101) surface. According to DFT, surface  $\text{O}_{\text{v}}$  sites are less stable than subsurface  $\text{O}_{\text{v}}$  sites in the absence of CO, but adsorbed CO stabilizes the surface  $\text{O}_{\text{v}}$  sites relative to subsurface vacancies. For this reason, the removal of  $\text{CO-Pd}_{\text{cus}}/\text{O}_{\text{v}}$  species by reaction or desorption creates a thermodynamic driving force for subsurface oxygen atoms to move into surface  $\text{O}_{\text{v}}$  sites and generate surface  $\text{O}_{\text{cus}}$  atoms. Using DFT, we identified a relatively facile pathway wherein a subsurface O-atom, bonded directly underneath a  $\text{Pd}_{\text{cus}}$  atom, can move into the surface  $\text{O}_{\text{v}}$  site to regenerate an  $\text{O}_{\text{cus}}$  atom at the surface. These results reveal that oxygen migration from the bulk reservoir provides an efficient route for regenerating reactive O-atoms at the PdO(101) surface during adsorbate oxidation, and should be taken into account in kinetic models of oxidation reactions on PdO(101). We are currently investigating CO oxidation on PdO(101) under isothermal conditions with CO and  $\text{O}_2$  in the gas-phase, aiming to achieve steady-state reaction conditions and characterize the kinetics for  $\text{O}_{\text{cus}}$  restoration via  $\text{O}_2$  dissociation.

## Characterization of propane $\sigma$ -complexes on PdO(101) by RAIRS

We used RAIRS and DFT to characterize propane  $\sigma$ -complexes adsorbed on the PdO(101) surface. The RAIR spectrum obtained from the propane monolayer on PdO(101) exhibits C-H stretch bands at  $\sim 2530$  and  $2620\text{ cm}^{-1}$  (Figure 2) that arise from Pd-coordinated C-H bonds of the adsorbed propane complexes. These softened C-H stretch bands are redshifted by 300 to  $400\text{ cm}^{-1}$  from gas-phase values, and thus reveal that  $\sigma$ -complex formation significantly perturbs C-H bonds of propane adsorbed on PdO(101). Diminution of the soft C-H stretch bands with increasing surface temperature to 250 K, concurrently with the appearance of a new C-H stretch peak at  $2789\text{ cm}^{-1}$ , demonstrates that adsorbed propane  $\sigma$ -complexes serve as precursors to initial C-H bond activation and that dissociation produces 1-propyl groups on the surface.

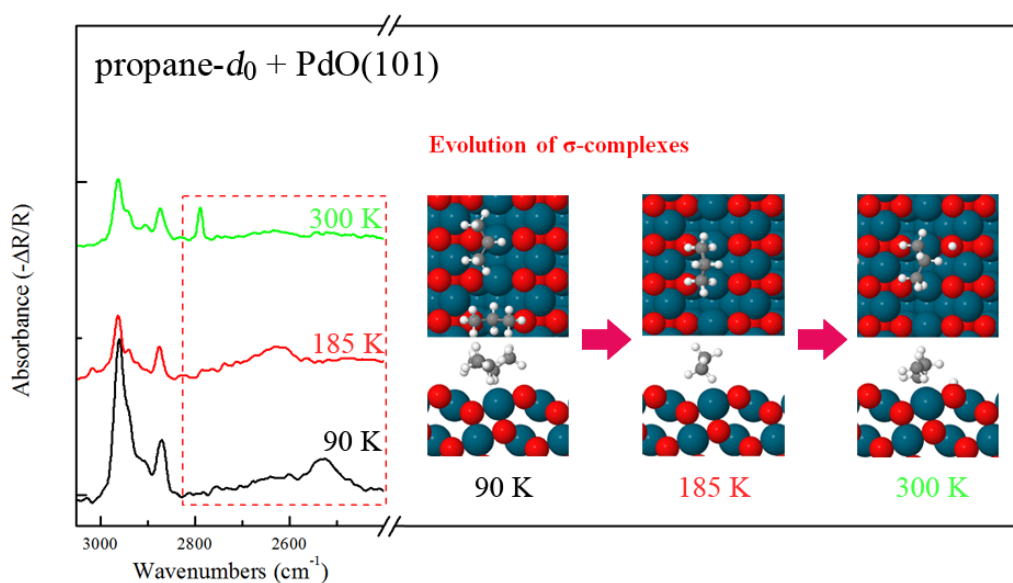


**Figure 2:** RAIR spectra (left) obtained from propane-saturated PdO(101) after heating to the temperatures indicated and images (right) of the propane configurations that evolve with temperature as predicted using DFT-D3.

We also find that the soft C-H stretch band at  $\sim 2620\text{ cm}^{-1}$  is dominant at low propane coverage, but that this band diminishes slightly while a second, soft C-H stretch band at  $\sim 2530\text{ cm}^{-1}$  intensifies with increasing propane coverage (Figure 2). RAIRS measurements of adsorbed propane- $d_2$  and  $d_6$  on PdO(101), in combination with DFT, demonstrate that these spectral changes arise from a change in the preferred bonding geometry of the propane complexes as a function of the propane surface coverage. At low coverage, propane complexes preferentially adopt a bidentate geometry along the  $\text{Pd}_{\text{cus}}$  row in which a single H-Pd  $\eta^1$  bond forms at each  $\text{CH}_3$  group, whereas at higher coverage, the propane complexes form both  $\eta^1$  and  $\eta^2$  complexes but coordinate to the  $\text{Pd}_{\text{cus}}$  atoms only through the  $\text{CH}_2$  group (Figure 2). The tendency for propane to coordinate to the surface Pd atoms only through the  $\text{CH}_3$  groups at low coverage is a key factor in determining the strong preference for propane to dissociate on PdO(101) via

primary C-H bond cleavage. This study is the first to provide spectroscopic evidence that adsorbed  $\sigma$ -complexes serve as precursors to alkane C-H bond cleavage on a solid surface, and identify the configurations of such species based on changes in the soft C-H stretch bands. Indeed, these findings demonstrate the utility of vibrational spectroscopy in characterizing alkane  $\sigma$ -complexes on oxide thin films.

### Publications Acknowledging this Grant in 2012-2015

1. “Vacancy-mediated processes in the oxidation of CO on PdO(101)”, J.F. Weaver, F. Zhang, T. Li, L. Pan and A. Asthagiri, *Acc. Chem. Res.* (2015) in press (DOI: 10.1021/acs.accounts.5b00101). (*Invited article* for a themed issue entitled “Microscopic Insights into Surface Catalyzed Chemical Reactions”)
2. “Molecular adsorption of NO on PdO(101)”, J. Choi, L. Pan, F. Zhang, J. Diulus, A. Asthagiri and J.F. Weaver, *Surf. Sci.* (2015) in press ([doi:10.1016/j.susc.2015.01.010](https://doi.org/10.1016/j.susc.2015.01.010)). (*Invited article* for a themed issue titled “Reactivity Concepts at Surfaces: Coupling Theory with Experiment”)
3. “CO oxidation on PdO(101) during temperature programmed reaction spectroscopy: Role of oxygen vacancies”, F. Zhang, L. Pan, T. Li, J. Diulus, A. Asthagiri and J.F. Weaver, *J. Phys. Chem. C* 118 (2014) 28647–28661.
4. “Intrinsic ligand effect governing the catalytic activity of Pd oxide thin films”, N.M. Martin, M. Van den Bossche, A. Hellman, H. Grönbeck, C. Hakanoglu, J. Gustafson, S. Blomberg, N. Johanson, Z. Liu, S. Axnanda, J.F. Weaver, and E. Lundgren, *ACS Catal.* 4 (2014) 3330-3334.
5. “CO oxidation on single and multilayer Pd oxides on Pd(111): Mechanistic insights from RAIRS”, F. Zhang, T. Li, L. Pan, A. Asthagiri and J.F. Weaver, *Catal. Sci. Technol.* 4 (2014) 3826-3834. (*Invited article* for a themed issue titled “Catalysis in the USA”).
6. “Effects of non-local exchange on core-level shifts for gas-phase and adsorbed molecules”, M. Van den Bossche, N.M. Martin, C. Hakanoglu, J. Gustafson, J.F. Weaver, E. Lundgren and H. Grönbeck, *J. Chem. Phys.* 141 (2014) 034706.
7. “Alkane activation on crystalline metal oxide surfaces”, J.F. Weaver, C. Hakanoglu, A. Antony and A. Asthagiri, *Chem. Soc. Rev.* 43 (2014) 7536-7547. (*Invited article* for a themed issue entitled “Catalysis for the Production of Renewable Energy”).
8. “CO adsorption on clean and oxidized Pd(111)”, N.M. Martin, M. Van den Bossche, H. Grönbeck, C. Hakanoglu, F. Zhang, T. Li, J. Gustafson, J.F. Weaver and E. Lundgren, *J. Phys. Chem. C.* 118 (2014) 1118–1128.

9. "Pathways and kinetics for methane and ethane C-H bond cleavage on PdO(101)", A. Antony, A. Asthagiri and J.F. Weaver, *J. Chem. Phys.* 139 (2013) 104702: 1-12.
10. "Inhibition of methane adsorption on PdO(101) by water and molecular oxygen", F. Zhang, C. Hakanoglu, J. Hinojosa, Jr. and J.F. Weaver, *Surf. Sci.* 617 (2013) 249-255.
11. "Dissociative adsorption of hydrogen on PdO(101) studied by HRCLS and DFT", N.M. Martin, M. Van den Bossche, H. Grönbeck, C. Hakanoglu, J. Gustafson, S. Blomberg, M.A. Arman, A. Antony, R. Rai, A. Asthagiri, J.F. Weaver and E. Lundgren, *J. Phys. Chem. C* 117 (2013) 13510–13519.
12. "Selectivity in the initial C-H bond cleavage of n-butane on PdO(101)", C. Hakanoglu, F. Zhang, A. Antony, A. Asthagiri and J.F. Weaver, *Phys. Chem. Chem. Phys.* 15 (29) (2013) 12075 - 12087. (**Invited article** for a themed issue entitled "Interfacial Phenomena in (De)hydrogenation Reactions")
13. "Surface chemistry of late transition metal oxides", J.F. Weaver, *Chem. Rev.* 113 (2013) 4164-4215. <http://dx.doi.org/10.1021/cr300323w> (**Invited article** for a special issue entitled, "Surface Chemistry of Oxides")
14. "Surface reactivity of oxide phases on Pd(111) generated during the growth vs reduction of PdO(101) films", C. Hakanoglu and J.F. Weaver, *Surf. Sci.* 611 (2013) 40-48.
15. "Pathways for C-H bond cleavage of propane  $\sigma$ -complexes on PdO(101)", A. Antony, A. Asthagiri and J.F. Weaver, *Phys. Chem. Chem. Phys.* 14 (2012) 12202-12.
16. "Dispersion-corrected density functional theory calculations of the molecular binding of n-alkanes on Pd(111) and PdO(101)", A. Antony, C. Hakanoglu, A. Asthagiri and J.F. Weaver, *J. Chem. Phys.*, 136 (2012) 054702: 1-9.
17. "Adsorption of CO<sub>2</sub> on a PdO(101) thin film", J.A. Hinojosa, Jr., A. Antony, C. Hakanoglu, A. Asthagiri and J.F. Weaver, *J. Phys. Chem. C* 116 (2012) 3007–3016.

Michael G. White

## **Influence of Cluster-Support Interactions on Reactivity of Size-Selected Metal Oxide Clusters**

M. Nakayama,<sup>1</sup> M. Xue,<sup>2</sup> P. Liu<sup>1</sup> and M. G. White<sup>1,2</sup>

<sup>1</sup>Chemistry Department, Brookhaven National Laboratory, Upton NY 11973

<sup>2</sup>Department of Chemistry, Stony Brook University, Stony Brook, NY 11794

### **Poster Abstract**

Metal-oxide interactions can strongly influence catalytic activity through electronic interactions which induce structural changes or creation of new active sites at the particle-support interface. For oxide supported Cu catalysts, which are of interest for promoting the water-gas-shift (WGS) reaction and methanol synthesis, the metal oxide-Cu electronic interactions are known to strongly influence activity. In this work, we are using size-selected deposition to explore the interfacial electronic structure of a number of small metal oxide clusters (Mo, W, Ti, Nb) on Cu(111) and Cu<sub>2</sub>O/Cu(111) surfaces as model “inverse” catalysts. Such inverse systems are useful for investigating the chemical role of the oxide, and in some cases, can be even more active than the conventional catalysts. The extent and direction of charge transfer at the interface are extracted from coverage dependent work function measurements using two-photon photoemission (2PPE) and theoretical DFT calculations. The trends observed for charge transfer are correlated with their ability to dissociate adsorbed water molecules, which is an important step in the WGS reaction. As O-vacancies can play an important role for adsorbate binding and water dissociation on oxide surfaces, both stoichiometric and sub-stoichiometric oxide clusters are being studied. These studies highlight the unique ability of cluster deposition to prepare well-defined “reduced” surface oxides by controlling the stoichiometry of the clusters rather than by post-deposition heating or chemical treatments.

### **FWP CO-009: Catalysis Science for Advanced Fuels**

#### **Subtask 2: Nanostructured Materials for Catalysis**

PIs: Ping Liu, Jose Rodriguez, Sanjaya Senanayake, Dario Stacchiola, Michael White

Postdocs: Wei An, David Grinter

Graduate Students: Shizhong Liu, Fang Xu, Meng Xue

### **Recent Progress**

#### **Chemical annealing of under coordinated copper sites (Stacchiola, Lead PI)**

Active metal nanoparticles present on catalysts present a variety of adsorption sites, with a significant higher number of under-coordinated atoms compared with a model flat Cu(111) surface. Therefore, investigating the adsorption of molecules on a controlled number of defect-sites on Cu(111) and monitoring the dynamic morphological changes during adsorption/desorption processes is desired for the understanding of catalytic reactions under reaction conditions. In order to study the effects of hydrogen absorption on the morphology of Cu surfaces, we prepared nano-pitted Cu(111) surfaces, with pits from one to several atomic layers. Fig. 1A shows the nanopits created on a Cu(111) sample by gentle sputtering of the

surface. No changes on the pits were observed when this surface was exposed to molecular  $H_2$  up to pressures of 1 atmosphere at 300 K. When the pitted surface is exposed to atomic hydrogen at 300 K, full reconstruction of the surface is observed even under small exposures (Fig. 1B-D). These adsorbate-driven morphological changes occur  $\sim 150$  K below the temperature required to remove the roughness of the pitted-Cu(111) by simply annealing in vacuum. These results highlight the importance of investigating the properties of the adsorption sites in the presence of adsorbates or under reaction conditions to identify dynamically formed active phases.

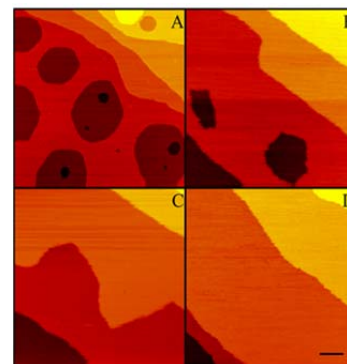


Fig. 1: STM images of pitted-Cu(111) before and after exposure to atomic hydrogen.

### CO oxidation on copper catalysts (Stacchiola, Lead PI)

The oxidation of CO is commonly used in surface science as a test reaction. The natural abundance of copper and its oxidation catalytic properties make it very attractive for practical uses. The Achilles heel of  $Cu_2O$  catalysts has been its deactivation by complete oxidation to  $CuO$ . The oxidation of CO on Cu(111) was tested in situ by IRRAS (Fig. 2). Copper oxide domains form even under reducing conditions at 300 K, and the surface reconstructs constantly through a redox cycle between  $CuO$ ,  $Cu_2O$  and  $Cu$ . The Cu atoms released during the redox cycle diffuse to the step edges leading to a flat surface with highly mobile step edges that are faceted along the  $\langle 110 \rangle$  direction. Metallic copper is the most active phase, but it cannot be stabilized under reaction conditions.  $Cu^+$  is also very active, and the formation of  $Cu^{2+}$  deactivates the catalysts. Strategies to stabilize structures with  $Cu^+$  cations, such as the formation of mixed-oxides, could lead to stable Cu oxidation catalysts.

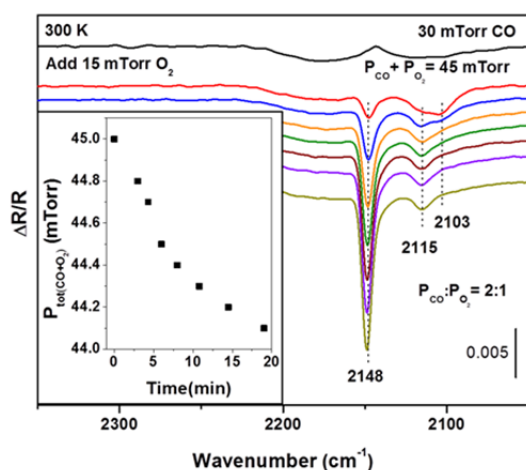


Fig. 2: *In situ* spectroscopic data for CO oxidation over Cu(111).

### Metal supported oxide on oxide nanostructures (Senanayake, Lead PI)

The interfacial interactions between two oxides are a rich source of active sites necessary for chemical conversion. Taking insights from model and theoretical studies we have studied  $CeO_2$ - $TiO_2$  (fluorite-anatase) powder catalysts aimed towards the Water gas shift and photocatalytic splitting of water. We have identified the chemical state of this interface and also the hierarchical nature of  $CeO_x$  atomic structures that can prevail on  $TiO_2$ , from 0-1D clusters, 2D plates and chains and 3D nanoparticles (Fig. 3). Each structural hierarchy can impart distinct electronic and chemical influence to the reactivity based on a combination of geometric / morphological, chemical ( $Ce^{3+}$  vs  $Ce^{4+}$ ) and electronic properties (charge transfer to  $TiO_2$  support). The

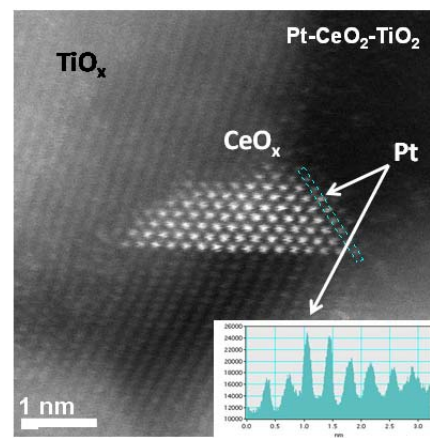


Fig. 3: STEM image of Pt-CeO<sub>x</sub>-TiO<sub>2</sub>.

addition of a metal to this mixed oxide support allows for a highly dispersed Pt of very low coordination (<0.5nm) that interacts strongly with the oxide-oxide support typical for a Strong Metal Support Interaction. Preliminary results have identified a direct ability to tune the reactivity of metals such as Pt using the electronic and chemical interactions with the support

### Size-Selected metal oxide cluster deposited on Cu surfaces (White, Lead PI)

In this work, we have explored the role of metal oxide structure, charge transfer and state of reduction on the reactivity of model inverse catalysts composed of small metal oxide nanoclusters ( $\text{MO}_x$ ;  $M = \text{Mo}, \text{W}, \text{Ti}, \text{Nb}$ ) on Cu(111) and  $\text{Cu}_2\text{O}/\text{Cu}(111)$  surfaces. The nanostructured surfaces were prepared by size-selected cluster deposition where metal-to-oxygen stoichiometry could be readily controlled. Two-photon photoemission (2PPE) measurements of coverage-dependent work function shifts were used to probe interfacial charge transfer and temperature programmed desorption and reaction (TPD, TPR) were used to assess activity for water dissociation. Experimentally, all the clusters on Cu(111) exhibit negative surface dipoles, indicative of  $\text{Cu} \rightarrow$  cluster charge transfer, with the dipoles for sub-stoichiometric and reducible oxides (i.e.,  $\text{Ti}_x\text{O}_y$  and  $\text{Nb}_x\text{O}_y$ ) being smaller. The observed trends are generally consistent with Bader charge analyses from DFT calculations, but in some cases, the calculations suggest that the intrinsic dipole of the adsorbed cluster (structure dependent) is more important than charge transfer. We find no evidence of water dissociation on  $\text{Mo}_x\text{O}_y$  and  $\text{W}_x\text{O}_y$  clusters ( $x/y = 3/9, 3/6$ ), which also exhibit the largest surface dipole moments. The  $\text{Ti}_x\text{O}_y$  clusters ( $x/y = 3/5, 3/6, 4/7, 4/8$ ) are found to be sensitive to thermal treatment and generally show low water activity as detected by desorption of molecular hydrogen. The  $\text{Nb}_x\text{O}_y$  clusters exhibit the highest activity (Fig. 4), with both stoichiometric ( $x/y = 3/7, 4/10$ ) and reduced clusters ( $x/y = 3/5, 4/8$ ) able to dissociate water on Cu(111). Only the reduced  $\text{Nb}_x\text{O}_y$  clusters show activity for water dissociation on the  $\text{Cu}_2\text{O}/\text{Cu}(111)$  oxide thin film surface, which is consistent with the much calculated lower energy barrier for water dissociation on Cu(111) versus  $\text{Cu}_2\text{O}(111)$ . Overall, these results suggest that both the reducibility and Lewis acid character of the Nb cation sites play a role in enhancing water dissociation.

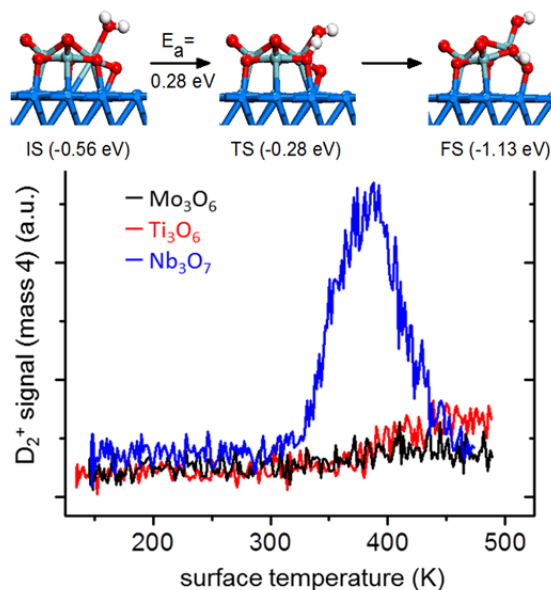


Fig. 4: Bottom: Thermal desorption curves for  $\text{D}_2$  following  $\text{D}_2\text{O}$  exposure of several metal oxide clusters deposited on Cu(111). Cluster coverage 0.3 ML. Top: DFT calculated energy pathway for water dissociation on  $\text{Nb}_3\text{O}_7$  on Cu(111). Red: oxygen; blue-green: Nb; blue: Cu.

### Methanol Synthesis from $\text{CO}_2$ and $\text{H}_2$ on a modified $\text{Mo}_6\text{S}_8$ cluster (Liu, Lead PI)

We investigated the methanol synthesis from  $\text{CO}_2$  and  $\text{H}_2$  on metal ( $M = \text{K}, \text{Ti}, \text{Co}, \text{Rh}, \text{Ni}$ , and Cu)-modified model  $\text{Mo}_6\text{S}_8$  catalyst using density functional theory (DFT). The results show that the catalytic behavior of a  $\text{Mo}_6\text{S}_8$  cluster is changed significantly due to the modifiers, via the electron transfer from M to  $\text{Mo}_6\text{S}_8$  and therefore the reduction of the Mo cation (ligand effect)

and the direct participation of M in the reaction (ensemble effect) to promote some elementary steps. With the most positively charged modifier, the ligand effect in the case of K-  $\text{Mo}_6\text{S}_8$  is the most obvious among the systems studied; however it cannot compete with the ensemble effect, which plays a dominate role in determining activity via the electrostatic attraction which stabilizes the  $\text{CH}_x\text{O}_y$  species adsorbed at the Mo sites of  $\text{Mo}_6\text{S}_8$ . In addition, the modifiers also vary the optimal reaction pathway from the reverse water-gas shift (RWGS) + CO hydrogenation to a pathway involving a formate intermediate. The addition of K improves methanol formation the most, while Ti, Co, Ni, and Cu decrease the activity of  $\text{Mo}_6\text{S}_8$ . The relative stability of  $^*\text{HCOO}$  versus  $^*\text{HOCO}$  is identified as a descriptor of the preferred mechanism and activity (Fig. 5). This study not only provides a better understanding of the reaction mechanism on modified  $\text{Mo}_6\text{S}_8$ , but also predicts some possible promoters to facilitate methanol synthesis on Mo sulfides.

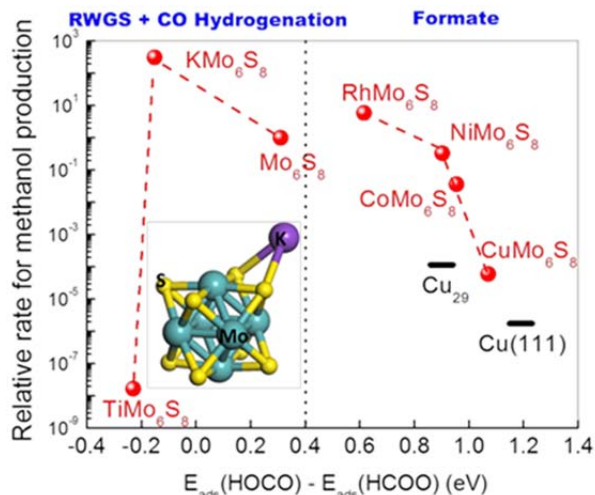


Fig. 5: Variation of the methanol synthesis rate versus the difference in HOCO and HCOO binding energies for various M- $\text{Mo}_6\text{S}_8$  clusters.

### Growth of Pt shell on Pd nanoparticles (Liu, Lead PI)

DFT calculations were used to obtain a better understanding of the growth mode of a  $\text{Pt}_{\text{ML}}$  shell on Pd nanoparticles. A hemisphere-like  $\text{Pd}_{174}$  nanoparticle model was employed to represent a  $\sim 2.2$  nm sphere-like truncated octahedral  $\text{Pd}_{405}$  nanoparticle (Fig. 6) containing  $\{111\}$  and  $\{100\}$  facets. Our previous studies demonstrated the capability of such a hemisphere model to describe the experimental electrochemical activities of core-shell nanoparticles. The results exhibit that the deposited Pt atom is likely to nucleate on the  $\{100\}$  or  $\{111\}$  terraces (Fig. 6) rather than at edges. The Pt growth on Pd from an adatom to a 2D tetramer is highly exothermic, suggesting that the 2D growth of Pt on Pd  $\{100\}$  is energetically preferred. It also shows that the growth from  $\text{Pt}_4$  to  $\text{Pt}_5$  favors the formation of a 2D planar rather than a 3D cluster because of the formation of additional strong Pt-Pt and Pt-Pd bonds. The Pt growth on Pd  $\{111\}$  is less preferential than that on  $\{100\}$  facets. From these results, we propose that growth of the Pt shell starts from the formation of an ordered Pt monolayer on Pd  $\{100\}$  facets, followed by the closure of an ordered Pt monolayer on Pd  $\{111\}$ . Overall, our DFT results clearly demonstrate that the epitaxial layer-by-layer growth of Pt is thermodynamically favorable on Pd nanoparticles. Moreover, the use of elevated temperatures during synthesis should

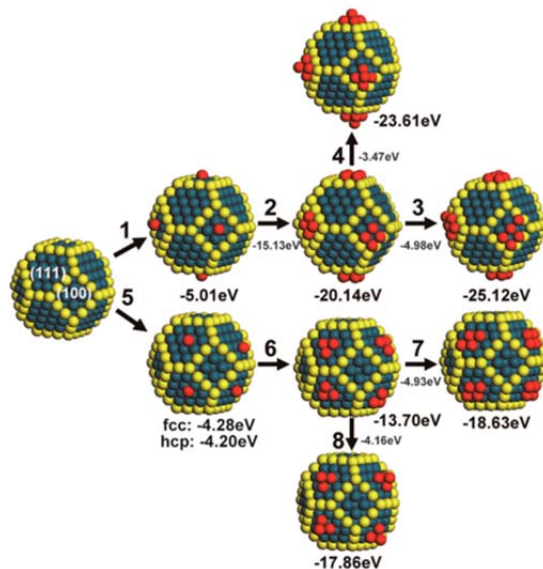


Fig. 6: DFT-calculated binding energies of Pt atoms (red) on  $\{100\}$  and  $\{111\}$  terraces of a Pd nanoparticle. Dark blue: Pd on terraces; yellow: Pd at edges and vertices; red: Pt.

facilitate the formation of a smooth and uniform Pt shell on Pd cores.

### Publications Acknowledging this Grant in 2012-2015

1. R. Palomino, R.; Magee J. W.; Llorca, J.; Senanayake, S. D.; White, M. G.; The Effect of Fe-Rh Alloying on CO Hydrogenation to C<sub>2+</sub> Oxygenates, *J. Catal.*, in press.
2. Nakayama, M.; Xue, M.; An, W.; Liu, P.; White, M. G.; Influence of Cluster-Support Interactions on Reactivity of Size-Selected Nb<sub>x</sub>O<sub>y</sub> Clusters, *J. Phys. Chem. C*, in press.
3. Liu, C.; Liu, P., Mechanistic Study of Methanol Synthesis from CO<sub>2</sub> and H<sub>2</sub> on a Modified Model Mo<sub>6</sub>S<sub>8</sub> Cluster, *ACS Catalysis* **2015**, *5*, 1004-1012.
4. Mudiyansele, K.; Xu, F.; Hoffmann, F.H.; Hrbek, J.; Waluyo, I.; Boscoboinik, J. A.; Stacchiola, D.; Adsorbate-Driven Morphological Changes on Cu(111) Nano-Pits, *PCCP* **2015**, doi: 10.1039/C4CP05088F.
5. Mudiyansele, K.; Baber, A. E.; Liu, Z.; Senanayake, S. D.; Stacchiola, D. J.; Isolation and Characterization of Formates on CeO<sub>x</sub>-Cu<sub>y</sub>O/Cu(111), *Catalysis Today* **2015**, *240*, 190–200.
6. Xu, F.; Mudiyansele, K.; Baber, A.E.; Soldemo, A.; Weissenrieder, J.; White, M. G.; Stacchiola, D. J.; Redox-Mediated Reconstruction of Cu(111) During CO Oxidation, *J. Phys. Chem. C* **2014**, *118*, 15902–15909.
7. J Graciani, J.; Mudiyansele, K.; Xu, F.; Baber, A. E.; Evans, J.; Senanayake, S. D.; Stacchiola, D. J.; Liu, P.; Hrbek, J.; Fernández-Sanz, J.; Rodriguez, J. A.; Highly Active Copper-Ceria and Copper-Ceria-Titania Catalysts for Methanol Synthesis from CO<sub>2</sub>, *Science* **2014**, *345*, 546-550.
8. Weissenrieder, J.; Gustafson, J.; Stacchiola, D. J.; Reactivity and mass transfer of low dimensional catalysts, *Chem. Rec.* **2014**, *14*, 857–868.
9. Zhang, Y.; Hsieh, Y.-C.; Volkov, V.; Su, D.; An, W.; Si, R.; Zhu, Y.; Liu, P.; Wang, J. X.; Adzic, R. R., High Performance Pt Monolayer Catalysts Produced via Core-Catalyzed Coating in Ethanol, *ACS Catalysis* **2014**, *4*, 738-742.
10. Baber, A. E.; Yang, X.; Kim, H. Y.; Mudiyansele, K.; Soldemo, M.; Weissenrieder, J.; Senanayake, S. D.; Al-Mahboob, A.; Sadowski, J. T.; Evans, J.; Rodriguez, J. A.; Liu, P.; Hoffmann, F. M.; Chen, J. G.; Stacchiola, D. J., Stabilization of Catalytically Active Cu<sup>+</sup> Surface Sites on Titanium-Copper Mixed-oxide Films, *Angew. Chem. Int. Ed. Engl.* **2014**, *53*, 5336-40.
11. An, W.; Baber, A.E.; Xu, F.; Soldemo, M.; Weissenrieder, J.; Stacchiola, D.; Liu, P., Mechanistic Study of CO Titration on Cu<sub>x</sub>O/Cu(111) (x≤2) Surfaces, *ChemCatChem.* **2014**, *6*, 2364 – 2372.
12. Magee, J. W.; Zhou, W-P.; White, M. G.; Promotion of Pt Surfaces for Ethanol Electro-Oxidation by the Addition of Small SnO<sub>2</sub> Nanoparticles: Activity and Mechanism, *Appl. Catal. B: Environ.* **2014**, *152–153*, 397–402.
13. Yang, Y.; Zhou, J.; Nakayama, M.; Nie, L.; Liu, P.; White, M.G., Surface Dipoles and Electron transfer at the Metal Oxide-Metal Interface: a 2PPE Study of Size-Selected Metal Oxide Clusters Supported on Cu(111), *J. Phys. Chem. C* **2014**, *118*, 13697–13706.
14. Agnoli, S.; Reeder, A. E.; Senanayake, S. D.; Hrbek, J.; Rodriguez, J. Structure and special chemical reactivity of interface stabilized cerium oxide nanolayers on TiO<sub>2</sub>(110), *Nanoscale* **2014**, *6*(2), 800-810.
15. Senanayake S.D., Mudiyansele K., Bruix A., Agnoli S., Hrbek J., Stacchiola D., Rodriguez J.A. The unique properties of the oxide-metal interface: Reaction of ethanol on an inverse model CeO<sub>x</sub>-Au(111) Catalyst, *J. Phys. Chem. C* **2014**, *118*, 25057-25064.

16. An, W.; Liu, P., Size and Shape Effects of Pd@Pt Core–Shell Nanoparticles: Unique Role of Surface Contraction and Local Structural Flexibility, *J. Phys. Chem. C* **2013**, *117*, 16144-16149.
17. Baber, A. E.; Mudiyansele, K.; Senanayake, S. D.; Beatriz-Vidal, A.; Luck, K. A.; Sykes, E. C.; Liu, P.; Rodriguez, J. A.; Stacchiola, D. J., Assisted Deprotonation of Formic Acid on Cu(111) and Self-assembly of 1D chains, *PCCP* **2013**, *15*, 12291-8.
18. Baber, A. E.; Xu, F.; Dvorak, F.; Mudiyansele, K.; Soldemo, M.; Weissenrieder, J.; Senanayake, S. D.; Sadowski, J. T.; Rodriguez, J. A.; Matolin, V.; White, M. G.; Stacchiola, D. J., In situ imaging of Cu<sub>2</sub>O under reducing conditions: formation of metallic fronts by mass transfer, *J. Am. Chem. Soc.* **2013**, *135*, 16781-4.
19. Liu, P.; Yang, Y.; White, M. G., Theoretical perspective of alcohol decomposition and synthesis from CO<sub>2</sub> activation. *Surf. Sci. Rep.* **2013**, *68*, 233-272.
20. Mudiyansele, K.; An, W.; Yang, F.; Liu, P.; Stacchiola, D. J., Selective molecular adsorption in sub-nanometer cages of a Cu<sub>2</sub>O surface oxide, *PCCP* **2013**, *15*, 10726-31.
21. Mudiyansele, K.; Kim, H. Y.; Senanayake, S. D.; Baber, A. E.; Liu, P.; Stacchiola, D., Probing adsorption sites for CO on Ceria, *PCCP* **2013**, *15*, 15856-62.
22. Mudiyansele, K.; Yang, Y.; Hoffmann, F. M.; Furlong, O. J.; Hrbek, J.; White, M. G.; Liu, P.; Stacchiola, D. J., Adsorption of Hydrogen on the surface and sub-surface of Cu(111), *J. Chem. Phys.* **2013**, *139*, 044712.
23. Nerko, D.; Axnanda, S.; Zhou, W.-P.; Lofaro, J.; White, M. G., Synthesis and Characterization of surface oxide films on CoGa (100), *Surf. Sci.* **2013**, *616*, 192-197.
24. Liu, P., Understanding the Behavior of TiO<sub>2</sub>(110)-Supported Pd<sub>7</sub> Cluster: A Density Functional Study. *J. Phys. Chem. C* **2012**, *116*, 25337-25343.
25. Baber, A. E.; Torres, D.; Muller, K.; Nazzarro, M.; Liu, P.; Starr, D. E.; Stacchiola, D. J., Reactivity and Morphology of Oxygen-Modified Au Surfaces, *J. Phys. Chem. C* **2012**, *116*, 18292-18299.
26. Rajasekaran, S.; Kaya, S.; Abild-Pedersen, F.; Anniyev, T.; Yang, F.; Stacchiola, D.; Ogasawara, H.; Nilsson, A., Reversible graphene-metal contact through hydrogenation, *Phys. Rev. B* **2012**, *86*, 075417.
27. Zhou, W.-P.; An, W.; Su, D.; Palomino, R.; Liu, P.; White, M. G.; Adzic, R. R., Electrooxidation of Methanol at SnO<sub>x</sub>–Pt Interface: A Tunable Activity of Tin Oxide Nanoparticles, *J. Phys. Chem. Lett.* **2012**, *3* (22), 3286-3290.
28. Hoffmann, F. M.; Hoo, Y. S.; Cai, T. H.; White, M. G.; Hrbek, J., Infrared study of Triruthenium Dodecacarbonyl interactions with Gold, *Surf. Sci.* **2012**, *606* (23-24), 1906-1913.
29. Axnanda, S.; Zhou, W. P.; White, M. G., CO oxidation on nanostructured SnO<sub>x</sub>/Pt(111) surfaces: Unique properties of reduced SnO<sub>x</sub>, *PCCP* **2012**, *14* (29), 10207-10214.
30. Zhou, J.; Zhou, J.; Camillone, N.; White, M. G., Electronic charging of non-metallic clusters: size-selected Mo<sub>x</sub>S<sub>y</sub> clusters supported on an ultrathin Alumina film on NiAl(110), *PCCP* **2012**, *14* (22), 8105-8110.
31. Yang, Y.; White, M. G.; Liu, P., A Theoretical Study of Methanol Synthesis from CO<sub>2</sub> Hydrogenation on Metal-Doped Cu(111) Surfaces, *J. Phys. Chem. C* **2012**, *116* (1), 248-256.
32. Liu, M. F.; Choi, Y. M.; Yang, L.; Blinn, K.; Qin, W. T.; Liu, P.; Liu, M. L., Direct Octane fuel cells: A promising power for transportation, *Nano Energy* **2012**, *1* (3), 448-455.

**Surface Mediated Thermocatalytic and Electrocatalytic Processes**

**— Reaction Mechanism and Catalyst Design**

Bingjun Xu, Marco Dunwell, Mathew J. Gilkey and Brian M. Murphy

Department of Chemical and Biomolecular Engineering, University of Delaware

**Presentation Abstract**

Understanding surface mediated reaction pathways is at the core of the rational design of catalytic materials. We employ a combination of kinetic, in-situ spectroscopic and isotopic labeling techniques to elucidate molecular level reaction mechanisms at gas-solid or liquid-solid interfaces for thermo- and electro-catalytic processes. *Efficient and selective upgrade biomass to fuels and valuable chemicals is main focus of the heterogeneous catalysis thrust.* Mechanistic studies of catalytic dehydration of lactic acid and its esters have identified the branching point, i.e., the dissociation of lactic acid or methyl lactate to form adsorbed sodium lactate, between the desired dehydration and undesired decarbonylation pathways on Na exchange zeolites. A ring activation mechanism has been proposed for the conversion of furfural to 2-methyl furan via catalytic transfer hydrogenation (CTH) based on isotopic labeling investigations. *On the electrocatalysis front, we focus our effort in understanding the fundamentals of several key reactions, e.g., CO<sub>2</sub> reduction reaction, hydrogen oxidation reaction (HOR).* By combining in-situ surface sensitive spectroscopy and isotopic labeling, we have identified that bicarbonate, rather than dissolved CO<sub>2</sub>, is the species reduced at Au surface. In addition, universal correlation among hydrogen binding energy, pH of electrolyte and HOR activities has been established by electrokinetic studies.

Related Publications:

1. M. Gilkey, P. Panagiotopoulou, A. Mironenko, G. Jennes, D. Vlachos, B. Xu, Mechanistic insights into metal-Lewis acid mediated catalytic transfer hydrogenation of furfural to 2-methylfuran, *ACS Catal.*, **2015**, *In press*.
2. A. Mironenko, M. Gilkey, P. Panagiotopoulou, G. Facas, D. Vlachos, B. Xu, Ring activation of furnace compounds on Ru-based catalysts, *J. Phys. Chem. C*, **2015**, *119*, 6075-6085.
3. B. Murphy, M. Davis, B. Xu, The effect of adsorbed molecule gas-phase deprotonation enthalpy on ion exchanged in sodium exchanged zeolites: an *in-situ* FTIR investigation, *Top. Catal.*, **2015**, *58*, 393-404.
4. J. Zheng, Z. Zhuang, B. Xu, Y. Yan, Correlating hydrogen oxidation/evolution reaction activity with the minority weak hydrogen-binding sites on Ir/C catalysts, **2015**, *under review*.

**Development and Applications of Quantitative and In situ Environmental Electron Microscopy to Structural Characterization of Supported Nanoparticles**

H. Ayoola<sup>1</sup>, C.S. Bonifacio<sup>1</sup>, M. France<sup>1</sup>, S.D. House<sup>1</sup>, L. Li<sup>1,2</sup>, Q. Zhu<sup>1</sup>, J.C. Yang<sup>1</sup>, S. Carencio<sup>3</sup>, C.H. Wu<sup>4</sup>, H. Bluhm<sup>3</sup>, J. J. Kas<sup>5</sup>, F.D. Vila<sup>5</sup>, J.J. Rehr<sup>5</sup>, K. Kislinger<sup>6</sup>, D. Su<sup>6</sup>, H.L. Xin<sup>6</sup>, E.A. Stach<sup>6</sup>, R. Henry<sup>7</sup>, C.T. Schamp<sup>7</sup>, Y. Chen<sup>8</sup>, R. Jin<sup>8</sup>, A.I. Frenkel<sup>9</sup>, R.G. Nuzzo<sup>10</sup>

<sup>1</sup>Dept. of Chem. and Petrol. Eng., Univ. of Pittsburgh, Pittsburgh, <sup>2</sup>RJ Lee Group, Monroeville, <sup>3</sup>Chem. Sci. Div., Lawrence Berkeley Natl. Lab., <sup>4</sup>Dept. of Chemistry, Univ. of California, Berkeley, <sup>5</sup>Dept. of Physics, Univ. of Washington, Seattle, <sup>6</sup>Center for Functional Nanomater., Brookhaven Natl. Lab., <sup>7</sup>Hitachi High Technologies America, Inc., Dallas, <sup>8</sup>Dept. of Chemistry, Carnegie Mellon Univ., Pittsburgh, <sup>9</sup>Dept. of Physics, Yeshiva Univ., New York, <sup>10</sup>Dept. of Chemistry, Univ. of Illinois Urbana-Champaign, Urbana

**Presentation Abstract**

Transmission electron microscopy (TEM) has proven to be a powerful tool to measure composition, chemistry and internal structure at the nanoscale and below. The three transformative developments in electron microscopy are (1) the emergence of aberration-corrected lenses that enable unprecedented spatial and spectral resolution; (2) the rapid advances in *in situ* capabilities for observing dynamic phenomena, especially under environmental conditions; and (3) quantitative electron microscopy. In this presentation, we will provide current examples of developments and applications of advanced TEM to characterizing supported nanoparticles. For example, we determined the environmental range of structural stability of bimetallic core-shell nanoparticles using ETEM and ambient pressure X-ray photoelectron spectroscopy (XPS); our results show that the Ni-Co core-shell reconfiguration is temperature-dependent and occurs in a stepwise process of surface oxide removal and metal segregation. As another example, we are determining the structure of  $\gamma$ -Al<sub>2</sub>O<sub>3</sub> by combining theoretical simulations of the electron energy-loss spectroscopy (EELS) using FEFF with experimental EELS data from a thin film of single crystal  $\gamma$ -Al<sub>2</sub>O<sub>3</sub>, synthesized through oxidation of (110)NiAl, to distinguish between different atomic structural models of  $\gamma$ -Al<sub>2</sub>O<sub>3</sub>.  $\gamma$ -Al<sub>2</sub>O<sub>3</sub> is arguably the most important heterogeneous catalyst material, yet still vaguely described as a defective spinel structure. We are also developing a quantitative Z-contrast scanning TEM (STEM) method where the absolute intensity of the Z-contrast image of the supported nanoparticle gives the number of atoms in it, providing 3-dimensional information. The goal of this project is to advance quantitative STEM such that the 3-dimensional arrangement of atoms in a nanoparticle is determinable from a single 2-D snapshot.

**Grant Number: DE FG02-03ER15476**

## Yolk-Shell Catalysts for Regular and Photo Catalysis

Yoon Jae Lee, Ilkeun Lee, Kerry M. Hanson, Yadong Yin, Christopher J. Bardeen  
and Francisco Zaera\*

Department of Chemistry, University of California, Riverside, California 92521, USA

Email: zaera@ucr.edu

### Presentation Abstract

Au@Void@TiO<sub>2</sub> yolk-shell nanostructures have been evaluated for use as catalysts in hydrogen photoproduction and for cryogenic oxidation catalysis. In terms of the production of hydrogen from water, the nanostructures have been used to investigate the role of the metal in this type of metal-semiconductor catalyst. Our results question the well-accepted explanation of the role of the metal as an electron trap after the absorption of photons and the generation of electron-hole pairs in the semiconductor, and has led us to propose an alternative pathway that requires the metal to act as a catalyst for the recombination of the hydrogen atoms made via the reduction of protons on the surface of the semiconductor instead. In terms of the ease with which catalysts made out of gold nanoparticles dispersed on titania supports oxidize carbon monoxide to carbon dioxide, we report on a unique gold/titania-based catalyst that, in addition to room-temperature catalysis similar to that seen by others, displays a second active regime at much lower temperatures, as low as 120 K. We show that this new catalytic regime follows a mechanism different to that operative at room temperature, and involves at least three titania-adsorbed CO species and a synergy between the CO and O<sub>2</sub> uptakes on the surface. New titanate sites, formed upon treatment of regular Au/TiO<sub>2</sub> catalysts with NaOH, appear to be responsible for the opening of this new reaction channel. Finally, we are presently investigating the surprising large changes in plasmon resonance wavelength that we observe in the gold nanoparticles of the Au@Void@TiO<sub>2</sub> nanostructures as a function of preparation details.

**DE-FG02-09ER16096: SISGR - Design and Characterization of Novel  
Photocatalysts With Core-Shell Nanostructures**

PIs: Francisco Zaera (PI), Christopher J. Bardeen (Co-PI), Yadong Yin (Co-PI)

Post-docs: Ilkeun Lee, Ji Bong Joo, Yoon Jae Lee, Kerry M. Hanson

Graduate Students: Robert Dillon, Qiao Zhang, Michael Dahl, Zhenda Lu, James Goebel

**RECENT PROGRESS**

Our project involves both the development of synthetic strategies for the making of new nanostructures, including metal-supporting nanorods and core-shell and yolk-shell nanoarchitectures, and the use of those, together with more conventional samples, to probe their photophysical behavior and their catalytic and photocatalytic performance.

*1. Synthesis.*

We continue to test the details of our synthesis of metal/TiO<sub>2</sub> core-shell and yolk-shell catalysts and to develop new strategies for the making of new nanostructures. For instance, we have developed a novel resin-protected calcination process for preparing hollow TiO<sub>2</sub> nanoshells with controllable crystallinity and phase. This method involves coating a template core with TiO<sub>2</sub> and then a protection layer through sol-gel processes and then crystallization of the TiO<sub>2</sub> shell by calcination. Through a systematic study on the crystallization behavior of the TiO<sub>2</sub> hollow shells with variation in core template and outer protection layer, we find that the grain growth and phase transformation of TiO<sub>2</sub> is determined by several parameters such as the protection material, core composition, and calcination conditions. In particular, the use of a crosslinked polymer as the protection layer for calcination, enables the production of TiO<sub>2</sub> shells with high crystallinity and controllable anatase-rutile mixed phases, which show significantly enhanced photocatalytic activity compared to those produced by SiO<sub>2</sub>-protected calcination. The photocatalytic activity could be further improved by improving the water dispersity of TiO<sub>2</sub> shells through base treatment. With the ease of achieving photocatalytic activity comparable to commercial Degussa-P25 TiO<sub>2</sub>, it is expected that the TiO<sub>2</sub> shells with controllable crystallinity

and phase could be further engineered by incorporating more active components for producing highly active composite photocatalysts.

We have also reported a novel photoreversible color switching system based on the photocatalytic activity of TiO<sub>2</sub> nanocrystals and the redox-driven color switching property of methylene blue (MB). This system rapidly changes from blue to colorless under UV irradiation and recovers its original blue color under visible light irradiation. We have identified four major competing reactions that contribute to the photoreversible switching, among which two are dominant: the decoloration process is mainly driven by the reduction of MB to leuco MB by photogenerated electrons from TiO<sub>2</sub> nanocrystals under UV irradiation, and the recoloration process operates by the TiO<sub>2</sub>-induced self-catalyzed oxidation of LMB under visible irradiation. Compared with the conventional color switching systems based on photoisomerization of chromophores, our system has not only low toxicity but also significantly improved switching rate and cycling performance. It is envisioned that this photoreversible system may promise unique opportunities for many light-driven actuating or color switching applications.

Nanostructured hybrid shells of r-GO/AuNP/m-TiO<sub>2</sub> have been synthesized using SiO<sub>2</sub> spheres as templates, followed by graphene oxide (GO) and Au nanoparticle (AuNP) deposition and TiO<sub>2</sub> coating, and then post-treatments of template removal and calcination. Evaluation of their photocatalytic activity by degradation of Rhodamine B (RhB) under the irradiation of UV, visible light, and simulated daylight demonstrated the superior photocatalytic performance of the sandwich-like hollow hybrid shells, which could be attributed to the porous nature of the hybrid shells and the enhanced charge separation and visible-light absorption of r-GO and AuNPs. Finally, colloidal barium-doped TiO<sub>2</sub> nanocrystals have been developed that enable the highly reversible light-responsive color switching of redox dyes with excellent cycling performance and high switching rates. Oxygen vacancies resulting from the Ba doping serve as effective sacrificial electron donors (SEDs) to scavenge the holes photogenerated in TiO<sub>2</sub> nanocrystals under UV irradiation and subsequently promote the reduction of methylene blue to its colorless leuco form. Effective color switching can therefore be realized without relying on external SEDs, thus greatly increasing the number of switching cycles.

## 2. Catalysis.

In terms of catalysis, this past year we have extended our work on the use of Au@Void@TiO<sub>2</sub> nanostructures for cryogenic temperature reactions. As we have reported before, the basic synthesis of those structures involves the sequential deposition of a sacrificial silica layer and a titania shell around well-defined gold nanoparticles followed by removal of the silica via NaOH etching. The resulting catalyst contains an amorphous titania shell with sodium titanate and silicon impurities that proved critical for the cryogenic activity; removal of those via HCl treatment kills most of the catalytic conversion. We have found that oxidation of carbon monoxide is possible with this Au@Void@TiO<sub>2</sub> catalyst at temperatures as low as 120 K, by a mechanism different than the one operative at room temperature that involves a weakly-adsorbed CO species with a C–O stretching frequency of 2162 cm<sup>-1</sup>, possibly at Au-TiO<sub>2</sub> interfacial sites.

In photocatalysis, it is well known that metals such as platinum or gold enhance semiconductor photoactivity, in particular in H<sub>2</sub> production. However, we have found that the commonly accepted explanation for this effect, that the excited electrons produced by absorption of light are trapped by the metal before they have the opportunity to recombine with their corresponding holes and return to the ground electronic state (left panel of Figure 1), does not explain a number of observations from our experiments, including time-dependent fluorescence measurement, evidence of O<sub>2</sub> production with titania alone if reducible ions such as Ce<sup>4+</sup>, Ag<sup>+</sup>, or IO<sub>3</sub><sup>-</sup> are

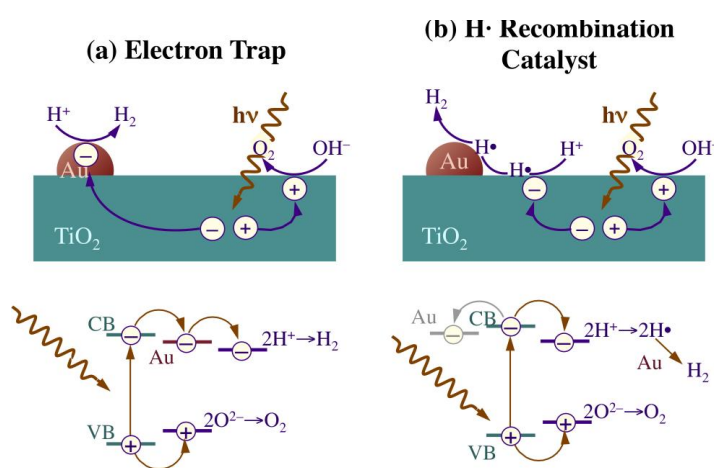


**Figure 1**

added to the water phase, and the observation of photocatalytic activity with NiO/titania catalysts but not with C/titania samples. Instead, an alternative mechanism is advanced where the reduced atomic hydrogen then migrates to the metal and recombines to yield the final molecular hydrogen product (Figure 1, right panel).

### Publications Acknowledging this Grant in 2014-2015

1. Wang, W.; Xie, N.; He, L. and Yin, Y. Photocatalytic Color Switching of Redox Dyes for Ink-Free Light-Printable Rewritable Paper, *Nat. Commun.* **2014**, *5*, 5779.
2. Moon, G. D. Joo, J. B., Lee, I. and Yin, Y. Decoration of Size-tunable CuO Nanodots on TiO<sub>2</sub> Nanocrystals for Noble Metal-free Photocatalytic H<sub>2</sub> Production, *Nanoscale*, **2014**, *6*, 12002-12008.
3. Dahl, M.; Liu, Y.; and Yin, Y. Composite Titanium Dioxide Nanomaterials, *Chem. Rev.* **2014**, *114*, 9853–9889.
4. Wang, W.; Ye, M.; He, L. and Yin, Y. Nanocrystalline TiO<sub>2</sub>-Catalyzed Photoreversible Color Switching, *Nano Lett.*, **2014**, *14*, 1681–1686.
5. Ding, D.; Liu, K.; He, S.; Gao, C. and Yin, Y. Ligand-Exchange Assisted Formation of Au/TiO<sub>2</sub> Schottky Contact for Visible-Light Photocatalysis, *Nano Lett.* **2014**, *13*, 5698–5702.
6. Zhang, T.; Zhao, H.; He, S.; Liu, K.; Liu, H.; Yin, Y. and Gao, C. Unconventional Route to Encapsulated Ultra-Small Gold Nanoparticles for High-Temperature Catalysis, *ACS Nano*, **2014**, *8*, 7297–7304.
7. Joo, J. B.; Dillon, R.; Lee, I.; Yin, Y.; Bardeen C. J. and Zaera, F. Promotion of atomic hydrogen recombination as an alternative to electron trapping for the role of metals in the photocatalytic production of H<sub>2</sub>, *Proc. Natl. Acad. Sci. U.S.A.*, **2014**, *111*, 7942-7947.
8. Zhang, Q.; Lee, I.; Joo, J. B.; Zaera, F.; Yin, Y. Core–Shell Nanostructured Catalysts. *Acc. Chem. Res.* **2013**, *46*, 1816-1824.

9. Lee, I.; Zaera, F. Catalytic Oxidation of Carbon Monoxide at Cryogenic Temperatures. *J. Catal.* **2014**, *319*, 155-162.
10. Zaera, F. New Advances in the Use of Infrared Absorption Spectroscopy for the Characterization of Heterogeneous Catalytic Reactions. *Chem. Soc. Rev.* **2014**, *43*, 7624 - 7663.
11. Ding, D.; Liu, K.; He, S.; Gao, C.; Yin, Y. Ligand-Exchange Assisted Formation of Au/TiO<sub>2</sub> Schottky Contact for Visible-Light Photocatalysis. *Nano Lett.* **2014**, *14*, 6731-6736.
12. Wang, M.; Han, J.; Xiong, H.; Guo, R.; Yin, Y. Nanostructured Hybrid Shells of R-Go/Aunp/M-TiO<sub>2</sub> as Highly Active Photocatalysts. *ACS Applied Materials & Interfaces* **2015**, *7*, 6909-6918.
13. Goebel, J.; Joo, J. B.; Dahl, M. and Yin, Y. Synthesis of Tailored Au@TiO<sub>2</sub> Core-Shell Nanoparticles for Photocatalytic Reforming of Ethanol, *Catal. Today*, **2014**, *225*, 90-95. Wang, M.; Han, J.; Xiong, H.; Guo, R.; Yin, Y. Nanostructured Hybrid Shells of R-Go/Aunp/M-TiO<sub>2</sub> as Highly Active Photocatalysts. *ACS Applied Materials & Interfaces* **2015**, *7*, 6909-6918.
14. Liu, H.; Joo, J. B.; Dahl, M.; Fu, L.; Zeng, Z.; Yin, Y. Crystallinity Control of TiO<sub>2</sub> Hollow Shells through Resin-Protected Calcination for Enhanced Photocatalytic Activity. *Energy Environm. Sci.* **2015**, *8*, 286-296.
15. Wang, W.; Ye, Y.; Feng, J.; Chi, M.; Guo, J.; Yin, Y. Enhanced Photoreversible Color Switching of Redox Dyes Catalyzed by Barium-Doped TiO<sub>2</sub> Nanocrystals. *Angew. Chem., Int. Ed.* **2015**, *54*, 1321-1326.

16. Lv, L.; Lu, Q.; Ning, Y.; Lu, Z.; Wang, X.; Lou, Z.; Tang, A.; Hu, Y.; Teng, F.; Yin, Y. and Hou, Y. Self-assembled TiO<sub>2</sub> Nanorods as Electron Extraction Layer for High Performance Inverted Polymer Solar Cells, *Chem. Mater.* **2015**, *27*, 44–52.

## FWP: ERKCC96

## Fundamentals of Catalysis and Chemical Transformations

**PIs:** Steven H. Overbury, Sheng Dai, Edward W. Hagaman, Michelle K. Kidder, Daniel A. Lutterman, David R. Mullins, Aditya (Ashi) Savara, Zili Wu

**Postdoc(s):** Peter Albrecht, Lance W. Gill, Amanda K.P. Mann, Zhenan Qiao, Li Zhang

**Collaborators:** Larry F. Allard, Ariana Beste, Huiyuan Zhu, Ken Herwig

**Student(s):** Andrew Binder

**Affiliations(s):** Oak Ridge National Laboratory

## RECENT PROGRESS

The principal goal of this program is to understand the role that atomic surface structure plays in controlling selectivity in catalysis at oxide surfaces. We have focused upon  $\text{CeO}_2$  as a catalytic oxide because of its reducibility that enables redox pathways and the fact that its bulk structure can accommodate a high oxygen deficit without large scale change in the bulk structure. We have used two approaches to meet this goal. In the first approach, we use highly oriented films with (100) and (111) orientation and explored surface chemistry within a UHV environment. In the second approach, we have used highly oriented nanoparticles, (cubes, rods and octahedra that terminate in specific crystallographic orientations) and explored their catalytic chemistry within a reactor environment. The combination of the two approaches and comparison of the surface chemistry on the different surfaces led to a new understanding of the structure-function relationships in oxide catalysis.

*Acetic acid adsorption on  $\text{CeO}_2(111)$ :* We have explored reaction pathways for C1 and C2 oxygenates reacting at flat surfaces and  $\text{CeO}_2$  nanoparticles with well-defined crystallographic terminations. To explore carboxylate function and ketonization reactions we have now studied adsorption and transformations of acetic acid adsorbed upon a model  $\text{CeO}_2(111)$  surface. A combination of ultra-high vacuum based methods was used including TPD, sXPS, NEXAFS and RAIRS, together with DFT calculations.[Calaza, 2015] Near 175 K, acetic acid adsorbs to form a mix of molecular and deprotonated acetic acid. Acetic acid desorbs at low temperature along with water which is produced from surface reactions. The water production is accompanied by reduction of the  $\text{CeO}_2$  surface. The resulting oxygen vacancies form strong adsorption sites that trap acetate.

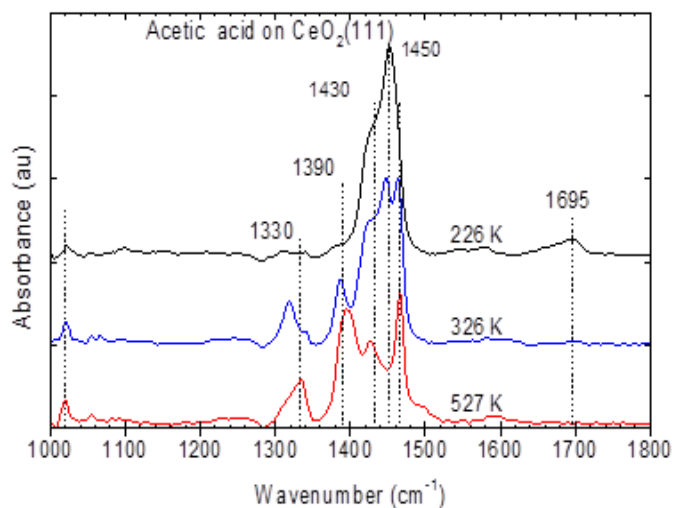


**Fig. 1.** Evolution of the reflection adsorption infrared spectroscopy (RAIRS) spectrum as a function of temperature for acetic acid adsorbed on  $\text{CeO}_2(111)$  surface.

From comparison of RAIRS measurements (**Fig. 1**) with modes computed by DFT, it is concluded that adsorbate states are best described by a mixture of bridge bonded  $\mu$ -acetate and acetate bonded at an oxygen vacancy (acetate/ $V_o$ ), and a small amount of the enolate of acetaldehyde, observed primarily on the more reduced surfaces. At temperatures near 500-600 K, a mixture of acetic acid, ketene, acetylene and acetone competitively desorbs. Acetate/ $V_o$  is the precursor to ketene and to acetylene, and its reaction with  $\mu$ -acetate leads to acetone. UHV conditions favor the unimolecular product (ketene) over the coupling product (acetone) during TPD. At higher temperature, further decomposition to form CO and  $CO_2$  is observed. The distribution of desorption products is strongly dependent upon the extent of reduction of the surface prior to adsorption. Increased reduction increases the ratio of  $H_2:H_2O$  and the ratio of  $CO:CO_2$ , and favors formation of acetaldehyde compared to acetone or ketene. It is suggested that in a catalytic reactor, the selectivity for acetone by ketonization of acetic acid should be sensitive to co-fed reducing or oxidizing gases in the reactor stream.

*Comparison of low and high surface area catalysts:* A motivating factor for the combination of both reactor based studies of faceted nanoparticles and UHV based studies of flat surfaces is to bridge the

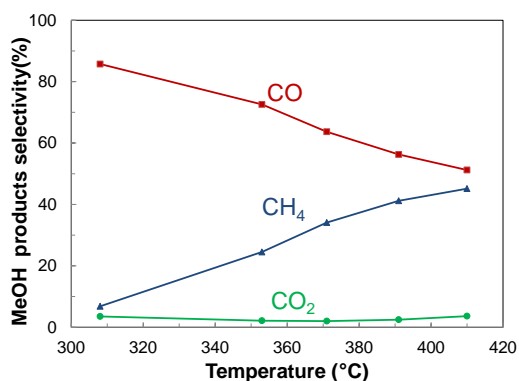


**Fig. 2.** Reaction selectivity for methanol decomposition reaction over meso structured  $CeO_2$  catalyst.

pressure gap between these two types of experiments on surfaces of comparable atomic structure. We have recently focused on methanol reactions as a model probe reaction for exploring this gap. Previously UHV based methanol TPD has shown variation in the product distribution between  $CeO_2(100)$  and  $CeO_2(111)$ . [Mullins, 2013b] When fully oxidized the (111) surface is relatively unreactive, leading to small amounts of formaldehyde but mostly recombinative methanol desorption. The (100) surface is more reactive, leading to formaldehyde and more aggressive dehydrogenation to CO. Pre-reduction of the surfaces leads to enhanced dehydrogenation which increases the CO product at the expense of formaldehyde. No methane is observed desorbing from any of these surfaces. Reactor based

TPD studies under inert gas flow from the methanol exposed (100) faceted cubes and (111) faceted octahedra indicate primarily CO as desorption product with only a minor amount of formaldehyde observed from the cubes, again with no evidence of methane desorption. But, steady state methanol decomposition reaction from high surface area mesostructured  $CeO_2$  indicate that although CO is the major product, substantial amounts of methane are also observed at higher temperature and conversion (**Fig. 2**). The partial dehydrogenation product, formaldehyde is not observed. The results suggest that the absence of readsorption in UHV environment vs multiple readsorption in a reactor environment are responsible for the different product selectivity.

*Bridging the pressure gap with ambient pressure XPS:* To further explore the effects of the pressure gap, we examined methanol adsorption as a function of pressure using ambient pressure XPS. Measurements at Beamline X1A1 at the National Synchrotron Light Source were carried out at  $10^{-5}$  torr and 0.1 torr to determine the surface species on  $CeO_2(100)$  when exposed to methanol, methanol plus oxygen, CO or  $H_2$ . In each case, the surface was initially fully oxidized. Changes in the Ce oxidation state, if any, were also monitored under reaction conditions. When  $CeO_2(100)$  was exposed to a mixture of methanol and  $O_2$  at a

nominal pressure of  $10^{-5}$  torr, the C 1s spectra indicated that the surface was primarily covered with methoxy accompanied by small amounts of formate and carbonate (**Fig. 3a**). As the temperature increased, the surface species decreased indicating that all of the C-containing species were being oxidized from the surface. There was never any indication of C build-up as occurred in the absence of  $O_2$  (not shown). When the pressure was increased to nominally 0.1 torr (**Fig. 3b**), the dominant surface species was formate. Further, the surface was virtually clean at 450 °C whereas a significant amount of methoxy and carbonate remained at 450 °C at the lower pressure. The valence band spectra (not shown) indicated that the surface remained fully oxidized at 0.1 torr. However, a small degree of reduction was evident when the reaction occurred at  $10^{-5}$  torr. The small degree of Ce reduction and the presence of less oxidized surface species at  $10^{-5}$  torr suggest that the reaction is limited by the availability of surface O. This occurs even though there is a greater relative amount of  $O_2$  at the lower pressure (5:1) compared to the higher pressure (2:1). Exposure of  $CeO_2(100)$  to CO and  $H_2$  showed that both gases were effective in reducing the Ce, and the measured extent of reduction increased as the pressure increased. CO produced a carbonate on the surface, whose coverage increased with temperature and pressure. When the CO was pumped away at 500 °C, the carbonate disappeared. These experiments demonstrate that there is a significant dependence on pressure in the reactivity methanol, CO and  $H_2$  on the  $CeO_2(100)$  surface. The build-up of C in the absence of  $O_2$ , the degree of Ce reduction at different  $O_2$  pressures, and the presence of more highly oxidized surface species at higher  $O_2$  pressures suggest that the oxidation of methanol is limited by the reaction and re-oxidation of lattice O on the surface. CO and  $H_2$  both reduce  $CeO_2(100)$  at elevated temperatures and pressures whereas they don't interact strongly with the surface at low exposures.

*Probing acid-base sites on  $CeO_2$ :* In addition to their well-known redox character, the acid-base property is another interesting but unresolved aspect of ceria-based catalysts. Reaction studies on the faceted nanoparticles suggested that the structural differences were related to structure induced variation in the anion base strength and cation acid strength of the (111) and (100) faces expressed by the octahedra and cubes. [Mann, 2014] To further explore this effect of surface structure on the acid-base property of ceria, the nature, type, strength and amount of acid and base sites on these ceria nanoshapes were investigated via in situ IR spectroscopy combined with various probe molecules. [Wu 2015] Pyridine adsorption shows the presence of Lewis acid sites (Ce cations) on the ceria nanoshapes. (**Fig. 4**) These Lewis acid sites are relatively weak and similar in strength among the three nanoshapes according to the interactions with both pyridine and acetonitrile. Both Brønsted (hydroxyl group) and Lewis (surface lattice oxygen) base sites are present on the ceria nanoshapes as probed by  $CO_2$  adsorption.  $CO_2$  and chloroform

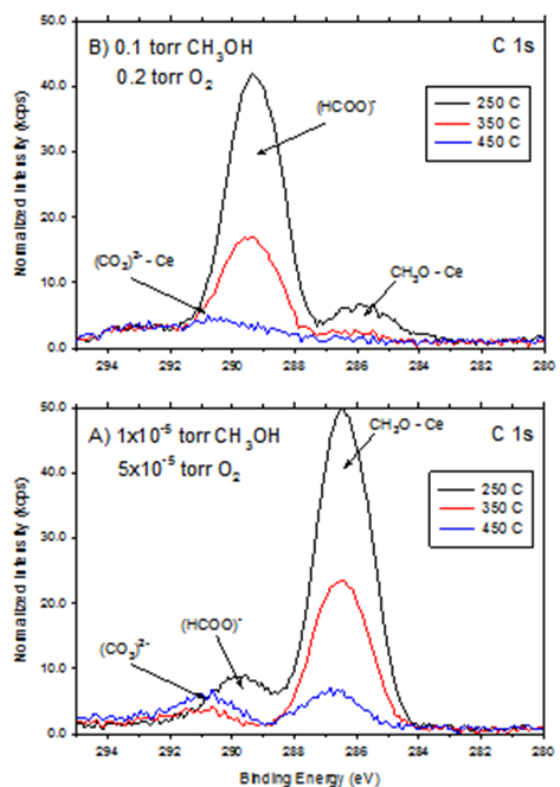


**Fig. 3.** C 1s photoemission spectra of  $CeO_2(100)$  immersed in A)  $1 \times 10^{-5}$  torr  $CH_3OH + 5 \times 10^{-5}$  torr  $O_2$  and B) 0.1 torr  $CH_3OH + 0.2$  torr  $O_2$  at the temperatures indicated.

adsorption indicate that the strength and amount of the Lewis base sites are shape dependent: rods > cubes > octahedra. The weak and strong surface dependence of the acid and base sites, respectively, are a result of both the surface structure dependent coordination unsaturation status of the Ce cations and O anions and the amount of defect sites on the three ceria nanoshapes. It was found that the nature of the acid-base sites of ceria can be impacted by impurities, such as Na and P residues that result from their use as structure-directing reagent in the hydrothermal synthesis of the ceria nanocrystals. This observation calls for caution in interpreting the catalytic behavior of nanoshaped ceria where trace impurities may be present.

*NMR studies of surface protons:* Since protons and hydroxyls results from adsorption of alcohols and water and contribute to the catalytic behavior of the oxide surfaces, we have further explored the behavior of protons on the faceted CeO<sub>2</sub> nanoparticles using NMR. <sup>1</sup>H Fast MAS NMR was used to characterize water and hydroxyl species on the (100)-surface dominated cubes. Multiple water resonances representing physisorbed (bulk) water, molecular water, both weakly and strongly hydrogen-bonded to the surface, have been identified. In addition, hydroxyl species (-OH) occur in isolated and in hydrogen-bonded configurations on the surface. <sup>1</sup>H-<sup>1</sup>H dipolar coupling strengths were characterized by MAS spinning side band intensities and T<sub>2</sub> relaxation measurements that assign weak dipolar coupling to all resonances on the surface. Water and hydroxylic species were identified through a combination of hydration and dehydration experiments and by molecular dynamics calculations. Water and Ce-OH species are differentially removed from the surface by heating the cubes in vacuum with loosely bound water largely eliminated by 100 °C and remaining species eliminated by 300 °C. (Fig. 5) Water hydration experiments of dry ceria cube surfaces show that water dissociates upon interaction with the surface to form two types of hydroxyl; those strongly hydrogen-bonded to surface oxygen and those isolated or weakly hydrogen-bonded to the surface, with the former predominating. The dominant ceria -OH resonances are strongly hydrogen-bonded, and their immediate formation from water suggests that the reaction occurs at surface defect sites (oxygen vacancies). Assuming the concentration of strongly hydrogen bonded -OH is a measure of oxygen vacancies, spin counting experiments show that the as much as 30 % of the surface of the nanocubes are occupied by oxygen vacancy sites. The high proportion of surfaces defects is a characteristic feature on nanoparticles. The instantaneous dissociation

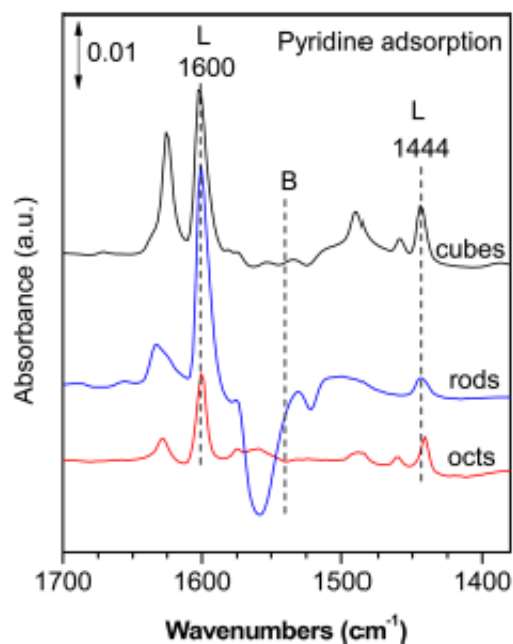


**Fig. 4.** Probing acid sites by pyridine adsorption using IR spectroscopy

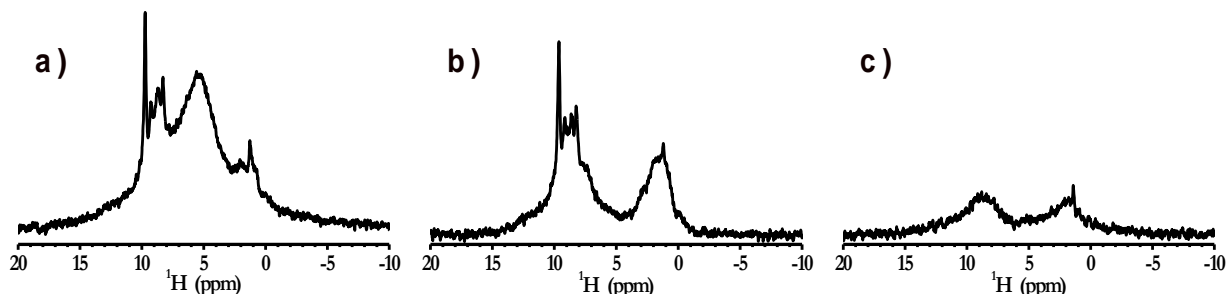


**Fig. 5** <sup>1</sup>H spectra of ceria cubes: (a) as received, RT; (b) evacuation at RT to 100 °C; (c) evacuation at 200 °C. Evacuation at RT for 2 h reduces the physisorbed water resonance to a concentration comparable to Ce-OH. Evacuation between 100 and 200 °C removes trace water and Ce-OH resonances.

of water on ceria cubes, show the dissociation is barrierless, consistent with DFT calculations. Attempts to exchange protic surface species on the water-passivated cube surfaces by washing with D<sub>2</sub>O fail under drastic exchange conditions. The hydroxylated ceria cubes surfaces behave as an hydrophobic surface. We posit that the catalytic properties of the cube surface are attained above a 300 °C temperature threshold, where the catalytic surface sites are accessible.

*Other oxide systems:* We are currently planning to expand our studies of oxide catalysis by working with other systems where well defined faceted crystallites with tunable cationic sites. The goal is to vary the acid-base properties of the surface sites while maintaining consistent structures, which can be achieved using iso-structural perovskites. To this end, we have initiated synthesis of perovskite catalysts. An ionic liquid-mediated synthetic strategy has been established for the preparation of meso-LaMO<sub>3</sub> perovskites

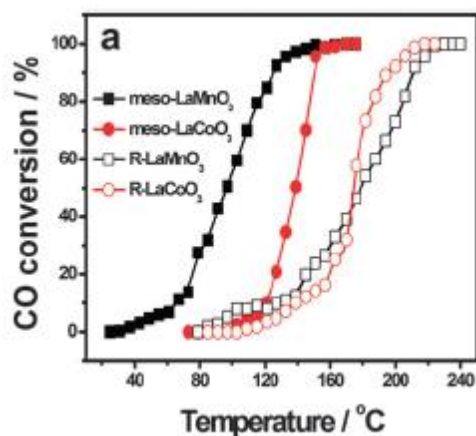


**Fig. 6** Light off curves for CO oxidation by meso-porous and bulk perovskites

(M= Mn, Fe,Co, Ni) with robust crystalline framework. [Lu, 2015] The synthesis takes advantage of the excellent thermal stability of ionic liquids to tightly crosslink the metal-containing species at high temperatures to construct a stable composition for nano-texture engineering. The high flexibility and compatibility of the synthetic strategy enables broad tunability of ionic liquids and metal precursors for the preparation of other kinds of perovskites. Benefiting from the pore structure and La–M ligand assembly, the resulting meso-LaMO<sub>3</sub> exhibits high activity and stability for CO oxidation. (**Fig. 6**) We believe the synthesis strategy may open up new opportunities for preparing functional mesoporous complex mixed oxides of various compositions with novel catalytic properties.

*Probing molecules tethered in oxide pores:* Previous work on intermolecular interactions between molecules, tethered to silica, have indicated the importance of hydrogen bonding and its effect on reactivity. Now we have performed IR measurements to further probe these interactions with the surface and its impact on reactivity. [Kandziolka, 2014] Benzyl phenyl ether was covalently grafted to a mesoporous silica (SBA-15), to create BPEa-SBA-15. The BPEa-SBA-15 was subjected to successive heating cycles up to 600 °C, with in situ monitoring by DRIFTS. It was found that the benzyl moiety coordinates to SBA-15 surface silanol hydroxyl groups via an aromatic–hydroxyl interaction. (**Fig. 7**) This interaction is evident from a red-shift of the aromatic C–H stretches, as well as a red-shift and broadening of the surface hydroxyl O–H stretches, which are features characteristic of a hydrogen bond between the aromatic ring and the surface. These features remain present during heating until ~ 400 °C whereupon the ether linkage of BPEa-SBA-15 is cleaved, accompanied by loss of the benzyl moiety. Aromatic–hydroxyl interactions are thus expected to be present under harsh conditions, and may need to be considered for accurate kinetic and mechanistic models in related chemical systems.

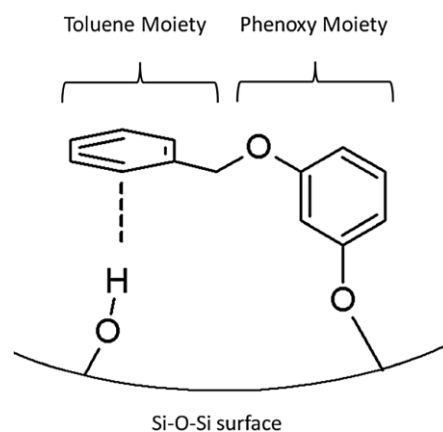


**Fig. 7** Depiction of BPEa-SBA-15, with the toluene moiety interacting

**Controlling reaction environments:** An important synthetic challenge is to hinder the interaction/contact between metal particles to prevent sintering. Similarly, tailoring voids and pores for controlling diffusion is another important goal. We have achieved both goals using a synthetic strategy to create a lab-in-a-shell catalyst that controls the reaction environment. These multifunctional core-shell nanospheres consist of a core of metal clusters and an outer microporous silica shell.[Qiao, 2014] Various metal clusters (e.g., Pd and Pt) were encapsulated and confined in the void space of hollow silica nanospheres containing entrapped polymer dots which act first as complexing agent for the metal ions and additionally as encapsulator for clusters, limiting growth and suppressing the sintering. The Pd clusters encapsulated

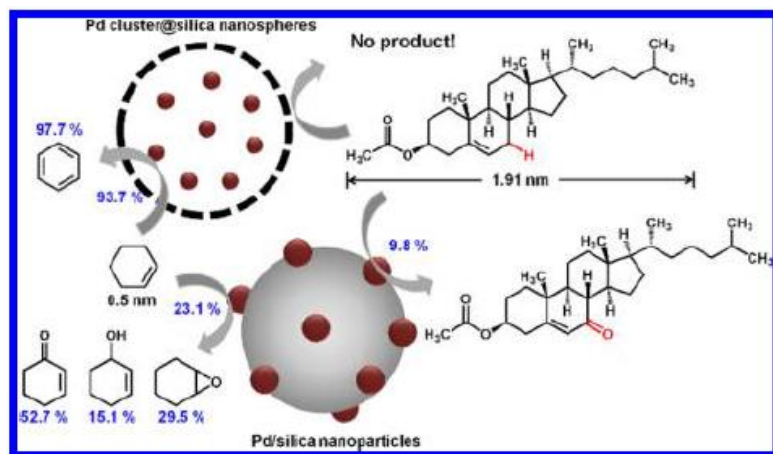


**Fig. 7.** Size-selective catalysis of Pd cluster@silica core-shell nanospheres.

in hybrid core-shell structures exhibit exceptional size-selective catalysis in allylic oxidations of substrates with the same reactive site but different molecular size (cyclohexene ~0.5 nm, cholesterol acetate ~1.91 nm). (Fig. 7) The solvent-free aerobic oxidation of diverse hydrocarbons and alcohols was further carried out to illustrate the benefits of such an architecture in catalysis. High activity, outstanding thermal stability and good recyclability were observed over the core-shell nanocatalyst.

### Publications Acknowledging this Grant in 2012-2015

- Beste, A.; Overbury, S. H., Pathways for Ethanol Dehydrogenation and Dehydration Catalyzed by Ceria (111) and (100) Surfaces. *J. Phys. Chem C* **2015**, *119*, 2447–2455.
- Calaza, F. C.; Chen, T.-L.; Mullins, D. R.; Xu, Y.; Overbury, S. H., Reactivity and reaction intermediates for acetic acid adsorbed on CeO<sub>2</sub>(111), *Catalysis Today* **2015**, 254 doi.org/10.1016/j.cattod.2015.03.033.
- Dong, Y.; Brooks, J. D.; Chen, T.-L.; Mullins, D. R.; Cox, D. F., Methylene migration and coupling on a non-reducible metal oxide: The reaction of dichloromethane on stoichiometric  $\alpha$ -Cr<sub>2</sub>O<sub>3</sub>(0001). *Surf. Sci.* **2015**, *632*, 28-38.
- Lu, H.; Zhang, P.; Qiao, Z.-A.; Zhang, J.; Zhu, H.; Chen, J.; Chen, Y.; Dai, S., Ionic liquid-mediated synthesis of meso-scale porous lanthanum-transition-metal perovskites with high CO oxidation performance. *Chem. Commun.* **2015**, *51*, 5910--5913.
- Mann, A. K. P.; Wu, Z. L.; Overbury, S. H. (2015). The Characterization and Structure-dependent Catalysis of Ceria with Well-defined Facets, in Catalysis by Materials with Well-Defined Structures (edition 1). Z. Wu and S.H. Overbury, Elsevier.
- Mullins, D., The Surface Chemistry of Cerium Oxide, *Surf. Sci. Reports* **2015**, *70*, 42 - 85.
- Wu, Z. L.; Mann, A. K. P.; Li, M. J.; Overbury, S. H., Spectroscopic Investigation of Surface Dependent Acid-base Property of Ceria Nanoshapes. *J. Phys. Chem. C* **2015**, *119*, 7340-7350.
- Wu, Z. L.; Overbury, S. H., *Catalysis by Materials with Well-defined Structures*, **2015**, Elsevier

- Zhang, P.; Li, H.; Veith, G. M.; Dai, S., Soluble Porous Coordination Polymers by Mechanochemistry: From Metal-Containing Films/Membranes to Active Catalysts for Aerobic Oxidation. *Adv. Mater.* **2015**, *27*, 234-239.
- Zhang, P.; Qiao, Z.-A.; Jiang, X.; Veith, G. M.; Dai, S., Nanoporous ionic organic networks: stabilizing and supporting gold nanoparticles for catalysis. *Nano Letters* **2015**, *15*(2), 823-828.
- Albrecht, P. M.; Jiang, D.-e.; Mullins, D. R., CO<sub>2</sub> Adsorption As a Flat-Lying, Tridentate Carbonate on CeO<sub>2</sub>(100). *J. Phys. Chem C* **2014**, *118*, 9042–9050.
- Baggetto, L.; Carroll, K. J.; Hah, H.-Y.; Johnson, C. E.; Mullins, D. R.; Unocic, R. R.; Johnson, J. A.; Meng, Y. S.; Veith, G. M., Probing the Mechanism of Sodium Ion Insertion into Copper Antimony Cu<sub>2</sub>Sb Anodes. *J. Phys. Chem. C* **2014**, *118* 7856.
- Bauer, J. C.; Toops, T. J.; Oyola, Y.; Parks, J. E.; Dai, S.; Overbury, S. H., Catalytic activity and thermal stability of Au-CuO/SiO<sub>2</sub> catalysts for the low temperature oxidation of CO in the presence of propylene and NO. *Catal. Today* **2014**, *231*, 15-21.
- Binder, A. J.; Toops, T.; Parks, J.; Dai, S., CuO-Co<sub>3</sub>O<sub>4</sub>-CeO<sub>2</sub> ternary mixed oxide outperforms PGM catalysts in CO oxidation with high resistance to inhibition by propene. *Science Commun.* **2014**.
- Kandziolka, M. V.; Kidder, M. K.; Gill, L.; Wu, Z.; Savara, A., Aromatic-Hydroxyl Interaction of an alpha-aryl ether Lignin Model-Compound on SBA-15, Present at Pyrolysis Temperatures. *Phys. Chem. Chem. Phys.* **2014**, *16*, 24188-24193.
- Li, G.; Jiang, D.-e.; Kumar, S.; Chen, Y.; Jin, R., Size Dependence of Atomically Precise Gold Nanoclusters in Chemoselective Hydrogenation and Active Site Structure. *ACS Catal.* **2014**, *4*, 2463-2469.
- Li, L.; Chai, S.-H.; Binder, A.; Brown, S.; Veith, G. M.; Dai, S., Catalytic CO Oxidation Over Gold Nanoparticles: Support Modification by Monolayer- and Submonolayer-Dispersed Sb<sub>2</sub>O<sub>3</sub>. *Catal. Lett.* **2014**, *144*, 912.
- Li, L.; Tian, C. C.; Chai, S. H.; Binder, A.; Brown, S.; Veith, G. M.; Dai, S., Gold nanocatalysts supported on heterostructured PbSO<sub>4</sub>-MCF mesoporous materials for CO oxidation. *Catal. Commun.* **2014**, *46*, 234-237.
- Lin, Y. Y.; Wu, Z. L.; Wen, J. G.; Poeppelmeier, K. R.; Marks, L. D., Imaging the Atomic Surface Structures of CeO<sub>2</sub> Nanoparticles. *Nano Lett.* **2014**, *14*(1), 191-196.
- Liu, Z.; Wu, Z.; Peng, X.; Binder, A.; Chai, S.; Dai, S., The Origin of Active Oxygen in a Ternary CuOx/Co<sub>3</sub>O<sub>4</sub>-CeO<sub>2</sub> Catalyst for CO Oxidation, *J Phys.Chem C* **2014**, *118*, 27870-27877.
- Luo, Z.; Nachammai, V.; Zhang, B.; Yan, N.; Leong, D. T.; Jiang, D.-e.; Xie, J., Toward Understanding the Growth Mechanism: Tracing All Stable Intermediate Species from Reduction of Au(I)-Thiolate Complexes to Evolution of Au<sub>25</sub> Nanoclusters, *J. Am. Chem. Soc.* **2014**, *136*(30), 10577-10580.
- Mann, A. K. P.; Wu, Z.; Calaza, F. C.; Overbury, S. H., Adsorption and Reaction of Acetaldehyde on Shape-Controlled CeO<sub>2</sub> Nanocrystals: Elucidation of Structure-function Relationships. *ACS Catal.* **2014**, *4*, 2437–2448.
- Pistner, A. J.; Lutterman, D. A.; Ghidui, M. J.; Walker, E.; Yap, G. P. A.; Rosenthal J., Factors Controlling the Spectroscopic Properties and Supramolecular Chemistry of an Electron Deficient 5,5-Dimethylphlorin Architecture. *J. Phys. Chem. C* **2014**, *118*, 14124-14132.
- Pistner, A. J.; Pupillo, R. C.; Yap, G. P. A.; Lutterman, D. A.; Ma, Y. Z.; Rosenthal, J., Electrochemical, Spectroscopic, and O-1(2) Sensitization Characteristics of 10,10-Dimethylbiladiene Complexes of Zinc and Copper. *J. Phys. Chem. A* **2014**, *118*, 10639-10648.
- Qiao, Z.-A.; Zhang, P.; Chai, S.-H.; Chi, M.; Veith, G.; Gallego, N.; Kidder, M.; Dai, S., Lab-in-a-Shell: Encapsulating Metal Clusters for Size Sieving Catalysis. *J. Am. Chem. Soc.* **2014**, *136* (32), 11260-11263.
- Ren, Y.; Ma, Z.; Dai, S., Nanosize Control on Porous beta-MnO<sub>2</sub> and Their Catalytic Activity in CO Oxidation and N<sub>2</sub>O Decomposition. *Mater.* **2014**, *7*, 3547.

- Savara, A., Vibrational spectra of CO adsorbed on oxide thin films: A tool to probe the surface defects and phase changes of oxide thin films. *J. Vac. Sci. Technol. A* **2014**, 32(2), PAGE NUMBER?.
- Savara, A.; Chan-Thaw, C. E.; Rossetti, I.; Villa, A.; Prati, L., Benzyl Alcohol Oxidation on Carbon Supported Pd Nanoparticles: Elucidating the Reaction Mechanism, *ChemCatChem* **2014**, 6, 3464-3473.
- Savara, A.; Weitz, E., Elucidation of Intermediates and Mechanisms in Heterogeneous Catalysis Using Infrared Spectroscopy. *Ann. Rev. Phys. Chem* **2014**, 65, 249-273.
- Tian, C. C.; Zhu, X.; Chai, S. H.; Wu, Z. L.; Binder, A.; Brown, S.; Li, L.; Luo, H. M.; Guo, Y. L.; Dai, S., Three-Phase Catalytic System of H<sub>2</sub>O, Ionic Liquid, and VOPO<sub>4</sub>-SiO<sub>2</sub> Solid Acid for Conversion of Fructose to 5-Hydroxymethylfurfural. *ChemSuschem* **2014**, 7, 1703-1709.
- Wu, Z.; Jiang, D.-e.; Mann, A. K. P.; Mullins, D. R.; Qiao, Z.-A.; Allard, L. F.; Zeng, C.; Jin, R.; Overbury, S. H., Thiolate Ligands as a Double-Edged Sword for CO Oxidation on CeO<sub>2</sub> Supported Au<sub>25</sub>(SCH<sub>2</sub>CH<sub>2</sub>Ph)<sub>18</sub> Nanoclusters, *J. Amer. Chem. Soc.* **2014**, 136(16), 6111-6122.
- Wu, Z. L., Multi-wavelength Raman spectroscopy study of supported vanadia catalysts: Structure identification and quantification. *Chin. J. Catal.* **2014**, 35, 1591-1608.
- Wu, Z. L.; Overbury, S. H., Infrared Spectroscopic insights into the role of supports in heterogeneous Au catalysis, *Heterogeneous Gold Catal. Catal.* **2014**, 512-532.
- Yu, Y.; Luo, Z.; Chevrier, D. M.; Leong, D. T.; Zhang, P.; Jiang, D.-e.; Xie, J., Identification of a Highly Luminescent Au<sub>22</sub>(SG)<sub>18</sub> Nanocluster, *J. Amer. Chem. Soc.* **2014**, 136(4), 1246-1249.
- Zhang, P.; Qiao, Z.-A.; Zhang, Z.; Wan, S.; Dai, S., Mesoporous graphene-like carbon sheet: high-power supercapacitor and outstanding catalyst support. *J. Matls Chem A* **2014**, 2(31), 12262-12269.
- Zhu, X.; Mahurin, S. M.; An, S.-H.; Chi-Linh, D.-T.; Tian, C.; Li, Y.; Gill, L. W.; Hagaman, E. W.; Bian, Z.; Zhou, J.-H.; Hu, J.; Liu, H.; Dai, S., Efficient CO<sub>2</sub> capture by a task-specific porous organic polymer bifunctionalized with carbazole and triazine groups. *Chem. Comm.* **2014**, 50(59), 7933-7936.
- Albrecht, P. M.; Mullins, D. R., Adsorption and Reaction of Methanol over CeOx(100) Thin Films, *Langmuir* **2013**, 29 4559-4567.
- Bauer, J. C.; Mullins, D. R.; Oyola, Y.; Overbury, S. H.; Dai, S., Structure Activity Relationships of Silica Supported AuCu and AuCuPd Alloy Catalysts for the Oxidation of CO. *Catal. Lett.* **2013**, 143(9), 926-935.
- Beste, A.; Buchanan, A. C., III, Computational Investigation of the Pyrolysis Product Selectivity for alpha-Hydroxy Phenethyl Phenyl Ether and Phenethyl Phenyl Ether: Analysis of Substituent Effects and Reactant Conformer Selection. *J. Phys. Chem. A* **2013**, 117, 3235-3242.
- Binder, A. J.; Qiao, Z. A.; Veith, G. M.; Dai, S., Deposition-Precipitation and Stabilization of a Silica-Supported Au Catalyst by Surface Modification with Carbon Nitride. *Catal. Lett.* **2013**, 143(12), 1339-1345.
- Galhenage, R. P.; Yan, H.; Tenney, S. A.; Park, N.; Henkelman, G.; Albrecht, P. M.; Mullins, D. R.; Chen, D. A., Understanding the Nucleation and Growth of Metals on TiO<sub>2</sub>: Co compared to Au, Ni and Pt. *J. Phys. Chem. C* **2013**, 117, 7191-7201.
- Ghidiu, M. J.; Pistner, A. J.; Yap, G. P. A.; Lutterman, D. A.; Rosenthal, J., Thermal versus Photochemical Reductive Elimination of Aryl Chlorides from NHC-Gold Complexes. *Organometallics* **2013**, 32(18), 5026-5029.
- Jiang, D.-e.; Overbury, S. H.; Dai, S., On the Structure of Au<sub>15</sub>(SR)<sub>13</sub> and its Implication on the Origin of the Nucleus in Thiolated Gold Nanoclusters. *J. Am. Chem. Soc.* **2013**, 135, 8786-8789.
- Li, M.; Wu, Z.; Overbury, S. H., Surface structure dependence of selective oxidation of ethanol on faceted CeO<sub>2</sub> nanocrystals. *J. Catal.* **2013**, 306, 164-176.

- Liu, Z. G.; Chai, S. H.; Binder, A.; Li, Y. Y.; Ji, L. T.; Dai, S., Influence of calcination temperature on the structure and catalytic performance of CuO<sub>x</sub>-CoO<sub>y</sub>-CeO<sub>2</sub> ternary mixed oxide for CO oxidation. *App. Catal., A* **2013**, *451*, 282-288.
- Moses-DeBusk, M.; Yoon, M.; Allard, L. F.; Mullins, D. R.; Wu, Z. L.; Yang, X. F.; Veith, G.; Stocks, G. M.; Narula, C. K., CO Oxidation on Supported Single Pt Atoms: Experimental and ab Initio Density Functional Studies of CO Interaction with Pt Atom on theta-Al<sub>2</sub>O<sub>3</sub>(010) Surface. *J. Am. Chem. Soc.* **2013**, *135*(34), 12634-12645.
- Mullins, D. R.; Albrecht, P. M., Acetaldehyde Adsorption and Reaction on CeO<sub>2</sub>(100). Thin Films, *J. Phys. Chem. C* **2013a**, *117*(28), 14692-14700.
- Mullins, D. R.; Albrecht, P. M.; Calaza, F. C., Variations in Reactivity on Different Crystallographic Orientations of Cerium Oxide. *Top. Catal.* **2013**, *56*, 1345-1362.
- Pistner, A. J.; Lutterman, D. A.; Ghidui, M. J.; Ma, Y.-Z.; Rosenthal, J., Synthesis, Electrochemistry, and Photophysics of a Family of Phlorin Macrocycles That Display Cooperative Fluoride Binding. *J. Am. Chem. Soc.* **2013**, *135*, 6601-6607.
- Pollock, J. B.; Cook, T. R.; Schneider, G. L.; Lutterman, D. A.; Davies, A. S.; Stang, P. J., Photophysical Properties of Endohedral Amine-Functionalized Bis(phosphine) Pt(II) Complexes as Models for Emissive Metallacycles, *Inorg. Chem* **2013**, *52*(16), 9254-9265.
- Qiao, Z. A.; Wu, Z. L.; Dai, S., Shape-Controlled Ceria-based Nanostructures for Catalysis Applications. *ChemSusChem* **2013**, *6*(10), 1821-1833.
- Ren, Y.; Ma, Z.; Morris, R. E.; Liu, Z.; Jiao, F.; Dai, S.; Bruce, P. G., A solid with a hierarchical tetramodal micro-meso-macro pore size distribution. *Nat. Commun.* **2013**, *4*.
- Tian, C.; Chai, S.-H.; Mullins, D. R.; Zhu, X.; Binder, A.; Guo, Y.; Dai, S., Heterostructured BaSO<sub>4</sub>-SiO<sub>2</sub> mesoporous materials as new supports for gold nanoparticles in low-temperature CO oxidation, *Chem. Comm.* **2013**, *49*, 3464-3466.
- Tian, C. C.; Oyola, Y.; Nelson, K. M.; Chai, S. H.; Zhu, X.; Bauer, J. C.; Janke, C. J.; Brown, S.; Guo, Y. L.; Dai, S., A renewable HSO<sub>3</sub>/H<sub>2</sub>PO<sub>3</sub>-grafted polyethylene fiber catalyst: an efficient heterogeneous catalyst for the synthesis of 5-hydroxymethylfurfural from fructose in water. *RSC Adv* **2013**, *3*, 21242-21246.
- Tian, C. C.; Bao, C. H.; Binder, A.; Zhu, Z. Q.; Hu, B.; Guo, Y. L.; Zhao, B.; Dai, S., An efficient and reusable "hairy" particle acid catalyst for the synthesis of 5-hydroxymethylfurfural from dehydration of fructose in water, *Chem. Commun.* **2013**, *49*, 8668-8670.
- Veith, G. M.; Lupini, A. R.; Baggetto, L.; Browning, J. F.; Keum, J. K.; Villa, A.; Prati, L.; Papandrew, A. B.; Goenaga, G. A.; Mullins, D. R.; Bullock, S. E.; Dudney, N. J., Evidence for the Formation of Nitrogen-Rich Platinum and Palladium Nitride Nanoparticles, *Chem. Mater.* **2013**, *25*(24), 4936-4945.
- Allard, L. F.; Overbury, S. H.; Bigelow, W. C.; Katz, M. B.; Nackashi, D. P.; Damiano, J., Novel MEMS-Based Gas-Cell/Heating Specimen Holder Provides Advanced Imaging Capabilities for In Situ Reaction Studies. *Microsc. Microanal.* **2012**, *18*(4), 656-666.
- Bauer, J. C.; Veith, G. M.; Allard, L. F.; Oyola, Y.; Overbury, S. H.; Dai, S., Silica-Supported Au-CuO<sub>x</sub> Hybrid Nanocrystals as Active and Selective Catalysts for the Formation of Acetaldehyde from the Oxidation of Ethanol. *ACS Catalysis* **2012**, *2*(12), 2537-2546.
- Beste, A.; Buchanan, A. C., III, The Role of Carbon-Carbon Phenyl Migration in the Pyrolysis Mechanism of β-O-4 Lignin Model Compounds: Phenethyl Phenyl Ether and α-Hydroxy Phenethyl Phenyl Ether. *J. Phys. Chem. A* **2012**, *116*, 12242-12248.
- Beste, A.; Buchanan, A. C., III, Kinetic Simulation of the Thermal Degradation of Phenethyl Phenyl Ether, a Model Compound for the β-O-4 Linkage in Lignin, *Chem. Phys. Lett.* **2012**, *550*, 19-24.

- Calaza, F. C.; Xu, Y.; Mullins, D. R.; Overbury, S. H., Oxygen Vacancy-Assisted Coupling and Enolization of Acetaldehyde on CeO<sub>2</sub>(111). *J. Am. Chem. Soc.* **2012**, *134*(43), 18034-18045.
- Fulvio, P. F.; Mayes, R. T.; Bauer, J. C.; Wang, X. Q.; Mahurin, S. M.; Veith, G. M.; Dai, S., "One-pot" synthesis of phosphorylated mesoporous carbon heterogeneous catalysts with tailored surface acidity. *Catal. Today* **2012**, *186*(1), 12-19.
- Hagaman, E. W.; Chen, B. H.; Jiao, J.; Parsons, W., Solid-state O-17 NMR study of benzoic acid adsorption on metal oxide surfaces. *Solid State Nucl. Magn. Reson* **2012**, *41*, 60-67.
- Jiang, D.-e.; Overbury, S. H.; Dai, S., Structures and Energetics of Pt Clusters on TiO<sub>2</sub>: Interplay between Metal–Metal Bonds and Metal–Oxygen Bonds. *J. Phys. Chem. C* **2012**, *116*(41), 21880-21885.
- Kintzel, E. J. J.; Kidder, M. K.; Buchanan, A. C., III; Britt, P. F.; Mamantov, E.; Zamponi, M.; Herwig, K. W., The Dynamics of 1,3-Diphenylpropane Tethered to the Interior Pore Surfaces of MCM-41. *J. Phys. Chem. C* **2012**, *116*, 923.
- Ma, G. C.; Binder, A.; Chi, M. F.; Liu, C.; Jin, R. C.; Jiang, D. E.; Fan, J.; Dai, S., Stabilizing gold clusters by heterostructured transition-metal oxide-mesoporous silica supports for enhanced catalytic activities for CO oxidation. *Chem. Comm.* **2012**, *48*(93), 11413-11415.
- Mullins, D. R.; Albrecht, P. M.; Chen, T.-L.; Calaza, F.; Biegalski, M. D.; Christen, H. M.; Overbury, S. H., Water Dissociation on CeO<sub>2</sub>(100) and CeO<sub>2</sub>(111) Thin Films. *J. Phys. Chem. C* **2012**, *116*, 19419–19428.
- Qian, H. F.; Jiang, D. E.; Li, G.; Gayathri, C.; Das, A.; Gil, R. R.; Jin, R. C., Monoplatinum Doping of Gold Nanoclusters and Catalytic Application. *J. Am. Chem. Soc.* **2012**, *134*(39), 16159-16162.
- Qiao, Z. A.; Huo, Q. S.; Chi, M. F.; Veith, G. M.; Binder, A. J.; Dai, S., A "Ship-In-A-Bottle" Approach to Synthesis of Polymer Dots@Silica or Polymer Dots@Carbon Core-Shell Nanospheres. *Adv. Mater.* **2012**, *24*(45), 6017-6021.
- Singh, J. A.; Overbury, S. H.; Dudney, N. J.; Li, M.; Veith, G. M., Gold Nanoparticles Supported on Carbon Nitride: Influence of Surface Hydroxyls on Low Temperature Carbon Monoxide Oxidation. *ACS Catal.* **2012**, *2*, 1138–1146.
- Tian, C. C.; Chai, S. H.; Zhu, X.; Wu, Z. L.; Binder, A.; Bauer, J. C.; Brown, S.; Chi, M. F.; Veith, G. M.; Guo, Y. L.; Dai, S., In situ growth synthesis of heterostructured LnPO<sub>4</sub>-SiO<sub>2</sub> (Ln = La, Ce, and Eu) mesoporous materials as supports for small gold particles used in catalytic CO oxidation. *J. Mater. Chem.* **2012**, *22*(48), 25227-25235.
- Wu, Z.; Li, M.; Overbury, S. H., Raman Spectroscopic Study of the Speciation of Vanadia Supported on Ceria Nanocrystals with Defined Surface Planes. *ChemCatChem* **2012**, *4*(10), 1653-1661.
- Wu, Z.; Li, M.; Overbury, S. H., On the Structure Dependence of CO Oxidation over CeO<sub>2</sub> Nanocrystals with Well-Defined Surface Planes. *J. Catal.* **2012**, *285*, 61-73.
- Wu, Z.; Schwartz, V.; Li, M.; Rondinone, A.; Overbury, S. H., Support Shape Effect in Metal Oxide Catalysis: Ceria Nanoshapes Supported Vanadia Catalysts for Oxidative Dehydrogenation of Isobutane. *J. Phys. Chem. C* **2012**, *3* 1517–1522.
- Wu, Z. L.; Li, M. J.; Mullins, D. R.; Overbury, S. H., Probing the Surface Sites of CeO<sub>2</sub> Nanocrystals with Well-Defined Surface Planes via Methanol Adsorption and Desorption, *ACS Catal.* **2012**, *2*(11), 2224-2234.
- Yang, X.; Wu, Z.; Moses-Debusk, M.; Mullins, D. R.; Mahurin, S. M.; Geiger, R. M.; Kidder, M. K.; Narula, C. K., Heterometal Incorporation in M-Exchanged Zeolites Enables Low Temperature Catalytic Activity of NO<sub>x</sub> Reduction. *J. Phys. Chem. C* **2012**, *116*, 23322-23331.
- Yunker, J. M. B., A.; Buchanan, I., A. C., Computational Study of Bond Dissociation Enthalpies for Lignin Model Compounds: β-5 Arylcoumaran. *Chem. Phys. Lett* **2012**, *545*, 100-106.

This page is intentionally blank.

# **Additional Abstracts**

This page is intentionally blank.

**Metal Carbide and Bimetallic Alloys as Low-cost and Active Electrocatalysts**

Jingguang Chen, Department of Chemical Engineering,  
Columbia University

**Presentation Abstract**

The electronic and catalytic properties of transition metals can be modified by incorporating carbon atoms to form carbides or by alloying with another metal to produce bimetallic alloys. The metal carbides and bimetallic alloys often demonstrate properties that are distinctively different from those of the pure parent metals. The goal of the current project is to use selected carbides and bimetallic alloys as model systems to unravel the relationship between the electronic/geometric structures and the chemical/catalytic properties to assist the rational design of catalytic materials. Furthermore, it is becoming apparent of the critical needs to identify alternative catalysts that can either replace Platinum (Pt) or substantially reduce the amount of Pt in many catalytic and electrocatalytic applications. During the past year we have focused on the utilization of carbide and bimetallic catalysts for the hydrogen evolution reaction (HER) from water electrolysis in three areas [1-7]: (1) utilization of monolayer precious metal over carbides in acid electrolyte, (2) discovery of non-precious bimetallic catalysts in alkaline environment, and (3) investigation of the effect of common impurities in tap water on the HER activity in both acid and alkaline.

**Grant number: DE-FG02-13ER16381**

**Grant Title: Structure-Property Relationship in Metal Carbides and Bimetallic Alloys**

**Part-time Postdoctoral Fellow:** Dr. Wencho Sheng, Dr. Qi Lu

**Graduate Students:** Yannick Kimmel (graduated in Dec. 2014), Elizabeth Mahoney

**Recent Progress:**

The primary objective of our DOE/BES sponsored research is to use carbide and bimetallic catalysts as model systems to demonstrate the feasibility of tuning the catalytic *activity, selectivity and stability*. Our efforts involve three parallel approaches, with the aim at bridging the “materials gap” and “pressure gap” between fundamental surface science studies and real world catalysis. For example, for the identification of low-cost HER electrocatalysts, we first performed DFT calculations to identify promising carbide or bimetallic surfaces using hydrogen binding energy (HBE) as a descriptor. The DFT-predicted HBE values were verified experimentally on selected single crystal surfaces. The polycrystalline films and porous catalysts of promising materials were then synthesized and characterized. Finally, these materials were tested for HER activity in electrochemical cells. Such combined approaches, all performed

within our own research group, allow direct and fast correlation between theoretical prediction and experimental verification for the discovery of catalysts and electrocatalysts.

As summarized in the publications listed below, the utilization of the three parallel approaches has led to the discovery of intriguing catalytic properties of carbide and bimetallic surfaces and catalysts. During the current funding period we have utilized these combined research approaches to explore the possibility of identifying and predicting carbide and bimetallic combinations with enhanced *activity, selectivity and stability* for several electrochemical reactions, including hydrogen evolution reaction (HER), CO<sub>2</sub> electroreduction, and direct alcohol oxidation. Below we will use two examples to highlight our recent results:

#### **A. Monolayer Precious Metal over TMCs as Low-Cost Electrocatalysts in Acid Electrolyte**

The motivation is to identify alternative electrocatalysts using a combination of theoretical and experimental methods. Fuel cells, electrolyzers, and photoelectrochemical cells are electrochemical devices that are commonly considered as core technologies in a clean energy future. Central to the operation of all of these devices are catalysts, more specifically electrocatalysts, which mediate charge transfer processes between the electrolyte and device electrodes with minimal losses in efficiency. Unfortunately, many state-of-the-art catalysts used in the aforementioned technologies are comprised of expensive Pt-group metals (Pt, Ru, Rh, Ir, and Pd). The high prices and limited supplies of these precious metals create potentially prohibitive barriers to market penetration and scale-up production of devices requiring large catalyst loadings for efficient operation.

To overcome this barrier to large-scale commercialization of the aforementioned electrochemical devices, many approaches have been taken to decrease or eliminate the loading of precious metals that are currently required for efficient operation. One of the commonly pursued approaches is the development of several classes of low-cost non-precious metal electrocatalysts, including multi-metallic and metal/nonmetal materials (oxides, carbides, sulfides, and nitrides). Since the discovery of the “Pt-like” properties of tungsten monocarbide (WC), tungsten carbides (W<sub>x</sub>C) and related transition metal carbides (TMC) have been extensively investigated, although the instability of TMCs has limited their use in many applications. Our efforts in the past year was to focus on the seven stable TMC substrates (WC, Mo<sub>2</sub>C, VC, NbC, TaC, TiC and ZrC) and their potential use as supports for one atomic layer, or monolayer (ML), of Pt for use in electrochemical applications. Although Pt is still utilized, this ML Pt-TMC electrocatalyst structure approaches the lower limit of Pt loading. By using a low cost support material such as TMC, the ML Pt-TMC structure offers great potential to drive down catalyst costs for various clean technology devices.

The limited demonstration of replacing Pt by TMCs is largely due to the fact that their “Pt-like” catalytic properties have only been observed for a limited number of catalytic reaction systems, and in some systems the catalytic activity and stability of TMCs are much lower than the Pt catalysts. Over the past few years our research group has attempted to overcome the shortcomings of pure TMC catalysts by modifying the TMC surface with ML amounts of precious metals, such as Pt and Pd. The hypothesis is that replacement of all but the top ML of bulk Pt catalysts with an electronically similar “Pt-like” TMC core will result in a ML Pt-TMC surface that should have electronic and catalytic properties similar to bulk Pt.

In order to probe the electronic similarities of ML Pt-TMC and bulk Pt catalysts, DFT calculations were used to determine the binding energies of hydrogen binding energy (HBE), which is known to be a descriptor to correlate with the HER activity in acid electrolyte. Parallel

experiments were performed on Pt/TMC surfaces to determine their HER activity and electrochemical stability. As summarized in Figure 1, a volcano type relationship is established between DFT-predicted HBE values and experimentally measured HER activity in acid electrolyte. Such correlation provides a design principle to identify other metal/TMC systems using on the HBE value as the design descriptor.

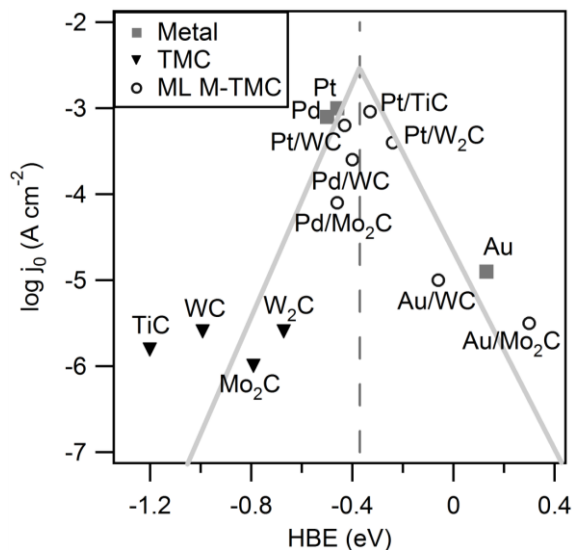


**Figure 2.** HER exchange current density ( $i_0$ ) as a function of DFT-predicted HBE values. (Results published in Kimmel et al., *Journal of Catalysis*, 312 (2014) 216).

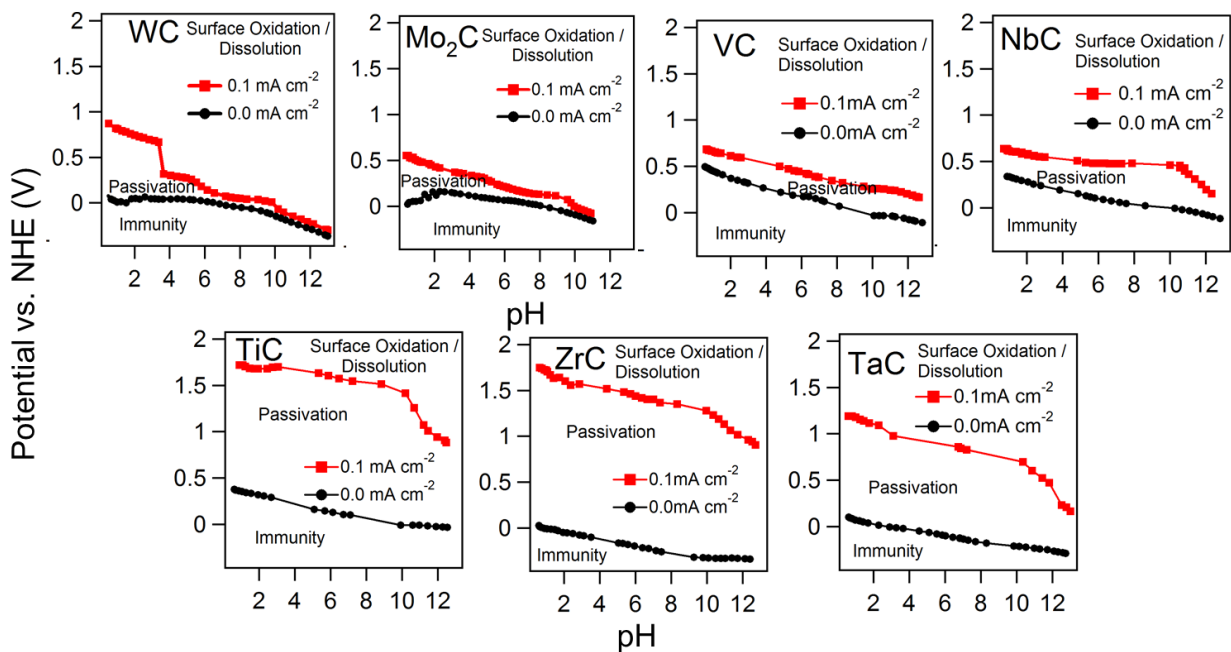


**Figure 3.** Approximate E-pH regions of stability of the seven common TMCs as determined from chronopotentiometric titration measurements in a deaerated  $\text{H}_2\text{SO}_4/\text{NaOH}$  supporting electrolyte at room temperature. (Results published in Kimmel et al., *ACS Catalysis*, 4 (2014) 1558).

We have also explored the electrochemical stability of all common TMC substrates for various potential electrochemical applications. Figure 2 summarizes the approximate E-pH (applied voltage vs. pH) regions of stability for the seven carbides, determined from chronopotentiometric titration measurements: (Region I - Immunity) a region of stability at negative potentials (E), (Region II - Passivation) a region of passivation centered at low pH and moderately oxidizing potentials in which the surface layers of TMC are oxidized into stable  $M_xO_{y(s)}$  surface species that limit further oxidation of the surface, and (Region III - Dissolution) a region of instability at positive potentials and neutral to alkaline pH, in which TMC undergoes successive oxidation and dissolution to form tungstate species. The results shown in Figure 3 should provide a guiding principle on the “stability window” for the utilization of TMC for a variety of electrochemical applications, a research area that has attracted much recent interest from many research groups around the world.

### B. Non-precious Bimetallic Catalysts for HER in Alkaline Environment

The advantage of using alkaline environment is that many non-precious metals are stable in this environment, therefore offering the possibility of developing non-precious metal electrocatalysts. Using the similar approaches of DFT prediction and experimental verification described above for TMC catalysts, we have established general trends between HBE and HER activity in alkaline for monometallic surfaces and used such correlation to identify several non-precious metal alloys, as shown in Figure 3.

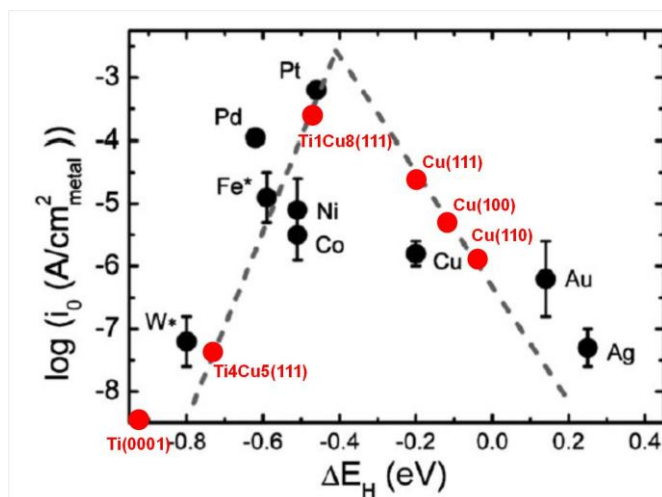


**Figure 3.** Correlating DFT-calculated hydrogen binding energy (HBE) with experimentally measured HER activity in alkaline electrolyte. (Results summarized in Publications: Sheng et al., *Energy & Environmental Science*, 7 (2014) 1719, and Lu et al., *Nature Communications*, 6 (2015) 6567)

Because of the difficulties in accurately calculating HBE values in alkaline electrolyte, we have carefully devised a way to experimentally measure the HBE values on Pt at pH ranging from 1 to 13. These values were then correlated with the HER and hydrogen oxidation reaction (HOR) activities. Such correlation allowed us to conclusively demonstrate that the strength of hydrogen binding is the dominant descriptor for HER/HOR activities in both acid and alkaline electrolytes. These results provided clarification to recent controversies in the literature and established the correlation between HBE values and HER activities in the entire pH range.

### Publications Acknowledging this Grant in 2013-2015:

1. W. Sheng, M. Myint, J.G. Chen\* and Y. Yan\*, "Correlating Hydrogen Evolution Reaction Activity in Alkaline Electrolyte to Hydrogen Binding Energy on Monometallic Surfaces", *Energy & Environmental Science*, 6 (2013) 1509-1512.
2. T.G. Kelly, S.T. Hunt, D.V. Esposito and J.G. Chen\*, "Monolayer Palladium Supported on Molybdenum and Tungsten Carbides as Low-cost HER Electrocatalysts", *International Journal of Hydrogen Energy*, 38 (2013) 5638-5644.
3. Q. Lu, J.G. Chen and J.Q. Xiao, "Design Nanostructured Electrodes for High-performance Supercapacitors", *Angewandte Chemie International Edition*, 52 (2013) 1882-1889.
4. W. Sheng, A.P. Bivens, M. Myint, Z. Zhuang, R.V. Forest, Q. Fang, J.G. Chen\* and Y. Yan\*, "Non-precious Metal Electrocatalyst with High Activity for Hydrogen Oxidation Reaction in Alkaline Electrolytes", *Energy & Environmental Science*, 7 (2014) 1719-1724.
5. Y.C. Kimmel, L. Yang; T.G. Kelly, S.A. Rykov and J.G. Chen\*, "Theoretical Prediction and Experimental Verification of Low Loading of Platinum on Titanium Carbide as Low-Cost and Stable Electrocatalysts", *Journal of Catalysis*, 312 (2014) 216-220.
6. W. Sheng, Z. Zhuang, M. Gao, J. Zheng, J.G. Chen\* and Y. Yan\*, "Correlating hydrogen oxidation/evolution reaction activity on platinum at different pH with measured hydrogen binding energy", *Nature Communications*, 6 (2015) 5848.
7. Y.C. Kimmel, X. Xu, W. Yu, X. Yang and J.G. Chen\*, "Trends in Electrochemical Stability of Transition Metal Carbides and Their Potential Use as Supports for Low-Cost Electrocatalysts", *ACS Catalysis*, 4 (2014) 1558-1562.
8. T.G. Kelly, K.X. Lee and J.G. Chen\*, "Pt-modified Molybdenum Carbide for the Hydrogen Evolution Reaction: From Model Surfaces to Powder Electrocatalysts", *Journal of Power Sources*, 271 (2014) 76-81.
9. T.G. Kelly and J.G. Chen\*, "Controlling C-O, C-C and C-H Bond Scission for Deoxygenation, Reforming, and Dehydrogenation of Ethanol using Metal-modified Molybdenum Carbide Surfaces", *Green Chemistry*, 16 (2014) 777-784
10. T.G. Kelly, A.L. Stottlemeyer, X. Yang and J.G. Chen\*, "Theoretical and experimental studies of ethanol decomposition and electrooxidation over Pt-modified tungsten carbide", *Journal of Electrochemical Society*, 161 (2014) E3165-3170.
11. E.G. Mahoney, W. Sheng, Y. Yan\*, and J.G. Chen\*, "Platinum-Modified Gold Electrocatalysts for the Hydrogen Oxidation Reaction in Alkaline Electrolytes", *ChemElectroChem*, 1 (2014) 2058-2063.
12. L. Yang, Y.C. Kimmel, Q. Lu and J.G. Chen\*, "Effect of pretreatment on the particle size and oxygen reduction activities of low-loading platinum on titanium carbide powder electrocatalysts", *Journal of Power Sources*, 287 (2015) 196-202.
13. I.J. Hsu, J.G. Chen\*, X. Jiang and B.G. Willis\*, "Atomic layer deposition synthesis and evaluation of core-shell Pt-WC electrocatalysts", *Journal of Vacuum Science and Technology A*, 33 (2015) 01A129
14. Q. Lu, G.S. Hutchings, W. Yu, Y. Zhou, R.V. Forest, R. Tao, J. Rosen, B.T. Yonemoto1, Z. Cao, H. Zheng, J.Q. Xiao, F. Jiao\* and J.G. Chen\*, "Highly Porous Non-precious Bimetallic Electrocatalysts for Efficient Hydrogen Evolution", *Nature Communications*, 6 (2015) 6567.

**Molecular-scale Understanding of Selective Oxidative Transformations Promoted by Au**Cynthia M. Friend  
Harvard University

The goal of this project is to develop a molecular-scale understanding the function of Au for promoting reactions of catalytic importance. We have evaluated the competition for binding sites of different reactants and products on O-covered Au(111) because it determines the relative concentrations of adsorbate species for a given temperature and partial pressure; thus, significantly affecting reaction selectivity. A major outcome of this aspect of our work is that weak, van der Waal's interactions, play a critical role in determining the stability of a homologous series of adsorbates; specifically demonstrated for alkoxides bound to Au(111). The stability of acetate, which is a model for carboxylate intermediates more generally, has been studied in detail. Carboxylates are strongly-bound poisons that lead to combustion on gold. The presence of excess  $O_{ads}$  on Au(111) significantly destabilizes acetate by 3-5 kcal/mol compared to clean Au(111). A similar destabilization also occurs on Au(110). Scanning tunneling microscopy (STM) studies show that acetate condenses into islands with excess Au on the clean surface but not in the presence of  $O_{ads}$ . Investigations of single-crystal Ag/Au alloy surfaces using and X-ray photoelectron spectroscopy (STM) are underway and will be compared to our studies of a porous alloy of Au with a ~3% Ag in an effort to understand the function of porous catalyst materials.

**Grant No. DE-FG02-84-ER13289: Molecular-scale Understanding of Selective Oxidative Transformations of Alcohols Promoted by Au and Au-based Alloys****Postdoctoral Associates:** Dr. Martin Schmid (Feodor Lynen Fellow)

Dr. Kara Stowers

Dr. Fanny Hiebel

**Graduate Students:** Dr. Cassandra Freyschlag Siler (DOE graduate fellowship, 2010-13)

Mr. Joshua Klobas

Mr. Yunfei Xu

**RECENT PROGRESS:**

Our DOE-sponsored work has focused on fundamental studies of the surface chemistry of Au, Ag and Au/Ag alloy surfaces using a combination of advanced surface science tools. The goal of this project is to develop a molecular-scale understanding the function of Au and Ag-Au alloys for promoting reactions of catalytic importance. The major accomplishments for this grant period are: (a) Investigation of the reactivity of fluorine-substituted oxygenates, e.g  $CF_3CH_2OH$  and  $CF_3COOH$ , in an effort to understand how the increase in electron density changes reactivity and selectivity; (b) Experimental determination of the relative binding strength of a series of adsorbates on O-covered Au(111) that play a role in selective oxidation reactions that establishes that van der Waal's interactions between alkyl groups and the surface play a critical role in determining the stability of a homologous series of adsorbates; (c) Excess

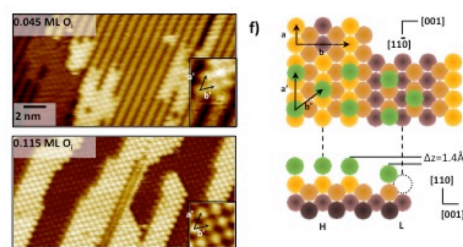


Figure 1: STM of acetate islands for two different coverages. A model of the structure shows the incorporation of Au into the structure.

O<sub>ads</sub> on both Au(111) and Au(110) significantly destabilizes acetate, a prototypical poison/site blocker, by 7-10 kcal/mol compared to the respective clean surfaces demonstrating that the accumulation of poisons can be altered under reaction conditions by controlling the amount of adsorbed oxygen; (d) Islanding and surface reconstruction play an important role in determining the stability of acetate bound to Au(110) based on scanning tunneling microscopy (STM) studies—acetate condenses into islands that recruit extra Au atoms in the absence of O<sub>ads</sub> (Fig. 1) but **not** in the presence of O<sub>ads</sub>; (e) There is substantial reconstruction and mass transport associated with the formation of thin-film, single-crystal Ag/Au alloys based on X-ray photoelectron spectroscopy and STM that are being used to understand the reactivity measured in ultrahigh vacuum (UHV) of a porous alloy of Au with a ~3% Ag that also functions as a catalyst under working conditions. These key contributions provide broad and predictive understanding of reactions of catalytic importance on O-activated Au.

### Publications acknowledging DOE support, 2014-15

‡Full support from DOE Grant No. DE-FG02-84-ER13289

†Partial support from DOE Grant No. DE-FG02-84-ER13289

1. ‡K. J. Stowers, R.J. Madix, and C.M. Friend, “Facile ester synthesis on Ag-modified nanoporous Au: Oxidative coupling of ethanol and 1-butanol under UHV conditions” *Catalysis Letters* (2015) Published on line/ In press.
2. ‡Wang, L., Stowers, K. J., Zugic, B., Biener, M. M., Biener, J. Friend, C. M., Madix, R. J., “Methyl Ester Synthesis Catalyzed by Nanoporous Gold: from 10<sup>-9</sup> Torr to 1 atm”, *Catal. Sci. Technol.*, 2015, 5, pp 1299-1306.
3. ‡Siler, C. G. F., Cremer, T., Rodriguez-Reyes, J. C. F., Friend, C. M., Madix, R. J., “Switching Selectivity in Oxidation Reactions on Gold: The Mechanism of C-C vs C-H Bond Activation in the Acetate Intermediate on Au(111)”. *ACS Catal.*, 2014, 4 (9), pp 3281-3288. DOI: 10.1021/cs500803n.
4. ‡Klobas, E. J., Schmid, M., Friend, C. M., Madix, R. J., “The Dissociation-induced Displacement of Chemisorbed O<sub>2</sub> by Mobile O Atoms and the Autocatalytic Recombination of O due to Chain Fragmentation of Ag(110)”. *Surface Science*, 2014. 630, pp 187-194. DOI: 10.1016/j.susc.2014.08.012
5. ‡Cremer, T., Siler, C.G.F., Rodriguez-Reyes, J. C. F., Friend, C. M., Madix, R. J., “Tuning the Stability of Surface Intermediates Using Adsorbed Oxygen: Acetate on Au(111)”. *J. Phys. Chem. Lett.*, 2014. 5 (7), pp 1126-1130. DOI: 10.1021/jz500192k.
6. ‡Xu, B., Madix, R. J., Friend, C. M., “Predicting Gold-Mediated Catalytic Oxidative-Coupling Reactions from Single Crystal Studies” *Acc. Chem. Res.*, 2014, 47 (3), pp 761-772. DOI: 10.1021/ar4002476.
7. ‡Bingjun Xu, Cassandra G. F. Siler, Madix, R. J., Friend, C. M. “Ag/Au Mixed Sites Promote Oxidative Coupling of Methanol on the Alloy Surface”. *Chem. A European Journal*. 20(16), 4646-4652. DOI: 10.1002/chem.201304837.

**Dramatic Improvement in a Re-Based Olefin Metathesis Catalyst via Ligand-Exchange-Mediated Activation on Chlorinated Alumina**

Alessandro Gallo,<sup>1</sup> Anthony Fong,<sup>1</sup> Julia Rieb,<sup>2</sup> Kai C. Szeto,<sup>3</sup> Mostafa Taoufik,<sup>3</sup> Laurent Delevoe,<sup>4</sup> Régis M. Gauvin,<sup>4</sup> Baron Peters,<sup>1,3</sup> Susannah L. Scott<sup>1,3</sup>

<sup>1</sup> Department of Chemical Engineering, University of California, Santa Barbara CA.

<sup>2</sup> Department of Chemistry & Biochemistry, University of California, Santa Barbara CA.

<sup>3</sup> C2P2 (CNRS-UMR 5265), Université Lyon 1, ESCPE Lyon, 43 Boulevard du 11 Novembre 1918, Villeurbanne, France. <sup>4</sup> UCCS (CNRS-UMR 8181), Université Lille Nord de France, USTL, Villeneuve d'Ascq, France.

Extensive chlorination of  $\gamma$ -Al<sub>2</sub>O<sub>3</sub> results in the formation of highly Lewis acidic domains free of surface hydroxyls, where methyltrioxorhenium (MTO) binds preferentially to give a low temperature olefin metathesis catalyst with very high activity and stability despite the absence of bulky or exotic ligands, and without the need for a pre-installed carbene initiating site. This grafted MTO undergoes exchange with the surface, acquiring a chloride ligand from modified alumina while donating an oxygen ligand to the support. IR, Raman, high field solid-state NMR, Re L<sub>III</sub>-edge EXAFS, and DFT calculations support facile O-Cl ligand exchange between MTO and Cl-Al<sub>2</sub>O<sub>3</sub>, to generate a [CH<sub>3</sub>ReO<sub>2</sub>Cl]<sup>+</sup> fragment associated with the support via a Lewis acid-base interaction with a bridging oxygen. The methyl group remains intact, and there is no evidence for a spectroscopically-observable methylene tautomer. Nevertheless, the chloride-promoted catalyst is dramatically more active and productive than MTO/ $\gamma$ -Al<sub>2</sub>O<sub>3</sub>, easily achieving a TON of 100,000 for propene metathesis in a flow reactor at 10 °C (compared to <5,000 for the non-chloride-containing catalyst). The increased activity results from a much larger fraction of active sites, as well as higher intrinsic activity for the Cl-containing sites; the high selectivity and remarkable stability are due to the absence of nearby Brønsted acid sites.

**DE-FG02-03ER15467: Hierarchical Design of Supported Organometallic Catalysts for Hydrocarbon Transformations**

**Lead PI:** Susannah L. Scott

**CoPIs:** Baron Peters, Albert E. Stiegman

**Postdocs:** Alessandro Gallo, Domenick Leto, Matthew Polinski

**Students:** Ryan Davis, Anthony Fong, Bryan Goldsmith, Youhong Wang, Taeho Hwang, Daniel Collier, Tony Ferrari, Yu Wu

**RECENT PROGRESS**

*The role of water in olefin epoxidation catalyzed by methyltrioxorhenium (MTO).* Olefin epoxidation by H<sub>2</sub>O<sub>2</sub> catalyzed by MTO is an order of magnitude faster when organic solvents are made semi-aqueous, although the rate constants for the epoxidation elementary steps are virtually independent of the solvent composition. These findings

implicate water in the activation of the pre-catalyst. We computed the free energies of activation for peroxy-complex formation using density functional theory, including solvation and a novel method to incorporate tunneling corrections for proton transfer steps. Computed rate constants for a water-assisted ligand exchange pathway are several orders of magnitude faster than the corresponding rates for direct ligand-exchange. The ligand exchange reactions are tetramolecular reactions involving two solvent H<sub>2</sub>O molecules transferring a proton from coordinated H<sub>2</sub>O<sub>2</sub> to the oxo ligand via a stepwise Grotthuss mechanism, Figure 1.

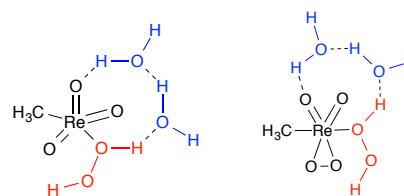


**Figure 1.** Cyclic transition states for proton transfer via a Grotthuss mechanism during ligand exchange.

Experiments confirmed our computational predictions that the rate of each step increases dramatically with water concentration Figure 2 (left). The kinetics were measured while keeping the total water concentration constant, but varying the H<sub>2</sub>O/D<sub>2</sub>O ratio. The observed rate constant  $k_n^{\text{obs}}$  (where  $n$  is the D-atom fraction) is related to the rate constant  $k_0^{\text{obs}}$  measured in the absence of D,  $k_n^{\text{obs}} = k_0^{\text{obs}} (1 - n + n\Phi^T)^m$ , where  $\Phi$  is the fractionation factor for each exchangeable H/D,  $m$  is the number of H/D transferred in the transition state T. Figure 2 (right) shows that  $m = 3$  for both ligand exchange steps. These findings suggest that efforts to catalyze epoxidation under anhydrous conditions may be unproductive; inherent rates are so slow as to be irrelevant.

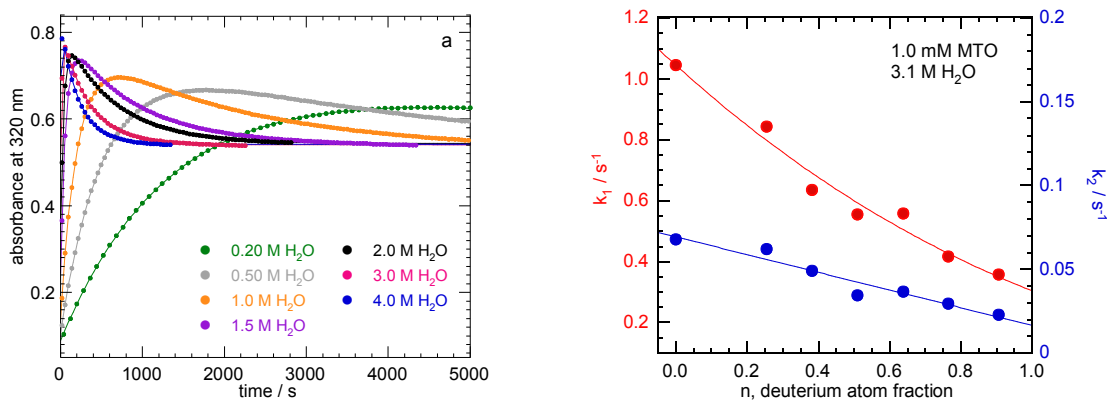


**Figure 2.** Left: Time-resolved kinetic profiles at 25.0 °C in CH<sub>3</sub>CN, at 320 nm, for the reaction of 1.0 mM MTO with 49.1 mM H<sub>2</sub>O<sub>2</sub>, in the presence of variable amounts of H<sub>2</sub>O (0.20 – 4.0 M), showing curve-fits obtained using biexponential kinetic equations. Right: Dependence on deuterium atom fraction ( $n$ ) of the rate constants  $k_1$  (red) and  $k_2$  (blue), showing curve-fits obtained using  $m = 3$ .

**New theory linking amorphous catalyst structures to reactivity.** Molecular or quasi-molecular catalysts grafted to amorphous supports have been widely studied by experimentalists, but they have been treated only superficially by theorists because the active site structure is generally unknown for amorphous catalyst materials. We used sequential quadratic programming (SQP) to reverse the structure-to-property paradigm: for each activation energy, we find the local site structure with the lowest energy. The rationale is that low energy sites will tend to be more common than strained high energy sites. We can thus predict the structural features that distinguish typical inactive sites from typical active sites. Our algorithm allows us to quantitatively predict the sensitivity of reaction kinetics to structural heterogeneities at sites on the amorphous support surface. Figure 3 shows results for a molybdenum carbene complex grafted to amorphous

SiO<sub>2</sub> as an olefin metathesis catalyst. The algorithm identified sites with activation barriers 10 kJ/mol lower than previous studies. More generally, it revealed that subtle structural variations in the surrounding SiO<sub>2</sub> environment can change activation barriers by as much as 40 kJ/mol! It generates representative structures of extremely active sites and completely dead sites. The structural changes in going from one extreme to the other reveal structure-activity relationships in a systematic way – a first for catalysts on amorphous supports.

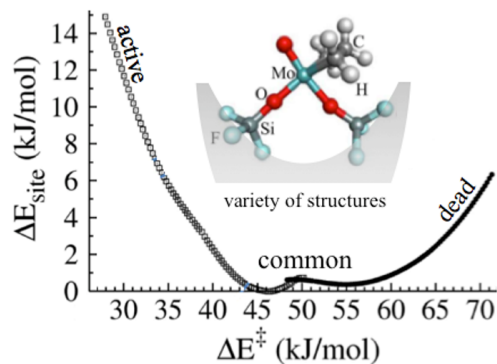


**Figure 3.** Results from our algorithm for understanding structure-property relationships for single-atom catalysts on amorphous supports, showing a Mo carbene grafted to amorphous SiO<sub>2</sub> and a deactivation pathway.

**Mechanism of Initiation in the Phillips Ethylene Polymerization Catalyst.** The structure and mechanism of the formation of the active sites for ethylene polymerization in the Phillips catalyst (Cr/SiO<sub>2</sub>) is one of the great, unsolved mysteries of heterogeneous catalysis. A mesoporous, optically transparent monolith of Cr<sup>VI</sup>/SiO<sub>2</sub> was prepared using sol-gel chemistry in order to monitor the reduction process spectroscopically. Using *in situ* UV-vis spectroscopy, we observed a very clean, step-wise reduction by CO of Cr<sup>VI</sup> first to Cr<sup>IV</sup>, then to Cr<sup>II</sup>. Both the intermediate and final states show XANES consistent with these oxidation state assignments, and aspects of their coordination environments were deduced from Raman and UV-vis spectroscopies. The intermediate Cr<sup>IV</sup> sites are inactive towards ethylene at 80 °C. The Cr<sup>II</sup> sites, which have long been postulated as the endpoint of CO reduction, were observed directly by high-frequency/high-field EPR spectroscopy. They react quantitatively with ethylene to generate organoCr<sup>III</sup> active sites, characterized by X-ray absorption and UV-vis spectroscopy.

The organoCr<sup>III</sup> sites are capable of initiating polymerization without recourse to an alkylating co-catalyst. Evidence for the formation of organic radicals suggests that the key step is a one-electron redox reaction, involving homolysis of a Cr-C bond. Solid-state <sup>13</sup>C CP-MAS NMR and Raman spectroscopy reveal that the resulting site contains a vinyl ligand, (≡SiO)<sub>2</sub>Cr<sup>III</sup>-CH=CH<sub>2</sub>, capable of initiating polymerization. Formation of the vinyl site is an incommensurate redox reaction, since Cr<sup>II</sup> undergoes 1e oxidation, while ethylene is ultimately reduced by 2e, Figure 4.

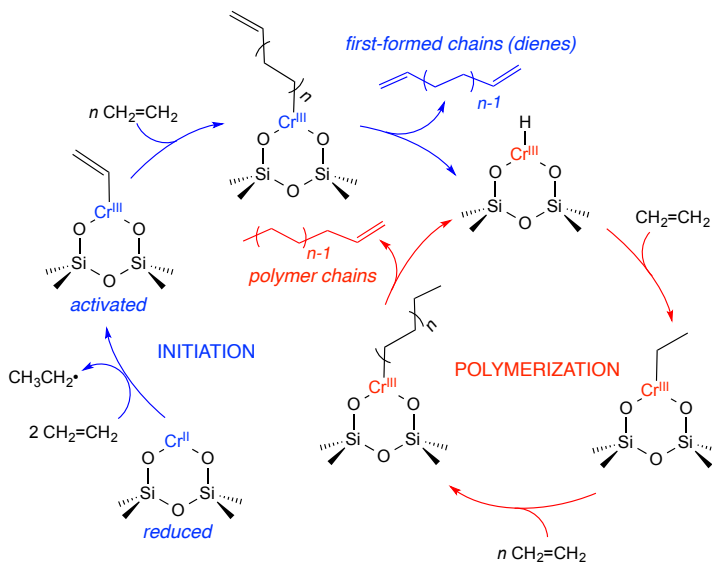


**Figure 4.** Proposed mechanism for initiation in the Phillips ethylene polymerization catalyst, involving formation of a vinylCr<sup>III</sup> site and liberation of ethyl radicals.

## Publications Acknowledging this Grant in 2012-2015

1. Peters, B. "Headspace diffusion limitations on heterogeneous catalysis in unstirred batch reactors", *Chem. Eng. Sci.* **2012**, *71*, 367-374.
2. Tovar, T. M.; Stewart S. M.; Scott, S. L. "Origin of the ZnCl<sub>2</sub> Effect on CH<sub>3</sub>ReO<sub>3</sub>/γ-Al<sub>2</sub>O<sub>3</sub> in Olefin Metathesis", *Top. Catal.* **2012**, *55*, 530-537.
3. Tao, Y. C.; Lita, A.; van de Burgt, L. J.; Zhou, H. D.; Stiegman, A. E., "Metal Site-Mediated, Thermally Induced Structural Changes in Cr<sup>6+</sup>-Silicalite-2 (MEL) Molecular Sieves", *Inorg. Chem.*, **2012**, *51*, 2432-2437.
4. Bhagat, S. D.; Chatterjee, J.; Chen, B. H.; Stiegman, A.E. "High Refractive Index Polymers Based on Thiol-Ene Cross-Linking Using Polarizable Inorganic/Organic Monomers", *Macromolecules*, **2012**, *45*, 1174-1181.
5. Wanglee, Y.J.; Hu, J. G.; White, R.E.; Lee, M.Y.; Stewart, S.M.; Perrotin, P.; Scott, S.L. "Borane-Induced Dehydration of Silica and the Ensuing Water-Catalyzed Grafting of B(C<sub>6</sub>F<sub>5</sub>)<sub>3</sub> to Give a Supported, Single-Site Lewis Acid, ≡SiOB(C<sub>6</sub>F<sub>5</sub>)<sub>2</sub>", *J. Am. Chem. Soc.* **2012**, *134*, 355-366.
6. Rosana, M. R.; Tao, Y. C.; Stiegman, A. E.; Dudley, G. B., "On the rational design of microwave-actuated organic reactions" *Chem. Sci.*, **2012**, *3*, 1240-1244.
7. Tiozzo, C.; Bisio, C.; Carniato, F.; Gallo, A.; Scott, S. L.; Psaro R.; Guidotti, M. "Niobium-silica catalysts for the selective epoxidation of cyclic alkenes: the generation of the active site by grafting niobocene dichloride", *Phys. Chem. Chem. Phys.*, **2013**, *15*, 13354-13362.
8. Hwang, T.; Goldsmith, B.; Peters, B.; Scott, S.L. "Water-Catalyzed Activation of H<sub>2</sub>O<sub>2</sub> by Methyltrioxorhenium: A Combined Computational-Experimental Study", *Inorg. Chem.* **2013**, *52*, 13904-13917.
9. Goldsmith, B. R.; Sanderson, E. D.; Bean, D.; Peters, B. "Isolated catalyst sites on amorphous supports: a systematic algorithm for understanding heterogeneities in structure and reactivity", *J. Chem. Phys.* **2013**, *138*, 204105.
10. Goldsmith, B. R.; Fong, A.; Peters, B. "Understanding reactivity with reduced potential energy landscapes: recent advances and new directions", in Reaction Rate Constant Computations: Theories and Applications, Eds Han, K.; Chu, T. Royal Society of Chemistry: Cambridge, **2013**, pp. 213-232.
11. Crosswhite, M.; Hunt, J.; Southworth, T.; Serniak, K.; Ferrari, A.; Stiegman, A.E. "Development of Magnetic Nanoparticles as Microwave-Specific Catalysts for the Rapid, Low-Temperature Synthesis of Formalin Solutions", *ACS Catal.* **2013**, *3*, 1318-1323.
12. Dudley, G. B.; Stiegman, A. E.; Rosana, M. R. "Correspondence on Microwave Effects in Organic Synthesis", *Angew. Chem. Int. Ed.*, **2013**, *52*, 7918-7923.
13. Hunt, J.; Ferrari, A.; Lita, A.; Crosswhite, M.; Ashley, B.; Stiegman, A.E. "Microwave-Specific Enhancement of the Boudouard Reaction", *J. Phys. Chem. C*, **2013**, *117*, 26871-26880.
14. Ma, S.; Guo, X.; Zhao, L.; Scott, S.L.; Bao, X. "Recent progress in methane dehydroaromatization: From laboratory curiosities to promising technology", *J. Energy Chem.*, **2013**, *22*, 1-20.
15. Xiao, P.; Davis, R.C.; Ouyang, X.; Li, J.; Thomas, A.; Scott, S.L.; Zhu, J. "Mechanism of NO reduction by CO over Pt/SBA-15", *Catal. Commun.*, **2014**, *50*, 69-72.
16. Ferrari, A.; Hunt, J.; Lita, A.; Ashley, B.; Stiegman, A. E. "Microwave-Specific Effects on the Equilibrium Constants and Thermodynamics of the Steam, Carbon and Related Reactions", *J. Phys. Chem. C*, **2014**, *118*, 9346-9356.
17. Chen, P.-K.; Rosana, M. R.; Dudley, G. B.; Stiegman, A. E., "Parameters Affecting the Microwave-Specific Acceleration of a Chemical Reaction" *J. Org. Chem.*, **2014**, *79*, 7425-7436.
18. Rosana, M. R.; Hunt, J.; Ferrari, A.; Southworth, T. A.; Tao, Y.; Stiegman, A. E.; Dudley, G. B., "Microwave-Specific Acceleration of a Friedel-Crafts Reaction: Evidence for Selective Heating in Homogeneous Solution" *J. Org. Chem.*, **2014**, *79*, 7437-7450.
19. Peters, B.; Scott, S.L. "Single atom catalysts on amorphous supports: a quenched disorder perspective" *J. Chem. Phys.*, **2015**, *142*, 104708.
20. Fong, A.; Yuan, Y.; Ivory, S.; Scott, S.L.; Peters, B. "Computational Kinetic Discrimination of Ethylene Polymerization Mechanisms for the Phillips (Cr/SiO<sub>2</sub>) Catalyst", *ACS Catal.* **2015**, *5*, 3360-3374.

This page is intentionally blank.

# Participant List

This page is intentionally blank.

## Catalysis Research Meeting

July 19-22, 2015

### Participant List

Abu-Omar, Mahdi  
Adzic, Radoslav  
Appel, Aaron  
Balbuena, Perla  
Bartels, Ludwig  
Bartlett, Bart  
Belkacem, Ali  
Bell, Alexis  
Bhan, Aditya  
Bligaard, Thomas  
Bond, Jesse  
Britt, Phillip  
Bullock, Morris  
Bunel, Emilio  
Campbell, Charles  
Cargnello, Matteo  
Celik, Fuat  
Chen, Jingguang  
Chen, Eugene  
Cox, David  
Crooks, Richard  
Datye, Abhaya  
Dauenhauer, Paul  
Davis, Robert  
Dixon, David  
Erlebacher, Jonah  
Figueroa, Joshua  
Finke, Richard  
Fout, Alison  
Friend, Cynthia  
Garrett, Bruce  
Gates, Bruce  
Gellman, Andrew

Gordon, Mike  
Gorte, Raymond  
Grabow, Lars  
Gunnoe, Thomas  
Harris, Alexander  
Head-Gordon, Teresa  
Henderson, Michael  
Henkelman, Graeme  
Hock, Adam  
Jaramillo, Thomas  
Jenks, Cynthia  
Jin, Rongchao  
Jones, William  
Jones, Christopher  
Katz, Alexander  
Kitchin, John  
Lercher, Johannes  
Liu, Ping  
Lutterman, Daniel  
Marceau, Diane  
McEwen, Jean-Sabin  
Miller, John  
Miranda, Raul  
Mullins, Charles  
Mustain, William  
Nguyen, SonBinh  
Nørskov, Jens  
Notestein, Justin  
Nuckolls, Colin  
Nuzzo, Ralph  
Overbury, Steven  
Oyama, S. Ted  
Ozkan, Umit

Peden, Charles  
Peng, Zhenmeng  
Pietraß, Tanja  
Pruski, Marek  
Rahman, Talat  
Ramasubramaniam, Ashwin  
Rappe, Andrew  
Rauchfuss, Thomas  
Ribeiro, Fabio  
Rodriguez, Jose  
Sadow, Aaron  
Savara, Aditya  
Schlögl, Robert  
Schneider, William  
Schwartz, Viviane  
Scott, Susannah  
Selloni, Annabella  
Sen, Ayusman  
Shaw, Wendy  
Sholl, David  
Slowing, Igor I.  
Stacchiola, Dario  
Suib, Steven  
Tonks, Ian  
Vicic, David  
Vlachos, Dionisios  
Wade, Christine  
Wang, Yong  
Weaver, Jason  
White, Michael  
Xu, Bingjun  
Yang, Judith  
Zaera, Francisco

## BENCHMARKING CATALYSIS SCIENCE

### Conclusions from the Breakout Sessions

The discussions held by the PIs during breakout sessions led to independent observations and conclusions that they will publish on their own in the open literature shortly. A reference to that publication will appear here when available.



## Toward Benchmarking in Catalysis Science: Best Practices, Challenges, and Opportunities

Thomas Bligaard,<sup>†</sup> R. Morris Bullock,<sup>‡</sup> Charles T. Campbell,<sup>§</sup> Jinguang G. Chen,<sup>\*,||,⊥</sup> Bruce C. Gates,<sup>#</sup> Raymond J. Gorte,<sup>g</sup> Christopher W. Jones,<sup>h</sup> William D. Jones,<sup>i</sup> John R. Kitchin,<sup>j</sup> and Susannah L. Scott<sup>\*,k</sup>

<sup>†</sup>SUNCAT - Center for Interface Science and Catalysis, SLAC National Accelerator Laboratory, Menlo Park, California 94025, United States

<sup>‡</sup>Center for Molecular Electrocatalysis, Pacific Northwest National Laboratory, Richland, Washington 99352, United States

<sup>§</sup>Department of Chemistry, University of Washington, Box 351700, Seattle, Washington 98195-1700, United States

<sup>||</sup>Department of Chemical Engineering, Columbia University, New York, New York 10027, United States

<sup>⊥</sup>Chemistry Department, Brookhaven National Laboratory, Upton, New York 11973, United States

<sup>#</sup>Department of Chemical Engineering & Materials Science, University of California, Davis, California 95616, United States

<sup>g</sup>Department of Chemical & Biomolecular Engineering, University of Pennsylvania, Philadelphia, Pennsylvania 19104, United States

<sup>h</sup>School of Chemical & Biomolecular Engineering, Georgia Institute of Technology, 311 Ferst Drive NW, Atlanta, Georgia 30332, United States

<sup>i</sup>Department of Chemistry, University of Rochester, Rochester, New York 14627, United States

<sup>j</sup>Department of Chemical Engineering, Carnegie Mellon University, 5000 Forbes Avenue, Pittsburgh, Pennsylvania 15213, United States

<sup>k</sup>Department of Chemical Engineering, University of California, Santa Barbara, California 93106, United States

\* Supporting Information

**ABSTRACT:** Benchmarking is a community-based and (preferably) community-driven activity involving consensus-based decisions on how to make reproducible, fair, and relevant assessments. In catalysis science, important catalyst performance metrics include activity, selectivity, and the deactivation profile, which enable comparisons between new and standard catalysts. Benchmarking also requires careful documentation, archiving, and sharing of methods and measurements, to ensure that the full value of research data can be realized. Beyond these goals, benchmarking presents unique opportunities to advance and accelerate understanding of complex reaction systems by combining and comparing experimental information from multiple, in situ and operando techniques with theoretical insights derived from calculations characterizing model systems. This Perspective describes the origins and uses of benchmarking and its applications in computational catalysis, heterogeneous catalysis, molecular catalysis, and electrocatalysis. It also discusses opportunities and challenges for future developments in these fields.

